*Indian Journal of Natural Sciences* www.tnsroindia.org.in ©IJONS

*Vol. 9 / Issue 50 /October 2018* *International Bimonthly* *ISSN: 0976 – 0997*

RESEARCH ARTICLE

# Screening and Molecular Identification of Endophytic Bacteria Isolated From Legumes Nodules and Roots Cultivated in *Acacia* Rhizosphere Soils Collected in an Arid Region, Tata-Akka in South of Morocco

K.Taoufiq[1,2], M.Faghire[1*], S.Tahrouch[1], M.Nejmeddine[3], M.Göttfert[4], K.Oufdou[2] and A.Hatimi[1]

[1]Laboratory of Plant Biotechnology, Department of Biology, Faculty of Sciences, University Ibn Zohr (UIZ), B.P 8106, Hay Dakhla, 80000, Agadir, Morocco

[2]Laboratory of Biology and Biotechnology of Microorganisms, Environmental Microbiology and Toxicology Unit, Faculty of Sciences Semlalia, Cadi Ayyad University, PO Box 2390, Marrakech, Morocco

[3]Laboratory of Cell Biology and Molecular Genetics, Faculty of Sciences, University Ibn Zohr (UIZ), B.P 8106, Hay Dakhla, 80000, Agadir, Morocco

[4]Technische Universität Dresden, Institut für Genetik, Helmholtzstr. 10, D-01069 Dresden, Germany

Received: 06 July 2018 Revised: 10 Aug 2018 Accepted: 13 Sep 2018

[*]**Address for Correspondence**
**M. Faghire**
Department of Biology,
Faculty of Sciences,
University Ibn Zohr (UIZ), B.P 8106,
Hay Dakhla, 80000, Agadir, Morocco
E mail: m.faghire@uiz.ac.ma



## ABSTRACT

A molecular characterization was used to assess the biodiversity of endophytic bacteria of some leguminous plants cultivated in the rhizosphere soil of *Acacia*, an autochthonous plant, collected in an arid region of South of Morocco, Tata-Akka region. Thus faba bean (*Vicia faba)*, chickpea (*Cicer arietinum)*, lentil (*Lens culinaris)* and common bean (*Phaseolus vulgaris)* were used to harbor the endophytic bacteria. A total of seventy-two isolates were obtained and characterized using PCR-ARDRA (Amplified Ribosomal DNA Restriction Analysis) of 16S rDNA. Our findings showed a high molecular biodiversity of our isolates, 40.9% of the isolated endophytic bacteria were *Ensifer meliloti* (*Sinorhizobium meliloti*) isolated in nodules of chickpea and common bean, 31.8% were *Rhizobium* sp. isolated in nodules and roots of common bean and lentil and 27.3% were *Enterobacter* sp. isolated in roots of faba bean, common bean, chickpea and lentil.

**Keywords**: Legumes, endophytic bacteria, *Acacia*, arid region, autochthonous plant, Tata-Akka, *Ensifer meliloti* , *Rhizobium* sp., *Enterobacter* sp.

## INTRODUCTION

In Northern Africa, salinity and drought are the most important abiotic constraints that limit the crops productivity. Morocco is among the regions affected by both these constrains [1, 2]. Indeed, Morocco is vulnerable to climate change, its arid and semi-arid regions would be more susceptible to drought and warm in the hot season [3]. The climate change affects the availability of water [3] which causes a high salinity of soils and reduces the productivity of many crops. It's well known that legumes are among the most important crops for human nutrition because they provide a high level of proteins compared to other plants [4]. In addition, the legumes play an important role in sustainable agriculture by offering many economic and environmental advantages, in particular their ability to fix nitrogen in symbiosis with rhizobia, for this reason they are mainly used to improve the fertility of saline soils [3, 4, 5, 6, 7]. However, legumes are sensitive to both drought and salinity, which limit their growth and production in many areas with particular severe drought and salinity conditions [3, 5, 6].

In recent years, the search of endophytic bacteria to ameliorate the production of legumes is becoming an issue of growing interest. Indeed, endophytic bacteria play an interesting role in improving the soil fertility, and by reducing the use of chemical fertilizers [8, 9, 10].The endophytic bacteria are defined as bacteria living within plant tissues without causing any harm or visible symptoms to plants [11]. In this symbiotic relationship, the host plants benefit extensively by harboring these bacteria [12]. They are called plant growth-promoting rhizobacteria (PGPR), they are naturally present in the soil, where they colonize plants's roots and promote plant growth [13].The Acacia, are a leguminous plants, trees or shrubs, that are natives to the tropical plains, these plants are distributed in areas of low rainfall or in areas where rainfall is seasonal, by this way they are widely distributed in arid and semi-arid regions and they tolerate many severe environmental conditions such as drought and salinity [14, 15, 16, 17]. In Morocco, the *Acacia* have a very important socio-economic role, many *Acacia* species are widely used in reforestation programs, in fertilization of soils and in dunes fixation [15, 16, 18, 19]. For example *Acacia cyanophylla* plants were introduced, in the Souss-Massa region in Morocco, by the Water and Forest Service of the Government to increase the biological stabilization of the coastal dunes [18, 19].

Several authors have reported also the use of *Acacia* species in traditional medicine [15, 17], indeed a study has been made in the region of Tata has shown that the population of this region uses *Acacia ehrenbergiana* and *Acacia tortilis* subsp. *Raddiana (Savi) Brenan*, in traditional medicine, bark, leaves, seeds, gum, flowers and fruits of both these species are used to treat several diseases such as hepatitis, lung diseases like asthma or to relieve fever [20].The studied area, Tata-Akka region, is among the most affected regions by both severe aridity and salinity conditions [16]. However, in these conditions, *Acacia*, which is a spontaneous plant, showed to be resilient and well adapted to the severe abiotic constraints that characterize this pre-saharan area [16].Thus Zahran [21, 22] have reported that the bacteria isolated from wild legumes in arid zones, present higher tolerance to several constraints such drought, salt stress and elevated temperatures,these bacteria may be used to inoculate wild, as well as, crop legumes, to ameliorate their productivity. These observations lead us to investigate the possibility of using the rhizosphere soil of *Acacia* that harbor endophytic bacteria to form a symbiosis with legumes. These bacteria can be then used to inoculate the plants in order to improve their tolerance to abiotic constraints, such as water deficiency and salinity. This work is the first report studying the biodiversity of legumes-endophytic bacteria isolated from the rhizosphere of *Acacia* in Tata-Akka region.

## MATERIALS AND METHODS

### Study area

Tata-Akka region is localized in the South East of Morocco, with an area of 26.274 km$^2$, it's located on the southern side of the Anti-Atlas Mountains. This region is characterized by hyper-aridity with a low rainfall around 100

mm/year, and large fluctuations in daily and annual temperature [20]. The average temperature in Tata, calculated in 13 years, is 22 °C. The highest temperatures are often recorded in the summer, which results in a high potential of evaporation that exceeds 2 m [16]. This presaharan climate causes a water deficiency and high soils salinity which induce seriously degraded vegetation and a progressive reduction of biological diversity in this ecosystem [16]. The region of Tata-Akka is characterized by two spontaneous species of *Acacia* which are *Acacia ehrenbergiana* and *Acacia raddiana* [20, 23].

### Collect of rhizospheric soils and soils mineral analysis

Samples of *Acacia* plants rhizospheric soils were collected in February 2015 from nine sites in the Tata-Akka region. Their positions were localized by the Global Positioning System (GPS). The samples have been subjected to a soil mineral analysis and stored at 4°C.The soil mineral analyses of major elements were conducted by X-ray fluorescence spectrometry (OLYMPUS).

### Plant materials

The legumes seeds used in this study were available in the market and were mainly used by the farmers. They belong to four legumes, which are faba beans, the common beans, lentils and chickpeas. Before planting, the surfaces of the seeds were disinfected with sodium hypochlorite NaClO (1/5) for 10 min, and washed extensively using sterile distilled water, and then putted to germinate in small pots containing rhizospheric soils (three seeds per pot of 20 cm of diameter and 30 cm of height). The seeds were germinated in the nine rhizospheric soils. Plants were grown in a temperature controlled glasshouse at 28 °C and irrigated with a nutrient solution. The plants were then harvested at the flowering stage.

### Isolation of endophytic bacteria

Roots of the plants were thoroughly washed under tap water to remove the soil particles, and then selected roots and nodules were cut in many fragments. Under aseptic conditions roots and nodules surface was disinfected with NaClO diluted at 1/3 for 5 min, and washed with distilled sterilized water for 3 to 5 times.After this step, the roots and nodules of each plant were individually crushed and homogenized in a sterilized mortar and pestle in sterilized water. The resulting suspensions were streaked, independently, onto Petri dishes containing yeast extract–mannitol (YEM) medium. This medium is routinely used for rhizobial isolation, purification and culture [24]. Petri dishes containing YEM were incubated for 24 hour at 28 °C. Colonies were selected after 24 hour by picking and repicking to obtain a final 72 isolates. All strains were stored in 40% (v/v) glycerol at -20 C°.

### Molecular characterization of the strains

Molecular characterization of the endophytic bacteria was done using the technique of Polymerase Chain Reaction combined with Amplified Ribosomal DNA Restriction Analysis (PCR-ARDRA) of 16S rDNA sequencing.The extraction of genomic DNA was conducted according to the protocol of Dhaese et al. [25]. Four ml of cultured bacteria were grown in liquid YEM medium for 2 days at 28 °C, and then collected by centrifugation. After washing with Tris-EDTA (TE) buffer, the pellets, containing bacteria, were resuspended in 300 µl of TE, then 100 µl of 5 % SDS and 100 µl pronase E (2.5 mg / ml in TE buffer pre-incubated for 90 min at 37 °C) were added to the suspension. After mixing, the solution was incubated for an over-night. The DNA was purified by two extractions with Tris-buffered phenol and one extraction with methylene chloride. The DNA was precipitated with 0.1 volume of 3 M sodium acetate and 2.5 volumes of ethanol. The identification was done by the 16S rDNA sequencing, using primers 16Sa (5'-CGCTGGCGGCAGGCTTAACA-3') and 16Sb (5'-CCAGCCGCAGGTTCCCCT-3') [26]. The PCR was performed using 100 ng of DNA, 1.25 units (U) of Dream Taq polymerase (product of Thermo Fisher Scientific) and 100 pmol of each

primer in a total volume of 50 µl (as suggested by the enzyme supplier). PCR conditions were: an initial denaturation at 95 °C for 5 min, 30 cycles of denaturation at 95 °C for 30 s, annealing at 55 °C for 30 s, and extension at 72 °C for 1.5 min. A final extension was conducted at 72 °C for 10 min. For visualization, the near full-length (approximately 1400-bp) 16S rDNA fragments were separated on 0.8% agarose gels and stained with ethidium bromide. Sequencing was done by GATC Biotech company (Konstanz, Germany) using primers 16Sa, 16Sb, and two internal primers 16SLOA (TAACGCATTAAACATTCCGCCTGG) and 16SLOB (TTAATCTTGCGACCGTACTCC). For blast searches, the resources of the National Center for Biotechnology Information were used. Phylogenetic analysis was conducted with Molecular Evolutionary Genetics Analysis (MEGA) version 5.2 [27].

## RESULTS

### Coordinates of studied sites

The coordinates of the studied sites are represented in Figure.

### Mineral analysis of soils samples

The Table 1 exhibits the analysis of the different soils samples used in this study.According to Boyer [28] mineral deficiency thresholds of phosphorus (P) is between 25 mg/kg and 100 mg/kg, 39 mg/kg for potassium (K), 20,655 mg/kg for magnesium (Mg), and 80 mg/kg for calcium (Ca). While Adeoye and Agboola [29], have reported 25 mg/kg as critical level of manganese (Mn) in soil. And according to Lindsay [30, 31] who have reported that plants require a critical content of soluble iron (Fe) in soil approximately equal to $10^{-8}$ M which corresponds to 0, 00056 mg/kg. Similarly Bonneau et al. [32] have reported that Al values higher than 7 meq/100 g (944.3 mg / kg) are toxic to plants whereas White and Broadley [33] have reported that only the values of chlorine in soil between 1.79 mg / kg and 3.57 mg / kg are needed by plants. The values below can be toxic for plants. According to the critical content values presented below, we conclude that our samples are rich on P, K, Fe and Mn, while the values of Mg and Ca are low. We record also a low content of aluminum (Al) and chlorine (Cl) in all samples except for site 5 where a high content of Cl is recorded.

### Molecular characterization of the strains

The molecular characterization of the 72 isolates has shown a genotypic diversity among these strains. *Ensifer meliloti* strains were isolated from nodules of chickpea and common bean represent 40.9 % of the isolates strains, while 31.8 % of strains isolated from nodules of common bean and lentil were closed to *Rhizobium* sp . *Enterobacter sp*. which represent 27.3% of isolates strains, were isolated from roots of faba bean, common bean, chickpea and lentil (as shown in **Table 2**). We noted that all legumes have formed typical nodules.

## DISCUSSION

The results obtained by mineral analysis of the rhizosphere of *Acacia* have shown that these soils are very rich in minerals and low in elements that can be toxic, such as Al and Cl. These results can be explained by the effect of the rhizosphere of *Acacia* that enriches the soil with root exudates that modifies positively the capacity of retention and adsorption of mineral elements by soil [34]. These conditions constitute a favorable environment for the development of microorganisms that, in their turn, ensure a high mineral fertility of soil [32, 34]. In addition the low leaching in this region with dry climate explains the high level of P, K and Mn [16, 35].The comparison of our samples soils with other soils on mineral elements such P and K shows a high level in this elements respect to other soils. P and K were very higher in our samples than in soils collected in many regions, in Sais region, which is an agricultural region in Northen central in Morocco [36] or with soils in Northern Spain where an autochtonous variety of chickpea in

alternance with barley were cultivated [37] as well as in soil samples collected in India [39].Many authors have affirmed that richness of soils in mineral elements can be attributed to microflora existing in soil. Thus Peix et al. [37] have shown that N, Ca, K and Mg content values were higher in soils inoculated with *Mesorhizobium mediterraneum* than in uninoculated soils. These suggestions were confirmed by previous studies by Grego et al. [34] that have shown that the rhizosphere of *Acacia raddiana* in two different biotopes, Tunisia and Senegal, is rich in active microflora. The results obtained by these authors have reported that several parameters such as the organic matter content, the microbial biomass, the soil respiration, the activity of the enzymes involved in the metabolism of nitrogen and phosphorus are higher and have a significance difference in the rhizosphere of *Acacia raddiana* compared to areas not influenced by the roots [34].

Thus, the microbial flora intervenes by several processes to improve the mineral quality of the soil, these processes include degradation of litter and mineralization of organic matter in soil, solubilization of insoluble phosphorus, and by enriching soil by nitrogen by fixing atmospheric nitrogen [6, 32, 37, 38, 40]. Other processes include elimination of toxic compounds such as Al and Cl [32, 41]. According to Bastviken et al. [42] up to 24% of inorganic chlorine initially added to the soil was incorporated into the microbial biomass in a week, with long-term formation of organic chlorine.The microorganisms have also a direct effect on plant growth, Saharan and Nehra [13 ] have reported that inoculation of crop plants with PGPR at an early stage of development of the plant has a positive effect on the plant growth by affecting positively the plant height and weight, the plant health, the plant vigor and by enhancement the seedling germination. In addition, the inoculation by these PGPR induce early flowering, increase the chlorophyll content and enhance nodulation in legumes [13].Elsewhere, several studies demonstrated that the effect of inoculation of legumes by some species of bacteria can ameliorate their tolerance to different stress like saline stress. Indeed, Faghire et al. [6] have previously demonstrated that the symbiotic nitrogen fixation was not affected by saline treatment (25 mM NaCl), using two varieties of common bean combined with *Rhizobium* strain CIAT899 and a local strain RhM11 isolated from Al Haouz region of Morocco. Faghire et al. [1] also showed that in common bean-rhizobia symbiosis; nodulation, shoot and root biomasses were not affected by salinity. Our molecular characterization of the strains showed that they belong to two groups, strains nodulating legumes or rhizobia and strains that not able to form nodules with leguminous plants.

Rhizobia group is among the most important group of the PGPR, the rhizobia-legumes symbioses is considered as a major atmospheric nitrogen fixing systems, thus symbiotic $N_2$ fixation represents a renewable source of N for agriculture and is the major source of nitrogen input in agricultural soils including those in arid regions [10, 21, 22].
The rhizobia are defined as soil bacteria that are able to form nodules and to establish a symbiosis with the roots or the stems of legumes, it is the process by which atmospheric nitrogen is fixed and reduced into ammonium which directly assimilated by plants [8,10]. Many studies have been done recently that show a great diversity among rhizobia, currently, we count more than 98 species belonging to 14 genera of $\alpha$- and $\beta$- proteobacteria, these genus are : *Rhizobium*, *Bradyrhizobium*, *Ensifer (Sinorhizobium)*, *Mezorhizobium*, *Microvirga*, *Azorhizobium*, *Phyllobacterium*, *Ocrhobactrum*, *Methylobacterium*, *Devosia* and *Shinella* these genus belong to the class of $\alpha$- proteobacteria, while the second class of $\beta$-proteobacteria contain *Burkholderia* and *Cupriavidus* (*Ralstonia*), and the third class is $\gamma$-proteobacteria which contains also some bacteria that are able to nodulate legumes and to fix nitrogen from atmosphere [8, 9,10].

Moreover Shiraishi et al. [9] showed that *Pseudomonas sp.,* class of $\gamma$-proteobacteria, belong to the group of rhizobia, inoculation tests and histological studies revealed that *Pseudomonas* sp. formed nodules on *Robinia pseudoacacia*. This result was confirmed by a phylogenetic analysis of symbiotic genes, both nodulation genes *nodA* and *nodC* and *nif* genes *nifH*, and *nifHD*, were used in this study. *Nif* genes are encoding for enzymes involving in the fixation of atmospheric nitrogen (nitrogenase enzyme…). The phylogenetic analysis of these symbiotic genes revealed that *Pseudomonas sp.* have high similarities with symbiotic genes of rhizobial species, these results indicate an horizontal gene transfer from symbiotic genes of rhizobia species in the soil to *Pseudomonas* sp. [9]. Certain rhizobial strains can nodulate only certain legumes, this process is called cross inoculation, for example *Rhizobium leguminosarum bv viciae*

can nodulate only some species like *Lens*, *Pisum*, *Vicia*, and *Lathyrus* spp, while *R. leguminosarum bv trifolii* can only nodulate species of *Trifolium* [43].Our findings, consisting on cross inoculation, are consistent with previous reports [44] that isolated *Sinorhizobium meliloti* in nodules of *Cicer arietinum* L. from soils of Kelaa de Sraghna region in Morocco, and in nodules of common bean from the oases in the south of Tunisia [45]. In the meantime, *Rhizobium* (*R. etli*, *R.tropici*, *R.gallicum*, and *R.phaseoli*) were isolated from nodules of *Phaseolus vulgaris* in saline soils from the Al Haouz region, Marrakech, Morocco [5], and from nodules of *Lens culinaris* in the soils in Algeria [46]. Consistently, both *Rhizobium* and *Ensifer* were shown to nodulate the *Phaseolus vulgaris* [5]. On the other hand *Enterobacter* (*E. cloacae*) was reported to be isolated from nodules of *Vicia faba* in Tunisia [47], while *Enterobacter aerogenes* was isolated from chickpea's nodules in India [48]. Furthermore Midekssa et al. [49] employed 16S rDNA sequence analysis to identify the isolates from roots of *Lens culnaris* Medik, they found that two species of *Enterobacrer sp*., *Enterobacter ludwigii* and *Enterobacter cloacae*, can be isolated from this leguminous plant.Finally *Enterobacter sp.* strains were able to colonize effectively the root of *Phaseolus vulgaris* [50]. The characterization of indigenous endophytic bacteria from *Acacia* plants rhizospheric soils collected from an arid region, such Tata-Akka region, may lead to the selection of efficient and effective inoculants strains for different species of legumes especially in soils affected by abiotic constrains like salinity.More investigations were needed to understand the mechanisms by which these strains of bacteria affect the growth of legumes in soil with severe conditions of drought and salinity.

## ACKNOWLEDGMENTS

This work was supported by the ministerial fellowship (Morocco) and also by the Alexander von Humboldt foundation.

## REFERENCES

1. Faghire M., Farissi M., Taoufiq Kh., Fghire R., Bargaz A., Mandri B., Oufdou Kh., Laury A., Drevon J.J., and Ghoulam C. (2013). Genotypic variation of nodules' enzymatic activities in symbiotic nitrogen fixation among common bean (*Phaseolus vulgaris* L.) genotypes grown under salinity constraint. Symbiosis 60: 115-122.
2. FARISSI Mohamed, BOUIZGAREN Abdelaziz, FAGHIRE Mustapha, BARGAZ Adnane, GHOULAM Cherki (2013). Agrophysiological and biochemical properties associated with adaptation of Medicago sativa populations to water deficit. Turk J Bot 37: 1166-1175.
3. Fnighire F., Laftouhi N.E., Saidi M. E. and Markhi A. (2014). Some Aspects of Climate Variability and Increasing Aridity in Central Morocco over the Last Forty Years: Case of Tensift Basin (Marrakech-Morocco). Journal of Environment and Earth Science 4(9): 42-51.
4. Broughton W.J., Hernandez G., Blair M., Beebe S., Gepts P. and Vanderleyden J. (2003). Beans (Phaseolus spp.) model food legumes. Plant and Soil 252: 55-128.
5. Faghire M. , Mandri B. , Oufdou K. , Bargaz A. , Ghoulam C. , Ramírez-Bahena M.H., Velázquez E. and Peix A. (2012). Identification at the species and symbiovar levels of strains nodulating *Phaseolus vulgaris* in saline soils of the Marrakech region (Morocco) and analysis of the otsA gene putatively involved in osmotolerance. Systematic and Applied Microbiology 35:156–164.
6. Faghire M., Bargaz A., Farissi M., Palma F., Mandri B., Lluch C., Tejera García N.A, Herrera-Cervera J.A, Oufdou K., and Ghoulam C. (2011). Effect of salinity on nodulation, nitrogen fixation and growth of common bean (*Phaseolus vulgaris*) inoculated with rhizobial strains isolated from the Haouz region of Morocco. Symbiosis 55: 69–75.
7. Benidire L., Lahrouni M., Daoui K., Zain el Abidine Fatemi Z.E.A., R.G., Göttfert M. and Oufdou K. (2018). Phenotypic and genetic diversity of Moroccan rhizobia isolated from Vicia faba and study of genes that are likely to be involved in their osmotolerance. Systematic and Applied Microbiology 41 (1) 51-61.
8. Zakhia F. and De Lajudie P. (2001). Taxonomy of rhizobia. Agronomie 21: 569-576.

9. Shiraishi A., Matsushita N. and Hougetsu T. (2010). Nodulation in black locust by the Gammaproteobacteria *Pseudomonas sp*. and the Betaproteobacteria *Burkholderia sp.* Systematic and Applied Microbiology 33: 269-274.
10. Berrada H. and Fikri Benbrahim K. (2014). Taxonomy of the Rhizobia: Current Perspectives. British Microbiology Research Journal 4(6): 616-639.
11. Hung P.Q. and Annapurna K. (2004). Isolation and Characterization of Endophytic Bacteria in Soybean (Glycine Sp.). Omonrice 12: 92-101.
12. Bandara W.M.M.S, Seneviratne G., and Kulasooriya S.A. (2006). Interactions among endophytic bacteria and fungi: effects and potentials. Journal of Biosciences 31(5): 645-650.
13. Saharan, B and Nehra, V. (2011) Plant Growth Promoting Rhizobacteria: A Critical Review. Life Science and Medical Research 21:1-30.
14. Ross J.H. 1981. An analysis of the African *Acacia* species: their distribution, possible origins and relationships. Bothalia 13: 389-413.
15. Benabid A. (2000). Flore et écosystèmes du Maroc. Evaluation et préservation de la biodiversité. Éditions Ibis Press, Paris. Librairie et éditions, Kalila Wa Dimna, Rabat.
16. Barathon J.J, El Abbassi H., and Lechevalier C. (2005). Les oasis de la région de Tata (Maroc) : abandon de la vie oasienne traditionnelle et adaptation à la vie urbaine. Annales de Géographie 644 : 449-461.
17. Fikri Benbrahim K., Berrada H., El Ghachtouli N. and Ismaili M. (2014). Les acacias: des plantes fixatrices d'azote prometteuses pour le développement durable des zones arides et semi-arides. International Journal of Innovation and Applied Studies 8 (1):46-58.
18. Hatimi A. (1999). Effect of salinity on the association between root symbionts and *Acacia cyanophylla* Lind.: growth and nutrition. Plant and Soil 216: 93-101.
19. Hatimi A., Bani-Aameur F., and Oihabi A. (2001). Caractérisation de souches de Rhizobiums autochtones des dunes: effet sur la croissance et la nutrition azotée d'*Acacia cyanophylla* Lindl. Acta Botanica Gallica 148 (3): 191-199.
20. Abouri M., El Mousadik A., Msanda F., Boubaker H., Saadi B., and Cherifi Kh. (2012). An ethnobotanical survey of medicinal plants used in the Tata Province, Morocco. International Journal of Medicinal Plant Research 1 (7): 099-123.
21. Zahran H.H. (2001). Rhizobia from wild legumes: diversity, taxonomy, ecology, nitrogen fixation and biotechnology. Journal of Biotechnology 91: 143-153.
22. Zahran H.H. (2009). Enhancement of Rhizobia–legumes symbioses and nitrogen fixation for crops productivity improvement. Microbial Strategies for Crop Improvement, pp.227-254 DOI: 10.1007/978-3-642-01979-1_11, 227-254.
23. El Ayadi F., Ait Aabd N., El Finti A., Msanda F., Baniaameur F., and El Mousadik A. (2011). Genetic variability of wild provenances of *Acacia tortilis* ssp. Raddiana (Savi) Brenan in south of Morocco. Asian Journal of Plant Sciences 10 (1): 43-51.
24. Vincent J.M. (1970). A Manual for the Practical Study of Root Nodule Bacteria. Oxford: Blackwell Scientific.
25. Dhaese P., De Greve H., Decraemer H., Schell J., Van Montagn M.I (1979). Rapid mapping of transposon insertion and deletion mutations in the large Ti-plasmids of *Agrobacterium tumefaciens*. Nucleic Acids Research 7: 1837-1849.
26. Van Berkum P. and Fuhrmann J.J. (2000). Evolutionary relationships among the soybean bradyrhizobia reconstructed from 16S rRNA gene and internally transcribed spacer region sequence divergence. International Journal of Systematic and Evolutionary Microbiology 50: 2165-2172.
27. Tamura K., Peterson D., Peterson N., Stecher G., Nei M., and Kumar S. (2011). MEGA5: molecular evolutionary genetics analysis using maximum likelihood, evolutionary distance, and maximum parsimony methods. Molecular Biology and Evolution 28(10): 2731-2739.
28. Boyer J. (1982). Fertilité et utilisation des sols. Initiation-Documentations techniques. Office de la recherche scientifique et technique outre-mer (Orstom), n° 52, Tome X, Paris, 384 p.
29. Adeoye G.O. and Agboola A.A. (1985). Critical levels for soil pH, available P, K, Zn and Mn and maize ear-leaf content of P, Cu and Mn in sedimentary soils of South-Western Nigeria. Fertilizer Research 6: 65-71.

30. Lindsay W. L. (1984). Soil and plant relationships associated with iron deficiency with emphasis on nutrient interactions, Journal of Plant Nutrition 7 (1-5): 489-500.
31. Lindsay W. L. (1995). Chemical reactions in soils that affect iron availability to plants. A quantative approach. In: Abadía J. (eds) Iron Nutrition in Soils and Plants. Developments in Plant and Soil Sciences, Springer, Dordrecht 59 :7-14..
32. Bonneau M., Landmann G., Garbaye J., Ranger J. and Nys C. (1994). Gestion et restauration de la fertilité minerale des sols. Rev . For. Fr. XLVI 5:579-585.
33. White P.J. and Broadley M.R. (2001). Chloride in Soils and its Uptake and Movement within the Plant: A Review. Annals of Botany 88: 967-988.
34. Grego S., Moscatelli M.C., Di Mattia E., Marinari S. and Cacciari I. (2003). Activité biochimique de la rhizosphère d'*Acacia raddiana* au nord et du sud du Sahara. In : Grouzis Michel (ed.), Le Floc'h E. (ed.) Un arbre au désert : *Acacia raddiana*. Paris : IRD, 231-247. ISBN 2-7099-1522-7.
35. Godfroy J. (1976). Evolution des teneurs des sols en éléments minéraux fertilisants sous culture bananière. Caractéristiques chimiques des sols de Cote D'Ivoire. Fruits, 31(2): 75-82.
36. Touhtouh D., Moujahid Y., El Faleh E.M. and EL Halimi R. (2014). Caractérisations physicochimiques de trios typesde sols du Sais, Maroc (Physicochemical characterizations of three types of soils of Sais, Morocco. Journal of Materials and Environnemental Scienece 5 (5): 1524-1534.
37. Peix A., Rivas-Boyero A.A., Mateos P.F., Rodriguez-Barrueco C., Martinez-Molina E., and Velazquez E. (2001). Growth promotion of chickpea and barley by a phosphate solubilizing strain of *Mesorhizobium mediterraneum* under growth chamber conditions. Soil Biology & Biochemistry 33: 103-110.
38. Peix A., Rivas R., Mateos P.F., Martınez-Molina E., Rodrıguez-Barrueco C. and Velazquez E. (2003). *Pseudomonas rhizosphaerae* sp. nov., a novel species that actively solubilizes phosphate *in vitro*. International Journal of Systematic and Evolutionary Microbiology 53: 2067-2072.
39. Shivanna A.M. and Nagendrappa G. (2014). Chemical analysis of soil samples to evaluate the soil fertility status of selected command areas of three tanks in Tiptur Taluk of Karnataka, India. Journal of Applied Chemistry 7: 01-05.
40. Rosas S.B., Andres J.A., Rovera M. and Correa N.S. (2006). Phosphate-solubilizing *Pseudomonas putida* can influence the rhizobia–legume symbiosis. Soil Biology & Biochemistry 38: 3502-3505.
41. Rodstedth M., Stahlberg C., Sanden P. and Oberg G. 2003. Chloride imbalances in soil lysimeters. Chemosphere 52: 381-389.
42. Bastviken D., Thomsen F., Svensson T., Karlsson S. , Sanden P., Shaw G., Matucha M. and Oberg G. (2007). Chloride retention in forest soil by microbial uptake and by natural chlorination of organic matter. Geochimica et Cosmochimica. Acta 71: 3182-3192.
43. Hirsch A.M., Lum M.R. and Downie J.A. (2001). What Makes the Rhizobia-legume symbiosis so special?. Plant Physiology 127: 1484-1492.
44. Maatallah J., Berraho E.B., Munoz S., Sanjuan J. and Lluch C. (2002). Phenotypic and molecular characterization of chickpea rhizobia isolated from different areas of Morocco. Journal of Applied Microbiology, 93: 531-540.
45. Mnasri B., Mrabet M., Laguerre G., Aouani M.E. and Mhamdi R. (2007). Salt-tolerant rhizobia isolated from a Tunisian oasis that are highly effective for symbiotic $N_2$ fixation with *Phaseolus vulgaris* constitute a novel biovar (bv. mediterranense) of *Sinorhizobium meliloti*. Archives of Microbiology 187: 79-85.
46. Riah N., Béna G., Djekoun A., Heulin K., De Lajudie P. and Laguerre G. (2014). Genotypic and symbiotic diversity of Rhizobium populations associated with cultivated lentil and pea in sub-humid and semi-arid regions of Eastern Algeria. Systematic and Applied Microbiology 37(5):368-75.
47. Fatnassi I.C., Chiboub M., Saadani O., Jebara M., and Jebara S.H. (2013). Phytostabilization of moderate copper contaminated soils using co-inoculation of *Vicia faba* with plant growth promoting bacteria. Journal of Basic Microbiology 53:1–9.
48. Singh O., Gupta M., Mittal V., Kiran S., Nayyar H., Gulati A. and Tewari R. (2013). Novel phosphate solubilizing bacteria '*Pantoea cypripedii* PS1' along with *Enterobacter aerogenes* PS16 and *Rhizobium ciceri* enhance the growth of chickpea (*Cicer arietinum* L.). Plant Growth Regul 73: 79–89.

49. Midekssa M.J., Löscher C.R., Schmitz R.A., and Assefa F. (2015). Characterization of phosphate solubilizing rhizobacteria isolated from lentil growing areas of Ethiopia. African Journal of Microbiology Research 9(25): 1637-1648.
50. Collavino M.M., Sansberro P.A., Mroginski L.A., and Aguilar O. M. (2010). Comparison of *in vitro* solubilization activity of diverse phosphate-solubilizing bacteria native to acid soil and their ability to promote *Phaseolus vulgaris* growth. Biology and Fertility of Soils 46: 727–738.

**Table 1. Elemental concentrations (mg / Kg) for analysis of the nine soils samples (S1 to S9).**

| | S1 | S2 | S3 | S4 | S5 | S6 | S7 | S8 | S9 |
|---|---|---|---|---|---|---|---|---|---|
| **K** | 7564 ± 87,81 | 5345 ± 58,31 | 6547 ± 61,02 | 6705 ± 64,24 | 7157 ± 68,29 | 7170 ± 69,40 | 6441 ± 61,36 | 6240 ± 62,21 | 5889 ± 57,89 |
| **Ca** | 9,11 ± 0,0668 | 5,76 ± 0,0366 | 2,73 ± 0,0172 | 5,56 ± 0,0343 | 6,26 ± 0,039 | 2,15 ± 0,0147 | 2,51 ± 0,016 | 3,33 ± 0,021 | 3,44 ± 0,0208 |
| **P** | 1731 ± 99,81 | 1570 ± 72,64 | 1403 ± 61,69 | 1531 ± 72,17 | 1361 ± 75,03 | 1500 ± 67,25 | 1304 ± 63,22 | 1388 ± 69,24 | 1340 ± 65,20 |
| **Mg** | 2,55 ± 0,4105 | 2,61 ± 0,3254 | 3,03 ± 0,308 | 3,19 ± 0,3228 | 2,66 ± 0,321 | 2,69 ± 0,324 | 2,83 ± 0,302 | 3,37 ± 0,320 | 2,88 ± 0,3026 |
| **Cl** | 2,09 ± 0,0879 | 2,03 ± 0,0620 | 2,17 ± 0,0587 | 1,31 ± 0,0624 | 7859 ± 663,85 | 2,05 ± 0,0665 | 1,26 ± 0,0618 | 1,11 ± 0,0668 | 1,37 ± 0,0616 |
| **Fe** | 1,48 ± 0,0163 | 2,37 ± 0,0191 | 2,66 ± 0,0192 | 2,35 ± 0,0183 | 2,35 ± 0,0187 | 2,97 ± 0,0221 | 3,25 ± 0,0227 | 1,89 ± 0,0151 | 1,93 ± 0,0149 |
| **Al** | 3,14 ± 0,0838 | 2,11 ± 0,0619 | 2,25 ± 0,0602 | 2,44 ± 0,0644 | 3,11 ± 0,0708 | 2,79 ± 0,0682 | 2,91 ± 0,0661 | 2,90 ± 0,0680 | 2,85 ± 0,0652 |
| **Mn** | 362 ± 34,94 | 229 ± 25,44 | 329 ± 24,52 | 292 ± 26,08 | 200 ± 25,54 | 871 ± 34,31 | 434 ± 26,70 | 233 ± 23,62 | 156 ± 21,57 |

**Table 2. Identification of some isolates by 16S rDNA sequencing and their correspondent strains**

| Strain | Isolates designation | Host plant | Site or Sol |
|---|---|---|---|
| *Ensifer meliloti* | PN101, PN121, PN,123, PN125, PN126, PN131, PN105, PN112, HN51 | chickpea and common bean | S1,S2,S4,S6,S7 ,S8 |
| *Enterobacter* sp. | HR26, HR57, PR113, PR135, LNR57, FR13 | common bean, chickpea, lentil and faba bean, | S1,S4,S7,S9 |
| *Rhizobium* sp. | HR46, HR48, HR33, HR38, HR46, LR142, LNR146, | common bean and lentil | S1,S3,S5,S6, |

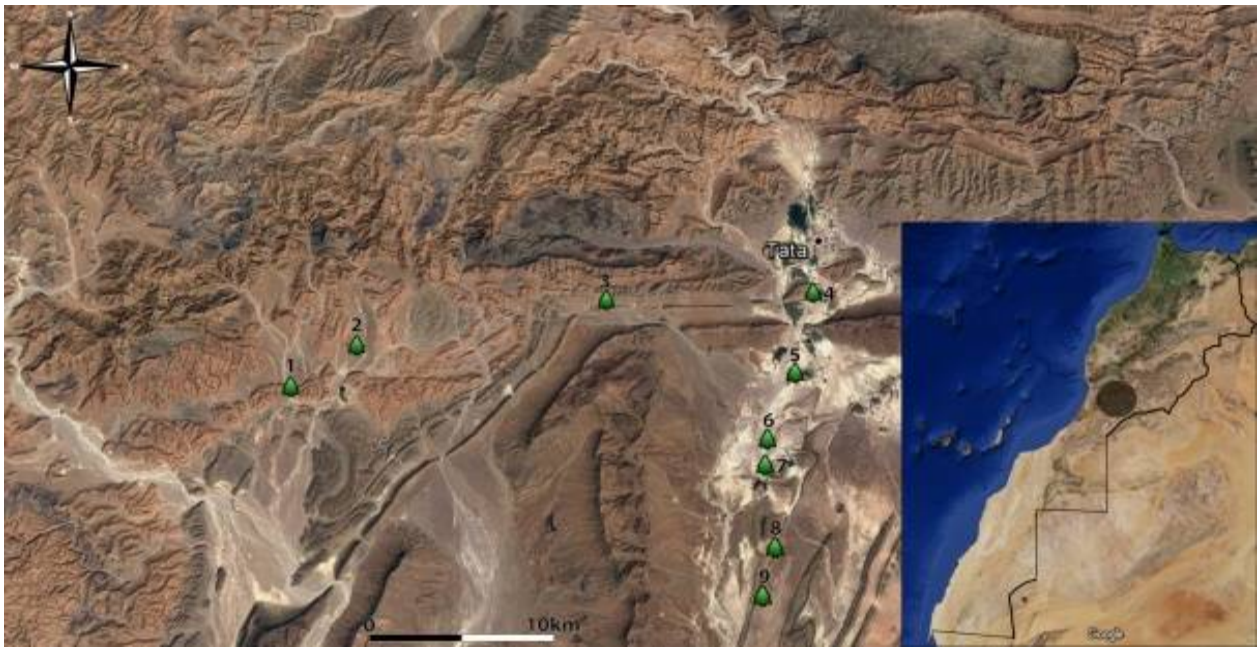


**Figure 1. Geographical Map showing the locations of all nine sampling sites of Tata - Akka region. The coordinates of the nine sites are: , site 1 (N 29°39'5,47" W 8°17'20,02"), site 2 (N 29°40'28,63" W 8°15'6,31"), site 3 (N 29°42'7,02" W 8°6'12,49"), site 4 (N 29°42'27,07" W 7°58'42,49"), site 5 (N 29°39'42,92" W 7°59'33,02"), site 6 (N 29°37'32,02" W 8°0'40,15"), site 7 (N 29°36'42,86" W 8°0'47,90"), site 8 (N 29°34'10,10" W 8°0'37,40") and site 9 (N 29°36'35,23" W 8°0'43,17")**

*Indian Journal of Natural Sciences* www.tnsroindia.org.in ©IJONS

*Vol. 9 / Issue 50 /October 2018* *International Bimonthly* *ISSN: 0976 – 0997*

RESEARCH ARTICLE

# Isolation and Identification of Important Food Borne Bacterial Strains from Fresh and Frozen Retail Bovine Meat in Baghdad Province

Jasim M.Fayyad* and Mohammed J. Alwan

College of Veterinary Medicine, University of Baghdad, Baghdad, Iraq

Received: 08 July 2018 Revised: 09 Aug 2018 Accepted: 13 Sep 2018

***Address for Correspondence**
**Jasim M.Fayyad**
College of Veterinary Medicine,
University of Baghdad,
Baghdad, Iraq.



## ABSTRACT

The current study aimed to determine the types and percentage of important food borne bacterial strains in fresh and retail bovine meat collected from different slaughter house and supermarkets in Baghdad city and evaluate antibiotic resistant of *Listeria monocytogenes* isolates, for this purpose,100 fresh and frozen bovine meat samples (fifty for each one).using routine microbiological methods for bacterial isolation and confirmed bacterial diagnosis by biochemical test and EPI20 system. The result revealed that six bacterial strains were isolated from fresh and frozen bovine meat including, 23(46%),29(58%) respectively *E.coli*, 3(6%),5(10%) respectively *L.monocytogenes*, 5(10%),7(14%) respectively Salmonella spp,2(4%),10(20%) respectively *Staph.aureus*, 2(4%),1(2%) respectively Campylobacter spp and 1(2%) both Pseudomonas spp, The high rate of *L.monocytogenes* strains were recorded in the frozen retail meat5(10%) followed by fresh meat 3(6%) with significant differences (P>0.05 ).PCR assay showed thatamong all strains of *L.monocytogenes* isolated from both fresh and frozen meat,8 isolates carried hemolysin gene.it was concluded that bovine meats considered a main source of food borne bacteria particularly *E.coli*.

**Keywords**: Meat ,bacterial strain isolation ,identification.

## INTRODUCTION

Food borne disease is considered important economic and public health problem worldwide, these disease are either infectious or toxic in nature that induced morbidity and mortality in population after consumption contamination food or water [1],the first one occur by consumption toxin production by pathogen and infection type occur directly by viable pathogen post consumption contaminated food by these organisms WHO recorded that food borne disease cause over 600 000000 cases of illness associated with 420 000 deaths together with 27000000 of lost life[2],`In USA,it was estimated that about $US78 billion cost of health care [3],and each person required

over $US1600 per year [4]. In India ,during 1980 to 2009 years, it was reported that 37 outbreaks of food poisoning [5],while in USA,foodborne disease cause 47.8 million cases lead to 127,839 hospitalization occur by contamination food and associated with 3037 death per year [6,7],reported that 48 million persons were infected by food borne disease per year in USA. In the United States, it was recorded that 10 pathogens associated with foodborne disease including Salmonella spp, which cause 31% of food related death, *Escherichia coli* O157:H7(3%), Listeria (28%), Shigella, Campylobacter (5%), in addition to viral and parasitic cases [8]. The main causes of food borne illness are bacteria which constitutes 66% of the problems[9].The most important invasive food borne pathogen is *L.monocytogenes* that form a major problem in meat and dairy industries worldwide [10],due to their wide distribution in the environment [11].

High mortality induced by these pathogen post consumption contaminated food (25% - 30% overall) [12],the source of outbreaks by these pathogen including raw meat, non-pasteurized milk, fishand vegetables dairy food including soft or semisoft cheese [13],in addition ready to eat foods [14], However, It was recorded that determined the incidence and prevalence of food borne pathogens could provide best information about control and prevent the outbreaks of food borne disease as well as to improve safety of food products,in addition to reduce costs induced by these disease [3,4]. in Iraq,there was no program to determine the type of food associated with these disease and their etiology ,therefore numerous studies were required to investigate food borne pathogens that were dependent on microbiological examination,therefore the aim of the present study were to investigate the type and percentage of pathogenic bacteria isolated from raw and frozen retail cattle meat in different markets in Baghdad and determine antimicrobial resistant of *L.monocytogens.*

## MATERIALS AND METHODS

One hundred fresh and frozen bovine meats(fifty each), were collected under septic condition from different supermarkets and slaughterhouse of Baghdad city /Iraq. The five grams of meat samples were homogenized with stomacher in 100ml of sterile normal saline,then culture on in MacConkey agar, blood agar and mannitol salt agar at 37C for 24hr ,then isolated colonies were culture on selective media to 24-48hr at 37C, morphology of the colonies were rerecorded according to color, shape, size, and microscopic examination by gram stain.

### Identification of bacterial strains

The suspected colonies were confirmed diagnosis by biochemical test, CAMP test, hemolysis in blood agar and EPI20 system

### Isolation of genomic DNA

Anovernight grown L.monocytogenes were centrifuged at 13000 rpm for 1 minute, then the pellet were transferred to 200ul of Buffer CL containing lysozyme (RNase A 5µl and Proteinase K 20µL), to Buffer BL, DNA extraction with G-spin ™ total DNA extraction kit protocol (Intron/Korea) according to the manufacture company.

### Confirmation of L.monocytogenes by polymerase chain reaction (PCR)

### Primers

The primer were obtained from [15],who consider being diagnosis*hyl* gene table1, PCR was performed in a final reaction volume 25 µl table2, in thermal cycle(Multi Gene Opti Max Gradient Thermal cycle/USA), with initial denaturation steps as 95C$^{o}$ for 3 min, thirty five amplification cycle, and final extraction step of 7 min at 72C$^{o}$, PCR product were resolved on 1% agarose gel electrophoresis and visualized by UV transilluminator apparatus.The

master mix reaction components were added to the stander PCR tube that containing the PCR premix. PCR product along with 100bp DNA ladder electrophoreses in 2% agarose gel containing red safe nucleic acid staining (30µl/500ml).then the agarose was run at 7V/c2 for 1-2 hrs.

## RESULTS

### Bacterial isolation

Bacterial inoculation showed colonies with varies size,shape and color, gram stain revealed certain isolated were gram negative and the other gram positive ,culturing on specific media biochemical test, and EPI20 system expressed several bacterial species were isolated from meat samples table(3). Table (**3**) showed that 50 fresh meat samples expressed 23 (46%) *E.coli*, 5(10%) E.coli O157:H7,3(6%) L.monocytogenes,5(10%) *Salmonella spp*,2(4%) *Staphylococcus aureus*,2(4%) Campylobacter and 1(2%) Pseudomonas spp isolates while frozen retail meat samples showed 29(58%) E.coli, 3(6%) *E.coli*O157:H7, 5(10%) *L.monocytogenes*, 10(20%) *Staphylococcus aureus*, 1(2%) *Campylobacter sp* and 1 (2%) *Pseudomonas sp.*

### Detection of *hyl* gene of L.monocytogenes

PCR assay were used to detect *hyl* gene of *L.monocytogenes,* the result showed that all *L.monocytogenes* isolated of meat sample, using PCR which amplified a product size of a proximally 209bp as show fig(1).

## DISCUSSION

The present finding revealed that 100% of raw and frozen retail bovine meat expressed positive bacterial isolates , these result may indicated generally poor hygiene treatment of the meat and these meat may contaminated with varies species of bacteria during handling,transmitted and storage in supermarkets particularly unstable electric source in Iraq.High percentage of bacterial positive isolates from frozen retail meat in the present study may indicated that these meat was considered one cause of gastroenteritis in people in Iraq, due to the retail meat widely consumption in Iraq. these idea was consistent with [16], who found in 2014, 4.1million cases of gastroenteritis cause by food borne pathogens on each year in Australia. The main bacterial species isolated from raw and frozen retail bovine meat are 23(46%),29(58%) respectively *E.coli*,5(10%),3(6%) E.coli O157:H7 respectively ,3(6%),5(10%) respectively *L.monocytogenes*,5(10%),7(14%) respectively *Salmonella.spp*,2(4%),10(20%) respectively *Staph.aureus*, 2(4%), 1(2%) respectively Campylobacter spp and 1(2%) both Pseudomonas spp and all of these bacterial isolates were pathogen for human, these result may supported idea that the food origin animals were considered important source of food borne disease [17], that effect human population during handling or consumption undercooking contaminated meat, these evidence was agreement with investigation of [18], who found that the beef and chicken meat may form important health risk for human due to contamination with fecal organism such as Salmonella spp and E.coli and other Enterobacteriaceae.

The current study revealed that large percentage of *Salmonella* isolated from meat , these result may indicated that the bacteria form a important food borne pathogens, these idea was agreement with [19], who recorded that the common cause of food borne illness are bacteria such as *Salmonella* that form 20.9%,,*Escherichia coli O157:H7* 1.4%, also the result of *Salmonella spp* isolated from meat in the current study may indicated that the meat was considered one cause of food poisoning and hospitalization illness in Iraq .

The present finding revealed high percentage of *Staph.aureus*10 (20%) were isolated from retail frozen bovine meat, these result may indicated that the retail meat is a main source of infected by these pathogen, these result was similar to those reported by [20], who recorded that 50 (32.5%) meat samples of cattle and pigs were positive for *S.aureus*

also In India,[21], recorded that *Staph.aureus* and *Salmonella* form the main etiological agents of food poisoning. on base of about idea, it was required better hygienic safety of retail and fresh bovine meat to prevent transmission food borne disease particularly large population of Iraqi people were dependent on retail meat consumption, these idea was in consistent with [22], who demonstrated that hygienic safety required to prevent spreading food borne disease worldwide. The current result showed that among fifty raw meat and fifty frozen bovine meat ,23(46%),29(58%) respectively*E.coli* positive isolates ,these result was similar to result of [23], in Egypt. isolated *E.coli* in high percentage from raw meat[24]. however,high percentage of *E.coli* isolated from raw bovine meat in the present study may be due to the meats contaminated from intestine or from the water during slaughtering and evisceration[25].High percentage of E.coli isolated from bovine meat may indicated that these pathogen is a main a cause of diarrhea in the individual ,these idea was agreement with [26], who reported that high incidence of diarrhea in developing countries due to food contaminated with enteropathogenic bacteria.

The current study revealed among raw bovine meat and frozen meat,5(10%) ,3(6%)*E.coli* O157:H7 respectively were positive isolates,these result may indicated poor general hygiene, and these pathogen widely spread in bovine meat due to widely spreading in the environment.[27], recorded that . *E.coli* O157:H7 can persist in soil, water and bovine feces for 90 days.the presence 8 *Escherichia coli* O157:H7 isolates in bovine meat may indicated these pathogen is important food borne disease in bovine cattle and highly distributed in these meat. The current study revealed that *L.monocytogenes*were isolated from 5(10%) of 50 samples of retail frozen bovine meat collected from different supermarkets in Baghdad city and from 3(6% ) of fresh bovine meat slaughter in abattoir these result were less than reported by [28], who isolated *L.monocytogenes* from 15(75%) of the frozen beef samples, 6(30.4%) of the 23 samples of local meat. these percentage of *L.monocytogenes* isolates in the current study may considered problem public health due to these pathogen can cause illness during handling or consumption of contaminated meat. this result may indicated that the meat may contaminated with L.monocytogenes , during the course of processing to the end[29]. the isolation of *L.monocytogenes* from meat is line with finding other studies in many countries,

The current study demonstrated that all isolates of *L.monocytogens* isolated from meat harboured virulence factors ,hemolysin-A gene (*hyl*), these result may indicated these pathogen is highly virulence that may cause human illness post consumption contaminated meat, these result was agreed with [30], who demonstrated that the *plcA, prfA, actA, hlyA* and *iap* virulence genes in 18 isolates of *L.monocytogenes* present in fish and shrimp meat,also demonstrated *plcA,*gene in bacterial isolated from bovine meat in the current study may indicated these pathogen was highly pathogenicity for human,these evidence was agreement with [31],who demonstrated that haemolytic species of Listeria such as *L.monocytogens* is highly pathogenicity for human and cause meningitis in nonimmunocompromised adult. Isolated of *L.monocytogens* from frozen meat in the present result may indicated that these pathogen can survive in frozen temperature these result was agreement with [32],who isolated *L.monocytogens* and *L.innocua* from 1.9% and 5.7% of the frozen and fresh sea-food samples, respectively. There are few studies about isolated *L.monocytogens* from bovine meat in Iraq and the current study may be the first report in Iraq describing virulence gene of *L.monocytogens* that isolated from bovine meat,numerous studies demonstrated virulence genes in *L.monocytogens* isolated from food products associated with public health risks due to consumption contaminated food products by these pathogenic *L.monocytogens*[33],The important emerging food borne pathogen is Listeria monocytogenes that associated with threat global food safety, these pathogen was isolated from varies food and food products such as dairy milk and meat .it has veterinary public health importance worldwide ,few studies were performed on the prevalence and characteristics of these pathogen in raw and frozen retail bovine meat in Iraq.

## REFERENCES

1. Adams M.R. and Moss M.O.(2003).“Significance of food borne diseases,” Food Microbiology, vol. 2(163): 160–164.

2. Havelaar A.H.; Kirk M.D.; Torgerson P.R.; Gibb H.J.; Hald T.; Lake R.J.; Praet N.; Bellinger D.C.; de Silva N.R and Gargouri N.(2010)."World Health Organization Global estimates and regional comparisons of the burden of foodborne disease in". PLoS Med. 2015, 12.
3. Scharff, R.L.(2012)."Economic burden from health losses due to foodborne illness in the United States". J. Food Prot: 75:123–131.
4. Guerra M.M.; Almeida A.M, and Willingham A.L.(2016)"An overview of food safety and bacterial foodborne zoonoses in food production animals in the Caribbean region". *Trop.* Anim. Health Prod. 48: 1–1.
5. Sudershan R. V.; Kumar R. N, and Polasa K.;(2012)."Foodborne diseases in India-a review," British Food Journal, 114(5): 661–680.
6. Scallan E.; Hoekstra R.M.; Angulo F.J.; Tauxe R.V.; Widdowson M.A.; Roy S.L.; Jones J.L. and Griffin P.M .( 2011)." Foodborne illness acquired in the United States – major pathogens". Emerg Infect. Dis. 17:7–15.
7. CDC,(2013)."Incidence and trends of infection with pathogens transmitted commonly through food". Foodborne Diseases Active Surveillance Network, 10 U.S. sites, 1996–2012. MMWR 62:283-287.
8. Mead P.S.; Slutsker L. and Dietz V.(1999)."Food-related illness and death in the United States," Emerging Infectious Diseases, 5(5): 607–625.
9. Addis M. and Sisay D.(2015).A Review on Major Food Borne Bacterial Illnesses. *Journal of Tropical Disease*. *3*(4): 1–7.
10. McCollum J.T.; Cronquist A.B. and Silk B.J. (2013)."Multistate outbreak of listeriosis associated with cantaloupe. *N Engl J Med*.;369:944–953.
11. Griffiths M.W.(2003)."Listeria: Properties and Occurrence," In: B. Caballero L. Trugo and P. M. Finglas Eds.; Encyclopedia of Food Science, Food Technology and Nutrition, 2nd Edition, London Academic Press, London,:3562-3573.
12. Al-Zeyara S.A.; Jarvis B. and Mackey B. M.(2010)."The Inhibitory Effect of Natural Micro flora of Food on Growth of Listeria monocytogenes in Enrichment Broths," International Journal of Food Microbiology, 145(1): 98-105.
13. Pesavento G.; Ducci B.; Nieri D.; Comodo N. and Lo-Nostro A.(2009)."Prevalence and Antibiotic Susceptibility of Listeria spp. Isolated from Raw Meat and Retail Foods," Food Control, 21(5):708-713.
14. Byelashov O.A.; Daskalov H.; Geornaras I.; Kendall P.A.; Belk K.E.; Scanga J.A.; Smith G.C. and Sofos J.N.(2010)."Reduction of Listeria monocytogenes on Frankfurters Treated with Lactic Acid Solutions of Various Temperatures," Food Microbiology,. 27(6): 783-790.
15. Shaw J.W; Alex C. and Clarence I.K.(2004)."Detection of PCR amplicons from bacterial pathogens using microsphere agglutination". J Microbiol Methods 56:395–400.
16. Humphrey T.; O'Brien S. and Madsen M.(2007)."Campylobacter as zoonotic pathogens: a food production perspective". International Journal of Food Microbiology. 117 (3): 237–57.
17. WHO.(2010).World Health Organization. World Health Organization Global Estimates and Regional Comparisons of the Burden of Foodborne Disease in 2010.
18. Wabeck C.J.(1972)."Feed and water withdrawal time relationship to processing yield and potential fecal contamination of broilers". Poultry Sci. 51:1119–1121.
19. *FSA(Food Stander Agency),(2011)*."Reducing the risk from E. coli 0157 – controlling cross-contamination". Food Standards Agency, United Kingdom. February 2011. Archived from the original on April 16, 2014. Retrieved 14 August 2016.
20. Nicoline F.T.;Eunice S.; Roland N.N. and Pascal O.B.(2015)."Detection of Pathogenic *Escherichia coli* and *Staphylococcus aureus* from Cattle and Pigs Slaughtered in Abattoirs in Vhembe District, South Africa". Scientific World Journal. 2015; 2015: 195972.
21. Sudershan R. V.; Naveen K.R.; Kashinath L. Bhaskar V. and Polasa K.(2014). "Foodborne Infections and Intoxications in Hyderabad India". Epidemiology Research International Volume 2014, Article ID 942961:5
22. Mor-Mur M. and Yuste J.(2010)."Emerging bacterial pathogens in meat and poultry: An overview". Food Bioprocess Technol. 3: 24-35.
23. Mayada G.; Helmut H.; Lutz G.and Herbert T.(2014)."Occurrence of Enterobacteriaceae in raw meat and in human samples from Egyptian retail sellers". Hindawi Publishing Corporation Volume 2014, Article ID 565671:6

24. Hussein H.S.(2007).“Prevalence and pathogenicity of Shiga toxin producing Escherichia coli in beef cattle and their products”. Journal of Animal Science, 85: E63–E72.
25. Scheutz F.; Teel L. D. and Beutin L.(2012).“Multicenter evaluation of a sequence-based protocol for subtyping Shiga toxins and standardizing Stx nomenclature,” Journal of Clinical Microbiology, 50: 2951–2963.
26. El-Rami F.E.; Elias A.R.; Fawwak T.S. and Alexander M. A.(2012). “Identification of virulence genes among antibacterial-resistance Escherichia coli isolated from poultry,” Advanced Studies in Biology, 4 (8):385–396.
27. Gagliardi J.V. and Karns J.S.(2002)."Persistence of Escherichia coli O157:H7 in soil and on plant roots". Environ. Microbiol. 4:89–96.
28. Hassan Z.; Purwati E.; Radu S.; Rahim RA. and Rusul G.(2001). "Prevalence of Listeria spp and Listeria monocytogenes in meat and fermented fish in Malaysia". Southeast Asian J Trop Med Public Health.,32(2):402-7.
29. Barros M.A.F.; Nero L.A.; Silva L.C., d'Ovidio L.; Monteiro, F.A.; Tamanini, R.; Fagnani R. Hofer E. and Beloti V.(2007)."*Listeria monocytogenes:* Occurrence in Beef and Identification of the Main Contamination Points in Processing Plants".Journal of Meat Science 76: 591-596.
30. Hassan M. and Shole Y.(2013)."Molecular characterization of *Listeria monocytogenes* isolated from fresh seafood samples in Iran". Published online 2013 Sep 13.
31. Lovett J. and Twedt R.(1988)."Listeria Outstanding symposia in food science and technology". Food Technol. 8: 188-191.
32. Rahimi E.; Yazdi F. and Farzinezhadizadeh H.(2012)."Prevalenceand antimicrobial resistance of listeria species isolated from different types of raw meat in Iran". J Food Prot. 75:2223–2227.
33. Lomonaco S.; Patti R.; Knabel S. J.; and Civera T.(2012)."Detection of virulence-associated genes and epidemic clone makers in *Listeria monocytogenes* isolates from PDO Gorgonzola cheese". Int. J. Food Microbiol. 160: 76–79.

**Table 1.The specific primer of *Listeria monocytogenes***

| Primer | | Sequence | Tm (°C) | Product size |
|---|---|---|---|---|
| ***hly A*** | F | CGCAACAAACTGAAGCAAAGGG | 66.7 | 209 bp |
| | R | TTGGCGGCACATTTGTCAC | 68.2 | |

**Table 2. Volume of PCR mixture of L.monocytogenes**

| Components | Concentration |
|---|---|
| Taq PCR PreMix | 5µl |
| Forward primer | 10 picomols/µl |
| Reverse primer | 10 picomols/µl |
| DNA | 1.5µl |
| Distill water | 16.5 µl |
| Final volume | 25µl |

**Table 3. Bacterial species were isolated from meat samples**

| sample | no | Bacterial isolates | | | | | | | | | | | | | |
|---|---|---|---|---|---|---|---|---|---|---|---|---|---|---|---|
| | 100 | *E.coli* | | *E.coli* O157 | | L.m | | *Sal. spp* | | *S.aureus* | | *Camp.spp* | | *Pseud.spp* | |
| Fresh meat | 50 | 23 | 46% | 5 | 10% | 3 | 6% | 5 | 10% | 2 | 4% | 2 | 4% | 1 | 2% |
| Frozen meat | 50 | 29 | 58% | 3 | 6% | 5 | 10% | 7 | 14% | 10 | 20% | 1 | 2% | 1 | 2% |

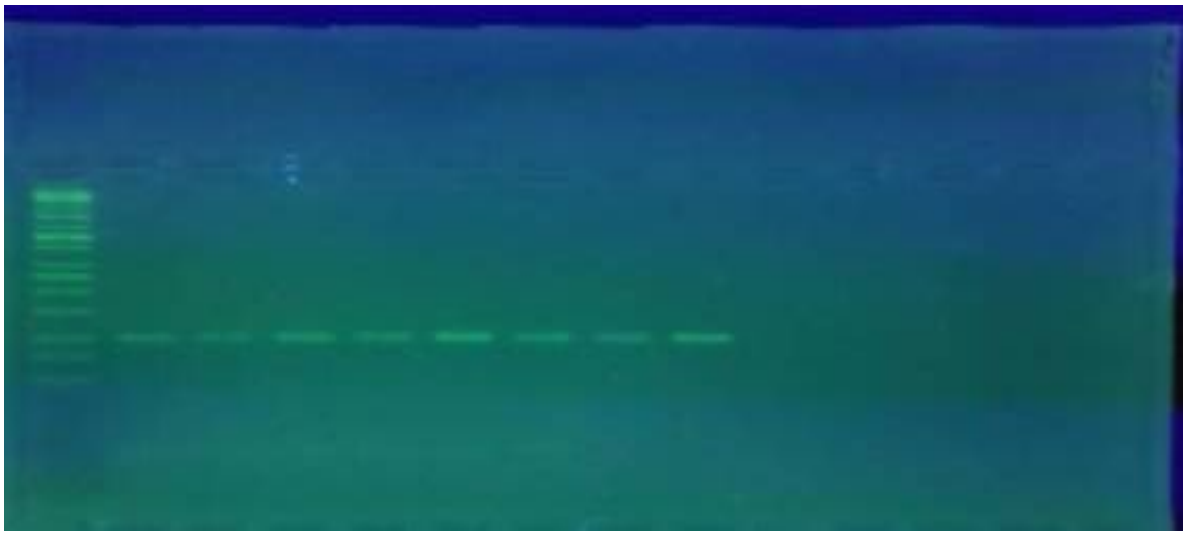

**Figure 1. PCR product the band size 209 bp. The product was electrophoresis on 2% agarose at 5 volt/cm². 1x TBE buffer for 1:30 hours. N: DNA ladder (100).**

*Indian Journal of Natural Sciences* www.tnsroindia.org.in ©IJONS

*Vol. 9 / Issue 50 /October 2018* *International Bimonthly* *ISSN: 0976 – 0997*

RESEARCH ARTICLE

# Assessment of the Irrigation and Drainage Networks in AL-Kufa District Using GIS

Ebtesam F. Khanjer[1*], Nawal K. Ghazal[2], Huda W.Abdulwadud[3] and Ali K. Hussein[4]

[1,2,3]Remote Sensing & GIS Department, College of Science, University of Baghdad, Baghdad, Iraq.
[4]Basic Science Department, College of Dentistry, University of Kufa, Iraq.

Received: 15 July 2018 Revised: 20 Aug 2018 Accepted: 26 Sep 2018

[*]**Address for Correspondence**
**Ebtesam F. Khanjer**
Remote Sensing & GIS Department,
College of Science,
University of Baghdad,
Baghdad, Iraq.



**ABSTRACT**

Applying this work in the province of Najaf, within the alluvial plain that has been chosen in the district of Kufa and its aspects such as AL-Abbassiya sub district, and AL- Huriya sub district which containing the irrigation and drainage networks. The implementation of the work is applied in two stages, the first phase represented as irrigation networks and its facilities, while the second phase as studying drainage networks. This study is carried out to know the problems of irrigation and drainage networks, the amount of water that isleaking from these projects and the impact on the area planted and the effect on the amount of production. Also to checkall regulators and pumps performance and which is idle or needs repairs.

**Key words:** Irrigation networks; Drainage networks;Regulators; Pump stations.

## INTRODUCTION

Iraq is one of the oldest countries in the world which have used irrigation, but it locates in the dry and semi-dry zone, it is due to nature of climatic characteristics, it cannot depend on rains in the construction of the agricultural economy, and secure the production of food and industrial crops. The dry and semi-dry zone have been known the amounts of rainfall are a few, and irregular in distribution and interrupted over some years.this causes drying to some areas, so the Iraqis have adopted since the early on the agriculture irrigated , which is based essentially on the water sources of Tigris Rivers and Euphrates, and streams them [1]. Irrigation and drainage networks are an important element in agricultural development and the important means for soil conservation and conservation, protection it.Thus develop earth element and increase productivity. The productive capacity of agricultural lands are mainly dependent on provision of water that needs its and this necessarily requires irrigation network with high efficiency to ensure for linking of irrigation water at the right time and the quantities required for the cultivated

lands. Drainage network should be the same of statue because it plays a big role in determining the productive capacity of agricultural land, which required being necessarily highly efficient in order to facilitate the disposal of excess water need. As excessive harm thirst and kill plantation, the excess water beats and kills it too; therefore the irrigation and drainage networks are interacting each other [2]. Irrigation can be defined asthe process that supplies soil to water by using methods and manners different.Manners different to reserve level wet suitable to crowofvegetation[3**]**,while the Drainage is defined as prevent excessive soil water pool (either on the soil surface or in the root zone of the plant) to provide continuous movement of water to bottom through the soil [4]. In this studied a GIS version 10.2 has been used to construct attribute table of the irrigation and drainage networks and their installations, which are represented regulators (head, cross and tail) and pumping stations (irrigation and drainage) addition to Geo-referenced and digitized map that collected from water resources directorate in AL-Najaf province.

## MATERIALS AND METHODS

### Material and software used can be listed by the following

**a)** Tables and Map (scale is 1cm=1,750meters)in Excel and JEPG form[6]
**b)** A GIS version 10.2
**c)** Adobe Photoshop version 13.0.1.3 of CC

### Study Area

AL-Najaf province locates in south-west part of Iraq,see Figure (1),which is represented by longitude (42°50'00'' E-45°44'00'' E) and latitude (29°50'00'' N-32°21'00'' N), covering an area of 2820288.47 hectares.It is bounded from the north by provinces of Babel and Karbala, while from east it is bounded by provinces Qadsia and Muthna, from south and south-west, it is bounded by Saudi Arabia kingdom. From west Anbar province. ***AL-Kufa*** district center locates about 8.99 km east of AL-Najaf district center, covering an area of 46447.18hectares [5]

## RESULTS AND DISCUSSION

### The Irrigation Networks Description

Al-Kufadistrict center consist of: Al-Abbassiya sub district and Al-Huriya sub district that depended mainly on the Euphrates River and its branches (Rivers of Al-Kufa and Al-Abbassiya) and streams branched from them. The total cultivated area covered by this project is 104349 donums, with a total irrigated area of 131563 donums, that included network of branch, main, secondary, field drains, and network of main and secondary unlined canals. River of Al-Abbassiya is entered Al-Najaf province, just 8 km from the branching point, where amount a length of main duct within study area 28 km as shown in Figure (2). it penetrates the sub district of Al-Abbassiya and Al-Huriya, controls of the discharge by the Al-Abbassiya head regulator, and it is branched group of branch streamson both sides (left/right ), about 13 branch within sub district of Al-Abbassiya and 7 within sub district of Al-Huriya, where amount of lengths about 177.1 km which are distributed on 113.7 km within sub district of Al-Abbassiya.

These have a total average discharge of about 39 $m^3$/sec with area is benefited of about 57000 donums. Where these branches are located in left side of Al-Abbassiya River, except streams of (AmAhaa and Abo hora) due to state slope ofsurface ;therefore, required made drains network which are doing on clearance of soil and vegetation from water surplus.Table (1) shows summarized of database included of stream name, location, length in km, discharge in $m^3$/sec, irrigated area in dounms, and canal type.

**Distribution of Regulators in the study area can be summarized are the following**

- On Al-Abbassiya River there are about 13 head Regulators to control water levels and discharges in the main streams.About 2 headsRegulators on the Al-Kufa River,*Alsayhee* of station Kufa north regulator for drainage water of the drain Kufa north to the Euphrates River by gravity.
- On Euphrates River there is Almasraf of drain Kufa northern regulator to control water levels and discharges in it, while about 9 headsRegulators on the main streams which are belonging to Al-Abbassiya River to control water levels and discharges in it and in the secondary streams.
- But there are 2 rear Regulator on the main stream,namely*Alhyal* regulator to control water levels and discharges in it and it prevents the passing water towards drain of Alhbaria. Alrakosregulator to control and manage water levels and discharges in it and it prevents the passing water towards drain of Shamia western.
- Alteyal, Alhyal, and Alhusseiny regulators are needed to maintence, which are determined by the balck color circle, that served a total irrigated area of 3972 dounms. While Alhmasi Alfryaa and Nagelregulators have been broken of gates that need to switch ,which are serveda total irrigated area of 4909 dounms, where thecircle in black color as shown in figure (3).
- Totally there are 27 Regulators have been distributed in Al-Kufadistrict center,2 regulators in center,15 regulators in Al-Abbassiya sub district,10 regulators in Al-Huriya sub district as seen in figure (3), and Table (2) showing details of the Regulators.

Al-Kufadistrict center has 10 pump stations, where these pump stations are distributed along of the sedimentary flatin the district center have wiped River by Al-Kufa and Al-Abbasia and branches them.The pump stations have been installed along to stream network in AL-Kufa district center.
The pump stations have been distributed by the following:

- There are 2 drainagepump stations for AL-Kufa district center for pumping water from the drain of Kufa southern and drain of the Kufa north to River of Al-Kufa.
- While there are 6 irrigation pump stations for Al-Abbasia sub district for pumping water from River by Al-Abbasia to Zaidi,Alaryan, Alamaa and Abograb, as illustrating in Figure (4) below.
- But 2 pump stations for Al-Huriya sub district, Tbar algazi irrigation station for pumping water from River of Al-Abbasia to Tbar algazi stream,while Hor Aban Najem drainage station pumps water from drain of 1.3 MD to marsh (Hor Aban Najem).

Table (3) illustrates summarized of database included of site name, location, easting and northing in (m), discharge in($m^3$/sec) a total number of pumps,power (KW), fuel type and head in (m).

## Drainage Network Description

The Plain region of sedimentary is characterized in Najaf province, the existence of a network of drainage main, branch, secondary, and field to discharge excess irrigation water of needed for crop agriculture in this region.Drainage networks have been studied, according to the spatial extension in the study area. The drain of Al-Kufadistrict center (Drains of Al-AbbassiyaRiver) can be summarized as the following:

## Drain of Al-Kufa western (Hafar)

The western drain works to discharge of land, water are located between the Rivers of Al-Kufa and Al-Qadisiya,see figure (5). It has a length of about 28 km with a mean discharge of 20 $m^3$\sec, and itis one of the longest drain in Al-Kufa sub distric, and it extends to the south, it goes of waters by gravity to River of Al-Kufa and assisted it by the decline of the surface.

**Drain Al-Kufa Alsyahee**

This drain stretches in agricultural lands is located on the left side of the Rivers of Al-Kufa. It has a length of 13 km with a mean discharge of about 10 $m^3$/s. It takes (north-south) extension,it benefits of agricultural land cultivated with various field crops in the discharge of excess water from the need, and it drains waterfrom its by gravity toRivers of Al-Kufa.

**Drain of Northern**

This drain extends in the land located at the right Rivers of Al-Kufa. It has a length of 12 km and mean discharge of 15 $m^3$\sec. And the nature of the surface of the region's significant impact on the drainage way of waters as they are by pumps located on the left side of the Rivers of Al-Kufa and then it ends in the Rivers of Al-Kufa. Table (4) illustrates summarized of database included indrain name, location, length in km, a discharge in $m^3$/sec and type.

## CONCLUSION

Outcomes of field investigation during interviews with the staff and the farmers are:

1. All streams unlined within Al-Kufadistrict center, where has caused water losses due to conveyance of water during a seepage process as well as growth of natural plants.
2. The drainage networks have taken directions (northern-southern) and (western-eastern) with slope surface of area. Drainage networks in AL-Kufa district center suffer many problems such as growth of natural plants as well as littering by the people of district.
3. About 18 Regulators are working with good method, served a total irrigated area is 76556 donums, while 3 Regulators need a maintenance that served a total irrigated area of 3972 dounms, but 2 Regulatorshave not employedgates and need to switch, which can servea total irrigated area of 4909 dounms, thus the agricultural production has been affected.
4. All Regulators in the study area are working manually.
5. The ID of (1, 2) for Kufa southern and Kufa northern stations isin need for rehabilitating. While about 8 pump stations are working with a discharge of 4.5 $m^3$\sec.
6. Drains which are located in south and north of Kufa are flowing into the Euphrates River, which negatively affects the quality of water for agricultural and drinking purposes, as well as there are three secondary streams are linked with drains of shamia western and Altoby

## REFERENCES

1. Mohammad Jafar Jawad Al-Samarrai, Modern irrigation and drainage projects in the provinces of Maysan, Dhi Qar and Basra, study of water resources geography, doctoral thesis College of Arts, University of Baghdad, 1999.
2. Hamid Alwan Mohammed Al-Saadi, Irrigation and drainage projects in the province of Diyala, Master Thesis, College of Arts, University of Baghdad, 1986.
3. Al-Asadi. Kfah Salih Bachay, The irrigation and drainage systems in the province of Maysan, Master Thesis, College of Arts, University of Basra, 1989.
4. Jamzoar W., Hankz J. , Jorinacc G.,The new all soils irrigated, translation Mahdi Ibrahim Odeh, Basra University Press, 1987, p. 272.
5. Agriculture directorate in AL- Najaf province.
6. Water resources directorate in AL- Najaf province

**Table 1. Attribute Table of Stream network in Al-Kufadistrict center[6].**

| Id | Stream name | Location | Length km | Dischar e $m^3$\s | Irrigated area\donum | Canal type |
|---|---|---|---|---|---|---|
| 1 | Tobar saed jowad | Al-Abbassiya sub district | 13 | 0 | 0 | unlined \main |
| 2 | River of abo hora | Al-Abbassiya sub district | 10 | 5 | 5000 | unlined \main |
| 3 | River of aladl | Al-Abbassiya sub district | 4 | 0.13 | 1000 | unlined \secondary |
| 4 | River of alhdari | Al-Abbassiya sub district | 12 | 7 | 12000 | unlined \main |
| 5 | Albdear | Al-Abbassiya sub district | 3 | 0 | 500 | unlined \secondary |
| 6 | Aleasa alawal | Al-Abbassiya sub district | 3 | 0 | 500 | unlined \secondary |
| 7 | Alfahee southern | Al-Abbassiya sub district | 1 | 0 | 1000 | unlined \secondary |
| 8 | Alafate | Al-Abbassiya sub district | 3 | 0 | 280 | unlined \secondary |
| 9 | River of Wahhabi | Al-Abbassiya sub district | 13 | 6 | 10000 | unlined \main |
| 10 | River of abograb | Al-Abbassiya sub district | 13 | 6 | 12000 | unlined \main |
| 11 | River of alaryan | Al-Abbassiya sub district | 13 | 0 | 5000 | unlined \main |
| 12 | River of alamaa | Al-Abbassiya sub district | 8 | 6 | 5000 | unlined \main |
| 13 | Almhana | Al-Huriya sub district | 3 | 0 | 354 | unlined \secondary |
| 14 | River of algazali | Al-Huriya sub district | 13 | 0 | 2100 | unlined \secondary |
| 15 | Tobar almoafat | Al-Huriya sub district | 2 | 0 | 282 | unlined \secondary |
| 16 | ALzyadi | Al-Huriya sub district | 2 | 0 | 2242 | unlined \main |
| 17 | Alteyal | Al-Huriya sub district | 6 | 1 | 1451 | unlined \secondary |
| 18 | River of bazel | Al-Huriya sub district | 4 | 1 | 650 | unlined \secondary |
| 19 | Tbar algazi | Al-Huriya sub district | 5 | 0 | 918 | unlined \secondary |
| 20 | Alhmasi alryesy | Al-Huriya sub district | 15 | 0 | 0 | unlined \secondary |
| 21 | Abo hlan | Al-Huriya sub district | 3 | 4 | 3420 | unlined \secondary |
| 22 | Tbar alsabaa | Al-Huriya sub district | 1 | 1 | 440 | unlined \secondary |
| 23 | Alhmasi alfryaa | Al-Huriya sub district | 14 | 0 | 5462 | unlined \secondary |

**Table 2. Details of Regulators inAL-Kufa distinct center [6].**

| ID | Regulator name | No. of gates | Easing /m | Northing /m | Discharg e $m^3/s$ | Location | Irrigate d area donum | State of Regulator | Structur e Name |
|---|---|---|---|---|---|---|---|---|---|
| 1 | Tobar gaze | 1 | 451846 | 3548658 | 2.5 | Al-Huriya | 585 | | Head |
| 2 | Alzadi | 3 | 450655 | 3548713 | 6 | Al-Huriya | 5000 | | Head |
| 3 | Alhmasi alryesy | 3 | 452217 | 3548818 | 6 | Al-Huriya | 1515 | | Head |
| 4 | Alhmasi alfryaa | 3 | 455896 | 3549002 | 6 | Al-Huriya | 4077 | Unemploye d of gates | Head |
| 5 | Alsabaa | 1 | 457374 | 3550551 | 1 | Al-Huriya | 363 | | Head |
| 6 | Alteyal | 2 | 456338 | 3552134 | 2 | Al-Huriya | 1867 | Need to be buried and cladding | Head |
| 7 | Nagel | 1 | 452751 | 3552329 | 1 | Al-Huriya | 832 | Unemploye d of gates | Head |
| 8 | Alhyal | 1 | 452834 | 3552439 | 1 | Al-Huriya | 83 | Need to be buried and | Rear |

| | | | | | | | | | |
|---|---|---|---|---|---|---|---|---|---|
| | | | | | | | | cladding | |
| 9 | Alhusseiny | 1 | 452828 | 3552451 | 1 | Al-Huriya | 2022 | Need to be buried and cladding | Head |
| 10 | Abo shahh shahad | 1 | 449260 | 3545550 | 2 | Al-Abbassiya | 1001 | | Head |
| 11 | Abo naman | 1 | 449192 | 3545729 | 2 | Al-Abbassiya | 1001 | | Head |
| 12 | Abo horha | 2 | 449623 | 3547768 | 5 | Al-Abbassiya | 8000 | | Head |
| 13 | Am hyayaa | 4 | 449287 | 3547807 | 6 | Al-Abbassiya | 9000 | | Head |
| 14 | Alamah | 2 | 447019 | 3551155 | 6 | Al-Abbassiya | 12000 | | Head |
| 15 | Alarway | 1 | 444708 | 3553331 | 4 | Al-Abbassiya | 5000 | | Head |
| 16 | Abo Gharb | 2 | 444414 | 3553962 | 6 | Al-Abbassiya | 10000 | | Head |
| 17 | Wahhabi | 2 | 442194 | 3554886 | 6 | Al-Abbassiya | 10000 | | Head |
| 18 | MC1 alyerway | 2 | 441090 | 3555706 | 30 | Al-Abbassiya | | | Head |
| 19 | Alhadary | 3 | 441309 | 3556742 | 3 | Al-Abbassiya | 10000 | | Head |
| 20 | Al adel | 1 | 441616 | 3556842 | 1 | Al-Abbassiya | 1000 | | Head |
| 21 | drain kufa north | | 442555 | 3545946 | | Al-Kufa | | | Head |
| 22 | kufa north | | 442576 | 3547140 | | Al-Kufa | | | Head |
| 23 | Alrakos | 2 | 451625 | 3540384 | 2 | Al-Abbassiya | 401 | | Rear |
| 24 | AL-qzaly | 1 | 455368 | 3552007 | 1 | Al-Abbassiya | 400 | | Head |
| 25 | Altraa | 1 | 459434 | 3550831 | 4 | Al-Huriya | 453 | | Head |
| 26 | Alkazmi | 2 | 444407 | 3551687 | 1 | Al-Abbassiya | 1200 | | Head |
| 27 | Am hyayaa | 4 | 449640 | 3547750 | 6 | Al-Abbassiya | 9000 | | Head |

**Table 3.Details of Attribute Table of Pump stations in AL-Kufa district center[6].**

| ID | Site Name | Location | Easting /m | Northing /m | Total Number of Pumps | Discharge of each Pump | Power (KW) | Fuel type | Head ( m) |
|---|---|---|---|---|---|---|---|---|---|
| 1 | Kufa southern | Al-Kufa | 448384 | 3538469 | 2 | 1m³\s+1/2m³/s | 2*90 | Electric | 13m |
| 2 | Kufa Northern | Al-Kufa | 442534 | 3547133 | 2+1 | 2*1m³/s+1*3/4m³/s | 2*112+170 | 3 Electric | 13m |
| 3 | Abo Gharb | Al-Abbassiya | 444663 | 3553221 | 2 | 1/2m³/s | 224 | Diesel | 13m |
| 4 | Wahhabi | Al-Abbassiya | 444412 | 3553925 | 2 | 1/2m³/s | 332 | Diesel | 13m |
| 5 | Hor aban najem | Al-Huriya | 459414 | 3559565 | 6 | 1/2m³/s | 110 | Diesel | 13m |
| 6 | Tobar al Gazee | Al-Huriya | 451825 | 3548596 | 1 | 1m³/s | 402 | Diesel | 13m |
| 7 | Zaidi | Al-Abbassiya | 450575 | 3548684 | 2 | 1/2m³/s | 402 | Diesel | 13m |
| 8 | Kazmi | Al-Abbassiya | 449402 | 3551607 | 7 | 1/2m³/s | 332 | Diesel | 13m |
| 9 | Alerian | Al-Abbassiya | 446651 | 3551866 | 1 | 1/2m³/s | 224 | Diesel | 13m |
| 10 | Cambary | Al-Abbassiya | 448298 | 3549226 | 1 | 1/2m³/s | 332 | Diesel | 13m |

**Table 4. Attribute Table of Drainage network in AL-Kufa district center[6].**

| Id | Drains name | Location | Length\km | Discharge m3\sec | Type |
|---|---|---|---|---|---|
| 1 | Drain of kufa northern | Al-Kufa district center | 12 | 15 | main drain |
| 2 | Drain of Kufa southern | Al-Kufa district center | 8 | 15 | main drain |
| 3 | Drain of shamia western | Al-Kufa district center | 28 | 20 | main drain |
| 4 | Drain of Kufa alsyahee | Al-Kufa district center | 13 | 10 | main drain |
| 5 | Drain of Jopan | Al-Abbassiya sub district | 28 | 3 | main drain |
| 6 | MS second | Al-Abbassiya sub district | 0 | 0 | |
| 7 | Drain of Euphrates east | Al-Abbassiya sub district | 15 | 3 | main drain |
| 8 | 1.3 MD | Al-Abbassiya sub district | - | - | - |
| 9 | Drain of Alqadeer | Al-Abbassiya sub district | 4 | 0 | Field drain |
| 10 | Alabyat | Al-Abbassiya sub district | 12 | 3 | main drain |

| | | | | | |
|---|---|---|---|---|---|
| 11 | Drain of Ashoka | Al-Abbassiya sub district | 3 | 1 | branch drain |
| 12 | Drain of Abo fywos | Al-Abbassiya sub district | 10 | 3 | main drain |
| 13 | Drain of Alaryan-Abo karab | Al-Abbassiya sub district | 10 | 3 | main drain |
| 14 | Drain of Amohii | Al-Abbassiya sub district | 10 | 3 | main drain |
| 15 | Drain of AM alyatia | Al-Huriya sub district | 2.5 | 0 | branch drain |
| 16 | Drain of Alhbaria | Al-Huriya sub district | 14 | 4 | branch drain |
| 17 | Drain of Alqzali and Alteel | Al-Huriya sub district | 6 | 2 | branch drain |
| 18 | Drain of Banihussain | Al-Huriya sub district | 12 | 5 | branch drain |
| 19 | Drain of Alkaze | Al-Huriya sub district | 3.5 | 0 | branch drain |
| 20 | Drain of Alhussieny | Al-Huriya sub district | 2.5 | 0 | branch drain |
| 21` | Drain of Alfra and Abo Halan | Al-Huriya sub district | 2 | 0 | branch drain |
| 22 | Drain of Alrapt | Al-Huriya sub district | 10 | 6 | branch drain |
| 23 | Drain of Altoby | Al-Abbassiya sub district | 2.2 | 0 | branch drain |
| 24 | Drain of Snayee | Al-Huriya sub district | 5 | 0 | branch drain |

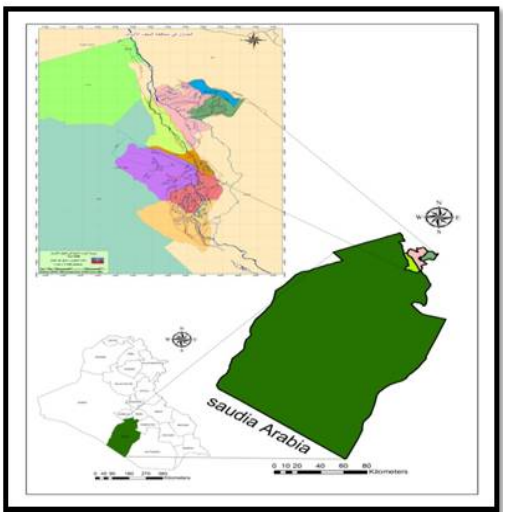


**Fig. 1. AL-Najaf province is located in the part of southern-western of Iraq**

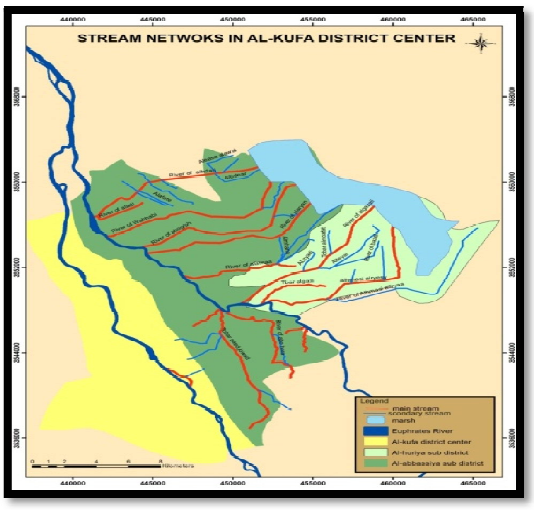


**Fig. 2. Stream networks in AL-Kufa district center.**

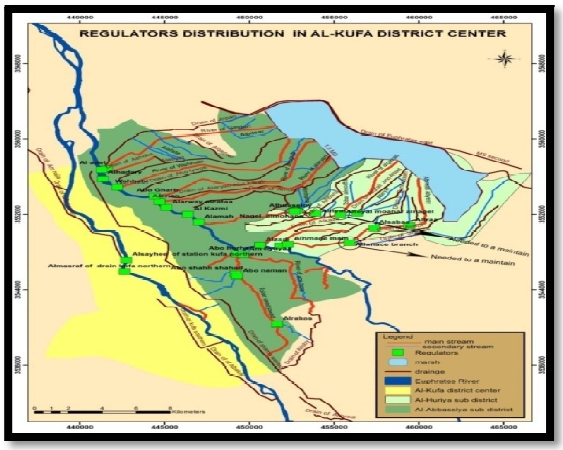


**Fig. 3. Geographic distribution of Regulator in AL-Kufa district center.**

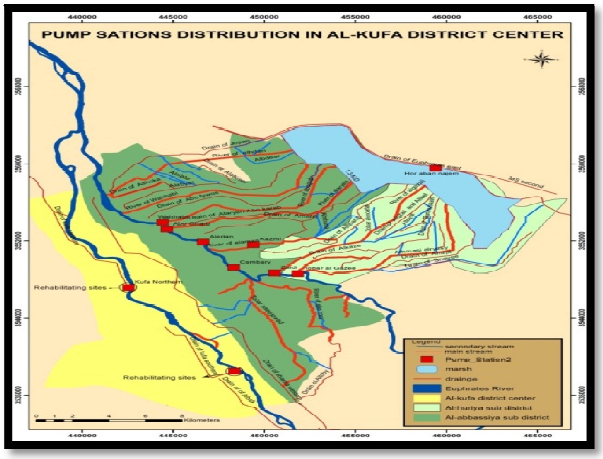


**Fig. 4. Pump station distribution in AL-Kufa district center.**


**Fig. 5. The Geographical extension of the drainage network in AL-kufa district center.**

*Indian Journal of Natural Sciences* www.tnsroindia.org.in ©IJONS

*Vol. 9 / Issue 50 /October 2018* *International Bimonthly* *ISSN: 0976 – 0997*

RESEARCH ARTICLE

# Genetic Study of Freezing Holstein Bull Semen at Different Seasons

Mohammad Yousif Mahmood* and Saad Akram Hatif

Department of Surgery and Obstetrics, College of Veterinary Medicine, University of Baghdad, Iraq

Received: 10 July 2018 Revised: 15 Aug 2018 Accepted: 17 Sep 2018

***Address for Correspondence**
**Mohammad Yousif Mahmood**
Department of Surgery and Obstetrics,
College of Veterinary Medicine,
University of Baghdad, Iraq



## ABSTRACT

The semen of 75 Holstein bulls samples were collected during different seasons, included 25 samples in warm season, 25 samples in cold season and, 25 samples in hot season .Samples were subjected to theflorescent microscopicalexamination to investigate the DNA fragmentation and light microscope examination to evaluate dead and live sperms.DNA was extractedin order to investigate theosteopontin (OPN) gene polymorphism. The results revealed that the fragmentation of DNA were13.00 ± 0.73,11.96 ± 0.5,and 14.00 ± 0.59 in the warm , cold ,and hot season respectively. The corresponding means of the viability of sperms were23.16 ± 1.66 , 23.4 ± 1.47,and23.96 ± 1.07.The result of OPN gene sequencing revealed5 genotype mutationsin the bulls (rs109637038, rs110254070, rs110329232, rs109659827, and rs380649619)which represented the genotyping and polymorphism in bulls. In conclusion the polymorphisms in the OPN genehave no significant effect on DNA fragmentation, dead and live of sperms in the semen freezing trough the different season.

**Keywords:** Bullsemen, DNA Fragmentation, OPN gene, Season.

## INTRODUCTION

Artificial insemination (AI) is a process by which sperm are collected from the male, processed stored and artificially introduced into the female reproductive tract for the purpose of conception (1). Deoxyribonucleic acid (DNA) is a nucleic acid that contains the genetic instructions for the development and function of living organisms.The DNA segments that carry genetic information are called genes, but other DNA sequences have structural purposes, or are involved in regulating the expression of genetic information (2).It could cause various physical and chemical damages to sperm membrane, outbreak to ROS, oxidative damage to membrane phospholipids and DNA (3)Osteopontin (OPN) is a ubiquitous, acidic glycoprotein with multi-function that has been found in higher concentrations in ejaculates of bulls that produce higher conception rates(4).

Osteopontin has also been shown to facilitate capacitation and viability of bovine sperm (5). Ejaculated sperm carries the bound OPN protein to the site of fertilization (6).Where it is thought to play a role in the sperm-egg interaction through OPN—integrin complexes present on the surface of the sperm and oocyte (7).

## MATERIALS AND METHODS

This study was carried out at the Artificial Insemination Center of Abou-Gharib West of Baghdad. The semen samples oftwenty five Holstein bulls (born in Iraqi) were routinely collected from all bulls weekly with the aid of an artificial vagina.All bulls have the same age 3-4 years. Semen samples were obtained from each test bull via straws and placed in ice for transport to the lab.Sperms DNA fragmentations were examined by using acridine orange stain (8-9).Alive and dead sperms had been assessed by using Eosin –Nigrosin stain and examined under light microscope Genomic DNA was extracted using a Relia prep blood g DNA mini prep system Kit No.A5081 ; Promega, USA , followed by PCR Amplification of OPN gene.The OPN gene was amplified using the universal primer, OPN4816F: 5'-TCC CTC CCT CTA CGT TTT CA-3' and OPN5528R: 5'-CAT CCC AAA AGG GCA TAG AA-3'. amplified the region between bp 4816 and 5528 of the OPN gene promoter region that also had reported polymorphisms(10). Sequences analyzer was used by Macro .gen in Korea. After that identify differences in genetic sequences among bulls .The Statistical Analysis was performed using SAS program (11). Least significant difference test was used to assess the difference amongparameters. $P<0.05$ is considered significant.

## RESULTS

OPN gene at 748bp separated on 1.5% agarose gels appearing as a stained single band represented the semen samples of bulls in A.I center in Iraq. Sequencing of OPN gene appeared five mutations in the sperms in deferent parameters obtained from Gene Bank. Subject represent of database of National Center Biotechnology Information (NCBI).PCR product of (OPN) gene, followed by sequencing appears 5 mutation types with numbers rs109637038, rs110254070, rs110329232, rs109659827 and rs380649619 at the samples of bulls in AI center in Iraq. Types of mutations distributed in the samples of semen, thirteen samples give mutation and 12 samples without mutation (Table 1). The results revealed 13.00 ± 0.73, 11.96 ± 0.5, and 14.00 ± 0.59 fragmentation of DNA in the warm , cold ,and hot respectively(Table 2).DNA fragmentsperms showed orange color while, the normal sperms gives green color under florescent microscope (Figure 2).Non-Significantdifferences were found between normal and sperms fragmented DNAthrough freezing storage.Eosin and nigrosin stained of sperms for dead and live investigation revealed 23.16 ± 1.66 in warm season, 23.4 ± 1.47 in cold season and 23.96 ± 1.47 in hot season (Table 3).Dead sperm take the pink color,alive spermsstill white in color(Figure 3 ).Non-Significant differenceswere found between seasons in different genotypes.

## DISCUSSION

The present study was concentrated on the effect of OPN genepolymorphism in Holstein bull, in sperm DNA fragmentation, and dead and live through freezing semen.We found no significant differences between semen samples in different seasons.The identification and genotyping of polymorphisms within the promoter region of bovine OPN gene may be useful for selecting bulls to improve sperm motility (12, 13). Due to extreme heat stress, bulls get physically exhausted and their reduced eagerness might result in higher reaction time and subsequently total time for successful ejaculation also increase, thus having an ultimate effect on production of sperms ( 14)**.** When freezing storage Initial motility and sperm concentration per-ejaculate were affected by age, season but freezing characteristics were due to individual variation (15).The fertilization rates are directly dependent upon both sperm progressive motility and DNA fragmentation (16). DNA integrity has been considered as an important parameter in the determination of spermatozoa ability to with stand the cryopreservation process, it is suggested that chromatin structure should be studied as an independent complementary parameter for the better assessment of the sperm

quality (17). Storage conditions and the cold shock caused by freezing and thawing, cold shock increases the susceptibility of semen to oxidative damage due to an increase ROS production, ROS have been shown to change cellular functions through the disruption of the sperm plasma membrane and damage to proteins and DNA (18, 19). The non-significant differences due to season in all bulls may be due to discard the low fertile bull and kept the good quality one in the center of A.I. Andrabiet al., (20) showed significant differences in spermtraits from one month to another due changes in photoperiod.In conclusion the polymorphisms in the OPN gene have no significant effect on DNA fragmentation, dead and live of sperms in the semen freezing trough the different season.

## REFERENCES

1. Januškauskas, A. and Žilinskas, H. (2002). Bull semen evaluation post-thaw and relation of semen characteristics to bull's fertility. Veterinarija ir Zootechnika, 17(39): 1-8
2. Peris, S.I.; Morrier, A.; Dufour, M. and Bailey, J.L. (2004). Cryopreservation of ram semen facilitates sperm DNA damage: Relationship between sperm andrological parameters and the sperm chromatin structure assay. Journal of Andrology., 25 (2): 224-233.
3. Meyers, S.A. (2005). Spermatozoal response to osmotic stress. Animal Reproduction Science, 89(1): 57-64.
4. Killian, G.J., Chapman, D.A. and Rogowski, L.A. (1993) Fertility-Associated Proteins in Holstein Bull Seminal Plasma. Biology of Reproduction, 49, 1202-1207.
5. Erikson, D.W., Way, A.L., Bertolla, R.P., Chapman, D.A. and Killian, G.J. (2007) Influence of Osteopontin, Casein and Oviductal Fluid on Bovine Sperm Capacitation. Animal Reproduction, 4, 103-112.
6. Souza, C.E.A., Moura, A.A., Monaco, E. and Killian, G.J. (2008). Binding patterns of bovine seminal plasma proteins A1/A2, 30kDa and osteopontin on ejaculated sperm before and after incubation with isthmic ampullary oviductal fluid. Animal Reproduction Science, 105, 72-89.
7. Gabler, C., Chapman, D.A. and Killian, G.J. (2003). Expression and Presence of Osteopontin and Integrins in the Bovine Oviduct during the Estrous Cycle. Reproduction, 126, 721-729.
8. Tejada, R.I.; Mitchell, J.C.; Norman, A.; Marik, J.J. and Friedman, S. (1984). A test for the practical evaluation of male fertility by acridine orange (AO) fluorescence. Fertility and Sterility, 42(1): 87-91.
9. Martins, C.F.; Dode, M.N.; Báo, S.N. and Rumpf, R. (2007). The use of the acridine orange test and the TUNEL assay to assess the integrity of freeze-dried bovine spermatozoa DNA. Genetics and Molecular Research, 6(1): 94-104.
10. Schnabel, R.D., Kim, J.J., Ashwell, M.S., Sonstegard, T.S., Van Tassell, C.P., Connor, E.E. and Taylor, J.F. (2005). Fine-mapping milk production quantitative trait loci on BTA6: Analysis of the bovine osteopontin gene. Proceedings of the National Academy of Sciences of the United States of America, 102, 6896-6901.
11. SAS. 2012. Statistical Analysis System, User's Guide. Statistical. Version 9.1th ed SAS. Inst. Inc. Cary. N.C. USA.
12. Abdolreza Salehi, Nasiri K, Aminafshar M, Sayaadnejad MB, and Sobhani R. (2015). The Association of bovine osteopontin (OPN) gene with milk production traits in Iranian Holstein bulls. Iran Journal of Biotechnology. 13(1): 43–48.
13. Rick, W .R ;Chance, L. W. and Lester TD. (2016). Association of osteopontin gene promoter single nucleotide polymorphisms with bull semen quality .Advances in Reproductive Sciences ,4,1-7.
14. Bhakat, M; Mohanty, T.K; Gupta, A.K. and Raina, V.S. (2009). Effect of season and management on semen quality of breeding bulls- a review. Agricultural Reviews. 30(2): 79-93.
15. Bhakat, M.; Mohanty, T.K.; Raina, V.S.; Gupta, A.K.; Khan, H.M.; Mahapatra, R.K. and Sarkar, M. (2011). Effect of age and season on semen quality parameters in Sahiwal bulls. Tropical Animal Health and Production, 43(6): 1161-1168.
16. Simon, L. and Lewis, S.E. (2011). Sperm DNA damage or progressive motility: which one is the better predictor of fertilization in vitro? Systems Biology in Reproductive Medicine, 57(3): 133-138.

17. Evenson, D.P.; Larson, K.L. and Jost, L.K. (2002). Sperm chromatin structure assay: its clinical use for detecting sperm DNA fragmentation in male infertility and comparisons with other techniques. Journal of Andrology, 23(1): 25-43.
18. Agarwal, A. and Said, T.M. (2003). Role of sperm chromatin abnormalities and DNA damage in male infertility. Human Reproduction Update, 9(4): 331-345.
19. Martorana, K.; Klooster, K. and Meyers, S. (2014). Suprazero cooling rate, rather than freezing rate, determines post thaw quality of rhesus macaque sperm. Theriogenology, 81(3): 381-388.
20. Andrabi, S.M.H.; Naheed, S.; Khan, L.A. and Ullah, N. (2002). Semen characteristics of crossbred (friesian x sahiwal) bulls at livestock research statlon, national agricul tural research centre, islamabad. Pakistan Veterinary Journal.22(4):181-187.

**Table 1.Distribution of types mutation in the samples**

| Sample number | Mutation number |
|---|---|
| 1,2,3,13,15,16,17,18 | (rs 109659827) |
| 8 | rs 109637038,rs 110254670,rs 110329232,rs 380649619 |
| 14,19,20 | rs 110329232, rs 109659827,rs 380649619 |
| 21 | rs 110329232,rs 380649619 |
| 4,5,6,7,9,10,11,12, 22,23,24,25 | 0 |

**Table 2. Effect of season on the normal and abnormal (Sperm DNA fragment)**

| Season | No | Normal DNA (Green) | Abnormal DNA (Orange) |
|---|---|---|---|
| Season 1 (warm) (10,11, month) | 25 | 87.00 ± 1.35 a | 13.00 ± 0.73 a |
| Season 2 (cold) (12,1,2 month) | 25 | 88.04 ± 1.09 a | 11.96 ± 0.55 a |
| Season 3 (hot) (3,4,5, month) | 25 | 86.00 ± 1.15 a | 14.00 ± 0.59 a |
| Level of sig. | --- | NS | NS |
| NS: Non-Significant. | | | |

**Table 3: Effect of the season on live and dead sperms**

| Season | No | Live (%) | Dead (%) |
|---|---|---|---|
| Season 1 (warm) (10,11, month) | 25 | 76.84 ± 3.92 a | 23.16 ± 1.66 a |
| Season 2 (cold) (12,1,2 month) | 25 | 76.6 ± 3.58 a | 23.4 ± 1.47 a |
| Season 3 (hot) (3,4,5, month) | 25 | 76.04 ± 2.52 a | 23.96 ± 1.07 a |
| Level of sig. | --- | NS | NS |
| NS: Non-Significant. | | | |

**Figure 1.Normal DNA of sperm (green color)stained by cridine Orange .**

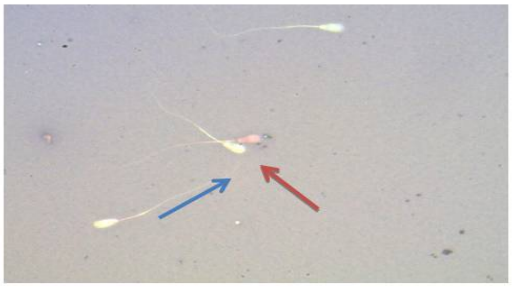

**Figure 2. Dead sperm (pink color) and a live sperm(white color) stained by Eosin – igrosin.**

*Indian Journal of Natural Sciences* www.tnsroindia.org.in ©IJONS

*Vol. 9 / Issue 50 /October 2018* *International Bimonthly* *ISSN: 0976 – 0997*

RESEARCH ARTICLE

# Treatment of Antibiotics, Resistant *Candida albicans* Using Cold Atmospheric Plasma Jet

Thikra K. Al-Kafiji* and Hammad R. Humud

Department of Physics, College of Science, University of Baghdad, Baghdad, Iraq

Received: 08 July 2018 Revised: 13 Aug 2018 Accepted: 12 Sep 2018

***Address for Correspondence**
**Thikra K. Al-Kafiji**
Department of Physics,
College of Science,
University of Baghdad,
Baghdad, Iraq.



**ABSTRACT**

Infection with antibiotics_ resistant Candida albicans has become world-wide concern and an effective treatment is urgently needed. Nonthermal atmospheric pressure plasma jet (APPJ) provides a very reactive chemistry, without thermal damage to heat-sensitive biological systems such as living cells and tissues. In this study, antimicrobial efficiency of plasma jet was investigated against the growth rate of Candida albicans using a simple device of plasma jet operating with pure Ar as working gas. The device was driven by an ac power supply operated at 7.5kV peak to peak, with frequency of 28 kHz. The effect of the plasma jet on the Candida albicans was studied using solid and liquid medium. The result showed the plasam jet significantly inactivated Candida albicans growth whereby more than 60% of Candida albicans was inactivated after only 2 min treatment with plasma jet. This study shows a simple and effective method of treatment against antibiotic-resistant Candida albican that can be consider as a platform for future clinical trials.

**Keywords:** Plasma jets**,** Candida albicans, Antibiotic- resistant, Growth rate, Cold plasma.

## INTRODUCTION

Candida Albicans is most common fungal pathogen presents in the oral cavity, and is best known for causing thrush in the mouths of babies, sore white and moist plaques in the mouth, on the tongue and the upper respiratory tract, as well as in some parts of gastrointestinal, and genital tracts of the human body. In addition, this fungus causes many types of diseases such as dermatocandidiasis that may cause morbidity and mortality of immunocompromised patients [1]. Recently, the development of antibiotic resistant pathogens has become a world concern, for instance Candida albicans has become resistant to antifungal drugs such as fluconazole and most of azole [2]. Thus, the

current treatment by available antifungal drugs like fluconazole or azoles derivatives has become unsuccessful [3]. For this reason, new antifungal therapies is of utmost importance for effective treatment of Candida albicans infection. Recently, has an impact on developing antimicrobial treatments is using the cold plasma. Atmospheric pressure plasmas system is cost-effective and convenient alternative to low-pressure plasma systems because the vacuum systems is not equired [4]. Physically, plasma is characterized as a matter with ionized state and equal number of negatively and positively charged particles (quasi-neutral). It consists of free radicals, electrons, ions, UV-radiation, and excited neutral and charged species independent of the gases used [5].

Plasmas are frequently subdivided into thermal and non-thermal Plasma. When the temperature of the electrons is similar to the temperature of ions, the plasmas are called thermal plasma. However, if the electrons have higher temperature than the ions, plasmas are known as a non-thermal plasma [6, 7]. Based on the operation systems, the produced plasma jet can increased to a number of centimeters into the surrounding ambient. Plasma jets show relatively less operational cost. When Plasma jets launched into the air high amount of reactive species are generated under ambient conditions. Plasma plume generates into the close environment and reacts with air molecules producing reactive oxygen and nitrogen species (RONS), such as atomic oxygen, ozone, superoxide, hydroxyl radicals, peroxide, nitrogen dioxide and nitric oxide, [8]. Generating excessive RONS may bring attention to using plasma jet for novel application such as antifungal treatments. One of the promising applications is the inactivation of microorganism Candida species [9]. These RONS react with cellular molecules, such as DNA and proteins, leading to inhibition of cell growth rates. Besides, plasma jet is safe and has no thermal damage to the living cells and tissues [4]. Application treatment using plasma medicine becomes a more and more important in research field. Therefore, further studies is needed to control plasma parameters to get reliable plasma sources for the different therapeutic application [10].

## Experimental Setup and Procedures 2- 1 Plasma torch

In this work type of plasma jet torch were constracted as shown in figure (1).The plasma jet torch has linear-field configuration, This figure shows a photograph at working of the non-thermal atmospheric pressure plasma torch. And the plasma jet length of flow 3 L/min is 3.5cm. It consists of teflon pipe with an inner diameter of ( 4.5mm ) and outer diameter(6.5mm ) and Aluminum foil, (10mm) width, is placed around the Teflon pipe, (10mm) away from its end. The Aluminum foil is connected to high voltage power supply, device operating with pure Ar as working gas. The device was driven by an ac power supply operated at the ends of the secondary coil is 7.5kV peak to peak, with frequency of 28 kHz .

## Fungi Preparation

Candida albicans isolate were obtained from Central Teaching laboratories in the City of Medicine, Teaching Hospital, Baghdad. The culture of Candida albicans were prepared under the following conditions: Firts, the fungi were cultured in the Sabouraud Dextrose Agar Medium that was prepared according to manufacture protocol., In brief, the amount of 65 g agar (15 g agar, 10 g peptone, 40 g dextrose) was dissolved in 1L distilled water. The medim PH was adjusted to 6.8 and autoclaved. The medium was cooled down to 45- 50ºC, casted in sterile Petri dishes and left for 24 h at 37 °C to solidify. The viable colonies were selected for the treatment and diluted with sterile physiological saline to produce equal to ($1* 10^6$ to $5* 10^6$ cell/ml) suspension (inoculum) were made as determined by 0.5 McFarland standard and spectrophotometric assays. and then kept stored in refrigerator at 4°C and used as needed.

### Sample Treatment by Plasma jet in the solid medium

The fungi suspensions prepared and medium plates containing Muller Hinton Agar inoculated of Candida albicans was examined using disk diffusion method (NCCLS document M44-A)[11]. The Candida albicans were taken from fresh stock cultures (24 hours) by the loop, suspended in normal saline, and adjusted using standard 0.5 McFarland turbidity ($5x10^6$ cell $ml^{-1}$) tubes, The fungus was absorbed on the surface of cotton swab by dipping into the suspension. The sterile cotton swab was streaked on the surface of the sold medium of Muller Hinton Agar. Fungus was treated with plasma at argon gas at a flow rate of 3 L/min, plasma plume was directed perpendicularly to the surfaces of agar plate.The distance between the plume and the surfaces of sold medium was 0.75mm, as shown in figure (2). The fungi sample was exposed to plasma jet for different time intervals (0.5, 1, 2, 3.5, 5 and 8 min). After the treatment, all plates were incubated for 24 h at 35 °C. For control experiments, samples were exposed to argon flow at the same flow rate without plasma ignition. After plasma exposure of Candida albicans for different time points, the plates were then incubated at 35 °C for the 24 hrs. . Plates containing Muller Hinton Agar with fungi cultures (untreated) were used as a control and each experiment was performed in triplicate. The diameter of the inhibition zone was precisely measured to calculate the antifungal activity of the test samples. The clear zone was considered as the zone of inhibition of microbial growth. The diameter of inhibition zones was measured using a meter ruler and the average value for each organism was recorded

### Sample treatment by plasma jet using liquid medium

The fungi suspensions had been also prepared in the same way as previously mentioned in paragraph (2-3). For inhibition rate investigation of the fungi samples, the influence of miniature plasma argon source efficiency was tested for different exposure times (0.5,1,2,3.5,5 and 8min).So using a (4.5 mL) Sabouraud Dextrose Broth was inoculated with fungal strain of ( 500 μL), standards (NCCLS document M27-A2) [12]. In the next stage, laboratory tube was placed in the incubator shaker platform (75 rpm). for 24 hours in 35 ºC. Cell viability was measured by the number of fungi cell in one ml of broth medium,and plotted in cell viability curve. It also was calculated by microscope counting using the heamocytometer method, based on these counts, the number of yeast per ml was calculated by the equation (2-1)

NO. of cell /ml = No. of cell in four squares × 4× 10 × 1000 × inverse of dilution if used ……2-1 [13].

## RESULTS AND DISCUSSION

### Antifungal activity of plasma jet in the liquid medium

Fungi deactivation by plasma jet was tested against the pathogen fungi Candida albicans. Microscopic examination was used to measure the growth rate of Candida albicans in the liquid medium (Sabouraud Dextrose Broth ) and solid medium (Muller Hinton agar). Figure (3) shows the microscopic measurements of the pathogen fungi Candida albicans growth in the liquid medium, that explain the antifungal activity of the plasma jet for six different time points ( 0.5, 1, 2, 3.5, 5 and 8 min). The figure illustrates the cell viability was calculated from equation (2-1), and shows the growth inhibition increased compared with the control, suggesting the cell viability decreased with increasing of the exposure time for all samples. A fast inactivation was observed for pathogen in the first 30 sec.

More than 60% of Candida albicans was inactivated after 2 min of applying the plasma jet. That result exhibits the maximum effect occurred after 8 min. Mean and standard deviation of the reduction in the growth rate of Candidia albicans in the suspension media after exposing to the plasma jet at different time points were shown in table (1). The results indicated there was high significant differences between the treatment in comparison with the control (**P < 0.01). The plasma-liquid system is considered as a high complex environment because of the plasma-water

interaction as well as the associated physical and chemical properties. The temperature of the plasma plume did not play a role in the plasma-water treatment; it was approximately the same as ambient air. Thus, it is not sufficient for the inactivation of fungi in water via pure thermal effects.

### Antifungal activity tests by applying plasma jet in the solid medium

Figure (4) shows the inhibition zone (IZ) of the Candida albicans culture grown in the solid medium. Muller Hinton agar plates cultured with Candida albicans were used to test the antifungal effect of plasma jet at six time points( 0.5, 1, 2, 3.5, 5 and 8 min). Figure (4) shows that the inhibition of growth rate increased compared of the control. The inhibition zone (IZ) area increased with increasing the period of timefor all samples. The diameters of inhibition zone area was 4, 8, 30, 32, 35 and 40 mm for the time periods 0.5, 1, 2, 3.5,5 and 8 min respectively. This result exhibits the maximum effect occurred after time 8 min which have inhibition zone diameter 40 mm. These results is supporting the microscopic measurements of candida albicans cultures in liquid medium. And these result is agreement with reported by previous studies [ 1,14].

Plasma jet acts though a complex mechanisms that include a synergetic mode of action to various reactive species, including ionized argon gas molecules, RNS and ROS or free electrons. Basically, plasma particles produce a major mechanical effect on the surface of living organisms. This mechanical effect is generated by charged particles in plasma jet that have a very important role in outer membrane rapture of fungi cells. Creating the electrostatic forces by charge accumulation on the cell membrane surface could conquer the membrane tensile strength and causing its rupture. These forces can generate pressure, causing transmogrification and distortion, leading to rupture of the cell membrane. Furthermore, the accelerating the cellular damage can be created by the cracks or holes that induced by charged particles and this will facilitate the invasion of free radicals [15, 16]

## CONCLUSION

Candida albicans inactivation by atmospheric pressure plasma jet indicates that. plasma jet is an effective tool to treat fungi infection. More than 60% of Candida was inactivated during a period of 2 min treatment by the plasma jet. Further research is required to understandi of the mechanisms of interactions among reactive plasma species and cellular structures.

## REFRENCES

1. Xiong Z., Lu X. P., , Feng A., , Pan Y., and Ostrikov K.," Highly effective fungal inactivation in He+O2 atmospheric-pressure nonequilibrium plasmas", PHYSICS OF PLASMAS Vol. 17, NO.123502 , pp. 1–6, 2010
2. Nelson D., Priscyla D. M., Priscyla D. M., Oswaldo L. Al. and Elisa E.," Antibacterial Effect of Silver Nanoparticles Produced by Fungal Process on Textile Fabrics and Their Effluent Treatment" Journal of Biomedical Nanotechnology, Vol.3, NO. 2, PP 203–208, 2007.
3. Peng S., Yi Su., Haiyan W., Weidong Z., Jose L. L., Wei L., Jue Z., Ruoyu L, and Jing F.," Atmospheric pressure cold plasma as an antifungal therapy", Applied Physics Letters,Vol. 98,NO. 021501 PP 1-3, 2011
4. Sohbatzadeh F., Mirzanejhad S., Shokri H. and Nikpour M.," Inactivation of Aspergillus flavus spores in a sealed package by cold plasma streamers", Theor Appl Phys ,Vol.10, PP99–106, 2016.
5. Boenig H. V., "Fundamentals of Plasma Chemistry and Technology", Technomic Publishing Co., Inc.: Lancaster, PA, 1988.
6. Vijay N., Ashok K. and Dwivedi H. K., "Atmospheric Non-Thermal Plasma Sources", International Journal of Engineering, Vol. 2 No.1, PP. 53-68, 2008.

7. Shailja S., Ramesh C., Supratim T., Hena R., Payal T., Amisha J. and Pulkit G., "The Bright Future of Dentistry with Cold Plasma – Review", IOSR Journal of Dental and Medical Sciences, Vol.13, No.10, PP. 6-13, 2014.
8. Aline C. B., Thalita M. C. Ni, Konstantin G. Ko., Gabriela de M. G. Li., Aline Vi. La. G.,c, Juliana N. M. M. de Car., Roberto Yz. H., Cristiane Y. K-It.," Cold atmospheric

**Table 1. Effect plasma jet of different time in Cell No. Viability of Candida albicans**

| Time (minute) | Mean ± SE of Cell Viability x $10^4$ (cell/ml) |
|---|---|
| Control | 1244.67 ± 44.49 a |
| 0.5 | 1056.00 ± 36.95 b |
| 1 | 757.33 ± 28.22 c |
| 2 | 469.33 ± 55.68 d |
| 3.5 | 229.33 ± 32.44 e |
| 5 | 186.67 ± 14.11 ef |
| 8 | 112.00 ± 18.47 f |
| LSD value | 107.75 ** |
| P-value | 0.0001 |

Means with the different letters in same column represent differed significant levels.** (P<0.01).

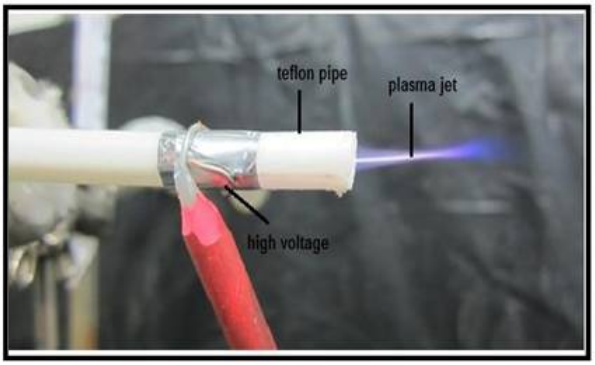


**Figure 1. Linear – field DBD plasma jet torch**

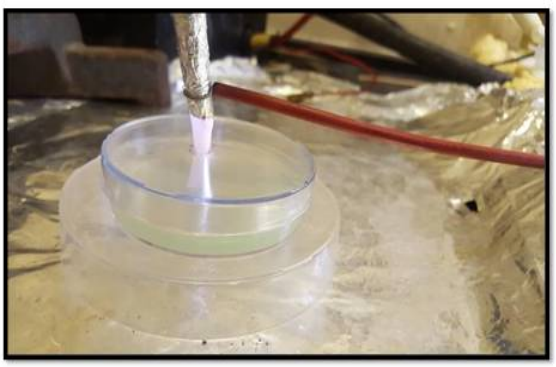

**Figure 2. Fungal sample in petri dish during exposure to plasma**

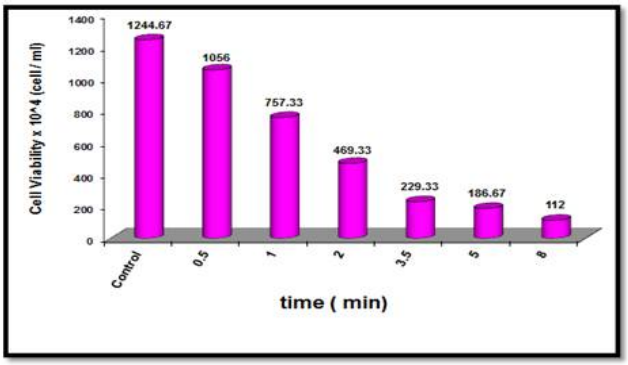


**Figure 3. Histogram effect plasma jet of different time in Cell No. Viability of *Candida* albicans growth in the liquid medium. All data are expressed as a mean ± standard deviation LSD test (ANOVA). Statistical significance was considered as p<0.01**

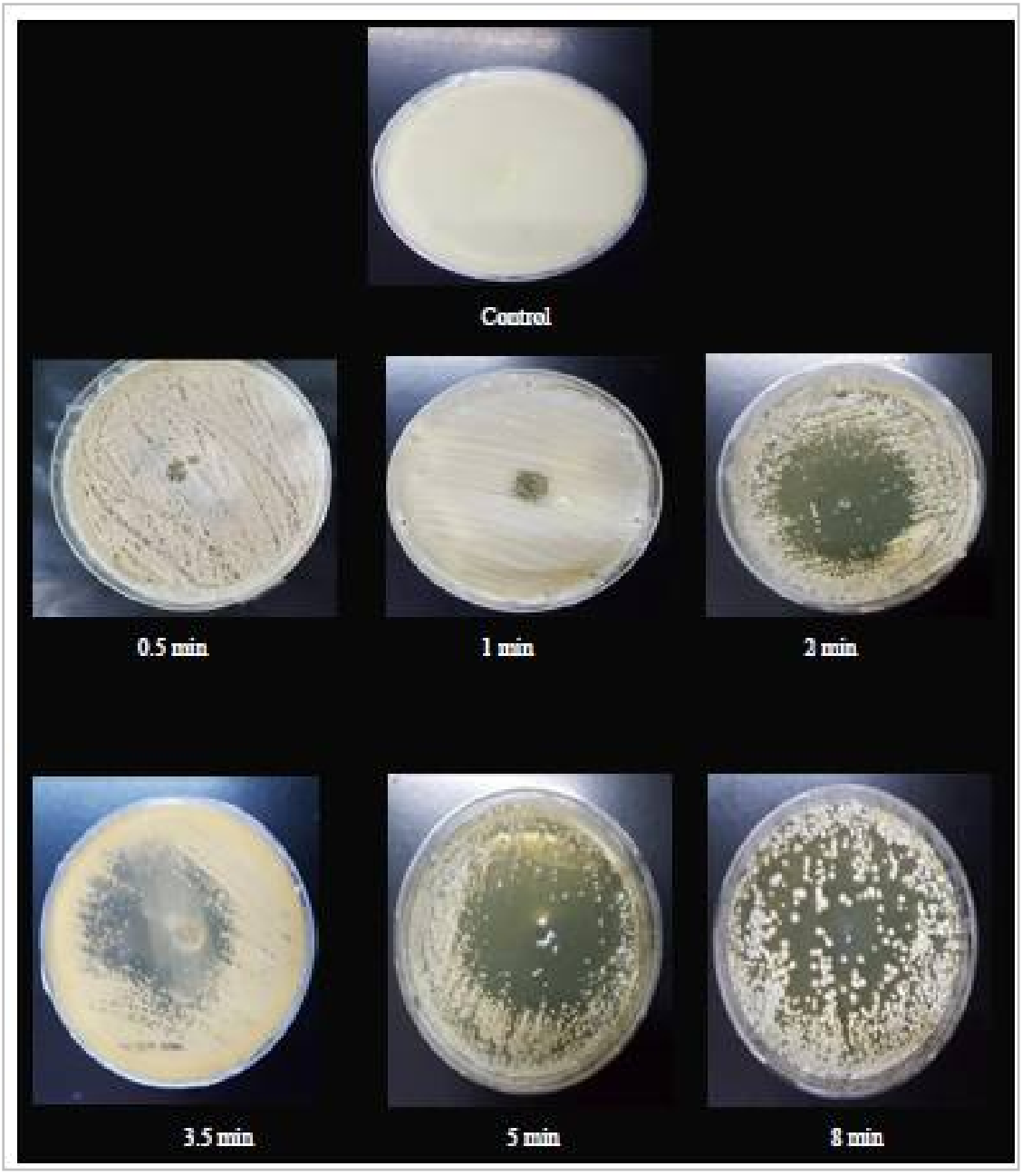


**Figure 4.shows the digital photographs inhibition zone (IZ) samples of the fungal Candida albicans samples in Petri dishes its of untried (control)and tried by exposure of plasma jet of (0.5,1,2,3.5,5and 8 min)**

*Indian Journal of Natural Sciences* www.tnsroindia.org.in ©IJONS

*Vol. 9 / Issue 50 /October 2018* *International Bimonthly* *ISSN: 0976 – 0997*

**RESEARCH ARTICLE**

# Investigation of Plasma Characteristics Produced by Laser - Induced Breakdown Spectroscopy in the Presence and Absence of a Magnetic Field

Marieam Ghreeb Jasim* and Qusay Adnan Abbas

Department of Physics, College of Science, University of Baghdad, Baghdad, Iraq

Received: 07 July 2018 Revised: 10 Aug 2018 Accepted: 13 Sep 2018

***Address for Correspondence**
**Marieam Ghreeb Jasim**
Department of Physics,
College of Science,
University of Baghdad,
Baghdad, Iraq.
Email: gmarieam@gmail.com, qusayiraqi@yahoo.com



**ABSTRACT**

Laser-induced breakdown spectroscopy of Cu plasma in the presence and absence of magnetic field has been investigated. The plasma was generated by employing Nd: YAG laser (532 nm, 9 ns) at various pulse laser ranging from (100 to 400 ) mj in a vacuum with different working pressure from 0.2torr to 0.8 torr. Both electron number density and electron temperature show an increasing trend with increasing the laser energy and decreasing with increase the working pressure. It is revealed that values of electron temperature and electron number density of copper plasma are higher in the presence of a magnetic field. The existence of magnetic field confinement effect is confirmed when the values of plasma parameter beta $\beta$, which is smaller than 1.

**Keywords**: LIBS , magnetic field confinement, electron temperature, OES, electron density.

## INTRODUCTION

Laser-induced breakdown spectroscopy (LIBS) it is new technicality a comparatively for elemental analysis and description of solids, liquids, gases and aerosol [1]. LIBS is an atomic emission spectrum analysis technicality. Which is a high pulsed laser energy is localized onto a small target volume leading to a breakdown of analytical into ions and free electrons, resulting to a plasma identify by both continuum and atomistic emission[2,3].The parameters of the Laser-generated plasma is progress quickly and are strongly related on irradiation conditions like Intensity of laser incident on a surface of the target and pulse laser duration, the wavelength of the laser, the spot size of radiance, gas ambient installation, and ambient pressure, which are temporary in nature [4,6]. The plasma generated by the

laser has become confined by use of the magnetic field. To control the energetic plasmas ineffectual ways and dynamical properties of the transient by using the magnetic field. The high intensity of the magnetic field pulse has been found to be useful in improving the radiation emitted from laser-induced breakdown plasma [2].Many physical phenomena like plume confinement, plasma instabilities, the transformation of plasma thermal energy into kinetic energy and Joule heating, effect emission improving may initiate in the expansion of laser-induced plasma in the existence of the magnetic field [7]. In laser generated plasma the used dynamic, play a basic role in deciding the characteristics of the plasma [8]. The plasma confinement degree was in good consent with simple magnetohydrodynamic (MHD) modeling. [9]. Plasma diagnostics method can be done through an account of the plasma electron temperature ($T_e$) and density ($n_e$). The strength of the different distribution functions describing the plasma state determines by the temperature, while the state of thermo- dynamical equilibrium of the plasma specifies by the electron density [10]. For the calculation of electron temperature the Boltzmann plot method it is one of the methods that are used [5,11]

$$\ln(\lambda_{mn} I_{mn}/g_m A_{mn}) = -\frac{1}{KT}(E_j) + \ln\left|\frac{N}{U(T)}\right| \quad \ldots\ldots\ldots\ldots \quad (1)$$

Where:

$\lambda_{mn}$ is wavelength, $I_{mn}$ intensity, $A_{mn}$ is the transition probability of upper (m) and lower (n) energy states, Em and $g_m$ are the upper states (m) energy and statistical weight, Te is the electron temperature, K is the Boltzmann constant, N (T) and U (T) are the total number density and partition function. The Stark broadening effect using to calculate the electron density requires a line which is free from self-absorption [12]:

$$n_e = \left[\frac{\Delta\lambda}{2\omega_s}\right] N_r \quad \ldots\ldots\ldots\ldots\ldots \quad (2)$$

$\omega_s$ is the theoretical line full width Stark broadening parameter, $N_r$ is the reference electron density, equal to $10^{16}$ ($cm^{-3}$) for neutral atoms and $10^{17}$ ($cm^{-3}$) for singly charged ions. Plasma parameter $\beta$ it is a measure of the effect of the external magnetic field on the plasma generated ,which is the ration of plasma pressure to the magnetic field pressure [13]

$$\beta = \frac{\sum nkT}{\frac{B^2}{2\mu^\circ}} \quad \ldots\ldots\ldots\ldots\ldots \quad (3)$$

where B is the magnetic field, $T_e$ is the electron temperature ,K is the Boltzmann constant and $n_e$ is the electron density.

## MATERIALS AND METHODS

LIBS system used for the detection spectral lines of laser - generated Cu plasma in the existence and without of magnetic field. Illustrated in Figure1 the experimental setup of The target were bombarded by Nd: YAG pulses laser (9 ns duration, 6 Hz frequency, and fundamental wavelength of 532nm) and laser pulse energy ranging from 100 mj to 400 mj on the target surface for the generation of Cu plasma, at an angle of 45°. To focused the laser on the target surface we used the convex lens with a focal length equal to 10 cm.The circularly shaped pellet of the copper target with diameter 3 cm is placed inside a vacuum chamber. The chamber was filled up with Argon gas at a pressure from (0.2 to 0.8 Torr).The vacuum chamber made of a cylindrical stainless steel tube. The two ends closed by Pyrex windows, by two stainless steel flanges, and with small quartz window fixed in it is center, that allows for a laser

pulse to shoot the Cu target. Two small pipes connected to pumping systems, while the other was used to deliver the argon gas with purity (99.9%).for applying a magnetic field ,two types of the permanent magnetic field were used (located under the target); the first is the outer and the second is the inner which is located inside the outer circular permanent. Figure (2) shows the radial profile of the magnetic field distribution along the Cu target. One can observe from this figure, the magnetic field intensity has nonuniform distribution along the target

The maximum value of the magnetic field is approximately 41 mT in the central region of the Cu target

## RESULTS AND DISCUSSION

### Emission intensity

Figure 3. Shows the variation in emission intensity of Cu (I) and Cu (II) for the selected spectral lines at various flounces in the absence and presence of a magnetic field. It is revealed that emission intensities typically show an increasing trend with increasing flounce. However, the line intensities of emission spectra in the presence of a magnetic field are higher than the absence of the magnetic field at different flounces. Also, We notice increasing of laser peak energy caused an increase in the intensities of the spectral lines because the mass ablation rate of the target also increases. The spectroscopic data for these lines are listed in Table 1.

### Electron temperature

The electron temperature (Te) is responsible for various excitation and ionization processes that occur in the laser-induced breakdown. To calculate the electron temperature plasma is assumed to be in local thermodynamical equilibrium (LTE), and the population of excited atoms follows the Boltzmann distribution. The value of (Te) was calculated according to Boltzmann plot method (equation (1)) by using the selected ionic Copper lines (CuI and Cu II) for the different Laser energy, with presence and without magnetic field at different working pressure. The electron temperature (Te) was calculated, using the relation between Ln $\left(\frac{I_{ji}\lambda_{ji}}{hcg_jA_{ji}}\right)$ versus upper energy level (Ej).The

Values of Te equal to the converse of the slope for the best line fitting. From figure (4) many features can be observed the electron temperature decreasing with increasing of gas pressure in the presences and absence of a magnetic field [15,16].The increasing of inelastic collisions of an electron with Ar atoms with increasing of gas pressure is responsible for decreasing of Te with increasing of pressure.The electron temperature increase in the presence of a magnetic field. The increasing of Te in the presence of a magnetic field can be explained as the magnetic fields will confinement the electrons in the region near the target surface. Therefore, the electron will gain the energy from the laser pulse and this will continue increases the electron temperature.

### Electron density

Plasma species are under the influence of electric field of fast moving electron and slow-moving ion. The perturbing electric field shifts the energy level of species, which is leading to broadening, regarding stark broadening. The electron number density can be related to the full width at half maximum [FWHM ($\Delta\lambda 1/2$)] of stark broadneing line by equation (2).The electron density ne increase with increasing laser energy from 100 to 400 mj and working pressure from 0.2 to 0.8 Torr in the presence and without magnetic field as shown in figures (5),as a result of increasing the ionization collision with increasing atoms density, the electron density is higher in presence of magnetic field than without magnetic field .The copper line (I) at wavelength of 510.5541 nm ,for this line (*w*m= 43 nm). And copper line (II) 512.07535 with (*w*m= 50nm) are used to calculate the electron number density [17].

**$\beta$ Value of plasma**

The values of $\beta$ are evaluated according to equation (3) ,from the figure (6) shown the variation of beta value along the Cu target at da ifferent gas pressure of wavelength 532 nm .It is clear from this figure that the $\beta$ value has a value is less than 1. This means that magnetic field pressure is great than plasma pressure. The beta value has the maximum value in the edge of Cu target. The variation of beta value along the target caused they non-uniform magnetic field distribution along the target surface.

## CONCLUSION

By using the laser produce copper oxide plasma, technique, the effect of the magnetic field was observed in the confirm the confinement of plasma through the measurement of plasma beta parameter, its value less than 1.Plasma characteristic like electron density and it is temperature, increasing with increase the laser energy from 100 to 400 mj and decrease with increasing working pressure. Also, we found that the electron temperature and its density with the existence of the field are higher than in the absence it. the measured value of beta decrease with increasing working pressure.

## REFERENCES

1. F. Anabitarte, A. Cobo, and J. M. Lopez-Higuera.2012."Laser-Induced Breakdown Spectroscopy: Fundamentals, Applications, and Challenges," *ISRN Spectrosc.*, vol. 2012, pp. 1–12.
2. V. N. Rai, H. Zhang, F. Y. Yueh, J. P. Singh, and A. Kumar. 2003. "Effect of steady magnetic field on laser-induced breakdown spectroscopy.," *Appl. Opt.*, vol. 42, no. 18, pp. 3662–9.
3. S. S. Harilal, C. V. Bindhu, M. S. Tillack, F. Najmabadi, and A. C. Gaeris. 2003. "Internal structure and expansion dynamics of laser ablation plumes into ambient gases," *J. Appl. Phys.*, vol. 93, no. 5, pp. 2380–2388.
4. J. Kaiser et al.. 2007. "Utilization of the Laser Induced Plasma Spectroscopy for monitoring of the metal accumulation in plant tissues with high spatial resolution," Mod. Reseach Educ. Top. Microsc., pp. 434–441.
5. J. A. Aguilera and C. Aragón. 2004. "Characterization of a laser-induced plasma by spatially resolved spectroscopy of neutral atom and ion emissions. Comparison of local and spatially integrated measurements," *Spectrochim. Acta - Part B At. Spectrosc.*, vol. 59, no. 12, pp. 1861–1876.
6. A. K. Sharma and R. K. Thareja. 2005. "Plume dynamics of laser-produced aluminum plasma in ambient nitrogen," *Appl. Surf. Sci.*, vol. 243, no. 1–4, pp. 68–75.
7. A. Arshad *et al.* 2016. "Effect of magnetic field on laser-induced breakdown spectroscopy of graphite plasma," *Appl. Phys. B*, vol. 122, no. 3, p. 63.
8. P. M. BELLAN. 2006. *FUNDAMENTALS OF PLASMA PHYSICS Fundamentals.*
9. C. Pagano. 2015."Influence of transverse magnetic field on expansion and spectral emission of laser," vol. 155205.
10. A. M. El Sherbini. 2012."Measurement of Plasma Parameters in Laser-Induced Breakdown Spectroscopy Using Si-Lines," *World J. Nano Sci. Eng.*, vol. 2, no. December, pp. 206 –212.
11. S. Waheed et al. 2017. "Effect of Magnetic Field on Laser Induced Breakdown Spectroscopy of Zirconium Dioxide ( ZrO 2 ) Plasma," Opt. - Int. J. Light Electron Opt.
12. A. M. El Sherbini. 2012."Measurements of Plasma Electron Temperature Utilizing Magnesium Lines Appeared in Laser Produced Aluminum Plasma in Air," Opt. Photonics J., vol. 2, no. 4, pp. 278–285.
13. M. S. Raju, R. Singh, P. Gopinath, A. Kumar. 2014.Influence of magnetic field on laserproduced barium plasmas: Spectral and dynamic behaviour of neutral and ionic species, J. Appl. Phys. 116 -153301.
14. W.L. Wiese and G.A. Martin, Wavelengths and Transition Probabilities for Atoms and Atomic Ions_ Part II, National Bureau of Standards, Washington, DC, (1980).
15. R. Fitzpatrick, "Introduction to Plasma Physics," Univ. Texas Austin, Austin, TX, 2006.

16. O. H. Chin and C. S. Wong, "Dependence of some plasma parameters on ap in a dc helium hollow cathode discharge," J. Fiz. MALAYSIA, vol. 23, no. 1–4, pp. 54–59, 2002.
17. J. Peng et al., "Comparative Study of the Detection of Chromium Content in Rice Leaves by 532 nm and 1064 nm Laser-Induced Breakdown Spectroscopy," Sensors, vol. 18, no. 2, p. 621, 2018

**Table 1 Spectroscopic parameters of Cu Lines[14]**

| wavelength (nm) | ion | Transitions | Transitions probabilityAji. gj | Ei | Ek |
|---|---|---|---|---|---|
| 488.97005 | Cu II | $3d^9 4p \rightarrow 3d^8 4s^2$ | $9.5\times10^5$ | 8.4205798 | 10.9554918 |
| 481.29476 | Cu II | $3d^9(^2D3/2)4d \rightarrow 3d^9(^2D3/2)4f$ | $6.5\times10^8$ | 14.534842 | 17.1101770 |
| 512.07535 | Cu II | $3d^9(^2D5/2)4d \rightarrow 3d^9(^2D5/2)4f$ | $1.0\times10^8$ | 14.430246 | 16.8507820 |
| 502.12785 | Cu II | $3d^9(^2D5/2)4d \rightarrow 3d^9(^2D5/2)4f$ | $2.2\times10^8$ | 14.392113 | 16.8606007 |
| 404.34879 | Cu II | $3d^9 4p \rightarrow 3d^8 4s^2$ | $1.03\times10^7$ | 8.7832224 | 11.8486266 |
| 406.2641 | Cu I | $3d^{10} 4p \rightarrow 3d^{10} 5d$ | $1.26\times10^8$ | 3.8166920 | 6.8676455 |
| 521.8202 | Cu I | $3d^{10} 4p \rightarrow 3d^{10} 4d$ | $4.5\times10^8$ | 3.8166920 | 6.1920251 |
| 515.3235 | Cu I | $3d^{10} 4p \rightarrow 3d^{10} 4d$ | $2.4\times10^8$ | 3.7858976 | 6.1911751 |
| 510.5541 | Cu I | $3d^9 4s^2 \rightarrow 3d^{10} 4p$ | $8.0\times10^6$ | 1.388948 | 3.8166920 |
| 578.2132 | Cu I | $3d^9 4s^2 \rightarrow 3d^{10} 4p$ | $3.30\times10^6$ | 1.6422256 | 3.7858976 |

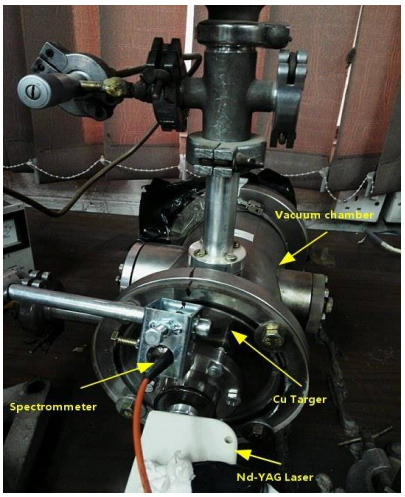


**Figure 1. The experimental set up of LIBS system**

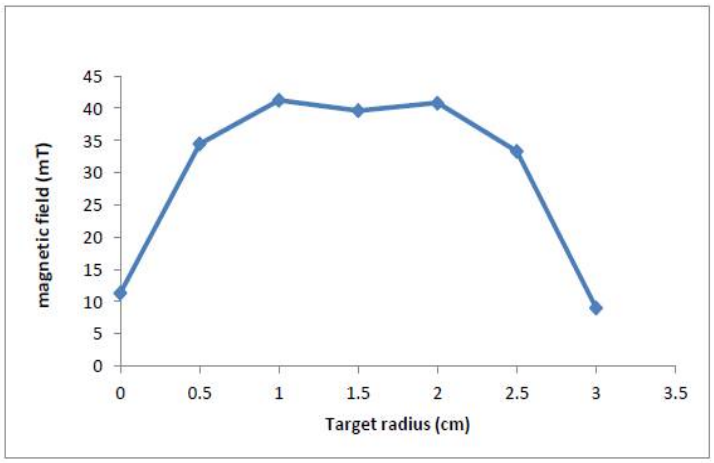


**Figure 2. The magnetic field distribution as function along the Cu target**

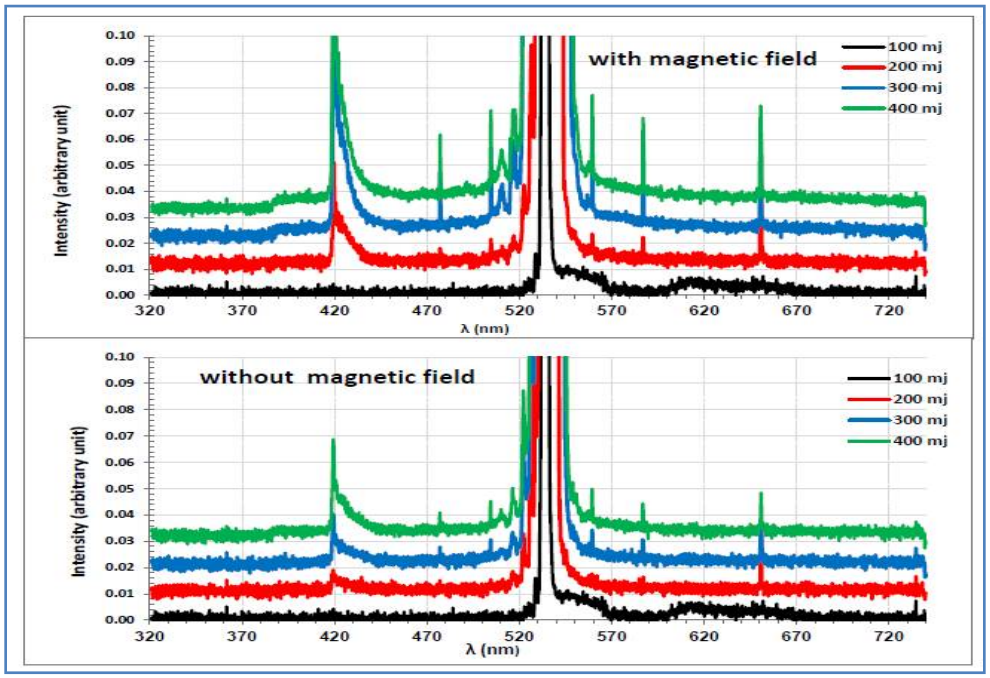


**Figure 3. Emission spectra of laser-induced copper target plasma with different laser energies**

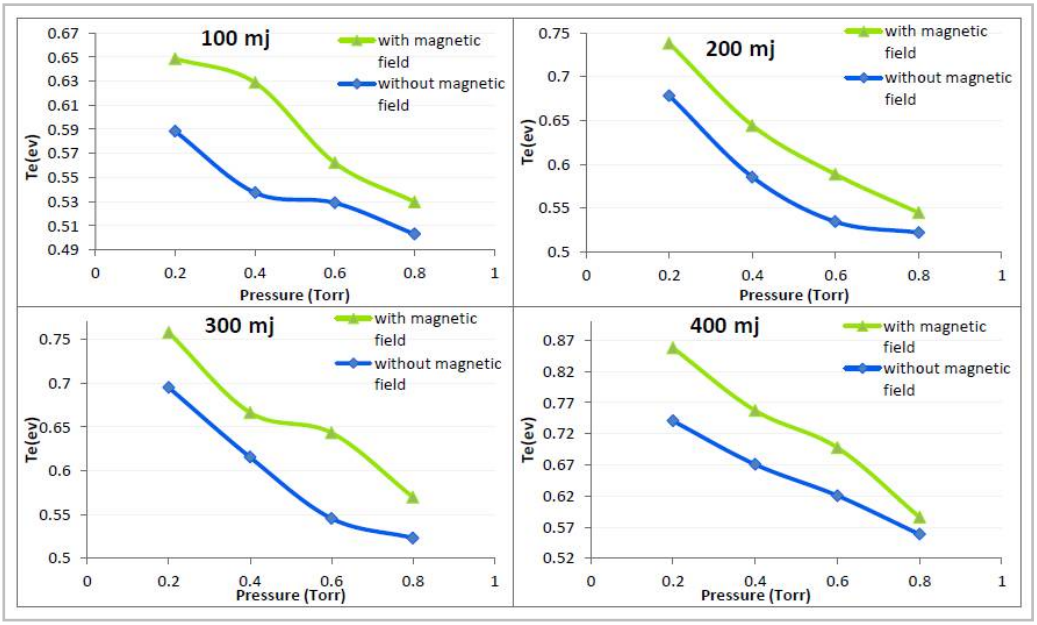


**Figure 4. The variation of electron temperature as a function of pressure in the copper target**

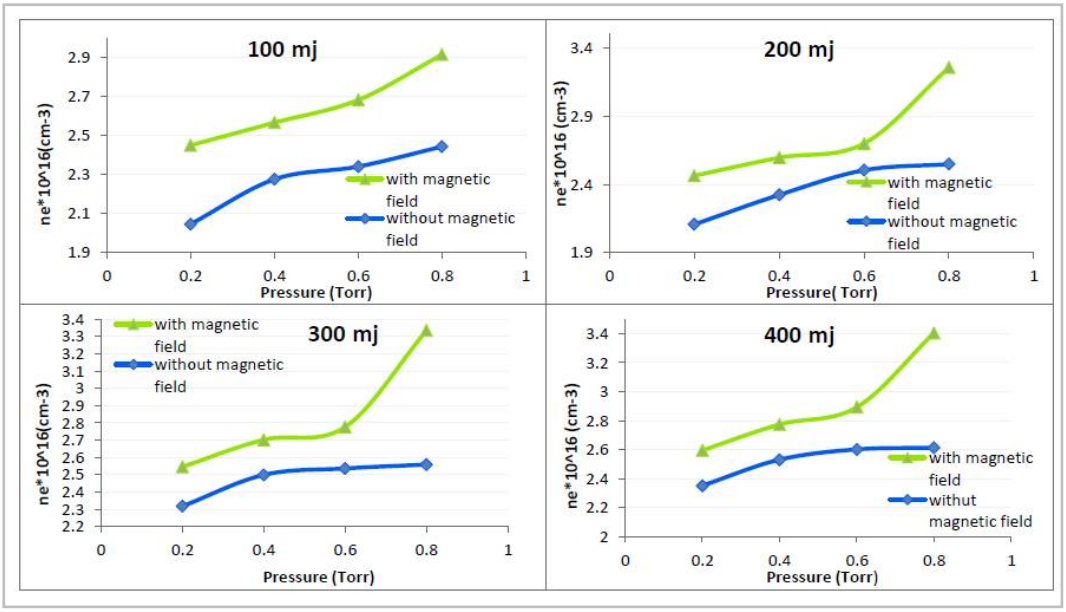


**Figure 5. The variation of electron density as a function of pressure in the copper target**

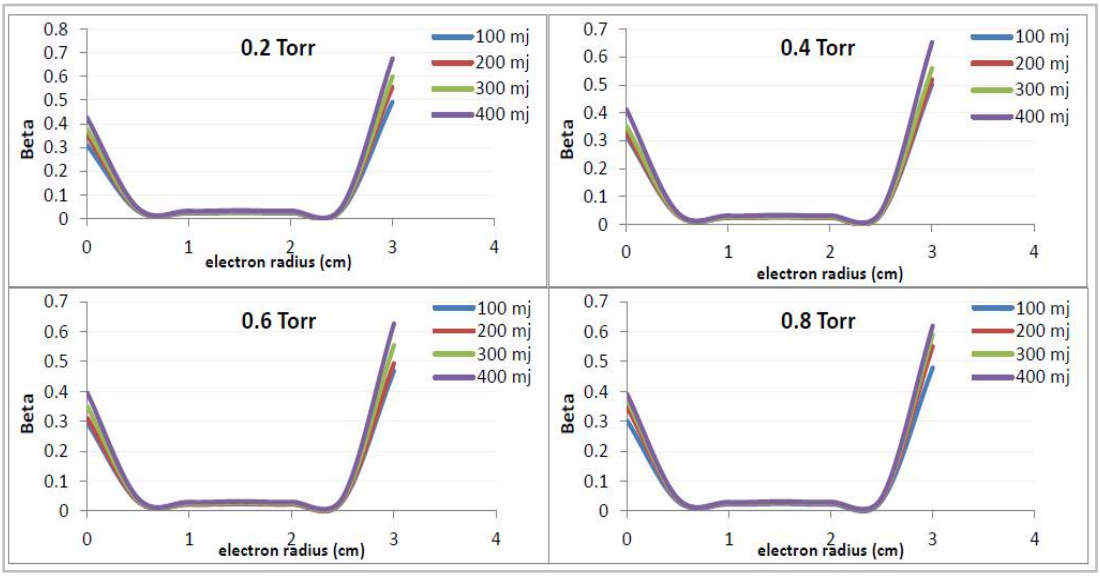


**Figure 6. The different of beta with the Target radius for a Copper target**

*Indian Journal of Natural Sciences* www.tnsroindia.org.in ©IJONS

*Vol. 9 / Issue 50 /October 2018* *International Bimonthly* *ISSN: 0976 – 0997*

**RESEARCH ARTICLE**

# Measuring the Electro - Optical Properties of Spatial Light Modulator Using Three Different Wavelengths

Farah G. Khalid[1]*, Sudad S. Ahmed[2], Samar Y. Al-Dabagh[1], Rawa K. Ibrahim[3], Aseel I. Mahmood[3], Kais Al Naimee[2]

[1]Department of Physics, Collage of Science for Women, University of Baghdad, Baghdad, Iraq.

[2]Department of Physics, Collage of Science, University of Baghdad, Baghdad, Iraq.

[3]Material Research Directorate, Ministry of Science and Technology, Baghdad, Iraq.

Received: 16 July 2018 Revised: 20 Aug 2018 Accepted: 24 Sep 2018

***Address for Correspondence**
**Farah G. Khalid**
Physics Department,
Collage of Science for Women,
University of Baghdad,
Baghdad, Iraq.
Email: rawak2070@gmail.com, farah_physicalaf70@yahoo.com



**ABSTRACT**

The characteristics of transmitting type twisted nematic liquid crystal based Spatial Light Modulators (SLMs) optical switch have been studied. Electro-optical properties of SLM represented by frequency response ,rise time ,fall time , and response time have been measured in this work using three different laser wavelengths; red ($\lambda$=632.8nm) ,green ($\lambda$=532 nm) , violet ($\lambda$=405 nm) . The results of investigations in the electro-optical properties of SLM make it acts as optical switch and possible major applications in electro-optic system. The optical switch for red laser showed faster rise time and faster response time than lasers at (532,405) nm due to the unique properties of the SLM.

**Keywords**: SLM; Nematic Liquid Crystal, electro-optical properties, optical switch.

## INTRODUCTION

Spatial Light Modulator (SLM) systems are based on liquid crystal(LC) micro displays which can be modulate light spatially in amplitude and phase, so they act as a dynamic optical element [1]. The optical function or information to be displayed can be taken directly from the optic design or an image source and can be transferred by a computer interface. Implementation is very easy due to the smart system architecture and by an easy addressing using (Video Graphics Array) VGA or (digital video interface) DVI signals directly from a computer graphics card. SLMs are made in five distinct technologies: liquid crystal devices, deformable mirror devices, electro-optics, acousto-optic and

magneto-optic devices [2]. Each type of device suits different types of applications; Liquid crystal spatial light modulators are available as reflective or transmissive [3]. Electrically or optically addressed [4], phase and or amplitude modulators. SLM is an important and useful device which can impose spatially varying modulation on light waves [5]. SLM has attracted increasing interest in various applications, such as diffractive optics [6], adaptive optics [7,8,9], optical tweezers[10], optical information processing and holographic projection[11,12,13] , due tothe high degree of flexibility, fast switching time, and good reconfigurable and reproducibility [14, 15].In this work, electro-optical properties of SLM optical switch were measured utilizing lasers at (632.8, 532, 405)nm wavelengths.

## MATERIALS AND METHODS

The electro-optical properties of SLM, which has an array of 90°nematic LC.,Holoeye LC2002 SLM from Sony has been measured. This type contains a Sony SVGA (800*600) LC micro display and driver electronics, the wavelength range of this SLM is (400-650) nm and LCD thickness is 20µm. The experiment was carried out at room temperature using .The block diagram of the experiment setup is shown in fig (1). Three different lasers were used to study the optical properties of SLM the first one is He-Ne laser ($\lambda$=632.8nm), the second is green semiconductor laser ($\lambda$=532 nm) and the third is violet semiconductor laser ($\lambda$=405 nm) .The SLM was set between two crossed liner polarizers type (Thorlaps) so that the angle between the polarizers is $90^0$.The photo detector used was from (THORLABS DET10A , Si Basied Detector) . The Oscilloscope type (ATTEN ADS 110Q2CAL, 100 MHZ) used to display the output signal. The block diagram of SLM optical switch system is shown in fig (1) . Fig(2) shows the photograph of the experimental setup

## RESULTS AND DISCUSSION

The Frequency response was calculated from the signal of the SLM optical switch device for the three lasers are shown in Fig.(3,4,5). The rise time, fall time, and the response time calculated from the signal of the response voltage of the SLM optical switch device that gets from the Oscilloscope as shown in Fig. (6,7,8) for the three lasers. Table (1) illustrate the electro-optical properties of SLM optical switch.The relationship between the response time and the wavelengths of the sources is shown in fig (9). It is clear from the figure that the relationship is inversely between the response time of the probe and the wavelength of lasers , means the longer greater the wavelength, the shorter the response time

## CONCLUSION

An investigation of the electro-optical properties of SLM by using three different sources have been carried out in this work, giving an assumption of how the SLM works as optical switch at different wavelengths .We noticed that red laser have the faster response time and rise time as compared to semiconductor lasers at (532, 405)nm because the SLM transmitted light at the red wavelength was the bigger than the green and the violet wavelengths. This means SLM is more active in the red wavelength when it works as optical witch.

## REFERENCES

1. J.W.Goodman, Introduction to Fourier Optics. New York: McGraw-Hill Book Co., 1968.
2. C.Warde and A. D. Fisher, "Spatial light modulators: applications and functional capabilities," in Optical Signal Processing, J. Horner, ed. (Academic, San Diego, Calif., 1987r. pp.477-523.
3. S.Ahderom, M. Raisi, K. Lo, K. E. Alameh, and R. Mavaddat, "Applications of Liquid Crystal Spatial Light Modulators in Optical Communications", ECU Publications, IEEE, p.p. 239-242, 2011.

4. Hossack, Will (1998) Spatial Light Modulators and Applications. http://www2.ph.ed.ac.uk/~wjh/teaching/mo/slms.html. Accessed 21 Nov 2015 .
5. Márquez, A., Iemmi, C., Campos, J., Escalera, J. & Yzuel, M. "Programmable apodizer to compensate chromatic aberration effects using a liquid crystal spatial light modulator". Opt. Express 13, 716–730 (2005).
6. Dou, R. & Giles, M. K. "Closed-loop adaptive-optics system with a liquid-crystal television as a phase retarder". Opt. Lett. 20, 1583–1585 (1995).
7. Love, G. D. "Wave-front correction and production of Zernike modes with a liquid-crystal spatial light modulator" Appl. Opt. 36, 1517–1520 (1997).
8. Laude, V. "Twisted-nematic liquid-crystal pixelated active lens" Opt. Commun. 153, 134–152 (1998).
9. Grier, D. G. "A revolution in optical manipulation". Nature 424, 810–816 (2003).
10. Karim, M. A. & Awwal, A. A. S. "Electrooptic displays for optical information processing". Proc. IEEE 84, 814–827 (1996).
11. Yu, F. & Lu, X. "A real-time programmable joint transform correlator", Opt. Commun. 52, 10–16 (1984).
12. Liu, H.-K., Davis, J. A. & Lilly, R. A. "Optical-data-processing properties of a liquid-crystal television spatial light modulator", Opt. Lett. 10, 635–637 (1985).
13. Mok, F., Diep, J., Liu, H.-K. & Psaltis, D. "Real-time computer-generated hologram by means of liquid-crystal television spatial light modulator", Opt. Lett. 11, 748–750 (1986).
14. Jun Liu1 and Jian Wang, "Demonstration of polarization-insensitive spatial light modulation using a single polarization-sensitive spatial light modulator", 25 March 2015
15. E.G. van Putten, I.M. Vellekoop, A.P. Mosk, "Spatial amplitude and phase modulation using commercial twisted nematic LCDs", Applied Optics, 47 (2008) 2076-2081.

**Table 1.electro-optical properties of SLM optical switch for the three laser sources**

| Laser Wavelength (λ) (nm) | Frequency Response (Hz) | Rise Time (ms) | Fall Time (ms) | Response Time (ms) |
|---|---|---|---|---|
| 632.8nm | 140 | 0.476 | 27.6 | 0.714 |
| 532 nm | 120 | 1.5 | 120 | 1 |
| 405 nm | 160 | 0.9 | 40 | 1.36 |

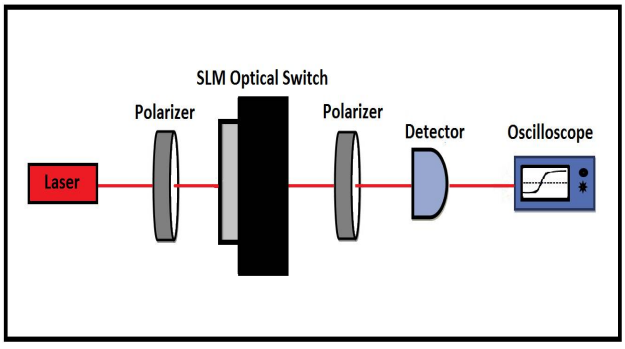


**Fig.1.Block diagram for measuring the electro-optical properties of theSLM optical switch system.**

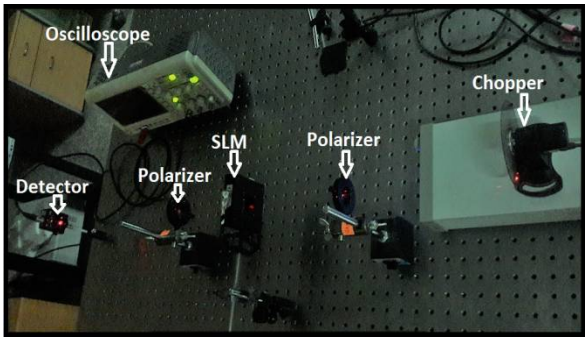


**Fig.2. Experimental setup of SLM optical switch.**

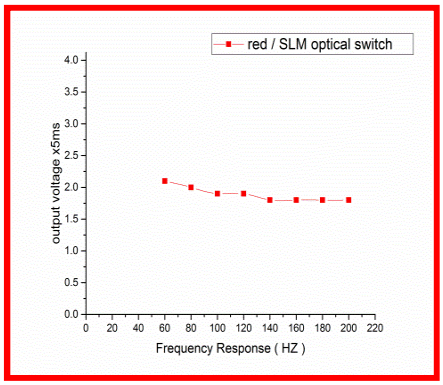


**Fig. 3.Frequency response of SLM Optical switch for red laser.**

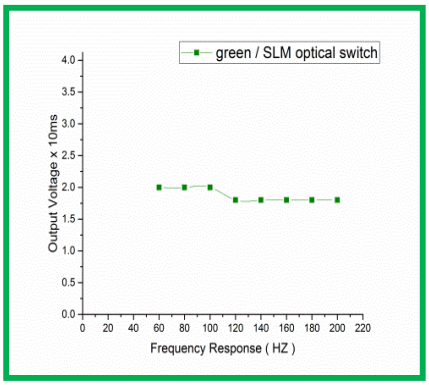


**Fig.4.Frequency response of SLM Optical switch for green laser**

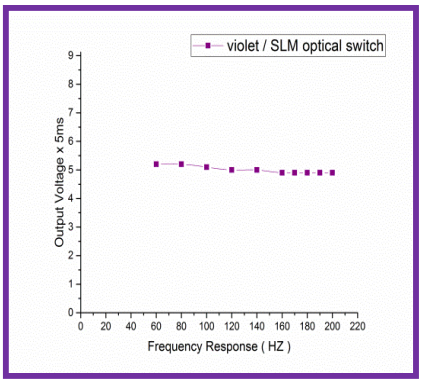


**Fig.5. Frequency response of SLM optical switch at violet laser**

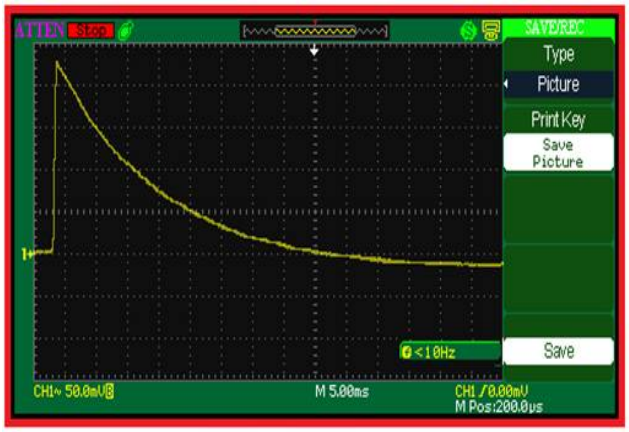


**Fig. 7.Oscilloscopes trace record of the optical switch signal of SLM optical switch for red laser**


**Fig. 6. Oscilloscopes trace record of the optical switch signal of SLM optical switch for green laser**

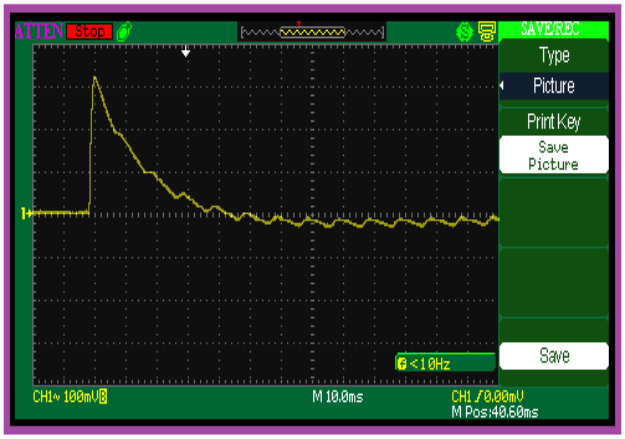


**Fig.8. Oscilloscopes trace record of the optical switch signal of SLM optical switch for violet laser**

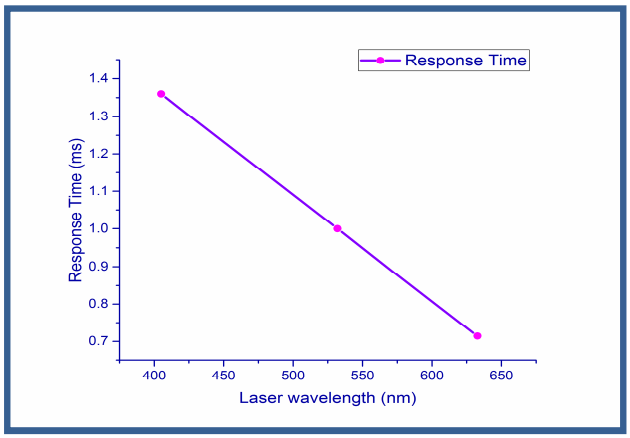


**Fig.9.Wavelength dependent Response time in SLM**

*Indian Journal of Natural Sciences* www.tnsroindia.org.in ©IJONS

*Vol. 9 / Issue 50 /October 2018* *International Bimonthly* *ISSN: 0976 – 0997*

RESEARCH ARTICLE

# Mitigative Effect of Different Mycotoxin Binders (Captex T2) with Inactivated *Saccharomyces cerevisiae* (Thepax) On T2 Toxin in Broiler Chickens

Momen Samir Ali* and Shaimaa Nabhan

Department of Microbiology, College of Veterinary Medicine, University of Baghdad, Baghdad, Iraq.

Received: 10 July 2018 Revised: 18 Aug 2018 Accepted: 24 Sep 2018

***Address for Correspondence**
**Momen Samir Ali**
Department of Microbiology,
College of Veterinary Medicine,
University of Baghdad,
Baghdad, Iraq.



## ABSTRACT

The main aim of this study was to Because these are no exhaustive researches about the pathological effect of T2-toxin in broiler chicken, so, this current study aimed to demonstrate the effect of T2-toxin in broiler chicken and compare between the mitigative effect of chemical and physical toxin binders (Captex T2) in presence and absence of inactivated *Saccharomyces cerevisiae (Thepax)* against T2 toxins in broiler chickens. The study included the followings:- The first step was carried out to determine the percentage of *F.sporotrichioides*in grains of poultry diet by collection 100 feed samples from different location of Baghdad province (AL-Taji, AL-Rashydia, AL-Madain and Abu-Ghraib) during Novmber 2017 to April 2018. These samples were divided into two parts, the first part for isolation and identification of *F.sporotrichioides* and the second part for detection of T2-toxin by ELISA. The result of this study showed 42% of poultry feed samples were contaminated with *F.sporotrichioides* and the AL-Madain showed significant increase in isolation of this fungus (65.3%) during January and February with (77.7%), while AL-Taji had the lowest ratio in all months of study (24%). The mean of T2-toxin was measured by ELISA technique and revealed to significant increasing in AL-Madain during January and February with 194.66_+3.52 ppb, while in Abu-Ghraib showed the significant decrease in March and April with 136.34_+1.85ppb. The second step of this study included extraction of T2-toxin from *F.sprortrichioides* and using 100 chicks divided into five groups with 20 chicks in each group. The 1st group was fed on normal feed without mycotoxin (control –ve group). The 2nd group was feed on normal feed but mixed with extracted T2-toxin without any toxin binder added. The 3rd group was fed as the 2nd group and treated with Captex T2+T2-toxin. The 4th group was fed as the 2nd group and treated with Thepax (2gm/kg).and the last group was fed as the 2nd group and treated with Captex T2+Thepax. The results showed that the T2-toxin caused significant decrease (P<0.05) in GSH concentration in the 2nd group while, there are no

significant differences (P<0.05) in the treated groups (G3, G4 and specially G5) when compared with control negative group due to the effect Captex T2 and Thepax and both of them.While T2-toxin caused a significant increased (P<0.05) in MDA and CAT concentration in the 2nd group while, the other groups showed no differences in these parameters when compared with the first group.On the other hand, the present study included detection of T2-toxin efficacy on the final body weight and revealed there was significant differences (P<0.05) between groups, the highest means appeared in the 5th group while, the lowest means showed in the 2nd group. The result of means of final body weight revealed there was significant differences (P<0.05) between groups, the highest means appeared in the 5th group while the lower mean showed in the 2nd group.

**Keywords:** Captex T2, Thepax, *F.sporotrichioides,* T2-toxin, ELISA and oxidative stress enzyme (GSH,MDA and CAT).

## INTRODUCTION

Contamination of poultry feed caused by fungal of secondary metabolites – mycotoxins is a major snag in poultry production that causes harmful effects on the performance and healthy, and through poultry meat consumption can causesseverity effect to human healthy. The poultry nutrition includes mostly grain as a source of carbohydrates, and potentially toxigenic fungi are the main contaminants of grain (Pleadin*et al*., 2015).Mycotoxins are secondary of fungal metabolites often found as polluters in agricultural commodities all over the world and possess a high risk for human and animal health, more than 400 different mycotoxins have been isolated and chemically characterized (da Rocha *et al*., 2014). The major of medically and agriculturally concern are aflatoxins, fumonisins, ochratoxins, trichothecenes, zearalenone (ZEA) and patulin (PAT), deoxynivalenol, T2-toxin, citrinin, patulin, penicillic acid, tenuazonic acid, , cytochalasins, fusarin C, and fusaric acid, are considered the kindes that major contaminate cereal grain,the best of the mycotoxins in these groups are produced by three fungal genera: *Aspergillus*, *Penicillium* and *Fusarium* (Ahmed and Jutta2015).Mycotoxins can result in significant decrease ofeconomiclly crop production and grain handling, feed manufacturers who incorporate mycotoxin-contaminated grain or feed ingredients in their product may encounter healthy of livestock problems or poor performance of animal, reduction of reproduction, suppression of growth, and finally animal death. (Tim 2016).

Trichothecenesare group of more than 100 fungal metabolites with the similar basic structure, are produced by a number of species of the genus *Fusarium*(McCormick *et al.,* 2011). They are common contaminants of poultry feeds and feedstuffs and can produce very bad effects on poultry healthy and productivity (Murugesan *et al*.,2015).The molecular mechanisms behind the toxic effects of the major mycotoxins are established and oxidative stress and the generation of free radicals have been shown to be implicated in mycotoxin toxicity (Wang *et al*., 2016). Indeed, the imbalance between free radicals and the antioxidant defence systems can cause chemical damage to DNA, proteins and lipids synthesis, as observed upon exposure to mycotoxins (Assi, 2017).Like other trichothecenes, T-2 binds and inactivates peptidyltransferase activity resulting in inhibition of protein synthesis and disruption of the mitochondrial morphology, endoplasmic reticulum and other membranes (Adhikari*et al*., 2017). Studies *in vitro* (Yang *et al*., 2016; Zhang *et al*., 2016) and *in vivo* (Chaudhari and Lakshmana, 2010) provided evidence that T-2-induced oxidative stress is associated with an increase in reactive oxygen spceies (ROS) generation and DNA, protein and lipid peroxidation leading to cell apoptosis.Current methods to decreasemycotoxin contamination in food and feed can be classified into several methods: the first one is Chemical methods such as ammoniation, acid treatments, hydrolysis of alkaline, by peroxidation, and ozonation, but their application in food and feed is limited due to their high costs and negative effects on the quality of raw materials as mentioned by (Park 2016; Aiko, 2016; and Fouler, 2016). Second type is Physical methods include the mechanical removal of more than contaminated fractions from raw materials (by sorting, cleaning, milling, dehulling), or by heat application, or by use of chemical adsorbents

(Vanhoutte, *et al.* 2016).Evenually the last type Biological methods consist of the biological agents were used and their enzymes, which are able to metabolize, damage or deactivate toxins into stable, less toxic compounds with minor impact on food sensory andquality of nutrition with chemical ones. (Commission Regulation 2015).Because these are no exhaustive researches about the pathological effect of T2-toxin in broiler chicken, so, this current study aimed to demonstrate the effect of T2-toxin in broiler chicken and compare between the mitigative effect of chemical and physical toxin binders (Captex T2) in presence and absence of inactivated *Saccharomyces cerevisiae (Thepax)* against T2 toxins in broiler chickens, through the following parameters:

1. Isolation and identification of *Fusariumsporotrichiodies*from poultry feed .
2. Detection of T2-toxin titer by ELISA technique.
3. Extraction of T2-toxin from *Fusariumsporotrichiodies.*
4. Determination of productive performance by measurement of definitive body weight, intake of feed and feed conversion ratio (FCR).
5. Evaluation of T2 toxin-induced oxidative stress enzymes.

## MATERIALS AND METHODS

Media used for Isolation and identification of Fungi,Potato-Dextrose Agar (PDA),Solutions and Buffers,Phosphate Buffer Saline (PH = 7.2) according to Hudson and Hay (1980),Normal saline Solution, Phosphate Buffer Saline with 0.01 % of Tween-80, Formaldehyde solution 10%,Stains,Lactophenol Cotton Blue.

### Collection of samples

One hundered Poultry feed samplescomprising of commercially prepared feed were collected during the period from Novmber 2017 to April 2018. These samples collected from different Poultry farms in Baghdad province (Al-Taji, Al-Madain, Al-Rashydia, Abu-Ghrab), tweenty five of Poultry feed samples, were collected from each place at regular intervals spread over the study period. One kg feed were collected from each of the four different places and kept in a polythene bag and stored in refrigerator prior to inoculation onto culture media every week to obtain a good fungal culture and remained poultry feed were used for evaluation and measurmentthe titer of T2-toxin that was found in these Poultry feed samples, by ELISA technique in Veterinary Directorate - Central Veterinary Laboratories and researches Department- Public health and food safety Laboratory these method of collection of samples was shown in diagram (1).

### Isolation of fungi from the surface disinfected grains

According to the method by (Albaldawy2007). Fifty grains of sample have been placed in (150 ml) sterilized flask, hen immersed for (one minute) with 2% solution hypochloride solution (NaOCI). Then the samples were washed two times with sterilized distilled for one minute.Then dried by sterilized filter paper.Five complete grains were added via sterilized forceps into a previously prepared plate, containing Potato-Dextrose Agar and incubation of all plates for (7) days at 25 °C with intermittent observation of the fungal growth.

### Diagnosis of *Fusariumsporotrichioides*

The present study focused on isolation of *F. sporotrichiodes* that produced T2 toxin according to Leslie &Summerell (2008).The identification of the *F.sporotrichiodes* has been depending on the colour of fungus on the PDA plate, shape, and examination under the microscope for microscopical appearance by taken small part from the fungal growth and mixed with one drop of lacto-phenol cotton blue and covered withcover slip and examined under the microscope by using (40 X ) Lens.

## ELISA Kit

### Test principles

Veratoxfor T2 testkitisa competitive directenzyme-linkedimmunosorbentassay (CD-ELISA) forthe quantitative analysisof T2-toxin insuchwareascorn, pellet, barley, oats, rice, rye, soy and wheat. The test kit is prepared for use by control of quality personnel and others familiar with food and feed probably contaminated by T2-toxin.

### Extraction of T2 toxin

**The extraction of T2 toxin included two parts**

***F. sporotrichioides* culture preparation**

Sections colonies that cultured on PDA medium were added to sterile rice substrate (50 g of rice in 50 mL sterile distilled water) and was incubated at (27±1) °C for 5 days, then 3 weeks was incubated at 10±2°C according toJoffe, A. Z. (1986) . Then growth medium was transferred onto a sterile aluminum foil and then was ovendried (45°C for 24-48 hours). The dry weight was powdered by electronic grinder. Afterward the extract was prepared and used for further analysis.

### Extraction preparation of T2-toxin

The grinded powder was mixed well to each 25 grams of the powder was added 100 mL of acetonitrile solution and water in 84:16. Then, for 12 hours was shacked vigorously in >210 rpm. The achieved extract was filtered twice by 9cm No.120 paper and then whatman paper 12.5cm No.1. The fat of the extract was removed by hexane by adding 2:1 ratio of hexane to extract and shacked for 5-10 min. subsequently; the upper phase which included fat was removed. The remained extract was used in rotary evaporator to dry it. Finally the powder was solved in 3mL of acetonitrile and water in 84:16 ratios.

### Measurment of the concentration of extracted T2-toxin

The measurment and evulation of T2-toxin that was extracted from poultry feed samples that measured by ELISA and compared with standard of T2-toxin that obatined from Neogen Kit, after that showed that ratio or value of extracted T2-toxin gave excellent value (infected value) when used this extracted in contaminated diet of poultry.

### Experimental study

### Experiment management

This study was performed by using (100) broiler chickens, they were placed in the animal house in college of Veterinary Medicine, from the period from 28/4/2018 – 11/6/2018. At room 3 x 4 m, this room was prepared before beginning of the experiment which include the following steps

1.The room was washed , cleaned by detol and disinfection by Activator (BenzalKonium chloride 6%) 1 liter /100 liter of water and after that disinfected all the room, after that closed all windows and door for 3 days to obtain a good condition for Poultry housing Hao, *et al* (2014).
2.Floor was covered by a litter containing wood mince ( 7 cm ) thick.
3.Supplied the room by a good quality thermometer for determination of temperature.

4.The room was provided by two 60-watt bulbs.
5.Plastic trays feeders for chickens were supplied in this experiment and then replaced by a metal feeder's 150 cm length in addition to plastic drinkers.

## Diet

All birds were fed daily from one day age to the end of this experiment on the basal diet which composed of Proteins, Corn, Soya bean, Mono Calcium- Phosphate, Lime salt, Methonine, Lysine, Vitamins and minerals (Hilbert *et al.*,2017).

## Health Care program

The broiler chicks were treated from first day to 24 days as protocol that shown below in table (1).

## Experimental design

Taken one hundered broiler chicks in this current experiment and after that was divided into five groups and each group contain tweenty broiler chicks that divided randomely, group one called negative control group while second group was called positive control group and all groups and feeding , type of treated of each group was showed below.

G1: Control negative (-Ve) group Poultry that fed on normal feed.
G2: Control positive (+ve) group poultry fed on contaminted fed by T2 toxin.
G3: Poultry fed on contaminated feed with T2 toxin + Captex T2.
G4: Poultry fed on contaminated feed with T2toxin + Thepax powder.
G5: fed on contaminated feed with T2 toxin + Thepax powder + Captex T2.

## The studied parameters

## Evaluation of Productive performance

## Final body weight

The chickens were weighted in the began of this experiment and in the end of the experiment inorder to obtain final body weight gain and after that was obtained average of final body weight gain according to the following equation:
Final Weight gain = Body weight at the end of the experiment – Body weight at the beginning of the experiment Hellwing,*et al* (2006).

### Feed Conversion Ratio (FCR)

Measuring nourish transformation of every group over the period of experiment was completed according the mathematical statement underneath Parks (2012).

$$\text{Feed conversion ratio} = \frac{\text{average of final feed intake (gm)}}{\text{average of final body weight gain (gm)}}$$

**Haematological parameters**

Samples were collected at 14 th, 21 th and 28 th days, from wing vein under a sterile conditions inorder to avoid any contamination that may be happened while collection of blood from broiler, after that put blood in sterile gel tube to obtain serum for measurement of oxidative stress (GSH, MDA and catalase). According to ISLAM (2017).Oxidative stress Measurments (GSH, MDA and CAT).

## RESULTS

The result of isolation of *F.sporotrichioides*in poultry feed by the surface disinfected grain with 2 % sodium hypochloride solution (NaOCI) showed the most predominant fungus was *F. sporotrichioides*depending on macroscopically,*F. sporotrichioides*was isolated by subculture potato dextrose agar (PDA) and incubation at 25 C for 7 days, the colonies were appeared as profuse mycelia and grow densely and rapidly. The number of Poultry feed samples that was given *F. sporotrichioides* is 42 from 100 samples of Poultry diet.The number and ratio of feed samples that contaminated by this fungus was showed the highest level in ratio and number of *F.sporotrichioides* in Al-median, that was showed a significant increase in *F.sporotrichioides* that isolated and identification in Novmber and December, when collected nine samples during these two months were showed seven positive samples from nine samples so that the highest ratio in this region was showed (77.7%), while during Junuary and February was showed six positive samples from nine samples inorder to the ratio was showed (66.6%), but during March and April were showed four samples positive from eight samples of poultry feed and the ratio was 50%, while in AL-Taji during all months were showed the lowest ratio specially during Junurary ,February, March and April. In AL-Rashydia during all months of this current study was showed the ratio and samples that was showed positive result for this fungus was 50% and all gave four positive poultry feed samples from eight samples.

The result of T2-toxin titer during Novmber and December in Al_median was (176.66 ppb) which the higher value in these months but the lower value in Novmber and December were showed in Abu-Ghraib as (145 ppb), while in Al-Rashydia and Al-Tajee the titer of T2-toxin was (154.67 ppb and 168.67 ppb) respectively. During January and Febuary months T2-toxin was recoded highest level of titer specially in Al-median that express (194.66 ppb) and other places showed abnormal values of T2-toxin titer, therefore during these months T2 was very active, the values of T2 titer in Abu-Ghraib, Al-Rashydia and Al-Tajee (158, 173 and 154 ppb) respectively in Poultry farms of Baghdad province, While the titer of T2 toxin in March and April were showed the lowest titer of this mycotoxin in Abu-Ghraib as (136.34 ppb) but the high value in these months were recorded in Al-Medain (155 ppb), in Al-Rashydia and Al-Tajee (151 and 142.66 ppb) respectively.

The results of means of the GSH at 14 days of poultry age was showed non significantdiferences (P< 0.05) between groups of this experiment, while the means of GSH at 21 days of poultry age was showed a significant differences (P<0.05) specially when compared control negative group (that fed on normal feed) and group of experiment. On the other hands the means of GSH at 28 days of broiler age also showed significant differences (P<0.05) and the level of titer was showed according to the groups of this experiment ( 4.10, 1.8, 3.13, 3.66 and 4.10 Micromole/L), but when compared each group alone according to 14,21,28 days of poultry age the result of means in first group (-Ve) that broiler fed on normal feed was showed no significant differences (P<0.05), but the result of means in second group according to the days of collected blood samples from broiler also showed significant differences (P<0.05) in (+Ve group that poultry fed in this group on contaminated feed by T2-toxin) as values (3.60, 2.53 and 1.80 Mm/L) respectively in 14,21,28 days. In group third (poultry fed on contaminated feed by T2-toxin + Captex t2 as toxin binder) the result of means of GSH in 14,21,28 days of poultry age was showed no significant differencs (P<0.05) and other two groups had also no significant differences between days of GSH that measurment during this current study.The result of means of MDA concentration (Mm/L) in all groups of experiment in 14 days were showed no significant differences (P> 0.05), as values ( 1.33, 1.35, 1.73, 1.93 and 1.60 micromole/L) respectively accroding to the

groups of broiler groups while the result of means of MDA in all groups of poultry experiment during 21 days of boiler age were showed significant differences (P<0.05), as values ( 1.93, 3.63, 3.10, 3.30, 1.53 micromole/L) respectively according to the groups of this experiment. The result of means of MDA enzyme that measurment from serum of broiler chicks in 28 days were showed significant differences (P < 0.05) as values were cleared (1.66, 3.93, 2.16, 1.86 and 1.46 (Mm/L) respectively, according to groups of experiment (G1, G2, G3, G4 and G5).

### And 28 days of Poultry age

The result of means of Catalase enzymes 14 days of broiler age revealed that there was no significant differences (P>0.05). On day 21 there was a significant differences (P < 0.05) in means of Catalase enzyme were reported between the groups (10.53,21.66, 12.86, 11.26 and 10.66 U/ml) according to the groups of this experiment while the result of means of Catalase in 28 days were showed a significanr differences (P < 0.05) and the titer of Catalase in 28 days in group 1 (poultry fed on normal feed) the mean of this oxidative stress enzyme (10.83 U/ml) but the mean in group 2 (Poultry fed on contaminated feed by T2-toxin) as value (19.76 U/ml), in group 3 (Poultry that fed on contaminated by T2-toxin + Captex T2) gave the mean of Catalase concentration (14.83 U/ml), in group 4 (poultry that fed on contaminated feed with T2-toxin + Thepax powder) eventually in group 5 (Poultry that fed on contaminated feed by T2-toxin + Captex T2 + Thepax powder) the result of means of Catalase (10.20 U/ml).

The result of means of final body weight of chicks revealed that there was significant differences (P<0.05) between groups of this current experiment. The mean of final body weight of group 1 (-ve that fed on normal feed) was (1,400 g.), and the mean of final body weight of group 2 (+ve that broiler chicks fed on contaminated feed with T2 toxin) was (1,200 g.), where as the mean of final body weight in group 3 (fed on contaminated feed by T2 + Captex T2 as toxin binder), group 4 (fed contaminated feed by T2 + Thepax ) and group 5 (that fed broiler chicks on contaminated feed by T2 + Captex + Thepax on the same poultry diet), 1,550 g. , 1750g. And 1950g. Respectively according to the groups of this experiment. The FCR in all groups of the experiment was showed significant differences (P<0.05), in group 1 the FCR was (1.845), in group 2 (2.164), where as in group 3 (1.661), in group 4 (1.46) and while in group 5 was (1.312), therefor there was significant differences between groups of the experiment, the excellent result of FCR and final body weight that recoded when used Thepax with captex T2 together in chicks feed contaminated by T2-toxin. The feed intake in all groups of this experiment as same as (50 Kg) for each group of chicks and each chick that intake (2.5 g.) of poultry diet.

## CONCLUSION

### From the present study, we can include the followings

1. The poultry feed exhibated contamination with *Fusarium sporotrichioides* with 42%.
2. During cold climate condition pressed influence the growth of *F.sporotrichioides* in the poultry feed which provide an ideal condition for the isolation of T2-toxin when compared with other climate condition.
3. AL-Madain showed the highest ratio of isolation *F.sporotrchioides* (65.3%), while AL-Taji showed the lowest ratio (24%) of *F.sporotrchioides* isolation.
4. Also, the mean of T2-toxin in poultry feed appeared in AL-Madain in January and February with (194.66 _+ 3.52), while the lower mean of T2 showed in Abu-Ghraib at March and April with (136.34_+1.85).
5. T2- toxin caused a significant decreased (P<0.05) in GSH concentration in the infected group, while there are no significant difference in the treated groups (G3,G4 and G5), when compared with control group due to the effect of Captex T2 and / or Thepax. Where as T2-toxin caused a significant increased (P>0.05) in MDA and CAT concentration in the infected group,but other groups showed no difference in these parameters when compare with control group.

6. The result of means of final body weight revealed there was significant differences (P<0.05) between groups, the highest means appeared in the 5th group while the lower mean showed in the 2nd group.

## DISSCUSION

The results of the present study showed that the isolation of this fungus from the poultry feed samples that was given 42 positive samples from 100 samples so the percentage of *F. sporotrichioides* was 42%, this fungus gave the highest level during cold climate season specially in January and Febraury the finding of this work were in consistent with (Richard *el al.,* 2007). Food safety is an imperative in food production worldwide. Poultry meat, eggs, and poultry products derived from them are crucial in safe food chain. As far as safety is concerned, special attention is directed towards possible contamination of food and poultry feed with fungi and to the risk of mycotoxin contamination (Radmila*et al.,* 2009). Previous studies confirmed the present results by reported that this fungus invade the poultry feed collected from broiler farms in Baghdad province was *Fusarium* specially *F.sporotrichioides* (Shareef, 2010), while Al-Anni, (2008) isolated *Fusarium* from diets of poultry fields of Agriculture College/Baghdad University. Other study in Pakistan revealed that contamination of poultry feed by *Fusarium* species and the most predominant fungus was *F.sporotrichioides* and other species of *Fusarium* that gave T2-mycotoxin.

Another study (Vesna*et al.,* 2011) they determine the *Fusarium* species these fungi incidence in Poultry feeds during a two years period (2007 and 2008) in Belgrade-Zemun, Republic of Serbia they found *Fusarium* (56.09 and 63.40%). Feeds are excellent media for the growth this very dangerous fungus and so, very high standard of hygiene is necessary to avoid feed contamination by this fungus. One of the best ways to control feed contamination and mycotoxin problem is to investigate of these genera of fungi in poultry diets (Stefi*et al.,* 2016). The most commonly used agricultural product for the production of poultry feed includes maize,grains, groud nut, soya, sorghum, wheat, barley etc., these agricultural products are exposed to various toxicogenic fungi both at harvest and storage (Sivakumar*et al.,* 2014). The fungal growth reduced nutritional value and could result in the production of mycotoxins (Frisvad*et al.,* 2006) and allergenic spores (Adhikari*et al.,* 2004) that constitute a risk factor for human and animal health. Fungi are the major contaminants of food and cause rapid quality deterioration (Boysen*et al.,* 2012). The previous study confirmed that the poultry feed were infected with *Fusarium* fungi occur due to the bad environmental condition during the storage may play an important role in the growth of these fungi and these results were in accordance to the finding of the literature (Magan and Aldred, 2007) which reported that climate represents the key agro-ecosystem driving force of fungal colonization and mycotoxin production. The most important parameters in the fungal growth and mycotoxin production are moisture and temperature. Storage temperatures between 25 C and 30 C and a relative humidity of 97% favour the growth of fungi and production of toxins during storage and about 25% of the worlod storages of cereals are affected by moulds every year (Freitas-Silva *et al.,* 2011). As well the insect activities on grains which cause physical damage (Al-Anni, 2008).

The result of T2-toxin titer that was measurment by ELISA was showed highest titer of this toxin in January and February while during November and December the titer of T2-toxin was showed moderate to high, but in March and April the titer of T2-toxin decline gradually accroding to climate conditions, recorded by ( Tangendjaja, *et al.* 2016) we found that the frequency ratio of T2-toxin titer according to climate condition. The LD 50 value of T2 toxin has been determined in some different experiments and has been estimated to 4.97 – 5.25 mg/kg b.w. in 1 –day-old chicks and 2.55 mg/kg b.w. in 7 –day-old chicks. The acute toxic effects developed 4-10 hours after dosing and are described as inappetence, (Pettersson, 1991). In the current study,high ratio of samples contained T2-toxin, which is still lower than that reported in Argentina (74.47%) of pellet and milled feed used for poultry production (Greco *et al*., 2014).The toxicogenic fungal contamination that was given T2-toxin these raw materials occurs during the pre-harvest and/or the post-harvest periods, and the finished feeds are exposed during production, processing, transportation, and storage (Greco *et al*., 2014). It has been observed that molds and mycotoxins presence vary depending on the geographical location and the year (del Pilar Monge *et al.,* 2012). Temperature and humidity play

important roles not only in the development of fungi but also in mycotoxins production(Greco *et al.,* 2014).T-2 is one of the most common and toxic trichothecenemycotoxins, it is an agriculture food contaminant and has been purportedly deployed in chemical warfare (Marin *et al.,* 2013). T-2 toxin has been the most extensively studied trichothecene in poultry. The three trichothecenes, croticin, diacetoxyscirpenol and T-2 toxin, cause oral necrosis and affect body weight gain in growing chicks. At a dietary inclusion rate of 5 µg/g of T-2 toxin a body weight reduction of 24% resulted, The level and incidence of mycotoxin contamination increases after feed is manufactured. Therefore, it is important to keep the time from the manufacture of feed to when it is consumed by the birds to as short as possible. Managemental practices like withdrawal of mycotoxin contaminated feed/feed ingredients or change of feed at the farm could provide partial protection to poultry from the toxicity as well as mycotoxin residues (Patil*et al.,* 2014). ELISA methods are relatively easy and rapid technologies for mycotoxin detection in contaminated feed/food (Asrani*et al.,* 2014).

There was non significant decrease or increase of GSH in 14 days of poultry age, while the means of GSH in 21 and 28 days of poultry age was showed a significant decrease in second group of this experiment when broiler chickens fed on contaminated feed by T2-toxin when compared with control group and other groups of experiment. The decrease in GSH when poultry fed contain high percentage of T2-toxin in diet of broiler these result agree with (Leal *et al.,* 1999) who found a significant decrease in GSH of chickens as result of poultry fed contaminated diet by T2-toxin. From other hand, T2-toxin interferes with all the metabolic processes in the body weight and inhibits protein synthesis. The present data agree with ( Rezar*et al.,* 2007). A delicate balance between antioxidants and prooxidants in cells is an important determinant of various physiological processes and maintenance of this balance is the main aim of so called an integrated antioxidant system built in the animal body. This system was developed during evolution to provide an antioxidant defence and give a chance for animals to survive in oxygenated atmosphere.The increase in MDA enzyme in group two of this experiment as result of broiler feed on infected diet by T2 toxin in 21 and 28 days of poultry age these result agree with (Leal *et al.,* 1999) we found that increase in MDA concentration was induced as well as marked increase in oxidative stress enzyme. (Rezar*et al.,* 2007) they found, that lipid peroxidation as detected by the amount of malondialdehyde increased in poultry but the changes varied by species of birds.The increase in Catalase enzyme in group two of this experiment as result of broiler feed on infected diet by T2 toxin in 21 and 28 days of poultry age as a result of poultry feed on contaminated feed by T2-toxin and these result agree with (He *et al.,* 2012) they found that exposure to T-2 toxin induced an increase in CAT. (Yang *et al.,* 2016) these found significant increase CAT activities in broiler as result of T2-toxin.

The result of means of final body weight that was showed a significant decrease in second group (that fed on contaminated feed by T2-toxin) and the feed conversion ratio was increasing in this group when compared with negative control group and other groups of this experiment, while when use Captex T2 in group 3 (that fed on infected diet by T2-toxin + Captex T2 as toxin binder) was given good final body weight and feed conversion ratio, but in group 4 (broiler fed on infected diet by T2-toxin + Thepax) was given better final body weight and feed conversion ratio when compared with group 2 and 3, while when used Captex T2 and Thepax in group 5 (that poultry in this group fed on contaminated feed by T2-toxin + Captex T2 + Thepax) was showed best final body weight and feed conversion ratio as compared with other groups of this experiment which agree with (Owens and McCracken, 2007) they found that feeding inactivated yeast (Thepax) and toxin binder (Captex T2) to broiler chicks improves body weight gain, feed conversion ratio (FCR) and survival rate. (Fazli*et al.,* 2008) they took about yeast (Thepax) acts as a prebiotic in feed poultry. Yeast is also an excellent source of selenium and chromium; two trace minerals which may have positive effects of broiler health (Celik*et al.,* 2001). It also acts as an antioxidant and its addition in broiler diet improves quality of broiler meat (Zhang *et al.,* 2005). Captex T2 contains a selected source of modified hydrated sodium calcium aluminosilicates; Captex T2 contains organic acid such as Propionic acid in order to control the residual presence of moulds (PERIC *et al* 2015).

## REFERENCES

1. Pleadin, J., Staver, M. M., Vahčić, N., Kovačević, D., Milone, S., Saftić, L., &Scortichini, G. (2015). Survey of aflatoxin B1 and ochratoxin A occurrence in traditional meat products coming from Croatian households and markets. *Food control*, *52*, 71-77.
2. da Rocha, M. E. B., Freire, F. D. C. O., Maia, F. E. F., Guedes, M. I. F., &Rondina, D. (2014). Mycotoxins and their effects on human and animal health. *Food Control*, *36*(1), 159-165.
3. Ismaiel, A., &Papenbrock, J. (2015). Mycotoxins: producing fungi and mechanisms of phytotoxicity. *Agriculture*, *5*(3), 492-537.
4. Qi, T. F., Renaud, J. B., McDowell, T., Seifert, K. A., Yeung, K. K. C., &Sumarah, M. W. (2016). Diversity of mycotoxin-producing black aspergilli in Canadian vineyards. *Journal of agricultural and food chemistry*, *64*(7), 1583-1589.
5. McCormick, S. P., Stanley, A. M., Stover, N. A., & Alexander, N. J. (2011). Trichothecenes: from simple to complex mycotoxins. *Toxins*, *3*(7), 802-814.
6. Wang, Z. L., & Song, J. (2006). Piezoelectric nanogenerators based on zinc oxide nanowire arrays. *Science*, *312*(5771), 242-246.
7. Assi, M., 2017. The differential role of reactive oxygen species in early and late stages of cancer. American Journal of Physiology – Regulatory, Integrative and Comparative Physiology 313: R646-R653.
8. Adhikari, M., Negi, B., Kaushik, N., Adhikari, A., Al-Khedhairy, A. A., Kaushik, N. K., & Choi, E. H. (2017). T-2 mycotoxin: toxicological effects and decontamination strategies. *Oncotarget*, *8*(20), 33933.
9. Zhang, X., Li, C. R., Wang, W. C., Xue, J., Huang, Y. L., Yang, X. X., ... &Qiu, J. F. (2016). A novel electrochemical immunosensor for highly sensitive detection of aflatoxin B1 in corn using single-walled carbon nanotubes/chitosan. *Food chemistry*, *192*, 197-202.
10. Chaudhary, M., &Rao, P. L. (2010). Brain oxidative stress after dermal and subcutaneous exposure of T-2 toxin in mice. *Food and Chemical Toxicology*, *48*(12), 3436-3442.
11. Karlovsky, P., Suman, M., Berthiller, F., De Meester, J., Eisenbrand, G., Perrin, I., ... &Dussort, P. (2016). Impact of food processing and detoxification treatments on mycotoxin contamination. *Mycotoxin research*, *32*(4), 179-205.
12. Vanhoutte, I., Audenaert, K., & De Gelder, L. (2016). Biodegradation of mycotoxins: Tales from known and unexplored worlds. *Frontiers in microbiology*, *7*, 561.
13. Hickert, S., Gerding, J., Ncube, E., Hübner, F., Flett, B., Cramer, B., &Humpf, H. U. (2015). A new approach using micro HPLC-MS/MS for multi-mycotoxin analysis in maize samples. *Mycotoxin research*, *31*(2), 109-115.
14. Leslie, J. F., &Summerell, B. A. (2008). *The Fusarium laboratory manual*. John Wiley & Sons.
15. Joffe, A. Z. (1986). *Fusarium species: their biology and toxicology*. John Wiley & Sons.
16. Hao, G., Chen, H., Du, K., Huang, X., Song, Y., Gu, Z., ... & Chen, Y. Q. (2014). Increased fatty acid unsaturation and production of arachidonic acid by homologous over-expression of the mitochondrial malic enzyme in Mortierellaalpina. *Biotechnology letters*, *36*(9), 1827-1834.
17. Hilbert, M., VAN DE LINDE, I., Lechevestrier, Y., &Koedijk, R. M. (2017). *U.S. Patent Application No. 15/315,184*.
18. Hellwing, A. L. F., Tauson, A. H., &Skrede, A. (2006). Effect of bacterial protein meal on protein and energy metabolism in growing chickens. *Archives of animal nutrition*, *60*(5), 365-381.
19. Parks, J. R. (2012). *A theory of feeding and growth of animals*(Vol. 11). Springer Science & Business Media.
20. Islam, M. T. (2017). Oxidative stress and mitochondrial dysfunction-linked neurodegenerative isorders. *Neurological research*, *39*(1), 73-82.
21. Resanović, R. M., Nešić, K. D., Nesić, V. D., Palić, T. D., &Jaćević, V. M. (2009). Mycotoxins in poultry production. *ZbornikMaticesrpskezaprirodnenauke*, (116), 7-14.
22. Shareef, A. M. (2010). Molds and mycotoxins in poultry feeds from farms of potential mycotoxicosis. *Iraqi Journal of Veterinary Sciences*, *24*(1), 17-25.
23. Al- Anni, F. (2008). Study of the toxicity and pathogenic22. ity of Ochratoxin A in poultry. Msc. thesis, Department of Microbiology University of Baghdad, Iraq.

24. Krnjaja, V. S., Lević, J. T., Stanković, S. Ž., &Stepanić, A. M. (2011). Fusarium species and their mycotoxins in wheat grain. *ZbornikMaticesrpskezaprirodnenauke*, (120), 41-48.
25. Stefi, A. L., Margaritis, L. H., &Christodoulakis, N. S. (2016). The effect of the non ionizing radiation on cultivated plants of Arabidopsis thaliana (Col.). *Flora-Morphology, Distribution, Functional Ecology of Plants*, *223*, 114-120.
26. Yang, J., Li, J., Jiang, Y., Duan, X., Qu, H., Yang, B., ... &Sivakumar, D. (2014). Natural occurrence, analysis, and prevention of mycotoxins in fruits and their processed products. *Critical reviews in food science and nutrition*, *54*(1), 64-83.
27. Adhikari, A., Sen, M. M., Gupta-Bhattacharya, S., &Chanda, S. (2004). Airborne viable, non-viable, and allergenic fungi in a rural agricultural area of India: a 2-year study at five outdoor sampling stations. *Science of the Total Environment*, *326*(1-3), 123-141.
28. Boysen, O., & Matthews, A. (2012). Impact of EU Common Agricultural Policy Reform on Uganda. *Overseas Development Institute Report, London*.
29. Magan, N., &Aldred, D. (2007). Post-harvest control strategies: minimizing mycotoxins in the food chain. *International journal of food microbiology*, *119*(1-2), 131-139.
30. Freitas-Silva, O., &Venâncio, A. (2011). Brazil nuts: benefits and risks associated with contamination by fungi and mycotoxins. *Food Research International*, *44*(5), 1434-1440.
31. Tangendjaja, B., Rachmawati, S., &Wina, E. (2016). Mycotoxin contamination on corn used by feed mills in Indonesia. *Indonesian Journal of Agricultural Science*, *9*(2), 68-76.
32. Pettersson, H. (1991). Nivalenol production byFusariumpoae. *Mycotoxin research*, *7*(1), 26-30.
33. Greco, M. V., Franchi, M. L., Rico Golba, S. L., Pardo, A. G., & Pose, G. N. (2014). Mycotoxins and mycotoxigenic fungi in poultry feed for food-producing animals. *The Scientific World.*
34. del PilarMonge, M., Magnoli, C. E., &Chiacchiera, S. M. (2012). Survey of Aspergillus and Fusarium species and their mycotoxins in raw materials and poultry feeds from Córdoba, Argentina. *Mycotoxin research*, *28*(2), 111-122.
35. Marin, S., Ramos, A. J., Cano-Sancho, G., &Sanchis, V. (2013). Mycotoxins: Occurrence, toxicology, and exposure assessment. *Food and Chemical Toxicology*, *60*, 218-237.
36. Asrani, R. K. (2014). Mycotoxicosis and its control in poultry: A review. *Journal of Poultry Science and Technology*, *2*(1), 1-10.
37. Patil, R. D., Sharma, R., &Asrani, R. K. (2014). Mycotoxicosis and its control in poultry: A review. *Journal of Poultry Science and Technology*, *2*(1), 1-10.
38. Leal, M., Shimada, A., Ruíz, F., & de Mejía, E. G. (1999). Effect of lycopene on lipid peroxidation and glutathione-dependent enzymes induced by T-2 toxin in vivo. *Toxicology Letters*, *109*(1-2), 1-10.
39. Rezar, V., Frankič, T., Narat, M., Levart, A., &Salobir, J. (2007). Dose-dependent effects of T-2 toxin on performance, lipid peroxidation, and genotoxicity in broiler chickens. *Poultry science*, *86*(6), 1155-1160.
40. He, S. J., Hou, J. F., Dai, Y. Y., Zhou, Z. L., & Deng, Y. F. (2012). N-acetyl-cysteine protects chicken growth plate chondrocytes from T-2 toxin-induced oxidative stress. *Journal of Applied Toxicology*, *32*(12), 980-985.
41. Yang, L., Yu, Z., Hou, J., Deng, Y., Zhou, Z., Zhao, Z., & Cui, J. (2016). Toxicity and oxidative stress induced by T-2 toxin and HT-2 toxin in broilers and broiler hepatocytes. *Food and Chemical Toxicology*, *87*, 128-137.
42. Owens, B. and McCracken, K.J. 2007. A comparison of the effects of different yeast products and antibiotic on broiler performance. Br. Poult. Sci. 48: 49-54.
43. Celik, K., Denli, M., Ertürk, M., Öztürkcan, O., & Doran, F. (2001). Evaluation of dry yeast (Saccharomyces cerevisiae) compounds in the feed to reduce aflatoxin b1 (AFB1) residues and toxicity to japanese quails (Coturnixcoturnix japonica). *Journal of Applied Animal Research*, *20*(2), 245-250.
44. Qi, H., Zhang, Q., Zhao, T., Chen, R., Zhang, H., Niu, X., & Li, Z. (2005). Antioxidant activity of different sulfate content derivatives of polysaccharide extracted from Ulvapertusa (Chlorophyta) in vitro. *International journal of biological macromolecules*, *37*(4), 195-199.
45. Peric, L., Steiner, T., Djukic-Stojcic, M., Bjedov, S., & Milosevic, N. (2015). Effects of phytogenic feed additive and enzyme on growth performance of broilers fed diets with reduced energy concentrations.

**Table 1. Health care program**

| Age | Health care and Vaccination |
|---|---|
| One day | Water contain sugar 50 gm/l, Newcastle vaccine (CEVAC) vitapest L by dropping in eyes and nose |
| 2 | Vitamin C 0.5 gm/l |
| 7 | Infectious Bursal disease vaccine (CEVAC) by drinking water |
| 8 | Vitamin C 0.5 gm/l |
| 14 | Infectious Bursal disease vaccine (Kindi Company) by drinking water |
| 15 | Vitamin C 0.5 gm/l |
| 23 | Infectious Bursal disease vaccine (Kindi Company) by D.W |
| 24 | Vitamin C 0.5 gm/l |

**Table 2. The number and ratio of Poultry feed samples that gave *F. sporotrichioides***

| Type of fungus | Number of isolates | Percentage |
|---|---|---|
| *F. sporotrichioides* | 42 | 42% |

**Table 3. Show the number and ratio of Poultry feed samples that contaminated with *F. sporotrichioides* according to months**

| Number of *F.sporotrichioides* according to months / Name of places | No. Of *F.sporotrichioides* during Nov.&Dec. | No.Of *F.sporotrichioides* during Jun.&Feb. | No.Of *F.sporotrichioides* during Mar.&Api. |
|---|---|---|---|
| AL-Median | 7/9 (77.7%) | 6/9 (66.6%) | 4/8 (50%) |
| Abu-Ghraib | 2/9 (22.2%) | 4/9 (44.4%) | 1/8 (12.5%) |
| AL-Rashydia | 4/8 (50%) | 4/8 (50%) | 4/8 (50%) |
| AL-Taji | 2/8 (25%) | 3/8 (37.5%) | 1/8 (12.5%) |

**Table 4. Measure of T2-toxin by ELISA technique (type of samples poultry feed).**

| Mean of T2 toxin titer according to months / Name of Place | Mean of T2-toxin titer during Novmber and December (ppb) | Mean of T2-toxin titer in January and Febuary (ppb) | Mean of T2-toxin titer in March and April (ppb) |
|---|---|---|---|
| AL_Median | 176.66±1.76 Ba | 194.66±3.52 Aa | 155.00±7.63 Ca |
| Abu-Ghraib | 145.00±7.63 ABc | A158.00±11.54bc | 136.34±1.85 Bb |
| AL_Rashydia | 154.67±5.69 Bbc | A173.00±4.72b | 151.00±2.64 Bab |
| AL_Tajee | 168.67±3.17 Aab | AB154.00±4.00c | 142.66±2.90 Bab |
| LSD | 16.105 | | |
| Means with a different small letter in the same column significantly different (P<0.05)<br>Means with a different capital letter in the same row significantly different (P<0.05) | | | |

**Table (4 – 4). Means of GSH concentration (Mm/L) in all groups at 14, 21 and 28 days of experiment**

| Time / Groups | 14 days | 21 days | 28 days |
|---|---|---|---|
| Group 1 (G1) – Ve Feed on normal feed | 3.73±0.17 Aa | 4.26±0.17 Aa | 4.10±0.40 Aa |
| Group 2 (G2) + Ve Feed on contaminated feed with T2 toxin | 3.60±0.20 Aa | 2.53±0.17 ABb | 1.80±0.34 Bb |
| Group 3 (G3) feed on contaminated feed with T2 toxin + Captex T2 | 3.40±0.30 Aa | 3.10±0.15 Ab | 3.13±0.08 Ab |
| Group 4 (G4) feed on contaminated feed with T2 toxin + Thepax powder | 3.13±0.14 Aa | 3.30±0.16 Ab | 3.66±0.32 Aab |
| Group 5 (G5) feed on contaminated feed with T2 toxin + Thepax powder + Captex T2 | 3.53±0.13 Aa | 3.80±0.52 Ab | 4.10±0.36 Aa |
| LSD | 0.7919 | | |
| Means with a different small letter in the same column significantly different (P<0.05) Means with a different capital letter in the same row significantly different (P<0.05) | | | |

**Table (4 – 5): Mean of MDAconcentrarion in all groups at14, 21 and 28 days of experiment**

| Time / Groups | 14 day | 21 day | 28 day |
|---|---|---|---|
| Group 1 (G1) – Ve Feed on normal feed | 1.33±0.13 Aa | 1.93±0.29 Ab | 1.66±0.08Ab |
| Group 2 (G2) + Ve Feed on contaminated feed with T2 toxin | 1.35±0.06 Ba | 3.63±0.44 Aa | 3.93±0.81 Aa |
| Group 3 (G3) feed on contaminated feed with T2 toxin + Captex T2 | 1.73±0.08 Ba | 3.10±0.15 Aa | 2.16±0.23 Bb |
| Group 4 (G4) feed on contaminated feed with T2 toxin + Thepax powder | 1.93±0.14 Ba | 3.30±0.17 Aa | 1.86±0.12 Bb |
| Group 5 (G5) feed on contaminated feed with T2 toxin + Thepax powder + Captex T2 | 1.60±0.11 Aa | 1.53±0.20 Ab | 1.46±0.17 Ab |
| LSD | 0.8259 | | |
| Means with a different small letter in the same column significantly different (P<0.05) Means with a different capital letter in the same row significantly different (P<0.05) | | | |

**Table (4 – 6): Mean of catalase enzyme concentration (U/ml) in all groups at 14, 21 and 28 days of experiment.**

| Time / Groups | 14 day | 21 day | 28 day |
|---|---|---|---|
| Group 1 (G1) – Ve Feed on normal feed | 11.66±0.66 Aa | 10.53±0.24 Ab | 10.83±0.27 Ac |
| Group 2 (G2) + Ve Feed on contaminated feed with T2 toxin | 10.66±0.88 Ba | 21.66±2.33 Aa | 19.76±1.48 Aa |

| | | | |
|---|---|---|---|
| Group 3 (G3) feed on contaminated feed with T2 toxin + Captex T2 | 11.86±0.42 Aa | 12.86±0.96 Ab | 14.83±1.82 Ab |
| Group 4 (G4) feed on contaminated feed with T2 toxin + Thepax powder | 10.20±0.50 Aa | 11.26±0.72 Ab | 12.66±0.88 Abc |
| Group 5 (G5) feed on contaminated feed with T2 toxin + Thepax powder + Captex T2 | 11.00±0.79 Aa | 10.66±0.72 Ab | 10.20±0.26 Ac |
| LSD | 3.0049 | | |
| Means with a different small letter in the same column significantly different (P<0.05)<br>Means with a different capital letter in the same row significantly different (P<0.05) | | | |

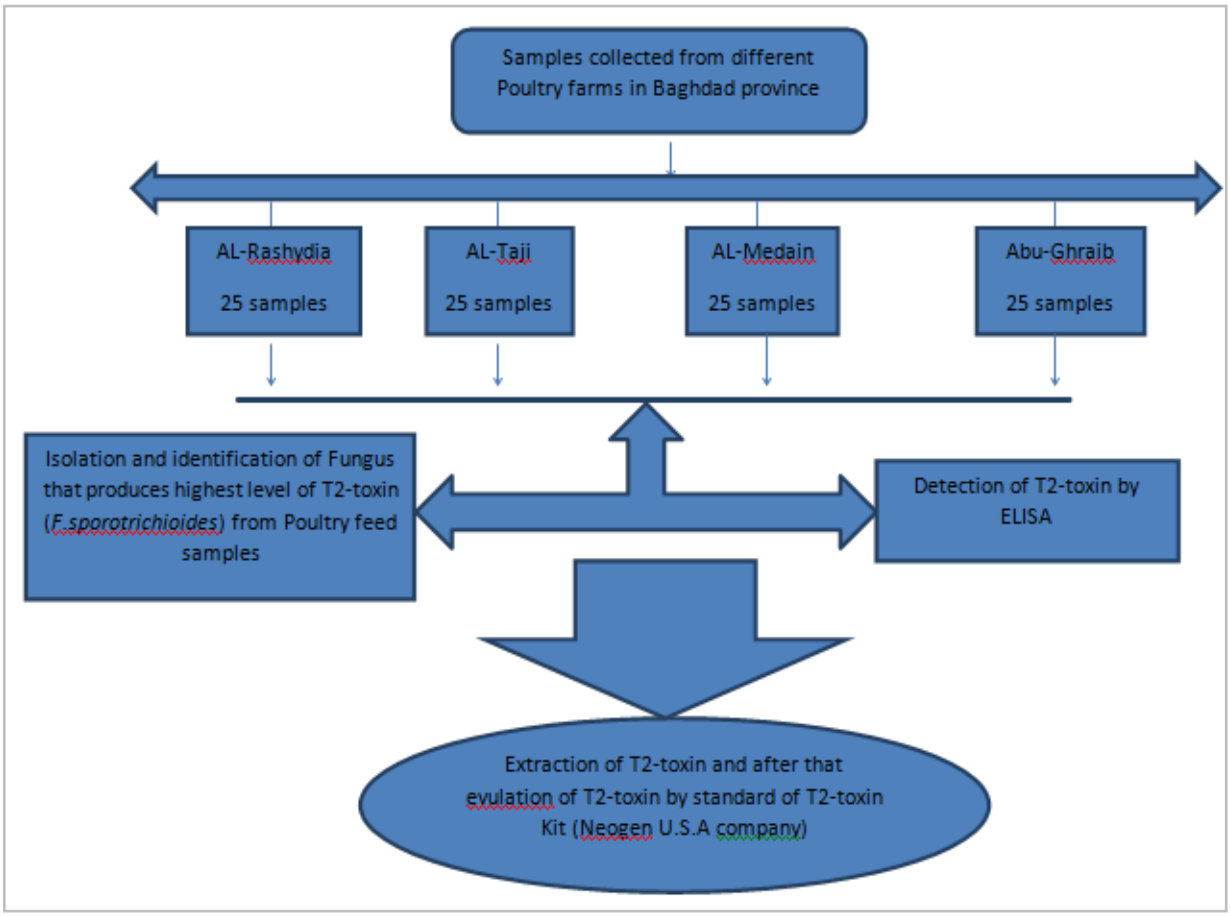


**Figure 1.method of collection of samples**

*Indian Journal of Natural Sciences* www.tnsroindia.org.in ©IJONS

*Vol. 9 / Issue 50 /October 2018* *International Bimonthly* *ISSN: 0976 – 0997*

RESEARCH ARTICLE

# Diagnostics Plasma for Rhodamine-B Using Laser-Induced Breakdown Spectroscopy

Adel Ch. Majeed[1]*and Ali A-K. Hussain[2]

[1]Ministry of Education, General Directorate of Education of Baghdad, Iraq.
[2]Department of Physics, College of Science, University of Baghdad, Iraq.

Received: 20 July 2018 Revised: 22 Aug 2018 Accepted: 25 Sep 2018

***Address for Correspondence**
**Adel Ch. Majeed**
Ministry of Education,
General Directorate of Education of Baghdad,
Iraq.
Email : adil.jasib@gmail.com, draliakh97@scbaghdad.edu.iq



## ABSTRACT

Diagnostics plasma for Rhodamine-B dye have been investigated using Laser-Induced Breakdown Spectroscopy (LIBS). The spectroscopic emission patterns at different laser pulse energies (600, 700, 800 and 900) mJ were recorded. There are many peaks corresponding to atomic and ionic lines for Carbon (C I, C II). It was found that the peaks intensities increase with increasing laser energies. The values of plasma temperature ($T_e$), plasma density ($n_e$), Debye length ($\lambda_D$), plasma frequency ($f_p$) and Debye number ($N_d$) for laser induced plasma were calculated from different laser energies employing lines parameters from the NIST of six selective ionic lines for spectroscopic pattern. The effect of different laser pulse energies on the ($T_e$) and ($n_e$) was examined. It was noticed that ($T_e$) and ($n_e$) increases with increasing of laser energy.

**Keywords**: LIBS, Rhodamine-B, Diagnostics plasma.

## INTRODUCTION

Laser-induced breakdown spectroscopy (LIBS) is one of the simplest technique for experimentally spectroscopic analytical [1]. LIBS also called laser-induced plasma spectroscopy (LIPS) [2]. Indeed, plasma could be generated at the sample surface, which makes it a distinguishable method from other techniques. Where, the sample does not need to be transported into the plasma source because the ablation and excitation processes are carried out by the laser pulse in a single step [3]. Furthermore, LIBS is a promising method in analytical chemistry, since it enables direct analysis of solids, without any chemical preparation [4]. LIBS technique typically consists of PLD system and a wide range spectral and spectrometer with a high sensitivity, fast response rate, time gated detector, which is coupled to a computer that can rapidly process and interpret the obtained data [1]. Nd:YAG laser is the most common laser

system used in LIBS is due to the easily configured to produce the power levels required for formation of induced plasma [5]. High-energy laser pulse of LIBS employs as the vaporization, atomization, and excitation source to create a high-temperature micro- plasma at the surface of the target. Each element has its unique emission lines as the "fingerprint" of the element [2]. The formation of laser induced plasma on a metal target in an ambient gas depends on different parameters like laser wavelength, laser power density, surface state and nature, gas pressure and nature, and interaction geometry [1]. Many advantages of LIBS are , multi-element detection capability, Rapid or real-time analysis, no sample preparation, It has versatile ability to sample gases, liquids, and solids equally well, can detect a wider range of elements [6], can be applied for analysis in-situ, can be carried out without physical contact with the examined sample [7].LIBS setup can be very simple. This simplicity allows being portable, the level of expertise needed to operate can be minimized easily with LIBS, the software can be easily designed to allow collected data quickly. However; with the speed of response LIBS does not sacrifice accuracy [8].

Briefly, there are two main steps leading to breakdown. First, there is a generation of a few free electrons which play a role of initial receptors of energy through three body collisions with photons and neutrals. Second, there is avalanche ionization in the focal region caused by collisions, ionization, more electrons, and energy absorption [9]. LIBS have been used in many applications; mainly due to its flexibility [10]. Field portable LIBS systems have been shown to be able to detect hazardous materials including bioaerosols [11]. LIBS has been identified along with Raman spectroscopy as a fundamental, next-generation instrument for characterization of mineralogical and organic material on expeditions on the Martian surface [12]. In laboratory uses range from industrial use (e.g. as metallic alloy composition measurements, steel and glass melt testing, etc. [13], [14] to detection of bacteria and other pathogens, LIBS can be used to discriminate between different strains of the same bacteria [15].Although, the organic dyes will cause serious environmental and biological problems, even capable to induce irritation to the skin, eyes, Rhodamine B (RhB) is one of the most commonly dyes, widely used industrial purposes, such as printing and dyeing in textile, paper, paints, leathers etc. As a result of decomposition with superior activity, the present promising application for the organic dye is photocatalysts based on semiconductor heterogeneous photocatalysis [16]. When it used as a laser dye Rhodamine B is tunable around 610 nm [17] The fluorescence yield is temperature dependent [18]. Its luminescence quantum yield is 0.65 in basic ethanol [19].

## MATERIALS AND METHODS

### Materials

Pure Rhadomine-B (99%) was purchased from MERCK company, appearance red to violet powder, Chemical formula $C_{28}H_{31}ClN_2O_3$ and Molar mass 479.02 $g{\cdot}mol^{-1}$

### Experimental Setup

The set-up consists of three main sections: PLD setup, plasma chamber and Spectrometer as well as the optical fiber were used for studying the plasma diagnostic, a schematic diagram illustrate the experimental setup as shown in Fig. 1.Nd:YAG laser (Huafei Tongda Technology–Diamond-288 pattern EPLS) is used in the present work. Table 3. Shows the main laser technical parametersFor the purpose of oxidizing target materials, PLD has been done inside the vacuum chamber at pressure 2.5 x $10^{-2}$ mbar. Nd: YAG laser beam is focused through Pyrex glass window into the vacuum chamber and impact the surface of the target with angle $45^0$ to the normal of the surface.

### Step of Libs Working

The step of LIBS working as follows

- Samples preparation was introduced the form of pellets. Pressing by hydraulic press operating (6-8) bar for 15min, usually 2 gm weigh entails pellet of 20 mm in diameter and approximately 5 mm of thickness.
- A small amount of ablating is produced when the sample was exposed to laser radiation and creates a super-heated plasma ionizing in the surface of the element. The excited atoms eventually de-excite and give off photons as they decay to their ground states.
- The optical fiber used to collect the light produced by the ablated plasma (it was set at an angle of about 45° to the laser beam axis to avoid splashing) and then carried on the entrance slit of the high resolution spectrometer responds to a wavelength between (200 – 900) nm with 3648 pixels.
- Then the spectrum was analyzed and compared with National Institute of Standards and Technology (NIST) data base [20] and evaluate the plasma parameters.

## RESULTS AND DISCUSSION

Figure 2 shows the spectroscopic patterns for emission from Laser Induced Plasma (LIP) at different pulse energies (600, 700, 800 and 900) mJ compared with atomic and ionic lines for Carbon (C I, C II) for Rhodamine-B [21]. There are many peaks corresponding to C II with some peaks corresponding to C I .It can be noticed that the peaks intensities increase with increasing laser energies as a result of increasing number of photons that excited atoms and then emissions with more photons by return to their stable levels The values of electron temperature ($T_e$) were calculated by Boltzmann Plot using the intensities of six CII lines for spectroscopic pattern samples with different laser energies, employing these lines parameters from the NIST [22] as shown in Figures 3 using the selected ionic lines for Rhodamine-B. The electron temperature ($T_e$) was calculated using the relation between $Ln\left(\frac{I_{ji}\lambda_{ji}}{hcg_jA_{ji}}\right)$ versus upper energy level ($E_j$). The equations of fitting lines were shown in the figures. The values of $T_e$ equal to the inverse of the slope for the best line fitting. Figure 4 illustrates the 656.28 nm CII peak profile for Rhodamine-B using different laser energies. The full width at half maximum ($\Delta\lambda$) were found by using Gaussian fitting, which used to calculate electron density at different laser energy using Stark Effect depending on the standard values of broadening for this line ($\omega_m$= 1.11 Å for C II peak $\lambda$=657.805 nm) [23]. It can be seen that the full width increase with increasing laser energy, indicates on increasing plasma density Table 2 shows the calculated values of plasma temperature ($T_e$), plasma density ($n_e$), Debye length ($\lambda_D$), plasma frequency ($f_p$) and Debye number ($N_d$) for laser induced plasma from Rhodamine-B targets using different laser energies. The variation of electron temperature ($T_e$) and electron density ($n_e$) with laser energy for the four samples were illustrated in figure 5. These figure showed that $T_e$ increases with increasing laser energy as a result of increasing energy transferred to electrons from photons. This increment cause to increase the $n_e$ due to increasing the probability of ionization collisions, which depend mainly on electron temperature [24]. At high laser energy $n_e$ being near stable as a result of reducing the ionization cross section.

## REFERENCES

1. Anusha Keloth, "Laser Induced Breakdown Spectroscopy (LIBS) and Time-Resolved Studies of Copper Plasma Excited By Nanosecond and Femtosecond Laser Pulses," Cochin University of Science and Technology, 2012.
2. Ningfang Yang, "Elemental Analysis of Soils Using Laser-Induced Breakdown Spectroscopy ( LIBS )," University of Tennessee - Knoxville, 2009.
3. E. M. Rodriguez Celis, "Laser Induced Breakdown Spectroscopy as a tool for discrimination and quantitative characterization of glass for forensic applications," 2009: 1–162.
4. D. A. Cremers, L. J. Radziemski, and John Wiley & Sons., Handbook of laser-induced breakdown spectroscopy. John Wiley, 2006.
5. W. Pierce et al., "Field-testing for environmental pollutants using briefcase sized portable LIBS system," 3rd Int. Conf. Laser Induc. Plasma Spectrosc. Appl., 2004;3,:1–14.
6. A. Sarkar, "Laser Induced Breakdown Spectroscopic Studies for Material Characterization," 2010:228.

7. N. M. Shaikh, B. Rashid, S. Hafeez, Y. Jamil, and M. A. Baig, "Measurement of electron density and temperature of a laser-induced zinc plasma," J. Phys. D. Appl. Phys., 2006;39:1384.
8. D. A. Cremers, Handbook of Laser-Induced Breakdown Spectroscopy. USA: Wiley, 2013.
9. L. M. C. S. and F. B. G. Celio Pasquini, Juliana Cortez, Laser Induced Breakdown Spectroscopy, Cambridge University Press, 2007;18.
10. A. W. Miziolek, V. Palleschi, and I. Schechter, Laser Induced Breakdown Spectroscopy. Cambridge University Press, 2006.
11. C. A. Munson, F. C. De Lucia, T. Piehler, K. L. McNesby, and A. W. Miziolek, "Investigation of statistics strategies for improving the discriminating power of laser-induced breakdown spectroscopy for chemical and biological warfare agent simulants," Spectrochim. Acta - Part B At. Spectrosc., 2005; 60:1217–1224.
12. F. R. Pérez and J. Martinez-frias, "Raman spectroscopy goes to Mars," Spectrosc. Eur.,2006; 18:18–21.
13. I. V. Cravetchi, M. Taschuk, Y. Y. Tsui, and R. Fedosejevs, "Scanning microanalysis of Al alloys by laser-induced breakdown spectroscopy," Spectrochim. Acta - Part B At. Spectrosc., 2004;59:1439–1450.
14. M. P. Mateo, S. Palanco, J. M. Vadillo, and J. J. Laserna, "Fast Atomic Mapping of Heterogeneous Surfaces Using Microline-Imaging Laser-Induced Breakdown Spectrometry," Appl. Spectrosc., 2000;54:1429–1434.
15. F. C. DeLucia et al., "Laser-induced breakdown spectroscopy (LIBS): a promising versatile chemical sensor technology for hazardous material detection," IEEE Sens. J., 2005;5:681–689.
16. R. Ameta and S. C. Ameta, Photocatalysis: principles and applications. CRC Press, 2017.
17. R. F. Kubin and A. N. Fletcher, "Fluorescence quantum yields of some rhodamine dyes," J. Lumin.,1982; 27:455–462.
18. T. Karstens and K. Kobs, "Rhodamine B and rhodamine 101 as reference substances for fluorescence quantum yield measurements," J. Phys. Chem., 1980;84:1871–1872.
19. K. G. Casey and E. L. Quitevis, "Effect of solvent polarity on nonradiative processes in xanthene dyes: Rhodamine B in normal alcohols," J. Phys. Chem., 1988;92: 6590–6594.
20. M. Ruiz et al., "Characterization of a laser plasma produced from a graphite target," in Journal of Physics: Conference Series, 2014;511: 012064.
21. J. E. Sansonetti and W. C. Martin, "Handbook of Basic Atomic Spectroscopic Data," Am. Inst. Phys., 2005;34: 4.
22. Y. Ralchenko, "NIST atomic spectra database," Mem. S.A.It. Suppl., 2005;8: 96–102.
23. A. Lesage, "Experimental Stark Widths and Shifts for Spectral Lines of Neutral and Ionized Atoms," 2002;31: 106-115.
24. N. S. J. Braithwaite, F. Hall, and B. Hill, "Introduction to gas discharges," Plasma Sources Sci. Technol., 2000;9:517–527.

**Table 1. Main laser technical parameters**

| Laser model | Q-switched Nd: YAG Laser first Harmonic oscillator (F H O) |
|---|---|
| Laser wavelength | (1064) nm |
| Pulse energy | (10-2000) mJ |
| Repetition Frequency | (1-10) Hz |
| laser pulse duration | 9 ns. |
| Cooling method | inner circulation water cooling |

**Table 2. plasma parameters from Rhodamine-B targets at different laser energies**

| Laser Energy (mJ) | $T_e$ (eV) | FWHM (nm) | $n_e \times 0^{17}$ ($cm^{-3}$) | $f_p \times 10^{12}$(Hz) | $\lambda_D \times 10^{-}$(cm) | $N_d$ |
|---|---|---|---|---|---|---|
| **600** | 8.302 | 0.900 | 5.797 | 600 | 2.812 | 54 |
| **700** | 9.008 | 1.100 | 7.086 | 700 | 2.649 | 55 |
| **800** | 9.548 | 1.200 | 7.730 | 800 | 2.611 | 58 |
| **900** | 9.700 | 1.250 | 8.052 | 900 | 2.579 | 58 |

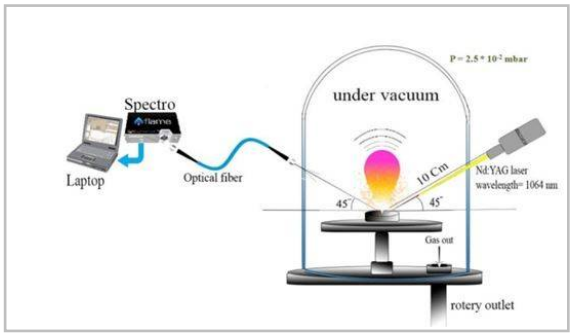


**Figure 1. Schematic of the experimental setup**

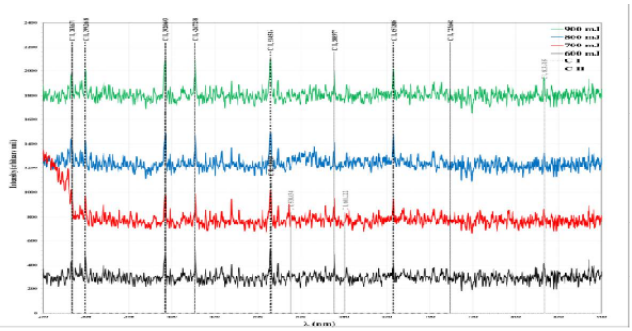

**Figure 2. Plasma emission patterns produced by LIP from Rhodamine-B target with different laser energies**

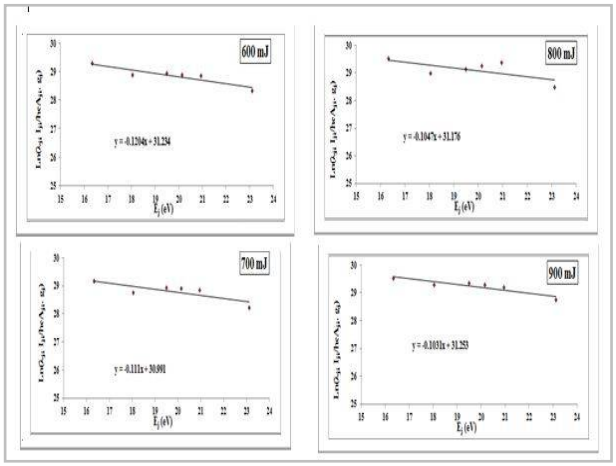


**Figure 3. Boltzmann plot for CII peaks using Rhodamine-B target at different laser energies.**

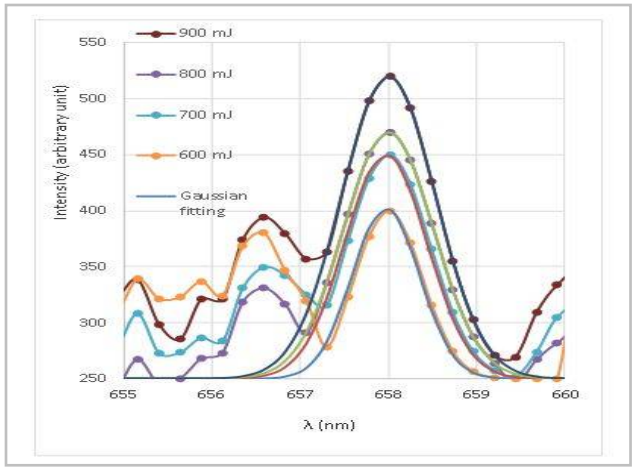


**Figure 4. Gaussian fitting for 657.8 nm C II peak emitted from Rhodamine-B targets at different laser Energies**

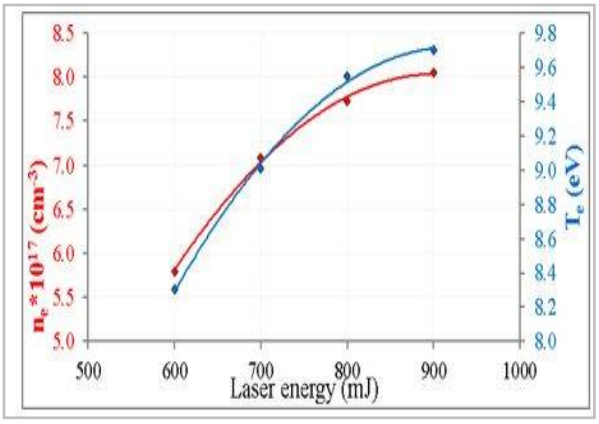


**Figure 5. variation of electron density and plasma temperature with laser energy for Rhodamine-B sample**

*Indian Journal of Natural Sciences* www.tnsroindia.org.in ©IJONS

*Vol. 9 / Issue 50 /October 2018* *International Bimonthly* *ISSN: 0976 – 0997*

RESEARCH ARTICLE

# Synthesis of Conducting Polythiophene, Multi-Walled Carbon Nanotubes Composites

Fatin A. Jassem*, Ahmed Abbas Hassan, and Muayed Khallel Ibrahim

Department of Physics, College of Science, University of Baghdad, Baghdad, Iraq.

Received: 21 July 2018 Revised: 24 Aug 2018 Accepted: 26 Sep 2018

***Address for Correspondence**
**Fatin A. Jassem**
Department of Physics,
College of Science,
University of Baghdad,
Baghdad, Iraq.
Email : fatin_adnan90@yahoo.com, ahmedabhasan27@yahoo.com, muayedalmuksusi@yahoo.com



## ABSTRACT

Conducting polythiophene (PTh)/multi-wall carbon nanotubes (MWCNTs) composites were synthesized by chemical oxidative polymerization method,Using NaClO4 as oxidant.The physical characterizations of the synthesized PTh nanoparticles were studied by Fourier transform infrared Spectroscopic (FTIR), and scanning electron microscopy (SEM). The resulting cable like morphology of the composite (MWCNTs – PTh) structures was characterized with elemental analysis;scanning electron microscopy (SEM) analysis revealed that the SWNT–PTh composites were core (MWCNTs) and shell (PTh) hybrid structures. Fourier transform infraredSpectroscopic analysis data for the composites were almost identical to those for PTh, supporting the idea that MWCNTs served as templates in the formation of a coaxial nanostructure for the composites, and also showed that the MWCNTs were modified by conducting PTh with an enhancement of various properties.

**Keywords:** conducting polymers; core-shell polymers; SEM; Nan composites; polythiophene; multi-wall carbon nanotubes,Optical Energy Gap**,** FTIR.

## INTRODUCTION

Since the first report on the electrochemical synthesis of polythiophene in 1981 polythiophene (PT) and its derivatives have been widely studied because of their good electrical properties and possible applications[1]. Polythiophenes with highconductivity have been prepared in anhydrous aprotic solvents of high dielectric constant and low nucleophility, such as acetonitrile and benzonitrile The presence of water causes the incorporation of carbonyl groups into the structure of the polymer [2], whereas its beneficial effect in trace amounts has not yet been confirmed. The synthesis conditions and the nature of a dopant anion strongly affect the morphology and properties of the material.

After the discovery of carbon nanotube (CNT) by Iijima's groups [3], single- and multi-walled carbon nanotube have been of great interest because of their unique structural, electrical and mechanical properties, as well as their potential applications in the fields including material chemistry [4–5], nanoscale devices field emission and scanning probe microscopy [6].Various polymers were applied to CNT for yielding CNT–polymer hybrid composites, which exhibit better dispersion in polymer matrix and enhance the properties of polymer composites like Young's modulus, tensile strength, electrical conductivity, solubility and so on. Ajayan et al. [7]Among the conjugated polymers, polythiophene (PTh) is one of the most studied polymers due to its flexibility, ease of doping, and good thermal and electrical stability that exhibit some unique advantages of PTh for the development of various applications [8]. PTh in both undoped and doped states have been studied for various applications, including organic field effect transistor, solar cells, sensors, electro chromic devices, and light emitting diodes .The important factors in these considerations are environmental stability in the presence of oxygen or moistur and easy control of electrical and optical properties [9].

## MATERIALS AND METHODS

The emploied materials and chemicals and their companies were listed in table (1):

### Preparation of Polythiophene Pure Solution

A solution of the polythiophene were prepared using (2ml) of Thiophene monomer and(0.8 gm) of Sodium perchlorate as a oxidized, in the presence of (50 ml) acetonitrile used as a solvent,Sodium perchlorate was solvent in the acetonitrile thenis addedThiophene monomer then are obtainedWithout colorsolutionsusing for sample preparation, one sample of this quantity can be obtained at 20 ° Cand 5 volts with intervals ranging from (5-10) minutesshown in table(2).

#### Preparation of Polythiophene /fMWCNTs Solution

After preparationthe polythiophene purewere mixed from fMWCNTs (0.01, 0.03 and 0.07) % with the compound solutionthen are obtained black colorsolutions,using for sample preparationone sample per concentration can obtainedat 20 ° C and 5 voltswith intervals ranging from (10-15)minuteshown in table (2).

#### Characterization

The morphology of the bulk samples was observed by scanning electron microscope (Hitachi FE-SEM model Inspect S50), Fourier-transform infrared spectra (FT-IR Shimadzu FTIR-8400S) and UV-visible-NIR Spectrometer (Shimadzu 1800).

## RESULTS AND DISCUSSION

#### FTIR Spectra

The chemically prepared PTh and PTh/MWCNT nanocomposites films with loaded with various ratios of MWCNT deposited on ITO glass substrate were analysed by FT-IR spectroscopy by making pellets with KBr are shown in Fig. the FT-IR spectrum of the PTh/MWCNT sample was shown peaks at 3423, 2928, 1721, 1637,1500, 784 , 692 and 600 $cm^{-1}$respectively [10]the region from 600-1500 $cm^{-1}$is a finger print region for PTh [11] the peaks at 1090-2928 $cm^{-1}$are low intensity peaks attributed to aromatic C-H stretching vibrations and C=C characteristic band 1637 $cm^{-1}$,the C-S bending mode has been identified at approximately 784 $cm^{-1}$[10] and C=O characteristic band 1721 $cm^{-1}$,the band at 3423$cm^{-1}$ originated from O–H stretching of water in KBr [11] The PTh/MWCNT composite shows almost the same

position of the peaks in a range of 600 -3423 cm-1. The ring stretching and deformation modes are having a minor shift in the peaks because of polaron/π transition interaction between the PTh and SWCNT surface. Results of the FTIR studies clearly indicated the polymerization of the monomer

### Field Emission-Scanning Electron Microscopy (FE-SEM)

FE-SEM observation can provide morphological information of many specimens of PTh/fMWCNT using Hitachi FE-SEM model Inspect S50 ,the magnification in the zoom ranges is (25-20000 )X. the acceleration voltage applied to the electron speed can be varied from (1-30) kV The FESEM micrographs of PTh/MWCNTs nan composites with various concentrations of SMCNTs suspended in the polymerization electrolyte on ITO substrate and interactive 3D surface of films. The polythiophene-MWCNT nanocomposites were subjected to scanning electronmicroscopy (SEM) to study the morphological features of the nanomaterial; The SEM image of pure PTh shows a granular structure [10] Shown in Fig (a) whereas the polythiophene-MWCNT composite fiber like nanostructure shown in Fig (b) [12-13]. Multiwalled carbon nanotubes (MWCNT) have shown a typical nano fibrous morphology. The fibre like morphology of nanocomposite materials could be attributed to the template effect of the carbon nanotube on the growing chain of polythiophene. [14]

### The Optical Energy Gap for PTh and (PTh/MWCNT)

The optical energy gap (Eg) for PTh and ( PTh/MWCNT)nancompositeshas been determined. A plot of $(\alpha h\nu)^2$versus $(h\nu)$ and itsextrapolation of the lineplotted to the $h\nu$ axis gives the energy bandgap show in Fig. respectively show the variation of $(\alpha h\nu)^2$versus $(h\nu)$ of composites samples prepared at at 20 ° C.Theplot is indicating the direct band gap nature of the polymer. The addition of MWCNT caused to shift the absorption edge to law energy side in the first stage , but continues addition of MWCNT caused shift to high energy side generally, the optical energy gap decreased by the effect of creation of localized states in the band gap which lead to visual decrease of energy gap energy[15].sometimes optical energy gap values increase with increasing the weight percentages of MWCNTs . This increasing is due to creation exciton (pair electron hole) between valance and conduction band this lead to increase the optical energy gap.[16]

## CONCLUSION

1. 1-FTIR spectrums analysis emphasized that there was changes , in structures, tacticity and geometry of PHT accompanied the change in doping ratio and doping with different additives.
2. Decreassing of temperature increasing optical energy gap for neat PTh and composites samples.
3. Optical energy gap changes according to type of dopant material.
4. The energy gap decrease as CNT added to the host polymer and then return to shift to higher energy for law preparation temperature while the energy gap increased and then return to shift to high energy side for high concentration of CNT at high preparation temperature.

## REFERENCES

1. L. Torsi, A. Tafuri, N. Cioffi, M.C. Gallazzi, A. Sassella, L. Sabbatini, P.G.Zambonin, Sens. Actuators B 93 (2003) 257.
2. R. Turcu, O. Pana, L. Bratu, M. Bogdon, J. Mol. Electron. 6 (1990) 1.
3. S. Iijima, T. Ichihashi, Nature 363 (1993) 603.
4. J.L. Bahr, J.M. Tour, J. Mater. Chem. 12 (2002) 1952.
5. R.H. Haughman, A.A. Zakhidov,W.A. de Heer, Science 297 (2002) 787.
6. H. Dai, J.H. Hafner, A.G. Rinzler, D.T. Colbert, R.E. Smalley, Nature 384 (1996) 147

7. P.M. Ajayan, Q. Stephan, C. Colliex, D. Trauth, Science 265 (1994) 1212.
8. M. Nicolas, F. Guittard, S. Geribaldi, Angew. Chem. Int. Ed. 45 (2006) 2251.
9. M. Fu, Y. Zhu, R. Tan, G. Shi, Adv. Mater. 13 (2001) 1874.
10. C. Bora, R. Pegu, B. J Saikia and S. K Dolui "Synthesis of polythiophene/graphene oxide composites by interfacial polymerization and evaluation of their electrical and electrochemical properties" DOI 10.1002/pi.4739 ,27 January (2014).
11. C. Bora, R.Pegu, B. J Saikia and Swapan K Dolui, DOI 10.1002/pi.4739 Accepted article published: 21 March (2014)
12. T.S. Swathy, M. Anne Jose, M. Jinish Antony "AOT assisted preparation of ordered, conducting and dispersible core-shell nanostructured polythiophene - MWCNT nanocomposites" S0032-3861(16)30846-1(2016)
13. Saini, V.Li ,Z. Bourdo, S. Dervishi, E.Xu, Y. Ma, X.Kunets, V. P. Salamo, G. J. ,Viswanathan, T. Biris, A.R. Saini, D. Biris, A. S. " electrical, optical, and morphological properties of P3HT-MWNT nanocomposites prepared by in situ polymerization. " J. Phys. Chem. C 113 : 8023 (2009)
14. Kuila, B. K. Malik, S. Batabyal, S.K.Nandi, A. K. In-situ "synthesis of soluble poly (3- hexylthiophene)/multiwalled carbon nanotube composite Morphology, structure, and conductivity". Macromolecules 40: 278 (2007)
15. S. M. Hasan, N. M. Hasan, F. Sultan and G. Al-Zaidi, "The Effectof Gamma Radiation on The Optical Properties of (PC-PS) Polymer Blend", International Review of Physics, vol. 7, no.1, p. 125, (2013)
16. I. A. Al-ajaj, A. SH. Khalel , A. B. H. AL-Safee"Study of The Mechanicaland Electrical Properties of Epoxy/MWCNTs Composite"(2014).

**Table 1.materials and chemicals used in this study**

| Substance | States | Molecular Formula | provider |
|---|---|---|---|
| Thiophene (monomer ) | Liquid | $C_4H_4S$ | Sigma Aldrich |
| Acetonitrile | Liquid | $CH_3CN$ | Sigma Aldrich |
| Sodium perchlorate | Solid | $NaClO_4$ | Sigma Aldrich |
| fMWCNTs | Solid | C | Nanostructured & Amorphous Materials, Inc, diameter (10-30 ) nm and length of 1-2$\mu$m |

**Table 2. Summary of the preparation processes**

| MWCNTs rate | Temperature (°C) | Tim(minuet) | Voltage (Volt) |
|---|---|---|---|
| 0.07 | 20 | 13 | 5 |
| 0.03 | 20 | 12 | 5 |
| 0.01 | 20 | 8 | 5 |

**Table 3. Optical properties of PTh and PTh/MWCNT at 20 ° C.with different doping ratio (0.01,0.03 and 0.07) wt.%**

| Sample(20 °C) | Eg (eV) |
|---|---|
| 0.01%CNT | 2.6 |
| 0.03%CNT | 2.7 |
| 0.07%CNT | 1.55 |
| Pure | 1.50 |

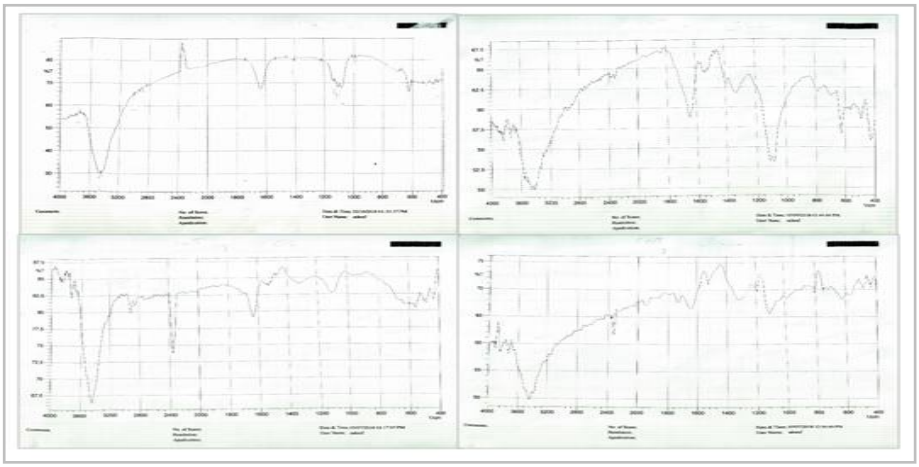

**Figure 1.FT-IR spectrum of PTh and PTh/MWCNT at 20 ° Cwith different doping ratio (0.01,0.03 and 0.07) wt.%**

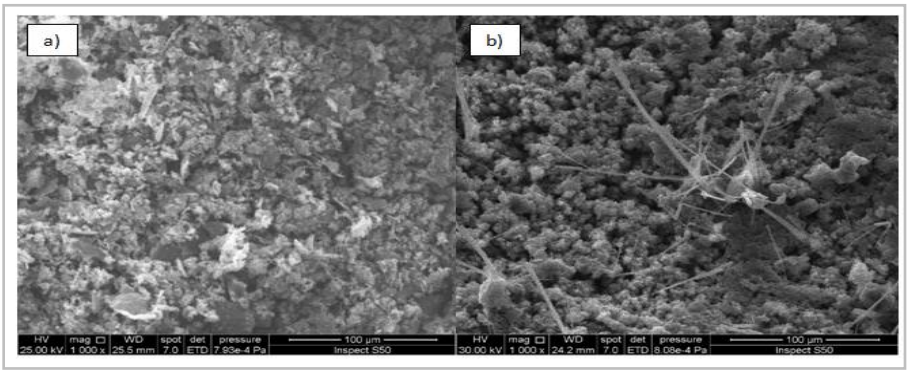


**Figure 2.Scanning Electron Microscopy Images of the ( a ) PTh and ( b ) PTh/MWCNT**

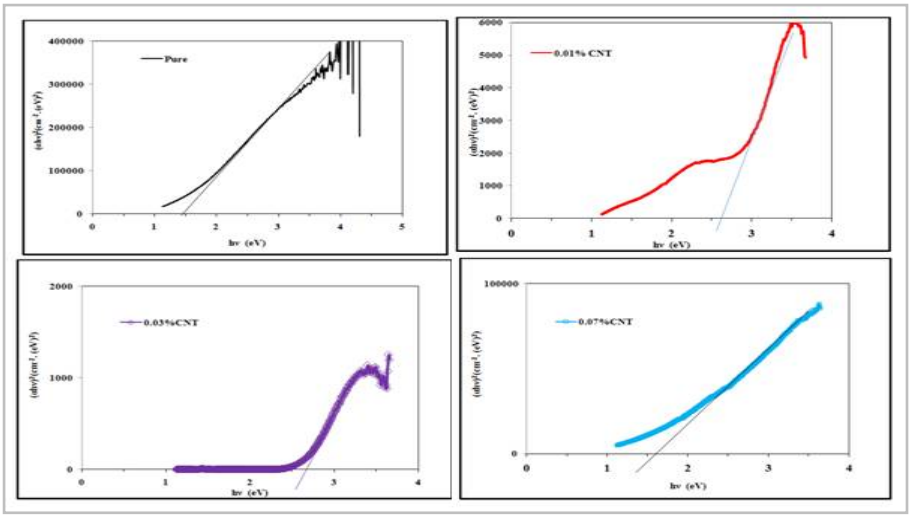


**Figure 3.Energy Gap of PTh and PTh/MWCNT at 20° C.with different doping ratio (0.01,0.03 and 0.07) wt.%**

*Indian Journal of Natural Sciences* www.tnsroindia.org.in ©IJONS

*Vol. 9 / Issue 50 /October 2018* *International Bimonthly* *ISSN: 0976 – 0997*

RESEARCH ARTICLE

# A Comparison Between Er, Cr: YSGG 2780 nm Laser and Bur in Root-End Surgery: Retrograde Cavity Preparation

Doaa A. Almiran[1]*, Salah A. Alkurtas[2] and Mohammed A. Al-Maliky[3]

[1,3]Department of Biomedical Applications, Institute of laser for postgraduate studies, University of Baghdad, Baghdad, Iraq
[2]Oral and Maxillofacial Department, Akarkh General Hospital, Iraq.

Received: 19 July 2018 Revised: 24 Aug 2018 Accepted: 26 Sep 2018

***Address for Correspondence**
**Doaa A. Almiran**
Department of Biomedical Applications,
Institute of laser for postgraduate studies,
University of Baghdad,
Baghdad, Iraq
Email : al.meran1988@gmail.com



## ABSTRACT

The Aim of the study was to compare between Er,Cr:YSGG 2780 nm laser and carbide fissure bur in retrograde cavity preparation regarding the micromorphological variations under scanning electron microscope, temperature changes and duration of retrograde cavity preparation.3.75 W, 15 Hz, 30% water, 60% air, 31.84 J/Cm$^2$. Twenty teeth of single canals were obturated and apex resected with carbide cross cut bur with 0° bevel. Retrograde cavity was prepared using carbide fissure bur in ten samples and the remaining were prepared using MZ6 glass tip of 660 µm diameter. Temperature on external root surface and average time for cavity preparation were recorded. Samples were prepared for SEM and examined to evaluate dentinal cracks, roughness, smear layer and opened dentinal tubules. Whenever required**,** $x^2$ test/Fisher exact and Kruskal–Wallis test were used. The level of significant was set at $P \leq 0.05$.There are statistical significant differences between bur group and Er,Cr:YSGG laser group in the terms of dentinal cracks, surface roughness, smear layer removal and opened dentinal tubules, temperature on the external root surface and the duration of cavity preparation. While the difference in the term of quantitative assessment of opened dentinal tubules was very highly statistically significant.
Er,Cr:YSGG laser showed higher percentage of dentinal cracks, rougher surface, better smear layer removal and more opened dentinal tubules and longer time for preparation than bur. There was no elevation of temperature on external root surface.

**Keywords:** retrograde cavity, Er,Cr:YSGG laser, cracks, roughness, dentinal tubules.

## INTRODUCTION

Root end surgery is treatment of choice when non-surgical revision is unsuitable due to the nature of the periapical pathosis or if the non-surgical treatment will result in excessive demolition of either the tooth or the restoration. The technique includes root end resection and retrograde cavity preparation [1]. It is difficult to reach the goal of ideal retrograde cavity preparation and a good retrograde filling with the classical procedures where bur fail to debride the apical canal and it is likely to result in smear layer while ultrasonic retrograde cavity preparation creates dentinal cracks and/or chipping [2]. Several studies evaluated the efficiency of Er,Cr:YSGG 2780 nm laser in the preparation of retrograde cavity and revealed that it didn't result in cracks or chipping [3-5] but resulted in rough surface with opened and wide dentinal tubules [6]. Er,Cr:YSGG laser showed better results than both bur and ultrasonic retrotips in retrograde cavity preparation [2, 7]. On the other hand, laser should be used with caution so as to avoid excessive and unnecessary dentin removal when used for retrograde cavity preparation [8]. The Aim of this study was to compare between Er,Cr:YSGG 2780 nm laser and carbide bur in retrograde cavity preparation considering the micromorphological changes (such as cracks, roughness of dentin surface, smear layer and opened dentinal tubules) under scanning electron microscope, temperature and duration of the cavity preparation procedure.

## MATERIALS AND METHODS

### Sample preparation

Twenty extracted human single rooted teeth of single canal and mature apices had been used in this study after approval of the university of Baghdad on the research proposal (number 17 on 12 July 2017). The teeth were free of calcification, root caries and resorption, developmental anomalies or crack lines. The soft tissue remnants and hard deposits were removed with hand scaler, then the samples were kept hydrated in isolated tubes filled with 0.1% thymol at 4°C until the time it have been used in this study.The teeth were rapped with wet gauze to prevent the dehydration during canals preparation and obturation. Standard access cavities were prepared with carbide round bur under copious amount of water flow. Barbed broach was used to remove the pulpal tissue. K-files #10 moved down into the canal until the file was just visible at the apical foramen and the working length was determined by substracting 0.5 mm from this length. Root canals were prepared with the conventional technique using hand-operated ProTaper files. The instrumentation sequences began with SX file for coronal flaring until reach a final size at F4 file.

Irrigation of root canal with disposable syringe with a 30-gauge end closed and double sided vent needle. The irrigation protocol as follow: one ml of 5.25% NaOCl before instrumentation and 2 ml of it between instruments changes, root canals received final irrigation with 1 ml of 17% Ethylendiaminetetraacetic acid (EDTA) for one minute. Followed by 3 ml of 5.25% NaOCl then washed with 5 ml of normal saline, with emphasis that the irrigant reached the apical end of the canal. Dryness of root canal with ProTaper paper point F4, followed by obturation with cold lateral condensation technique using Gutta-Percha F4 (DiaDent,Korea) and AH Plus sealer (Dentsply ,Maillefer,USA) along with accessory Gutta-Percha. Finally the access cavity was filled with Tetric-N ceram.Teeth were stored in normal saline sodium chloride BP (0.9% w/v) at 37$^0$C in a water bath. All the teeth were stabilized in the water bath with their crowns immersed in water and the temperature on the external apical root surface was stabilized at 37 °C at the starting point of the resection or retrograde cavity preparation process.

The root-end resection was performed at about 3 mm from the roots apical end and at 0° to the long axis of the root with slow speed surgical handpiece 40,000 rpm (NSK ,China) and cross cut carbide bur (ELA,Germany). Twenty teeth were randomly divided into two groups, according to the method of retrograde cavity preparation. For the purpose of standardization, the same rate of water was used in both laser and bur group which was set at 11 ml/min with the aid of Beker and a clock watch.The temperature was recorded during cavity preparation procedure using a

thermocouple which was hold to the external root surface at 1mm from the resected root-end and connected to digital thermometer (AMPROBE TMD®-56, Everett, WA, USA). The average time for preparation of retrograde cavity was recorded for each sample.

### Retrograde cavity preparation

In group 1, the retrograde cavity preparation performed using slow speed angled handpiece (20.000 rpm) along with carbide fissure bur (MEDIN ,a.,s.,Czech Republic) each single bur was used for 5 samples preparation. The water flow was set to be 11ml/min supplied through IV administration set up. While in the group 2, retrograde cavity prepared using Er,Cr:YSGG pulsed laser (Biolase, waterlase, Iplus, CA, USA) delivered through MZ6 glass tip of 660 µm diameter and 6 mm length (calibration factor is 1.00), the parameters used according to manufacturer instructions for class I comfort preparation (average power 3.75 W, frequency 15 Hz, fluence 31.84 J/cm$^2$,water level 30% and air level 60%).The MZ6 tip placed about 1.5 mm away from the hard tissue so as to obtain spot size of 1mm diameter and the cavity irrigated with normal saline using irrigation needle of double sided vent 30-gauge at every 1 mm cavity preparation depth to prevent the charring inside the retrograde cavity (figure 1). For the purpose of standardization, the diameter of the cavity is 1 mm in all samples with 3 mm depth and this confirmed with diameter of periodontal probe. At the end of the preparation in both groups, the retrograde cavity irrigated with normal saline to remove the debris and remnants from the cavity. Each single laser tip was used for retrograde cavity preparation of single tooth and then discarded.

### Scanning electron microscope evaluation

Teeth were sectioned with diamond wafering blade (Ted Pella,USA) under copious amount of normal saline flow. The sectioning was accomplished with two cuts, one of them was horizontal at the cementoenamel junction while the other was longitudinal that separated the root into two equal halves buccal (labial) and palatal (lingual). Samples were dehydrated and fixed following Marchesan et al. protocol [9]. All specimens were examined at x50 by single observer to detect the presence or absence of dentinal cracks. On the middle and at about 1 mm from the incisal edge of the retrograde cavity wall, the area was observed at x400 to evaluate surface roughness by two calibrated examiners in a double-blinded fashion using scoring system described by Duarte et al. at which 0 :smooth surface, 1: surface with slight roughness, 2: surface with moderate roughness, 3: surface with severe roughness [10], and observed at x2000 to evaluate smear layer and opened dentinal tubules by three calibrated blind examiners using scoring system described by Hulsmann *et al.* at which score 1: dentinal tubules completely open, score 2: more than 50% of dentinal tubules open, score 3: less than 50% of dentinal tubules open, score 4: almost all dentinal tubules covered with smear layer [11]. All specimens were observed at 10 kV. To assess the number of opened dentinal tubules, SEM micrograph at x2000 was quantitatively evaluated with the aid of Image J software program (manual method) to count the number of partially and completely opened dentinal tubules. Data obtained from SEM observations were evaluated using Chi square test, Fisher exact test and the Kruskal–Wallis test whenever it was required and the level of significant was set at ($P \leq 0.05$).

## RESULTS

### Dentinal cracks

Samples were evaluated under SEM at x50 by single observer**.** Group 1 showed presence of crack in 3 (30%) samples while the rest 7 (70%) revealed no cracks. On the other hand, group 2 showed dentinal cracks in 7 (70%) sample while the rest 3 (3)% showed no cracks. The statistical analysis was performed using $x^2$ test/Fisher's exact test. The difference between group 1 and 2 was statistically significant at which P value is 0.04 (Table 1 and figure 2 ).

### Roughness

The samples examined under SEM at x400 for analysis of surface roughness by two examiner in a double-blind fashion (Table 2 and figure 3). The analysis of the interexaminer agreement of the scores obtained for the surface roughness by the Kruskal–Wallis test determined significant differences between the groups ($P \leq 0.05$). Bur group produced significantly smoother surface than the Laser group ($P \leq 0.05$). The analysis of scores obtained for the cut quality by the Kruskal–Wallis test revealed no significant differences inside the groups (Examiner 1 and Examiner 2) ($P > 0.05$). The comparison between the groups for the surface roughness was performed using the Kruskal–Wallis and Dunn tests. The significant level was established at 5%. Significant statistical differences ($p \leq 0.05$) occurred in the comparisons between Bur and Laser groups (Table 3).

### Smear layer and open dentinal tubule

The samples examined under SEM at x2000 to evaluate the smear layer and opened dentinal tubules by three well calibrated examiners (figure 4). The statistical analysis was performed using $x^2$ test/Fisher's exact test, a comparison on the level of individual samples between group 1 and 2 showed fluctuation in the term of statistical difference from no significant, significant to highly significant differences. Overall difference between group 1 and 2 was statistically significant at which P is 0.05. To confirm the results obtained by $x^2$ test/Fisher's exact test, another test was carried out which is the Kruskal–Wallis test which also revealed statistically significant difference between group 1 and 2 (P value $\leq 0.05$) (table 4 and 5).

### Quantitative assessment of opened dentine tubules

The $x^2$ test/Fisher's exact test was used to assess the number of opened dentinal tubule statistically. Statistical difference between group 1 and 2 was very highly significant at which P value is 0.001, as laser resulted in greater number of opened dentinal tubules than bur (Table 6 and figure 5).

### Temperature

There was no temperature elevation above 37°C in both groups. The recorded temperature was below 37 °C (below the starting point temperature) during retrograde cavity preparation in both bur and laser groups. The lowest temperature reached during retrograde cavity preparation at the external root surface was considered for each sample in both groups and involved in the statistical analysis. The statistical analysis was performed using $x^2$ test/Fisher's exact test. Group 1 reached lower temperature at the external root surface than group 2. The difference between group 1 and 2 was statistically significant (table 7).

### Duration of preparation procedure

The average time consumed in retrograde cavity preparation in both groups was calculated. The difference was statistically significant. Laser took longer time to prepare the retrograde cavity (table 8).

## DISCUSSION

Various techniques and devices have been advocated for retrograde cavity preparation .Traditionally, preparation with burs in high-speed handpieces shows lack of parallelism, inaccessible root tip and perforation of the root lingually[12].The success rate is approximately 60% while using ultrasonic retrotips for retrograde cavity preparation results in dentinal cracks and smear layers which can threaten the apical seal [13]. Er:YAG 2940 nm and Er,Cr:YSGG

2780 nm lasers are highly absorbed by water-rich tissues [14]. The hydroxyl group of the (carbonated) hydroxyapatite mineral of the tissues shows a small absorption at around 2800 nm [15]. Therefore, the aim of study was to compare between Er,Cr:YSGG 2780 nm laser and carbide bur in retrograde cavity preparation considering the morphological changes, temperature and the duration of preparation.

The finding of this study revealed that preparation of retrorograde cavity with Er,Cr:YSGG laser associated with more cracks than with carbide fissure bur. This is contradict with the previous studies as laser revealed absence of vibration or pressure exerted during cavity preparation which predispose cracks [3]. The incidence of cracks in this study might be related to the small diameter of retrograde cavity thus insufficient water spray from the handpiece reaching the full depth inside the cavity; on the other side, increasing the diameter to 1.5 mm resulted in defect at the apical end of the cavity in both methods of preparation (bur and laser) due to the thin remained dentin in apical cross section therefore retrograde cavity preparation of 1 mm diameter was the choice for this study.The proper interaction between retrofilling material and retrograde cavity surface depends on both the materials characteristics and the surface conditions of the cavity. Smear layer removal is necessary to provide a proper interface which lead to better adaptation of the material. Er,Cr:YSGG laser is highly absorbed by water, causing microexplosions of the water content of dentin, which results in debris and smear layer removal that will increases the number of opened dentinal tubules and the root dentin permeability [6].

Two methods for evaluation of opened dentinal tubules were used in this study to overcome the subjectivity of the evaluation. Both of them revealed that Er,Cr:YSGG laser treated cavity showed larger number of opened dentinal tubules which is coincide with studies conducted by Ishizaki et al.[16] and Yamazaki et al.[17] The cut quality analysis by the Kruskal–Wallis test revealed no significant differences inside both groups which indicate the standardization of cutting was achieved for all samples. On the other hand, laser preparation resulted in rougher surface than bur, this is coincide with a study conducted by Winik et al. who suggested that this roughness can affect the interface between the filling material and retrocavity according to the viscosity of the filling material which results in increase or decrease the seal between them [6]. From another point of view, Er:Cr:YSGG laser ablation results in a micro-retentive surface (irregular intertubular dentin surface) which will lead to enhancement of the mechanical bond between retrograde filling material and dentinal wall [13]. The preparation with laser results in rough surface because of its pulsed cutting mode which impair uniform cutting of dentine [10].Er:Cr:YSGG laser preparation cut the dentin in a way that the temperature of root surface during cavity preparation remains low due to the energized water molecules, which is critical for the surrounding bone [2]. The recorded temperature was low in both groups. The recorded temperature in this study was far below 37°C, which can be related to the limitations of the in vitro study as the blood circulation and surrounding periodontium have an effect on maintaining the steady temperature at the operation site.

Er,Cr:YSGG results in charring more than Er:YAG laser under the same conditions, this is because Er,Cr:YSGG laser has higher heat deposition within the tooth [18]. Tissue charring occurs when the tissue dehydrated and then burned. The end products of this process is carbon which is a high absorber of all wavelengths, thus it becomes a “heat sink” as the lasing continues and the heat conduction will then result in broad collateral thermal trauma [19]. Continuous drilling of 3 mm depth and 1 mm diameter retrograde cavity resulted in charring because the tip was impeded inside small diameter cavity and the water spray didn’t reach the full depth of the cavity during lasing process, to overcome this problem every 1 mm of retrograde cavity preparation followed by normal saline irrigation with irrigation needle 30-gauge, this procedure continued till reach 3 mm depth and this resulted in absence of charring using this new method.The average time consumed in retrograde cavity preparation using laser was longer than bur and this is coincide with a study conducted by Batista de Faria-Junior et al.[4]. The most critical part of SEM analysis is the preparation of a sample. Dehydration and drying procedures may create artifacts in hard tissues. There are two approaches for SEM analysis, direct and indirect approaches. The direct one consists of the dehydration and drying of the original sample while indirect approach is carried out by taking impressions with appropriate material thus prevent creation of artifacts but it lacks the detailed information of the tooth structure [12].In this study, no crack was

detected at the evaluation of 10 random samples with direct method and at 10 kV of SEM analysis, therefore we suggested that direct method is suitable and doesn't produce artifact in this protocol of dehydration and SEM setting. Further studies are required to evaluate different laser parameters to prepare retrograde cavities.

## CONCLUSION

Within the limitation of the in vitro study and the conditions of the current research, using Er,Cr:YSGG 2780 nm laser according to the manufacturer instructions for class I comfort preparation to prepare retrograde cavity resulted in several morphological and surface characteristics compared to bur. Advantages of Er,Cr:YSGG 2780 nm laser :

- Better smear layer removal and more opened dentinal tubules than bur. .
- Reduction in temperature on the external root surface thus it will prevent damage to the surrounding periodontium and bone during retrograde cavity preparation. Laser resulted in decrease of root surface temperature below the starting point of 37°C by 10.9 ±1.6 °C because of the Er,Cr:YSGG laser cooling system.

Disadvantages of Er,Cr:YSGG 2780 nm laser:

- Higher percentage of dentinal cracks.
- Rough surfaces of the prepared cavity walls (this characteristic can be considered as disadvantage or not, depending on the type of material will be used as a retrograde filling).
- Laser took longer time to prepare retrograde cavity.

## REFERENCES

1. Gutmann JL. and Lovdahl PE. *Problem Solving in Endodontics - E-Book: Prevention, Identification and Management*. 2010: Elsevier Health Sciences.
2. Chaudhry S, Yadav S, Oberoi G ,Talwar S, Verma M. *Evaluation of root-end cavity preparation using erbium, chromium:yttrium, scandium, gallium, and garnet laser, ultrasonic retrotips, and conventional burs.* Journal of Dental Lasers 2016; 10: p. 43-46.
3. Wallace JA. *Effect of Waterlase laser retrograde root-end cavity preparation on the integrity of root apices of extracted teeth as demonstrated by light microscopy.* Aust Endod J 2006; 32: p. 35-9.
4. Batista de Faria-Junior N, Tanomaru-Filho M, Guerreiro-Tanomaru JM, de Toledo Leonardo R, Camargo Villela Berbert FL. *Evaluation of ultrasonic and ErCr:YSGG laser retrograde cavity preparation.* J Endod 2009; 35: p. 741-4.
5. Rahimi S, Yavari HR, Shahi S, Zand V, Shakoui S, Reyhani MF *et al. Comparison of the effect of Er, Cr-YSGG laser and ultrasonic retrograde root-end cavity preparation on the integrity of root apices.* J Oral Sci 2010; 52: p. 77-81.
6. Winik R, Araki AT, Negrão JA, Bello-Silva MS, Lage-Marques JL. *Sealer penetration and marginal permeability after apicoectomy varying retrocavity preparation and retrofilling material.* Brazilian Dental Journal 2006; 17: p. 323-327.
7. Arslan S, Bala O, Berk G, Kayaoglu G. *Comparison of Crack Formation in Retrograde Cavities prepared with Ultrasound,Er,Cr:YSGG Laser or Bur : An ex vivo Study.* J Contemp Dent 2013; 3: p. 1-6.
8. Camargo Villela Berbert FL, De Faria-Junior NB, Tanomaru-Filho M, Guerreiro-Tanomaru JM, Bonetti-Filho I, Leonardo Rde T *et al. An in vitro evaluation of apicoectomies and retropreparations using different methods.* Oral Surg Oral Med Oral Pathol Oral Radiol Endod 2010;110: p. e57-63.
9. Marchesan MA, Brugnera-Junior A, Souza-Gabriel A. E, Correa-Silva S. R, Sousa-Neto M. D. *Ultrastructural analysis of root canal dentine irradiated with 980-nm diode laser energy at different parameters.* Photomed Laser Surg 2008; 26: p. 235-40.
10. Duarte MA, Domingues R, Matsumoto MA, Padovan LE, Kuga MC. *Evaluation of apical surface roughness after root resection: a scanning electron microscopic study.* Oral Surg Oral Med Oral Pathol Oral Radiol Endod 2007; 104: p. e74-6.

11. Hulsmann M, Rummelin C, and Schafers F. *Root canal cleanliness after preparation with different endodontic handpieces and hand instruments: a comparative SEM investigation.* J Endod 1997; 23: p. 301-6.
12. Aydemir S, Cimilli H, Hazar Yoruc AB, Kartal, N. *Evaluation of two different root-end cavity preparation techniques: A scanning electron microscope study.* Eur J Dent 2013; **7**: p. 186-90.
13. Roghanizad N, Fekrazad R, Kalhori AM K, Khalilak Z, Esmaeili AM, de Fatima Zanirato Lizarelli R. A *comparison of Er, Cr: YSGG laser with ultrasonic preparation on the seal of retrograde cavities.* Laser Therapy 2015; **24**: p. 33-37.
14. Freitas PM and SimÃµes A. *Lasers in Dentistry: Guide for Clinical Practice* 2015: Wiley.
15. Parker S, Darbar A, Featherstone J, Iaria G, Kesler G, Rechmann P, Michael D, Joel W, Harvey A. *The Use of Laser Energy for Therapeutic Ablation of Intraoral Hard Tissues* J Laser Dent 2007; 15: p. 78-86.
16. Ishizaki NT, Matsumoto K, Kimura Y, Wang X, Kinoshita J, Okano SM *et al. Thermographical and morphological studies of Er,Cr:YSGG laser irradiation on root canal walls.* Photomed Laser Surg 2004; 22: p. 291-7.
17. Yamazaki R, Goya C, Yu DG, Kimura Y, Matsumoto K. *Effects of erbium,chromium:YSGG laser irradiation on root canal walls: a scanning electron microscopic and thermographic study.* J Endod 2001; 27: p. 9-12.
18. Diaci J and Gaspirc B. *REVIEW Comparison of Er:YAG and Er,Cr:YSGG lasers used in dentistry.* Journal of the Laser and Health Academy 2012; 1: p. 1-13.
19. Convissar RA. *Principles and Practice of Laser Dentistry - E-Book*. 2nd ed ed. 2015: Elsevier Health Sciences.

**Table 1. $X^2$ test/Fisher's exact test of dentinal crack in retrograde cavity.**

| Groups | Dentinal cracks | |
|---|---|---|
| | With cracks (Yes%) | Without cracks (No%) |
| Bur Samples (10) | 3(30%) | 7(70%) |
| Laser Samples (10) | 7(70%) | 3(30%) |
| *P*- Value ($x^2$ test/Fisher's exact test) | 0.04 | 0.04 |

**Table 2. Roughness scores by two observers (scanning electron microscope).**

| Samples | Group 1 (Bur retrograde cavity group) | | Group 2( Laser retrograde cavity group ) | |
|---|---|---|---|---|
| | Examiner 1 | Examiner 2 | Examiner 1 | Examiner 2 |
| 1 | 0 | 2 | 2 | 2 |
| 2 | 1 | 1 | 3 | 2 |
| 3 | 1 | 1 | 3 | 2 |
| 4 | 1 | 1 | 2 | 2 |
| 5 | 2 | 1 | 2 | 1 |
| 6 | 1 | 1 | 2 | 2 |
| 7 | 0 | 1 | 3 | 2 |
| 8 | 0 | 1 | 2 | 2 |
| 9 | 1 | 2 | 2 | 2 |
| 10 | 0 | 0 | 3 | 2 |

**Table 3: Descriptive, Kruskal–Wallis and Dunn tests of surface roughness.**

| Groups | Median | Minimum | Maximum |
|---|---|---|---|
| Bur | $1^a$ | 0 | 2 |
| Laser | $2^b$ | 1 | 3 |
| Kruskall–Wallis and Dunn tests | Different letters show significant statistical differences ($p \leq 0.05$) | | |

**Table 4. Descriptive and $x^2$ test/Fisher's exact test of smear layer and dentinal tubule scores using $x^2$ test/Fisher's exact test.**

| Samples | Group 1 (Bur retrograde cavity group ) Mean±SD | Group 2 ( Laser retrograde cavity group ) Mean±SD | *P*- Value ($x^2$ test/Fisher's exact test) |
|---|---|---|---|
| 1 | 4±0 | 1.67±0.58 | 0.01 |
| 2 | 3.33±0.6 | 2.33±0.58 | 0.05 |
| 3 | 4±0 | 4±0 | NS |
| 4 | 4±0 | 3.33±0.57 | NS |
| 5 | 4±0 | 4±0 | NS |
| 6 | 4±0 | 4±0 | NS |
| 7 | 3±0 | 2.66±1.3 | NS |
| 8 | 4±0 | 2±0 | 0.01 |
| 9 | 4±0 | 1.33±0.57 | 0.01 |
| 10 | 2.66±0.5 | 1±0 | NS |
| Total | 3.7±0.11 | 2.6±0.45 | 0.05 |

**Table 5. Descriptive, Kruskall–Wallis and Dunn tests of smear layer and dentinal tubule scores.**

| Groups | Median | Minimum | Maximum |
|---|---|---|---|
| Bur | $4^b$ | 2 | 4 |
| Laser | $2.5^a$ | 1 | 4 |
| Kruskall–Wallis and Dunn tests | Different letters show significant statistical differences ($p \leq 0.05$) | | |

**Table 6. Descriptive and $x^2$ test/Fisher's exact test of number of opened DTs in retrograde cavity groups.**

| Groups | Number of opened dentinal tubules |
|---|---|
| Bur Samples (10) | 57.41 ± 23.5 |
| Laser Samples (10) | 225.3 ± 65.9* |
| *P*- Value ($x^2$ test/Fisher's exact test) | 0.001 |

**Table 7. Descriptive and $x^2$ test/Fisher's exact test of temperature measurements of retrograde cavity groups .**

| Groups | Temperature (°C) |
|---|---|
| Bur Samples (10) | 22.9 ± 2.9* |
| Laser Samples (10) | 26.1 ± 1.6 |
| *P*- Value ($x^2$ test/Fisher's exact test) | 0.05 |

**Table 8. Descriptive and $x^2$ test/Fisher's exact test of average time of retrograde cavity preparation.**

| Groups | Average time of preparation (minute) |
|---|---|
| Bur Samples (10) | 1.21 ± 0.2* |
| Laser Samples (10) | 2.5 ± 0.8 |
| *P*- Value ($x^2$ test/Fisher's exact test) | 0.05 |

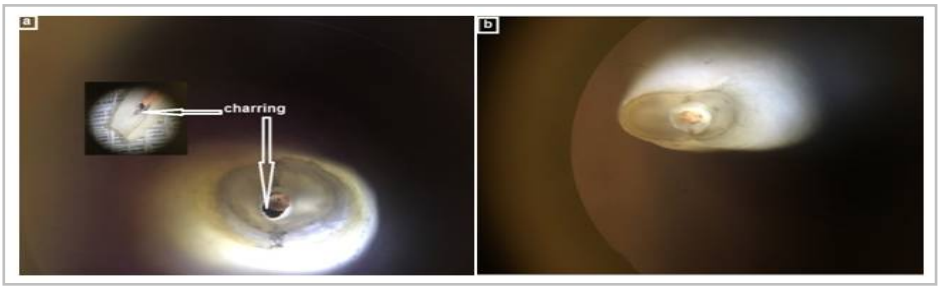


**Figure 1. (a) Retrograde cavity with charring (b) retrograde cavity without charring.**

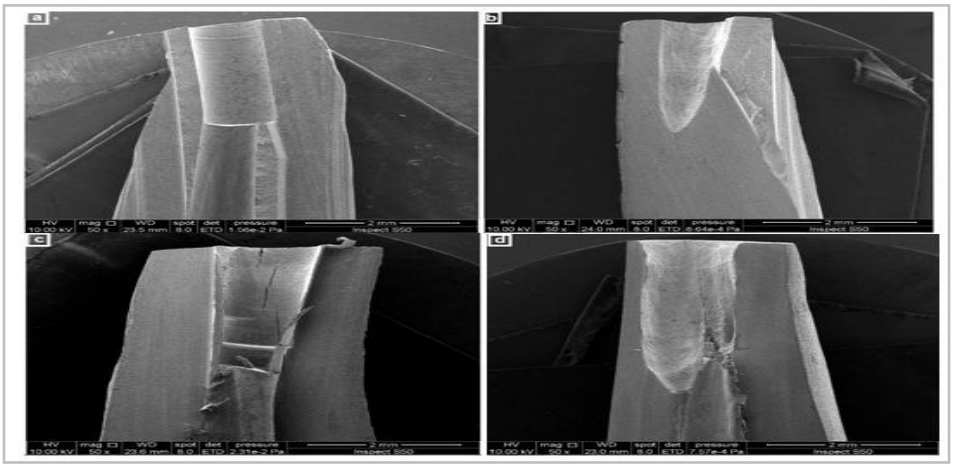


**Figure 2. SEM of retrograde cavities at x50 shows(a) retrograde cavity prepared by carbide fissure bur without dentinal crack .(b) retrograde cavity prepared by laser with MZ6 tip without dentinal crack.(c) retrograde cavity prepared by carbide fissure bur with dentinal crack.(d) retrograde cavity prepared by laser with MZ6 tip with dentinal crack.**

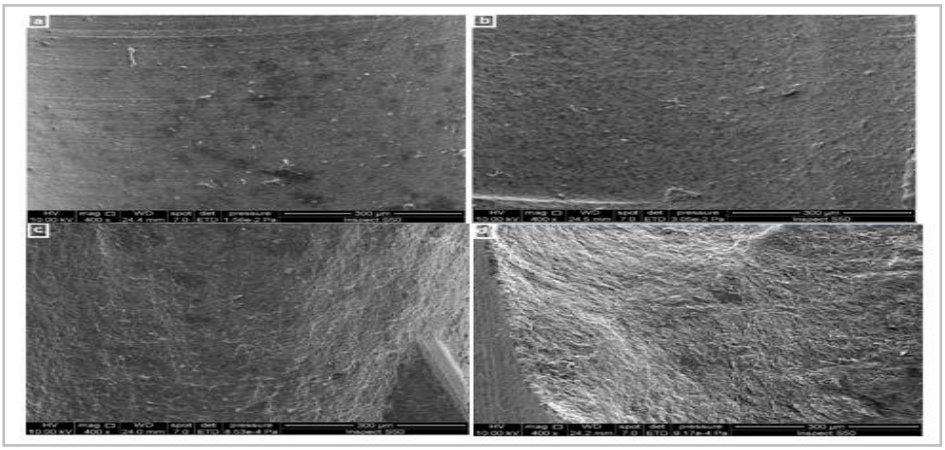


**Figure3. SEM of retrograde cavities at x400 shows surface roughness (a) retrograde cavity prepared by carbide fissure bur score 0 .(b) retrograde cavity prepared by carbide fissure bur score 1.(c) retrograde cavity prepared by laser with MZ6 tip score 2.(d) retrograde cavity prepared by laser with MZ6 tip score 3.**

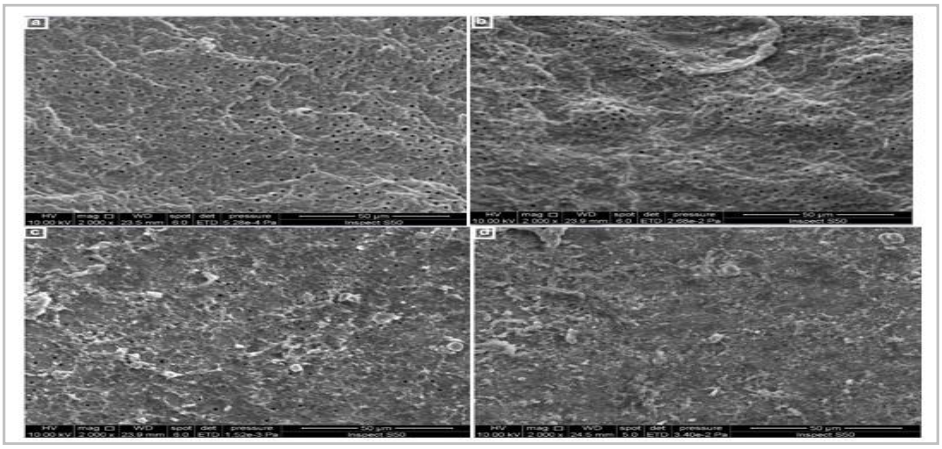

**Figure 4. SEM of retrograde cavities at x2000 shows smear layer and opened dentinal tubules (a) retrograde cavity prepared by laser with MZ6 tip score 1 .(b) retrograde cavity prepared by laser with MZ6 tip score 2.(c) retrograde cavity prepared by carbide fissure bur score 3.(d) retrograde cavity prepared by carbide fissure bur score 4.**

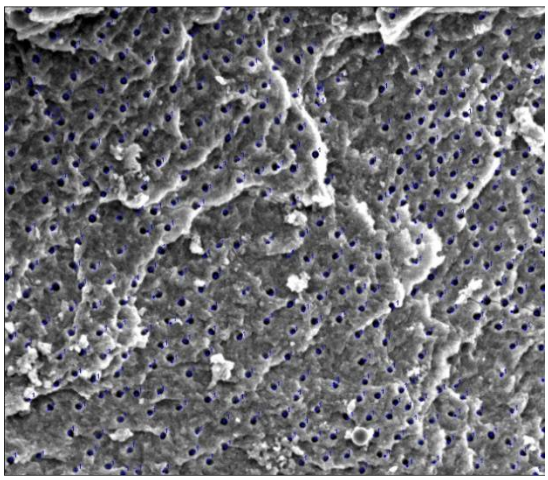

**Figure 5. Counting opened dentinal tubule with Image J software program.**

*Indian Journal of Natural Sciences* www.tnsroindia.org.in ©IJONS

*Vol. 9 / Issue 50 /October 2018* *International Bimonthly* *ISSN: 0976 – 0997*

RESEARCH ARTICLE

# Synthesis, Characterization and Evaluation of Phormidium Sp. Based Biochar and its Activation Efficacy for Removal of Safranin-O from the Aquatic System

Vyan A. Qadir[1]*, Sewgil S. Anwer[2], Shameran J. Salih[3] and Baref Z. Rashid[4]

[1,3]Department of Chemistry, Koya University, Daniel Mitterrand Boulevard, Koya KOY45, Kurdistan Region, Iraq.

[2]Department of Clinical Biochemistry, College of Health Science, Hawler Medical University, Erbil, Kurdistan Region, Iraq.

[4]Technical Institute, Department of Pharmacy, Wrme St. , Mardin 327 , Alley 76, Sulemaniyah, Kurdistan Region, Iraq

Received: 20 July 2018 Revised: 25 Aug 2018 Accepted: 28 Sep 2018

*Address for Correspondence
**Vyan A. Qadir**
Department of Chemistry,
Koya University,
Daniel Mitterrand Boulevard,
Koya KOY45,
Kurdistan Region, Iraq



## ABSTRACT

The potential application of Phormidium Sp. for biosorption of textile waste effluent was examined. This study addresses the adaptation of the microalgae Phormidium Sp.based biochar in textile waste effluent and the investigation of the best removal process. Synthetic dyes have an adverse effect on aquatic ecosystem and their toxic substances have to be removed from the effluent before their discharging. Microbial processes for the treatment of textile wastewater have the advantage of being environment friendly, cost effective and producing less sludge. The capacity of microalgae based biochar to carry out dye decolorization has received much attention. Microorganisms are examined as a significant source for decolorizing the textile dye effluent. Recent studies have been focused on the decolorization or degradation of azo-dyes using yeast, fungi, bacteria and algae. Biosorption is simply defined as the removal of substances from solution by biological material. Such substances can be organic, inorganic, gaseous and soluble or insoluble forms. . Nevertheless, the more work should be done to confirm the ability of microalgae to be considered as a promising alternative of biological treatment to reduce the pollution load resulted from the textile wastewaters proposed to be drained into the public water bodies.

**Keywords:** Phormidium Sp, Biochar, Weber-Morris Model, Safranin O, Textile waste effluent

## INTRODUCTION

Microalgae are the most organisms that found in every type of environment [1].Industrial and environmental development has created a serious problem by emitting waste water containing many different kinds of pollutants including heavy metals. The algae have many features that make them ideal for the selective removal and reducing the concentration of heavy metals, which include high bio sorption capacity, high tolerance to heavy metals, ability to grow both autotrophically and heterotrophically. However, large surface area/volume ratios, phototaxy, phytochelatin production and its potential for genetic manipulation [2].. Biosorption using algae is one of the new developed and promising metal removal methods Since the function groups on the cell wall of algae are found to be responsible for metal uptake, cell wall constituents of different groups of algae are compared. Mechanisms for metal adsorption and absorption are introduced [2, 3]. Biochar is a high carbon content solid carbonized material produced by pyrolysis of biomass under anoxic or aerobic conditions. It can improve soil structure, increase soil fertility, and increase crop yield R&R. Biochar also has a certain adsorption capacity for heavy metals R&R and organic matter R, which can be used for contaminated soil remediation. VersusThe daily salvage is up to thousands of tons. Phormidium Sp.cannot be directly eaten by poultry and livestock. The large amount of cyanobacteria recovered cannot be treated in a timely and effective manner. Long-term accumulation leads to rot, odor and decomposition releases a large amount of nutrient salt particles such as nitrogen and phosphorus, hydrogen sulfide gas and microcystins. , causing secondary pollution to the environment R. Phormidium Sp. is an excellent biomass material. If it is prepared into biochar, and then used as a activator for the removal of refractory pollutants such as dyes, it can not only provide a new resource for the utilization of Phormidium Sp. At present, there are few reports on related research. Therefore, the author selected cyanobacteria as raw materials to prepare a variety of biochar under different conditions. Based on the characterization of physicochemical properties of Phormidium Sp. Biochar safranin-O was used as a typical organic pollutant to study the preparation conditions for biochar activation.The influence of Safranin-O efficiency, the influencing factors and activation mechanism of the sorption process, and the evaluation of its recycling performance, in order to provide scientific basis and technical support for the application of Phormidium biochar in the activated advanced adsorption technology.

## MATERIALS AND METHODS

All reagents used were of analytical purity, water sample was collected from pond in Erbil spread on agar plate contain BG11 medium and incubated at 28°C under continuous illumination (1700Lx) and pH 7.5 [4]. The algal cell purified by sub culturing then the purified algal cell was transfer to liquid BG11 medium to obtain biomass. Isolated and purified microalgal culture was identified according to morphological properties [5].The basic dye, safranin O (dye content ≥85 %, molecular formula $C_{20}H_{19}ClN_4$, MW 350.84 and $\lambda max$ = 520nm) was obtained from Sigma-Aldrich and used without further purification. Double distilled water was used for the preparation of all experimental solutions.

### Dry biomass

The biomass collected after incubation in BG11 medium microalgal cell harvested by centrifugation at 5000 rpm for 10min. and the sample dried in oven at 80 °C for 12hr as described [5].

### Synthesis of biochar

The dried cyanobacteria are pulverized, impregnated with 7.5mol•$L^{-1}$,phosphoric acid or sodium hydroxide solution for 8h, then transferred to a muffle furnace, pyrolyzed at set temperature for 2h, cooled and rinsed with double distilled water. The filtrate was neutral, dried, and ground through a 500 μm pore size sieve for use. The preparation

of Phormidium Spbiochar refers to the literature [5, 6], the pyrolysis temperature is 500 ° C, and the obtained biochar is named PSpB.

### Batch sorption

Biosorption of safranin O onto PSpB, was investigated in a batch mode system. Adsorption studies were conducted at 180rpm using mechanical agitation for 2h, 100 mL of a 20 $mg{\cdot}L^{-1}$safranin O solution was added to the Erlenmeyer flask. Then, PSpB were sequentially added, sealed, and placed in a constant temperature (centrifugation radius of 12 mm) at 25±1 °C [7, 8]. After sampling at the set time, the sample was filtered through a 55mm pore size filter and measured by a UV-visible spectrophotometer ((UV/Vis) Agilent Technology Cary) at a wavelength of 520 nm to calculate the residual safranin O concentration. The default values for safranin O and PSpB dosing are 5 $mmol{\cdot}L^{-1}$ and 0.25$g{\cdot}L^{-1}$. In the pH experiment, the initial pH of the safranin O solution was adjusted to a set value using a 0.1 $mol{\cdot}L^{-1}$ hydrochloric acid or sodium hydroxide solution [9]. The initial concentration of the safranin O solution was recorded as $C_o$ ($mg{\cdot}L^{-1}$), and the remaining concentration was recorded as C ($mg{\cdot}L^{-1}$), and the removal effect of the dye was represented by $C/C_o$.

$$q_e = C_o - C\frac{V}{W} \quad \text{.....(1)}$$

$$R = \frac{C_o - C}{C_o} \times 100 \text{.....2)}$$

## RESULTS AND DISCUSSION

Isolated and purified microalgae strain observed under microscope and culture showed filamentous with thin layer and without akinet and heterocyst, the cells were cylindrical shape and the strain is identified as Phormidium sp. as shown in Fig 1[3,5,9]. Figure1: Cultural and Microscopic observation of Phormidium sp. (a-in liquid medium, b-under microscope) Microalgae being ubiquitous in nature possess a high potential of adaptation to diverse environments [7]. The same characteristics showed by isolated Phormidium from Spanish river [7,8]. Microalgae have been suggested as ideal candidates for waste water treatment system.

### Biochar characterization

SEM images of Phormidium Sp. and the biochar produced at 500 °C were shown in Fig2. PSpB exhibited a complex morphology due to the heterogeneous components. The biochar from Phormidium Sp. developed high porosity, presenting longitudinal pores with sizes ranging from micro to macro pores (10-200 µm). The large pores are originated from the vascular bundles of the raw biomass and they are important for improving the removal process as it can provide habitats for symbiotic microorganisms [10,13]. They can also act as release routes of pyrolytic vapors generated in the process [11,12]. [13] Reported that biochar presents good performance as adsorbent for elemental mercury removal from coal combustion, which can be improved using physical or chemical activation processes.

### Modeling of Biosorption kinetics

The mechanism of biosorption kinetics and the potential rate controlling steps involved in the process of adsorption has been studied using kinetic models such as pseudo-first order, pseudo-second order and intraparticle diffusion model[15,16]. The linear forms of these models are obtained by equation (3), (5) and (5). The Lagergren pseudo-first-order model illustrated the adsorption kinetic data, which is the earliest known equation describing the adsorption

rate based on the adsorption capacity. The integral form of the pseudo-first-order model is generally expressed as [8,11,23].

$$\text{Log } (q_e - q_t) = \text{Log } qe - \frac{k_1}{2.303} t \quad \text{.....(3)}$$

Where $k_1$(L $min^{-1}$) and predicted qe can be determined from the slope and intercept of the liner plot between log (qe-qt) and t, respectively[11].

The biosorption kinetic may be described by the pseudo second-order model. The differential equation is generally known and described as [17,20].

$$\frac{dq_t}{d_t} = K_2 (q_e - q_t)^2 \quad \text{.....(4)}$$

Where $k_2$(g $mg^{-1}min^{-1}$) is the second-order rate constant of adsorption. Integrating Eq. (4) for the boundary conditions qt =0-qt at t =0-t is simplified and linearized to obtain[17, 21,22];

$$\frac{t}{q_t} = \frac{1}{k_2 q_e^2} + \frac{1}{q_e} t \quad \text{.....(5)}$$

The second-order rate constants were used to calculate the initial biosorption rate given by the following equation [20]:

$$h = K_2 q_e^2 \quad \text{.....(6)}$$

Where $q_e$and $q_t$(mg/g) are the biosorption capacities at equilibrium and time t, respectively $k_1$ ($min^{-1}$) and $k_2$ (mg. g/min) are pseudo-first and pseudo-second order rate constant [21]. Pseudo –second order model was developed based on the assumption that the rate controlling step is chemisorption involving valance force due to sharing or exchange of electrons between safranin O and PSpB molecules[5], tabulated data are present in table1. Fig. 3 presents the plot of pseudo-first order kinetic for adsorption of safranin O onto PSpB at different initial concentrations. Nevertheless, the higher ($R^2 > 0.99$) for the pseudo-second order kinetics (Fig.4) indicate the fitness of this model and it was suggested that chemisorption might be a rate controlling step [18,22]. Furthermore, the $q_e$ values calculated using pseudo-second equation agreed well with the experimental $q_e$indicating that the biosorption of safranin O onto PSpB could be well represented using the pseudo-second order kinetic model [19].

## Biosorption mechanism

## Intraparticle diffusion model

The biosorption proceeds in several steps involving transport of solute molecules from the aqueous phase to the surface of the solid particles and then interior of the solid. According to Weber and Morris (1963)[17,22], for most adsorption processes the amount of adsorption varies almost proportional with $t^{1/2}$, which can be expressed as

$$q_t = K_{id} t^{\frac{1}{2}} \quad \text{.....(7)}$$

Where qt is the adsorption capacity at time t, $t^{1/2}$ is the half life time in second and Kid (mg $g^{-1}min^{-1/2}$) is the rate constant of the intraparticle diffusion model [9,11,24].The Intraparticle diffusion model suggest that the final sorption equilibrium was the intraparticle diffusion initiates to slow down due to quit low concentration of safranin O ions left in the solution.

### Liquid film diffusion model

In the transport of the adsorbate molecules from the liquid phase to the solid phase, the boundary layer plays an important role in adsorption and the equation of the liquid film diffusion model can be written as

$$\ln(1-q_t/q_e) = -K_{fd}t \quad \text{.....(8)}$$

Where qt/qe is the fractional attainment of equilibrium, and $K_{fd}$ is the film diffusion rate constant[15,19,24].

## CONCLUSION

Based on the current work, it is concluded that Phormidium Sp. based biochar is highly efficient sorbent for removal of safranin O from the textile waste effluent. Scanning electron microscopy showed enormous surface area that applicable to generate more sites with different sorbent classes.In turn, the theoretical values of qe mostly agree with the experimental data, both facts suggest that the pseudo-second order kinetic model ($R^2$ = 0.995) is more likely to predict the kinetic behavior for the whole range of time studied. On the other respect, the microalgae based biochar can be an alternative to assist in the textile culture effluent treatment, reducing the environmental impact caused by their pollutants. The algal biochar generated may be useful as fertilizers, feedstock or for biofuel production.

## REFERENCES

1. Mcgregor GB. Freshwater cyanobacteria of north-eastern Australia: 2. Chroococcales. Phytotaxa. 2013 Sep 20;133(1):1-30.
2. Chekroun KB, Baghour M. The role of algae in phytoremediation of heavy metals: a review. J Mater Environ Sci. 2013;4(6):873-80.
3. Rippka R. [1] Isolation and purification of cyanobacteria. InMethods in enzymology 1988 Jan 1 (Vol. 167, pp. 3-27). Academic Press.
4. Sadettin S, Dönmez G. Bioaccumulation of reactive dyes by thermophilic cyanobacteria. Process Biochemistry. 2006 Apr 1;41(4):836-41.
5. Holt J.G., Rieg,N., Smeath ,P.H.,Staley, J.T. Williams, S.T. Berges manual of determinative bacteriology ,9th ed.787.
6. Anwer S. Effect of temperature ph and light intensity to growth rate ChroococcusPallidus. Journal of Koya university.2010: 15 67-80.
7. Becker,E.W. Microalgae biotechnology and microbiology.Measurment of algal growth. Cambridge.University press 56-62.
8. Crini G, Badot PM. Application of chitosan, a natural aminopolysaccharide, for dye removal from aqueous solutions by adsorption processes using batch studies: a review of recent literature. Progress in polymer science. 2008 Apr 1;33(4):399-447.
9. Salih SJ, Rashid BZ. Cranberry Stem as an Efficient Adsorbent and Eco-Friendly for Removal of Toxic Dyes from Industrial Wastewater. Physico Studies. International Journal of Pharmaceutical Chemistry. 2015;5(6):207-17.

10. Mittal A, Jhare D, Mittal J. Adsorption of hazardous dye Eosin Yellow from aqueous solution onto waste material De-oiled Soya: Isotherm, kinetics and bulk removal. Journal of Molecular Liquids. 2013 Mar 1;179:133-40.
11. Rashid BZ, Omar RA, Salih SJ. Characterization and Antimicrobial Efficiency of Silver Nanoparticles Based Reduction Method. International Journal of Current Microbiology and Applied Sciences. 2016;5(8):802-10.
12. Salih SJ. Removal of Basic Dyes from Aqueous Solution by Chloroacetic Acid Modified Ferula Communis Based Adsorbent: Thermodynamic and Kinetic Studies (Doctoral dissertation, Eastern Mediterranean University (EMU)-DoğuAkdenizÜniversitesi (DAÜ)).
13. Faraj RH. Potential of PistachiThiosemicarbazone Sorption: Kinetic Studies, Optimization.
14. Tsibranska I, Hristova E. Modelling of heavy metal adsorption into activated carbon from apricot stones in fluidized bed. Chemical Engineering and Processing: Process Intensification. 2010 Oct 1;49(10):1122-7.
15. Harmsen PF, Huijgen W, Bermudez L, Bakker R. Literature review of physical and chemical pretreatment processes for lignocellulosic biomass. Wageningen UR-Food &Biobased Research; 2010.
16. Ekpete OA, Horsfall MJ. Preparation and characterization of activated carbon derived from fluted pumpkin stem waste (Telfairiaoccidentalis Hook F). Res. J. Chem. Sci. 2011 Apr;1(3):10-7.
17. Salih SJ, Anwer SS, Faraj RH. A Biosorption of Mercury from Wastewater Using Isolated Aspergillus Sp. Modified 1, 10-Phenanthroline: Hill Isotherm Model. Science Journal of University of Zakho. 2017 Dec 30;5(4):288-95.
18. Thajeel AS. Isotherm, kinetic and thermodynamic of adsorption of heavy metal ions onto local activated carbon. Aquatic Science and Technology. 2013 May 27;1(2):53-77.
19. Lian L, Cao X, Wu Y, Lou D, Han D. Synthesis of organo-functionalized magnetic microspheres and application for anionic dye removal. Journal of the Taiwan Institute of Chemical Engineers. 2013 Jan 1;44(1):67-73.
20. Salih SJ, Smail AK. Synthesis, characterization and evaluation of antibacterial efficacy of zinc oxide nanoparticles. Pharmaceutical and biological evaluations. 2016 Jun 11;3(3):327-33.
21. Sekirifa ML, Hadj-Mahammed M, Pallier S, Baameur L, Richard D, Al-Dujaili AH. Preparation and characterization of an activated carbon from a date stones variety by physical activation with carbon dioxide. Journal of Analytical and Applied Pyrolysis. 2013 Jan 1;99:155-60.
22. Sailh SJ, Omar NS, Sailh SJ. Kinetic Uptake and Isothermal Dynamics for the Removal of a Malachite Green (Aniline Green) from Simulated Wastewater using Natural Adsorbents.
23. Patil AK, Shrivastava VS. Alternantherabettzichiana plant powder as low cost adsorbent for removal of Congo red from aqueous solution. International Journal of ChemTech Research. 2010;2(2):842-50.
24. Binupriya AR, Sathishkumar M, Swaminathan K, Kuz CS, Yun SE. Comparative studies on removal of Congo red by native and modified mycelial pellets of Trametesversicolor in various reactor modes. Bioresource Technology. 2008 Mar 1;99(5):1080-8.
25. Park HJ, Jeong SW, Yang JK, Kim BG, LEE SM. Removal of heavy metals using waste eggshell. Journal of Environmental Sciences. 2007 Jan 1;19(12):1436-41.

**Table 1: biosorption kinetic model parameters obtained using spectral study**

| Pseudo-first order kinetic model | | | | Pseudo-second order kinetic model | | | | | |
|---|---|---|---|---|---|---|---|---|---|
| **Initial CV Conc. (mg/l)** | **$K_1$** | **$q_{e(exp)}$ (mg/g)** | **$q_{e(the)}$ (mg/g)** | **R2** | **$K_2$** | **$q_{e(exp)}$ (mg/g)** | **$q_{e(the)}$ (mg/g)** | **h (mg/g.min)** | **R2** |
| 200 | 0.0374 | 156 | 53.372 | 0.990 | 0.0012 | 156 | 166.766 | 34.33 | 0.995 |
| 100 | 0.0529 | 78 | 48.753 | 0.989 | 0.0013 | 78 | 91.909 | 11.75 | 0.995 |
| 50 | 0.0529 | 92 | 33.735 | 0.989 | 0.0025 | 92 | 101 | 25.64 | 0.996 |

***a.Phormidium* in liquid medium** **b. *Phormidium* under microscope**

**Figure1: Cultural and Microscopic observation of Phormidium sp. (a-in liquid medium, b-under microscope)**

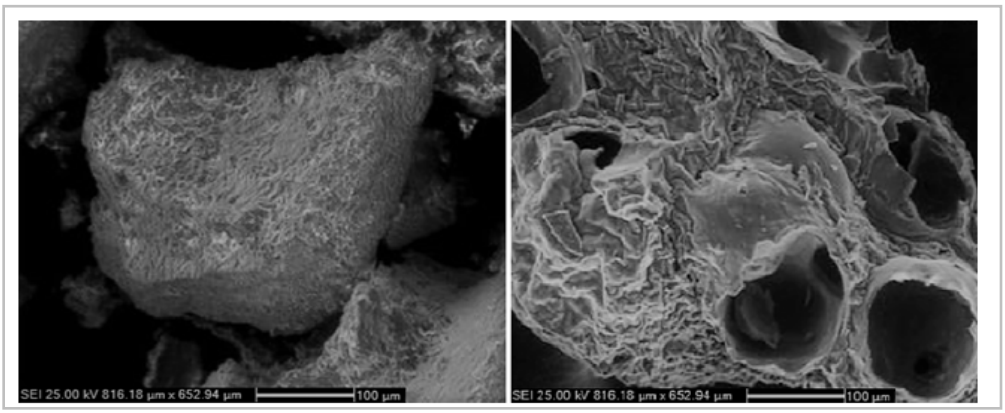


**Figure2: SEM images of the Phormidium Sp. based biochar obtained at 500 °C**

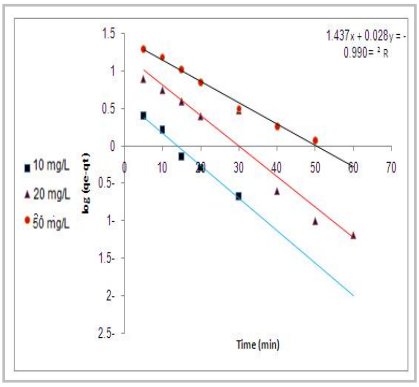


**Figure3:Pseudo-first order kinetic model for biosorption of safranin O onto PSpB at different initial concentration**

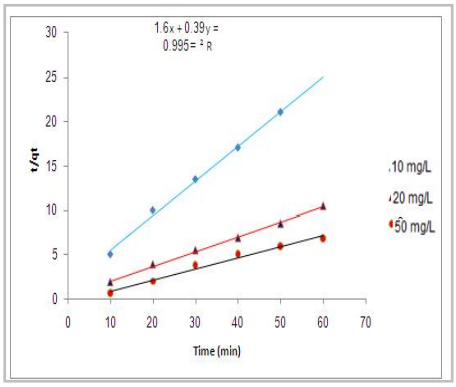


**Figure4: pseudo-second order kinetic model for biosorption of safranin O onto PSpB at different initial concentration**

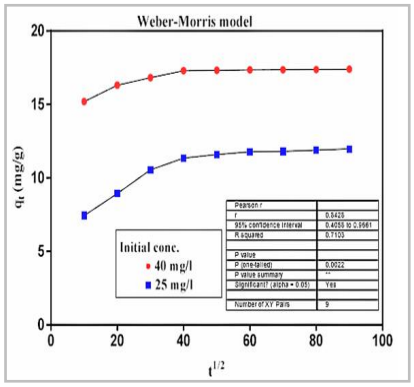


**Figure5: Intraparticle diffusion kinetic model**

*Indian Journal of Natural Sciences* www.tnsroindia.org.in ©IJONS

*Vol. 9 / Issue 50 /October 2018* *International Bimonthly* *ISSN: 0976 – 0997*

RESEARCH ARTICLE

# Fuzzy Filter Convergence in Fuzzy Bitopological Space

Amer Himza Almyaly[1]* and Zainab Hayder Abid AL-Aali[2]

The College of Science, Department of Mathematics, AL-Muthanna University, Iraq.

Received: 18 July 2018 Revised: 24 Aug 2018 Accepted: 29 Sep 2018

***Address for Correspondence**
**Amer Himza Almyaly**
The College of Science,
Department of Mathematics,
AL-Muthanna University, Iraq.



**ABSTRACT**

The aim of this paper to define the convergent and cluster point of fuzzy Filter in fuzzy Bitopological, Supra fuzzy topological and least upper fuzzy topological space. We explain the equivalent and difference between the concepts in those spaces.

**Keywords:** Least upper fuzzy topology, Fuzzy Filter, Fuzzy Bitopology and Supra fuzzy topology.

## INTRODUCTION

The concept of fuzzy Filter introduced by Parada and his Colleague [4]. He so defined the convergent and cluster point of fuzzy Filter in fuzzy topological space. Here, we will introduce same concepts but in fuzzy Bitopological space, Supra fuzzy topological space and least upper fuzzy topological space. We also build some theorems, remarks and examples which necessary to prove the relations between our concepts. Throughout this paper, $I^X$ will denote the set of all fuzzy sets in $X$, the symbols $N, \mathcal{N}$ and $\aleph$ are different according to the space type.

### Preliminaries

**Definition 1.1 [2]**

Let $X$ be a nonempty set, a fuzzy point $p_x^t$ in $X$ is fuzzy set with support $x \in X$ and value $t \in [0,1]$.

**Definition 1.2 [3]**

A fuzzy set $N$ in fuzzy topological space fts $(X,T)$ is a neighborhood of fuzzy point $p_x^t$, if there exist fuzzy open set $U$ such that $p_x^t \in U \leq N$. The collection of all neighborhoods of fuzzy point $p_x^t$ in $X$ is denoted by $N_{p_x^t}$.

**Definition 1.3 [5 and 4]**

A fuzzy Filter $\mathcal{F}$ (short, Filter $\mathcal{F}$) on $X$ is a nonempty collection of subsets of $I^X$ with the properties:

[1] If $F_1, F_2 \in \mathcal{F}$ then $F_1 \wedge F_2 \in \mathcal{F}$.
[2] If $F \in \mathcal{F}$ and $F \leq F'$ then $F' \in \mathcal{F}$.
[3] $0 \notin \mathcal{F}$.

**Example 1.1**

The set of all neighborhoods $N_{p_x^t}$ of some fuzzy point $p_x^t$ in $X$ is Filter.

**Definition 1.4 [5 and 4]**

A Filter $\mathcal{F}$ is converges to fuzzy point $p_x^t$, if $N_{p_x^t} \subset \mathcal{F}$.

**Remark 1.1**

If Filter $\mathcal{F}$ is converges to some fuzzy point $p_x^t$, then $\mathcal{F}$ is finner of $N_{p_x^t}$ or $N_{p_x^t}$ is coarser of $\mathcal{F}$.

**Definition 1.5 [4]**

A Filter $\mathcal{F}$ has cluster fuzzy point (short, cluster point) $p_x^t$ in fts $(X, T)$ iff $\forall N \in N_{p_x^t}$ then $N \wedge F \neq 0, \forall F \in \mathcal{F}$.

**Definition 1.6 [4]**

A collection $\mathcal{B}$ of subsets of $I^X$ is a base for some Filter $\mathcal{F}$ iff $\mathcal{B} \neq \emptyset$ and

[1] If $B_1, B_2 \in \mathcal{B}$ then $B_3 \leq B_1 \wedge B_2$ for some $B_3 \in \mathcal{B}$.
[2] $0 \notin \mathcal{B}$.

The collection $\mathcal{F} = \{F \in I^X : \exists B \in \mathcal{B}\ s.t.\ B \leq F\}$ is Filter. We said $\mathcal{F}$ is generated by $\mathcal{B}$. A collection $\mathcal{B}$ of subsets of $\mathcal{F}$ is a base for $\mathcal{F}$ iff for each $F \in \mathcal{F}$ there is some $B \in \mathcal{B}$ such that $B \leq F$.

## Fuzzy Filter in fbts

**Definition 2.1 [1]**

A fuzzy bitopological space fbts is a triple $(X, \tau_1, \tau_2)$, where $\tau_1$ and $\tau_2$ are arbitrary fuzzy topologies on X.

**Definition 2.2**

Let $p_x^t$ be an fuzzy point in $X$ and $(X, \tau_1, \tau_2)$ is an fbts. $N$ is said to be neighborhood of $p_x^t$ if there some fuzzy set $\mu \in \tau_1 \cup \tau_2$ such that $p_x^t \in \mu$ and $\mu \leq N$. Now, we recall the definition (1.4) to define the convergent of Filter in fbts.

**Definition 2.3**

A Filter $\mathcal{F}$ is converge to fuzzy point $p_x^t$ in fbts $(X, \tau_1, \tau_2)$ if $N_{p_x^t} \subset \mathcal{F}$.

**Remark 2.1**

In the next, let us denoted for the set of all neighborhoods of $p_x^t$ in fts $(X, \tau_1)$,$(X, \tau_2)$ and fbts $(X, \tau_1, \tau_2)$ by $N'_{p_x^t}$, $N''_{p_x^t}$ and $N_{p_x^t}$, respectively.

**Proposition 2.1**

Let $(X, \tau_1, \tau_2)$ be a fbts. A Filter $\mathcal{F} \subseteq I^X$ is converge to $p_x^t$ in $(X, \tau_1, \tau_2)$ iff it converges to fuzzy point $p_x^t$ in fts $(X, \tau_1)$ and $(X, \tau_2)$ together.

**Proof**

Fixed fuzzy point $p_x^t$ which belong to $X$.
$\Rightarrow$ Since $N'_{p_x^t}, N''_{p_x^t} \subseteq N_{p_x^t}$ , therefore, $N'_{p_x^t}, N''_{p_x^t} \subseteq \mathcal{F} \Rightarrow \mathcal{F}$ converges to fuzzy point $p_x^t$ in $(X, \tau_1)$ and $(X, \tau_2)$ together.
$\Leftarrow \forall N \in N_{p_x^t}$ in fbts $(X, \tau_1, \tau_2)$, $N$ is neighborhood of $p_x^t$ in fts $(X, \tau_1)$ or $(X, \tau_2)$, therefore, $N \in \mathcal{F} \Rightarrow N_{p_x^t} \subset \mathcal{F}$, i.e, $\mathcal{F}$ is converge to $p_x^t$ in $(X, \tau_1, \tau_2)$.

**Remark 2.2**

If the Filter $\mathcal{F} \subseteq I^X$ converges to $p_x^t$ in fts $(X, \tau_1)$ or $(X, \tau_2)$, then is not necessary $\mathcal{F}$ converges to $p_x^t$ in fbts $(X, \tau_1, \tau_2)$, as following example.

**Example 2.1**

Let $X = \{a, b\}$ and let $\tau_1 = \{X, \emptyset, \{p_a^{0.5}\}\}$ and $\tau_2 = \{X, \emptyset, \{p_a^{0.2}, p_b^{0.5}\}\}$. The Filter which converge to $p_a^{0.2}$ in $\tau_1$ is not necessary converge to same point in fbts $(X, \tau_1, \tau_2)$, since the neighborhood $\{p_a^{0.2}, p_b^{0.5}\}$ of $p_a^{0.2}$ in fbts $(X, \tau_1, \tau_2)$ is not neighborhood of $p_a^{0.2}$ in fts $(X, \tau_1)$. The proposition (2.1) and example (2.1) are leading to the following question (What the difference between the set of all neighborhoods $N'_{p_x^t} or N''_{p_x^t}$at fixed fuzzy point $p_x^t$ and the set of all neighborhoods $N_{p_x^t}$ at same fuzzy point $p_x^t$ in fbts $(X, \tau_1, \tau_2)$?). We note, from example (2.1), $N'_{p_a^{0.2}} \subsetneq N_{p_a^{0.2}}$ since $\{p_a^{0.2}, p_b^{0.5}\} \in N_{p_a^{0.2}}$ and $\notin N'_{p_a^{0.2}}$. This mean, for any fixed fuzzy point $p_x^t$ in $X$, $N_{p_x^t} = N'_{p_x^t} \cup N''_{p_x^t}$. Therefore we can conclude the following:

**Remark 2.3**

The set of all neighborhoods $N_{p_x^t}$ at fuzzy point $p_x^t$ in fbts $(X, \tau_1, \tau_2)$ is not necessary Filter, as following example.

**Example 2.2**

From example (2.1), $\{p_a^{0.5}\}, \{p_a^{0.2}, p_b^{0.5}\} \in N_{p_a^{0.2}}$ but $\{p_a^{0.5}\} \wedge \{p_a^{0.2}, p_b^{0.5}\} \notin N_{p_a^{0.2}}$.
Now, we recall the definition (1.5) to define the cluster fuzzy point of Filter in fbts.

**Definition 2.4**

A Filter $\mathcal{F}$ has cluster fuzzy point (shor. cluster point)in fbts $(X,\tau_1,\tau_2)$ iff $\forall N \in N_{p_x^t}$in fbts $(X,\tau_1,\tau_2)$ then $N \wedge F \neq 0, \forall F \in \mathcal{F}$.

**Proposition 2.2**

Let $(X,\tau_1,\tau_2)$ be fbts. A Filter $\mathcal{F} \subseteq I^X$ has cluster point $p_x^t$ in $(X,\tau_1,\tau_2)$ iff it has same point as cluster point in $(X,\tau_1)$ and $(X,\tau_2)$ together.

**Proof**

Fixed fuzzy point $p_x^t$ which belong to $X$.
$\Rightarrow$ If $\mathcal{F}$ has cluster point $p_x^t$ in $(X,\tau_1,\tau_2)$ then $N \wedge F \neq 0, \forall N \in N_{p_x^t}$and $\forall F \in \mathcal{F}$.i.e, $\forall N' \in N'_{p_x^t}$ and $\forall N'' \in N''_{p_x^t}$, $N', N'' \wedge F \neq 0, \forall F \in \mathcal{F} \Rightarrow \mathcal{F}$ has cluster point $p_x^t$ in $(X,\tau_1)$ and $(X,\tau_2)$ together. $\Leftarrow$ It's easy.

**Remark 2.4**

If the Filter $\mathcal{F} \subseteq I^X$ has cluster point $p_x^t$ in fts $(X,\tau_1)$ or $(X,\tau_2)$, then is not necessary $\mathcal{F}$ has same point $p_x^t$ as cluster point in fbts $(X,\tau_1,\tau_2)$, as following example.

**Example 2.3**

From example (2.1). Let $\beta = \left\{\{p_b^{0.5}\},\{p_a^{0.2},p_b^{0.5}\}\right\}$ is base for some filter $\mathcal{F} \subseteq I^X$, this filter has cluster point $p_a^{0.2}$ in $(X,\tau_1)$, since $\forall N' \in N'_{p_a^{0.2}}$ then $N' \wedge F \neq 0$ $\forall F \in \mathcal{F}$. But $\{p_a^{0.5}\}$ is neighborhood of $p_a^{0.2}$ in $(X,\tau_1,\tau_2)$ and $\{p_a^{0.5}\} \wedge \{p_b^{0.5}\} = 0$, therefore, $p_a^{0.2}$ is not cluster point for filter $\mathcal{F}$ in $(X,\tau_1,\tau_2)$. The following, the relation between the convergence and cluster point.

**Proposition 2.3**

Let $(X,\tau_1,\tau_2)$ be a fbts and let $\mathcal{F} \subseteq I^X$ be filter which converges to fuzzy point $p_x^t$ in $(X,\tau_1,\tau_2)$ then $p_x^t$ is cluster point for $\mathcal{F}$.

**Proof**

From definitions (1.3), (2.3) and (2.4).

**Remark 2.5**

The converse is not true ingeneral as following.

**Example 2.4**

we recall example 2.1. Let $\mathcal{F} \subseteq I^X$ is Filter generate from base $\beta = \{\{p_a^{0.2},p_b^{0.5}\}\}$, then $\mathcal{F}$ has cluster point $p_a^{0.2}$ in $(X,\tau_1,\tau_2)$, but $\mathcal{F}$ is not converges to $p_a^{0.2}$ since the neighborhood $\{p_b^{0.5}\} \notin \mathcal{F}$.

## Fuzzy Filter in sfts

**Definition 3.1, [1]**

A family $\eta \subseteq I^X$ is called supra fuzzy topology if it is closed under arbitrary union and contains $X$. The space $(X,\eta)$ is called supra fuzzy topological space sfts. There more, if we have $\tau_1$ and $\tau_2$ are fuzzy topologies on $X$ and generated the family $\tau_s$ which is a supra fuzzy topology on $X$ then $(X,\tau_s)$ is called the associated supra fuzzy topological space asfts of fbts $(X,\tau_1,\tau_2)$.

**Example 3.1**

From example 2.1, $\tau_s = \{\phi, X, \{p_a^{0.5}\}, \{p_a^{0.2}, p_b^{0.5}\}, \{p_a^{0.5}, p_b^{0.5}\}\}$ is asfts of fbts $(X,\tau_1,\tau_2)$.

**Remark 3.1**

It's obvious from example 3.1, $\tau_1 \cup \tau_2 \subsetneq \tau_s$.

**Definition 3.2**

Let $p_x^t$ be an fuzzy point in $X$ and $(X,\eta)$ is sfts, $\mathcal{N} \in I^X$ is neighborhood of some fuzzy point $p_x^t$ if there some fuzzy set $\ell \in \eta$ such that $p_x^t \in \ell \leq \mathcal{N}$. The collection of all neighborhoods of fuzzy point $p_x^t$ is denoted by $\mathcal{N}_{p_x^t}$.

**Definition 3.3**

A filter $\mathcal{F} \subseteq I^X$ is converge to fuzzy point $p_x^t$ in sfts $(X,\eta)$ if it contains $\mathcal{N}_{p_x^t}$.

**Proposition 3.1**

Let $(X,\tau_s)$ be asfts of fbts $(X,\tau_1,\tau_2)$. A filter $\mathcal{F} \subseteq I^X$ is converge to $p_x^t$ in $(X,\tau_s)$ iff converges to same point in $(X,\tau_1,\tau_2)$.

**Proof**

$\Rightarrow$Let $\mathcal{F} \subseteq I^X$ is converge to $p_x^t$ in $(X,\tau_s) \Rightarrow \mathcal{N}_{p_x^t} \subseteq \mathcal{F}$, but $N_{p_x^t} \subseteq \mathcal{N}_{p_x^t} \Rightarrow N_{p_x^t} \subseteq \mathcal{F} \Rightarrow \mathcal{F}$ is converge to $p_x^t$ in $(X,\tau_1,\tau_2)$.
$\Leftarrow$Let $\mathcal{F}$ is converge to $p_x^t$ in $(X,\tau_1,\tau_2)$. $\forall \mathcal{N} \in \mathcal{N}_{p_x^t}$ then $\mathcal{N} \in N_{p_x^t}$ or contains element $N \in N_{p_x^t}$ such that $N \leq \mathcal{N}$ and from the definition of filter then $\mathcal{N} \in \mathcal{F} \Rightarrow \mathcal{F}$ converges to same fuzzy point in $(X,\tau_s)$.

**Remark 3.2**

As in remark 2.3 and from example 2.2, we can conclude the set of all neighborhoods $\mathcal{N}_{p_x^t}$ of some fuzzy point $p_x^t$ in sfts is not necessary filter.

**Definition 3.4**

A filter $\mathcal{F} \subseteq I^X$ has cluster fuzzy point $p_x^t$ (shor. cluster point)in sfts $(X,\eta)$ if $\forall \mathcal{N} \in \mathcal{N}_{p_x^t}$in sfts $(X,\eta)$then $\mathcal{N} \wedge F \neq 0, \forall F \in \mathcal{F}$.

**Proposition 3.2**

A filter $\mathcal{F} \subseteq I^X$ has cluster point $p_x^t$ in $(X, \eta)$ iff $\mathcal{F}$ has same cluster point $p_x^t$ in fbts $(X, \tau_1, \tau_2)$.

**Proof**

It's obvious, as in proposition 3.1.

**Remark**

From proposition 2.3, remark 2.5 and example 2.4, if a filter $\mathcal{F} \subseteq I^X$ converges to fuzzy point $p_x^t$ in sfts $(X, \eta)$ then $p_x^t$ is cluster point for $\mathcal{F}$ and the converse is not necessary.

## Fuzzy Filter in lufts.

**Definition 4.1, [1]**

Let $(X, \tau_1, \tau_2)$ be a fbts and let $\tau_\ell \subseteq I^X$ be least upper fuzzy topology of $\tau_1$ and $\tau_2$ on $X$, then $(X, \tau_\ell)$ is called least upper fuzzy topological space lufts of $\tau_1$ and $\tau_2$ on $X$.

**Example 4.1**

From example 2.1, $\tau_\ell = \{\phi, X, \{p_a^{0.5}\}, \{p_a^{0.2}, p_b^{0.5}\}, \{p_a^{0.5}, p_b^{0.5}\}, \{p_a^{0.2}\}\}$.

**Remark 4.1**

It's obvious, $\tau_s \subsetneq \tau_\ell$.

**Remark 4.2**

we will denoted for set of all neighborhoods of some fuzzy point $p_x^t$ in lufts $(X, \tau_\ell)$ of $\tau_1$ and $\tau_2$ on $X$ by $\aleph_{p_x^t}$.

**Definition 4.2**

A filter $\mathcal{F} \subseteq I^X$ is converge to fuzzy point $p_x^t$ in lufts $(X, \tau_\ell)$ if it contains $\aleph_{p_x^t}$.

**Proposition 4.1**

Let $(X, \tau_\ell)$be lufts of fbts $(X, \tau_1, \tau_2)$. A filter $\mathcal{F} \subseteq I^X$ is converge to $p_x^t$ in $(X, \tau_\ell)$ iff converges to same point in asfts $(X, \tau_s)$.

**Proof**

$\Rightarrow$ Let $\mathcal{F} \subseteq I^X$ is filter which converges to some fuzzy point $p_x^t$ in lufts $(X, \tau_\ell) \Rightarrow \aleph_{p_x^t} \subseteq \mathcal{F}$, but $\mathcal{N}_{p_x^t} \subseteq \aleph_{p_x^t} \Rightarrow \mathcal{N}_{p_x^t} \subseteq \mathcal{F} \Rightarrow$ $\mathcal{F}$ converges to same fuzzy point $p_x^t$ in asfts $(X, \tau_s)$. $\Leftarrow$ Let $\mathcal{F} \subseteq I^X$ is filter which converges to fuzzy point $p_x^t$ in asfts $(X, \tau_s) \Rightarrow \mathcal{N}_{p_x^t} \subseteq \mathcal{F} \Rightarrow \forall U \in \tau_s$ such that $p_x^t \in U$ then $U \in \mathcal{F}$ and from definition filter, we can conclude for each neighborhood $\aleph$ of $p_x^t$ then $\aleph \in \mathcal{F} \Rightarrow \mathcal{F}$ is fuzzy filter which converges to $p_x^t$ in lufts $(X, \tau_\ell)$.

**Proposition 4.2**

A fuzzy filter $\mathcal{F} \subseteq I^X$ has cluster point $p_x^t$ in lufts $(X, \tau_\ell)$ then $\mathcal{F}$ has cluster point $p_x^t$ in asfts $(X, \tau_s)$.

**Proof**

Its obvious, as proposition 4.1.

**Remark 4.3**

The converse is not true ingeneral.

**Example 4.2**

Let $X = \{a, b, c\}$, $\tau_1 = \left\{\phi, X, \{p_a^{0.5}, p_c^{0.5}\}\right\}$ and $\tau_2 = \left\{\phi, X, \{p_c^{0.5}, p_b^{0.5}\}\right\} \Rightarrow$
$\tau_s = \{\phi, X, \{p_a^{0.5}, p_c^{0.5}\}, \{p_c^{0.5}, p_b^{0.5}\}, \{p_a^{0.5}, p_c^{0.5}, p_b^{0.5}\}\}$. Let $\beta = \{\{p_a^{0.5}, p_b^{0.5}\}\}$ is base for filter $\mathcal{F}$ which has cluster point $p_c^{0.5}$ in $\tau_s$. Now, $\tau_\ell = \{\phi, X, , \{p_a^{0.5}, p_c^{0.5}\}, \{p_c^{0.5}, p_b^{0.5}\}, \{p_a^{0.5}, p_c^{0.5}, p_b^{0.5}\}, \{p_c^{0.5}\}\}$, now $\mathcal{F}$ has not cluster point $p_c^{0.5}$ in $\tau_\ell$ since $\{p_c^{0.5}\} \wedge \{p_a^{0.5}, p_b^{0.5}\} = 0$.

## REFERENCES

1. A. Kandil, A. A. Nouh and S. A. El-Sheikh, "On Fuzzy Bitopological Spaces", Fuzzy Sets and Systems; Vol. 74, PP. 353-363, (1995).
2. C. K.Wong, "Fuzzy Points and Local Properties of Fuzzy Topology", J. Math. Anal. App., Vol. 46, PP. 316-328, 1974.
3. C. L. Chang, "Fuzzy Topological Spaces", J. Math. Anal. Appl., Vol. 24, PP. 182-190, 1968.
4. M.A. DE Prada Vicente and M. Saralegui Aranguren, "Fuzzy Filters", Journal of Mathematical Analysis And Applications, Vol.129, PP.560-568, 1988.
5. M. Muthukumari, A. Nagarajan and M. Murugalingan, "Convergence of Fuzzy Filters", Intjr. Of Mathematical Sciences and Applications, Vol.5, No.2, PP.207-210, 2015.

*Indian Journal of Natural Sciences* www.tnsroindia.org.in ©IJONS

*Vol. 9 / Issue 50 /October 2018* *International Bimonthly* *ISSN: 0976 – 0997*

RESEARCH ARTICLE

# Calculating the Area Vacant Lands for Baghdad City Using Objective Classification Method for High Resolution Satellite Images

Jalal Ibrahim Faraj[1*] and Faleh Hassan Mahmood[2]

[1]Department of Physics, College of Science, University of Baghdad, Iraq.
[2]Remote Sensing Unit, College of Science, University of Baghdad, Iraq.

Received: 20 July 2018 Revised: 23 Aug 2018 Accepted: 25 Sep 2018

[*]**Address for Correspondence**
**Jalal Ibrahim Faraj**
Department of Physics,
College of Science,
University of Baghdad, Iraq.
Email: jalalibrahimskb355@gmail.com, faleh_sine@yahoo.com



## ABSTRACT

This study aims at classifying and calculating vacant lands from high resolution satellite images of Baghdad city by Objective Classification tool in ERDAS program. Such a classification method is regarded as being the latest and most advanced method of image classification. The methodology followed a seven-step, beginning with image processing, followed by classifying the images to calculate vacant lands, and finally an accuracy test was performed. A final thematic map was produced showing the location, number and area of the vacant lands. The results showed that the areas of these lands were about 11 km² (13 % of the study area). The study recommends applying the object classification method for man-made geographical features, as opposed to other types of classifications which are more suitable for natural environmental features.

**Keywords**: Vacant lands, Classification, Satellite images, remote sensing, supervised classification.

## INTRODUCTION

Object-Oriented classification techniques based on image segmentation are gaining interest as methods for producing output maps directly storable into Geographical Information System (GIS) databases [1]. This approach considers not only identification of land cover on a pixel level, but also organization of such pixels into groups (segments) that correspond to real world objects. It involves partitioning image into meaningful objects called segments. The basic processing units of object-oriented image analysis are segments, so-called image objects, and not the single pixels [2]. IMAGINE Objective in ERDAS 2011 version [3] is one of the software solutions to object-oriented classification and feature extraction available in the market. Compared to other tools, it is relatively new and less explored by users. It

is less complex than some of the other tools, which limits its possibilities while making it easier to use [4]. IMAGINE Objective tool employs feature models which work on objects produced by image segmentation and various other pixel-based algorithms which, after being victories, can be processed by geometric and textural parameters [5]. With object-oriented analysis it is possible to get better results from remote sensing information.

**Area of Study**

The study area is Baghdad city. It is the capital and the main administrative center of Iraq. Baghdad is located in the central part of Iraq on both sides of Tigris River with geographic coordinates: Latitude (33°25'46″) to (33°24'21″) N, Longitude (44°15'55″) to (44°17'38″) E. Baghdad is the largest and most heavily populated city in Iraq. Baghdad is suited in a plain area of an elevation between (31-39 m) above sea level. No natural boundaries exist that limits the aerial extension of the city. The Tigris River passes through the city dividing it into two parts; Karkh (Western part) and Rusafa (Eastern part). The area is bounded from the east by Diyala River, which joins the Tigris River southeast of Baghdad. The Army Canal, 24 km long, recharges from the Tigris River in the northern part of the city and terminates in the southern part of Diyala River [6]. Figure-1 shows area of study "Baghdad city"

### Importing of GeoEye-1 Images

GeoEye-1, launched in September 2008, is the latest in a series of commercial high-resolution Earth observation satellites. In the experiment, we choose GeoEye-1 images with 1.65m high resolutions, which was achieved in 2012 and located in Baghdad, Iraq. The size is 14000 × 38000 pixels and it covers an area of about 85 square kilometers.

### Problem statement

The percentage of vacant lands in the city of Baghdad is a true problem because of the difficulty of obtaining housing, so it is necessary to determine the area of vacant lands and create the thematic map using the objective classification tool of being more efficient and modern within the programs of remote sensing. In terms of their ability to classify earthly phenomena in various patterns, especially when using very high-resolution satellite images. The study depends on the objective classification method to calculate the vacant land in the city of Baghdad and through a sample of the city.

**Major objective**

This study tries to achieve a number of goals:

1. The use of remote sensing techniques in extracting vacant land in part of the Baghdad city by the Objective Imagine tool in the ERDAS program.
2. Illuminate steps for advanced classification using objective classification of vacant lands and to produce the thematic map with the highest possible accuracy
3. display thematic map showing the distribution of vacant lands in the study area and Learn about the engineering characteristics.

## Materials and methods

The vacant lands extraction methodology includes the following steps:

### Raster Pixel Processor (RPP)

Single Feature Probability SFP is used to perform pixel based classification. SFP is a pixel cue that computes the probability metric (a number between 0 and 1) to each pixel of the input image based on its pixel value and the training samples. The vacant lands to be extracted are selected by the user as training samples and based on the pixel values of the training samples, the probability values are assigned. Higher probability values are assigned to those pixels whose values are similar to ones of pixels in the training samples. Lower probability values are assigned to pixels whose values are significantly different from the values of pixels in the training samples. The training samples must be chosen very carefully and should not include any background pixel. Pixels other than the pixels that are similar to the training pixels are considered as the background pixels. During the training phase, pixels that are representing the individual objects are submitted to compute pixel cue metrics to train the pixel classifier. During the automated extraction phase candidate pixels from imagery are submitted to the pixels classifier for query to measure how closely they resemble to the training pixels. The output of this step is a pixel probability layer in which each pixel value represents the probability that it is the object of interest. Twelve training samples are selected from the satellite image and seven background pixels are selected. The GeoEyeimage used in this study is shown in Figure 1.Input the test image tiff into ERDAS program 14000 columns and 38000 Rows with.

### Raster Object Creators (ROC)

At this level the raster objects were created using the "segmentation" creator for all feature models. Segmentation is a way of partitioning raster images into segments based on pixel values and locations. Pixels that are spatially connected and have similar values are grouped in a single segment. This operator performs segmentation on the raster image specified by the Input variable parameter. The result is a thematic image where pixel values represent class IDs of contiguous raster objects. The Pixel Probability Layer input (product of the previous level) is used to compute the pixel probability zonal mean of each segment and that zonal mean was used as the value of the segment Pixel Probability attribute. In Figure 2 is presented the result of segmentation.

### Raster Object Operators (ROO)

Afterwards, the processing of the objects created previously followed, using several operators. Size filter and probability filter were used in order to filter out very small, very big and low probability objects. Moreover, morphological filters like dilation and erosion implemented so as to include (or remove for erosion) pixels that belong (or not) to the raster object. Finally, the "reclump" operator was very useful to perform a clump operation. The input layer of this operator is usually a layer of raster objects which have been split, joined or filtered by other operators, and no longer have correct clump values. This operator renumbered the raster objects so that each raster object (group of contiguous pixels) has a unique value. In Figure 3 is presented the final result of ROO level

### Raster To Vector Conversion (RVC)

At this level the objects automatically were converted by the software from raster to vector format.

### Vector Object Operators (VOO)

These operators perform operations on the vector objects, and produce a new Vector Object Layer. These operations may be necessary to change the shape of the vector objects by generalizing, smoothing, etc. This operator simplifies polylines and polygons by removing unnecessary vertices. It helps remove noise and improves the performance of downstream processing for removing noise and pixel artifacts in a polygon or polyline a tolerance value must be entered. This algorithm creates trend lines from each arcs starting point, and to other arcs. Then the distance is

measured for each vertex to its trend line. If the distance of the vertex to the trend line is greater than the tolerance, the vertex is then removed. Thus, a tolerance of 0 will not remove any vertices and a larger tolerance will remove many vertices. The value of tolerance entered in this model is 0.50 meters, In Figure 4 is noted the final result of VOO level.

**Vector Object Processor (VOP)**

The Vector Object Processor node performs classification on vector objects. Vector object classification involves specifying one or more cues which are used by an Object Classifier. The cues include metrics which measure some property of vector objects. The Object Classifier uses the cues to assign a probability to each object in a group of vector objects.

**Vector Cleanup Operators (VCO)**

Vector Cleanup Operators allow the user to manipulate the Vector Objects after they have been processed by the Vector Object Processor. Vector Cleanup Operators typically clean up the set of vector objects to produce a nice final output. Some Vector Cleanup Operators will use the Probability attribute generated by the Vector Object Processor in the operation. Some typical operations: Reshaping the existing vector objects for a more presentable output, Eliminating Vector Objects that do not meet some criteria or that have low probability, matching vector objects to a template or fitting them to a fixed shape or shape type such as an orthogonal polygon, combining multiple input Vector Objects into a single vector object, splitting vector objects into multiple new vector objects, Converting polygon objects into polylines, and vice-versa This operator smoothens the polygon objects in a vector layer. The smoothing factor is specified to control how much smoother the objects become. Enter any value between 0 and 1. 0 indicates no smoothing is applied to the objects, while 1 applies the greatest smoothing. For less smoothing, choose less than 0.5. For more smoothing (for example, to cut sharp turns more), choose more than 0.5. The value taken here is 0.5. The bigger the factor, the smoother is the polygon objects, In figure 6 is presented the final result of vacant lands extraction model

## RESULTS AND DISCUSSION

The method described above automatically extracts vacant lands from satellite images. The original GeoEye image and the extracted vacant lands from that image are shown in Figure 1 and Figure 5, where using the developed feature extraction models in detected the vacant lands in the image. The results show that the similarity of the vacant lands and building roofs lead to spectral overlap because of the dust found on the building roofs. Note from the figure 5 as we move away from the city center towards the outskirts, increasing the vacant lands due to decreasing population density and also we note from table 1 the ratio of vacant lands to study area is 13% which can be regarded as fairly acceptable and the area of vacant lands is 11km$^2$.

## CONCLUSION

The stability of dust particles on the roofs of buildings and streets due to the frequency of dust storms lead to reduce the accuracy of classification and creates a great similarity between the properties of reflected radiation from vacant lands and other phenomena which may be classified as vacant lands. The existence of building debris, cars or any other phenomenon within the vacant lands also lead to reducing the accuracy of classification, therefore to increases the accuracy of classification, we select more points within all part of the image.

## REFERENCES

1. Grignetti, A., F. Giannetti, and D. Coaloa, 2011. Identification of death trees in forest areas through object and pixel oriented approaches applied to IKONOS images. *RivistaItaliana Di Telerilevamento,*. 43(1), 3-17.
2. Benz, U.C 2004. Multi-resolution object- oriented fuzzy analysis of remote sensing data for GIS- ready information. *Isprs Journal of Photogrammetry and Remote Sensing*, 58(3-4): p. 239-258.
3. "Imagine Objective, User's Guide 2011,"
4. ChepkocheiL. C., 2011,Object-oriented image classification of individual trees using ERDAS Imagine Objective: Case study of Wanjohi area, Lake Naivasha Basin, Kenya, proceedings, Kenya Geothermal Conference, November 21-22,.
5. Lack N. and S. Bleisch, 2010, Object-based change detection for a cultural-historical survey of the Landscape - From cow trails to walking paths, The International Archives of the Photogrammetry, Remote Sensing and Spatial Information Sciences,, vol. XXXVIII-4/C7.
6. Bushra Q. Al-Abudi1, Mohammed S. Mahdi and Yasser Ch. B., 2016. Study of Land Cover Changes of Baghdad Using Multi-Temporal Landsat Satellite Images, *Iraqi Journal of Science*, 57(3B), 2146-2160.

**Table 1. Metadata for Vacant lands**

| The description | The value |
|---|---|
| The area for Baghdad city | 204.2 $km^2$ |
| The area study | 84 $km^2$ |
| Ratio of the study area for Baghdad city | 41% |
| Number of vacant lands | 3559 |
| The area of vacant lands | 11 $km^2$ |
| Ratio of the vacant lands for study area | 13% |
| Max value for vacant lands | 550113 $m^2$ |
| min value for vacant lands | 13 $m^2$ |
| Mean value for vacant lands | 3013.29 $m^2$ |
| Standard deviation for vacant lands | 14679.07 $m^2$ |

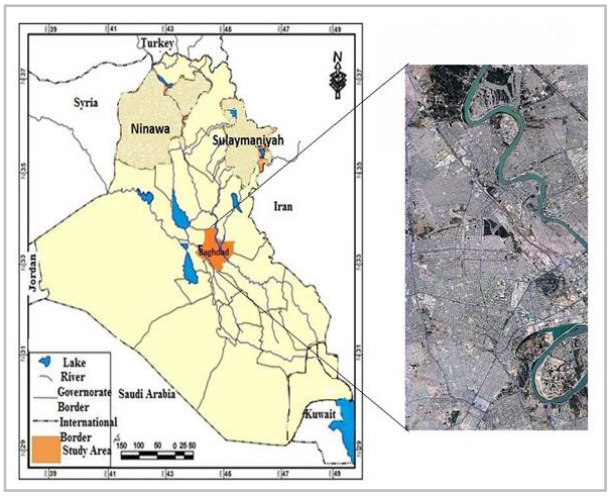


**Figure 1. Area of study "Baghdad city"**

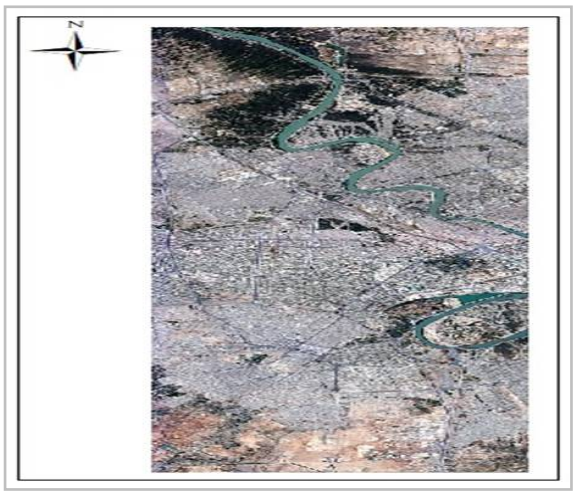


**Figure 2. GeoEye-1 Satellite Image**

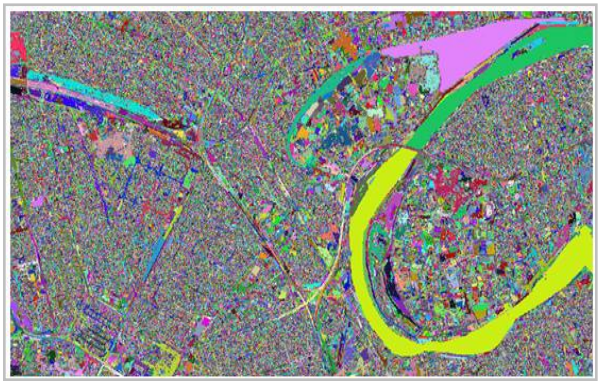

**Figure 3. Final result of segmentation for subset image**

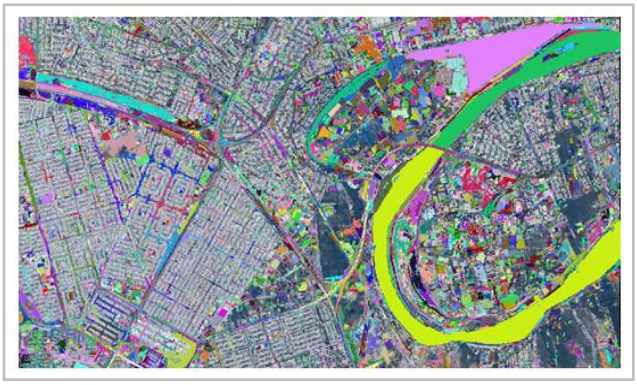

**Figure 4. The final result of ROO level for subset image**

**Figure 5. The final result of VOO level for subset image**

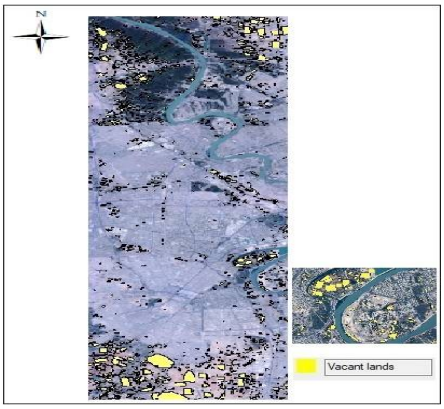


**Figure 6. The final result of vacant lands extraction Model**

*Indian Journal of Natural Sciences* www.tnsroindia.org.in ©IJONS

*Vol. 9 / Issue 50 /October 2018* *International Bimonthly* *ISSN: 0976 – 0997*

RESEARCH ARTICLE

# Classification of Residential Group in the City of Baghdad from Trees and Green Areas using High-Resolution Satellite Images

Gheidaa Sabeeh Al-Hassany[1*] and Alaa Hassan Harif[2]

Unit of Remote Sensing, College of Sciences, University of Baghdad, Iraq.

Received: 20 July 2018 Revised: 25 Aug 2018 Accepted: 28 Sep 2018

[*]**Address for Correspondence**
**Gheidaa Sabeeh Al-Hassany**
Unit of Remote Sensing,
College of Sciences,
University of Baghdad, Iraq.
Email: gheidaa_sab@yahoo.com, AlaaHarif@Scbaghdad.edu.iq



## ABSTRACT

In this research, scenes of a high resolution satellite images of the city for the years 2002 and 2017 of Baghdad were studied from where containing green spaces (gardens) and untapped areas by analyze and classify the extracted scenes by applying remote sensing techniques for the analysis and classification of satellite images in the Geographic information system by using ArcMap GIS program. The scenes of high resolution satellite images were captured by the satellite landsat 8 for the sensor ETM+ with spatial resolution (0.5*0.5) meter square for the one pixel. The reason for this study is that people in most of the cities of Iraq, especially in the capital Baghdad, cut houses and villas into small houses because of the high prices of real estate and high rents and the growth of families may be the area of these small houses sometimes forty square meters Previously, a third of the area of houses occupied by gardens and after the shredding The areas occupied by these gardens have declined and in many of these houses after the cutting and construction of small houses the area has completely disappeared gardens and to study the change in the use of land in one of the residential areas in the capital Baghdad and show deterioration and decline in the survey In these areas, we classified the same area in the first two phases of 2017 and the second in 2002

**Keywords:** High-resolution, satellite images, ArcGIS, PCA, Baghdad, classification

## INTRODUCTION

### Satellite imagery (SI)

Earth images or images of planets clipped by satellites of images running by regimens and interested people. Images of satellites were produced by NASA are published by NASA EO (Earth Observatory) and are obtainable free to all

interested people. In this century SI became vastly obtainable when reachable, simple for using software with access to SI database was given by several companies and organizations.Images of satellites became widely applicable in meteorology, Sea science, fishing, farming, Ecology, forests, landscape, geology, cartography, urban planning, and wars. Images are in visible electromagnetic region and in other. In addition to above, there is a radar image; it is used in the field of elevation maps [1].

## Resolution of image

SI resolution in RS has the types: spatial, spectral, temporal, and radiometric. These types are defined as following:

- Spatial Resolution: representation the size of image pixels with the size of the surface area (i.e. $m^2$) being measured on the ground, determined by the sensors' IFOV (instantaneous field of view).
- Spectral Resolution: is known as the size of the interval of wavelength interval (discrete segments of the ES electromagnetic spectrum) and no. of intervals the sensors are measuring.
- Temporal Resolution: Usually known as a period of time that separated between the collected images for the same location.
- Radiometric resolution is defined as the ability of any imaging system for recording various levels of brightness and the no. of gray-scale levels of the sensor, it is usually having the expresses: 8_bit {0_255}, 12_bit {0_4095} or 16_bit {0_65,535}.
- Geometric resolution: is the sensor ability to effectively image a portion of the ground in one pixel and is usually has the express: GSD. Ground sample distance has a meaning of contain the inclusive optic and systemically noises sources in addition to Its usefulness for comparison the best equality of sensors can recognizes the feature on the earth locations for one pixel. [2]

Google Earth GE is a program of computers renders a three dimension represent and recognition of ground surface depending on SI. It is mapping the ground surface by the superimposition of images acquired from SI, Aerial Photography and GISData for a 3D Globe, to allow the user to seeing towns and buildings at different directions. GE allows user to searching reach the address for most countries, and has their coordinates.User can use the GE to add his special data, letting this data obtainable to groups like forums. GE has the ability to view different types of images overlaid on the ground in addition to a WebMapService customer. [*3*] GE's imagery is exhibited on a digital Globe, which exhibits the Earth surface in one image (compositing image) at afar range. Next a zoom in afar appropriate, the difference among images may be finer details when the imagery transitions into various images of the interested location, which don't have the same date or time from area to the next. The collected images are recaptured from Satellites or Aircraft [4]. Before NASAs launching and the USGS, Landsat-8 satellite, Google cooperated slightly with SI from Landsat-7, which had problems in a hardware Lead to diagonal holes in the image [5] In 2013, GE used Data mining to solve the problem, providing what was qualified as a successor to the Blue-Marble image of earth, with a single large image of the globe. This was carried out by combining multiple sets of images possessed from Landsat-7 for elimination the cloud effects and diagonal gaps, for creation a single mosaic image [6] GE recently deal with Landsat-8 to provide images in a higher resolution and with greater frequency.[*7*] Imagery Resolution ranges from 15 m of resolution to 15 centimeters. GE Mostly showing areas in 2D and 3D for some areas are available, most of them typically cities. [*8*]

## Classification and High Resolution Images

Classification process (CP) for urban places of very high resolution imagery (VHRI) is a quite complicated mission. Impervious urban land cover (IULC) like structures, streets, and car-park are very close in their spectral to be recognized using only the spectrally traditional information of VHRI. In addition to that information is required for recognizing such features to classify. Recently, a very high resolution SI data (Spatial Resolution $\leq 1$ meter) was available since 1999 then the classification of urban land cover data becomes an emanating domain for researching in the RS communities. For the rezone of the sub-meters Spatial Resolution, VHRI has a highly potential in deep details

and precise mapping of urban land covers [9].For recognition IULC like structures, streets, and car-park and flagged places supplemental information would be inserted into the CP. Moreover information may be the spatially measures extracted either from the scene, in the texturally form, morphologically, and contextually measures, or from ancillaries data [10]. At the last decade, a significant amount of research has utilized spatially measures extracted from the scene such as morphology, texture and context in the CP of VHRI over IULC [11]. Shadow is a darkness feature in optically image, it is an active feature that reducing the spectrally values of the shading object and then it is influence in the classifying of land cover [12]. According to that, the classifier must firstly extract and exclude shadows from the subsequently classification. Later, the covering feature by shadow then must be assigned to street or building depending on its nearer pixels to these classes. As mentioned, in this paper, the considered shadows are of buildings and not shadow under trees. Trees shadows were added in the class of trees. After the extraction of shadows, they would be added to their corresponded features class. Some of buildings have level roofs then shadows of the top covers parts of the lower levels. Shadows may be covering the roads, but mostly of shadows in the scenes are cast by houses, most of the shadow areas belong to streets or upper floor surfaces. It should be noted that this rule may not be necessary responsible to other locations have differences urban structures.

PCA is a statistical procedure that uses an orthogonal transformation to convert a set of observations of possibly correlated variables into a set of values of linearly uncorrelated variables called principal components (or sometimes, principal modes of variation). The number of principal components is less than or equal to the smaller of the number of original variables or the number of observations. This transformation is defined in such a way that the first principal component has the largest possible variance (that is, accounts for as much of the variability in the data as possible), and each succeeding component in turn has the highest variance possible under the constraint that it is orthogonal to the preceding components. The resulting vectors are an uncorrelated orthogonal basis set. PCA is sensitive to the relative scaling of the original variables.

## Multivariate Data Transformation: Principal Component Analysis

Principal Component Analysis PCA, in mathematic have the definition: "An orthogonal linear transformation that transforms the data to a new coordinate system such that the greatest variance by some projection of the data comes to lie on the first coordinate (called the first principal component), the second greatest variance on the second coordinate, and so on" [ 13 ] PCA is utilized to transform the data attributes in a multi-band raster from the input multivariate attribute space to new space whose axes are rotated with respect to the old space. The new axes aren't correlated. The main goals of PCA transformation are the compression of data by reducing redundancy, emphasizing the variances in raster bands, and let the data be more explainable.The result of applying a PCA technique is a multi-band raster have equal number of bands to the old raster (one band per axis in the new multivariate space). The first principal component will have the greatest variance; the second will show the second most variance not described by the first, and so third. Many times, the first three to four layers of the new raster from the PC function may contain more than 95 % of the variances. The other layers resulting of PC raster may be dropped and the described multivariate procedures may be performed on this new raster vice the old raster. The new raster contains less number of layers and more than 95 % of the variances of the old raster, then a faster computation, and accuracy will be obtained.The PC function may has an input multi-band raster to be identified, the number of PCs into which the data be transform, the statistics output file title, and the output raster title. The output raster will contain the same number of bands as the specified number of components. Each band will depict each component.

## The concept of PCA in Arc_GIS program

Theoretically, a two-layer raster is used, a shift and rotate processes of the axes and a transforming of the data is done as following:

- The data is graphed in a scatter-plot.

- In scatter-plot, points are bounding with a calculated ellipse (as shown in fig. 1).
- The major axis of calculated ellipse is determined (as shown in fig. 2). The major axis will become the new x-axis, the first principal component (PC1). PC1 depicts the greatest variation because it is the largest transect that can be drawn through the ellipse. The direction of PC1 is the eigenVector and its magnitude is the eigenValue. The angle of the x-axis to PC1 is the rotation angle that is used in the transformation.

A calculation of the orthogonal perpendicular line to PC1 is done. It represents the PC2 and the new y-axis (as shown in fig. 3).The new axis describes the second most variance not described by PC1.Using the eigenVectors, the eigenValues, and the calculated covariance matrix of the input of the multi-band raster, a linear formula defining the shift and rotation is created. This formula is applied to transform each cell value relative to the new axis. [14].

### Study region

Baghdad has 11 districts, Al-Adhamiya is one of these districts, Al-Fahama is a sub-district located in Al-Adhamiya District then HaiUr is located in Al-Fahama sub-district. It is a large residential area, it is bordered to the east by Al-Sader City and it is bordered to the west by Al- Shaab, from the north it is bordered by Al-Shaab and Al-Sader and from the south by Al-Benoge City. The area of study is located in the northern outskirts of Baghdad province, north of Fahama sub-district in Hei-Ur between longitude 44.425491$^{o}$ and latitude 33.421750$^{o}$ south to longitude 44.428885 and latitude 33.424658 north. This region was chosen to observe the change in green areas in the period between the years 2002 (as shown in fig. 4) to 2017 (as shown in fig. 5).

## MATERIALS AND METHODS

The data of a high resolution image is a correlated data and have a redundant. To avoid that, PCA technique was applied to each one of the two images data before the classification techniques.Polygon technique (A technique in the Tools of ArcGIS program) is applied in the study scene taken from a Landsat-8 satellite image (high resolution image) in order to determine and distinguish the green lands in the resulted raster of classification from the rest of the details of a scene like houses and streets and then study these green lands. The following steps were followed to apply the method

1. The Google Earth image**s for the years 2002 and 2017 of the study region** were utilized in ArcGIS program.
2. UTM project was chosen for the coordinates because it is a convenient for small spaces (lease than one zone).
3. A geo-reference technique was applied to each image to give their real coordinate.
4. The scene of HeiUr was extracted from the original Landsat satellite image by using the techniques of spatial analyst tools, as following:
   A. A zooming command was activate on the interested region (the studied area) to let the recognition of the selection of the boundaries be possible.
   B. A polygon shape file is created to detect the boundaries lines and curves points as a vertex of the created polygon to be as a mask to extract the studied region. As shown in Fig.6. Then the extracted study region was result as shown in fig.7.
5. To avoid the mix with houses shadows a polygon shape file process was applied to extract the shadow regions to reduce the errors in the classes as following:
   A. A zooming command was activate on the interested region (the studied area) to let the recognition of the selection of the boundaries be possible.
   B. A polygon shape file is created to detect the boundaries lines and curves points as a vertex of the created polygon to be as a mask to extract the houses shadows. As shown in Fig.8. Then the extracted regions was result as shown in fig. 9

6. PCA technique was applied to each one of the two extracted scenes data to de_correlate the data of each one. The resulted PCA raster of each image were shown in fig.10
7. A collection process was applied for each scene data with the PCA of that scene. Then the resulted raster is illustrated in fig. 11.
8. Perform normalization technique (i.e. Using Unique Values Criterion) on the resulted raster of collection process pixel values (as shown in fig. 12) to produce different ranges of classes to make the account process of each class be possible.
9. The classification process was applied of each resulted raster from the Unique Values Criterion process by the symbology in the properties day lock box, as shown in fig. 13
10. The account of each class pixels was multiplied by the spatial resolution value for each satellite image to calculate class area for each of them. These calculations are illustrated in bellow.

The length of each block = 181.4 m
The width of each block = 228.8 m
The total area of each block =41504.32 $m^2$
The selected green and other regions = The total area of any block – The extracted areas from the block
Then the results of the calculation are illustrated below in table1:

# RESULTS AND DISCUSSION

The utilized data (images of Landsat-8 satellite) were chosen to be the studied regions for this paper. These two images are a high spatial resolution images (0.5 meter*0.5 meter for the pixel). As shown in the steps of the methodology that the extraction technique was done to reduce the mix among classes then the PCA technique was applied too for each scene to de-correlate the data then the classification process was applied successfully and the pixels of the green areas were appeared clearly in each scene. These steps give a perfect result for this type of image to avoid the high redundancy among the pixels and reducing them to minimize the mix among the classes. Table- (1) represents the number of points (pixels), the area of each class and the percentage of classes' areas obtained by implementing the classification method.

## CONCLUSION

High-resolution satellite images, up to a few centimeters in diameter, can be defined as rich images in fine detail, but these details are highly correlated. It is very useful when dealing with such images to apply PCA technique, especially in the field of classification because it is very effective to transform the image data to uncorrelated data by reducing the high redundancy among the pixels.The application of the PCA technique in ArcGIS is very easy and perfect, for two important rezones first is the high construct of the facilities of the image data and the second is the possibilities offered by the Arc_GIS program for many technologies In the past has been more complicated steps to let be applied because the pre-processing of multi-temporal satellite images are less developed than it is now

## REFERENCES

1. Shall, Andrea (September 6, 2008). *"GeoEye launches high-resolution satellite".* Reuters. *Retrieved 2008-11-07.]*[https://en.wikipedia.org/wiki/Satellite_imagery
2. Campbell, J. B. 2002. Introduction to Remote Sensing. New York London: The Guilford Press][ https://en.wikipedia.org/wiki/Satellite_imagery
3. *"Keyhole Markup Language — Google Developers". Developers.google.com. 2012-03-01. Retrieved 2013-06-15.*] [https://en.wikipedia.org/wiki/Google_Earth
4. "How images are collected". Google. Retrieved August 6, 2017.

5. "SLC-*off Products: Background" United States Geological Survey. Retrieved August 6, 2017.*
6. *."Only clear skies on Google Maps and Earth". Google. June 26, 2013. Retrieved August 6, 2017.*
7. *"Google Earth and Maps get sharper satellite imagery with new update". Tech Crunch. June 27, 2016. Retrieved August 6, 2017.*
8. *"Dive into New Google Earth". Retrieved 2009-02-03.* http://en.wikipedia.org/wiki/Google_Earth
9. Pacifici, F.; Chini, M.; Emery, W.J. A neural network approach using multi-scale textural metrics from very high-resolution panchromatic imagery for urban land-use classification. *Remote Sens. Environ.* 2009, *113*, 1276–1292.
10. Salehi, B.; Zhang, Y.; Zhong, M.; Dey, V. A review of the effectiveness of spatial information used in urban land cover classification of VHR imagery. *Int. J. GeoInf.* 2012, *8*, 35–51.
11. www.mdpi.com/journal/remotesensing] [*Remote Sens.* 2012, *4*, 2256-2276; doi:10.3390/rs4082256, ISSN 2072-4292] [Object-Based Classification of Urban Areas Using VHR Imagery and Height Points Ancillary Data, Bahram Salehi 1,*, Yun Zhang *Received: 10 June 2012; in revised form: 20 July 2012 / Accepted: 26 July 2012 / Published: 3 August 2012.*
12. Lu, D.; Hetrick, S.; Moran, E. Land cover classification in a complex urban-rural landscape with Quickbird imagery. *Photogram. Eng. Remote Sensing* 2010, 76, 1159–1168.
13. Jolliffe I.T. Principal Component Analysis, Series: Springer Series in Statistics, 2nd ed., Springer, NY, 2002, XXIX, 487 p. 28 illus. ISBN 978-0-387-95442-4
14. Jensen, John R. Introductory Digital Image Processing: A Remote Sensing Perspective. Prentice–Hall. 1986

**Table 1: Illustrated results of the calculation**

| | The green regions | | The percentage from the total area | The other regions | | The percentage from the total area |
|---|---|---|---|---|---|---|
| | Number of pixel region | The area | | Number of pixel region | The area | |
| 2003 scene | 68653 | 17163.25 $m^2$ | 41.35% | 97364.28 | 24341.07 $m^2$ | 58.65% |
| 2017 scene | 53387 | 13346.75 $m^2$ | 32.16% | 112629 | 28157.25 $m^2$ | 67.84% |

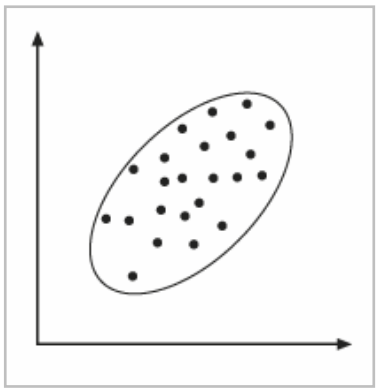

**Figure 1: A calculated ellipse is Bounding the points in the scatter-plot**

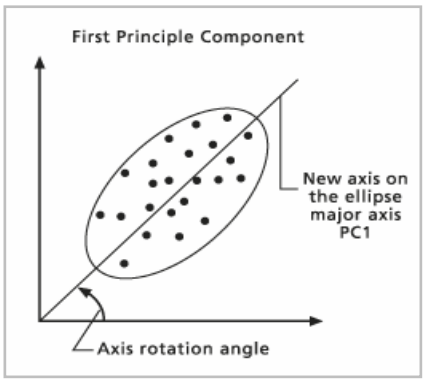


**Figure 2: A determination of the ellipse major axis was done**

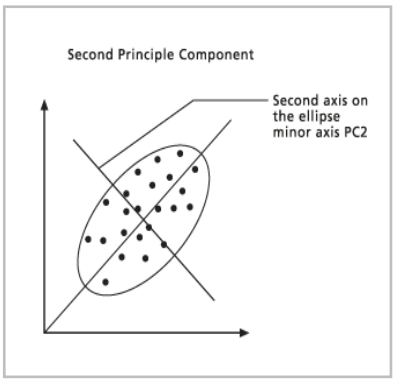


**Figure 3: Illustrates the calculated orthogonal perpendicular line to PC1.**

**Figure 4: The northern outskirts of Baghdad province, north of Fahama sub -district, Hei_Ur in 2017.**

**Figure 5: The northern outskirts of Baghdad province, north of Fahama sub -district, Hei_Ur in 2002**

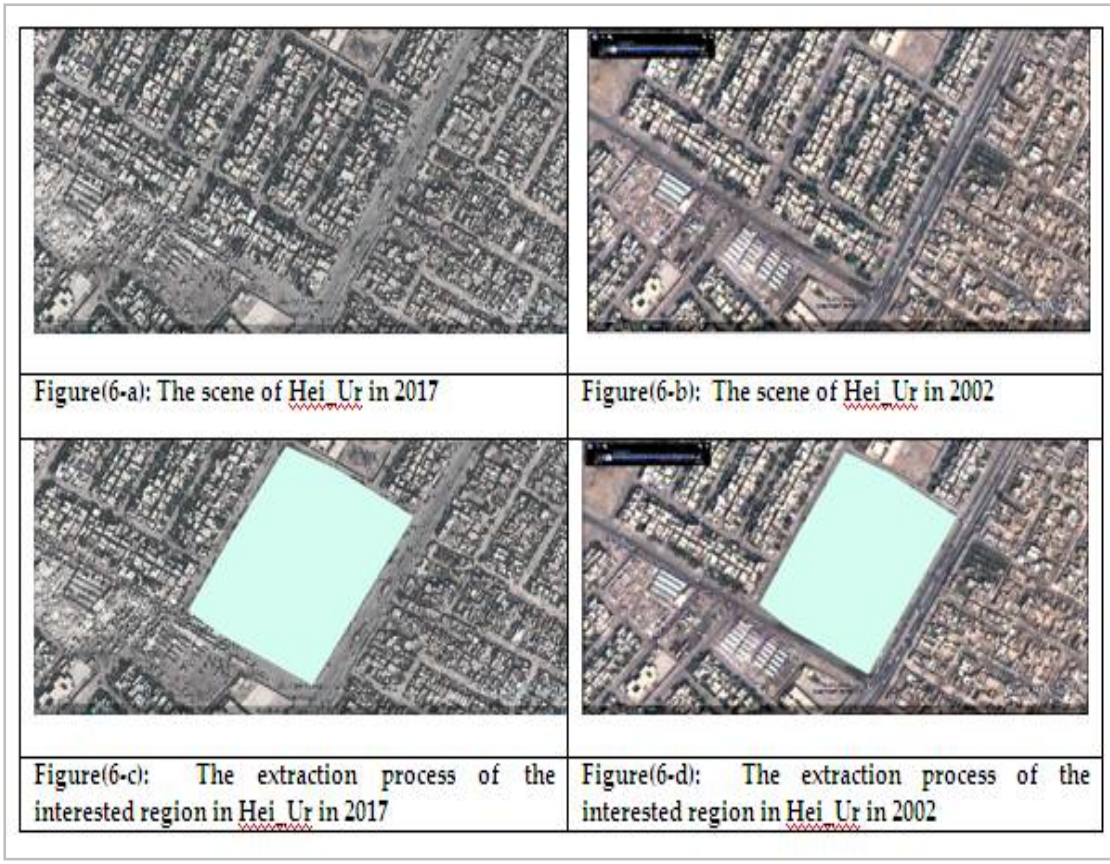


**Figure 6: The extraction process of the interested region in each scene**

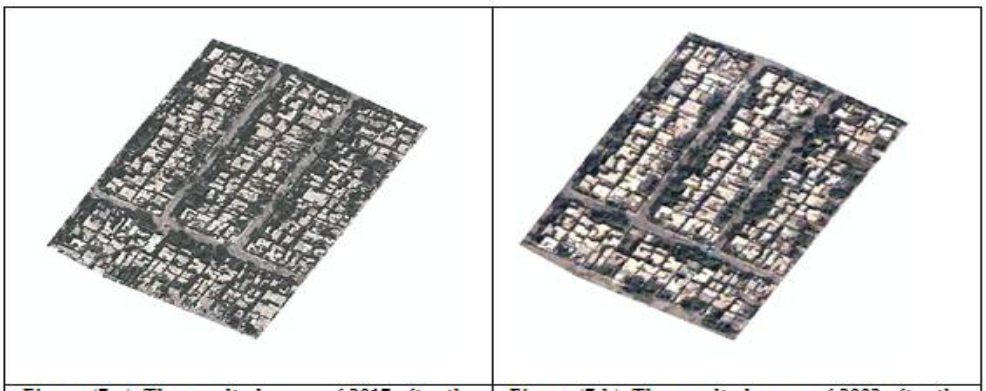

Figure (7-a): The resulted scene of 2017 after the extraction process

Figure (7-b): The resulted scene of 2002 after the extraction process

**Figure7: The resulted two scenes of 2017 and 2002 after the extraction process**

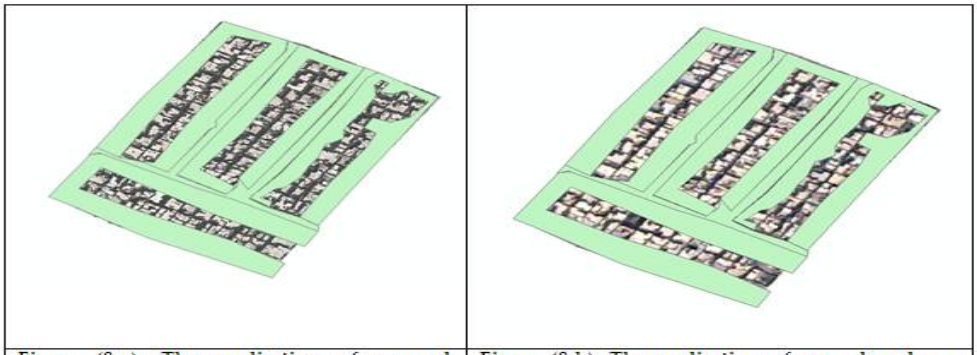

Figure (8-a): The application of a mask polygon shape file process on the 2017 extraction scene

Figure (8-b): The application of a mask polygon shape file process on the 2002 extraction scene

**Figure 8: The application of a mask polygon shape file process on the 2017 and 2002 two extraction scenes to extract the shadow regions**

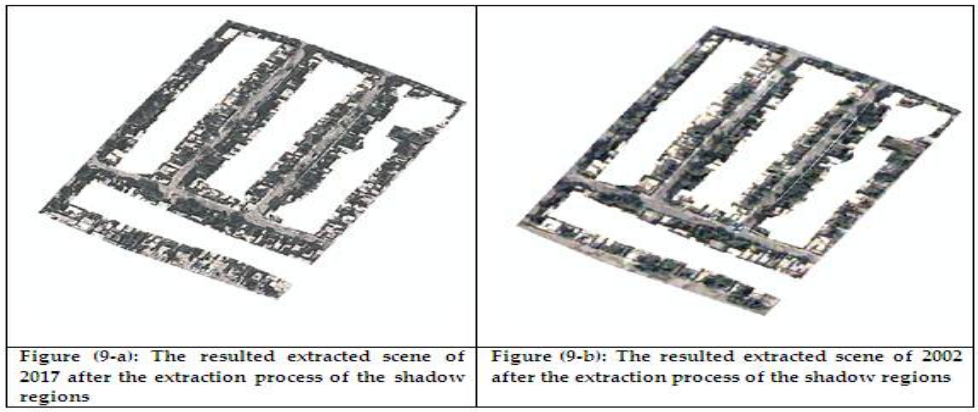

Figure (9-a): The resulted extracted scene of 2017 after the extraction process of the shadow regions

Figure (9-b): The resulted extracted scene of 2002 after the extraction process of the shadow regions

**Figure 9: The resulted two extracted scenes of 2017 and 2002 after the extraction process of the shadow regions**

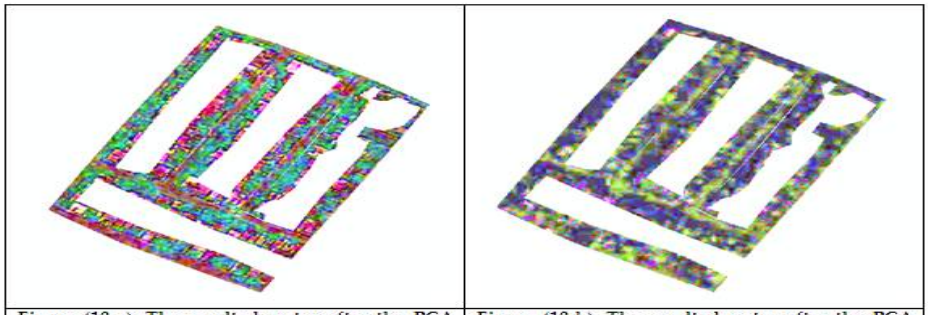

Figure (10-a): The resulted raster after the PCA application on the extracted scene of 2017

Figure (10-b): The resulted raster after the PCA application on the extracted scene of 2002

**Figure10: The resulted PCA raster of each image**

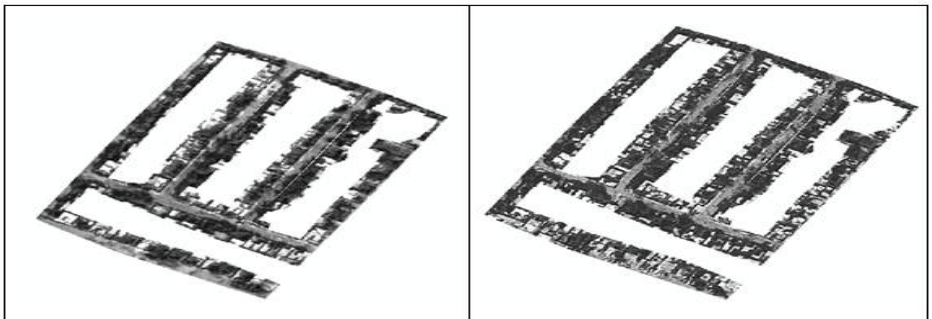

Figure (11-a): The resulted raster of after the collection process application on the extracted scene of 2017

Figure (11-b): The resulted raster of after the collection process application on the extracted scene of 2002

**Figure 11: The resulted raster of each image after the collection process application**

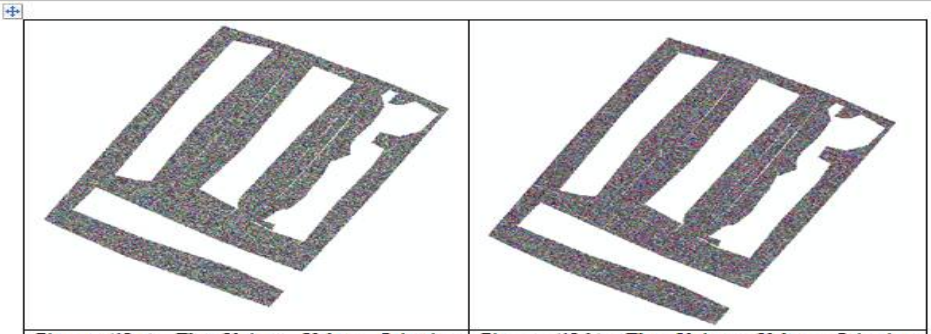

Figure (12-a): The Unique Values Criterion process application of 2017 resulted raster from the collection process.

Figure (12-b): The Unique Values Criterion process application of 2002 resulted raster from the collection process.

**Figure 12: The Unique Values Criterion process application of each resulted raster from the collection process**

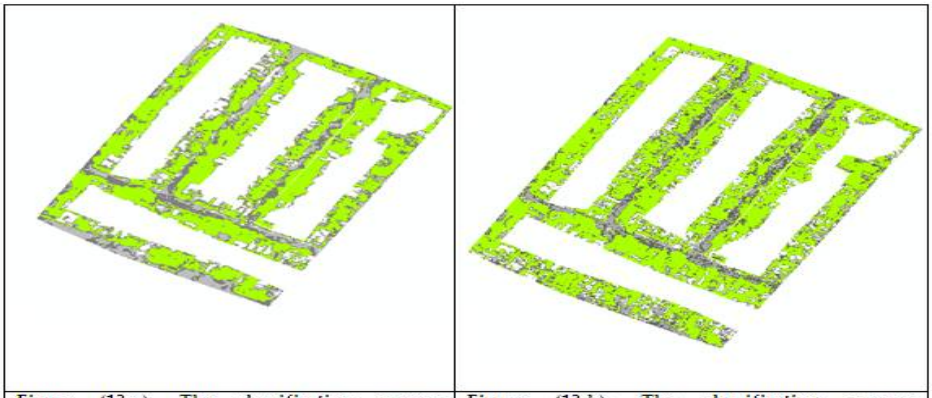

Figure (13-a): The classification process application of 2017 resulted raster from the Unique Values Criterion process.

Figure (13-b): The classification process application of 2002 resulted raster from the Unique Values Criterion process.

**Figure 13: The classification process application of each resulted raster from the Unique Values Criterion process.**

*Indian Journal of Natural Sciences* www.tnsroindia.org.in ©IJONS

*Vol. 9 / Issue 50 /October 2018* *International Bimonthly* *ISSN: 0976 – 0997*

RESEARCH ARTICLE

# A Retrospective Studyon Pet Birds Rearing in Kerala State of India

P.C.Divya, Joseph Mathew, Sabin George*, A.Kannan, K.Shyama, and M.K.Muhammad Aslam

Department of Livestock Production Management, College of Veterinary and Animal Sciences, Mannuthy, Thrissur, Kerala, India.

Received: 16 July 2018 Revised: 18 Aug 2018 Accepted: 25 Sep 2018

***Address for Correspondence**
**SABIN GEORGE**
Department of Livestock Production Management,
College of Veterinary and Animal Sciences,
Mannuthy, Thrissur, Kerala, India.
Email: sabingeorg@gmail.com



## ABSTRACT

A study on the socio-economic profile of pet bird owners and details of birds maintained as pets by the pet bird owners was taken up in Ernakulam district of Kerala. Data were collected from pet bird owners in their own premises by personal interview using a pre-tested questionnaire.Mainly the owners of the dogs were the male members of the family. Self-employed people and businessmen were more interested in bird keeping.Pigeons were the most preferred variety followed by budgerigars.The number of birds owned per household was 1-50 for than halfof the households surveyed. The birds were mostly kept for recreation and business purpose.

**Keywords**: Socio-economic profile, bird keeping, self-employed people, pigeon keeping

## INTRODUCTION

Rearing of pet birds not only act as a tool for stress alleviation in the modern society but also open an avenue for entrepreneurship for unemployed youth. Pet bird owners are on the increase here in India. There are more than 400 varieties of pet birds to choose from.Birds remain the most popular specialty or exotic pet, second only to fish. Although birds have been popular as pets for thousands of years it is now easier than ever to maintain them successfully. The wide range of prepared foods enables bird keepers to offer all types of birds a balanced diet and modern equipment and accessories have greatly eased care, feeding, and breeding of all species. Even though pet bird population is increasing in India, systematic studies on distribution, management, and marketing of pet birds are scarce and scanty. Statistics on pet bird population in India or in Kerala is not available. The information regarding the management practices followed at the household level is meager. Hence it is a need of the time to develop certain strategies to augment this sector. The present study was conducted to analyze the socio-economic profile of pet bird owners of Kerala and the distribution pattern of pet birds, taking Ernakulam district as a sample.

## MATERIALS AND METHODS

A total of 33 pet bird owners from Ernakulam district of Kerala who maintain pet birds were surveyed. A purposive random sampling method of survey utilizing a structured questionnaire and personal interview was conducted in the study area. Details regarding breeding, feeding, housing, management, marketing, health status and disease problems of pet birds were studied. A detailed questionnaire was prepared to incorporate the details regarding the socio-economic profile of the pet bird owners and the management details such as selection of birds, housing, feeding, breeding, health care, training, welfare and major constraints in bird keeping. A pilot study was also carried out to test the efficacy of the questionnaire. The data collected were analyzed for mean and standard error using SPSS package and the results were categorized and tabulated [1].

## RESULTS AND DISCUSSION

The average age of pet bird owner was 41.88±2.11years.This is almost in agreement with the finding of Anderson [2]. He reported that the bird owners are in the age range of 41 to 50. This also indicates the need for attracting men and unemployed youth to the sector. The average family size was 4.06±0.2numbers. Mainly self-employed (48.4 percent) and businessmen (18.1 percent) were engaged in pet bird rearing.12.1 percent of the owners were private employees, 9 percents were students and 6 percent each were un-employed and retired people. This may be because self-employed and businessmen are getting more spare time for taking care of the birds than the employed people. Bird owners were the male members of the family in 93.9 percent of the households surveyed.This result is in contrast to the findings [2, 3, 4]. According to those three studies in the US, the majority of the bird owners were females. The male dominating family structure existing in Kerala and the socio-cultural difference may be the reasons for such a result. Lack of awareness on the prospects of pet bird rearing among women may be the other reason.Among all, 60.6 percent of the bird owners were undergraduates, 15.1 percent were having high school education, 3 percent were diploma holders, 3 percent were postgraduates, 6 percent were professionals, 6 percent had higher secondary education and 6 percent hadlower primary education only. The female bird owners were found to be unemployed.

The financial status of the pet bird owners was also surveyed. About 24 percent of the pet bird owners reported to had an annual income above 2 lakhs, 42.4 percent had it ranging between one and two lakh rupees, while 30.3 percent had a range of fifty thousand to one lakh whereas 3 percent had less than fifty thousand rupees.This finding is in accordance with findings of American Veterinary Medical Association (AVMA) survey [4],that household income levels were not a big determining factor in the ownership of birds. More than fifty percent (54.5%) of the pet bird owners had land holdings less than 10 cents, 12.1 percent had 10-20 cents, 27.2 percent had 20-50 cents and 6 percent had 1-2 acres. This is due to the fact pet bird rearing is more oriented towards the peripherals of the urban area where individual land holdings may be lesser compared to rural areas. Pet bird rearing is an important entrepreneurial opportunity for persons with fewer land holdings in Kerala. A total 42.4 percent of the owner's practices animal husbandry in their land, 9 percent practice agriculture, 9 percent practice both agriculture and animal husbandry while 39.4 percent were not practicing both.

Nearly 27.2 percent of the pet bird owners had 1-2 years of previous experience in bird keeping, 24.2 percent had 5-10 years, 24.2 percent had 10-20 years, 12 percent had 20-30 years and 6 percent each had 30-40 and more than 40 years of experience. None of the pet bird owners had attended any training programme in bird rearing.All the owners had the opinion that there is a need for institutional training regarding pet bird rearing and management.Nonavailability of training facilities in any of the institutions in Kerala may be the main reason for this. This calls for the urgent need for starting such training programs in educational institutions. The number of pet bird owners surveyed was 33. For 91 percent of the owners, pet bird rearing is an auxiliary occupation while for 9 percent it is the main occupation. Nearly 60.6 percent of the owners had registered the birds with Kerala Pigeon Society ie. 60.6 percent of the pet bird owners surveyed had social participation. Seventy-fivepercent of the members of the Kerala Pigeon Society always

attended the meeting of the organization conducted on second Sundays of every month. There will be seminars, shows and sales of birds in these meetings while 20 percent of the owners attended the meeting sometimes whereas 5 percent never attended the meeting. The occupation pattern of the bird owners is presented in Figure 1.The details pertaining to holding and distribution pattern of birds surveyed are presented in Table 1. Almost half of the pet bird owners (51.5 percent) had less than 50 birds,30.3 percent had 51-100 birds, 3 percent had 100-150 birds and 6 percent each had >300 and >500 birds. The most preferred variety of birds was Pigeons followed by Budgerigars. Cockatiels, African lovebirds, finches, Diamond Doves, Pheasants, African grey parrot were also reared by some owners. Some of the popular birds reared are presented in plate 1.The male and female ratio of the birds reared was almost 50 percent.This result is in contrast to the findings by the American Veterinary Medical Association (AVMA) survey (2002), Anderson (2003) and Gaskins et al (2011). According to those three studies in the US, the majority of the bird owners were females. The male dominating family structure existing in Kerala and the socio-cultural difference may be the reasons for such a result. Lack of awareness on the prospects of pet bird rearing among women may be the other reason

## REFERENCES

1. Snedecor GW, Cochran WG. Statistical Methods, 8th Ed. The Iowa State University Press, Ames, Iowa, USA; 1994.
2. AndersonPK. A Bird in the House: An Anthropological Perspective on Companion Parrots.Soc Anim2003;11:393-418
3. Gaskins LA, Bergman L. Surveys of Avian practitioners and pet owners regarding common behavior problems in psittacine birds. J Avian Med Surg2011;25:111-118.
4. American Veterinary Medical Association. U.S Pet Ownership &Demographics Sourcebook. Schaumburg, IL;2002

**Table1. Details of pet birds maintained by pet owners in Kerala**

| Sl. No. | Variables | | Percent |
|---|---|---|---|
| 1. | Number of birds per household | 1-50 | 51.5 |
| | | 51-100 | 30.3 |
| | | 101-200 | 3 |
| | | 300-400 | 6 |
| | | >500 | 6 |
| 2. | Type of birds owned | Pigeons | 75.7 |
| | | Budgerigars | 39.4 |
| | | Cockatiels | 6 |
| | | African love birds | 3 |
| | | Finches | 9 |
| | | Diamond doves | 12.1 |
| | | Pheasants | 3 |
| | | African grey parrot | 3 |
| 3. | Sex of the birds (%) | Male | 50 |
| | | Female | 50 |

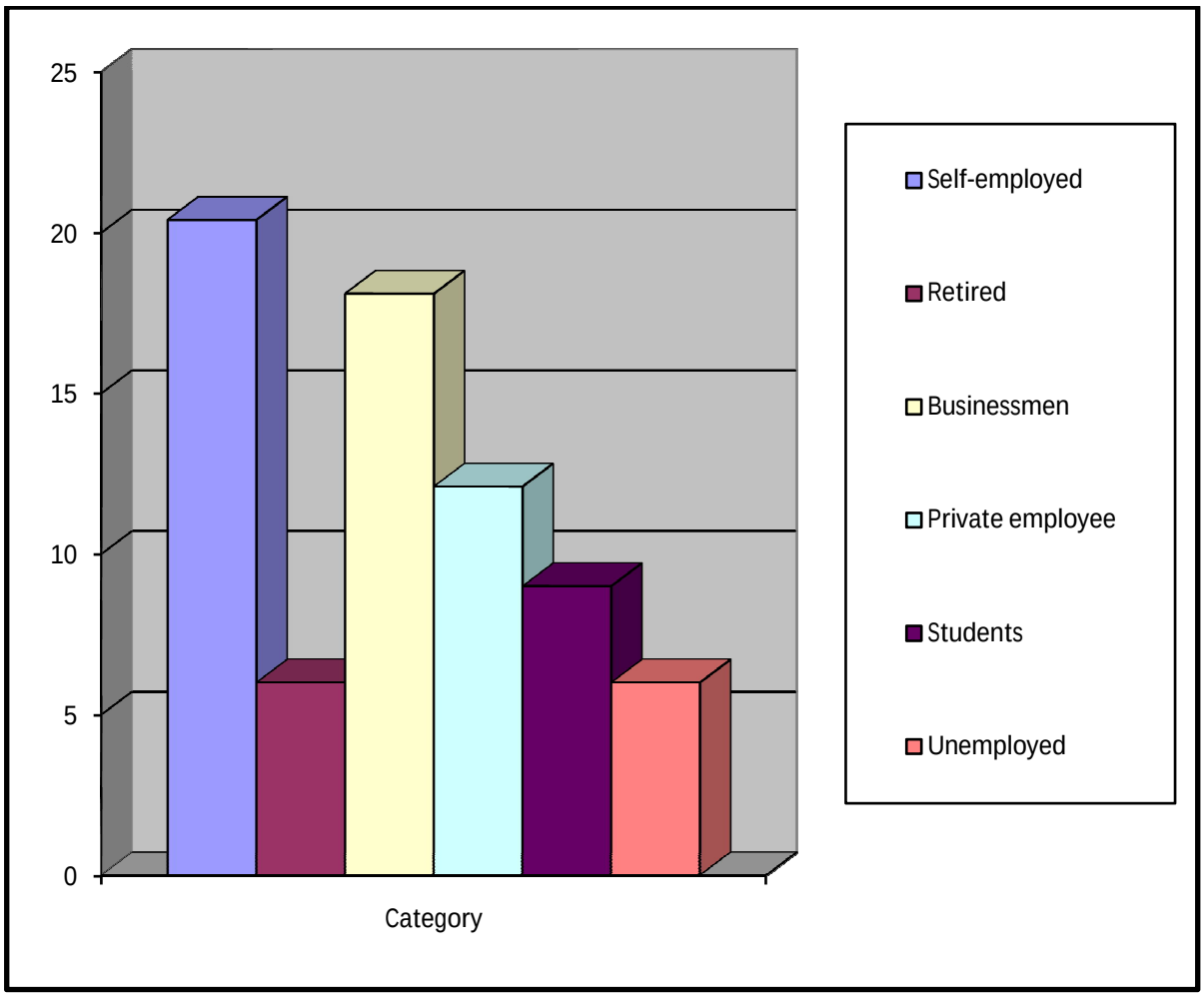


**Figure 1. Occupation pattern of the pet bird owners in Ernakulam**

*Indian Journal of Natural Sciences* www.tnsroindia.org.in ©IJONS

*Vol. 9 / Issue 50 /October 2018* *International Bimonthly* *ISSN: 0976 – 0997*

RESEARCH ARTICLE

# Enhanced Synthesis of Biogenic Silver Nanoparticles by Microwave Radiation, and Its Antibacterial Activity

Nada K. Abbas[1*], Israa Al-Ogaidi[2,3] and Shurooq S. Mahmood[1]

[1]Department of Physics, College of Science for Women, University of Baghdad, Baghdad, Iraq.
[2]Department of Biotechnology, College of Science, University of Baghdad, Baghdad, Iraq.
[3]Department of Chemistry and biochemistry, Fulbright College of Arts and Sciences, University of Arkansas, Arkansas, USA.

Received: 20 July 2018 Revised: 24 Aug 2018 Accepted: 26 Sep 2018

[*]**Address for Correspondence**
**Nada K. Abbas**
Department of Physics,
College of Science for Women,
University of Baghdad, Baghdad, Iraq.
Email: nadabbs@yahoo.com, Biotechphd2011@yahoo.com, shurooq_88@yahoo.com



## ABSTRACT

Biologically synthesis of metallic (AgNPs) nanoparticles was used instead of the physical and chemical approaches. In this work, AgNPs were synthesized by using banana peels extract (BPE) as a (reducing agent) was achieved by using microwave oven.Plant extracts are non-toxic, inexpensive, eco-friendly and thus can be an economic and efficient alternative for the large-scale synthesis of nanoparticles. BPE was found to reduce the silver ions ($Ag^{+}$ to $Ag^{0}$) and capping agent. The AgNPs were prepared by reaction of BPE with silver nitrate as aqueous solutions ($AgNO_3$) when the reaction conditions were altered the concentration of $AgNO_3$, BPE content, pH and reaction time in microwave oven. The formation of AgNPs was confirmed by UV–Vis spectroscopy, XRD, TEM, AFM, DLS, Zeta potential and FTIR. AgNPs showed effective antibacterial activity against Gram-positive and Gram- negative bacteria.

**Keywords**: Silver nanoparticles; Biomaterial; Green synthesis; Biosynthesis; Banana peels extract; Quantum confinement effect; Antibacterial.

## INTRODUCTION

Nanotechnology represents the activities of atoms and molecules. Noble metallic nanoparticles have now become the subject of focused research[1]. It is known that the chemical routes use toxic chemicals to synthesis of nanoparticles. The need in this time; Is the development of methods for the synthesis of nanoparticles by environmentally benign methods. Researchers in this field are eagerly looking into biological systems for non-toxic or environmentally

friendly systems[2] The biologically systems of the microorganisms and plant origin have provided ecofriendly methods for the synthesis of nanoparticles (NPs).[3,4]The fabrication, characterization and application of biologically synthesized nanomaterials havebecome an important branch of nanotechnology[5] Bioinspired techniques frequently lead to the synthesis of nanostructures that are uniform in the size and shape[6].The attempts of biosynthesis of nanoparticles were started as the physical and chemical processes were costly. It was observed that in many times, chemical synthesis methods lead to the presence of some of the toxic chemicals absorbed on the surface of nanoparticles that may have adverse effects in medical applications[7] This problem can be resolved by synthesizing nanomaterial's by green methods[8] Green synthesis provides advancement over chemical and physical methods as it is cost effective, environment friendly, rapid and easily scaled up for large scale synthesis and in this method there is no need to use high pressure, energy, temperature and toxic chemicals[9]. Biological entities have been shown to serve as both reducing and stabilizing agents for the synthesis of metallic nanoparticles[3]. Among the different categories of biological compounds, phytochemicals are emerging as a useful natural resource for the fabrication of metallic nanoparticles[10].Several biologically systems including bacteria, fungi and algae have been used in this regard[3]. In comparison with microbes, plant synthesis of nanoparticles provides an environmentally friendly alternative to large quantities of nanomaterials, does not contain harmful chemicals, eliminates the detailed process of preserving cell cultures, facilitates product retrieval and also presents a dual nature such as noise reduction and reduction at same time[11].Using plant can be suitably scaled up for large-scale synthesis of nanoparticles[12], the prospect of using plant for the synthesis of the nano-sized metals at ambient conditions, without any additive protecting nanoparticles from aggregating, template- shaping nanoparticles or accelerants like ammonia[13].

Plant materials such as *Pomegranate Polyphenols*[14],*Murraya koenigii*[15],*Calotropis gigantean* [16], *Ananas comosus*[17],*Acacia leucophloea*[18] and *Glucose*[19] have been used as fuels to synthesize various nanomaterial's. The methods that using plant extracts include phytochemicals which is act as a reductant agent in the presence of metal salts. All that indicate the formation of size of nanoparticles depende of source, the structure and the weretype of phenolic phytochemical[20] The wastes of fruit are highly perishable, seasonal and it's a problem for the processing industries. Can be recovered this problem by utilizing its high value compounds, including the dietary fiber fraction that has a great potential in the preparation of the functional foods whereas bananas are consumed all over the world, after consumption of the pulp, the peels in general are discarded[21]. Banana is herbaceous plant and belongs to Musaceae family which is originated from the tropical area of south Asia[22]. However, the peel of banana represent 40% of the total weight of the fresh banana and the peel are often discarded as waste product after the inner flesh portion is eaten. The peel of banana contains Potassium, Calcium, Sodium, Iron, Manganese, Copper, Bromine, Rubidium, Strontium, Zirconium and Niobium, they are also the good sources of polyphenols, carotenoids, dietary fibre, proteins, essential amino acids, polyunsaturated fatty acids and other which possess diverse beneficial effects on human health[23] and consider as a good source of antioxidants for foods and functional foods against cancer and heart disease, is used for allergies and skin irritations as a good home remedy[24].Banana peel can be utilized for various useful applications such as bio-fuel manufacturing, bio-sorbents, pulp and paper making, cosmetics, energy related activities, organic fertilizer, environmental cleaning, biotechnology related processes and in nanotechnology[25].

Silver nanoparticles are important materials that have been studied extensively, its play a thoughtful role in the biology and medicine fields. It's can be synthesized by various physical, chemical and biological methods[26].Such nanoparticles possess unique electrical, optical as well as biological properties and are thus applied in catalysis, biosensing, nanodevice fabrication, imaging, molecular diagnostics, in therapies, drug delivery, in medicine also in devices which used in several medical procedures, antibacterial agents in the health industry, textile coatings, food storage and a number of environmental applications[26,27]. Although many of new antibacterial agents development in the last few decades; none of them have been improved its activity against multidrug-resistant bacteria[28].Recently, nanotechnology has very important in the biomedical areas and pharmaceutical as alternative antibacterial agent strategy because re-emergence the appearance and infectious diseases of antibacterial-resistant strains especially within gram negative bacteria[29].There is an increasing interest for silver nanoparticles on account of the antimicrobial properties[30].Silver is a nontoxic, safe inorganic antibacterial agent that is capable of killing about 650 types of diseases

causing microorganisms[31].Silver products are known for its sturdy inhibitory and bactericidal effects, in addition to a wide spectrum of antimicrobial activities, which has been practiced to prevent and treat various diseases, most notably infections. They are also being projected as generation antimicrobial agents in a future.[32] This study was carried out to synthesize AgNPs by a Biogenic method by using the banana peels extract as an inexpensive source, abundantly available and as a waste. The present study differs from earlier reports by using microwave oven. Microwave oven saves time, fast-paced, distributes the heat evenly, retains the vital basic components in the plant which works as a reducing and stabilizing agent for the development of nanoparticles as well as to improve the structural properties of nanoparticle such as the size, uniformly distributed and stability of particles, and the optical properties of nanoparticle such as the Surface Plasmon Resonance (SPR) and optical band gap (Eg). In addition, the nanoparticles have been characterized utilizing UV-Visible spectroscopy, X-Ray diffraction (XRD), Transmission Electron Microscopy (TEM), Atomic Force Microscopy (AFM), Dynamic Light Scattering (DLS), Zeta Potential (ZP) and Fourier Transform Infrared Spectroscopy (FT-IR) analysis. Besides, an application of these nanoparticles that are biologically synthesized as antibacterial agents Gram-positive bacteria (*Staphylococcus aureus*) and Gram-negative bacteria (*Pseudomonas aeruginosa*, *klebsiella pneumonia* and *Escherichia coli*) has also been investigated with different concentrations of AgNPs.

## MATERIALS AND METHODS

### Preparation of Fresh Banana Peels Extract (BPE)

Banana Peels Extract (BPE) was prepared according to[33] with slight modification; which include the use of microwave oven to cut short the time also to preserve the vital resources in the banana peels. Fresh banana was washed repeatedly three times with tap water and three times with distilled water for remove the dust and any organic impurities present in it. Then, the banana peels that remains after the pulp is been consumed were removed and dried on paper toweling and cut it into small pieces (Figure 1, *A*). To prepare aqueous BPE, about 100 g of the banana peels were taken into a 250 mL beaker contained 100 mL of distilled water and then the peels were boiled in the microwave oven (700W, 2.45GHz) for 2 min. After that, the peels were crushed and the solution thus formed was filtered by a gauze swabs to remove insoluble fractions and macromolecules. This filtrate was treated with equal volumes of chilled acetone and the resultant precipitate was centrifuged in 1000 rpm for five min. This precipitate was resuspended in distilled water and stored in refrigerator at 4 ºC for used in further experiments. This extract was used as a reducing aswell as stabilizing agent for development metallic silver nanoparticles.

### Synthesis of the Silver nanoparticles from BPE

AgNPs were synthesized according to the procedure of[33] with slight modification. AgNPs were synthesized by using Microwave oven; this shortens reaction time and produces nanoparticles with uniformly sized. Silver nitrate ($AgNO_3$) was the source of silver in all experiments; it was dissolved in distilled water. In a typical reaction procedure, mixture contained 2.5 mL of peels extract was added to 47.5 mL of 2.25 mM aqueous solutions of silver nitrate. The reaction mixture was kept for incubation in a microwave oven (700W, 2.45GHz) for 190 sec under static conditions till the resulting solution colour changes from pale yellow to reddish brown (Figure 1, *B*). The change in colour indicates the reduction of silver ions. No additional reducing agent or surfactants were needed for the synthesis of AgNPs. After that, the AgNPs which formed in the reaction solution were recovered by centrifuged at 13,000 rpm for 10 min, the supernatant was discarded and their pellets were re-dispersed in distilled water to get rid of any uncoordinated biological molecules. The centrifugation and re-dispersion in distilled water was repeated twice to ensure better separation of free entities from the AgNPs. The reaction conditions were altered to study the effect that on the nanoparticle synthesis with respect to concentration of silver nitrate (1.0, 1.25, 1.50, 1.75, 2.0, 2.25 and 2.50 mM). The BPE content was varied (0.5, 1.0, 1.5, 2.0, 2.5, 3.0, 3.5 and 4 mL) while keeping the $AgNO_3$

concentration at a level of mM. The effect of pH was studied by adjusting the pH of the reaction mixtures (2.5 mL BPE, 2.25 mM $AgNO_3$) to 2.0, 3.0, 3.5, 4.0, 4.5, 5.0 and 6.0. To study the effect of reaction time was evaluated by incubating the reaction mixtures with optimum composition containing 2.5 mL BPE, and 2.25 mM $AgNO_3$ at pH 6 for (40, 70, 100, 130, 160, 190 and 220 sec) in microwave oven. The total volume of mixture reaction for all experiments was 50 mL (includes Banana peels extract as well as aqueous solutions of silver nitrate).

## UV-Vis spectra analysis of the Silver nanoparticles

It is generally recognized that UV–Visible spectroscopy could be used to examine size and shape of controlled NPs in aqueous suspensions. The Ultraviolet–Visible spectra of the bioreduction AgNPs were monitored periodically as a function of wavelength within range from 190 to 1100 nm by using UV- VIS Spectrophotometer (UV-1800 Shimadzu, Japan). For the sample analysis, one mL of the sample in a cuvette was diluted to two mL with distilled water. The UV-Vis spectra for the resulting diluents were monitored for all samples prepared at a resolution of 1 nm at room temperature. UV-Vis spectroscopy indicated a strong Surface Plasmon Resonance band at 410 nm and thus indicating the fabrication of AgNPs.

## Characterization of the Silver nanoparticles

In order to study the structural properties of AgNPs, the crystalline structure was recorded by X-ray diffractometer (XRD-6000, Shimadzu, Japan), the source of radiation is Cu ($k\alpha$) with wavelength of ( $\lambda$=1.5405Å ), voltage 60 kV and current 80 mA, at scanning speed of 5 degree/min in 2θ range from 20° to 80°, these measurements were carried out on dried and finely grounded samples on Nano-Filter paper. The size and shape of the silver nanoparticles were determined by TEM and AFM. For TEM, a drop of aqueous the silver nanoparticles samples was loaded on a carbon coated copper grid, and it was allowed to dry in room temperature, the micrographs were monitored by use TEM (model CM120, Phillips Holland) can be operated up to 120 KV. The surface morphology, particle size distribution and root mean square of roughness of the AgNPs were performed by using atomic force microscope AFM (AA3000 Scanning Probe Microscope SPM, tip NSC35/AIBS from Angstrom Advanced Inc., USA). The average particle size of the Silver nanoparticles in aqueous medium was used to determine hydrodynamic diameter by DLS (Brookhaven NanoBrook 90 Plus, USA). Besides, the particle size distribution and a surface charge of AgNPs were determined by Zeta Potential Analyzer (Brookhaven NanoBrook ZetaPlus, USA). In order to determine the functional groups which present in biomolecules in the plant extract surface and their possible involvement in the synthesis of silver nanoparticles, Fourier Transform Infrared (FTIR) Spectroscopy measurements was carried out. The test samples were independently dried and blended with KBr to obtain a pellet. The FTIR Spectrometer where detected by used (TENSOR 27, Bruker Optik GmbH, Germany) ranging from 400 to 4000 $cm^{-1}$.

## Activation and preparation of the Bacterial isolates

The bacterial isolates used in this study were obtained from Department of Biotechnology, College of Science, University of Baghdad, they were Gram-positive bacteria (*Staphylococcus aureus*) and Gram-negative bacteria (*Pseudomonas aeruginosa*, *klebsiella pneumonia* and *Escherichia coli*) were used to evaluate the antibacterial activity of prepared silver nanoparticles. Bacterial isolates were streaked on brain heart infusion agar and incubated for 18 hours at 37□. Then single colony was picked up from media plate and inoculated into 5 mL of brain heart infusion broth then incubated for overnight at 37°C

### Antibacterial Activity of the Silver nanoparticles

The antibacterial efficacy of the biogenic synthesized silver nanoparticles was investigated utilizing agar well diffusion method against each of the previously mentioned microorganisms. The tested bacteria were swabbed

uniformly on Mueller Hinton agar plates employing sterile cotton swab, then four wells of 6-mm diameter were made employing sterile well borer. Freshly synthesis of AgNPs solutions (prepared with 2.5 mL of BPE, 2.25 mM of $AgNO_3$ at pH 6.0 incubated for 190 sec) samples (50µL) with various concentrations (70, 35 and 17.5 µg $mL^{-1}$) were added into the corresponding wells. The samples were then incubated overnight at 37°C. After the incubation period, the zone of inhibition (in mm diameter) was observed and tabulated. After the incubation period, positive test results were registered when a zone of inhibition (in mm diameter) was observed around the well.

## RESULTS

### Visual observation and UV-Vis spectra analysis

The formation of the microwave accelerated green synthesis of stable Silver Nanoparticles was monitored with color change and UV-Vis spectroscopy. The preliminary detection of silver nanoparticles was carried out by visual observation of the color changes of the reaction solutions. These changes were attributed to the excitation of Surface Plasmon Resonance (SPR) in the metal nanoparticles. Noble metals are known to exhibit unique optical properties due to the property of Surface Plasmon Resonance (SPR)[34]. Typically, UV–Vis spectroscopy is used for observed SPR. Characteristic Surface Plasmon Absorption band was investigated at 410 nm for the reddish brown colored, indicating the generation of silver nanoparticles (Figure 2, *A*), due to the reduction of silver metal ions $Ag^+$ into silver nanoparticles Ag° via the active molecules present in the BPE[35].

### Effect of silver nitrate concentration

Silver nanoparticles synthesized from silver nitrate with different concentrations ranged from 1.0 to 2.50 mM were observed color change from yellowish brown to light reddish brown colors. The SPR peak of AgNPs became distinct with increased of concentration for $AgNO_3$, the maximum peak intensity was obtained at 2.25 mM of silver nitrate (Figure 2, *B*). A variation in the metal salt concentration and biological material is known to influence nanoparticle synthesis[36].

### Effect of BPE

AgNPs synthesized from 2.25 mM of $AgNO_3$ with banana peels extract concentration (0.5-4 mL) was observed the reaction mixtures containing 0.5, 1.0 and 1.5 mL of BPE developed a light reddish brown color, while those containing 2.0 up to 4.0 mL of BPE developed darker reddish brown color. The SPR peaks were proportionally more intense and From (Fig. 2, C) it was found that from Ag + ions the optimal concentration of AgNPs was 2.50 mL. There was also a small increase in the intensity of the SPR range from 0.5 to 4 mL. The increase in SPR band intensity is because the fabrication of more AgNPs due to of high initial concentration of Ag+ ions. According to Mie's theory, only a single SPR band is expected in the absorption spectra of the spherical metallic nanoparticles, whereas anisotropic particles could give rise to two or more SPR bands, this depending on the particles shape[37], our results, suggest that our silver nanoparticles were spherical, as a result of the emergence of one peak for SPR

### Effect of pH

The effect of pH on the formation of AgNPs was evaluated by UV–visible spectroscopic studies and is given in (Figure 2, *D*). The color of reaction mixture and the intensity of the SPR peaks were pH dependent; when the reaction was conducted at pH 2.0 neither color change nor characteristic SPR peak of silver nanoparticles were observed. At pH values 2.0-4.0 we obtained a white precipitate and we not observed color change also. We observed varying shades of reddish brown color at pH values 4.5-6.0. The highest color intensity was obtained at pH 6.0. It is clear that the

manufacture of nanoparticle depends mainly on the pH of the reaction medium. The absorption value gradually increased with the pH increase in the range from 2 to 6, indicating that the composition of the nanoparticle particles is high in the basic pH of the acid pH. The formation of nanoparticles is rapid, neutral, and the primary pH may be ionization of the phenolic group present in the extract[39]. The slow rate of formation and aggregation of AgNPs at acidic pH could be related to electrostatic repulsion of anions present in the solution[40]. In agreement[41], reported that at pH 2.0 no reaction occurred while at pH 11 highly monodispersed nanoparticles were obtained with an average size of 23 ± 2 nm.A variety of biomolecules are postulated to be involved in biological nanoparticle synthesis, such biomolecules are likely to be inactivated under the extremely acidic conditions (pH 2.0)

## Effect of incubation period in Microwave oven

Spectroscopy of reaction solutions were registered after 40, 70, 100, 130, 160, 190 and 220 sec consecutively. The spectroscopy show that there was an increased in the intensity of absorbance with the increased of concentration of AgNPs with the reaction time (Figure 2, *E*). The intensity of the reddish brown color was directly proportional to the incubation time of reaction mixture. The rate of silver ions reduction was walking slowly during the first 40 sec, as described by the low AgNPs that were synthesized by the biologically method using the Debye-Scherrer equation[48]: absorbance values in wavelength 410 nm and in color intensity. Tangible increase in the absorbance together with color intensity was detected after longer time periods up to 220 sec.We obtained the maximum reduction of silver ions after 190 sec. This increasing in absorbance along with color intensity can be ascribed to an increasing in the number of silver nanoparticles with time.42 It has been reported that the time required for complete reduction of the metal ions during biosynthesis of metal nanoparticles using bacteria and fungi range from 24 to 124 h.43 The rapid generation of nanoparticles was owing to the preparation in microwave oven and excellent reducing potential of the active components of banana peel extract and their polymeric stabilization within a narrow size spectrum

### Optical band gap of the Silver nanoparticles

We calculated absorption coefficient ($\alpha$) wich associated with the strong absorption region of the sample from absorbent (A) and the thickness of sample (t) by using the relation:

$\alpha = 2.303A/t$ ……(1)

Whereas the optical band gap of AgNPs was calculated using the Tauc relation:44

$$\alpha = \frac{B(h\nu - Eg)^n}{h\nu} \quad \text{……(2)}$$

Where, $\alpha$ is the absorption coefficient, *B* is a constant, $h\nu$ is the energy of incident photons and exponents *n* whose value depends upon the type the transition which may have values 1/2, 2, 3/2 and 3 corresponding to the allowed direct, allowed indirect, forbidden direct and forbidden indirect transitions, respectively.45 Figure 3, *A,B* showed the variation of ($\alpha\ h\nu$)1/n vs. photon energy, $h\nu$ for Ag nanoparticle for the sample that attended in the standard conditions (synthesized with 2.5 mL of BPE, 2.25 mM silver nitrate at pH 6.0 incubated for 190 sec), with n values of 1/2 and 2, respectively. We calculated a allowed direct and indirect band gap of AgNPs to be 4 and 3 eV, respectively. These values very higher than reported values as zero eV in bulk silver and 2.6 eV in silver dimer nanoparticles.46 The increasing in the band gap of the AgNPs with the decreasing in particle size may be due to a quantum confinement effect.47

### X-Ray diffraction (XRD) analysis

The crystalline nature of Ag nanoparticle for the sample that attended in the standard conditions (synthesized with 2.5 mL of BPE, 2.25 mM silver nitrate at pH 6.0 incubated for 190 sec) was confirmed through X-ray diffraction

pattern analysis. This used to characterize crystallographic structure, preferred orientation and grain size. XRD analysis showed numbers of Bragg reflection peaks at 2θ values of 38.47°, 44.43°, 64.25° and 77.15° (Figure 4, *A*), which correspond to crystal facets of (111), (200), (220) and (311) planes of the face-centred cubic (FCC) structure of silver, respectively. XRD results clearly showed that the AgNPs formed by the reduction of Ag+ ions by the banana peels extract were crystalline in nature which is in agreement with the standard diffraction pattern of JCPDS No. 89-3722. A few unassigned peaks (28.06°, 32.52°, 46.66°, 54.98° and 67.85°) were also found along with the characteristic peaks. May be these Bragg peaks have resulted due to the organic compounds which are present the extract and responsible for silver ions reduction and stabilization of resultant nanoparticles.41 Can be calculated the average particle size for AgNPs that were synthesized by the biologically method using the Debye-Scherrer equation:48

$$D = \frac{K\lambda}{\beta cos\theta} \quad \text{.....(3)}$$

Where: *D* is the mean size of the ordered (crystalline) domains, which might smaller or equal to the grain size, *K* is a dimensionless shape factor, with a value close to unity. The shape factor has a typical value of about 0.9, but varies with the actual shape of the crystallite, $\lambda$ is the X-ray wavelength and $\beta$ is the line broadening at half the maximum intensity (FWHM), after subtracting the instrumental line broadening, in radians. This quantity is also sometimes denoted as $\Delta(2\theta)$, and $\theta$ is the Bragg angle. It was found that the average size was approximately 12 nm.

## Transmission Electron Microscopy (TEM)

Transmission electron microscopy (TEM) has been employed to characterize the size, shape, and morphology of the biosynthesized silver nanoparticles. The image obviously showed that particles size was in the range from 8 to 14 nm as clearly in (Figure 4, *B*). The larger AgNPs might because the aggregation of the smaller ones, due to the TEM measurements. These results detected that the particles have spherical shape and it's uniformly distributed (mono dispersed) without any important agglomeration. It is evident that Ag nanoparticles were highly stabilized by using BPE as well as Microwave oven. Radiation by microwave creates the uniform size of nanoparticles owing to the homogeneous heating of the media, that rise the accelerate nucleation reaction of nanoparticles in addition to depletion energy is lower by microwave method in comparison with classical heating method.30,49

## Atomic force microscopy (AFM)

The aqueous silver nanoparticles sample was deposited on a glass substrate, and it was allowed to dry in room temperature. The AFM images were used to characterize the structure morphology and size of the AgNPs. Figure 4, *C* showed lateral and 3D AFM image for the biosynthesis Ag nanoparticle. From AFM pictures we can see that the size of nanoparticles is bigger. The sizes of nanoparticles obtained from the AFM images appear bigger than the values that we get from XRD and TEM measurements. We interpret those results to several reasons; first explanation relates the Silver nanoparticles tend to form aggregates on the surface during deposition. Second explanation related to the shape of the tip AFM may cause misleading cross sectional views of the sample.50,51 So, the width of the nanoparticle depends on probe shape. The resultant images for AgNPs were showed have spherical shape. The particle size of the AgNPs was found to be more or less homogenous in size and its size were found to be 49 nm .

## Dynamic Light Scattering (DLS) measurements

Can be determined the average particle size by DLS method. DLS was employed to analyzing quantitative size distributions and a more precise quantity of monodispersity in colloidal solutions.52 The average particle size was found to be 13.5 nm as revealed in the size distribution graph (Figure 5, *A*). As it is clear there high homogeneity of the AgNPs produced. The result of DLS confirming the results were obtained by XRD and TEM. The size of the

particle was very close to the results of TEM and XRD. By compared with33 who used banana peels extract to prepare Ag nanoparticles, the result of DLS was 23.7 nm. Maybe the size improvement due to use Microwave oven.

## Zeta Potential (ZP)

The stability of the biosynthesized AgNPs obtained from Banana peels extract were performed by using Zeta potential analysis (Figure 5, *B*). Zeta potential values reveal information regarding the surface charge and stability of the synthesized AgNPs. We found that the zeta potential value of the colloidal solution to be -32.45 mV, indicating the stability of the synthesized nanoparticles. This stability may be attributed to the complex composition of the Banana peels extracts that may have acted as coating agents for the AgNPs. In comparison with other published processes for the synthesis of AgNPs, the current preparations did not require additional steps for coating to make the AgNPs stable and to prevent aggregations.53

## FTIR Spectroscopy analysis

We identified functional groups to extract cortices and predict their role in the formation of AgNPs using FTIR analysis. The band strength was analyzed in different regions of the spectrum for BPE and Ag nanoparticles (this before and after interaction with AgNO3, respectively) and shown in Fig. 5, C. The figure illustrate shifts in the following peaks:3427 to 3436, 2928 to 2923, 2345 to 2341, 1605 to 1626, 1056 to 1033, 773 to 772, and 470 to 463 cm-1. We note that the broad and intense absorption peak at about 3427 cm -1 corresponds to the O-H expansion vibrations of phenols and carboxylic acids. The shift from 3427 to 3436 cm -1 may refer to the participation of the O-H functional group in the AgNPs installation. The peak at about 2345 cm -1 is due to N-H expansion or extended C = O oscillations. The peak shift from 2345 to 2341 cm -1 may be involved in that these groups participate in the process of manufacturing nanoparticles. The peak at 1626 cm-1 may be assigned to C = O and stretch in the carboxyl or C = N bending in the amide group. The shift at this peak (from 1626 to 1605 cm -1) indicated the potential for the participation of BMBs in the synthesis of nanoparticles.Corresponds the peak at 773 and 772 cm-1 with C-H expansion of aromatic compounds. Broad peaks around 470 and 463 cm -1 are associated with AgNPs with oxygen from hydroxyl groups. Banana husks consist mainly of pectin and cellulose and hemicelluloses54 and the functional groups associated with these polymers as well as the proteinaceous matter may be involved in reducing the silver salt to Ag0.

## Antibacterial activity of the silver nanoparticles

Antibacterial activity has been shown to be excellent against clinically isolated human pathogens such as Gram positive bacteria viz., , Staphylococcus aureus and Gram negative bacteria viz., using AgNPs viz., *Pseudomonas aeruginosa*, *klebsiella pneumonia* and *Escherichia coli* with various concentrations of AgNPs (70, 35 and 17.5 μg mL-1) (Figure 6). The diameter of inhibitory zone was measured and tabulated in (Table 1). The result showed the *Staphylococcus aureus* bacteria showed larger zones of inhibition, than *Escherichia coli* bacteria compared with the *Pseudomonas aeruginosa*, *klebsiella*, which may due to the variation in cell wall composition. For Gram positive bacteria the cell wall composed of a thick peptidoglycan layer, consisting of linear polysaccharide chains cross linked by short peptides, therefore forming more rigid structure leading to difficult penetration of the AgNPs, while in Gram negative bacteria the cell wall possesses thinner peptidoglycan layer.55 The biologically synthesized Ag nanoparticles by using different plant extracts also showed a similar potent antibacterial activity.56-58.The high antibacterial activity is certainly because the silver cations that released from AgNPs that act as reservoirs for the Ag+ bactericidal agent. Big changes in the membrane structure of bacteria as a result of the interaction with silver cations lead to the increasing membrane permeability of the bacteria.59,60

## DISCUSSION

Silver nanoparticles have emerged as a typical antimicrobial nanomaterial, which applied in daily life, industry and medicine. Biosynthesis of Silver nanoparticles were produced by the direct interaction in microwave oven of silver nitrate with banana peels extract in aqueous media without the intervention of any external chemicals. The technique of using Plant extracts were ecofriendly, Inexpensive, and so can be effective and economical alternative to wide range synthesis of nanoparticles .Optimum conditions for the reaction were 2.25 mM silver nitrate, 2.50 mL BPE content, pH=6 and the reaction time was 190 sec. The formation of AgNPs was confirmed by UV–Vis absorption spectroscopy characteristic due to surface plasmon resonance (SPR) peak at 410 nm. The optical band gap of AgNPs was calculated for allowed direct and indirect band gap to be 4 and 3 eV, respectively. This is very higher than reported values as zero eV in bulk silver. The increase in the band gap of the AgNPs with the decrease in particle size may be due to a quantum confinement effect. X-ray diffraction (XRD) analysis confirmed the presence of AgNPs, it has crystalline nature with a cubic structure and the value of average grain size is about 12 nm. Transmission electron microscopy (TEM) showed mono-dispersed spherical shaped nanoparticles, confirmed the crystallinity of nano particles and the size of nanoparticles were in the range from 8 to 14 nm. Atomic force microscopy (AFM) image has proved that very helpful in the determining morphological features. Dynamic light scattering (DLS) studies revealed that the average particle size of Ag nanoparticles was found about 13.5 nm. The Zeta potential analysis (ZP) value for Ag nanoparticles obtained was -32.45 mV, indicating the moderate stability of fabrication of nanoparticles, which suggesting the BPE can be used as a reducing and stabilizing agent for the preparation of AgNPs.The presence of water-soluble organic compounds like flavonoids, polyphenols, phenol derivatives etc. in the BPE was revealed by Fourier transform infrared spectroscopy (FT-IR) spectroscopy which were found to be responsible for the reduction of Ag+ ions to Ag nanoparticles and the stabilization of particles as a capping agent. The produced AgNPs shows a clear bacterial resistance against *Staphylococcus aureus*, *Pseudomonas aeruginosa*, *klebsiella pneumonia* and *Escherichia coli*.

## REFERENCES

1. Kumar V, Yadav SK. Plant-mediated synthesis of silver and gold nanoparticles and their applications. J Chem Technol Biotechnol 2009;84(2):151-157.
2. Bunghez IR, Ion RM, Pop S, Ghiurea M, Dumitriu I, Fierascu RC. Silver Nanoparticles Fabrication Using Marine Plant (Mayaca fluviatilis) Resources. Analele Ştiinţifice ale Universităţii. Alexandru Ioan Cuza. Secţiunea Genetică şi Biologie Moleculară. TOM XI. 2010:89-94.
3. Thakkar KN, Mhatre SS, Parikh RY. Biological synthesis of metallic nanoparticles. Nanomed Nanotechnol Biol Med 2010;6(2):257-262.
4. Vijayraj D, Anarkali J, Rajathi K, Sridhar S. A facile green synthesis of silver nanoparticles using the medicinal plant Leucas aspera and their antibacterial activity. Nano Biomed Eng 2012;4(2):95-98.
5. Chen J, Zhao JX. Upconversion Nanomaterials: Synthesis, Mechanism, and Applications in Sensing. Sensors 2012;12(3):2414- 2435.
6. Wu LQ, Payne GF. Biofabrication: using biological materials and biocatalysts to construct nanostructured assemblies. Trends Biotechnol 2004;22(11):593-599.
7. Parashar UK, Saxena PS, Srivastava A. Bioinspired synthesis of silver nanoparticles. Digest Journal of Nanomaterials and Biostructures 2009;4(1):159-166.
8. Begum NA, Mondal S, Basu S, Laskar RA, Mandal D. Biogenic synthesis of Au and Ag nanoparticles using aqueous solution of black tea leaf extracts. Colloids and surfaces B, Biointerfaces 2009:71(1):113-118.
9. Forough M, Farhad K. Biological and green synthesis of silver nanoparticles. Turkish J Eng Env Sci 2010;34:281-287.
10. Park Y, Hong YN, Weyers A, Kim YM, Linhardt RJ. Polysaccharides and phytochemicals: a natural reservoir for the green synthesis of gold and silver nanoparticles. IET Nanobiotechnol 2011;5(3):69-78.
11. Saxena A, Tripathi RM, Zafar F, Singh P. Green synthesis of silver nanoparticles using aqueous solution of Ficus

benghalensis leaf extract and characterization of their antibacterial activity. Materials Letters 2012;67(1):91-94.
12. Jancy M, Inbathamizh L. Green synthesis and characterization of nano silver using leaf extract of morinda pubescens. Asian J Pharm Clin Res 2012;5(1):159-162.
13. Huang J, Li Q, Sun D, Lu Y, Su Y, Yang X, Wang H, Wang Y, Shao W, He N, Hong J, Chen C. Biosynthesis of silver and gold nanoparticles by novel sundried Cinnanonum camphora leaf. Nanotechnology 2007;18(10): 105104-105115.
14. Abdelmonem AM, Amin RM. Rapid Green Synthesis of metal nanoparticles using pomegranate polyphenols. Int J Sci Basic Appl Res 2014:15(1):57-65.
15. Christensen L, Vivekanandhan S, Misra M, Mohanty AK. Biosynthesis of silver nanoparticles using murraya koenigii (curry leaf): an investigation on the effect of broth concentration in reduction mechanism and particle size. Adv Mat Lett 2011;2(6):429-434.
16. Sivakumar J, Premkumar C, Santhanam P, Saraswathi N. Biosynthesis of silver nanoparticles using Calotropis gigantean leaf. Afr J Basic Appl Sci 2011:3(6):265-270.
17. Ahmad N, Sharma S. Green synthesis of silver nanoparticles using extracts of Ananas comosus. Green Sustain Chem 2012;2(4):141- 147.
18. Murugan K, Senthilkumar B, Senbagam D, Saleh Al Sohaibani. Biosynthesis of silver nanoparticles using Acacia leucophloea extract and their antibacterial activity. Int J Nanomedicine 2014;9(1):2431-2438.
19. Israa Al-Ogaidi. Detecting the antibacterial activity of green synthesized silver (Ag) nanoparticles functionalized with ampicillin (Amp). Baghdad Science Journal 2017;14(1):117-125.
20. Rao KJ, Puria S. Green synthesis of silver nanoparticles from aqueous Aegle marmelos leaf extract. Mater Res Bull 2013;48:628-634.
21. Many JN, Keerubavathi M. Synthesis of silver nanoparticle using fresh banana peel Musa (AAB) extract. Science & Technology. 2016;2(5):73-82.
22. Leslie S, Cobley. An Introduction to the Botany of Tropical Crops (2nd Edition). Longman Group Limited London 1976:153-15.

## Abbreviations

AgNPs, Silver nanoparticles; BPE, Banana peels extract; SPR, Surface plasmon resonance; XRD, X-ray diffraction; TEM, Transmission electron microscopy; AFM, Atomic force microscopy; DLS, Dynamic light scattering; ZP, zeta

## Potential Analysis

FTIR, Fourier transform infrared spectroscopy.

## Conflict of interest

The authors declare that there are no conflicts of interest.

## Author contributions

Authors contributed equally to the work, the design of the experiments and developed, read the text and modified, were involved in interpretation of results and approved the final manuscript.

## Funding Sources

The authors wish to thank MSc Sarah Lafta Hamad, Department of Biotechnology, College of Science, University of Baghdad, Baghdad, Iraq, for providing the bacterial isolates. The funding sources had no influence in the study design; in the collection, analysis and interpretation of data; in the writing of the report; and in the decision to submit the paper for publication.

**Correspondence to**

N.K. Abbas, Department of Physics, College of Science for Women, University of Baghdad, Baghdad, Iraq.
Email: nadabbs@yahoo.com
I. Al-Ogaidi, Department of Biotechnology, College of Science, University of Baghdad, Baghdad, Iraq.
Email: Biotechphd2011@yahoo.com

S.S. Mahmood, Department of Physics, College of Science for Women, University of Baghdad, Baghdad, Iraq.
Email: shurooq_88@yahoo.com

**Table 1: Results of the antibacterial activity of biologically synthesized AgNPs**

| Name of the Microorganisms | Diameter of inhibition zone (mm) | | |
|---|---|---|---|
| | 70 µg/mL | 35 µg/mL | 17.5µg/mL |
| *Staphylococcus aureus* | 19 | 18 | 16.5 |
| *Escherichia coli* | 18 | 17 | 17 |
| *Pseudomonas aeruginosa* | 17 | 13 | 13 |
| *klebsiella pneumonia* | 14 | 13 | 11.5 |

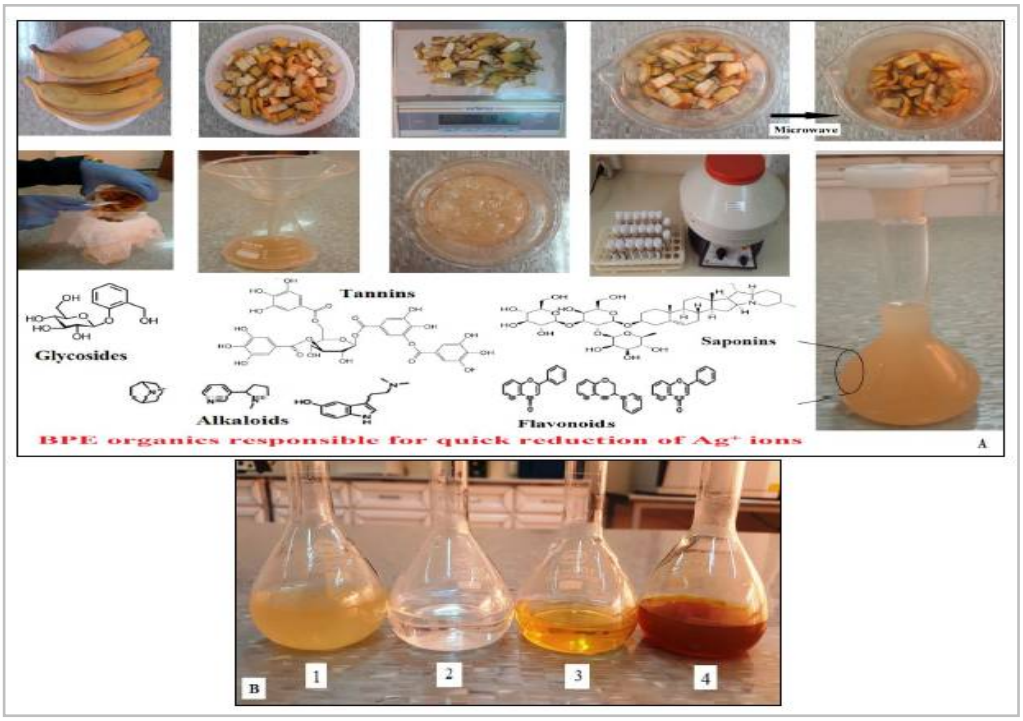


**Figure 1. (A) Steps of preparation process of BPE (1) A fresh Banana peels clean, (2) Cut it into small pieces, (3) Weight about 100 g of peels, (4) 100 g of the banana peels into 100 mL of distilled water, (5) After boil in the microwave oven for 2 min, (6) Crushed the peels and filtered, (7) The filtrated solution, (8) Treated this filtrate with equal volumes of chilled acetone, (9) Centrifuged for the resultant precipitate at 1000 rpm for five min, (10) The precipitate was resuspended in distilled water.(B) Volumetric flask containing samples of (1) Banana peels extract. (2) Silver nitrate. Colour change of the reaction mixture of BPE and AgNO3 indicating the formation of AgNPs (3) Before and (4) After bioreduction in Microwave oven.**

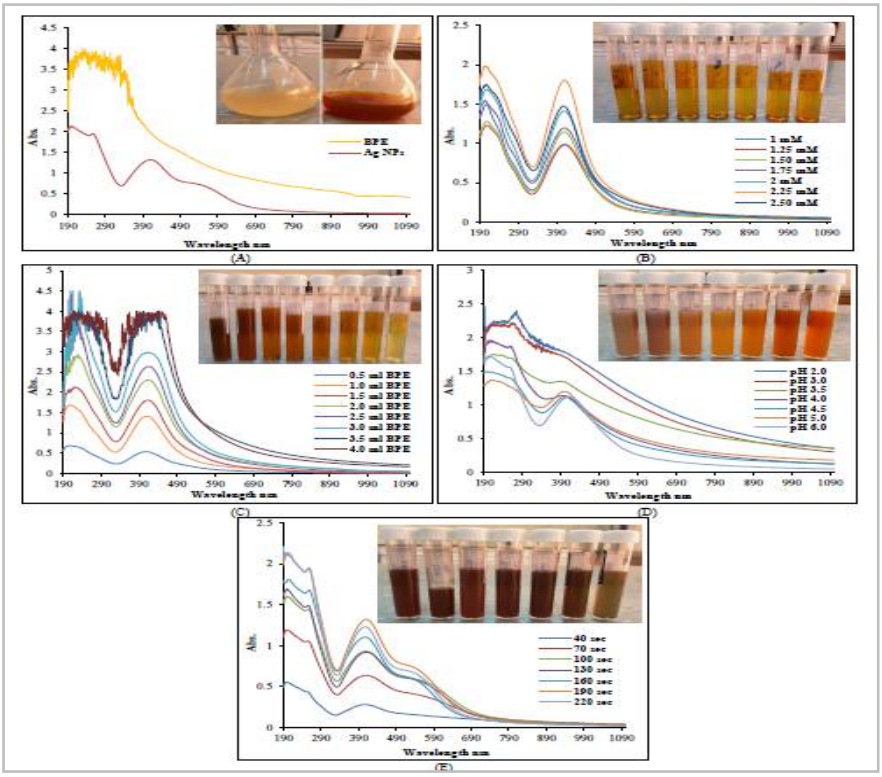


**Figure 2. UV-Vis absorption spectroscopy of biosynthesized silver nanoparticles as a function of the wavelength, showing the surface Plasmon resonance peak of silver nanoparticles at 410 nm (A) inset showing the color change upon formation of silver nanoparticles. (B) The effect of the AgNO3 concentration on AgNPs (1.0, 1.25, 1.50, 1.75, 2.0, 2.25 and 2.50 mM). (C) The BPE concentration was varied (0.5, 1.0, 1.5, 2.0, 2.5, 3.0, 3.5 and 4 mL) while keeping the AgNO3 concentration at a level of 2.25 mM. (D) The effect of pH was studied by adjusting the pH of the reaction mixtures (2.50 mL BPE, 2.25 mM AgNO3) to 2.0, 3.0, 3.5, 4.0, 4.5, 5.0 and 6.0. (E) The effect of reaction time was evaluated by the reaction mixtures with optimum composition (2.50 mL BPE, and 2.25 mM AgNO3 at pH 6.0) for 40, 70, 100, 130, 160, 190 and 220 sec.**

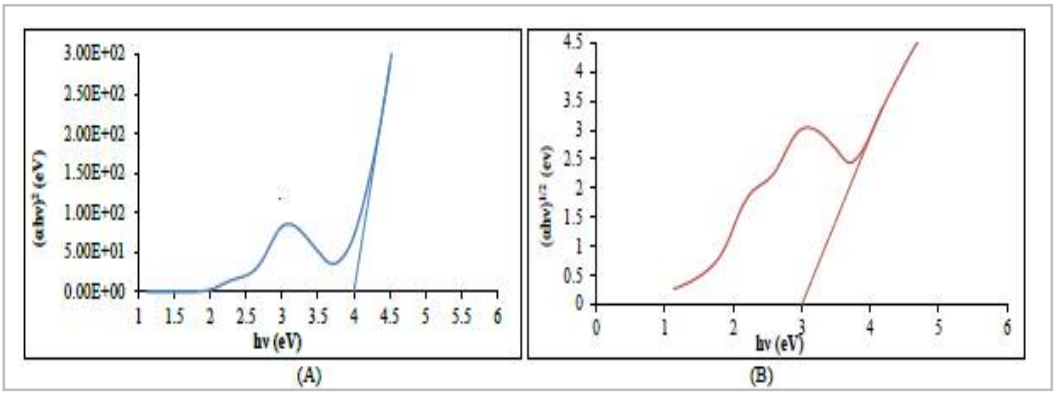


**Figure 3. (A) Variation of ($\alpha h\nu$)2 with $h\nu$ for AgNPs as a function of the wavelength at *n* value of 1/2. (B) Variation of ($\alpha h\nu$)1/2 with $h\nu$ for AgNPs as a function of the wavelength at *n* value of 2.**

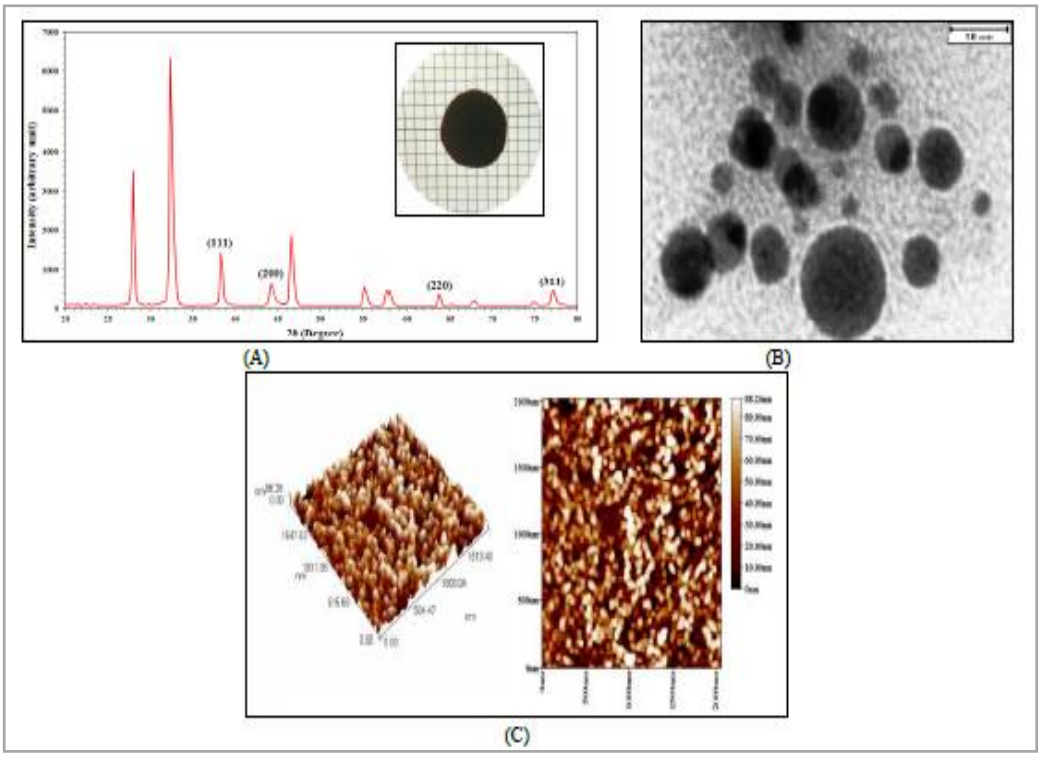


**Figure 4. (A) XRD pattern of Biosynthesized AgNPs using BPE. (B)TEM image of bio-reduced silver nanoparticles. (C) Atomic force microscopy of AgNPs.**

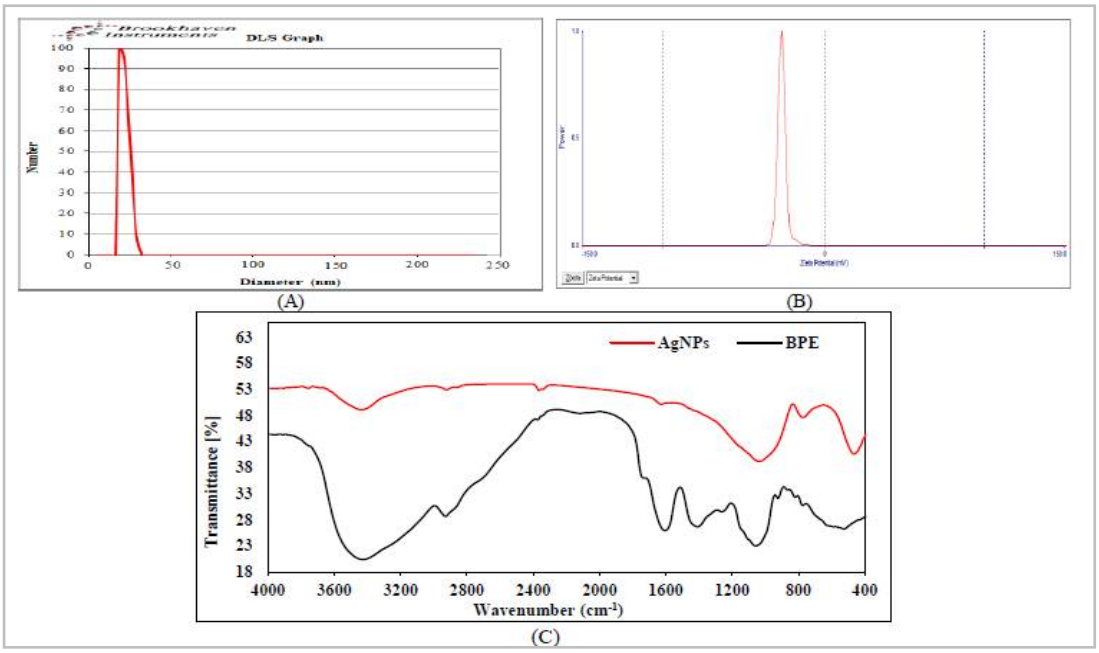


**Figure 5. (A) Graphs showing Particle Size distribution of silver nanoparticles. (B) Graph result for zeta potential. (C) FTIR spectrums of BPE extract alone, and synthesized AgNPs using BPE.**

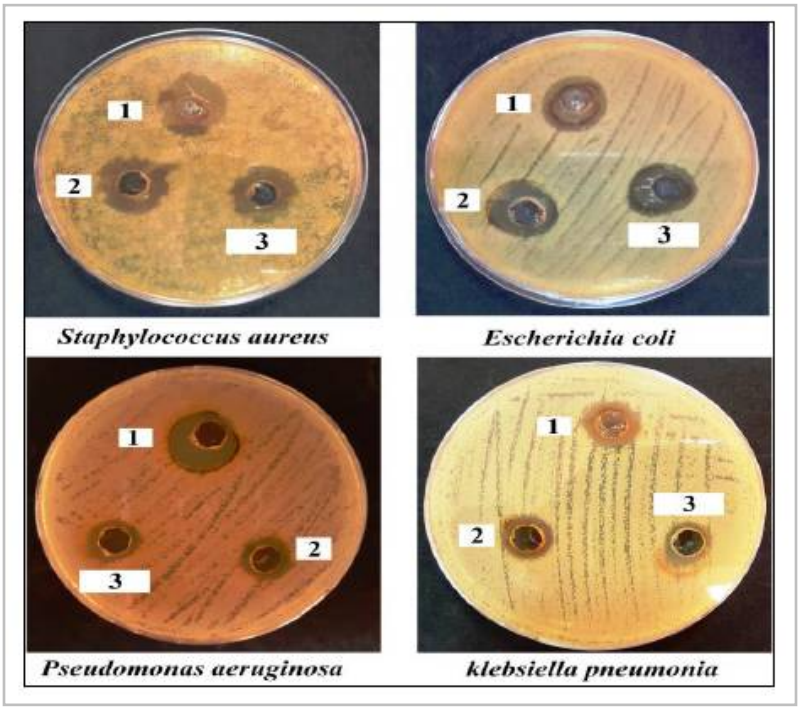


**Figure 6. Activity of AgNPs against bacteria with clear zones of inhibition with various concentrations of AgNPs (1) 70, (2) 35 and (3) 17.5 μg mL-1.**

*Indian Journal of Natural Sciences* www.tnsroindia.org.in ©IJONS

*Vol. 9 / Issue 50 /October 2018* *International Bimonthly* *ISSN: 0976 – 0997*

RESEARCH ARTICLE

# The Nuclear Energy Levels in $^{42}$Ca Calculated By the Use of Different Interactions

Firas Z. Majeed[1] and Sadeq S. Mashaan[2]*

[1]Department of Physics, College of Science, University of Baghdad, Baghdad, Iraq.
[2]Department of Computer, Al-Musaib Technical College, Al-Furat Al-Awsat Technical University, Babylon, Iraq.

Received: 12 July 2018 Revised: 18 Aug 2018 Accepted: 22 Sep 2018

***Address for Correspondence**
**Sadeq S. Mashaan**
Department of Computer,
Al-Musaib Technical College,
Al-Furat Al-Awsat Technical University,
Babylon, Iraq.
Email:sadeq278@ymail.com



## ABSTRACT

The shell model is an essential section of nuclear theory and a basic theoretical tool for the microscopic description of nuclear structure. Nuclear energy levels with even-even nucleons that were present outside closed($^{40}$Ca consider as inert core), which are occupied in fp-shell ($1f_{7/2}$,$2p_{3/2}$,$1f_{5/2}$,$2p_{1/2}$) have been studied. The use of four interactions to calculate the nuclear energy levels of $^{42}$Ca. FPD6, GXPF1 and KB3G interactions had been adopted and compared with experimental data, it's agreement with some results are achieved,for the case of Gogny-p2as an effective interaction to study energy levels in $^{42}$Ca through nuclear shell model and considering of full space (no core) technique of frozen occupying particles, i.e. making of particles to be active but still in its orbitals. Harmonic Oscillator potential is used to generate single particle wave functions in fp-shell and considering $^{40}_{20}Ca_{20}$ as an inert core. The cod OXBASH computer programing is used to the process of this study.

**Keywords**: nuclear, energy levels, shell model, $^{42}$Ca, Gognyinteraction, fp-shell.

## INTRODUCTION

Many different microscopic and microscopic theories have been performed to study nuclei excitations. The multi-nucleon shell model with mixed configurations is one of these theoretical models. In this model, the nucleon target is imagined as an inert core with addition effective nucleons distributed over a limited number of orbits, which called model space orbit. Shell-model calculations carried out within a model-space in which the nucleons are restricted to occupy a few orbits are unable to reproduce the calculated static moments or transition strengths without scaling

factors[1]. The shell model is an essential section of nuclear theory and a basic theoretical tool for the microscopic description of nuclear structure. The fundamental assumption in the nuclear shell model is that each nucleon moves independently in an average field includes a strong spin-orbit term and produced by the nucleons itself. The nucleons then arrange themselves into group of levels, the "shells", well separated from each other. According to this approximation, the nucleus is considered to be consisting of an inert core made up by shells filled up (closed shell) with neutrinos and protons plus a certain number of external nucleons called valence nucleons [1].

## The $^{42}$Ca nucleus

The shell model has played an indispensable role in the study nuclear structure, since it was conceived by Mayer and Jensen. The shell model several has important and basic features such as the independence of model assumption, the usage realistic nucleon- nucleon interaction, and the common Hamilton for various types of eigenstates, and for different nuclei. The shell model continues to provide the main theoretical tool for understanding all properties of nuclei [2]. The nucleus $^{42}Ca_{22}$ have 20 protons and 22 neutrons, two neutrons play essential role in the shell model space, outer the closed shell when the inert core $^{40}$Ca is under consideration. One can say it have configurated sub states energy levels. The shell-model calculations with the GXPF1 and KBG3 interaction were performed with effective charges that include a polarization isovector charge [3]. The FPD6 as an effective interaction in the isospin formalism, in fp-model space with a $^{40}$Ca core had been used to generate energy levels [4]. The isotopes of calcium lying between doubly magic $^{40}$Ca and $^{48}$Ca provide a unique laboratory probe for examining the foundation of fp shell model calculations. Available spectroscopic information on odd mass Ca isotopes, mean charge radii, excitation energies, B(E2 : $0_1^+$ $2_1^+$) values and electric quadruple moments of the $2_1^+$ states in even mass Ca nuclei have all indicated that $^{40}$Ca was not a good closed shell nucleus. Already in 1967 it had been postulated that a breakdown of the Z = 20 shell closure, caused by the promotion of sd-shell protons into the fp-shell, was responsible for the observed spectroscopic properties [5].

The Ca isotopes have been the subjects of much experimental and theoretical interest. This is in large part due to the fact that $^{40}$Ca and $^{48}$Ca, which occupy the ends of the stable isotope series for this element, are both doubly magic nuclei within shell model theory. For this reason, knowledge concerning the structure of the ground- and excited-state charge distributions of these two isotopes is of particular value in elucidating the general systematic of nuclei in this region [6]. Nuclei with valence nucleons in the *fp* shell have been intensively studied and discussed in recent years following the striking progress in the development and refinement of large-scale shell model calculations [7]. The level schemes and transition probabilities were studied for $^{42}$Ca [8]. the core is taken $^{40}$Ca for nuclei in the *fp* shell, by generating the wave functions of a given level schemes and transition probabilities in known nuclei by adopting code OXBASH [9] and FPD6, GXFP1 and KB3G interactions[10]. Protons and neutrons interact inside the nuclei with a non integrable interaction.It was shown that is possible to reproduce the energy statistics of nuclear energy levels analyzing the fluctuations of an ensemble of nuclear states produced by random interactions. The contribution was analyzed the characteristics of the fluctuations and distributions of the energy levels in order to understand the independent scale nature of the 1/f-noise nuclear energy levels[11]. The energy distribution of calcium nucleus had been studied by several methods and it has been demonstrated its complexity. The interaction was taken as a harmonic oscillator mean field added with the monopole part realistic interaction of the KB3G [12]. This interaction had been derived by minimally modifying the monopole strength in the original Kuo-Brown interaction [13]. The two body interaction (multipole part(is composed by an ensemble of random interactions (two body random ensemble or TBRE) [14].The Hilbert space selected is the full fp shell: it is the harmonic oscillator shell for $\eta$ = 3,which has demonstrated to be a very good truncation to study this nucleus. The shell model calculation is performed with the code ANTOINE [15], which works in the m-scheme. As one were interested in the evolution of the energy levels statistic, and therefore in its correlation, used the method of power spectra [16-19].

### Perturbation theory

For the application of perturbation theory it is advantageous to make the influence of the residual interaction[20]:

$H^{(1)} = \sum_{1=k<l}^{A} W(k,l) - \sum_{k=1}^{A} U(k)$ .....(1)

Noticing thatany product of *a* single-particle functions $\Phi_a^{(0)} \equiv \emptyset_{a1}(r(1)) \ldots . \emptyset_{aA}(r(A))$ satisfies the Schrodinger equation

$H^{(0)}\Phi_a^{(0)} = E_a^{(0)}\Phi_a^{(0)}$ .....(2)

The first-order perturbation theory is

$|\Phi_\Gamma\rangle = |\Phi_\Gamma^{(0)}\rangle + |\Phi_\Gamma^{(1)}\rangle$ .....(3)

$|E_\Gamma\rangle = |E_\Gamma^{(0)}\rangle + |E_\Gamma^{(1)}\rangle$ .....(4)

Where $|\Phi_\Gamma^{(1)}\rangle$ and $|E_\Gamma^{(1)}\rangle$ represent the supposedly small changes in the wave function and the energy of the unperturbed state[20].

### Binding energies and excitation energies

The binding energy $E^b$of a nucleus is defined as the negative value of the total energy needed to decompose the nucleus into free protons and neutrons. Often the binding energy is given with opposite, positive sign. With the negative sign used here, however, there is a more direct connection with the expectation value of the Hamiltonian of the nuclear system. The absolute value of the binding energy is the largest for the nucleus in its ground state. The excitation energy $E_x(n)$of the *n*th excited state follows from the binding energy $E^b(n)$ of the nucleus in that state taken with respect to the ground-state binding energy$E^b(0)$ [20], i.e.

$E_x(n) = E^b(n) - E^b(0)$ .....(5)

A meaningful description of a nucleus can be made in terms of an inert core of closed shells and two extra nucleons in the orbit ϱ not occupied by core nucleons (as shown in fig.1). The various terms contributing to the total binding energy of this nucleus can be written down at once from the definition of the binding energy given above as[20]

$E_\Gamma^b(core + \rho^2) = 2e_\rho + E_\Gamma^{(1)}(\rho^2) + E^b(core$.....(6)

Here the term $2e_\rho$ represents the negative value of the energy needed to remove the two particles from the potential well in which they are assumed to move independently in the orbit ϱ. It is usually assumed that this potential well does not depend on the number of particles outside the core. The contribution to the binding energy from the mutual nuclear interaction of the two outer-core particles is given by$E_\Gamma^{(1)}(\rho^2)$. This term depend not only on the orbit ϱ, but also on the spin Jrand isospin Tr of the two particle system. The last term, Eᵇ(core), represents the binding energy of the particles in the core[20]. When it is assumed that the closed-shell core is inert (i.e. it will maintain its closed-shell configuration and thus cannot be excited), it follows that the term Eᵇ (core) is a constant.In the case of two active particles outside a core one has

$H_{12}^{(1)} = V(1,2)$.....(7)

And for total Hamiltonian

$H = H_{core} + H_{s.p.}(1) + H_{s.p.}(2) + V(1,2)$ .....(8)

The binding energy of the nucleus with two particles outside the core in the orbit ϱ and coupled to spin and isospin Γ is given by the expectation value

$E_{\Gamma}^{b}(A) = \left\langle \Phi_{\Gamma}^{(0)}(1,\dots,A) \middle| H \middle| \Phi_{\Gamma}^{(0)}(1,\dots,A) \right\rangle$ .....(9)

Of the total Hamiltonian in the state $\Phi_{\Gamma}^{(0)}(1,\dots,A)$ of the complete nucleus.

**States of mixed configuration**

We have restricted our discussion to unperturbed states $\Phi_{\Gamma}^{(0)}$. Each of these states represents a pure shell-model configuration. For example, considering two active orbits ϱ and $\lambda$, one has pure states $\Phi_{\Gamma}^{(0)}(\rho_{\alpha}^{n}\lambda_{\beta}^{m})$ each with a given particle distribution specified by $\varrho^n$ and $\lambda^m$ and a given set of intermediate quantum numbers $\alpha$ and $\beta$ with $J_\alpha + J_\beta = J_\Gamma$ and $T\alpha + T\beta = T\Gamma$[20].

**Energy Matrix Element With Oscillator Function:**

The Hamiltonian describing the independent motion of two particles in a harmonic-oscillator potential can be separated in $(r_1, r_2)$ space and also in the relative and center of mass coordinate system of the two particles [21]

$$H = \frac{p_1^2}{2m} + \frac{1}{2}m\omega^2 r_1^2 + \frac{p_2^2}{2m} + \frac{1}{2}m\omega^2 r_2^2 \quad \text{.....(10)}$$

$$= \frac{p^2}{2m} + \frac{1}{2}m\omega^2 r^2 + \frac{P^2}{2m} + \frac{1}{2}m\omega^2 R^2$$

Where the latter coordinates and their canonically conjugate momenta are [21]**.** It may be shown that this transformation is independent of the magnetic number $\mu$. The transformation bracket vanishes for all combinations of its parameters which do not satisfy the total angular momentum:

$$\vec{\lambda} = \vec{l_1} + \vec{l_2} = \vec{l} + \vec{L} \quad \text{.....(11)}$$

and the degenerated eigen value (energy) in this case is [4]:

$$E(n_1 l_1, n_2 l_2) = \left(2n_1 + l_1 + \frac{3}{2}\right)\hbar\omega + \left(2n_2 + l_2 + \frac{3}{2}\right)\hbar\omega \quad \text{.....(12)}$$

The wave function $\phi_{nl}(\vec{r})$ describes states with energy $\left(2n + l + \frac{3}{2}\right)\hbar\omega$ has the form:

$$\phi_{nl}(\vec{r}) = R_{nl}(\alpha r) Y_{lm}(\theta,\varphi) \quad \text{.....(13)}$$

where $R_{nl}(\alpha r)$ is the radial wave function and given by:

$$R_{nl}(\alpha r) = \left[\frac{2^{l-n+2}(2l+2n+1)!!\,\alpha^{2l+3}}{\sqrt{\pi}\,n!\left[(2l+1)!!\right]^2}\right]^{\frac{1}{2}}\left[\exp\left(-\frac{\alpha^2}{2}r^2\right)\right] r^l$$

$$\times \sum_{k=0}^{n} \frac{(-1)^k\, 2^k\, n!\,(2l+1)!!\left(\alpha^2 r^2\right)^k}{k!(n-k)!(2l+2k+1)!!} \quad \text{.....(14)}$$

and $Y_{lm}(\theta,\varphi)$ is the angular wave function and $\alpha^2 = \frac{m\omega}{\hbar}$.

The single-particle energies are calculated according to [20]:

$$e_{nlj} = (2n+l-\frac{1}{2})\hbar\omega + \left\{\begin{array}{ll} -\frac{1}{2}(l+1)\langle f(r)\rangle_{nl} & for\ j=l-\frac{1}{2} \\ \frac{1}{2}l\langle f(r)\rangle_{nl} & for\ j=l+\frac{1}{2} \end{array}\right\} \quad \text{.....(15)}$$

with:

$$\langle f(r)\rangle_{nl} \approx -20A^{-2/3} MeV$$

$$\hbar\omega = 45A^{-1/3} - 25A^{-2/3}$$

**The Realistic Gogny-p2 Effective N-N Interaction**

The realistic Gogny-p2 effective NN interaction, which is used in electron scattering ($V_{res}$ =*v*12) is expressed as a sum of the central potential part $v_{12}^{(c)}$, spin-orbit potential part $v_{12}^{(LS)}$, long range tensor part $v_{12}^{(TN)}$, and density dependence part $v_{12}^{(DD)}$ as follows [22]:

$$v_{12} = v_{12}^{(c)} + v_{12}^{(LS)} + v_{12}^{(TN)} + v_{12}^{(DD)} \quad \text{.....} \quad (16)$$

The four potentials are expressed as: [23]

$$\left.\begin{aligned} v_{12}^{(c)} &= \sum_n (t_n^{(SE)} P_{SE} + t_n^{TE} P_{TE} + t_n^{(SO)} P_{SO} + t_n^{(TO)} P_{TO}) e^{-(\mu_n r_{12})^2} \\ v_{12}^{(LS)} &= \sum_n (t_n^{(LSE)} P_{TE} + t_n^{(LSO)} P_{TO}) \nabla^2 \delta(\mathrm{r}_{12})(r_{12}) L_{12}.(\vec{S}_1 + \vec{S}_2) \\ v_{12}^{(TN)} &= \sum_n (t_n^{(TNE)} P_{TE} + t_n^{(TNO)} P_{TO}) f_n^{(TN)}(r_{12}) r_{12}^2 S_{12} \\ v_{12}^{(DD)} &= \{t^{(DD)} P_{SE}.[\rho(r_1)]^{a^{(SE)}} + t^{(DD)} P_{TE}.[\rho(r_1)]^{a^{(TE)}} \delta(r_{12}) \end{aligned}\right\} \quad \text{.....(17)}$$

Where

$f_n^c(r_{12}) = e^{-(\mu_n r_{12})^2}$, $f_n^{LS} = \nabla^2\delta(r_{12})$represented Gogny interaction[24, 25].

The relative coordinate is denoted by $\vec{r}_{12} = \vec{r}_1 - \vec{r}_2$ and $|\vec{r}_{12}| = r_{12}$ Correspondingly, the relative momentum is defined by $\vec{P}_{12} = \frac{(\vec{P}_1 - \vec{P}_2)}{2}$, $\vec{L}_{12}$ is the relative orbital angular momentum, $\vec{L}_{12} = \vec{r}_{12} \times \vec{P}_{12}$ , $\vec{S}_1$ and $\vec{S}_2$ are the nucleon spin operators, and **S12**is the tensor operator which is defined as[26, 27].

## RESULTS AND DISCUSSION

Energy levels in $^{42}$Ca are sketched in the unit of MeV with the assigned symbol $J_k^\pi T$where$J$ represented the total spin, $\pi$is the parity, $T$is the isospin and $k$represents the order sequence of energy levels for the same ($J^\pi T$)state and the firstorder of sequence is $k$ = 0. For the figures(2, 3), where we compare the calculated results of energy levels in $^{42}$Ca using FPD6, GXPF1,KB3G and Gogny-p2interactions in comparison with exp. data, it is clear that for the case of fp-shell model space and $^{40}$Ca as an inert core all of the calculated results are for from agreement, but in some how the order of sequence is predictedfor the produced multipolarities($J_k^\pi T$ = $0_k^+1, 1_k^+1, 2_k^+1, 3_k^+1$ *and* $4_k^+1$)where$k$ = 0,1,2, … ,9, and our analysis about $^{42}$Ca is that it is a two particles system (with $^{40}$Ca as inert core) and from the allowed ($J^\pi T$) states ther are four stateswith J=0, three states with J=1, seven states with J=2, four states with J=3 and six states with J=4; but the exp. data show that there are ten states with J=0, ten states with J=1, ten states with J=2, three states with J=3 and two states with J=4. So, if we compare them, we'll predict that fp-shell model space with four orbitals ($1f_{7/2}$,$2p_{3/2}$,$1f_{5/2}$,$2p_{1/2}$)will not enough and the need for extending the model space(fp) toward higher configuration, or toward the closed shell orbits, or the two options, is necessary especially when we analyses the value of J=0.

Figure (2) represented $^{42}$Ca energy levels scheme by use nuclear shell model with FPD6, GXPF1 and KB3G interactions (by using fp-shell model space) with inert core $^{40}$Ca for ($J_k^\pi T$)s ($0_k^+, 1_k^+, 2_k^+, 3_k^+$, *and* $4_k^+$, *where* $k$ = 0,1,2, … ,9), for the energy states, compared with available experimental data respectively, i.e. in ground state $0_0^+$ all results are conformed with available experimental data ($\Delta$=0), $2_0^+$ , and $4_0^+$are closer with values of available experimental data, compare exp. data, (at $J = 2_0^+$) the deviation $\Delta$= 0.971, 1.113, 1.382, (at $J = 4_0^+$) $\Delta$= 3.927, 4.166, 4.271 respectively Clearly, there are neared between the energy values that's have same $J_k^\pi T$for all cases, so the FPD6 and KB3G interactions closer of available experimental data. And one find new energy states are making in high orders of$J_k^\pi T$.

The energy levels of calculated results are distributed over arrange of 18 MeV in comparison with the experimental one 12 MeV. Less than 3 MeV the results are in same manner expect the order of sequence, but after this region the deviation are very clear especially for the highly angular momentum values and highly excited energy levels for the same $J_k^\pi T$ multipolarities in the case of FPD6, GXPF1 and KB3G.When the use of Gogny-p2 effective interaction achieved, and the results are sketched in fig(3). The order of sequence between this option and in the comparison with experimental data (exp. data) it is clear that the order of sequence is as same that of the other interactions, but it deviates in some states by the values of MeV less than that of exp. data.

Figure (3) represented $^{42}$Ca energy levels scheme by used nuclear shell model with FPD6, GXPF1 and KB3Ginteractions (with using fp-shell model space) with inert core $^{40}$Ca for ($J_k^\pi T$)s ($0_k^+, 1_k^+, 2_k^+, 3_k^+, and\ 4_k^+, where\ T$ = 1, $k$ = 0,1,2, … ,9, $T$ = 1), for the energy states, compared with results of Gogny-p2(no core) interaction. You can see conform in ground state $0_0^+$in all result interactions withavailable exp. data, i.e. compare exp. data (at $J = 2_1^+$) with same state of FPD6, GXPF1, KB3G andGogny-p2interactions, the deviation $\Delta$=0.853, 1.648,0.764,0.487, (at $J = 3_0^+$) $\Delta$= 1.958,2.531,1.72,0.394, respectively. So from the result one can say Gogny-p2interaction best of the others compare with exp. data, with some of energy states lying under the ground states and up outer of scheme range (just in Gogny-p2interaction). Gogny-p2 interaction in frozen spsd-shell and active fp-shell will produce states lying under the ground state with energy level spacing $\Delta$=-0.15 MeV for $J_k^\pi T = 4_0^+1$,and $\Delta$=-0.4 MeV for $J_k^\pi T = 2_0^+1$, meaning that the calculated ground state is not $J_k^\pi T = 0_0^+1$ but it is $J_k^\pi T = 2_0^+1$, or if we unescapably consider that $J_k^\pi T = 0_0^+1$is ground state, so $J_k^\pi T = 2_0^+1, 4_0^+1$ is a self $\gamma$-ray emitting state.

## CONCLUSIONS

Realistic Gogny-p2 effective interactionis very useful to reproduce energy levels in $^{42}$Ca especially for the low laying states.

- Shell model enhances the calculation where the particles in full shell are included and make them occupying of inert core and make the other active to reproduce nuclear properties.
- Energy levels are in fair agreement with the fitting interactions (FPD6, GXPF1 and KB3G).
- Energy levels calculated by realistic (Gogny-p2) interaction is in betteragreement with exp. data, in comparison withthe results of the other interactions(FPD6, GXPF1 and KB3G).

## REFERENCES

1. Fadhel Mahmood Hmood, a thesis, University of Baghdad, College of Science (2016).
2. A. N. Bohr and B.R. Mottelson, CERN, Geneva, E 84 016224(1957).
3. R. du Rietz, et al, Phys. Rev. Lett. 93, 222501 (2004).
4. A.K. Hamoudi, Nucl. Phys. A 892, 21 (2012).
5. M.J. Taylor,et al. Phys. Let.B, 605, 265–272 (2005) .
6. R. A. Eisenstein, et al, Phys. Rev., 188, 4 (1969).
7. K.-H. Speidel, et al, Prog. Part. , Nucl. Phys., 49 , 91-154 (2002).
8. F. M. Hussain and Musaab Khudhur, Jour. of Infor. Engin. and Applic. Vol.3, No.10 (2013).
9. Oxbash for windows, B. A, Brown , A. Etchegoyen, N.S. Godwin, W. D. M.Rae, W.A.Rcihter, W.E.Ormand,
10. E.K.Warburton, et al, MSUNSCL, report number 1289 (2004).
11. V. Vel´azquez et al, Jour. Phys. A 475, p 1742 (2013).
12. Poves A and Zuker A P, Phys. Reports 70 235 (1981).
13. Kuo T T S and Brown G E, Nucl. Phys. A 114 241 (1968).
14. Papenbrock T and Weidenmuller H A Phys. Rev. C 73 014311 (2006).
15. Caurier E and Nowacki F Code ANTONIE (Strasbourg: CRN) (1989).
16. Faleiro E, et al, Phys. Rev. Lett. 93 244101 (2004).
17. G´omez J M G, et al,Phys. Rev. Lett. 94 084101 (2005).

18. Molina R A, et al, Phys. Lett. B 644 25 (2007).
19. Landa E, et al, Phys. Rev (2011).
20. P. J. Brussaard and P. W. M. Glademans, "Shell-model Application in Nuclear Spectroscopy" North-Holland Publishing Company, Amsterdam (1977).
21. R. D. Lawson, "Theory of the Nuclear Shell Model" Clarendon Press, Oxford (1980).
22. H. Nakada, Phys. Rev. C68. 014316 (2003).
23. H.Nakada, phys.Rev. C78, 054301(2008).
24. J.F. Berger, M. Girod, D. Gogny, Comput. Phys. Commun. 63, 365, (1991).
25. S. Hilaire, M. Girod, Eur. Phys. J. A 33(2), 237, (2007).
26. B. A. Brown, phys. Rev. C58(1), 220, (1998).
27. Y. Waghmare, R. K. Gupta and N. Kumar, Pro. of Theo. Phy., 31(5), 765, (1964).

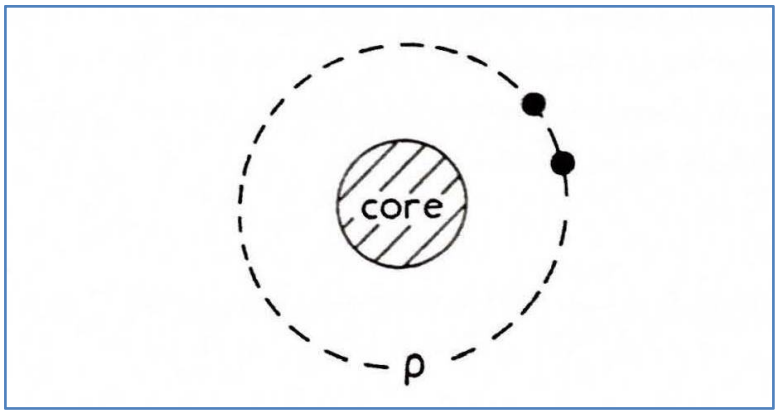


**Fig. 1. Schematic illustration of a nucleus described by an inert core and two particles in the orbit ϱ.**

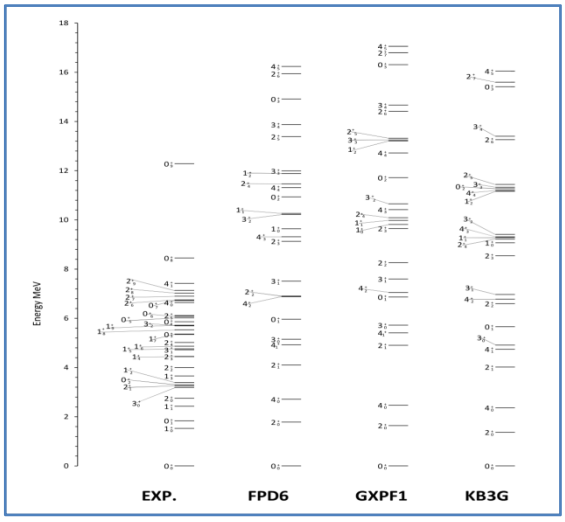


**Fig. (2)the energy levels scheme of $^{42}$Ca by use FPD6, GXPF1 and KB3G interactions(by using fp-shell model space) with inert core $^{40}$Ca for ($J^{\pi}_{T}$)s even party, ten orders compare with exp. Data**

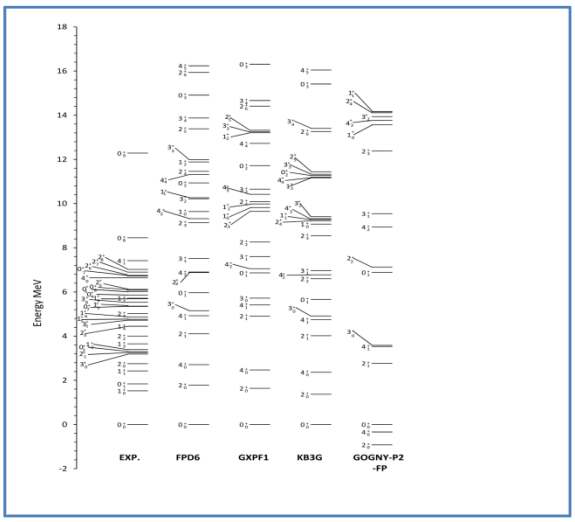


**Fig. (3) the energy levels scheme of $^{42}$Ca by used FPD6, GXPF1 and KB3Ginteractions (by using fp-shell model space) with inert core $^{40}$Ca for ($J^{\pi}_{k}T$)s for the energy states, with results of Gogny-p2(no core) interaction.**

*Indian Journal of Natural Sciences* www.tnsroindia.org.in ©IJONS

*Vol. 9 / Issue 50 /October 2018* *International Bimonthly* *ISSN: 0976 – 0997*

RESEARCH ARTICLE

# The Change Effect of Graphene Ratio on the Behavior of the Electrical Double-Layer Capacitors (EDLCs)

Hanaa H. Salman[1]* and Harith I. Jaafar[2]

[1]College of Education, University of Al-Qadisiyah, Iraq.
[2]College of Science, University of Baghdad, Baghdad, Iraq.

Received: 17 July 2018 Revised: 22 Aug 2018 Accepted: 27 Sep 2018

***Address for Correspondence**
**Hanaa H. Salman**
College of Education,
University of Al-Qadisiyah, Iraq.
Email: hanayara90@yahoo.com, harith ibrahem@yahoo.com



## ABSTRACT

In this study,the electrical properties of EDLCs were investigated (Graphene)as active material as electrode .The electrodes were prepared from aluminum plates with dimensions (5×5)$cm^2$ and covered by nano graphene material with different weights (0.04,0.06,0.08,0.l,0.2 and 0.3)gm., and sodium sulphate ($Na_2SO_4$) was used l.7M concentration as an electrolyte solution. The capacitor is charged with 3volt, the method for testing these capacitors were including charge and discharge curve. The results showed an increase in the charge current by increasing the weight of graphene, while the discharge current become stable .there was an improvement in the voltage drop and an increase in storage energy.

**Keywords:** supercapacitor ,graphene, ,electricaldouble-layer, stored energy.

## INTRODUCTION

Supercapacitor (SCs) is a new device of stored energy, It has large capacitance, high power density, enhanced thermal operating rang, long cycle life, low cost of maintenance, and environment friendly [l,2]. Energy is stored in the duble –layer capacitor as charge separation in the double –layer formed at the interface between the liquid electrolyte and the solid electrode material surface in the micro pores of electrodes after the cur when a voltage is applied rent flow ,the electrons charged across the double layer and form a capacitor [3]. Fig.l shows the structure of electrical double layer capacitor. A supercapacitor cell consists of separator ,two electrodes and an electrolyte ,the electrodes are made up of an active material ,which high surface area ,it separated by membranes ,the separator which allows the mobility of the charged ions and forbids the electronic conductance ,the system impregnated with an electrolyte ,it maybe organic (solid state)or aqueous [4]. Ectrical double layer capacitors (EDLCs), that can use different active materials(carbon ,graphene ,oxides or conducting polymers).the storage energy at the electrolyte – active materials interface through reversible ion adsorption onto active materials surface ,thus charging the so- called 'double-layer

capacitance' .this double –layer capacitance ,firstly defined by Helmholtz(l879) and later refined by Gouyand Chapman ,Stern and Geary [5].Y .MengCAI et al,(20ll)[7], the effect of the electrolytesolution on super capacitors l properties, used Graphene Sheetas the electrode for has been investigated .They found that The specific capacitance increases from l54.l F/g for pure to 23l.0 F/g for the Nanocomposite. B .Andres et al,(20l2)[8], study supercapacitors with graphene foil and Silver electrodes materials,the paper used as separator between two electrode materials were investigated,the supercapacitors with a grapheme – gold nanoparticle composite as electrodes"showed a specific capacitance of up to l00 F/g and energy density can be increased by using other electrolytes (aqueous electrolyte)". M.B.Tayel et al ,(20l5)[9],investigated the fabrication of supercapacitor based on graphene and polyaniline for energy storage application ,the result indicated that graphene PANI double layers exhibited high porosity and large surface area,and the specific capacitance as high as 9l5.78F/g in polyaniline /graphene supercapacitor.H .Mustafa ,A. Zdunek,(20l7)[6], investigated super capacitor, used graphene ,carbon black , PAN electrodes, the $H_2SO_4$ was used IM concentration as an electrolyte solution"Electrodes fabricated from a lower carbon mixture with PAN and graphene showed the highest capacitances whereas electrodes fabricated from higher carbon with PAN ,graphene and carbon black had significantly lower capacitance values".

M.H.Mustafa,A.Zadunek,(20l7)[l0], Study supercapacitorNanofiber Electrodes Graphene –Based .A strong influence of initial electro spinning mixture concentration on capacitance and electrode structure was also observed .Electrodes fabricated from a lower carbon mixture containing PANA and graphene showed the highest capacitance where as electrode fabricated from higher carbon mixtures of PANA ,graphene and carbon black had significantly lower capacitance values.L. Huang *et al.(*20l8)[ll], study super capacitors with Flexible paper and Graphite was coated on paper with pencil drawing as electrode. Showed a high electrical conductivity of l0.0S.$cm^{-l}$and could be directly used a supercapacitors electrodes, and high energy density of ll0.3 Wh.$Kg^{-l}$at a power density of l2l.9 W.$Kg^{-l}$

## MATERIALS AND METHODS

### Materials

1. Graphene Nano powder with specification thickness:6-8nm and surface area:l20-l50$m^2$/g was used ,manufactured by company sky spring nanomaterial,Inc.…,
2. Commercial aluminum plates with thickness (0.99mm) and dimensions (5×5) $cm^2$.
3. separator:A thin sheet of fibrous texture of o.33 mm thick is inserted between the two electrodes of super capacitors before adhesion them together .
4. Electrolyte solution $Na_2SO_4$ with l.7M concentration.

### Methodes

The aluminum plates used basis of electrodes with dimension 5×5$cm^2$ .Clean and cut a according to the dimension mentioned .The end of the plates were punctures with a diameter(3mm), for the purpose of the placing the wires at the ends of the plates as positive and negative electrode and connecting them to the electrical circuit.After the preparation and configuration of the electrodes leave a side and then bring the mix and (polyurethane epoxy and hardener) which is used adhesive and conductive. Bring the mixture with a weight 3gm from polyurethane epoxy and 2gm hardener they are well-blended .The mixture is distributed equally and homogenously over the effective area of each electrode .Then we prepare the active materials (nano graphene) that covers the electrodes.A layer of graphene is placed according to the weights mentioned plates(0.04, 0.06, 0.08,0.l,0.2 and 0.3). The separator (fibrous texture) is the placed between aluminum plates(electrodes), and infused with electrolyte solution $Na_2SO_4$.The electrodes are then connected to gather and the nylon wrap is clamped with a thermal-nylon knob.The EDLCs were manufactured to be connected to the circuit for the purpose of conducting tests.

## RESULTS AND DISCUSSION

The circuit consists of two parts . The First part is the Charging circuit when the switch closed and the second part is the discharge part when the key is opened. l-the charge-discharge circuit The circuit concatenation between the supply voltage D.C.,EDLCs manufacture (C) required to calculate its capacity,Ameter for measurement of charge current ($I_{ch}$), avometer (V), key to close and open the circle ,resistance l0Kohm , ameter for measurement of discharge ($I_{dch}$),curvature device fig.2. After connected the capacitor with electric circuit described in the fig.2switch is closed and charging is capacitor, For 0.04 gmnano graphene, the first period for charge voltage was 3volt , after 30 minute and during the discharging process ,a drop in the voltage was observed thel.5V fig( 3) . After 30 minute the voltage was drop to 0.8V using out resistance (l0KOhm). For second period , anther charging process (3volte)was done for 30 minute, a drop in the voltage was observed (l.65 V), after 30 minute the voltage was drop to( 0.9V) in second curve. This method was used for all sample groups (capacitors) manufactured from the nano –graphene with weight (0.06,0.08,0.l,0.2and 0.3) gm. Through this curve, the capacitance was calculated by applying E q .(l) $t_2$-$t_l$ is the time interval of the voltage drop between 40%v_max and 80%v_max. Vl: is 80% of 3V= 2.4V, V2:is 40% of 3 V=l.2V, Tl:Time with voltage Vl(sec), T2:Time with voltage V2(sec), I:Discharge current determine from $V_C$ and resistance load (R) , $V_C$ voltage on capacitors.

$$C = I\frac{dt}{dv} \qquad Eq(1)$$

were C : capacitance(F). I : discharge current(A).

"The stored energy in supercapacitors calculated by multiplying the capacitance by the vo1tage v to the power of 2, Eq.2"

$$\mathbf{E} = \frac{1}{2}.\mathbf{c}.\mathbf{v}^2 \qquad \mathbf{Eq(2)}$$

In two electrode symmetric cell configuration, specific capacitances can be calculated from the equation:

$$\mathbf{C = 2(I\,\Delta t/m\,\Delta V)} \qquad \mathbf{Eq(3)}$$

where I is the constant discharge current, Δt is the discharging time, m is the mass of one electrode, and ΔV is the voltage drop upon discharging. Energy density (E) and power density (P) can becalculated from the following equations:

$$\mathbf{E = [C\,(\Delta V)2]/8} \qquad \mathbf{Eq(4)}$$

$$\mathbf{Eq(5) P = E/\Delta t}$$

where E, C, ΔV, P and Δt are the specific energy, specific capacitance, potential. window, specific power and discharge time, respectively [l3].The applied voltages which used to be charge the(EDLCs) was(3 volt), the EDLCs have electrodes from graphene and electrolyte solution is $Na_2SO_4$and( fibrous texture) a separated.The electrolyte solution is placed on the separator between electrodes and when connecting the EDLCs with electrical circuit, we charged the capacitor with 3volt, the current will be pass between two electrodes and willlead to ionization of the electrolyte solution$Na_2SO_4$ and transfer of positive ions Na to the negative electrode and negative ions SO to the positive electrode stay on the surface of active material.It was observed that, when the weight for (graphene) increased, the charging current ($I_{ch}$) will increase dueto the increased surface area of the electrode with presence of graphene ,which spread on the surface of the electrode .This leads to direct contact points which gives more ions which dissolved from the solution. For the discharge current($I_{dch}$), it was found(Table l) that the current is constant maybe due to the output circuit which have constant resistance(load) was (l0KΩ)fig. 2.For the drop voltage($V_{drop}$),

when the EDLCs in the process of discharge , ($V_{drop}$ )will occurred this due to, an internal electric field will be generated between the electrodes, resulting in the disintegration of the ions and their direction or deviation to electrodes. In the process of discharge will be occur a drop in voltage due to the rearrangement or direct association of decaying ions with the electrolyte solution that is not adjacent to the electrodes or the effective medium. When the ratio of the active substance is increased, the results shown(Table l) is active material(graphene) which has high surface area on which all ionized ions from the electrolyte will be stabilized and which are initially adhered to, this will reduce the number of ionsthat are(non-polarized)or (not attached) to the electode(free) this in turn will be effect the process of reduction in ($V_{drop}$) after charge process. For the capacitance values, note the increase of the values by increasing the weight of the active material(graphene) due to the increase of the surface active material.Because of the increase in capacity, the stored energy increase as well as because of its dependence on the voltage square

## REFERENCES

1. K. Patel and R. Desai , (IJEIT),2,Issue l,(20l2).
2. D.Majumdar , Innovative energy and Research,.5,Issue 2,(20l6).
3. Y.Zhang,l.Wei ,X.Shen, H.liang,WSEAS TRANSCTIONS onCIRCUITS and SYSTEMS ,8,Issue 6,(2009).
4. A .Shneuwly and R.Gallay,"Properties and application of supercapacitors from the state –of-the art to future trendes",Proceeding PCIM ,2000.
5. P.Simon and Y.Gogotsi,OATAO ,Philosophical Transaction A:Mathematical ,Physical and Engineering Sciences,.368, (20l0),PP.3457-3467,ISSN l364-503X
6. M.H .Mustafa and A.Zdunek,Int.J.Electrochem. Sci.,l2, (20l7)PP.29l7-2932
7. Y .Meng CAI ,Z. Yi Qin L .Chen.2l,Issue 6, (20ll)PP.460-466
8. B .Andres ,S .Forssberg ,A . Vilches , R .Zhang ,H. Andersson ,M. Hummelgard ,J .Strom, H.Olin ,Nordic Puip and paper Research Journal , 27,2,(20l2).
9. M. Tayel ,M .MSoliman, M.E.Harb,copyright to IJAREEIE,4,Issue l0,(20l5).
10. M.H.Mustafa ,A.Zdunek,Int.J.Electrochem.Sci , (20l7),PP.29l7-2932
11. Huang ,W.Rao,l.Fan,J,Xu,Z.Bai,W.Xu, H.Bao,Journal/Polymers,(20l8)
12. S .Ban ,J .Zhang ,l .Zhang, K .Tsay, D .song , X .Zou, acta 90 (20l3), pp. 542-549
13. H. Wang, H. Yi, X. Chen, X. Wang,(ESI) for Journal of Materials Chemistry A This journal is © The Royal Society of Chemistry 20l3

**Table I. shows electrical properties of capacitor with different weights of active materials (graphene)**

| Material (graphene) gm | $I_{ch}$(A) | $I_{dch}$(A) | $V_{drop}$(V) | C(farad) | E (stored energy Wh) | $C_{specific}$ ($Fg^{-l}$) | E density ($WhKg^{-l}$) | P density ($wkg^{-l}$) |
|---|---|---|---|---|---|---|---|---|
| 0.04 | 3.4 | 0.2l | l. 5 | 0.008 | l4.04 | 0.4l66 | 74.9 | 7.4 |
| 0.06 | l.5 | 0.2l | l.25 | 0.0l | 75.6 | 0.250 | 45 | 0.75 |
| 0.08 | 4.2 | 0.2l | l | 0.0l4 | 72 | 0.486l | 87.498 | 0.87 |
| 0.l | 5.7 | 0.2l | l | 0.03 | 2l6 | 0.3333 | 59.99 | 0.299 |
| 0.2 | ll | 0.2 | 0.75 | 0.05 | 360 | 0.9533 | l7l.59 | 0.6599 |
| 0.3 | l2.8 | 0.2 | l | 0.047 | 4248 | 0.l666 | 29.988 | 0.l |

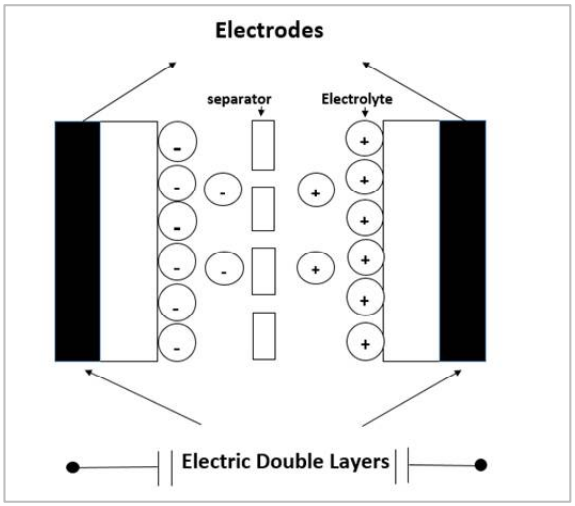


**Fig. 1. Principle of a double layers capacitor [3]**

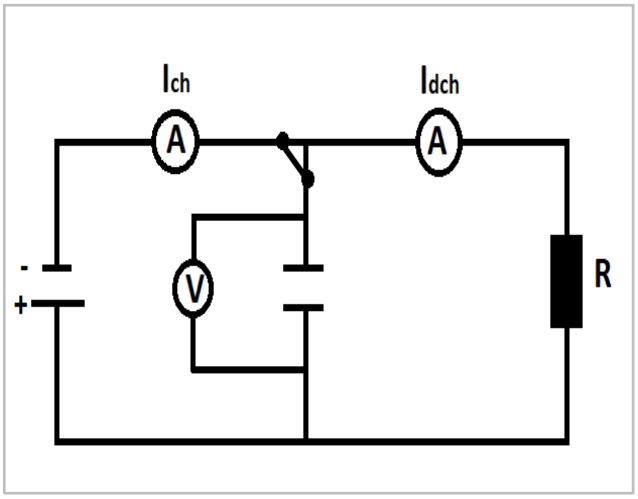


**Fig.2 Charge and discharge circuit diagram [I2].**

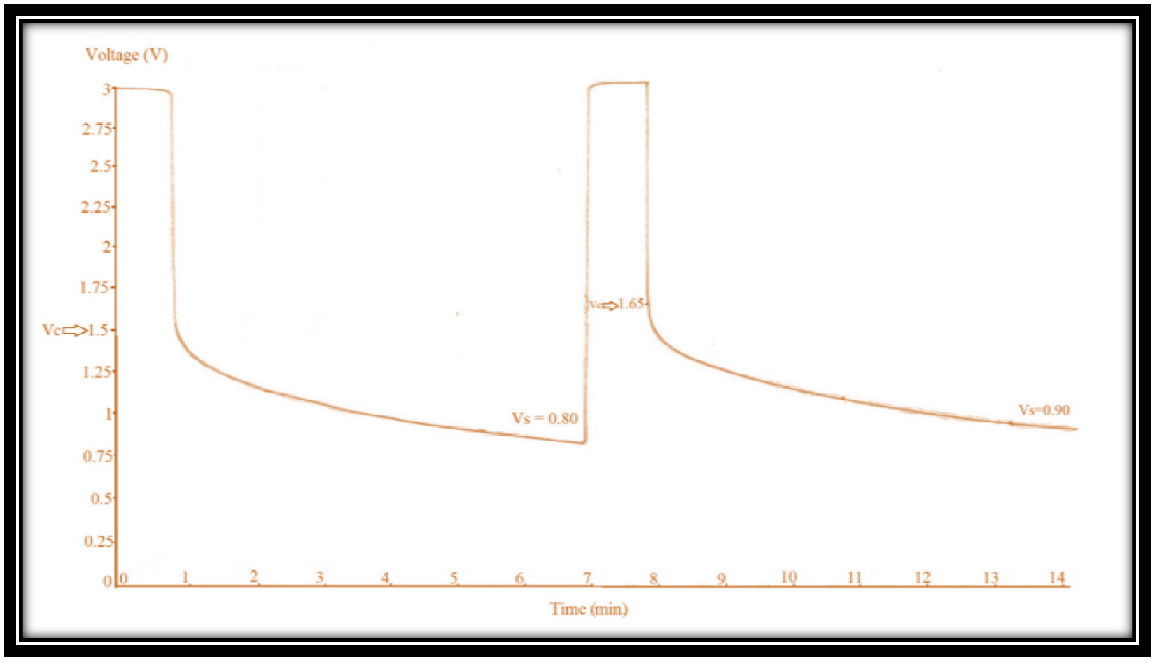


**Fig 3. Charge - discharge curve**

*Indian Journal of Natural Sciences* www.tnsroindia.org.in ©IJONS

*Vol. 9 / Issue 50 /October 2018* *International Bimonthly* *ISSN: 0976 – 0997*

RESEARCH ARTICLE

# Preparation of Polystyrene Conductive Polymer Nanocomposites Based on Silver-Gold Nanoparticles for Optoelectronic Application

Nahida.J.H*

School of Applied Science, University of Technology, Iraq.

Received: 13 July 2018 Revised: 18 Aug 2018 Accepted: 25 Sep 2018

***Address for Correspondence**
**Nahida.J.H**
School of Applied Science,
University of Technology, Iraq.
Email: nahidajoumaa61@yahoo.com



## ABSTRACT

Conventional conductive composite as polystyrene (PS) and methyl orange/polystyrene (MO/PS) show promising conductivity for these applications. In this research paper,polystyrene (PS) and methyle orange/polystyrene (MO/PS) composites were prepared at different concentrations (3.6, 6.7 and 12.5 wt/ wt%), the optimum one was doped with gold (Au), and silver (Ag) nanoparticles. The optical, electrical, and morphology properties of the involved samples were studied using, (UV–Vis) spectrophotometer, Hall system, scanning electron microscope (SEM), and atomic force microscope(AFM).The results show increase and shift in absorption spectra towards the longer wavelength with MO ratio specially at 3.6% MO/PS, and (Au, Ag nanoparticles) incorporation. It was induced by the energy change in the lowest unoccupied molecular orbital (LUMO) of legend, causing the ($\pi$-$\pi^*$), and ($d\pi$-$\pi^*$) transition to occur at higher or lower energy. It was seen decrease in energy gap with (MO) ratio, and (Au, Ag (nanoparticles) incorporation increase. There was significant increase in PS conductivity from ($8.83^{-8}$, to $4.26\times10^{3}$ $(cm.\Omega)^{-1}$ at (3.6%MO) addition, that means that the (PS) electrical conductivity could be controlled by MO orange addition and could be transferred from insulator to conductor material.

**Keywords:** conductive, polystyrene, microscope, molecular, energy.

## INTRODUCTION

Since the discovery of intrinsically conducting polymers, researchers have explored their unusual electronic properties for a wide range of applications. Due to the presence of conjugated p-electron backbone these polymers exhibit electronic properties such as low energy optical transmission, low ionization potential and high electron affinities. These unique properties make these materials suitable for applications as thin film transistors, organic light emitting diodes, sensors, super-capacitors, organic solar cells and electrochromic displays.Many research groups have extensively investigated conducting polymers for these applications and a number

of excellent reviews are available (1-5). Polymers are known as dielectric materials (6). It faced a significant interest by many researchers. Its conductivity was improved by filler addition (7,8). It was found that its conductivity depends on material type and the process method. The conducting polymers are characterized by its conjugated bonds, which was alternated with single bonds in back bone structure (9). The conducting, and semi conducting polymers advantages are attributed to its low density, and good workability (10). Many studies were carried out about the conducting poly heterocyclic polymers because of its environmental stability (11). The polymer conductivity, and physical properties can be enhanced by filler addition (polymer composites) at different concentrations. The polymer conducting of modified polymers can be achieved by using selected elements (12). Raid A. Ismail, et. al. also reported that the electrical and photoresponse properties of (Ag-PS/P-Si) and (Au-PS/P-Si) hetrojunctions were studied.The rectification characteristics of junction were improved after nanoparticles incorporation (13). Zhu and Schmauder (6); Ahmad and Mamat (14); Aly A .(15) and Sangawar VS, Golchha MC (2013) (16) proved that the optical, magnetic,and mechanical properties of PS after embedding metal or semiconducting nanoparticles into the polymer matrix .Sheikholeslami M, Vajravelu K.(17),and Deshmukh SH,and etals(18) found that addition of metal nanoparticles can enhance the thermal conductivity and heat transfer of fluid (17,18). Here, we carry out a first study on the preparation and characterization of (MO/PS) composites at different \concentration, and gold and silver nanoparticles were added to the sample of best absorption spectrum to study its effect on electrical conductivity of (PS).

## MATERIALS AND METHODS

### Materials

All the materials were used with analytical grade. Polystyrene (PS) was supplied from ICI London. Methyl Orange (MO) was purchased from sigma Aldrich USA. Diachloromethane were purchased from GCC Iraq while Au and Ag nanoparticles were purchased from Sigma Aldrich USA.

### Method

The Polystyrene (PS) were used as matrix. The samples were prepared by casting method. (PS) grains were dissolved in diachloromethane ($CH_2Cl_2$) solvent of high purity (99.99%) ,which were provided from (GCC), at different concentration (6-10 wt./vol%). The solution were shacked till get homogeneous solution, and cased in clean Petri dishes, left it 24 hours to dry. It was found that 7wt.% /vol was of best concentration. The film was clear without bubbles, and defects. Methyl orange (MO) ($C_{14}H_{14}N_3NaO_3S$) was added at different concentrations 3.6, 6.7 and 12.5 (w/w) to (PS). The previous method was followed to prepare composite films. Figure 1. shows photographs of (PS) solution before and after (MO) addition.Ag and Au (nanoparticles) were prepared by laser ablation in ethanol. The laser energies of (750 mJ) with 200 laser pulses, and (600 mJ) with 300 laser pulses were used to prepare collide Au and Ag nanoparticles respectively, which were prepared in concentration of 0.4 and 0.5 mg/ ml respectively.

### Conductive polymer composite Characterization

The prepared films were evaluated spectrophotometrically by using UV/VIS Spectrophotometer (UV1800 Shimadzu). The surface morphology of the films were investigated using AFM (atomic microscopy (CSM-500). The surface morphology were analysed using Scanning Electron Microscope (SEM) (ZEISS GeminiSEM 500) with the emission current at 5.00 KV. The electrical measurement was carried out by using Hall system (HMS-3000) to get (carrier concentration, mobility, resistivity, and conductivity) for the samples involved.

## RESULTS AND DISCUSSION

As shown in Figure 3 the high porosity (which is 94%) for (PS) structure was confirmed by the SEM images of (MO), and (MO/PS), (MO/PS;Au), and (MO/PS;Ag) composites. Circular pores were shown in their results. It reveals that micros pores structure was highly interconnected (19). Au and Ag nanoparticles filled (PS) micro spheres, and micro particles of MO were aggregated on the prose wall as shown in Fig. 3b (3). As it could be seen, gold-decorated and silver-decorated micro spheres increase as proved by the result. Observing of Figures (3c and 3d), (Ag) (nanoparticles) formation as well as free (Ag) (nanoparticles) attached on (PS) surface as PS core would be fill with (Au) and (Ag) (nanoparticles). The growth and nucleation condition can be attributed to this process which was shown for (Au) (nanoparticles) (4). The growth and nucleation condition dependent, of prose structure was proved in Figures (3c and 3d). It shows that the prose was partially or completely filled with (Au) and (Ag) (nanoparticles, and other particles (MO) would be aggregated on the wall of the pores (20). Observing of Figures (4a-4d) which show AFM images of (MO/PS), (MO/PS;Au) and (MO/PS; Ag) composites. This images proved that (MO) good distributed over all (PS) Matrix aligned vertically in a good contact with (PS) pores. (AFM) analysis was used to obtain the root mean square (RMS) of surface roughness and samples involved in (AFM) analysis was given in figure 5.

As observed, these results enhanced the uv-vis spectrophotometric evaluation as increase in (RMS) of roughness with (MO), (Au) addition, and decrease with (Ag) addition (21,22). Figure 6 show that the absorption spectra of (PS), and (MO/PS) composites at different concentrations. Figures 7 and 8 show the absorption spectra of the samples involved after Au, and Ag (nanoparticles incorporation). As shown, absorption increase, and shifted toward the longer wave length. The shift is as a result of change in energy of the lowest unoccupied molecular orbital (LUMO) of legend, causing the $(\pi\text{-}\pi^*)$, and $(d\pi\text{-}\pi^*)$, transition to occur at higher or lower energy (5) (Zhu W.,and etals(2013). Localized state formation in the energy gap, and ion mobility, which increased in its ability to penetrate the polymer chain caused the absorption increase. These lead to the enhancement of AFM results in roughness increase with MO. Au, and Ag nanoparticles ratio increase (23).The optical energies gap was measured by $(\alpha h\nu)=A\ (Eg\text{-}h\nu)^r$. Observing of Figures 9-11 show that the relationship between $(\alpha h\nu)^2$ and $(h\nu)$; It was proved that (PS) was of direct transition type. Extrapolation of linear part at $(\alpha h\nu)^2 = 0$ was used to obtain the optical energy gap (See the figures below). Modifying the electronic structure of (PS) matrix which was induced by appearance of various poloronic and localized states formation was found to have led to decrease in energy gap with (MO) ratio increase. The increase with methyl orange that was attributed to defect formation in composite structure was seen at (3.6% MO) of the lowest energy gap, though it was less than (PS) energy gap. In relation to the decrease in the (PS) electrical resistivity, Figures 12 and 13 display the decrease in energy gap with MO%, and Au, Ag (nanoparticles addition) (See the figures below). The energy gap of the samples involved is given in Table (I).

From the study of the electrical properties of PS and (MO/PS) before and after Au, Ag (nanoparticles) addition, it was proved that there was nonlinear relationship between the carrier concentration and MO% that was attributed to the no compatibility between the (PPS and (MO). It shows further that (PS) was of (P-type). The carrier type converted to N-type after MO addition. MO and (Au and Ag) (nanoparticles addition) result in increased the carrier concentrations as it was seen in figures 14 and 15, and mobility decrease, that was attributed to impurities scattering, and it was in a good agreement with figures 16 and 17. The dye will create defects in matrix structure that will act as localized states in energy gap, which results in increase in total energy of the carrier concentration and complex ion formation as MO ratio, and (Au, Ag) nanoparticles addition increase. As shown, the reason to take high concentration of dye is that the negative ion mobility is high in comparison with positive ion, so the positive ion mobility needs high concentrations of counter ions and that each polaron moves close to the opposite charge field. It is observed in figures 18 and 19 that the resistivity behaviour decreased with free radical in polymer chains increase. Intermolecular charge transition enables the polymer conductivity to be induced by electron hopping from onepolymer chain to another. This conductivity may be limited to bad contact among phases.

The conductivity mechanism was achieved by charging hopping or inters soliton hopping. The charge was captured by appositive charge of doping materials, whereas natural solition will be delocalized and capable to interact with any chain, which has charged solition; the electron will transfer from defect to another as a result of this interaction (redox reaction). By this, the donor will be oxidized, whereas the accepter will be reduced by free energy. It was provided by potential oxidation by (P-type doping) electron acceptor or by potential reduction (n-type doping) electron donor since the organic polymer did not contain intrinsic charge carriers, Figures 20 and 21 shows that as a result of doping, charges, like polaron, bipolaron, and soliton, defect (5).

## CONCLUSIONS

There were significant increase in PS conductivity at (3.6% MO) ratio from ($1.79\times10^{-12}$ to$4.54\times10^{3}$), that means that the (PS) conductivity could be controlled by MO orange addition and could be transferred from insulator to conductor material. In this work it could be synthesized low cost conductor polymer system in simple method. The study proved the (3.6% MO/PS) is of higher value than that of samples which incorporated with Au, and Ag ((nanoparticles) of higher cost. The samples involved suggested being use in optoelectronic applications, and many other electric applications.

## REFERENCES

1. Aldemir DA, Kökce A, Özdemir AF (2017) Temperature effects on the electrical characteristics of Al/PTh–SiO2 /p-Si structure. Bull Mater Sci 40:1435–1439.
2. Ismar E. (2018) Facile synthesis of poly [1-p(tolylsulfonyl) pyrrole] via Ce(IV)-pyrrole redox initiating system and polyacrylonitrile blended nanofibers. 1–9.
3. Das TK, Prusty S (2012) Review on Conducting Polymers and Their Applications. Polym Plast Technol Eng 51:1487–1500.
4. Zhan C, Yu G, Lu Y, et al (2017) Conductive polymer nanocomposites: a critical review of modern advanced devices. J Mater Chem C 5:1569–1585.
5. Bakhshi AK, Bhalla G (2004) Electrically conducting polymers: Materials of the twentyfirst century. J Sci Ind Res 63:715–728
6. Zhu K, Schmauder S (2003) Prediction of the failure properties of short fiber reinforced composites with metal and polymer matrix. Comput Mater Sci 28:743–748.
7. Karrar,M.A.,(2013):MSC Thesis,Study of dyes effect on optical ,properties of (PS),Univrsity of technology/School of Applied Science.
8. Mort,G.P.(1989); Electronic properties of polymer science,and Technology,John and Sons.
9. Ali K M (2014) Study of Methyl Orange Effect on the Optical and Electrical Properties of Polystyrene (PS). 39–53
10. Heinze J (1990) Electronically Conducting Polymers. Top Curr Chem 152:1–47.
11. Polymers E (2005) Structure and Property of Electronic Polymers. Chem Mater 1–45.
12. Zhang Y, Gu C, Schwartzberg AM, et al (2006) Optical trapping and light-induced agglomeration of gold nanoparticle aggregates. Phys Rev B - Condens Matter Mater Phys 73:1–9.
13. Raid A. Ismail1• Nahida J. Almashhadani1• Rand H. Sadik(2017), Preparation and properties of polystyrene incorporated with gold and silver nanoparticles for optoelectronic applications, Appl Nanosci DOI 10.1007/s13204-017-0550-6
14. Ahmad T., Mamat O. (2011), " The Development and Characterization of Zirconia-Silica Sand Nanoparticles Composites ". World J Nano Sci Eng 01:7–14.
15. Aly A, Mahmoud M, Omar A (2012) Enhancement in mechanical properties of polystyrene filled with carbon nano-particulates (CNPS). World J Nano Sci Eng 2:
16. Sangawar VS, Golchha MC (2013) Evolution of the optical properties of Polystyrene thin films filled with Zinc Oxide nanoparticles. 4:2700–2705.

17. Sheikholeslami M, Vajravelu K (2017) Nanofluid flow and heat transfer in a cavity with variable magnetic field. Appl MathComput 298:272
18. Deshmukh SH, Burghate DK, Akhare VP, et al (2007) Electrical conductivity of polyaniline doped PVC –PMMA polymer blends. 30:51–56.
19. Prize TN (2000) Advanced Information - The Nobel Prize in Chemistry 2000. 1–16
20. Kutorglo EM, Hassouna F, Kopecký D, et al (2017) Synthesis of conductive macroporous composite polymeric materials using porogen-free method. Colloids Surfaces A Physicochem Eng Asp.
21. Zhang Y, Chen Y, Liu Y, et al (2018) Highly porous single-ion conductive composite polymer electrolyte for high performance Li-ion batteries. J Power Sources 397:79–86.
22. Yılmaz Baran N, Saçak M (2018) Preparation of highly thermally stable and conductive Schiff base polymer: Molecular weight monitoring and investigation of antimicrobial properties. J Mol Struct 1163:22–32.
23. Zhu W, Wu Y, Yan C, Wang C, Zhang M, Wu Z (2013) Facile synthesis of mono-dispersed polystyrene (PS)/Ag composite microspheres via modified chemical reduction. Materials 6:5625

**Table 1 The energy gaps of the Samples involved**

| Polymer system | Eg (eV) | Polymer system | Eg (eV) | Polymer system | Eg (eV) |
|---|---|---|---|---|---|
| PS | 3.9 | PS | 3.9 | 0 | 3.9 |
| MO/PS; 1Au | 1.6 | MO/PS; 1Au | 1.7 | 3.6 | 2.3 |
| MO/PS; 2Au | 1.5 | MO/PS; 2Au | 1.6 | 6.7 | 3.1 |
| MO/PS; 2.4Au | 1.4 | MO/PS; 2.4Au | 1.3 | 12.5 | 2.9 |

**Table 2 The electric characteristic of PS and MO/PS at different concentration**

| MO% | Carrier Concentration ($m^{-3}$) | Mobility ($m^2$/VS) | Resistivity ($\Omega$.cm) | Conductivity $(\Omega.cm)^{-1}$ |
|---|---|---|---|---|
| 0 | 1.96 $E^{+10}$ | 6.19 $E^{+01}$ | 1.68 $E^{+11}$ | 8.83 $E^{-09}$ |
| 3.6 | 6.04 $E^{+20}$ | 5.16 $E^{+01}$ | 2.35 $E^{-04}$ | 4.26 $E^{+03}$ |
| 6.7 | 8.56 $E^{+08}$ | 4.56 $E^{+01}$ | 1.44 $E^{+08}$ | 5.37 $E^{-09}$ |
| 12.5 | 1.23 $E^{+09}$ | 8.68 $E^{+01}$ | 1.11 $E^{+08}$ | 9.30 $E^{-09}$ |

**Table 3 The electric characteristic of MO/PS, Au, and Ag addition (cc)**

| **Au-addition (cc)** | **Carrier Concentration ($m^{-3}$)** | **Mobility ($m^2$/VS)** | **Resistivity ($\Omega$.cm)** | **Conductivity $(\Omega.cm)^{-1}$** |
|---|---|---|---|---|
| 1 | 1.42 $E^{+09}$ | 2.36 $E^{+02}$ | 4.06 $E^{+07}$ | 7.42 $E^{-08}$ |
| 2 | 3.06 $E^{+10}$ | 3.92 $E^{+02}$ | 2.53 $E^{+08}$ | 3.04 $E^{-08}$ |
| 2.4 | 7.49 $E^{+08}$ | 1.20 $E^{+02}$ | 5.39 $E^{+07}$ | 9.30 $E^{-08}$ |
| **Ag-addition (cc)** | **Carrier Concentration ($m^{-3}$)** | **Mobility ($m^2$/VS)** | **Resistivity ($\Omega$.cm)** | **Conductivity $(\Omega.cm)^{-1}$** |
| 1 | 7.49 $E^{+08}$ | 1.20 $E^{+02}$ | 1.51 $E^{+10}$ | 1.64 $E^{-08}$ |
| 2 | 7.36 $E^{+08}$ | 3.04 $E^{+01}$ | 4.79 $E^{+10}$ | 3.08 $E^{-09}$ |
| 2.4 | 1.43 $E^{+10}$ | 1.84 $E^{+02}$ | 1.80 $E^{+08}$ | 5.87 $E^{-09}$ |

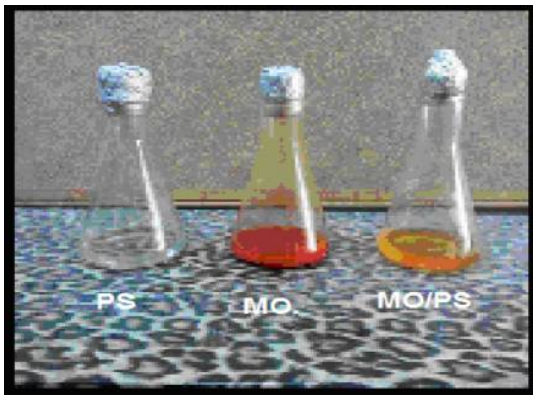


**Fig.1.Prepared solitions of PS, MO and MO/PS**

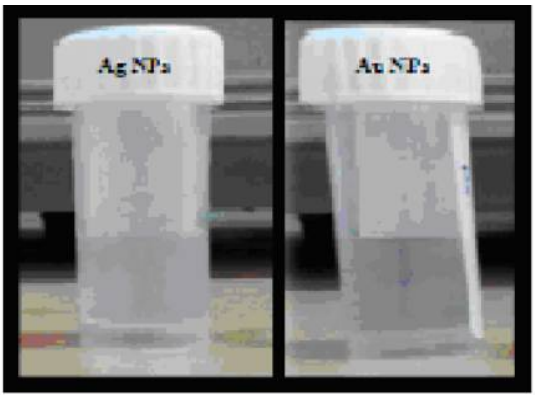


**Fig.2.Prepared colloidal (Ag)NPs and (Au)NPs**

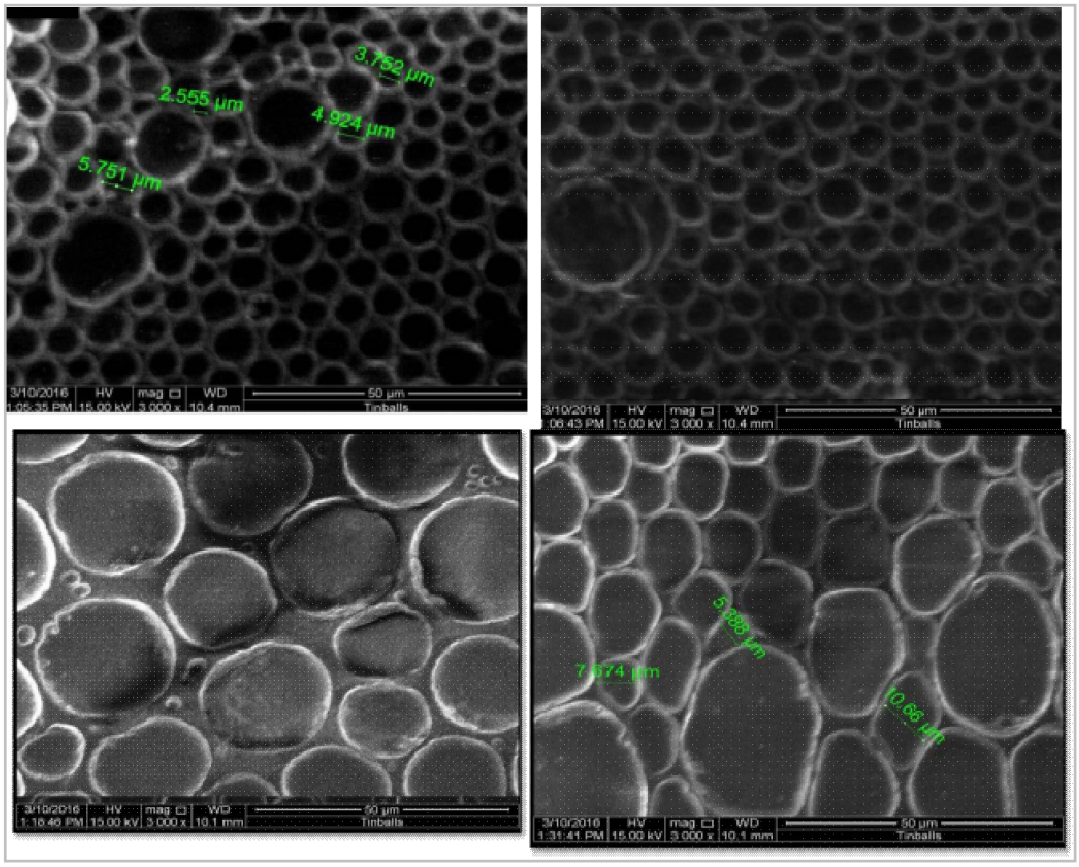


**Figure 3 SEM images of a (PS) matrix, b (MO/PS ) c (MO/PS:Au),d (MO/PS:Ag).SEM magnification of (X3000).**

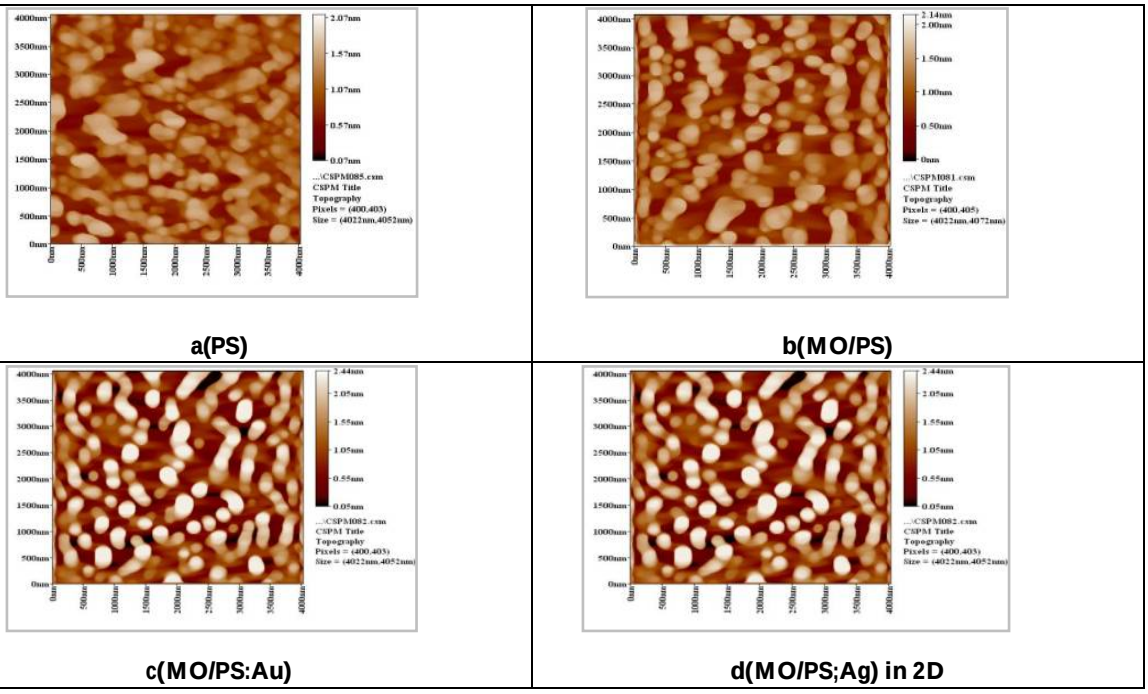

a(PS) b(MO/PS)

c(MO/PS:Au) d(MO/PS;Ag) in 2D

**Fig.4: AFM image**

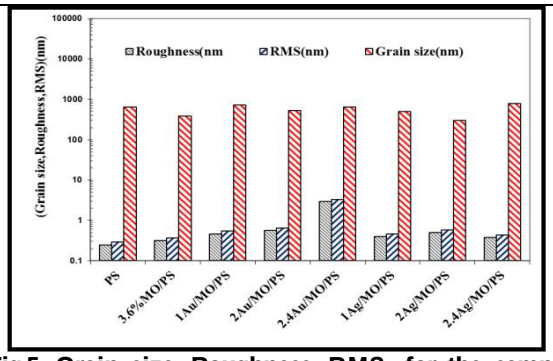


**Fig.5. Grain size, Roughness, RMS for the samples involved**

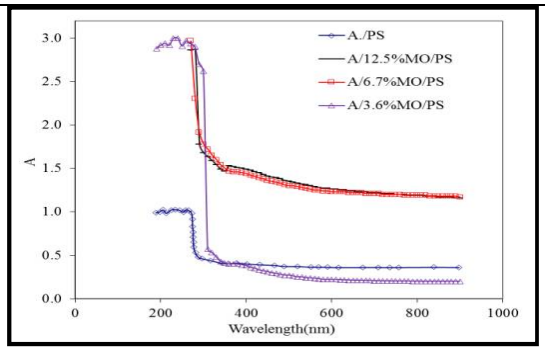


**Fig. 6. absorption spectra of PS.and MO/PS composites at different concentrations**

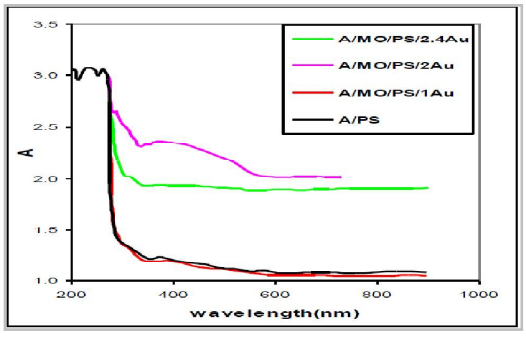


**Figure 7 absorption spectra of PS. and MO/PS composites after Au incorporation**

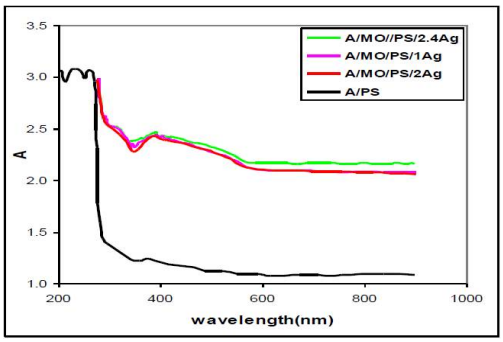


**Figure 8 absorption spectra of PS.and MO/PS composites after Ag incorporation**

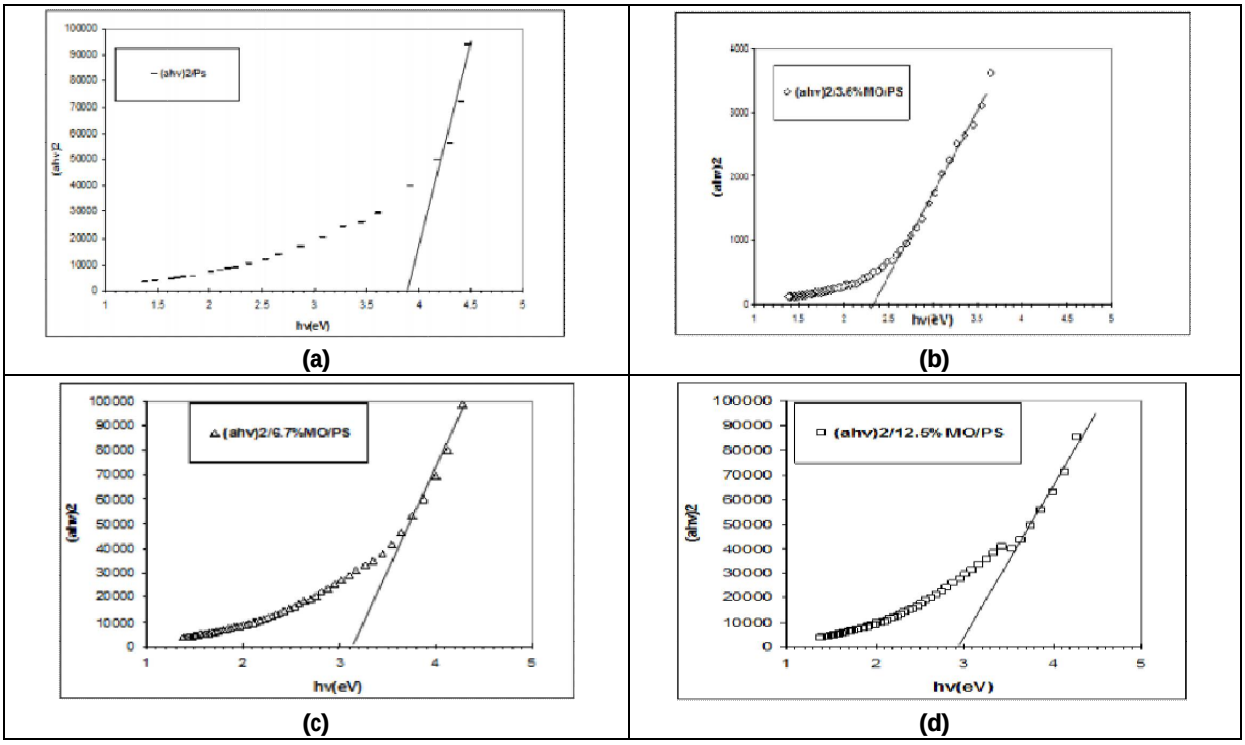


**Figure 9 (a-d) The relationship of $(\alpha h\nu)^2$ with $(h\nu)$ for PS and MO/PS composites**

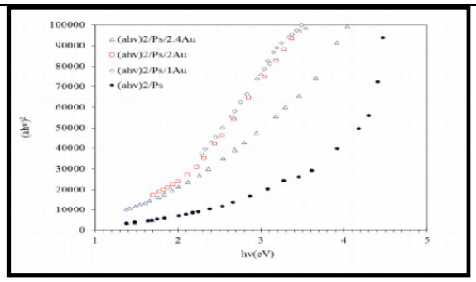


**Figure 10. The relation of $(\alpha h\nu)^2$ with $(h\nu)$ for PS and MO/PS composites after Au incorporation**

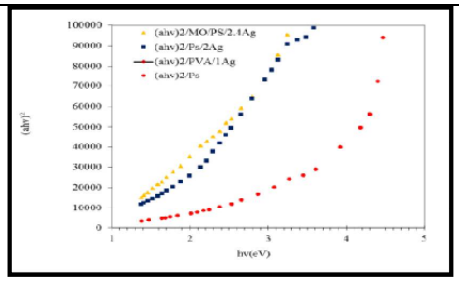


**Figure 11. The relationship of $(\alpha h\nu)^2$ with $(h\nu)$ for PS and MO/PS composites after Ag incorporation**

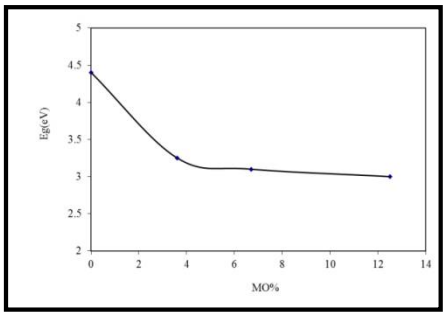


**Figure 12. The relationship between the energy gab and MO%**

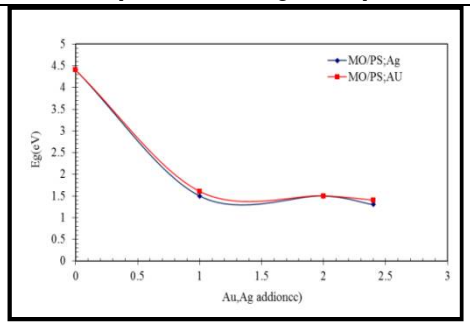


**Figure 13. The relationship between the energy gab and AU,Ag addition(cc)**

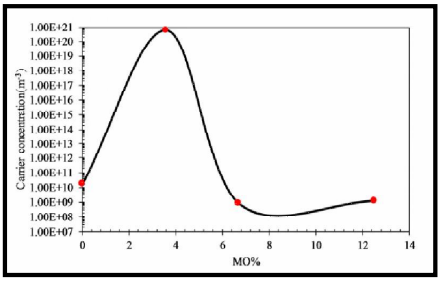


**Figure 14. The relationships between the carrier concentrations and MO ratio**

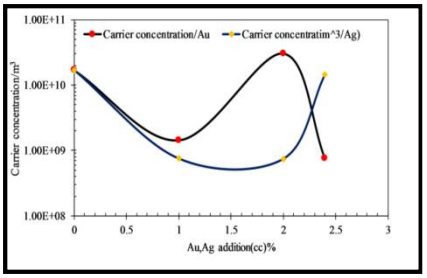


**Figure 15. The relationships between the carrier concentrations and Au, Ag addition (cc)**

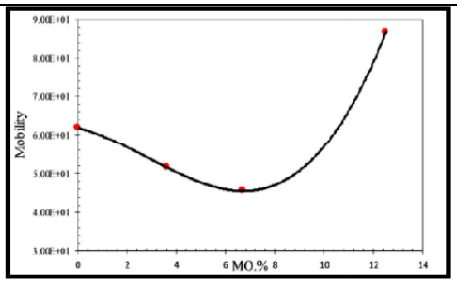


**Figure 16. The relationships between the mobility and MO ratio**

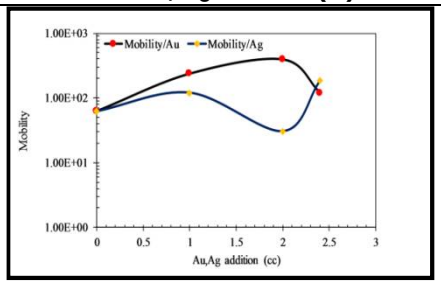


**Figure 17. The relationships between the mobility and Au, Ag addition (cc)**

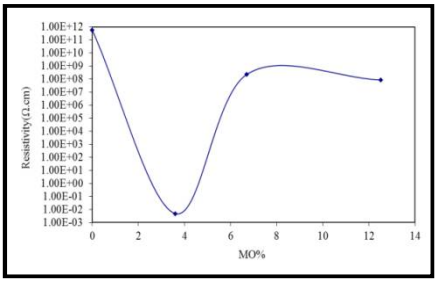


**Figure 18. The relationships between the resistivity and MO ratio**

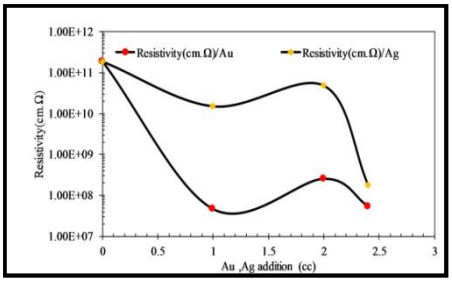


**Figure 19. The relationships between the resistivity and Au,Ag addition(cc)**

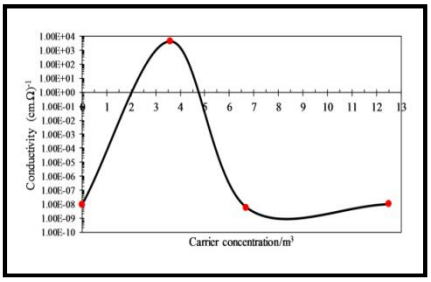


**Figure 20. The relationships between the conductivity and MO ratio**

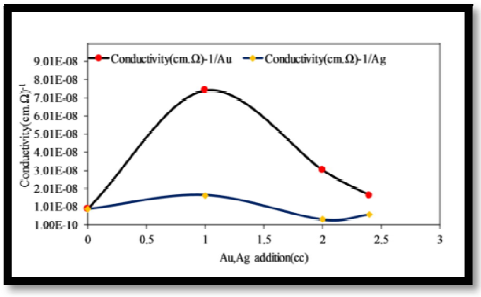


**Figure 21. The relationships between the conductivity and Au, Ag addition (cc)**

*Indian Journal of Natural Sciences* www.tnsroindia.org.in ©IJONS

*Vol. 9 / Issue 50 /October 2018* *International Bimonthly* *ISSN: 0976 – 0997*

RESEARCH ARTICLE

# Effect of Thickness for ($Bi_xSb_{2-x}Te_3$) Thin Films on the Thermal Properties

Hussain. M. Selman[1*], Salma M. Shaban[1] and Falah I.Mustafa[2]

[1]Deptartment of Physics. College of Science, University of Baghdad, Iraq.
[2]Solar Energy Research Center, Renewable Energy Directorate, Ministry of Higher Education and Scientific Research, Baghdad, Iraq.

Received: 02 July 2018 Revised: 06 Aug 2018 Accepted: 10 Sep 2018

[*]**Address for Correspondence**
**Hussain. M. Selman**
Deptartment of Physics,
College of Science,
University of Baghdad, Iraq



## ABSTRACT

In this study The( $Bi_xSb_{2-x}Te_3$) alloys with different values of percentage of (Bi) (x=0,0.1,0.3,0.5, and 2) and different thickness, have been prepared, Thin films of these alloys are prepared using thermal evaporation technique under vacuum of ($1\times10^{-5}$ ) Torr on glass substrates, at R.T. Thermoelectric properties of( $Bi_xSb_{2-x}Te_3$) thin film were calculated from (300 K to 423 K) The values of Seebeck coefficient, decreases when increasing of Bi percentage in all samples of ( $Bi_xSb_{2-x}Te_3$) thin film, also power factor showed same manner which decrease when increases the (Bi) percentage in( $Bi_xSb_{2-x}Te_3$) thin film for different thickness. Thermal conductivity $K_{el}$ for the deposited ($Bi_xSb_{2-x}Te_3$) thin film, decreases by increasing Bi percentage for different thickness, , from ($4.163*10^{-5}$ w/k.cm at x=0 to $0.98*10^{-5}$ at x=2) for thickness100nm ,as well as ( $5.071*10^{-5}$ w/k.cm at x=0 to $1.556*10^{-5}$ )at x=2) for thickness 300nm, and ($12.052*10^{-5}$ w/k.cm at x=0 to $3.385*10^{-5}$) at x=2) for thickness 500nm. Finally we found that the figure of Merit (ZT) decreases by increasing (Bi) percentage for all investigated ($BixSb2_{-x}Te_3$) thin films, for different thickness from (0.537 at x= 0 to 0.204 at x=2) for thickness 100nm, also from (0.769 at x=0 to 0.250 at x=2) for thickness 300nm, and from (0.988 at x=0 to 0.276 at x=2) for thickness 500nm.

**Key words:** Thermoelectric, Bi, $Sb_2$, $Te_3$, Parameter

## INTRODUCTION

Know, the world is depending on the fossil fuels this type of fuel generates risky waste on the environment, so the researchers started to looking for a new source of clean energy, herefore the work on the raw materials that innervates the devices and technologies so that it can be a clean energy sources, this raw materials are chemical compounds it able to convert the energy heat to electrical energy or vice versa. These materials are found in (1820) by

scientists in Western Europe, the thermoelectric material can defined as a material has a high figure of [1].These materials have a low thermal conductivity, high Seebeck coefficient and high electrical conductivity, which give a high dimensionless figure of merit, and that gives a good explanation to how much the materials have a thermoelectric properties, and it useful for the thermoelectric applications**.** The term of "thermoelectric" can be know as the relationship between the heat and electricity, so when were applying a temperature orientation on a thermoelectric junction, an electric current have been produced (by producing a voltage difference and it causes the movement of charge carriers inside the material [2]. The German physicist T. J.Seebeck who first discovered the Seebeck effect in (1821).Seebeck's first observed that, when we put acompass needle near of a closed loop composed of two deferent metals, it will be deflected, and there is a temperature difference between the junctions which has been proved there was an electric current generation in a closed loop is event of the temperatures difference at both ends of the junction . The charge carriers (electrons or holes) in the material are responsive to the temperature difference that causes diffusion of the charge carriers from the hot side to the cold side; as a result these can give a rise to the thermoelectric voltage). The relation between the difference voltage and difference temperature is called Seebeck effect that can be written as:[3]

$\Delta V = (S_A - S_B)\,\Delta T$ ……..……(1)

where, $S_A$ and $S_B$ are the Seebeck coefficients of the terminals to material A and B, respective $\Delta V$: difference of voltage in(Volt), $\Delta T$: applied temperature in K. The charge carriers of the cold side can be raised by increasing in the temperature difference, and this leads to increasing in the thermoelectric voltage. The voltage difference ($\Delta V$), is called electromotive force (emf.), which was generated when happen a temperature difference ($\Delta T$) between two different terminals of semiconductors or metals as mentioned in the equation (1), therefore we can defined Seebeck coefficient as the electric field strength that is enhanced by a set temperature gradient in the material, So the Seebeck coefficient is most important indication parameter on the thermoelectric materials[4].The aim of finding materials for future generation for thermoelectric applications is to improvement the figure of merit. There are two methods to use thermoelectric material , the first one is power generation ,which is depends on the Seebeck coefficient to convert the heat to electrical power, the second is thermoelectric cooling ,which (runs inversely with power generation), which converts the applied electrical current so that the heat can be pumped from the cold to hot junction ,the cold junction will speedily drop under ambient temperature[5].The ($Bi_xSb_{2-x}Te_3$) thin films possess properties making them thermoelectric nature at room temperature, and this demeanor could be explaining in the coming sections. Seebeck's coefficient (thermo power) of a material is a measure of the magnitude of the induced thermoelectric voltage in response to a temperature difference across that sample. a good thermoelectric material should show a value of (S) in the range of few hundred of ($\mu V/K$), which is given by the equation (2)[6]:

$S = -\frac{dV}{dT}$…… (2)

Where $\frac{dV}{dT}$:is the voltage gradient with temperature Thermal conductivity is the property of material ability measurement to behaviour heat. Thermal conductivity is the ratio of heat flux (Q) through the material and the negative gradient in temperature ($-\nabla T$) as show in equation (3).

$K = -\frac{Q}{\nabla T}$…….…….. (3)

Lattice thermal conductivity linked with the crystal structure, defects and grain limitations, etc. The thermal conductivity that is consists of lattice Phonon thermal conductivity ($K_{ph}$), and electronic thermal conductivity ($K_{el}$) as shown in eq (4) [7].

$K = K_{ph} + K_{el}$……..…. (4)

The lattice phonon ($K_{ph}$) has no high value in polycrystalline alloy with compared of (Kel), for that the($K_{ph}$) is proportional inversely to the unit cell mass and for the grain size , However, the electronic thermal conductivity ($K_{el}$) can be calculated from the"Wiedemann-Franz" law as show in eq.(2).

$K_{el} = L\,\sigma\,T$…… (5)

Where L= 2.445*10-$^{8}$WΩ/K2 is Lorentz number [71], σ : is the electrical conductivity and T is temperature. In (1910) is the first attempt to explaining the thermoelectric efficiency way was scattered by Altemkirch, then Abrahm. And Loffe formulated the ($Z$) parameter ,which included into the modern dimension less figure of merit $ZT$, The last was used to evaluation the thermoelectric material's quality. The part ($S^2\sigma$) in the relation (2) referred to the power factor as seen in eq. (2),which represented the electrical transportation properties of a thermoelectric material [8]. so the most important factor that measures the thermoelectric efficiency is the dimensionless figure of merit (ZT) as shown in eq (1-6) [9].

$ZT = \left(\frac{S^2\sigma}{k}\right)T$…… (6)

Where (S) is the Seebeck's coefficient, (σ) is the electrical conductivity, and (K)is the thermal conductivity . And the power factor (p.f) can be determined from the eq. (7).

$p.f = S^2\sigma$…….. (7)

## MATERIALS AND METHODS

This work includes an explanation of the preparation method of ($Bi_x Sb_{2-x} Te_3$) alloys with x= (0 , 0.1 , 0.3 , 0.5 ,2) , and thin films, the mechanism of measurement to the structural and electrical properties with nearby electric circuits which is used in this measurement. In the beginning raw materials are obtained as powder to prepare the alloys, these raw materials are (Bi with purity 99.9%, Sb purity 99.96% and Te purity 99.999%) powders. Alloys have been prepared from this raw materials in the magnitude which is mentioned above, by melting them in the quartz ampoules under vacuum with pressure about ($10^{-3}$) Torr. By using thermal evaporation method Thin films are prepared, the vaporized material is deposited on the glass substrate to investigate the thermoelectric properties (seebeack coefficient, thermal conductivity and figure of merit) [8**].** In order to measure how the thermoelectric properties of the material there are many types like; Peltier coefficient, Seebeck's coefficient and thermal conductivity can be used for this purpose. We will study Seebeck and thermal conductivity in this research. Seebeck coefficient deals with difference of the temperature between two terminals of the materials so that can be tested in depending on the equation (2) , it also gives information about the type of material whether it is (p-type ) or (n-type). Seebeck coefficient is also used to determine the Figure of Merit (ZT) as the relation (1-6). So it we need some tools in order to start the test, we use two blocks of aluminum one is at room temperature, and the other one is related with heater to rising the temperature gradually, and also with thermocouple to clogging the block temperature rising of. The thin film with width of (1.5) cm and length of (5) cm and the thermoelectric (TE) film is on the sample's edges are in contact with the aluminum block. Every side of the sample has the same temperature since the aluminum block is at the contact position. Seebeck voltage can be measured by investigation of keithely close to the contact points. All parts must be covered during the measurement to ensure minimized loss of radiation. The thermal conductivity can be measured from electrical conductivity, using equation (5 ) , the power factor and figure of merit can be measured by using Seebeck's values as in the eq. (7).The high ratio of the electrical conduction to the thermal conductivity makes from (Bi , Sb ,Te) a good thermoelectric material.

## RESULTS AND DISCUSSION

The information about thermoelectric properties of theprepared ($Bi_xSb_{x-2}Te_3$ ) thin films is obtained, by measuring the Seebeck coefficient, thermal conductivity , figure of merit and power factor.

### Seebeck coefficient

The investigation of the thermoelectric properties for deposited ($Bi_xSb_{x-2}Te_3$ ) thin films for different percentage of Bi (x=0,0.1 ,0.3 ,0.5 and2) and different thickness (100nm, 300nm, and 500nm ), Seebeck coefficient had been calculated by measuring the voltage difference as a function of temperature in the range of (300to 423)K, by using the equation (2). It was observed from a figure (3-1) a linear conduct between the voltage and temperature, which indicates that increasing in voltage lead to increasing of temperature.Also its found that Seebeck coefficient decreases with increasing (Bi) percentage, as seen in figure (4) and this result agree with Z. Li [10] and G. Zheng [11]. The Seebeck coefficient sign show that the $Bi_xSb_{x-2}Te_3$ thin films were p-type, this conduct is attributed to the preparation condition to the low excess of (Te) and there is no excess in (Sb) and (Bi) percentage that are responsible for transferring their conductivity type from n- to p- type.Also its noticed that seebeck coefficient increases with increasing the thickness (100nm,300nm, and 500nm) as shown in figure (2), it can be see that (S) is equal to( 114.2 µv/k when x=0), it decreases to be (73.44 µv/k at x=2) for thickness (100nm) while it equal to ( 137.2 µv/k when x=0), it decreases to be (78.57 µv/k at x=2) for thickness (300nm), and it equal to ( 155.5 µv/k when x=0), it decreases to be (82.25 µv/k at x=2) for thickness (500nm) All results are listed in Table (1).

### Power Factor

Its calculate the power factor for deposited $Bi_xSb_{2-x}Te_3$ thin films for different thickness by using equation (7). It can be observed that, as the (Bi) percentage (x=0, 0.1, 0.3, 0.5, and 2) increases the power factor decreases, in addition of that the power factor increased with increases the thickness , as shown in figure (3), this behavior is attributed to the decreasing in carrier concentration with increasing of (Bi) percentage, as mentionable previously in our results of Hall effect, this conduct agree with J.Song et al[12] ,these results listed in Table (1).

### Thermal Conductivity

Thermal conductivity can be obtained from eq. (7) which calaulated from as deposited $Bi_xSb_{2-x}Te_3$ thin films, lattice Phonon thermal conductivity ($k_{ph}$) has been neglected because of a small value for the material under study. It was observed that $K_{el}$ decreases sharply with increasing of (Bi) percentage and in the same time with increasing the thickness from (100nm to 500nm) as show in figure (3-4). Table (1) show the results of thermal conductivity and the electrical conductivity. These results are agree with X. Han [87] and L. X. Dong [13].

### Figure of Merit (ZT)

We calculated the figure of merit (ZT) by using eq. (6) of $Bi_xSb_{2-x}Te_3$ thin films at 300 K. It is found that ZT decreases from( 0.537 at x=0 to 0.204 at x=2 for thickness 100nm) as well as from ( 0.769 at x=0 to 0.25 at x=2 for thickness 300nm) and from ( 0.988 at x=0 to 0.276 at x=2 for thickness 500nm) with increasing (Bi) percentage for all the investigated samples which have agreement with N. Gao [14], as shown in fig. (5),the values of Figure of merit and other parameter are listed in the Table (3-1).

## CONCLUSION

From the study of ,electrical properties for( $Bi_2Sb_{2-x}Te_3$) thin films with different(Bi) percentage (0 ,0.1 ,0.3 , 0.5 , and 2) and different thickness (500nm, 300nm, and 100nm) which deposited by thermal evaporation technique at R.T. the thermoelectric properties were determined by Seebeck coefficient , power factor , thermal conductivity and figure of merit which represented as the most important parameter to have the knowing about the efficiency of thermoelectric materials. all the Seebeck co efficient, power factor, the thermal conductivity and figure of merit decreasing with increasing the Bi percentage but they increases with increasing the thickness, from (0.537 at x=0 to 0.204 at x=2 for thickness 100nm) as well as from (0.769 at x=0 to 0.25 at x=2 for thickness 300nm) and from ( 0.988 at x=0 to 0.276 at x=2 for thickness 500nm).

## REFERENCES

1. W.Qu, M.Plötner, , and W.J. Fischer, "Microfabrication of thermoelectric generators on flexible foil substrates as a power source for autonomous microsystems", Journal of Micromechanics and Microengineering,Vol.11,No.146(2001).
2. N. Fuschillo "Thermoelectric Phenomena" ,Thermoelectric Materials and Devices, Edited by, Irving B. Cadoff and Edward Miller
3. G.S. Nolas, J. Sharp, H.J. Goldsmid, Thermoelectrics: basic principles and new materials developments. Springer Verlag, (2001).
4. A.muto, masschusetts,"Solar Thermoelectric Energy Converter device" institute of technology ,p. 8, (2008)
5. Gross, A.J. Low Power, Integrated, Thermoelectric Micro-coolers for Microsystems Applications. Ph.D. dissertation, University of Michigan,(2010).
6. A.F. Ioffe, L.S. Stilbans, E.K. Iordanishvili, and T.S. Stavitskaya. Termoelektricheskoe Okhlazhdenie. U.S.S.R. Academy of Sciences, (1949).
7. TS Kim, TK Kim, SJ Hong, BS Chum. Mater SciEng; 90(1): 2-6. (2002).
8. T.M. Tritt, In Editors in Chief: K. H. Buschow, Robert W. Cahn, Merton C. Flemings, Bernard Ilschner, Edward J. Kramer, and Subhash Mahajan,Thermoelectric materials: Principles, structure, properties, and applications, Encyclopedia of Materials: Science and Technology,. Elsevier, Oxford, second edition,pp1–11, (2001).
9. G. J. Snyder and E. S. Toberer, Nat. Mater.,Vol. 7, No.105 (2008).
10. Z. Li, G. L. Zhao1, P. Zhang, S. Guo, J. Tang " Thermoelectric Thermoelectric Performance of Micro/Nano-Structured Bismuth- Antimony-Yelluride Bulk from Low Cost Mechanical Alloying" (2012).
11. G. Zheng , X. Su , H. Xie , Y. Shu , T. Liang , X. thermoelectric She , W.L. Y.Yan ,Q. Z. C.Uher , M. G. Kanatzidis and X. Tang ," High thermoelectric performance of p-BiSbTe compounds prepared by ultra-fast thermally induced reaction",(2017).
12. Junqiang Song, Qin Yao, Ting Wu, Xun Shi, and Lidong Chen, Electron. Mater. Lett., Vol. 9, No. 6 (2013).
13. L. X. Dong and Y. H. Park, "Structure and Transport Properties of $(Bi_{1-x}Sb_x)_2Te_3$Thermoelectric Materials Prepared by Mechanical alloying and Pulse Discharge Sintering ", (2002).
14. N. Gao, B. Zhu, X.Y. Wang, Y.Yu, and F.Q. Zu,"Simultaneous optimization of Seebeck, electrical and thermal conductivity in free- solidified Bi0.4Sb1.6Te3 alloy via liquid-state manipulation", (2018).

**Table 1. The parameters of thermoelectric properties, Seebeck coefficient, electrical conductivity, thermal conductivity, power factor and figure of merit of $Bi_xSb_{x-2}Te_3$ for different compositions (X=0, 0.1, 0.3, 0.5, and 2) and different thickness.**

| Thickness T(nm) | X | s(µv/k) | σ(Ω.cm)^-1 | k( w/cm.K) | p.f(µw/k.cm) | ZT |
|---|---|---|---|---|---|---|
| 100 | 0 | 114.2 | 5.714 | $4.163*10^{-5}$ | 0.0745 | 0.537 |
| | 0.1 | 98.79 | 3.93 | $2.868*10^{-5}$ | 0.0384 | 0.398 |
| | 0.3 | 86.41 | 2.53 | $1.849*10^{-5}$ | 0.0189 | 0.304 |
| | 0.5 | 81.6 | 1.8 | $1.315*10^{-5}$ | 0.0120 | 0.272 |
| | 2 | 73.44 | 1.34 | $0.98*10^{-5}$ | 0.00725 | 0.204 |
| 300 | 0 | 137.2 | 6.96 | $5.076*10^{-5}$ | 0.1311 | 0.769 |
| | 0.1 | 121.1 | 4.57 | $3.334*10^{-5}$ | 0.0671 | 0.599 |
| | 0.3 | 104.5 | 3.53 | $2.578*10^{-5}$ | 0.0386 | 0.446 |
| | 0.5 | 93.53 | 2.54 | 1.853*10-5 | 0.0222 | 0.357 |
| | 2 | 78.57 | 2.13 | $1.556*10^{-5}$ | 0.0131 | 0.250 |
| 500 | 0 | 155.5 | 16.54 | $12.052*10^{-5}$ | 0.3999 | 0.988 |
| | 0.1 | 131.4 | 13.66 | $9.95*10^{-5}$ | 0.2358 | 0.706 |
| | 0.3 | 111.6 | 9.34 | $7.805*10^{-5}$ | 0.1163 | 0.509 |
| | 0.5 | 103 | 7.14 | $5.207*10^{-5}$ | 0.0758 | 0.433 |
| | 2 | 82.25 | 4.64 | $3.385*10^{-5}$ | 0.0314 | 0.276 |

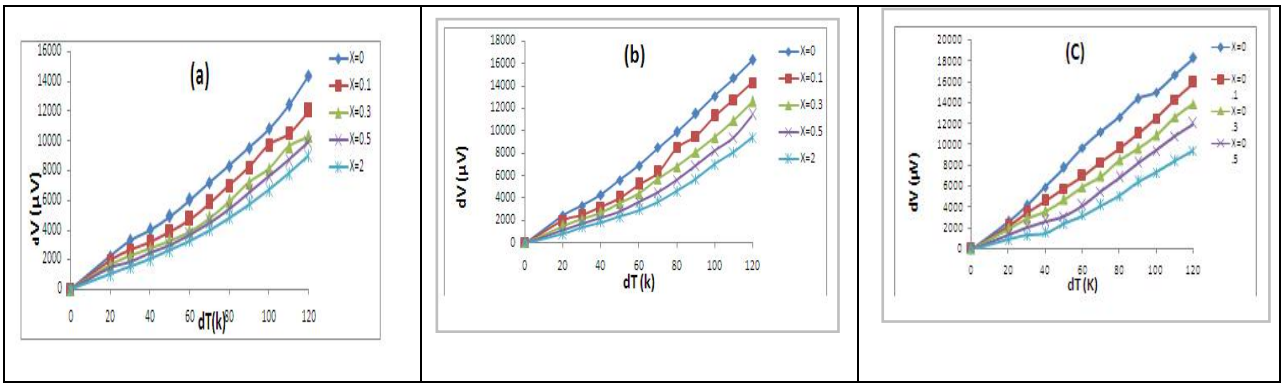


**Figure 1. the linear relation between the voltage and the temperature of $Bi_xSb_{2-x}Te_3$ thin films for different thickness: a(100nm), b(300nm), C (500nm).**

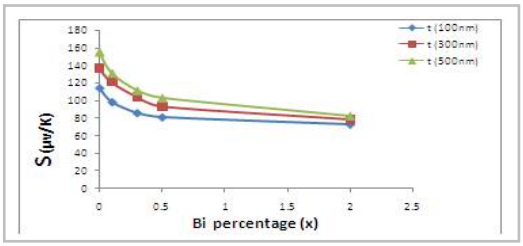


**Figure 2. the variation of Seebeck coefficient(S) with (Bi) percentage of $Bi_xSb_{2-x}Te_3$ thin films for different thickness.**

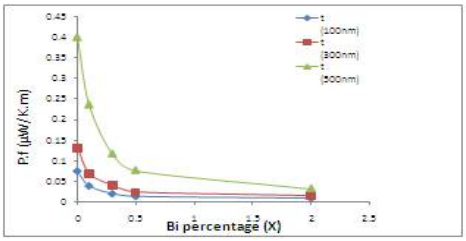


**Figure Power factor of $Bi_xSb_{2-x}Te_3$ thin films with deferent Bi percentage for different thickness**

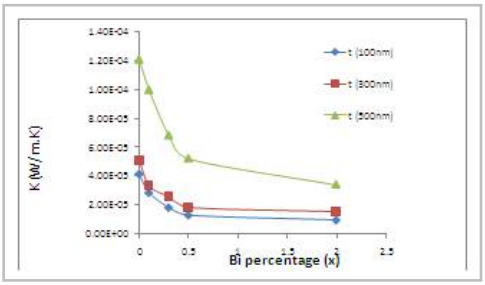


**Figure 4. Thermal conductivity for $Bi_xSb_{2-x}Te_3$ thin films with Bi percentage for different thickness.**

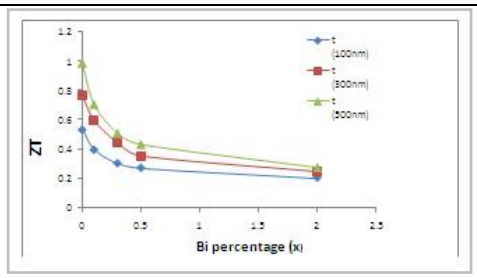


**Figure 5. the figure of merit of $Bi_xSb_{2-x}Te_3$ thin films with Bi percentage for different thickness.**

*Indian Journal of Natural Sciences* *www.tnsroindia.org.in ©IJONS*

*Vol. 9 / Issue 50 /October 2018* *International Bimonthly* *ISSN: 0976 – 0997*

RESEARCH ARTICLE

# Identification, Architecture & The Gross Structure of the Kidney in Adult Local Breed Ram in Iraq ( *Ovis ovis* ) by Using Corrosion Cast & Latex Techniques.

Nabeel Abd Murad AL-Mamoori[1*], Maha Abdul-Hadi Abdul- Rida[2] and Saffia Kareem Wally Alumeri[3]

Department of Anatomy and Histology, College of Veterinary Medicine AL-Qadisiyah University, Iraq.

Received: 02 July 2018 Revised: 08 Aug 2018 Accepted: 10 Sep 2018

[*]**Address for Correspondence**
**Nabeel Abd Murad AL-Mamoori**
Department of Anatomy & Histology,
College of Veterinary Medicine,
AL-Qadisiyah University, Iraq
Email : Nabeel.almamorri@qu.edu.iq



## ABSTRACT

Used ten specimens in the present study to distinctive anatomical, morphometric and blood supply features of the kidneys in adult ram (Ovis *ovis*) by using corrosion cast and latex injection techniques. The kidney was bean shape, brown in color and smooth consist from two surfaces, two borders and two pols. The mean weight, length, width, thickness, length medial and lateral borders of the right kidney was 58.003± 2.74, 6.5± 0.20, 4.075± 0.11, 3.075± 0.04, 9.22± 0.48 and 11.675± 0.29, while the mean weight, length, width, thickness, length medial and lateral borders of the left kidney was 58.237± 0.07, 6.575± 0.5,3.825± 0.37,3.1± 0.14 , 8.825± 0.27 and 10.8± 0.26 respectively. The parenchyma of the kidney divided into many regions differ in the color and texture was capsule, cortex and medulla.The renal pelvis a wide origin of the ureter within the kidney take saddle shape extend in horizontal plane at the level of renal crest and apex of renal pyramid. It send extension toward the renal pyramid refer to major and minor calyces. The renal artery divided into 2-3 segmental arteries. The segmental artery divided into 6-7 branches called interlobar artery. The interlobar arteries give the arcuate artery. The arcuate artery gives off several branches of the cortical radiate artery. The renal vein divided into 3-4 of segmental veins. The segmental vein divided into 6-7 branches called interlobar vein. The interlobar vein divided into the arcuate vein. The arcuate vein give off several branches of the cortical radiate vein.

**Keywords:** Kidney, morphology, corrosion cast, latex, ram, *Ovis ovis.*

## INTRODUCTION

The Sheep were regarded an important source of production of wool, meat and milk (1).The Awassi breeds have wide spread throughout the Asia area and the greater numbers of Awassi is found in Iraq. It is numerically the most important sheep and concentrated in the middle of the country (2).The total number of sheep in Iraq at 1980 (8,526,480) and (21,526) in AL-Qadisiyah province (3). The urinary system consists of two kidneys (right and left), two ureters (right and left), urinary bladder and urethra. The kidneys play very an importance role in maintenance homeostasis and excretion of metabolic waste products and other functions such as syntheses and secretions hormones renin and erythropoietin (4 and 5). It is located in the dorsal part of the abdominal cavity on each side of the caudal vena cava and abdominal aorta. In the most domestic animals the right kidney extend cranial more than left kidney. The kidneys in the most animal bean shape with smooth surface except in the cattle are lobulated with rough surface (6 and 7). This study design to providing anatomical information and data about the kidney in adult rams by using corrosion cast technique and latex injection technique.

## MATERIALS AND METHODS

### Morphological and biometrical study

Used ten specimens of the kidney of adult rams. It collected from AL-Diwaniyah abattoir immediately after slaughtering the rams. Make incision from thoracic inlet into the pelvic cavity and removed the internal organs to exposure the kidney. Dislocation of the kidneys with kept on the major blood vessels which supply the kidney (renal artery and vein) and part from ureter. Removed the adipose tissue which covered the kidneys and washing the kidneys by using tap water to remove the some of the impurities found. Finally recorded the weight, length, width and thickness of right and left kidneys.

### Corrosion cast technique

Used this technique to exposure the internal appearance of blood vessels and ureter by following steps:

1. Inject the renal artery, vein and ureter with warm normal saline solution 0.9 % or tap water to cleaning and discharge the clot or sediment which may be found in the blood vessels or ureter, let the specimen five minutes after injection with warm water.
2. Inject the renal blood vessels and ureter by mixture of self-cure denture material set (Powder and liquid 1 to 4), It consist of 20% monomethyl-methacrylate powder and 80% polymethyl-methacrylate liquid and adding the suitable dyes ( Red, blue and yellow ballpoint pen ink) to differentiate the blood vessels and the ureter (8).
3. Let the specimen at room temperature for 24 hours for polymerization.
4. Put the specimen in drain opener (It consist of a mixture of NaOH, Na2CO3 and NaClO take a granules shape dissolved 1 kg of drain opener in 5 liters of tap water) in at the room temperature for 72–96 hour to corrosion casted.
5. Washing the specimens with tap water and photographed.
6. Finally, to exposure the internal shape of the blood supply and renal pelvis put the polymerized kidney in square container and adding enough amount from tap water and freezing after that make longitudinal section by using special saw.

### Latex techniques

Used this technique to exposure the external appearance of blood vessels by following steps:

1. Inject the renal artery and vein with warm normal saline solution 0.9 % or tap water to cleaning and discharge the clot or sediment which may be found in the blood vessels, let the specimen five minutes after injection with warm water.
2. Inject the renal artery and vein with the red colored latex substance (2 : 3 latex with ammonia mixed with carmine stain) using blunt needle and syringe.
3. Used small pieces of tissue paper to prevent any leakage of latex from the damaged small arteries by pressing on the site of oozing.
4. Put the specimens in 10% formalin for 24 hour to fixed the tissue and setting of the injected material.
5. Finally made longitudinal section of the kidney to exposure the blood supply of the kidney by dissecting the blood vessels carefully and photographed.

## RESULTS

### Morphology of Kidney

### External Appearance of the Kidney

The kidneys (right and left) was bean shape, brown in color and smooth from outer surface embedded within adipose tissue. Each kidney consists from two surfaces (dorsal and ventral), two borders (lateral and medial) and two pols (cranial and caudal). The dorsal surface was strongly convex and the direction toward the vertebral columns, while the ventral surface slightly convex and toward the abdominal viscera. The medial border was concave in the middle region to formation the hilum to enter the renal artery with nerve and leave the renal vein and ureter while the extremities of border convex (Fig.1). The hilum was depression area connect the renal sinus where the ureter found, artery, vein, nerves and lymph vessels are pass through it. It can be see extend on ventral surface more than dorsal surface. The medial border of the right kidney toward the caudal vena cava, while the medial border of the left kidney toward the abdominal aorta. The lateral border convex from side to side (Fig.1). The mean weight, length, width, thickness, length medial and lateral borders of the right kidney was 58.003± 2.74, 6.5± 0.20, 4.075± 0.11, 3.075± 0.04, 9.22± 0.48 and 11.675± 0.29, while the mean weight, length, width, thickness, length medial and lateral borders of the left kidney was 58.237± 0.07, 6.575± 0.5 , 3.825± 0.37, 3.1± 0.14 , 8.825± 0.27 and 10.8± 0.26 respectively ( Table. 1 ).

#### Internal Appearance of the Kidney

To show the internal structure of kidney make longitudinal section of the parenchyma of the kidney can be see many regions or layers differ in the color and texture was capsule strong a fibrous membrane layer, transparent cover the outer surface of the kidney and easily dislocation resembling nylon bag (Fig.2). The cortex located beneath the capsule rough texture, brown in color and take radiate appearances which consist from cortical artriol and veniole. The cortex send part of it called renal columns toward the medulla separated renal pyramid. The medulla located ventral to cortex dorsal to renal pelvis, rough texture, light-brown in color, it divided into many regions pyramidal in shape called renal pyramid (Fig.2,3,10&11 ). The renal pyramid part of medulla has pyramidal in shape, it consist of base and apex, the base toward the cortex while the apex toward the renal pelvis.The apex of pyramid form renal papillae which refer to apical portion of the pyramid which projection in the minor calyces of the renal pelvis. It form the horizontal ridge of the medulla formed of the fusion of the renal papillae that projects into the renal pelvis called renal crest (Fig.2,3,10&11).The renal pelvis a wide origin of the ureter within the kidney. It is located in the renal sinus receives the urine from the renal papillae and transport into the ureter. When inject with cast resin the renal pelvis take saddle shape extend in horizontal plane at the level of renal crest and apex of renal pyramid. The renal pelvis see send extension toward the renal pyramid resemble the butterfly wings closed this refer to major and minor

calyces which surrounded the renal pyramid. The region between the extension (butterfly wings closed) see the blood vessels pass through it (Fig.2,3,7,8 and 9 ).

### Blood supply of Kidney

By uses the corrosion cast technique and latex injection technique can be seen the blood vessels that supply the kidneys and as following**:**

### Renal artery

The abdominal aorta give arises two branches of renal artery from the ventral side of it, to supplies the right and left kidneys through the hilum (Fig.1). The renal artery when reaches into entrance of the hilum of kidney divided into 2-3 segmental arteries (Fig.4,6,7 and13). The segmental artery extend into short distance &when reaches into the apex of the renal pyramid divided into 6-7branches called interlobular artery that supply medulla region (Fig.7,12&13).The interlobular arteries pass through the renal columns between the sides of renal pyramid and form the external boundaries of it which resemble the network of arteries. When it reaches into the base of the renal pyramid give branch extend along the base resemble of arch called arcuate artery ( Fig.7,10 and 13). The arcuate artery extend along the renal pyramid and give off several branches extend toward the cortex has radiate shape called cortical radiate artery that supply cortex region and capsule ( Fig. 4,6,7,10,11,12 and 13).

### Renal vein

The caudal vena cava give arises two branches of renal vein from the ventral side of it, which enter the kidney through the hilum of kidney ( Fig.1 ). The course of renal vein resemble of the renal artery.The renal vein when reaches into entrance of the hilum of kidney divided into 3-4 of segmental veins (Fig.5,6,7,8 and 13). The segmental vein extend into short distance with segmental artery in the same course and when reaches into the apex of the renal pyramid divided into 6-7 branches called interlobular vein (Fig.7,8 and 13 ). The interlobular vein pass through the renal columns with interlobular artery and form the external boundaries of the renal pyramid. When it reaches into the base of the renal pyramid give branch extend along the base resemble of arch called arcuate vein( Fig.7,8,12 and13).The arcuate vein extend along the base of renal pyramid in the same course of arcuate arteries and give off several branches extend toward the cortex take radiate shape called cortical radiate vein( Fig.7,8,10,11,12 and 13).

## DISCUSSION

### Morphology of Kidney

The kidney was bean shape, brown in color and smooth from outer surface. Each kidney consist from two surfaces, two borders, two pols and this result agreement with 6,7 and 9in small ruminants, horse, dog & cat, and disagreement with 7,9 and 10 in bovine show the kidney is lobulated ovoid in shape, while in one humped camel the kidney has smooth surface bean–shaped with grayish.The mean weight, length, width, thickness, length medial and lateral borders of the right kidney was 58.0035±,6.5±,4.075±,3.075±,9.225±,and 11.675±, while the mean weight, length, width, thickness, length medial and lateral borders of the left kidney was 58.237± , 6.575± , 3.825± , 3.1± , 8.825± and 10.8± respectively and this result disagreement with 12 show the mean weight, length, width, thickness, length medial and lateral borders of the right kidney was 66.41, 6.10, 3.60, 2.29 , 10.88 , and 11.87 cm, while the mean weight, length, width, thickness, length medial and lateral borders of the left kidney was 65.67, 6.30, 3.59, 2.20, 11.80 and 11.83 respectively in goat, this differ may be due to type and age of animal.The renal pelvis is a wide origin of the ureter within the kidney. The renal pelvis see send extension toward the renal pyramid resemble the butterfly wings closed this refer to major and minor calyces which surrounded the renal pyramid. This result agree with 7 and 9

show the renal pelvis bifurcated to major calices and then to miner calices, except in large ruminant where the major calices attached directly to the ureter. This differ due to structure and type of kidney (unilobular or multilobar).

### Blood supply of kidney

The renal artery arises from the ventral side of abdominal aorta and before entrance of the hilum of kidney divided into segmental artery, this result agree with 6,7,13,14 and 15 in sheep, buffalo, dog and horse. But disagree with 16 explain found the accessory renal arteries originating directly from aorta out of 100 specimens, it is recorded as 2%. The segmental artery has 3-4 branches extend into short distance and when reaches into the apex of the renal pyramid each one divided into 6-7 branches called interlobar artery that supply medulla region this result agree with 17 in goat show the segmental artery divided into 4 division, but disagree with 12 and 17 in buffalo show the number of interlobular artery 4-5 while 14 show the renal artery in kangal dog divided into two branch dorsal and ventral branch. The right dorsal artery gave 5 to 6 segmental arteries, while the right ventral artery give 4 to 6 segmental arteries, but the left dorsal artery give off 5-7 segmental arteries and the left ventral artery 6 to 8 segmental arteries. These differ due to species of animal. The interlobular arteries pass through the renal columns between the sides of renal pyramid and give arcuate artery, this result agree with 9. The renal vein when divided into 3-4 of segmental veins. The segmental vein extend into short distance with segmental artery in the same course divided into 6-7 branches called interlobular vein. This result disagree with 18 in pig show renal vein divided into cranial, middle and caudal renal veins. Each one branched into 8-9 interlobar veins. The interlobular vein pass through the renal columns with interlobular artery and branched into arcuate vein This result agree with 18 in pig.

## REFERENCES

1. Warriss A,. "Meat Science an Introductory Text", *School of Veterinary Science University of Bristol UK. CABI publishing*. 2000; 2: 1-4.
2. Owen J B., "Sheep Production Textbook". ELBS. 1981; 1st ed: 5 - 9.
3. AL-Sadi H I., "Animal Wealth in Iraq and Means of Improving it". *University of Mosul press*. 1980: 203-204.
4. Frandson R D., Wilke W L., and Fails AD., "Anatomy and Physiology of Farm Animals". Wiley Blackwell. 2009; 7th ed. 23: 383.
5. Mescher A L., "Junqueira's Basic Histology text and atlas". Mc. Graw-Hill Education. 2013; 13th ed. 19: 385-397.
6. May N D., "The Anatomy of the Sheep. Brisbane" Australia University of Queen land Press.1970; 3rd Ed: 161-207.
7. Dyce K M., Sack W O and Wensing C J., "Textbook of Veterinary Anatomy" W.B. Saunders Company, Philadelphia. London. New York. 2010; 4 th Ed: 104 - 637.
8. Mishra G P., Bhatnagar S., and Singh B., "Anatomical Variations In Arterial Pattern Of Lower Segmental Artery And It Relation With Collecting System". International Journal of Anatomy and Research, 2014; 2: 403-05.
9. Al-Asadi F S., "Some morphological studies on the kidney of the sheep with technique to its arterial segmentation". Basrah. J. Vet. Res. 2006;5.1:44-46.
10. Sisson S B., "A text book of veterinary anatomy". W.B. Saunders Company, Philadelphia. London. New York. 1911; 469-483.
11. Getty R., "The anatomy of domestic animal" W.B. Sanders, Co. 1975; 5th ed.1.
12. Khan H., Rind M M., Ahmad R., Ahmad N., and Shah G., "Gross Anatomical Study on Normal Kidneys of Adult Goat". Journal of animal and veterinary advances. 2003; 2(9): 539-541.
13. Al- Kinanny A F., "Anatomical , Histological and Radiological study of the kidney and the ureter of Buffalo "Bubalus bubalis" in Iraq". A Thesis University of Baghdad 2006.
14. Beatriz P S., Sampaio A P., Henry R W., Favorito L A., and Francisco J B., "Dog Kidney: Anatomical Relationships Between Intrarenal Arteries and Kidney Collecting System" 2007;6:1017–1022.
15. Ozdemir D., Zekeriya O., and Ismail M., "Intrarenal Segmentation of the Renal Arteries in the Kangal Dog" Kafkas -niv Vet Fak Derg. 2009; 15: 41- 44.

16. Chandragirish S., Nanjaiah C M., Suhas Y S., Saheb S H., "Study On Accessory Renal Artery". Int J Anat Res.2014; 2(4):712-15.
17. Gahlot R., Pahuja K., and Gahlot N K., "Study of renal arterial segmentation in mammals by corrosion cast". Asian J. Pharm. Hea. Sci.2014; Vol(4); 1154-1157.
18. Farag F M., "The Intrarenal Venous Architecture of the Pig Kidney (Sus scrofa)". J. Vet. Anat. 2013; 6: 31 – 45.

**Table 1: Biometrical observation in right and left kidney in adult ram. Mean and stander error**

| The parameter | Right kidney | Left kidney |
|---|---|---|
| Weight | 58.003 ± 2.741 | 58.237 ± 0.070 |
| Thickness | 3.075 ± 0.047 | 3.1 ± 0.143 |
| Wide | 4.075 ± 0.110 | 3.825 ± 0.375 |
| Length of kidney | 6.5 ± 0.204 | 6.575 ± 0.507 |
| Length of medial boarder | 9.225 ± 0.488 | 8.825 ±0.273 |
| Length of lateral border | 11.675 ± 0.296 | 10.8 ± 0.263 |

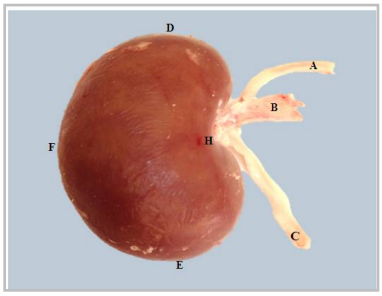


**Fig. ( 1 ) External Appearance of the Kidney in Ram Show: A- Renal artery. B- Renal vein. C- Ureter. D- Cranial pole. E- Caudal pole. F- Lateral border. H- Hilum in the medial border.**

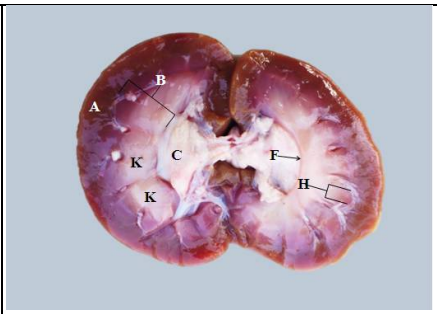


**Fig.( 2 ) Internal Appearance of the Kidney in Ram Longitudinal Section Show: A- Cortex, B- Medulla,C- Renal pelvis, F- Renal crest,H- Arcuate artery, K- Renal pyramid.**

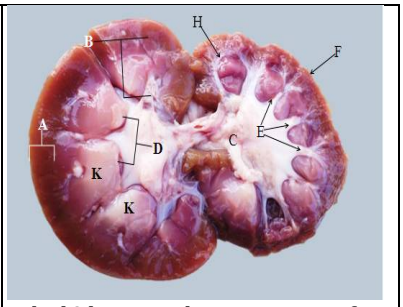


**Fig.( 3 ) Internal Appearance of the Kidney in Ram Longitudinal Section Show: A- Cortex. B- Medulla. C- Renal pelvis. D- Renal papillae. E- Minor calyxes. F- Capsule. H- Arcuate artery. K- Renal pyramid**

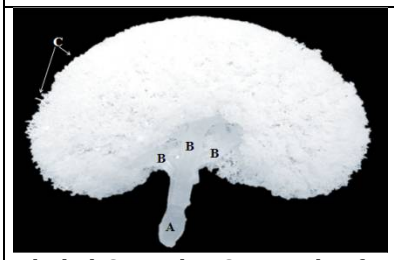


**Fig.( 4 ) Corrosion Cast Resin of Arterial supply of the Kidney in Ram Show: A- Renal artery. B- Segmental artery. C- Cortical artery**

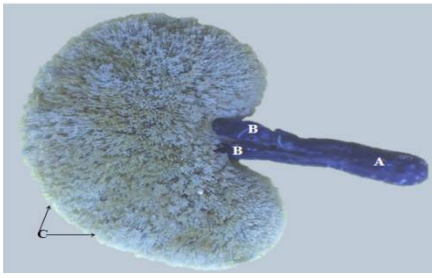


**Fig.( 5 ) Corrosion Cast Resin of Venous supply of the Kidney in Ram Show: A- Renal vein. B- Segmental vein. C- Cortical vein.**

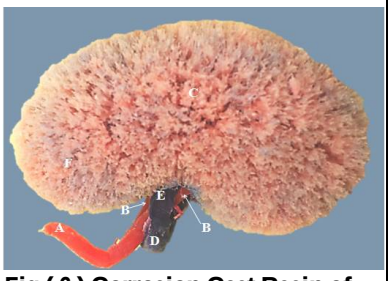


**Fig.( 6 ) Corrosion Cast Resin of Arterial and venous supply of the Kidney in Ram Show: A- Renal artery. B- Segmental artery. C- Cortical artery D- Renal vein. E- Segmental vein. F- Cortical vein.**

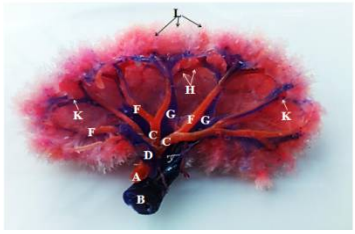

**Fig.( 7 ) Corrosion Cast Resin of the Blood supply of Kidney in Ram Longitudinal Section Show: A- Renal artery, B- Renal vein, C- Segmental artery, D- segmental vein. F- Interlobular artery, G- Interlobular vein. H- Arcuate artery. K- Arcuate vein, L- Cortical artery and vein.**

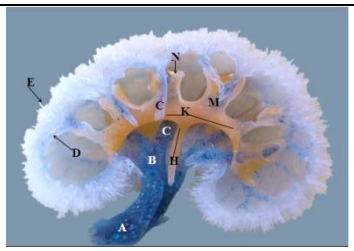

**Fig.( 8 ) Corrosion Cast Resin of Renal vein and Ureter of the Kidney in Ram Longitudinal Section Show: A- Renal vein. B- Segmental vein. C- Interlobular vein, D- Arcuate vein. E- Cortical vein, H- Ureter, K- Renal pelvis. M- Major calyces, N- Minor calyces.**

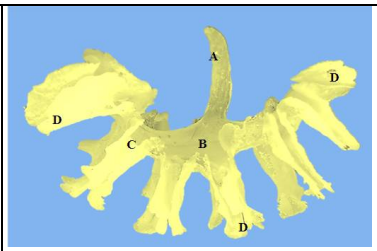

**Fig.( 9 ) Corrosion Cast Resin of Ureter and Renal pelvis of the Kidney in Ram Show: A- Ureter, B- Renal pelvis. C- Major calyces. D- Minor calyces.**

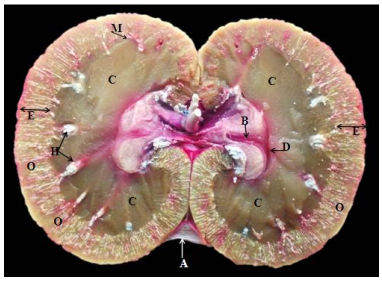

**Fig.(10 ) Longitudinal Section of the Kidney in Ram used Latex with Carmine Stain Show:A- Capsule. B- Ureter. C- Medulla. D- Renal crest. E- Cortex.H- Interlobular artery. O- Cortical artery and vein. M- Arcuate artery.**

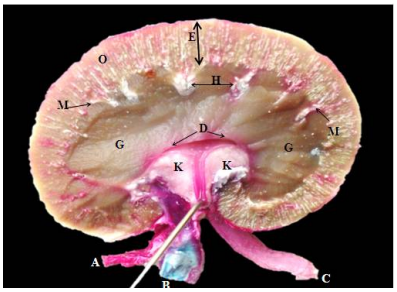

**Fig.(11 ) Longitudinal Section of the Kidney in Ram used Latex with Carmine Stain Show: A- Renal artery. B-Renal vein. C- Ureter, D-Renal crest, E- Cortex. G- Medulla. H- Interlobular artery. K- Adipose tissue, O- Cortical artery and vein. M- Arcuate artery.**

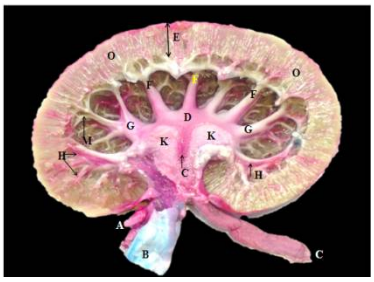

**Fig.(12 ) Longitudinal Section of the Kidney in Ram used Latex with Carmine Stain Show: A- Renal artery. B-Renal vein. C- Ureter. D-Renal pelvis. E- Cortex. F- Minor calix.G- Major calix. H- Interlobular artery. K- Adipose tissue. O- Cortical artery and vein. M- Arcuate vein.**

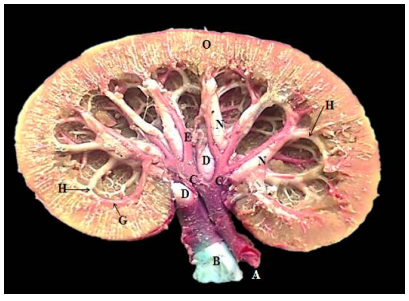

**Fig.(13 ) Longitudinal Section of the Kidney in Ram used Latex with Carmine Stain Show: A- Renal artery, B-Renal vein. C- Segmental artery, D- Segmental vein,E- Interlobular artery,N-Interlobular vein. G- Arcuate artery.H- Arcuate vein,O- Cortical artery and vein.**

*Indian Journal of Natural Sciences* www.tnsroindia.org.in ©IJONS

*Vol. 9 / Issue 50 /October 2018* *International Bimonthly* *ISSN: 0976 – 0997*

RESEARCH ARTICLE

# The Prevalence and Synergistic Effect of Heat Treatments and Hydrogen Peroxide against of *Staphylococcus aureus* Isolated From Imported and Locally Produced Cream in Baghdad.

Haider Flaiyih Hassan* and Zina Saab Khudhir

Department Public Health, College of Veterinary Medicine, University of Baghdad, Iraq

Received: 20 June 2018 Revised: 25 July 2018 Accepted: 28 Aug 2018

***Address for Correspondence**
**Haider Flaiyih Hassan**
Department Public Health,
College of Veterinary Medicine,
University of Baghdad, Iraq



## ABSTRACT

The current study evaluated the sensitivity of *Staph. aureus* isolates in the broth for heat treatment (48 and 50°C for 30 and 60 minutes respectively ) and to different concentrations of hydrogen peroxide (0.01% , 0.02% and 0.04% for 30 and 60 minutes respectively) which isolated from imported and locally produced cream in Baghdad .Results indicated that the high prevalence levels of contamination with *Staph .aureus* that were found in both Buffalos raw milk and the locally produced cream which is pointed out the potential the public health hazards. Complete elimination of viable *Staph .aureus* was not achieved when the cultured nutrient broth was subjected to 50°C for 60°C minutes. There were 6.57±0.02 and 6.14±0.04 log cfu/ml survivors after 30 and 60 minutes of incubation in the nutrient broth that supplemented with 0.01% $H_2O_2$ respectively whereas , there were 6.33±0.06 and 5.65±0.18 log cfu/ml survivors after 30 and 60 minutes of incubation in the nutrient broth that supplemented with 0.02% respectively , while the starting initial count in the control (before heating) 7.07±0.02 log cfu/ml was reduced to 4.54±0.03 log cfu/ml after 30 minutes of heating and 4.19±0.04 log cfu/ml after 60 minutes of exposure to the heat processing. In conclusion, *Staphylococcus aureus* cultures were $H_2O_2$ tolerant and exhibit viable cell until the end of 60 minutes of incubation at 37°C in the nutrient broth that supplemented with 0.04% $H_2O_2$ and the supplementation of the nutrient broth with 0.04% $H_2O_2$ and heating at 50°C for 60 minutes acted synergistically in the reduction of *Staph .aureus* counts.

**Key words:** Hydrogen peroxide, *Staphylococcus aureus*, Baghdad

## INTRODUCTION

Cream is considered as one of the food products that can be contaminated either from the dairy animal that suffering from mastitis or from the carrier human and is considered a good medium for the growth and multiplication of the pathogenic and non- pathogenic microorganisms (1). Cream is one of the best dairy products that enriched with necessary elements for building human body (2). The locally produced cream is called Gaimar it is a very popular locally dairy produced in Iraq. Gaimar is usually made from the rich fatty raw milk of buffaloes, which are prevalent in the marshes of Southern Iraq. In addition, Gaimar is also made in other Iraqi regions like the middle of Euphrates region, the western and the north regions of Iraqi villages. Since all the locally produced cream are sold directly to the consumers, it is a very important to observe the health conditions during the different stages of production and exposure to various sources of pollution starting from its handling, storage and supply to the consumption hydrogen peroxide was used as effective and affordable way by farmers in tropical developing countries to extend the keeping quality of raw milk during transportation to the market or to processing plants (3). Many attempts put to improvement the safety of dairy products as cream during food preservation and processing system by different sub-lethal and stressor conditions such as control pH values, storage temperature and oxidative stress by different concentrations of $H_2O_2$ (4).The main objectives of this study are isolation and identification of *Staphylococcus aureus* bacteria from the imported and locally produced cream samples by the conventional and rapid methods and studying the synergetic effect of hydrogen peroxide as antimicrobial agent against *Staphylococcus aureus* bacteria at concentrations of (0.01%, 0.02% and 0.04%) for 30 and 60 minutes and heating stress at 48 and 50$^{O}$C for 30 and 60 minutes respectively

## MATERIALS AND METHODS

A total of 150 samples including Buffaloes' raw milk, locally produced cream and imported cream (50 samples for each) were collected randomly at weekly intervals from different retail markets and local vendors in Baghdad province. All examined samples were collected in sterilized bottles and poly ethaline bags and transported to the veterinary public health laboratory, Department Public Health, College of Veterinary Medicine, University of Baghdad in the ice box and the bacteriological analysis was done immediately upon samples arrival. The study began from 1/12/2017-1/6/2018. Isolation and enumeration the *Staph .aureus* bacteria from different samples and stress conditions by heat treatments and different concentrations of hydrogen peroxide. Evaluation the sensitivity of *Staph. aureus* isolates by heat treatment at (48 and 50$^{O}$C for 30 and 60 minutes respectively and different concentrations of hydrogen peroxide treatment at (0.01% ,0.02% and 0.04% for 30 and 60 minutes respectively),which were determined by the standard plating technique. *Staphylococcus aureus* isolates were obtained by plating on the Mannitol agar, Baird Parker agar supplemented with 5% egg yolk tellurite emulsion and selective chromogenic agar that were further tested by conventional and rapid biochemical identifications tests such as Gram stain test,Catalase test, Coagulase activity and DNase test. Rapid biochemical tests such as detection of the *Staph. aureus* coagulation by Dry spot staphytect -plus test and Electronic ™ Staph. plus system (ERIC Rapid system) with standard colors chart . Further serological test as Masta ™ Staph agglutination kit was used as a rapid Latex test for the identification of *Staphylococcus aureus* bacteria (5)

### Statistical analysis

Statistical analysis of data was performed using SAS (Statistical Analysis System - version 9.1). One-way, Two way ANOVA and Least significant differences (LSD) post hoc test were performed to assess the significant differences among means. Also unpaired t test was used to compare the means of two groups. $P < 0.05$ was considered tatistically significant.

## RESULTS AND DISCUSSION

The conventional techniques for isolation of *Staph .aureus* bacteria is regarded as the golden standard methods but it takes many days to complete the isolation and identity of the survivor pathogenic microorganisms ,selective plating , biochemical characterizes and serological confirmation by the commercial latex agglutination tests were involved for the identification of *Staph. aureus* bacteria in both raw milk and cream (6). The typical colonies of *Staph. aureus* bacteria were appeared on the selective differential chromagar-Staph. as mauve in color with the ability to grow on the mannitol salt agar (MSA) and fermented the mannitol sugar and produced the golden yellow colonies that surrounded by yellow zone around the colonies ( 7). All the isolates that grown on the (5% v/v) of sheep blood agar at 37$^{O}$C for 24 hrs gave β - hemolysis pattern . Further conventional and rapid biochemical and serological tests for identifications were done including the gram's reaction, coagulase test, catalase test , Dryspot *Staph. aureus* test and Latex Mast Staph . The positive results for all positive *Staph. aureus* isolates were indicated by the agglutination of the Latex . The number of colonies in each bacterial dilution was multiplied by the reciprocal of the dilution factor and calculated as the colony forming units (cfu/ml) per milliliter of raw milk or gm of imported and locally produced cream (Table 1). All of the *Staphylococcus aureus* isolates in this study were positive to the different commercial selective media as chrom-agar and Baird Parker agar supplemented with 5% egg yolk tellurite emulsion and mannitol salt agar. The current results were in agreement with Arshad., (8) who reported that out of (33) staphylococcal bacteria isolates from bovine milk samples (32) isolates were *Staphylococcus aureus* which were able to produce positive results as ferment the mannitol sugar . *Staphylococcus aureus* produced the coagulase enzyme which clot the plasma into gel, due the conversion of the fibrinogen to fibrin that leading to clotting of the plasma. The coagulase activity test is very important differentiating test between the coagulase positive *Staphylococcus aureus* and the other cogulase – negative staphylococci (9). The catalase test was performed for all the *Staphylococcus aureus* isolates and all of bacterial isolates produced catalase enzyme and this test was used for the differentiation of *Staphylococcus aureus* from the different *staphylococci* species where the positive reaction appeared bubbles gas as a result of converting the hydrogen peroxide to water and oxygen.

The higher significant (P≤0.05) prevalence levels of contamination were found in both the raw milk and locally produced cream where 47 (94%) isolates out of 50 locally produced cream samples were identified as *Staph. aureus* while the lowest significant (P≤0.05) prevalence level of contamination was found in the imported cream were only 1 (2%) isolate out of 50 imported cream samples was found positive for the presence of *Staph .aureus* bacteria as shown in Tables 2 and Table 3 .Such high prevalence levels of contamination with *Staph. aureus* bacteria in both raw milk and locally produced cream pointed out the potential public health hazard. Dehkordi *et al*. (10) reported that milking process, procedure of cream manufacturing, handling, the contamination during the storage in the retail stores and improperly cleaned utensils were the major factors that influence in the prevalence rates of *Staphylococcus aureus* between different kinds of cream products. Also the genetic difference of dairy animal species may be a another reason for the differences in the occurrence of *Staphylococcus aureus* in the farms dairying systems (11). Petersson Wolfe *et al*.,(12) recorded that the higher prevalence rate of occurrence of *Staphylococcus aureus* may be occurred in the traditionally dairy products which associated with the milking animals as (Buffalos and cows) because *Staphylococcus aureus* was the major causative agent of subclinical mastitis in the dairy Buffalos and cows.

Both the milk production and the cream manufacturing process that may introduce such organism to the such products and present the potential public health hazard. The imported cream production conditions under good hygienic measurements inside the dairy plants .The microbial populations (counts) were proved to be efficient as an indicator of good or poor sanitation techniques in the milk production and the manufacturing process .The average mean log values (log cfu/ml or gm) of total *Staph. aureus* counts in the Buffalos raw milk and both the imported and locally produced cream samples (50 samples for each products) are shown in Table 4.The current data revealed that there were significant (P≤0.05) differences in the average mean log values of the viable *Staph. aureus* counts between each of the raw milk and cream samples ,the average mean log value of the viable *Staph. aureus* counts in the Buffalos

raw milk samples was 7.68±0.02 log cfu/ml and in the locally produced cream samples was 7.19±0.05 log cfu/gm. Such high *Staph. aureus* counts that were found in all of the above mentioned dairy products reflected the high contamination level that could be attributed to the neglected hygienic techniques and very poor sanitary practices during were reflected on the lowest significant ($P \leq 0.05$) *Staph. aureus* counts where the average mean log value of viable *Staph. aureus* count in the 50 imported cream samples was 3.27±0.04 log cfu/gm. Many reports illustrated that the *S. aureus* food poisoning is attributed to ingestion of contaminated food specially raw milk and other dairy products in which the enterotoxigenic strains of staphylococcus can grow and multiple to reaching about the $10^5$ CFC/g of food.(13) *Means with a different small letter in the same column significantly different (P<0.05) between raw milk and different cream samples The viability of the of *Staph. aureus* when incubated in the nutrient broth supplemented with 0.01%or 0.02% or 0.04% of hydrogen peroxide over the two time periods of incubation at 37°C for 30 and 60 minutes are shown in Table 5. The count of survivor cells of *Staph. aureus* was monitored immediately before supplementation of nutrient broth with hydrogen peroxide to sever as a control (without the addition of $H_2O_2$ to it).The microbial cells of the stressed *Staph. aureus* by each $H_2O_2$ concentration were enumerated for the total survivor cells after 30 and 60 minutes of incubation at 37°C.

Supplementation of nutrient broth with different concentrations of Hydrogen peroxide significant ($P \leq 0.05$) influenced the inactivation degree of the *Staph. aureus* where there were significant ($P \leq 0.05$) decrease in the viable counts of stressed *Staph. aureus* that subjected to the different concentrations (0.01%or 0.02% or 0.04% ) of hydrogen peroxide after incubation time of 30 and 60 minutes. Culture of *Staph.aureus* was tolerant and exhibited viable cells until the end of the 60 minutes broth that supplemented with 0.04% of hydrogen peroxides (exhibited survivor cells).The time exposure to each concentration of $H_2O_2$ at 37°C of incubation had a significant ($P \leq 0.05$) influence on the viability loss of stressed *Staph. aureus* by the $H_2O_2$ from 30 to 60 minutes. There were 6.57±0.02 and 6.14±0.04 log cfu/ml survivors after 30 and 60 minutes of incubation in the nutrient broth that supplemented with 0.01% $H_2O_2$ respectively whereas there were 6.33±0.06 and 5.65±0.18 log cfu/ml survivors after 30 and 60 minutes of incubation in the nutrient broth that supplemented with 0.02% respectively .The viability of the stressed *Staph. aureus* that subjected to 0.04% $H_2O_2$ was not lost after 60minutes of incubation at 37°C ,where similarly with the nutrient broth that supplemented with 0.04% $H_2O_2$ there were 5.62±0.02 and 5.50±0.06 log cfu/ml survivors after 30 and 60 minutes of incubation at 37°C respectively .The result established the statistically significant ($P \leq 0.05$) influence of $H_2O_2$ on the of the *Staph. aureus*. Increasing the $H_2O_2$ concentration up to 0.04% $H_2O_2$ in nutrient broth resulted in a further significant ($P \leq 0.05$) increase of the antimicrobial effectiveness of $H_2O_2$ against *Staph. aureus* where the starting initial count of *Staph. aureus* in the control of about 7.07±0.02 log cfu/ml was reduced to5.50±0.06 log cfu/ml after 60 minutes of incubation at 37°C(resulted in a decrease of survivor count of about 1.5 log cfu/ml.

The conclusion was an increase of $H_2O_2$ concentration resulted in a decrease of viable count of *Staph. aureus* after 60 minutes of incubation at 37°C. * Different small letters in the same column significant (P<0.05) differences between the exposure times. *Horizontal different capital letters revealed significant (P<0.05) differences between the different concentrations of $H_2O_2$. The mean log values of *Staph. aureus* that were enumerated in the cultured nutrient broth immediately before and after heating to each of 48 and 50°C for two exposure time points of 30 and 60 minutes are shown in Table 6.Heating of the cultured nutrient broth that inoculated with *Staph .aureus* at different temperatures and processing times had significantly ($P \leq 0.05$) influenced the inactivation degree of the *Staph .aureus* in the broth. Heating of the nutrient broth that cultured with *Staph .aureus* at 48°C for 30 and 60 minutes produced a significant ($P \leq 0.05$) partial reduction of *Staph .aureus* counts where the starting initial count in the control (before heating) of 7.07±0.02 log cfu/ml was reduced to 4.54±0.03 log cfu/ml after 30 minutes of heating and 4.19±0.04 log cfu/ml after 60 minutes of exposure to the heat processing whereas increasing the heating temperature to 50°C for 30 and 60 minutes of exposure resulted in a further increase in the inactivation degree of *Staph .aureus* and produced additional significant ($P \leq 0.05$) reduction of *Staph .aureus* counts in the cultured nutrient broth to 3.44±0.02 log cfu/ml and to 3.10±0.02 log cfu/ml after 30 and 60 minutes of exposure to the heating temperature respectively. Complete inactivation or elimination of viable *Staph .aureus* was not achieved when the cultured nutrient broth was subjected to the 50°C for 60 minutes *Means with a different small letter in the same column significantly different (P<0.05)

between the exposure times. *Means with a different capital letter in the same row significantly different (P<0.05) between the different heat treatments. In the food production , preservation and storage the heating process ,osmotic and acid stress the most frequently stressors conditions used ,due the *S. aureus* bacteria is a highly adaptable organism to the surrounding environmental circumstances that which lead to affect in the bacterial cell's morphology and physiology, therefore in the modern dairy production techniques the multiple-hurdle such as hydrogen peroxide and heat methods are use in the current study which applied to inhibited the bacterial growth and multiplication, such these methods can increase the food safety, and extend the shelf life of different kinds of dairy products (14). The viability of *Staph .aureus* in the nutrient broth that supplemented with 0.04% of $H_2O_2$ and heated at 50$^O$C for 60 minutes is shown in Table 7. The count of survivor cells of *Staph .aureus* was monitored immediately before the supplementation with $H_2O_2$ or heating at 50$^O$C to serve as a control. The microbial cells of *Staph .aureus* that stressed by 0.04% $H_2O_2$ were enumerated before and after the heating process at 50$^O$C for 60 minutes.

Supplementation of the nutrient broth with 0.04% $H_2O_2$ significantly (P<0.05) influenced the inactivation degree of the *Staph .aureus* where there was a significant (P<0.05) decrease in the viable count of *Staph .aureus* that stressed by 0.04% $H_2O_2$ .The viability of *Staph .aureus* that subjected to the stressed of 0.04% $H_2O_2$ was not lost after 60 minutes of incubation at 37$^O$C,where there was 5.50±0.06 log cfu/ml survivors at the end of incubation period . More over heating of the stressed *Staph .aureus* by 0.04% $H_2O_2$ at 50$^o$C for 60 minutes produced additional significant (P<0.05) reduction of the Staph .aureus count to 3.67±0.01log cfu/ml, both the supplementation of nutrient broth with 0.04% $H_2O_2$ and heating temperature at50$^o$C at synergistically in the reduction of *Staph .aureus* count in the cultured nutrient broth. *Means with a different small letter in the same row significantly different (P<0.05) between the $H_2O_2$ concentration 0.04% alone and that associated with heat treatment at 50$^O$C. These results agree with another reports who recorded that Hydrogen peroxide, in combination with another substance as thiocyanate ion, can used to control *Staph. aureus* and *Listeria monocytogenes* in milk at different storage temperature(15).And agree with study who recorded that ozonation treatment and refrigeration storage acted as synergistic for inhibition of *Staph. aureus* in raw milk (16).

## REFERENCES

1. Senan.,S.; Malik., R. K. and Vij.,S.(2016). Food and Industrial Microbiology. available at htpp://Agrimmon.com
2. Gasmalla.,M.A.A.;Tessema.,H.A.;Salaheldin.,A.;Alahmad.,K.;Hassanin.,H.A.M. and Aboshora.,W.(2017). Health Benefits of Milk and Functional Dairy Products. MOJ Food Processing and Technology. 4(4): 00099/
3. Oogai., Y.; Kawada.,M. M.; Komatsuzawa., H.(2016). *Staphylococcus aureus* SrrAB A_ects Susceptibility to Hydrogen Peroxide and Co Existence with Streptococcus sanguinis. PLoS ONE 11(7): e 0159768.
4. Medveďová., A ;Studeničová.,A.; Valík., Ľ. and Horvathova., Z. (2014). Prevalence and growth dynamics of enterotoxinogenic *Staphylococcus aureus* isolates in Slovakian dairy products. Czech J. Food Sci., 32: 337–341.
5. Bharathy.,S.; Gunaseelan.,L.; Porteen.,K.. and Bojiraj.,M.(2015). Prevalence of *Staphylococcus .aureus* in raw milk: can it be a potential public health threat?. International Journal of Advanced Research , 3 ( 2): 801-806.
6. Najim.,H.N.; Abd.,A.H.A. and Khudhir.,Z.S.(2012). Laboratory manual for milk testing. pp 11-66.
7. Hasan., Z.A.(2016). Isolation and identification of *Staphylococcus .aureus* and methicillin resistant *Staphylococcus .aureus* (MRSA) from tonsils by chromagar media. J.Bio. Innov 5(4), pp: 570-573
8. Arshad., M.; Muhammad., G.; Siddique., M.; Ashraf., M. and Khan., H. (2006). Staphylococcal mastitis in bovine and some properties of Staphylococcal isolates. Pakistan Veterinary Journal. 26(1),20
9. FDA, (2002). Bacteriological Analytical Manual. 9th Edn., AOAC International, Arlington, VA., USA. Finegold, S.M. and W.J. Martin, 1982. Bailley and Scott Daignostic Microbiology 6th Ed., C.V. Mosby Co.st. Louis, Toronto, London.
10. Dehkordi.,A.A.;Tajbakhsh.,E.;Tajbakhsh.,F.;Khamesipour.,F.; Shahraki.,M.M.and Momeni., H.(2015). Molecular Typing of *Staphylococcus aureus* Strains from Iranian Raw Milk and Dairy Products by Coagulase Gene Polymorphisms. Advanced Studies in Biology, 4, 169-177 HIKARI Ltd.

11. Katsande., S; Matope., G; Ndengu., M and Pfukenyi DM. (2013).Prevalence of mastitis in dairy cows from smallholder farms in Zimbabwe. Onderstepoort Journal of Veterinary Research.; 80(1):1-7.
12. Petersson-Wolfe, C. S., Mullarky, I. K. and Jones G. M.( 2010). *Staphylococcus. aureus* mastitis: Cause, detection, and control. Virginia Cooperative Extension: 1–7. Accessed Jul. 18, 2017. https:// www.pubs.ext .vt .edu/ 404/ 404 -229/ 404 -229 .html
13. Salandra, G., Goffredo, E. et al. (2008): Occurrence, characterization and antimicrobial resistance pattern of Staphylococcus species isolated from dairy products in southern Italy. Int. J. Food Microbiol., 9: 327360.
14. Leistner, L. and Grahame, W.G. ( 2005). Update on hurdle technology approaches to food preservation. In P. M. Davidson, J. N. Sofos, and A. L. Branen, eds. In Antimicrobials in Food. Boca Raton, FL: CRC Press, pp. 621–631.
15. Gaya, P., M. Medina and M. Nunez, 1991. Effect of the Lactoperoxidase system on *Listeria .monocytogenes* behavior in raw milk at refrigeration temperatures. Applied Environ. Microbiol., 57: 3355-3360.
16. -Zina,S,K and Mahmood., M,R.(2017). The efficacy of ozone treatment on the microbiological quality of raw milk at different storage temperatures Journal of Entomology and Zoology Studies; 5(5): 930-934.

**Table.1 The cultural, biochemical and serological characterizations of *Staphylococcus aureus* isolates that isolated from imported cream and both raw milk and locally produced cream.**

| Microorganism | Medium | Cultural characteristics | Positive results | | |
|---|---|---|---|---|---|
| | | | Conventional biochemical characteristics | Serological properties (Rapid test) | |
| | | | | Dryspot *staph. aureus* | Latex mast staph |
| *Staph. aureus* | Chromogic-agar | Shining Mauve colonies | Gram positive | Agglutination | Agglutination |
| | Mannitol salt agar | Golden Yellow colonies | Catalase positive (oxygen bubbles) | | |
| | Baird-Parker agar with egg yolk emulsion | shining black colonies | D-ANase production | | |
| | Blood agar | β-hemolysis | Coagulase positive (agglutination) | | |

**Table. 2 The prevalence rate of *Staph .aureus* in the locally produced cream and raw milk samples that collected from Baghdad city**

| Sources of samples | Number of examined samples | Number of positive Samples | Isolation percentage% |
|---|---|---|---|
| Cream | 50 | 43 | 86 |
| Raw milk | 50 | 47 | 94 |
| Total | 100 | 90 | 90 |
| Chi square value | 1.77 | | |
| P | 0.18 | | |

**Table . 3 The prevalence rate of *Staph. aureus* in the cream and raw milk samples**

| Source of samples | Number of examined samples | Number of positive Samples | Isolation percentage% |
|---|---|---|---|
| Raw milk | 50 | 47 | 94 |
| Locally produced cream | 50 | 43 | 86 |
| Imported cream | 50 | 1 | 2 |
| Total | 150 | 91 | 60.66 |
| Chi square value | 108.84 | | |
| P | <0.0001 | | |

**Table .4 *Staphylococcus aureus* bacterial counts log cfu /ml or g of the examined raw milk and both imported and locally produced cream samples.**

| Sources of samples | Number of samples | Total bacterial counts |
|---|---|---|
| | | Mean±SE $Log_{10}$ cfu /ml or g |
| Raw milk | 50 | 7.68±0.02 a |
| Local produced cream | 50 | 7.19±0.05 b |
| Imported cream | 50 | 3.27±0.04 c |
| LSD | | 0.1252 |

**Table 5 Sensitivity of *Staph. aureus* to different concentrations of $H_2O_2$ at different exposure times**

| Exposure times (Minutes) | ($log_{10}$ cfu/ml ) Mean±SE | | | |
|---|---|---|---|---|
| | Control | Different concentrations H2O2% | | |
| | 0 | 0.01 | 0.02 | 0.04 |
| 30 | 7.07±0.02 Aa | 6.57±0.02 Ba | 6.33±0.06 Ca | 5.62±0.02 Db |
| 60 | 7.07±0.01 Aa | 6.14±0.04 Bb | 5.65±0.18 Cc | 5.50±0.06 Cc |
| LSD | 0.2316 | | | |

**Table 6 Sensitivity of *Staph .aureus* for heat treatment for 48 and 50°C at different exposure times**

| Exposure times (minutes) | (log10 cfu /ml) Mean±SE | | |
|---|---|---|---|
| | Different heat temperatures | | |
| | (37°C) (Control) | 48°C | 50°C |
| 30 | 7.07±0.02 Aa | 4.54±0.03 Ba | 3.44±0.02 Ca |
| 60 | 7.07±0.01a Aa | 4.19±0.04 Bb | 3.10±0.02 Cb |
| LSD | 0.0912 | | |

**Table 7 Synergistic effects of $H_2O_2$ at concentration 0.04% and heat treatment at 50°C for 60 minutes on the viability of *Staph .aureus***

| Exposure time (minutes) | ($log_{10}$ cfu/ml ) Mean±SE | | |
|---|---|---|---|
| | (Control) | $H_2O_2$ concentration 0.04% | $H_2O_2$ concentration 0.04% associated with heat treatment at 50°C |
| 60 | 7.07±0.01 a | 5.50±0.06 b | 3.67±0.01 c |

*Indian Journal of Natural Sciences* www.tnsroindia.org.in ©IJONS

*Vol. 9 / Issue 50 /October 2018* *International Bimonthly* *ISSN: 0976 – 0997*

RESEARCH ARTICLE

# Investigation of Medical Diagnosticx-Ray Shielding by Polymer Composite

BushraM.Mahmood[1*], Hayder S.Hussain[2] and NabaaA.Najiph D[1]

[1]Medical Physicist College of Medicine, Al-Mustansirya University, Iraq
[2]Department of Physics, College of Scinece University of Baghdad, Iraq

Received: 19 June 2018 Revised: 23 July 2018 Accepted: 28 Aug 2018

[*]**Address for Correspondence**
**BushraM.Mahmood**
Medical Physicist College of Medicine,
Al-Mustansirya University, Iraq
Email : boshramajid00@gmail.com, dr.hyder_hussain@yahoo.com, Nabaanaji2012@gmail.com



## ABSTRACT

This study deals with the shielding properties of polymer compositeagainst diagnostic x- rays emitted frommedical x-ray tube with voltage range(80-135) kV Polymer composites(PU/EP /lead),with lead ratio (40, 50,60 and 70)%wt.for differentsizes of lead particles had been prepared. The shielding propertiesof the prepared samples have been determined using the narrow beam transmission method of x-ray tube voltage by Geiger-Mullerdetector (GM) which used to measure the x-ray transmittedthrough polymer compositesThe average attenuation for the lead composite varies from 90.25% to 99.17%, acceptance testing of compositeused as shielding applicationagainst diagnostic x-rays. Additionally theresults show a directly relationship, between the thickness of the shielding material and the attenuation percentage. The result, also show that, a reversal relationship, between the attenuation percentage and the energy of the x-ray photon. The results showthat, the samples prepared of good absorption for diagnostic x-ray So, The displayed results indicated that the constructed materials show good radiation protection properties.

**Keywords:** Polymer Composite, diagnosticx-ray, Geiger-Muller, transmission

## INTRODUCTION

Ionizing radiation can cause harm to both the humans and the environment.The most important source of ionizing radiation is that used inmedicine for diagnostic and therapeutic purpose However, there are three principles for protection against the hazards of radiation to keep the radiation dose received by hospital personnel under normal working conditions. These are time, distance, and shielding , As Low As Reasonably Achievable ALARA [1] Staying as less time as possible around the radiation sources and staying as far as possible away from the radiation sources can cause less radiation exposure.Shielding is the best technique for a radiation worker to protect themselves from the hazardous effects of radiation. Shielding material reduces the exposure dose by interacting the radiation itself

with material and reducing the intensity of the radiation [2]Radiation shields are commonly used in hospitals, clinics and dental offices to protect medical patients and workers from unintentional direct and secondary radiation exposure during diagnostic imaging. Shields take many forms: Lead aprons, CT Breast Shields, CTeye shield, ThyroidCollar, vial shields, fixed and portable leadbarriers.[3]. The choice of shielding materials and the design of the shield depends" on the type and the energy of the radiation itself.X-rayare the most penetrating of ionizing radiation following gamma-rays that are known to be harmful to human health"[4]. Therefore, highdensity materials are used toprotect life from such hazardous radiation, aslead bricks orhighdensity concretewhich is often used. In addition, other metallic shieldsinclude copper, bismuth, tungsten, steel, etc. However lead is superior over allthese shieldingmaterialsbecause of its higher atomic number, density, and low cost [5]. But however, lead is toxic and leadaprons are so heavy for personal shielding [6]**.**

Nowadays, researchers are generally studying various polymers and highdensity metals for radiation protection.Observations ofinconsistencies in shielding performance with recommendations to improve standardized methods for acceptance testing.Several researchers have been studied for developing new shielding materials for ionizing electromagnetic radiation.in (2009, Harish, et all). Used unsaturated polyester resin as matrix material and used lead (II) oxide as filler. They found linear attenuation coefficient of the composite with 50% filler amount as 0.206 $cm^{-1}$. Thus they reported that their composite's attenuation performance was better than cement, copper and silver [7]. In the same yearPlions.A.A,etall had been studied on polymer-bismuth bricks that could be used as an alternative to lead bricks and they reported their attenuation performances nearly same as lead bricks for radiation energies below 400 keV[8].In (2012Dong Yu, et al) hadbeen studied effects of WO3 particle size in WO3/Epoxy resin radiation shielding material[9].In (2013, NoorAzman., et al) had been studied" characterization of micro-sized and Nano-sized tungsten oxide-epoxy for radiation shielding of diagnostic X-ray"[4].

In the same yearDhameer A. Mutlak and Ahmed .H. Ali had been studied the properties of gamma shielding by using epoxy /lead powder and lead shut composite and found linear absorptioncaffeine[10]. In (2014),E. ErenBelgin et alhad been studied A Novel Metal Oxide Filled Polyethylene Based Composite Shielding Material for Protection from Harmful Effects of Ionizing Electromagnetic Radiation [5].In (2016Noor M.A) had been prepared samples of polymers composite of polyurethane with epoxy added deferent ratio of lead( powder ,Nano) used as Bremsstrahlung Radiation shielding [12]. Several more recent studies using clinical beams have examined different aspects of the attenuation properties of some commercial radiation aprons.Likein (2011, Abdullah.H.,etal)had been measured the attenuation percentage for four groups of commercial lead composite aprons [13]. In (2003 Christodoulou et al)had been stayedEvaluation of the transmitted exposure through lead equivalent apron sued in a radiology department, including the contribution from backscatter try to improve standardized methods for acceptance testing [14].in (2016Yücel,H. et al)had been studied, the X-ray attenuation properties of some protective materials made fromelastomers loaded by high-Z elements (such as Sb, Sn, W, Ba, etc.) determined in terms of the attenuation ratio using both narrow and broad-beam geometry conditions[15]

## THEORY AND EVALUATION

When anincidentx-ray photons passing through absorbermaterial some pass without interact with matter and some are absorbed orscattered in a single event through various interaction processes *photoelectric effect*, *Compton Effect*, and *pair formation*. The attenuation of x-ray when they pass through an absorber of thickness (x) can be expressed by the exponential law [16].

$$I = I_o e^{-\mu x} \ldots\ldots\ldots\ldots (1)$$

where ($I_o$) is incident x-ray, (I)isattenuatedof X- ray X is thickness of absorber material And $\mu$is thelinear attenuation coefficientof absorber ($cm^{-1}$). The linear attenuation coefficient depends on photon energy and attenuator atomic

number (*Z*)[17]. High energy radiation is scattered principally by electrons, and so are best shielded by elements with high atomic number (Z) [18]. Thus Lead ( Pb) which an atomic number of (82) is expected to shield better than (polyurethane/epoxy) alone. So, (Lead/ polyurethane/epoxy) composites would be expected to increase the radiation shielding characteristics. Thus, one object of this work was to study the enhancement of the radiation shielding afforded to polyurethane /epoxy /lead composites.

### Percent attenuation calculations

Shielding is mainly achieved by wearing protective lead aprons of 0.25 or 0.5 mm thickness, which have been cited to attenuate over 90% and 99% of the radiation dose, respectively[18]. Percent attenuation (%Att.) Values of the composite materials can calculated by the equation [13]:

$$\mathbf{Attenuation\%} = \left[\mathbf{1} - \left(\frac{\textbf{measurment with shielging}}{\textbf{measurment without shielding}}\right)\right] \mathbf{x\ 100\%} \;..\mathbf{(2)}$$

### Effective atomic numberand density percent for composite

The values of the effective atomic number of the compound's or the mixtures can be calculate from the atomic number value of each element addition to the percentage of its presence in the compound or mixture equation [3]

$$\text{Zeff} = \frac{n1z1^{2} + n2z2^{2} +}{n1z1 + n2z2 +} \ldots\ldots\ldots\ldots\ldots\ldots\ldots\ldots\ldots\ldots\ldots\ldots\ldots\ldots. \quad (3)$$

Where n1, n2 represent the (wt %) in composites and z1, z2 are the atomic numbers of each element in composite . The "theoretical density values ($\rho_{comp}$) were calculated from Eq. (4) with an assumption of the samples being void free" [7].

$$P_{composit} = \frac{\mathbf{100}}{\left[\frac{\mathbf{M}}{\boldsymbol{\rho}\mathbf{m}} + \frac{\mathbf{F}}{\boldsymbol{\rho}\mathbf{f}}\right]} \ldots\ldots\ldots\ldots\ldots\ldots\ldots\ldots\ldots\ldots\ldots\ldots\ldots\ldots\ldots\ldots\ldots\ldots. (4)$$

where , M = wt % of the matrix, F = wt % of the filler, ϱm =density of matrix and ϱf = density of the filler, with unit of gm/cm³.

### Heavinessϱ composite

To verify the heaviness of the polymers composites, lead was assumed as standard and normalized to 100%. With reference tolead, the percentage of the other conventionalshielding materialalong with the composite using the following relation [20]:

$$\mathbf{\%of\ heaviess} = \frac{\textbf{Density of given material}}{\textbf{Density of lead}} \mathbf{x\ 100} \ldots\ldots. \mathbf{(5)}$$

## MATERIALS AND METHODS

The materials used to prepare the composite samples as a shield with different thicknesses of this work are; Epoxy Resin (EP) EUXIT 50 (Swiss Chem.), polyurethane (PU) EUXIT TG10 (Swiss Chem.) Polyurethane (PU) EUXIT101 and Lead Nano, powder and shot/ball.

**Sample Preparation**

**Preparation of EP/PU Blends**

**Epoxy Resin (EP)**

An exact amount of special hardener is added to the resin with weight ratio of hardener to resin (1:3) using a sensitive electronic balance of sensitivity (0.01gm). The content is mixed thoroughly by a fan type stirrer until the mixture becomes homogeneous.

**PolyurethaneTG10**

A sufficient amount of isocyanate hardener is Also added to resin (polyol) with weight ratio of hardener to resin (1:9). The content is also mixed thoroughly by a fan type stirrer before adding epoxy to the mixture. The epoxy/polyurethaneTG10 blends are prepared with weight ratio of both polymers as (%EP+%PU) multiple blends with differentratio and different thickness were dune Also made another blends but used the polyurethaneTG10 polyol (without hardener) with epoxy(PUTG10polyol+%EP) by the same manner of the previous preparation were prepared the blend. The (resin )/polyurethane PU101 blends are prepare with weight ratio of both polymers as( EP%+ PU101%) made multiple blend with different ration this blends appear flexible . mixture becomes ready after they are stored at room temperature for 72 hours. The best compatibility blends after made the bending test according to ASTM (American Society For Testing and Materials) standard D-790, and tensile test D638[21]was(60%EP+ 40%PUTG10) ,( 80%EP+20%PUTG10 polyol) and (30resin+70%PU101 The mixture was placed in a circular templates it'sdiameter proportional to the diameter detector for the most accurate results as shown in figure (1).

**Preparation of lead /Ep/pucomposites**

By the same manner of the previous preparation of blend, using the best ratio of blends, the lead/EP/PU composites will beprepared as shown in figure (2).

**X-ray Transmissions measurement**

The x-ray transmission through the prepared samples wasstudied using beams generated from a diagnostic x-ray machine(Sedecal, model A-6553001 fixed) inthe range from(40 - 150 kV ) tube voltages. For all beams, the exposure was set at 10 mA .in time 0.1 sec "The distance between the x-raytube and the detector was set at 100 cm,and the x-ray beam was well collimated relativeto the center of the detector for a dimension of about (3x3)cmaccording to the samples size .Arriving to the" detectortype (wallac/ RDA-31) which measurement range was0.05-400mR. $h^{-1}$"[22].Connected bysensor withthedetector A Geiger-Muller (GM) tube produced by IRaqiCenter of Radiation Protection. The primary x-ray beam ($I_o$) and the transmitted x-ray beam (I ) were measured using a detector The exposure produced by the primary x-ray beam was measured inthe absence of sample between the x-ray tube and the detector. Meanwhile, the transmitted x-ray beam (I) was measured with present samples The transmission of protective composite is dependent on the incident energy of the photons and the thickness of the protective material [14].

## RESULTS AND DISCUSSION

The shielding effect of the examined composite was studied in terms of x-ray transmissions with the energies of (80, 100, 120 and 135) kV. The attenuation percentage was obtained by applying equation (5). The thickness of each composite was fixed at (10mm) and the X-ray tube current was set at (10mA) as shown in table( 3) column (3) intables (3,4,5) its apparent density of each samples increased with the increment of filler content, a phenomenon which was also observed by "Harish.et al 2009[7]."who stated that " increase with lead particles loading values, Increasing filler content in composites with a fine dispersion of high density filler should offer more interaction probability of photons and hence better shielding properties"This findings are important for the X-rays which are considered as the most penetrating radiations as compared to other ionizing radiations. Their interaction depends on the probability of their collision with the atoms of the materials during the interaction.

To increase the probability, must be interact the density of the material they are passing through needs to be increased.whichmeans the materials should have a lot of atoms with an assumption that the materials are free from voids as explanation by AzmanNZet al .2013[4]. It was found that the average attenuation or (shielding effect) of the lead composites varies from (93. %) to (99.17 %), where the attenuation percentage of the examined composites decreased with increasing the x-ray tube voltage ,the resultsagreement withChristodoulou, E.G et al 2003 ,. These findings also are in agreement with Azman NZet al., 2012. [23] who published that the "probability for the photoelectric interaction to occur depends on ($Z^3/E^3$) where (Z) is the atomic number of the absorbing material, and E is the photon (X-ray) energy while Compton scattering is dominant in the high energy photons,the probability of Compton scattering is weakly dependentof the atomic number (Z) and X-ray energy (E) The transmissions of the diagnostic x-ray were measured by using the Geiger-Muller detector and are represented in figure (3). There was a clear difference in the transmission percentage of the composites with the change in the tube's voltage, these composites exhibited different levels of attenuation at the same beam quality.

It was found that the (P-Y) composite which was loaded with 70% lead powder showed the most effective shielding for the voltage range (80 to 135) kV, where it exhibited consistent protection over the diagnostic energy range (over 100 kV), where the shielding protection of lead is dominant [13]and very low transmission was achieved with attenuation percent of (99.17%).A higher X-ray transmission was appeared with the (P-B) composite which was loaded by70% lead powder, where the average attenuation percentage was (98.3%), r= 0.9856. This result can be explained by thedispensability of the lead powder through the Blend (B) which has a density effect of (1.0988 $gm/cm^3$ ) while the blend (Y) has a density effect of (1.0144 $gm/cm^3$ ) so that the lead powder particles has been easily concentrated through the blend (Y), this homogeneous concentration helped in increasing the resistance against the X-ray. The average attenuation percentages of the (F-Y), (K-B), and (K-y) were found lower than the average attenuation percentage of the two previously discussed composites (98.55% with r=0.8918, 97.8% with r=0.95712, 93% with r=0.9974) respectively, the (F-Y) composite showed a higher attenuation percentage as compared with the (K-B, and K-Y) composites because of the existence of 40%.

Nano lead particles in its composition, while (k-B and K-Y) Composites containing Lead powder 50% but the density of (K-B) Sample larger than (K-Y)sample. The same transmission measurement test was repeated with the (Z-Y, H-Y, and H-G) composites of the thickness (4mm), at x-ray tube current of (10mA) and the average attenuation percentages were found for each of them as listed in table (4). The results of table 4 showed that the highest average attenuation percentage was appeared with the (H-G) composite which was loaded with a 70% Nano lead particles and it had a density effect of (3.105 $g/cm^3$ ), this composite exhibited an excellent attenuation for the diagnostic x-ray (99.15% and r=0.90453) as shown in figure (4)while the (H-Y) composite showed a less attenuation percentage and higher x-ray transmission (97% with r=0.98523) as compared with the (H-G) composite because it has a lower density effect (2.797 $g/cm^3$). The (Z-Y) composite showed the lowest average attenuation percentage (90.25% with r=0.99245) and the highest transmission of the diagnostic x-ray as compared with the other two previous samples, this

composite contained 50% of Nano lead particles with a density effect of (1.8622 g/cm$^3$). The results of table ( 5) showed the change in the attenuation percentage of the x-ray with this composite where the average attenuation was (80.75%). When increasing the Composite's thickness as in (D-$Y_2$) composite led to a noticeable increase in the attenuation percentage value (95.138%). For this reason, this composite exhibited an excellent shielding effect for the diagnostic x ray. The attenuation x-ray increases with increase thickness of composite this result perfectly applicable with the theoretical concept of the equation (1). The regression lines of figure (5) describes the transmission of the x-ray through the composites with the change of the x-ray tube voltage through (D-Y1 and D-Y2)

### Composites' Heaviness Results

The Lightness of each polymer composite was evaluated in comparison to lead heaviness which is considered as a standard andnormalized to 100% by using the equation (5). It was found that the composite (H-G) had the highest heaviness while the lightest composite was the (F-Y) as shown in table (6 )and figure ( 6 )It was observed that the heaviness percentage of the composite increase with increasing the filler concentration. These results proved that the polymer composites exhibited excellent lightness when they are compared to the conventional radiation shielding material like lead; they showed an appreciable performance particularly at higher filler concentration (preferably 40% and above) for the diagnostic x-ray .The results of the current study is in complete accordance with Harish. V.,et al 2012 [20] and Abbas J. Al-Saadi.2014 [24] who proved that polymer composite exhibits considered lightness when it was compared with the conventional radiation shielding material like lead, and concrete.

## CONCLUSIONS

In the present work a new material had been tested for radiation shielding applications in order to meet needs for lightweight multifunctional shielding materials. The current study included the following conclusions:

1. Composite of thickness 2mm flexible elastic, and easily shapeable. And lightnesscan be used in medical application as shielding likeaprons, gloves as sample D-$Y_2$
2. Samples which flexible and lighting with thickness 4mm can be used as CT-scan Breast Shield, eye shield, Thyroid Collar, as(H-Y) composite
3. Composite sample (H-G) of the thickness (4mm) isrigid.This it can be used as fixed and portable lead barriers,
4. Transmission of diagnostic x-ray increased with increasing tubevoltage, for all samples
5. As the composite sample thickness increases , the attenuation will be increase accordingly.
6. The density of the composite sample increases with increasing the lead ratio and the attenuation of X- ray by polymers composites increased with increasing the samples density. Therefore, polymer composite is preference attenuation than pure polymer blend.

## REFERENCES

1. Munro L, Ostensen H, Ingolfsdottir G, World Health Organization. Basics of radiation protection for everyday use: how to achieve ALARA: working tips and guidelines.2004.
2. Erol A, Pocan I, Yanbay E, Ersoz OA, Lambrecht FY. Radiation shielding of polymer composite materials with wolfram carbide and boron carbide.Radiation Protection and Environment. 2016 Jan 1;39(1):
3. affer HI, Hussain HS. Dependence of gamma-ray absorption coefficient on the size of lead particle.Baghdad Science Journal. 2011;8(27-613:(عدد خاص بمؤتمر الفيزياء.
4. Noor Azman, N.Z.,S.A. Siddiqui.R. Hart.R, Low,I.M,. Microstructural Design of Lead Oxide–Epoxy Composites for RadiationShielding Purposes.Wiley Periodicals Inc. J. Appl. Polym. Sci. 2013: 128: 3213–3219.
5. Belgin, E. E, Aycik, G.A.,A Novel Metal Oxide Filled Polyethylene Based Composite Shielding Material for Protection from Harmful Effects of Ionizing Electromagnetic Radiation. ,2014; 48000, Mugla, Turkey , ISITES.

6. Nambiar S, Yeow JT. Polymer-composite materials for radiation protection. ACS applied materials & interfaces. 2012 Oct 26;4(11):5717-26.
7. Harish V, Nagaiah N, Prabhu. T. B , T.K.Varughese ,.Preparation and characterization of lead monoxide filled unsaturated polyester based polymer composites for gamma radiation shielding application .J application polymer Sci 2009 ; 112,3:1503-1508.
8. Plionis A.A., Garcia S.R., Gonzales E.R., Porterfield D.R., Peterson D.S.. Replacement of lead bricks with non-hazardous polymer-bismuth for low-energy gamma shielding. J Radio analytical and Nuclear Chem., 2009; 282: 239–242.
9. Dong,Yu, ChangShu-Quan, Zhang Hong-Xu ,Ren Chao , Kang Bin , Dai Ming-Zhu , Dai Yao-Dong , "Effects of WO3 particle size in WO3/epoxy resin radiation shielding material", Chin. Phys. Lett.2012 : 29, 10 .
10. Mutlak DA, Ali AH. Study the enhancement of the radiation shielding afforded to epoxy/lead composites. Journal of university of Anbar for Pure science. 2013;7(2).
11. Aowd NM. Investigation of Bremsstrahlung radiation in polymer composites Using beta Radiation. Master thesis ,university of Baghdad, college of science ,department of physics , 2016
12. Shousha HA, Rabie N, Hassan GM. Experimental investigation of commercially available lead composite aprons used for diagnostic X-rays. Radiation Effects and Defects in Solids. 2011 Dec 1;166(12):935-41.
13. Christodoulou, E.G.; Goodsitt, M.M.; Larson, S.C.; Darner, K.L.; Satti, J.S.; Chan, H.P. *Med. Phys*. 2003, *30* (6),1033–1038.
14. Yücel,H, Güllüoğlu, E , Çubukçu S, Üncü1 Y.A,. Measurement of the Attenuation Properties of the Protective Materials Used as a Thyroid Guard and Apron for Personnel Protection against Diagnostic Medical X-rays. , 2016. Journal of Physical Science, 2016; 27(1), 111–128,
15. Martin.E.M,.Physics for Radiation Protection. 3rd Edition, Wiley-VCH Verlag& Co. KGaA, 2013.p 250.
16. Podgorsak EB. Radiation oncology physics. : A handbook for teachers and students Vienna: International Atomic Energy Agency (IAEA) 2005
17. Bushberg JT, Seibert JA, Leidholdt EM, Boone JM. The essential physics of medical imaging.therd edition LIPPINCOTT WILLIAMS & WILKINS, 2012..
18. Al.Dargazeli, S.S."Detection Of Nuclear radiation " Baghdad p 193 ,press,(1989) in Arabic
19. Harish. V,Nagaiah.N,Kummar.H.G.H." Lead oxides filled ioophthalic resin polmer composites for gamma radiation shielding applications"Journal of pure&applied physics, 2012:50.p.p 847-850.
20. Annual Book of ASTM-D790 standard, P405, (1984).AND - Annual book of ASTM-D638 standard vol 08.01 p254
21. koivukosi.J and Paatero.J .. Dose rate mapping and quantity analysis of radioactive deposition with simple monitoring instrument in finland after the chernobly accident. BOREL ENVIRMENT RESERCH ,vol 18 ,article ,Helsink .2013.
84:8.03 p254
22. Azman NZ, Siddiqui SA, Hart R, Low IM ,Ionescu, M., Low, I.M., A comparative study of X-ray shielding capability in ion-implanted acrylic and glass, Radiation Physics and Chemistry, 85 (2012) 102-106
23. Abbas J. Al-Saadi,.Variation of gamma ray attenuation parameters for Poly vinyl alcohol reinforced by lead acetate.ournal of Kerbala University , Vol. 12 No.3 Scientific . 2014

**Table 1. the blend codes**

| Sample choice | Blend code |
|---|---|
| 20% polyurethane ( PU)TG10 without hardener +80% epoxy (EP) | **B** |
| 70% polyurthan(PU)101 +30% resin | **Y** |
| 40 % polyurethane PU TG10+60%EP | **G** |

**Table 2. Composites' samples the blend with the lead ratio**

| Blend code | | | Lead size Pb Lead ratio | |
|---|---|---|---|---|
| Blen B | BlendG | Blend Y | | |
| N-B normal | | N-Y normal | Without pb | 0 |
| P-B | | P-Y | Powder 200µm, 500µm | 70% |
| K-B | | K-Y | Powder 200µm, 500µm | 50% |
| | H-G | H-Y | Nano | 70% |
| | Z-G | Z-Y | Nano | 50% |
| | | F-Y | Nano | 40% |
| | | D-Y | Nano | 60% |

**Table 3. average attenuation percentage of the diagnostic X-ray for different composites with thickness 10mm**

| No | Composites code | $\rho_{eff}$ | Attenuation % | | | | average % |
|---|---|---|---|---|---|---|---|
| | | | 80 kv | 100 kV | 120 kV | 135 kV | |
| 1 | K-Y | 1.862 | 96 | 94 | 92 | 90 | 93 |
| 2 | K-B | 2.0034 | 98.5 | 98 | 97.8 | 97 | 97.825 |
| 3 | F-Y | 1.5955 | 99.2 | 99. | 98 | 98 | 98.55 |
| 4 | P-B | 2.987 | 99.6 | 99. | 98.5 | 98.3 | 98.94 |
| 5 | P-Y | 2.797 | 99.5 | 99.2 | 99 | 99.17 | 99.17 |

**Table 4. Average attenuation percentages of the diagnostic X-ray for (Z-Y, H-Y, and H-G) composites with thickness 4mm**

| No | Sample code | $\rho_{eff}$ | Attenuation percentage% | | | | Average KV% |
|---|---|---|---|---|---|---|---|
| | | | 80kV | 100kV | 120kV | 135kV | |
| 1 | Z-Y | 1.8622 | 94 | 92 | 90 | 85 | 90.25 |
| 2 | H-Y | 2. 797 | 98.5 | 98 | 95 | 94.5 | 97 |
| 3 | H-G | 3.105 | 99.5 | 99.5 | 98.8 | 98.8 | 99.15 |

**Table 5. Attenuation percentage for the X-ray of (D-$Y_1$ and D-$Y_2$) composites**

| no | Sample code | $\rho_{eff}$ | Samples thickness | Attenuation percentage % | | | | Average kV |
|---|---|---|---|---|---|---|---|---|
| | | | | 80 kv | 100kv | 120 kv | 135kv | |
| 1 | D-$Y_1$ | 2.2359 | 1mm | 86 | 85 | 77 | 76 | 80.75 |
| 2 | D-$Y_2$ | 2.2359 | 2 mm | 97.272 | 97.05 | 94.23 | 92 | 95.138 |

**Table 6.samples heaviness as compared to lead normalized to 100%**

| Sample code | H-G | P-B | P-Y | H-Y | D-Y | K-B | Z-Y | K-Y | F-Y |
|---|---|---|---|---|---|---|---|---|---|
| heaviness | 27.38 | 26.34 | 24.664 | 24.662 | 19.717 | 17.666 | 16.421 | 16.221 | 14.069 |

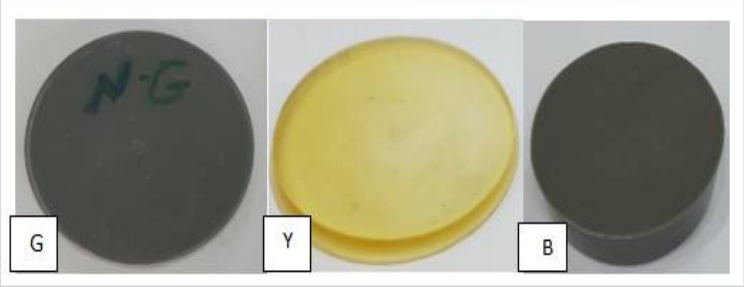


**Figure 1. Polymer blend samples.**

**Figure 2. Types of polymer composite**

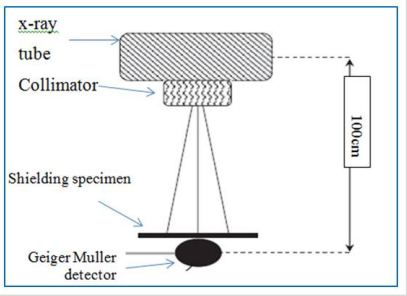


**Figure3. A diagram clarifying direct X-rays radiation dose measurement without and with a radiation specimen.**

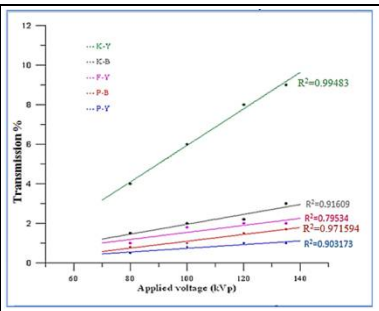


**Figure 4. The transmission of the diagnostic X-ray versus the X-ray tube voltage of (K-Y, K-B, F-Y, P-B, and P-Y) composites**

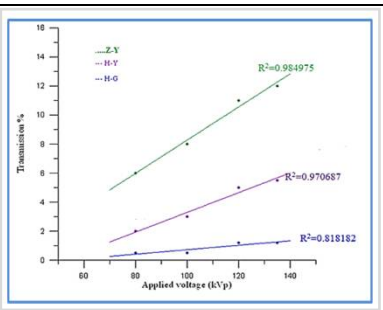


**Figure 5. The transmission of the diagnostic x-ray versus the x-ray tube voltage of (Z-Y, H-Y, and H-G) composites**

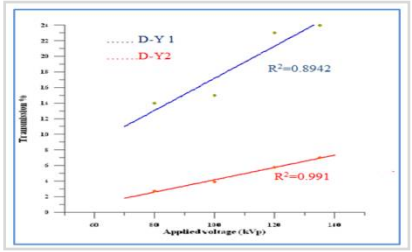


**Figure 6. The transmission of the diagnostic X-ray versus the X-ray tube voltage of (D-Y1 and D-Y2) composites**

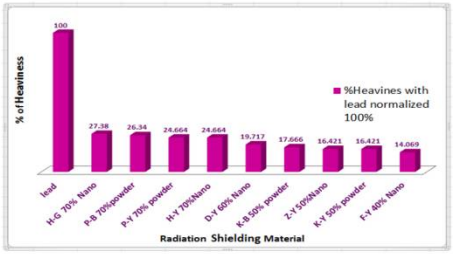


**Figure .7 diagram percentage of heaviness**

*Indian Journal of Natural Sciences* www.tnsroindia.org.in ©IJONS

*Vol. 9 / Issue 50 /October 2018* *International Bimonthly* *ISSN: 0976 – 0997*

RESEARCH ARTICLE

# The Effect of *Thymus vulgaris* on some Physiological and Antioxidant Parameters in Male Rabbits

Alia Hussein* and Noor Mahdi

Department of Biology, College of Science for Women, University of Baghdad, Iraq

Received: 23 June 2018 Revised: 25 July 2018 Accepted: 28 Aug 2018

***Address for Correspondence**
**Alia Hussein**
Department of Biology,
College of Science for Women,
University of Baghdad, Iraq
Email: no2000896@gmail.com



## ABSTRACT

The aim of this study is to explain the effect of 60mg/kg B.W. of thymus vulgaris on some physiological parameters in male rabbits .Twelve adult male rabbits were used in this study and were divided equally into two groups : first group was control (C) and received normal saline orally for four weeks , the second group (treated group)was intubated orally with *Thymus vulgaris*(T.v.) in dose 60mg/kg B.W. for four weeks .Blood samples were collected by heart puncture.from each animal at the end of experiment blood collected in gel activated tube without anticoagulant , anticoagulant serum was separated from coagulant blood by centrifugation . The results of this study showed that there were significant ($P<0.05$) increase in serum glutathione(GSH), significant decrease ($P<0.05$) in Malondialdehyde(MDA),significant decrease ($P<0.05$) in vitamin C(vit C), the value of vitamin E(vit E) concentration was non- significant increase ($P>0.05$) in animal received thymus vulgaris as compared with control group.The value of serum urea was reducedsignificantly in animals that received (T.v.)., non-significantincrease ($P>0.05$) in serum creatinine concentration , blood sugar concentration was reduced significantly ($P<0.05$) as compare with the control group. This study explain that there were non significant increase ($P<0.05$) in serum total protein , albumin ,globulin concentration , significant increase ($P<0.05$) inAspartate aminotransferase ( AST), there was non- significant increase($P>0.05$) in alanine aminotransferase (ALT) , while concentration of alkaline phosphatase (ALP) reduced significantly ($P<0.05$) in animal received (T.v.) as compared with control group .

**Keywords :** Thymus vulgaris , antioxidant factors , Kidney function , Liver enzyme

## INTRODUCTION

The medicinal variety is known as common Thyme or garden Thyme, the same variety that is most often used for seasoning. Medicinal preparations of common Thyme are made from the leaves and the flowers (Margar,2011). Thyme essential oil also has medicinal applications. Thyme is combined with other herbs to treat ailments that range from bronchitis and sore throat to gastritis and skin disorders. Drinking Thyme tea on a regular basis even helps with arthritis. In the Middle ages Thyme was used as a food preservative and an incense (Tribal,2002). Thyme is herbaceous plant of the platoon species, grows in mountainous areas, used as a beverage instead of or with tea, added to some food to give it an acceptable flavour, the plant is used in folk medicine frequently where it is prescribed to treat mouth infections, stomach, intestine and airways, coughing and gastroenteritis and expel intestinal worms, as well as to strengthen the heart (MohamedandOmar, 2013. The thyme *(Thyme vulgaris L.*) belong to the lamiacea family and aromatic native herbs in the Mediterranean region thymus vulgaris essential oil (TEO) is amixture of monoterpenean . The main compounds of this oil are the natural terpenoidthymol and its phenol isomer carvacrol (CVL) (Amiri,2012), (Nickavar*et al*,2005). Which have antioxidant (Hoferl*et al*, 2009)6 ,antimicrobial (Youdim*et al,*1999) ,antitussive(Barnes,*et al*,2007) , expectorant (Dorman*et al*,, 2000), antispasmodic effects(Monographs ,2009)..Terpenoids flavonoid aglycones , flavonoids glycosides and phenolic acids were also found in thymus spp. (Vila*et al*,2002) .Thyme (thyme Vulgaris L.) is an aromatic plant of the Mediterranean flora commonly used as spices and for medicinal purposes , thyme is traditionally used for its antiseptic (Brasseur,1983) , antispasmodic(Essawiand Srour,2000) and antitussive effects .Further more , thyme possesses antimicrobial , antifungal(Miura,*et al*2002), antioxidative and antiviral properties(Solimam and Badeaa,2002). The essential oil derived from thyme (thyme Vulgaris L.) is amixture of monoterpenes and one of the main compounds of this oil is a natural terpenoidthymol (Hudaib*et al*,2002) .Thymol exhibits multiple biological activities including antinflammatory (Braga*et al,*2006) immunomodulating (Suzuki and Funuta,1988) antioxidant(Aeschbach*et al*, 1994), antibacterial (Didry*et al*,1994)(Venturini*et al*,2002)antifungal (Mahmoud,1994) and free radical scavenging properties (Fujisaw and Kadoma,1992). The herb is also a rich source of many important vitamins such as B-complex, folic acid, beta carotene, vitamin A, K, E and C

## MATERIALS AND METHODS

Thymus vulgaris preparation dry thyme leaves powder was prepared after grinding and mixed with distilled water .And the dose wasprepared by using 60mg/kg B.W.(Wilson,2002) for treated group and dosed for four weeks.

### Experimental Design

This study was carried out at the animal house of Biology Department at the College of Sciences for Women /University of Baghdad .Twelve adult malerabbits weighting 1000-1250g were used in this study .The animals were housed for two weeks for acclimation, they were housed in cages within a room with controlled temperature and humidity, and they were kept under good hygienic conditions. The animals were maintained on anatual 12h light and 12h dark cycle, received a balanced diet, water adlibitum throughout the experiment period.

### Control Group

Received standard diet and distilled water orally daily for four weeks. 2- Treated Group: received orally Thymus vulgaris atadose of 60mg/kg B.W. for four weeks. At the end of experimental period, blood samples were collected from overnight fasted animals by cardiac puncture without anticoagulant in gel activated tubes and serum separated coagulant blood by centrifugation at 5000rpm for 10 minutes and stored at (-20C°)for studying the following parameters, glutathione, malondialdehyde, Vitamin C, Vitamine E. Concentration Glutathione according to diamond

enzyme kit (Beutleretal, 1963), malondialdihyde according to ( Ohkawaet al ,1979), vitamin C according to (Lin, 1982), vitamin E according to (Bieriet al,1979). Concentration serum urea, creatinine, blood sugar according to diamond enzyme kit (Palton and Crouch, 1977),(Henry, 1974). Total protein was estimated by (Doumas, 1971). Serum albumin concentration wasestimated according to kit (Young, 1995). The concentration of serum globulin was estimated indirectly by measuring of albumin in serum and then it was subtracted from theresult of serum globulin concentration (total serum protein – serumalbumin concentration = serum globulin). Determination of serum AST and serum ALTperformed by using enzymatic kit (Reitman and Frankel, 1975),ALP was measured according to (Belfield and Goldberg ,1971). The crude data were analyzed by using statistical analysis system (SAS) and the significance was considered at P<0.05(SAS,2012)

## RESULTS AND DISCUSSION

Table (1) Expained that acomparison in antioxidant and oxidative stress between treated group and control group There was significant increase that was (7.76+_0.49) mmol/L in treated group as compared with control group (5.10+_0.22) mmol/L. Malondialdehyde concentration (MDA) that was indicator for oxidative stress (Lipid peroxidation) decrease significantly (P<0.05)in treated group (0.93+_0.06)mmol/L as compared with control group (1.26+_0.08)mmol/L. There was significant decrease (P<0.05) in VitC concentration that was (0.19+_0.08)mg/dl in treated group as compared with control group (0.34+_0.05)mg/dl. While there was non - significant change in Vit E concentration in treated group as compared with control.

The results obtained in table (1) revealed that, administration of thyme to normal rabbits exhibited a significant increase in glutathione (GSH) as compared with controled group. Glutathione (GSH) is a non-enzymatic biological antioxidant and one of the most abundant naturally occurring tripeptides. GSH is capable to remove free radicals such as H2O2, superoxide radicals and alkoxy radicals produced during oxidative stress, maintenance of membrane protein thiols detoxification of foreign chemicals and biotransformation of drugs (Alin*et al*,2010). These results may be attributed to the antioxidant activity of thyme. This suggestion was supported by the finding of (Archana*et al*, 2009) who mentioned that, TOH could optimally antagonized radiation-induced toxicity, which may be due to its free radical scavenging potential, by normalizing the intracellular antioxidant levels, also by its anti-lipid peroxidative potential. This results of the increase (GSH) agreement with (Hussein*et al*,2013) This observation increase thoughts that the thyme have an effective protective mechanism in response to ROS and may be associated with decreased the oxidative stress and free radical mediated tissue injury due to its ability to scavenges the free radical and this is one of the majorantioxidant mechanism to hinder the chain reaction of lipid peroxidation (Seung*et al*,2005) agreement with(Swayeh,2014) However, administration of thyme to intoxicated rabbits exhibited a significant decrease in malondialdehyde (MDA) as compared with controlled group. The recorded results may be related to the antioxidant properties of phenolic compounds found in the thyme (Baranauskiene*et al*,2003).

It is well documented that he leaves and flowers of plant containing numerous aromatic chemicals. Phenolic phytochemicals are thought to promote optimal health partly via their antioxidant and free radical scavenging effect there by protecting cellular component against free radical induced damage (Dapkevicius,*et al*2002) agreement with (Archana*et al*, 2009).Decrease in (MDA) that thyme may protect the liver by preventing the increase of MDA because it scavenges the free radicals and this scavenging is one of the major antioxidant mechanisms to inhibit the chain reaction of lipid peroxidation agreement with (Abu-Raghifl*et al*,2016). Vitamin C is one of the naturally occurring antioxidant in nature (Traikovich,1991),(Sies and Wihelm,1995). Vitamin C is the major water – soluble antioxidant within the body (Wang*et al*,2007). However, administration of thyme to rabbits exhibited a significant decrease in Vitamin C. this is because vitamin C is generally unstable when it has inclement storage in terms of light, temperature, humidity and diseases. Perhaps, the other reason is the high rate of vitamin C in thyme essential oil treatments due to greater impact of the oil to control decay.(Burton and Ingold,1986). Vitamin E functions as a chain-breaking antioxidant that prevents the propagation of free radical reactions (Burtonand Ingold,1986),There was

non-significant inchanges vitamin (vit.E).Table (2)Explained that there was significant decrease(P<0.05) in urea concentrationthat was (53.66+_2.45mg/dL) in treated group as compared with control group that(79.33+_3.62mg/dL). Creatinine (Cr.) concentration (P>0.05) in treated group as compared with control group . Blood sugar there was significant decrease in blood sugar (P<0.05)in treated group that was (80.33+_2.5)mg/dL as compared with control that was (105.33+_4.95mg/dL).

While there was none-significant in the value of creatinine in treated group compared with control. While there was decreased blood sugar concentration of effect thyme showed significant reduction in glucose as compared with group control. These results were in agreement with (Al-Amin*et al*,2006), (Goyal and Kadnur,2006)and (Iranloye*et al*,2011). (Iranloye*et al*,2011) concluded that thyme has hypoglycemic effect, enhances insulin synthesis and this may be due the reduction in blood glucose by thyme oil to the action of carvacrole or thymol which is an insulin mimetic and possibly the ability of the plants oil to alter the inhibitory activity of alloxan on glucokinase which is the glucose sensor of the β cells (Parivash*et al*,2011). While there was decrease urea concentration by the reduction of blood urea, in animals that thyme may contains some effective compound that influence removing certain waste products from plasma that interfered with a mechanism of reabsorption urea in the nephrons(Jagetia*et al*,2003). The thyme could prevent the depletion of antioxidant concentration and antioxidant enzymes Activity in the kidneys by instructive the effect of urine flow rate on the renal Eliminating of a substance such as creatinine and urea the (Frondoza*et al*,2004). The presence of polyphenols and flavonoids in the thyme might be responsible for the antioxidant nephroprotective activities and the reduction of serum urea, creatinine (Afshari*et al*,2007). This result explained that this plant has protective effect on kidney function

Table (3) revealed that there was non –significant change (P>0.05) in serum total protein , Albumin , Globulin , Alanine aminotransferase( ALT), and Alkalin phosphates (ALP) while there was significant increase inserum Aspartate aminotransferase( AST ) that was (29+_0.36 mg/dL)in treated group as compared with control (12+_0.13mg/dL).

## REFERENCES

1. Margar, E. 2011.Recognition for plant heritage thyme collection. Brickell Award for National Plant Collection Holder. Plant Heritage.3ed
2. Tribal,H.V. 2002. Hoopa quality control plan. Hoopa valley tribalenvironmental protection agency .14th : 38.
3. Mohamed, A. ; Omar , A .A .2013.Study to find thyme oil dose thatKin 50% of mice and minimal dose that kill all mice and maximum nonlethal Dose . Nature and science. 11 :(12) . (52-53).
4. Amiri, H. 2012. "Essential oils composition and antioxidant properties of three Thymus species," Evidence-Based Complementary and Alternative Medicine. Academic Editor VassyaBankova ; 495.
5. Nickavar , B.; Mojab, F.; and Dolat-Abadi, R.2005."Analysis of the essential oils of two Thymus species from Iran," Food Chemistry;90(4): 609–611.
6. Höferl, M.; Buchbauer, G.; Jirovetz ,L.; Schmidt, E.; Stoyanova , A.; Denkova, Z.; Slavchev, A. and Geissler, M.2009."Correlation of antimicrobial activities of various essential oils and their main aromatic volatile constituents," Journal of Essential Oil Research; 21 (5): 459–463.
7. Youdim, K. A.; Damien Dorman, H. J and Deans, S. G. 1999. "The antioxidant effectiveness of thyme oil, α-tocopherol and ascorbylpalmitate on evening primrose oil oxidation," Journal of Essential Oil Research;11 (5) 643–648.
8. Barnes, J.; Anderson, L. A. and Philipson, J. D. 2007. Herbal Medicines, Pharmaceutical Press, 3rd ed;296.
9. Dorman, H. J. D. and Deans, S. G. 2000. "Antimicrobial agents from plants: antibacterial activity of plant volatile oils," Journal of Applied Microbiology,88(2) 308–316.
10. Monographs ,E. (2009) .The scientific foundation for herbal medicinal products. Wiley Inter science.2ed .24(3).
11. Vila, R.; Stahl-Bisk up, E. and Saez, F.2002."Flavonoids and furtherpolyphenols in the genus Thymus," in Thyme: The Genus ThymusMedicinal and Aromatic Plants—Industrial Profiles ,Taylor& Francis ,New york ,USA: 75.

12. Brasseur, T. 1983."Etudes botaniques, phytochimiques et pharmacologiquesconsacrées au thym". Journal de Pharmacies de Belgique.;38(5):261–272.
13. Essawi, T. and Srour, M. 2000.Screening of some Palestinian medicinal plants for antibacterial activity. Journal of Ethnopharmacology.;70(3):343–349
14. Miura, K.; Kikuzaki, H. and Nakatani, N. 2002. Antioxidant activity of chemical components from sage (Salvia officinalis L.) and thyme (Thymus vulgaris L.) measured by the oil stability index method. Journal of Agricultural and Food Chemistry.;50(7):1845–1851.
15. Soliman, KM. and Badeaa, R.I. 2002. Effect of oil extracted from some medicinal plants on different mycotoxigenic fungi. Food and Chemical Toxicology.;40(11):1669–1675
16. Hudaib, M.; Speroni, E.; Di Pietra, A.M. and Cavrini, V. 2002.GC/MS evaluation of thyme (Thymus vulgaris L.) oil composition and variations during the vegetative cycle. Journal of Pharmaceutical and Biomedical Analysis.;29(4):691–700.
17. Braga, P.C.; Dal Sasso, M.; Culici, M.; Bianchi, T.; Bordoni, L. and Marabini , L. 2006. Anti-inflammatory activity of thymol: inhibitory effect on the release of human neutrophil elastase. Pharmacology; 77(3):130–136.
18. Suzuki, Y. and Furuta, H. 1988. Stimulation of guinea pig neutrophil superoxide anion-producing system with thymol. Inflammation.;12(6):575–58.
19. Aeschbach, R.; Löliger, J.; Scott, B.C.; Murcia, A.; Butler, J.; Halliwell, B. and Aruoma, O.L.1994. Antioxidant actions of thymol,carvacrol, 6-gingerol, zingerone and hydroxytyrosol. Food and Chemical Toxicology. 32(1):31–36.
20. Didry, N.; Dubreuil, L. and Pinkas, M. 1994. Activity of thymolcarvacrol, cinnamaldehyde and eugenol on oral bacteria.Pharmaceutical Act.Helvetiae . 69(1):25–28.
21. Venturini , ME.; Blanco, D. and Oria, R.2002. In vitro antifungal activity of several antimicrobial compounds against Penicilliumexpansum. Journal of Food Protection. 65(5):834–839.
22. Mahmoud, A. 1994.Antifungal action and anti a flatoxigenic properties of some essential oil constituents.Letters in Applied Microbiology. 19(2):110–113.
23. Fujisawa, S. and Kadoma, Y. 1992.Effect of phenolic compounds on the polymerization of methyl methacrylate.Dental Materials. 8(5):324–326
24. Wilson J.X.2002. The physiological role of dehydroascorbic acid. FEB Lett.527:5–9.
25. Beutler, E.; Duron, O. and Kelly, B.M. 1963. Improved method for the determination of blood glutathione. J. Lab. Clin. Med. 61: 882-888.
26. Ohkawa, H.; Ohishi, N. and Yagi, K. 1979. Assay for lipid peroxides in animal tissues by thiobarbituric acid reaction. Anal.Biochem. 95(2): 351-358.
27. Lin, p. 1982. Determination of vitamin C by spectrophotometric method.Clin.Chem 28: 2225-2228.
28. Bieri, G.; Tolliver, J.T. and Catignani, G.L. 1979. Simultaneous dtermination of alpha tocopherol and retinol in plasma or red cells by high pressure liquid chromatography. Am. J. Clin. Nutr. 32: 2143-2149.
29. Palton,C.J.andCrouch,S.R.1977.Enzymatic determination of serum urea by modified Berthelot reaction. Anal. Chem.;49:464-469.
30. Henry,R.J. 1974.Principle and techniques ,Clinical chemistry ,2nd ed. Harper and Row .:525.
31. Doumas, B.T.1971. Standards for total serum protein assays .A collaborative study. Clin. Chem., 21(8):1159-1166
32. Young,D.S. 1995.Effect of drugs on clinical laboratory tests 4th ed. AACC,press.
33. Reitman,S.,andFrankel,S.1975. Acolourimetric method for the determination of serum glutamic oxaloacetic and glutamic pyruvic transaminases .Am.J.Clin.Path.,28:56.
34. Belfield ,A.and Goldberg, D.M.1971. Revised assay for seum phenyl phosphatase activity using 4- amino-antipyrine. Enzyme.,12:561-573.
35. SAS.2012.Statistical Analysis System,Uses Guide Statistical.Version 9.1 th end. SAS.Inst. Inc. Cary.N.C.USA.
36. Alin, K.V.K.; Satish, R.; Rama, T. Anil, K.; Babul, D. and Samhitha J. 2010.Hepatoprotective effect of FlemingiaStrobilifera R.Br. onParacetamol induced hepatotoxicity in rats. Int J Pharm Res. 2: 1924-1931.

37. Archana, P. R.; Rao, B. N.; Ballal, M.; Rao, B. S.S. 2009. Thymol, a naturally occurring monocyclic dietary phenolic compound protects Chinese hamster lung fibroblasts from radiation-induced cytotoxicity. Mutation Research 680: 70–77.
38. Hussein, S.A.; Omayma, A. R.; AbdElmaksoud, H.; Afaf ,D. A.M. and Alshaimaa, M. S.2013.antioxidant effect of thyme on pirimiphos methyl induced toxicity in rats . Benha veterinary medical journal .24(1): 184-195.
39. Seung, L.; Katumi, U.; Takayki, S. and Kwang-Geum L.2005. Identification of volatile components in basil and thyme leaves and their antioxidants properties, Food.Chem., 91(1).131-137.
40. Swayeh, N.H.; Abu-Raghif, A.R.; Qasim,B.J. and Sahib H.B.2014. The Protective Effects of Thymus vulgaris Aqueous Extract against Methotrexate-Induced Hepatic Toxicity in Rabbits. Int. J. Pharm. Sci. Rev. Res. 29(2): 187-193.
41. Baranauskiene, R.; Venskutonis, P.R.; Viskelis, P. and Dambrauskiene, E. 2003. Influence of nitrogen fertilizers on the yieldand composition of thyme (Thymus vulgaris) J. Agric. Food Chem. 51: 7751–7758.
42. Dapkevicius, A.; van Beek, T.A.; Lelyveld, G.P.; van Veldhuizen, A.; de Groot, A.; Linssen, J.P.H., and Venskutonis, R. 2002. Isolation and structure elucidation of radical scavengers from Thymus vulgaris leaves. J. Nat. Prod. 65: 892–896
43. Archana, P.R.: Rao,B.N.; Ballal, M. ; Rao, B.S.S.(2009). Thymol, anaturally occurring monocyclic dietary phenolic compound protects Chinese hamster lung fibroblasts from radiation – induced cytotoxicity .Mutation Research 680:70-77.
44. Abu-Raghif1,A.R.; Sahib, A.S. and Hasan,S.A. 2016. Hepatoprotective effects of thyme extract in Cisplatin-induced liver toxicity in rabbits.Der Pharmacia Lettre.8 (18):22-26.
45. Traikovich S.S. 1999.Use of Topical Ascorbic acid and its effects on Photo damaged skin topography. Arch Otorhinol Head Neck Surg.125:1091 -8.
46. Sies, H. and Wilhelm,S. 1995. Vitamins E, C, Beta – Carotene and other carotenoides as antioxidants. Am.J.Clin.Nut., 62:315S- 321S.
47. Wang,C.Y.;Wang ,S.Y.;Yin,J.J.Parry,J.;and Yu,L.L.2007.Enhancing antioxidant ,antiproliferation, and free radical scavenging activities in straw with berries with essential oils .J.Agric.Food Chem. 55:6527-6532
48. Burton, G. W. and Ingold, K. U. 1986. Vitamin E: application of the principles of physical organic chemistry to the exploration of its structure and function. Acc. Chem. Res. 19, 194–201.
49. AL-Amin,Z.M.;Thomson,M.;Al-Qattan,K.K.;Peltonen-Shalaby R, Ali M.2006.Anti-diabetic andhypolipidaemic properties of ginger in streptozotocin induced diabetic rats ,Br.J.Nutr;96(4):660-666
50. Goyal,R.K.andKadnur,S.V.2006.Beneficial effects of Zingiberofficinale on gold thioglucose induced obesity Fitoterapia ;77:160-163
51. Iranloye,B.O.;Arikawe,A.P.;Rotimi,G.andSogbade ,A.O. 2011.Anti-diabetic and anti-oxidant effects of zingiberofficinale on alloxan induced and insulin-resistant diabetic male rats Niger,J.Physiol.Sci.,23,26(1):89-96.
52. Parivash,R.;Najmeh,K.;Sedigheh,A.and.Mahbubeh,S. 2011.Anti-daibetic effects of walnut oil on alloxan-induced diabetic rats.Afrrican journal of pharmacy and pharmacology .5:2655-2661.
53. Jagetia,G.C.;Baliga,M.S.andUlloor,J.N.2003.Influence of ginger rhizome (*ZinbiberOfficinale*) on survival,glutathione and lipid peroxidation in mice after whole body exposure to gamma radiation Radiat.Res.160:548-592.
54. Frondoza CG, Soharbi A, Phan S, LindmarkL.2004.An in vitro screening assay for inhibitors of proinflammatory mediators in herbal extracts using human synoviocyte cultures.Invitro Cell Dev.Biol.Anim;40:95-101.
55. Afshari AT, Saadatian R, RasmiY, Saboory E, Allameh B.2007.The effect of ginger on diabetic nephropathy plasma antioxidant capacity and lipid peroxidation in rats.Food Chemistry ;101(1):148-153.

**Table 1. The effect of *Thymus vulgaris* in a dose of 60mg/kg B.W. on antioxidants parameters in control and treated male Rabbits**

| The Group | Mean ±SE | | | |
|---|---|---|---|---|
| | GSH(mmol/L) | MDA(mmol/L) | Vit.-C (Mg/dl ) | Vit.E (Mg/dl) |
| Control | 5.10±0.22 | 1.26±0.08 | 0.34±0.05 | 3.33±0.12 |
| Treatment | 7.76±0.49 | 0.93±0.06 | 0.19±0.08 | 2.70±0.08 |
| LSD value | 1.763* | 0.288* | 0.093* | 0.607 NS |
| P<0.05), NS: non- significant.* | | | | |

Values are expressed as mean ±SE n=6 for each group.

**Table 2. The effect of *Thymus vulgaris* in a dose 60 mg/kg B.w .inUrea (Ur), creatinine (Cr.), blood sugar (B. Sugar) parameters in control and treated male rabbits**

| The Group | Mean ±SE | | |
|---|---|---|---|
| | Urea(mg/dl) | Cr. (mg/dl) | B. sugar (mg/dl) |
| Control | 79.33± 3.62 | 0.86 ± 0.07 | 105.33 ± 4.95 |
| Treatment | 53.66± 2.45 | 0.78 ±0.03 | 80.33 ± 2.15 |
| LSD value | 7.912* | 0.193 NS | 17.47* |
| *(p<0.05), NS: Non-Significant. | | | |

Values are expressed as mean ±SE n=6 for each group

**Table 3. The effect of thymus vulgaris in a dose 60 mg/kg B.w .in Total protein, Albumin, Globulin, Aspartate aminotransferase (AST), Alanin aminotransferase (ALT) and Alkaline phosphatase (ALP) in control and treated male rabbits**

| Group | Mean ± SE | | | | | |
|---|---|---|---|---|---|---|
| | Total protein (mg/dl) | albumin (mg/dl) | Globulin (mg/dl) | AST(mg/dl) | ALT (mg/dl) | ALP (mg/dl) |
| Control | 6.96± 0.27 | 4.00 ±0.09 | 2.94 ±0.05 | 12.00 ±0.13 | 24.00±0.33 | 1.6471.00± |
| Treatment | 7.60± 0.44 | 4.50 ±0.08 | 3.16 ±0.11 | 29.00 ± 0.36 | 28.00±0.74 | 64.00±1.53 |
| LSD value | NS 0.893 | 0.926 NS | 0.561 NS | 4.279* | 6.118NS | 9.205* |
| *(p<0.05), NS: Non-Significant. | | | | | | |

*Indian Journal of Natural Sciences* www.tnsroindia.org.in ©IJONS

*Vol. 9 / Issue 50 /October 2018* *International Bimonthly* *ISSN: 0976 – 0997*

**RESEARCH ARTICLE**

# Synthesis and Optical Characterization of CdO Doped ZnO Nanoparticles by Pulsed Laser Deposition Technique

Zeina saleh Mahdi* and Ali H. khidhir

Department of Physics, College of Science, University of Baghdad, Iraq.

Received: 06 July 2018 Revised: 10 Aug 2018 Accepted: 13 Sep 2018

***Address for Correspondence**
Zeina saleh Mahdi
Department of Physics,
College of Science,
University of Baghdad, Iraq.
Email : Zeina-sm-2012@yahoo.com, alzurfialiali@gmail.com



**ABSTRACT**

In this work, cadmium oxide (CdO), zinc oxide (ZnO), and their composites nanofilms were obtained at room temperture with different concentrations of zinc oxide (x= 0.3, 0.5, and 0.7)%wt. on to glass substrates by pulsed-laser deposition (PLD) technique characterized by x-ray diffraction (XRD), atomic force microscopy (AFM), and UV-visible device. The XRD pattern of the films showed polycrystallographic phases with (111), (101), (100), and (200) reffered to orientations and they have hexagonal and cubic nature. Optical properties were studied for the prepared films using an ultravioet-visible and near-infraredspectrophotometers. In addition to the refractive index, extinction coefficient and dielectric constant were determined.

**Keywords:**(CdO)1-X(ZnO)X puled laser deposition growth; Atomic Force Microscopy; X- Ray diffraction; optical properties.

## INTRODUCTION

During the last years, the researchers have focused on one-dimensional semiconductor nanomaterials due to their unique properties, among these materials, cadimiume oxide (CdO) is n-type semiconductor with ranging direct band gap of 2.2-2.7 eV and an indirectband gap of 1.98 eV[1]. CdO has many attractive properties such large energy band gap, high transmission coefficient in visible spectral domain remarkable luminescence characteristics etc[2]. This materials have been widely studied for optoelectronic applications in transparent conducting oxides (TCO)[3], solar cells [4], photovoltaic[5], photodiodes[6], as well as, other types of applications like IR heat mirror[7], gas sensors[8], low emissive wondows, thin-film resistors,...etc.[9-10]. Zinc oxide (ZnO) is a promising material and it has unique desirable properties such as wide band gap of 3.37 eV and large exciton energy around 60meV. ZnO is thermally

more stable in hexagonal wurtzite structure at room temperature than in cubic zinc bland structure[11]. The desirable physical and chemical properties of ZnO has received great attention and make it viable for the design of optical, electrical, and magnetic devicessuch as photo detectors, $NO_2$ gas sensor, ZnO based on$LED_s$ , transistors, sensors, solar cells, optical switches, photo-catalyst,….etc. Also, ZnO can be employed in biomedical applications[12].A variety of techniques have been used employed to prapare CdO nanostructure such as plsed-laser deposition (PLD) technique[13], spray pyrolysis[14], chemical vapour deposition[15], sol-gel method[16], and DC magnetron sputtering[17]. In this work pulsed-laser deposition technique used to prepare CdO doped ZnO nanostructure.The structural and optical properties of the films have been studied[18].

## MATERIALS AND METHODS

Cadmium oxide with a purity 99.99% and zinc oxide with purity 99.99% were mixed at different concentration of ( x= 0.3, 0.5 and 0.7) wt. %. The powder of precursor was mixing together using agate mortar then the mixture was pressed into pellets (1.5 cm) in diameter and (0.2 cm) thick, using hydraulic piston type, under pressure of 6.5 tons . Finally the pellets were sintered in air at (550K) for 2 h. The thickness of (CdO)1-x(ZnO)x thin film was measured using an optical interferometer method employing He-Ne laser 632nm with incident angle 45°. This method depends on the interference of the laser beam reflected from thin film surface and then substrate, the films thickness( t) was determined using the following formula [20]:

t=λ/2. Δx/x … (1)

where x is fringe width, Δx is the distance between two fringes and λ is wavelength of laser He – Ne (632.8nm).

### PLD and Thin Film Preparation

The (CdO)1-x(ZnO)x films were deposited on glass substrates of (2.5×7.5 cm) which are cleaned with dilated water using ultrasonic process for 20 minutes to deposit the films at room temperature by PLD technique using Nd:YAG with $\lambda$( = 1064 nm) at energy 400 mJ, repetition frequency (6Hz) for 200 laser pulse is incident on the target surface making an angle of 45° with it . The distance between the target and the laser was set to (10 cm), and between the target and the substrate was (1.5 cm), under vacuum of ($3\times10^{-3}$ mpar).

### Characterization

The crystal and phase structure of (CdO)1-x(ZnO)x thin films were examined using XRD analysis type (SHIMADZU 6000 X-ray diffract meter system). The surface roughness and topography of deposited thin films was investigated using Atomic Force Microscopy (AFM) micrographs type (Digital Intruments, CSPM-AA3000). The optical properties of the films were investigated by a double –beam UV/VIS Spectrophotometer (Metertech) SP8001in the range (300-1100) nm.

## RESULTS AND DISCUSSION

### X-ray diffraction results (XRD)

XRD studies were carried out in order to get an idea of the nature of the crystal structure of CdO, ZnO and CdO:ZnO films prepared by PLD technology at( x=0.3,0.5 and 0.7)% under Vacuum (P=2.5 x $10^{-2}$ mbar) Through the study of diffraction X-ray, we can understand the crystalline growth of films prepared by PLD on a glass slide at room substrate temperature**.**

Figure (1) shows the x-ray diffraction (XRD) patterns of CdO, ZnO and CdO:ZnO composite films with different ZnO contents at room temperature. The peaks of ZnO (100) (101) planes can be clearly seen for the film with 0.3% ZnO, and the peak intensity of ZnO increases with the increasing of ZnO content of the composite. It is also seen that as the content of ZnO increases the peak of CdO (111) (200) decreases. Table (1) shows the structural parameters like $2\Theta$, FWHM, inter-planar spacing, and Crystalline size of pure CdO, ZnO and CdO:ZnO with different x content (0.3, 0.5 and 0.7)% at RT

## Atomic force microscopy (AFM)

The grain size (grain diameter) and average roughness of CdO, ZnO and (CdO):(ZnO) films prepered at RT with different content of (x=0.3, 0.5 and 0.7)%wt are shown in table (2). Figure(2) depicts the surface morphology of the films analyzed by (AFM) (Scanning probe Microscope type) (AA3000). From the images, it was observed that the surfaces of the films exhibited a certain degree of roughness and the film become rougher when the concentration increases. This result indicates that the growth of larger grains with increasing concentration leads to an increase in the surface roughness. It is observed that the average grain size increases with increasing of concentration and the values of the average grain size variable from (50.7-62.57nm) depending on film concentration as shown in table (2). This may be due to the bigger clusters formed by the coalescence of two or more grains [21]. It is clear from this table, that there are minimu difference between the value of grain size measued by (FAM) and by (XRD) analysis. The former one measure the grain size directly which give the exact value which, the latter measure the grain size through Scherer's equation which needs so me correction.

### The Optical Properties of the Films

Figure (3) shows the transmission spectrum of pure films CdO, ZnO and CdO:ZnO at different concentrations (0.3, 0.5, and 0.7) of zinc oxide films deposited at room temperature. It can be observed that the transmittance pattern of all deposited thin films increases with increasing of ($\lambda$). Also, as shown in Figure (3) and Table (3) that the transmission values of pure CdO and doped ZnO films at x= (0.3, 0.5 and 0.7) wt. % are 51.18%, 43.51%, 31.79 % and 25.85% respectively, in the 350 nm wavelength. The increments in values of transmittance observed for pure film and decrease with increasing of concentration thin films. This decrease in transparency is related to the structural properties of the film characteristics, because it is known that the changes in transmittance depend on the material characteristics of the films [22]

The absorption coefficient ($\alpha$) is very important factor for designing solar Cell. The variation of the absorption coefficient ($\alpha$) with wavelength of the deposited CdO:ZnO films on glass at different concentrations (0.3, 0.5, 0.7) of ZnO at RT is shown in fig (4). It is possible to know the nature of the electronic transitions from the knowledge of the value of the absorption coefficient. If the value of the absorption coefficient is high ($\alpha > 10^4$ $cm^{-1}$), this means that a direct electronic transmission. The absorption coefficient ($\alpha$) was calculated in the fundamental absorption region from the following equation [23]:

$$\alpha = 2.303A/t \quad \text{.... (2)}$$

A is absorbance and t is the thickness of sample. We can see from the figure and table (3) that ($\alpha$) for films increases with increasing of the concentration ZnO. . The absorption coefficient increases rapidly at wavelength less than cut off wavelength. The reason for increase the absorption coefficient with wavelength is to generate donor levels (i.e localized states) within forbidden energy gap and conduction band. The optical energy gap values ($Eg^{opt}$) of pure CdO, ZnO and their composite films, deposited on glass substrate at room temperature have been determined by using Tauc equation as illustrated from equation[24].

$$(\alpha h\nu) = A(h\nu - Eg)^{1/2} \quad \text{....(3)}$$

The Tauc equation is used to find the type of the optical transition by plotting the relations $(\alpha h\upsilon)^{1/2}$,$(\alpha h\upsilon)^{1/3}$,$(\alpha h\upsilon)^{2/3}$,and $(\alpha h\upsilon)^2$ versus photon energy ($h\upsilon$ and selects the optimum linear part. It is found that the relation for r=1/2 yields linear dependence, which describes all films have allowed direct transition. The optical energy gap ($Eg^{opt}$) is then determined by the extrapolation of the portion at $(\alpha h\upsilon)^2=0$ as shown in Fig. (5) For different composite ratio. We can observe that the increasing of ZnO content from leads to increase the optical band gap from 2.34 eV to 2.60 eV at RT. The increasing of $Eg^{opt}$ with increasing of ZnO content maybe due to decrease of particle size. This result is consistent with previous researches [25]. All values of are tabulated in Table (3).

Fig.(6) shows the variation in refractive index with wavelength for pure CdO, ZnO and CdO:ZnO films in the wavelength range of (300-1100)nm for RT and for different concentrations (X=0.3, 0.5 and 0.7) of ZnO. It can be noticed from these figure that the refractive index increases with increasing the concentration of ZnO. The refractive index values were calculated using Eq. (4).

$$n=1+R/1-R+\sqrt{4(1-R)^2-K^2} \qquad \ldots(4)$$

The variation of the refractive index (n) and the extinction coefficient (k) with wavelength for the films as shown in Figs. 6 and 7, respectively. It can be noticed from Figure (6) and Table (3) that the refractive index decreases with the increasing concentration of ZnO (2.599-2.292). The behavior of (k) can be ascribed to high absorption coefficient. And from Figure (7) and Table (3) it can see that the extinction coefficient increases with increasing the concentration of ZnO (0.533-1.077).

### Dielectric Constant Measurements

The variation of the real (□r) and imaginary (□i) parts of the dielectric constant Values versus wavelength in the range (300-1100) nm for CdO, ZnO and CdO:ZnO films with various concentration of ZnO (0.3, 0.5 and 0.7) at RT, with various as shown in the figures (8-9). The behavior of □r is similar to that of the refractive index because of the smaller value of ($k^2$) compared with ($n^2$) according to equation (4), while □i is mainly depends on the k values in equation (5).

$$\varepsilon r = n^2-k^2 \qquad \ldots.(4)$$

$$\varepsilon i = 2nk \qquad \ldots.(5)$$

## CONCLUSION

In this paper the structural, morphological, and optical properties of CdO films which are deposited using the PLD technique were investigated. By structural and optical properties of the films were analyzed by means of XRD, AFM, and UV–Vis-NIR spectrophotometry. The XRD characterization shows a polycrystalline films, with hexagonal and cubic structure and many peaks. The AFM investigations show no cracks in the film and a larger grains with increasing concentration of ZnO leads to an increase in the surface roughness. It is observed that the average grain size increases with increasing of concentration. As well as the refractive index, n, and the extinction coefficient, k, in the 200 to 800 nm wavelength range. The optical properties indicate the increase in band gap energy due to reduction of particle size Compared with the bulk material.

## ACKNOWLEDGEMENTS

We thank University of Baghdad, College of Science, Department of Physics, Plasma Physics Lab. for postgraduate studies and dr.kadhim A. Aadim for supporting this work.

## REFERENCES

1. Guillermo Santana, Arturo Morales-Acevedo, Osvaldo Vigil, L´ıdiceVaillant, Francisco Cruz, Gerardo Contreras-Puente. Structural and optical properties of (ZnO)x(CdO)1-x thin films obtained by spray pyrolysis. Thin Solid Films. 2000;373:235-238.
2. Ilican S, Caglar M, Caglar Y, Yakuphanoglua F. CdO:Al films deposited by sol–gel process: a study on their structural and optical properties. Optoelectronics and advanced materials – RAPID communications. 2009;3( 2):135–140.
3. Wenting Dong, Congshan Zhu. Optical properties of surface-modified CdO nanoparticles. Optical Materials. 2003;22:227–233.
4. S.Aksoy, Y.Caglar. Electrical Properties of n-CdO/p-Si Heterojunction Diode Fabricated by Sol
5. Gel.World Academy of Science, Engineering and Technology. 2011;59.
6. Eskizeybek V, Avcı A, Chhowalla M. Structural and optical properties of CdO nanowires synthesizedfromCd(OH)2 precursors by calcinations. Cryst. Res. Technol. 2011;46(10):1093–1100. [6]. Zhiyong Zhao DL, Morel CS Ferekides. Electrical and optical properties of tin-doped CdO films deposited by atmospheric metalorganic chemical vapor deposition. Thin Solid Films. 2002;413. 203–211.
7. Baranov AM, Malov YA, Zaretsky DF, Tereshin SA. Solar cells based on the heterojunction a-C/p-Si. Solar Energy Materials & Solar Cells. 2000;60:11-17.
8. Champness CH, Ghoneim K, Chen JK. Optimization of CdO layer in a Se-CdO Photovoltaic cell. Can. J. Phys. 1985;63:767.
9. Kondo R. Okhimura H, Sakai Y. Electrical properties of Semiconductor Photodiodes with Semitransparent films. Jpn. J. Appl. Phys. 1971;10:176.
10. Mishra RL, Sharmaa AK, Prakash SG. Gas sensitivity and characterization of cadmium oxide (CdO) semi conducting thin filmdeposited by spray pyrolysistechnique.Digest Journal of Nanomaterials and Biostructures.2009;4(3):511– 518.
11. Gomez Daza O, Arias-Carbajal Readigos A, Campos J, Nair MTS, Nair PK. Formation of Conductive CdO Thin Films on Photoconductive CdS Thin films for Window Layer Applications inSolar Cells. Mod. Phys. Lett. B. 2001;17:609-612.
12. Yan M, Lane M, Kannewurf CR, Chang RPH. Highly conductive epitaxial CdO thin films prepared by pulsed laser deposition. Appl. Phys. Lett. 2001;78:02342.
13. Peter ChritovShindov. CdO thin films deposited by spray pyrolysis. Electronics; 2004.
14. Osvaldo Vigil, Francisco Cruz, Arturo Morales-Acevedo, Gerardo Contreras-Puente, Vaillant L, Santana G. Structural and optical properties of annealed CdO thin films prepared by spray pyrolysis. Material Chemistry and physics. 2001;68:249-252.
15. Hani Khallaf, Chia-Ta Chen, Liann-Be Chang, Oleg Lupan, Aniruddha Dutta, Helge Heinrich

A. Shenouda, Lee Chow. Investigation of chemical bath deposition of CdO thin films using three differentcomplexing agents. Applied Surface Science. 2011;257:9237–9242.

16. Sakthivel S, Mangalaraj D. Cadmium Oxide Nano Particles by Sol-Gel and VapourLiquid-Solid Methods. Nano Vision. 2011;1(1):47-53.
17. Subramanyam TK, Srinivasulu Naidu B, Uthanna S. Studies on dc magnetron sputtered cadmium oxide films. Applied Surface Science. 2001;169(170):529-534.
18. Balu AR, Nagarethinam VS, Suganya M, Arunkumar N, Selvan G. Effect of the solution concentration on the structural, optical and electrical properties of silar deposited Cdo thin films. Journal of electron devices. 2012;12:739-749
19. Oprea C, Ciupina V, Prodan G. Investigation of nanocrystals using TEM micrographs and electron diffraction Technique. Rom. J. Phys. 2008;53.223–230.
20. D. JuSeo, "Structural and Optical Properties of CdO Films Deposited by Spray Pyrolysis", Journal of the Korean Physical Society, vol.45 no.3, pp. 1575-1579, 2004.

21. G. Aytaç, "Effect of Au Nanoparticles Doping on The Properties of TiO2 Thin Films", Materials Science (Medžiagotyra), vol. 20, no.1, p. 1392–1320, 2014.
22. AbdulhusseinK. Elttayef, Ahmed K. Abass, Huda M. Mutlak," the structural and surface morphology properties of CdO thin films prepared via R.F. magnetron sputtering", International Journal of Application or Innovation Engineering And Management, Vol. 4, Issue7, 2015.
23. K. Usharani et al., "characteristic analysis on the sutability of CdO thin films towards Optical Device Applications-Substrate Temperature Effect", Int. J. Thin. Sci. Tec., Vol.4, No.2, PP.89-96, 2015.
24. Asama NatikNaje, "optical characterstics of CdO Nanostructure", physical review and research international, Vol.3, No.4, PP.472-478, 2013.
25. Hassan Karami, "investigation of sol-gel synthesized CdO-ZnOnanocomposite for CO gas sensing", Int. J. Electrochem. Sci., Vol.5, PP.720-730, 2010.

**Table 1. Structural parameters like inter-planar spacing, crystallite size and miller of bulk CdO, ZnO and CdO:ZnO with different concentrations.**

| Sample | 2θ (Deg.) | FWHM (Deg.) | $d_{hkl}$ Exp.(Å) | G.S (nm) | hkl | $d_{hkl}$ Std.(Å) | Phase |
|---|---|---|---|---|---|---|---|
| CdO | 31.8927 | 0.5812 | 2.8038 | 14.22 | (002) | 2.8137 | Hex. Cd |
| | 33.0104 | 0.1342 | 2.7113 | 61.77 | (111) | 2.7108 | Cub. CdO |
| | 34.6647 | 0.5364 | 2.5856 | 15.52 | (100) | 2.8137 | Hex. Cd |
| | 38.2861 | 0.2236 | 2.3490 | 37.63 | (200) | 2.3477 | Cub. CdO |
| | 55.2757 | 0.2234 | 1.6606 | 40.16 | (220) | 1.6600 | Cub. CdO |
| | 65.9165 | 0.2236 | 1.4159 | 42.36 | (311) | 1.4157 | Cub. CdO |
| | 69.2697 | 0.5364 | 1.3553 | 18.01 | (222) | 1.3554 | Cub. CdO |
| 0.3 ZnO | 31.7139 | 0.4024 | 2.8192 | 20.53 | (100) | 2.8137 | Hex. ZnO |
| | 32.9210 | 0.2235 | 2.7185 | 37.08 | (111) | 2.7108 | Cub. CdO |
| | 36.1401 | 0.4024 | 2.4834 | 20.78 | (101) | 2.4754 | Hex. ZnO |
| | 38.1967 | 0.4917 | 2.3543 | 17.11 | (200) | 2.3477 | Cub. CdO |
| | 55.1863 | 0.3128 | 1.6630 | 28.67 | (220) | 1.6600 | Cub. CdO |
| | 65.9165 | 0.4917 | 1.4159 | 19.26 | (311) | 1.4157 | Cub. CdO |
| 0.5 ZnO | 31.8033 | 0.3128 | 2.8114 | 26.42 | (100) | 2.8137 | Hex. ZnO |
| | 33.0551 | 0.4024 | 2.7078 | 20.60 | (111) | 2.7108 | Cub. CdO |
| | 34.4411 | 0.3577 | 2.6019 | 23.26 | (002) | 2.6035 | Hex. ZnO |
| | 36.2742 | 0.2240 | 2.4745 | 37.34 | (101) | 2.4754 | Hex. ZnO |
| | 38.3308 | 0.4470 | 2.3464 | 18.82 | (200) | 2.3477 | Cub. CdO |
| | 47.4963 | 0.5811 | 1.9128 | 14.94 | (102) | 1.9110 | Hex. ZnO |
| | 55.3204 | 0.3129 | 1.6593 | 28.68 | (220) | 1.6600 | Cub. CdO |
| | 56.5723 | 0.3575 | 1.6255 | 25.24 | (110) | 1.6245 | Hex. ZnO |
| | 62.8316 | 0.3129 | 1.4778 | 29.76 | (103) | 1.4772 | Hex. ZnO |
| | 65.9165 | 0.4024 | 1.4159 | 23.54 | (311) | 1.4157 | Cub. CdO |
| 0.7 ZnO | 31.9374 | 0.2235 | 2.7999 | 36.99 | (100) | 2.8137 | Hex. ZnO |
| | 33.1893 | 0.2300 | 2.6971 | 36.06 | (111) | 2.7108 | Cub. CdO |
| | 34.5753 | 0.2288 | 2.5921 | 36.38 | (002) | 2.6035 | Hex. ZnO |
| | 36.4083 | 0.2210 | 2.4657 | 37.86 | (101) | 2.4754 | Hex. ZnO |
| | 38.4650 | 0.2235 | 2.3385 | 37.66 | (200) | 2.3477 | Cub. CdO |
| | 47.6751 | 0.2287 | 1.9060 | 37.99 | (102) | 1.9110 | Hex. ZnO |
| | 55.4098 | 0.3130 | 1.6569 | 28.68 | (220) | 1.6600 | Cub. CdO |
| | 56.7064 | 0.2234 | 1.6220 | 40.42 | (110) | 1.6245 | Hex. ZnO |
| | 62.9657 | 0.2235 | 1.4750 | 41.69 | (103) | 1.4772 | Hex. ZnO |
| | 66.0060 | 0.3576 | 1.4142 | 26.50 | (311) | 1.4157 | Cub. CdO |
| | 68.0179 | 0.3128 | 1.3772 | 30.65 | (112) | 1.3782 | Hex. ZnO |
| | 69.2250 | 0.3129 | 1.3561 | 30.86 | (222) | 1.3554 | Cub. CdO |
| | 77.0939 | 0.2683 | 1.2361 | 37.87 | (202) | 1.2377 | Hex. ZnO |
| ZnO | 31.8927 | 0.1341 | 2.8038 | 61.64 | (100) | 2.8137 | Hex. ZnO |
| | 34.5306 | 0.1786 | 2.5954 | 46.60 | (002) | 2.6035 | Hex. ZnO |
| | 36.3636 | 0.1788 | 2.4686 | 46.79 | (101) | 2.4754 | Hex. ZnO |
| | 47.6751 | 0.2234 | 1.9060 | 38.89 | (102) | 1.9110 | Hex. ZnO |
| | 56.7064 | 0.2682 | 1.6220 | 33.67 | (110) | 1.6245 | Hex. ZnO |
| | 62.9210 | 0.2682 | 1.4759 | 34.74 | (103) | 1.4772 | Hex. ZnO |
| | 68.0626 | 0.3575 | 1.3764 | 26.82 | (112) | 1.3782 | Hex. ZnO |
| | 72.7124 | 0.3130 | 1.2994 | 31.52 | (004) | 1.3017 | Hex. ZnO |

**Table 2. Average roughness, grain size and RMS for the (CdO)1-x(ZnO)x thin films at concentration different of ZnO at room Temperature obtained from (AFM)**

| Temperature | Sample | Ave. grain size (nm) | Ave. Roughness (nm) | R.M.S (nm) |
|---|---|---|---|---|
| RT | CdO | 50.7 | 0.84 | 0.97 |
| | 0.3 ZnO | 51.11 | 1.56 | 1.79 |
| | 0.5 ZnO | 61.81 | 1.74 | 2.13 |
| | 0.7 ZnO | 62.57 | 2.55 | 2.94 |
| | ZnO | 62.95 | 0.83 | 0.96 |

**Table 3. Transmittance spectra (T) for nano-films, Absorption coefficient, refractive index (n), Extinction coefficient (k) and Dielectric Constant in the wavelength of 300 nm with different concentration of ZnO.**

| samples | T% | $\alpha$ ($cm^{-1}$) | K | n | εr | εi | Eg (eV) |
|---|---|---|---|---|---|---|---|
| CdO | 51.18 | 133983 | 0.533 | 2.599 | 6.469 | 2.772 | 2.34 |
| 0.3ZnO | 43.51 | 166415 | 0.662 | 2.644 | 6.552 | 3.503 | 2.35 |
| 0.5ZnO | 31.79 | 229229 | 0.913 | 2.506 | 5.446 | 4.573 | 2.51 |
| 0.7ZnO | 25.85 | 270558 | 1.077 | 2.292 | 4.095 | 4.938 | 2.6 |
| ZnO | 21.03 | 311886 | 1.242 | 2.010 | 2.499 | 4.992 | 2.8 |

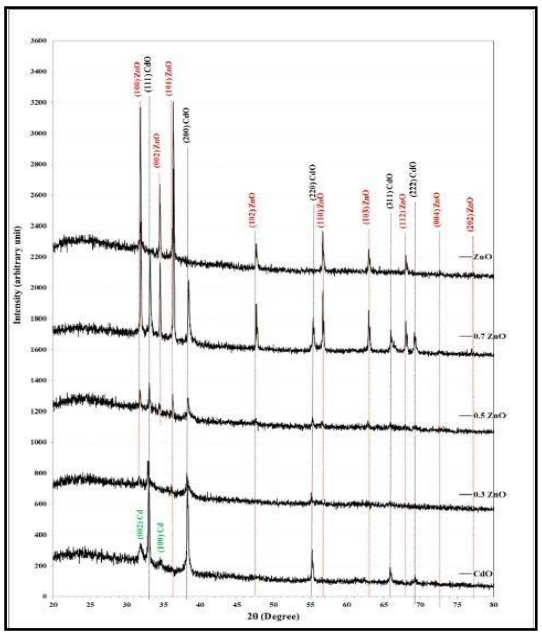


**Fig. 1. X-ray diffraction patterns of CdO, ZnO and CdO:ZnO with different concentrations (x= 0.3, 0.5, 0.7)%wt.ZnO at room temperature (R.T.).**

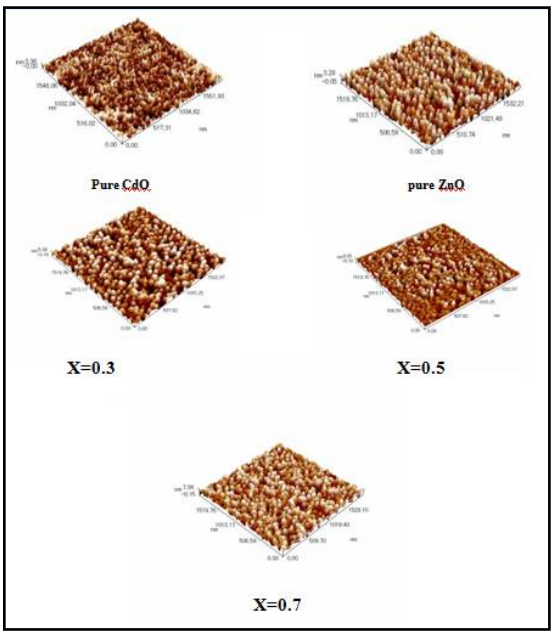


**Fig. 2. 3D image for surface morphology of the pure CdO, ZnO and CdO:ZnO nano- films analyzed by AFM test at a different concentrations at room temperature**

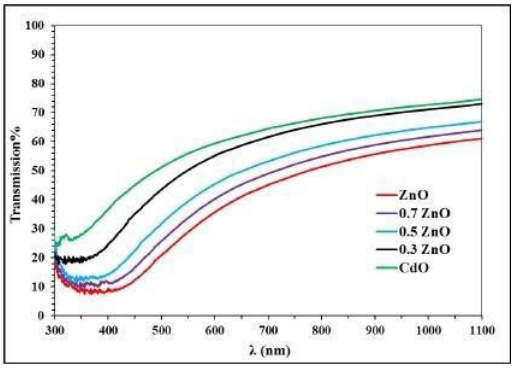


**Fig. 3. The variation of the transmittance spectra as function of wavelength at different concentrationsof ZnO.**

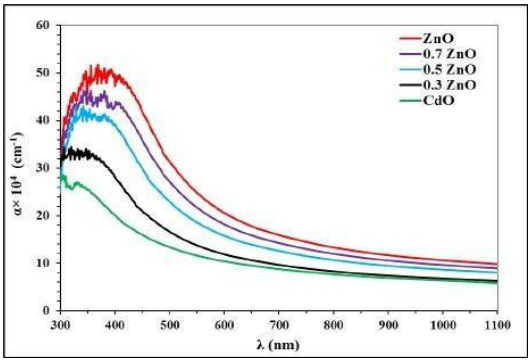


**Fig. 4. Absorption coefficient as a function of wavelength for CdO, ZnO and CdO:ZnO films at different concentrations of ZnO**

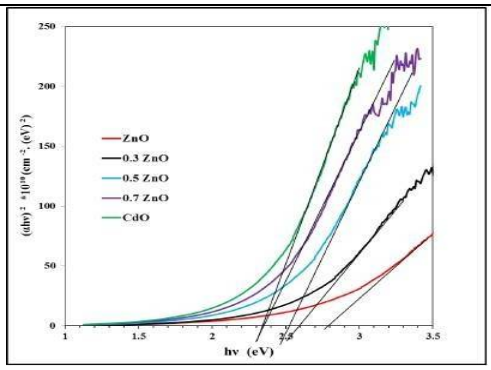


Fig.5. The variation of $(\alpha h\nu)^2$ **as a function of Photon energy for CdO, ZnO and CdO:ZnO nano-films at different concentrations of ZnO.**

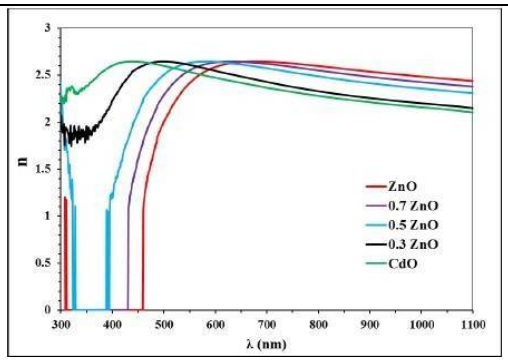


**Fig. 6. The variation of refractive index as a function of wavelength for CdO, ZnO and CdO:ZnO films at different concentrations of ZnO.**

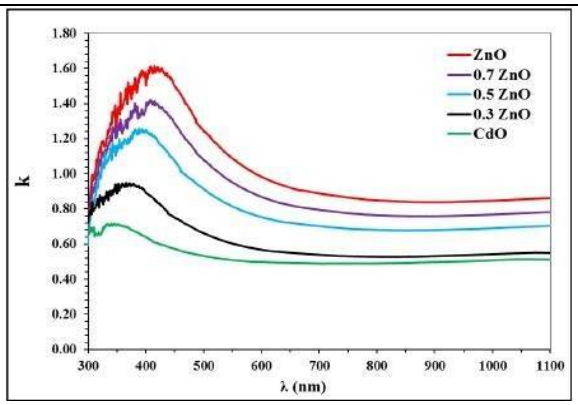


**Fig. 7. The variation of the extinction coefficient various wavelengths of CdO, ZnO and CdO:ZnO films at different concentrations of ZnO.**

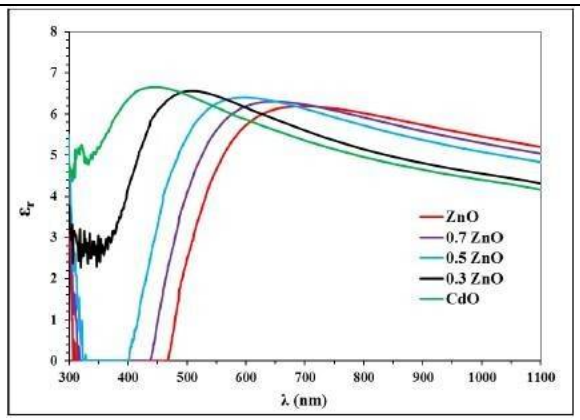


**Fig. 8. The Variation of the Real Part of Dielectric Constant (εr) With Wavelength of CdO, ZnO and CdO:ZnO films at different concentrations of ZnO.**

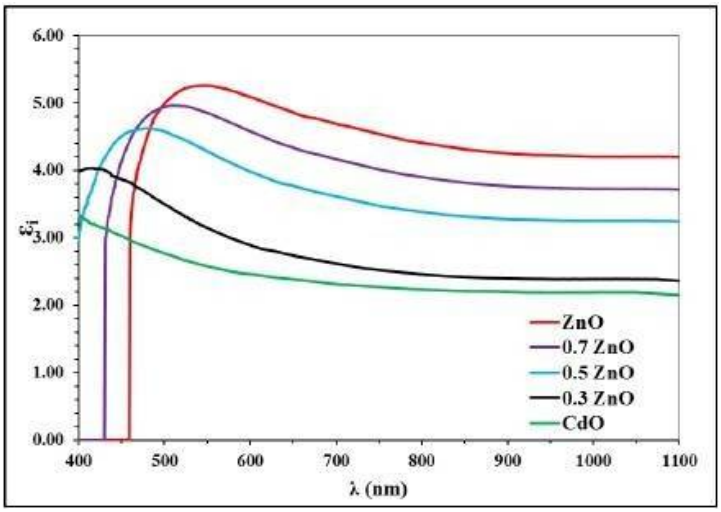


**Fig. 9. The Variation of the imaginary Part of Dielectric Constant (εi) with Wavelength of CdO, ZnO and CdO:ZnO films at different concentrations of ZnO.**

*Indian Journal of Natural Sciences* *www.tnsroindia.org.in ©IJONS*

*Vol. 9 / Issue 50 /October 2018* *International Bimonthly* *ISSN: 0976 – 0997*

RESEARCH ARTICLE

# Evaluation of Histological Changes Resulting From Cutaneous *Leishmaniasis* Infection Before and After Treatment In Diyala, Iraq

Saba Dawod Salman, Nagham Y. Al-Bayat and Thekra Atta Ibrahim.*

Department of Biology, College of Education for Pure Science, University of Diyala, Iraq.

Received: 17 July 2018 Revised: 20 Aug 2018 Accepted: 26 Sep 2018

***Address for Correspondence**
**Thekra Atta Ibrahim**
Department of Biology,
College of Education for Pure Science,
University of Diyala, Iraq.



## ABSTRACT

Histological changes in patients with cutaneous leishmaniasis at Baqubah Teaching Hospital were studied for the period from Oct. 2017 to Aug. 2018. Forty-five tissue biopsies were taken from 110 patients diagnosed with cutaneous leishmaniasis, from different age groups (biopsies were divided into two groups: pre-treatment, and post-treatment); women were the most exposed to infection 54,54% than men 45,45%. The age group 21-30 revealed more exposure to infection 29.09% than the other groups, while the age groups less than one 10 years or 41 years or more were the least infected with 10.90% with a significance level of 0.001 and P-Value = 0.001. A pathological histological changes study was carried out at different stages of the disease, the study included pre-treatment, post-treatment processes. Pathological changes in the epidermis included hyper keratosis and hyper epidermis, these changes appeared in 85% and 90% of patient in pre-treatment stage and decreased to 52,38 % and 80,95% of them in through treatment stage. Necrosis in the epidermis and dermis layers appeared in 60% of the patients and decreased to 42% of them with significant differences at P-Value=0.05

**Key words:** Leishmaniasis, phagocyte, papilloma, promastigote , sand fly.

## INTRODUCTION

Leishmaniasis is considered a Vector-Borne Disease, its transmitted by the female sand fly's sting, whereas the cause of the disease is due to a protozoan parasite from the *Leishmania* species(1). *Leishmania* exist in two basic body forms: the promastigote, tin the Invertebrate; and the amastigote, the amastigote form in the vertebrate host, including humans(2) . it is also considered one of the large-scale epidemics, it spreads across four continents including Asia, Europe, Africa and America(3). this disease settles in 88 countries including Iraq(4).Leishmaniasis stimulates the immune response significantly because the parasite exists inside the phagocytes, which is an immune system cell, and because the immune system has an important role in defending and securing the body from pathogens,

extracellular or intracellular, the system is stimulated when leishmania parasite enters the body(5). Given the importance of the disease and the rise of numbers of infected persons in the last years in Iraq (specially in Diyala province), this study was carried on to epidemically study this disease which infected people from Diyala's center (Baqubah city).

## MATERIALS AND METHODS

### Collection of Data

Data was collected from patients diagnosed with leishmaniasis by dermatologists and in accord with the clinical symptoms. A questionnaire form was made to record required information by asking infected people for their name, age, gender and marital status, and inspecting lesion form, number of lesions, place of lesion, period of infection, presence of rodents in the house of the infected or in the surrounding area, also they were asked about their place of residence (rural or city), and does the patient suffer from other diseases.

#### Collection of Samples

#### Histological Biopsies

The study included 110 patient diagnosed with cutaneous leishmaniasis by the specialized doctor, forty-five biopsies were taken from the patients' infected skin. Biopsies were collected by a tool called the 'punch', this process is carried out after sterilizing the tool and the place from which the biopsy was taken with 70% ethyl alcohol, and local anesthesia with 2% xylocaine, all carried out by specialists.Samples were preserved in 10% formalin solution until necessary examinations are made. Samples were divided into tow groups: first group: pre-treatment, second group: post-treatment.Samples were collected during the period 08/01/2017 to 30/10/2017.

## RESULTS AND DISCUSSION

The Study's' results revealed that among the 110 patients, at the Dermatology Unit at Baqubah Educational Hospital with cutaneous leishmaniasis (CL), 45.45% were males (50 males out of 110) and 54.54% were females (60 females out of 110); patients' ages ranged from 1 year to more than 41 years. Results revealed no significant differences in the cases of cutaneous leishmaniasis among males and females at a probability level of 0.05 with a value of P-value 0.390. This is agree with (6), which revealed no significant differences between males and females with leishmaniasis; it also revealed that the highest infection rate was for ages ranging from 20-30 years, and that is not agree with previous studies which stated that the most vulnerable to infection were those at the age of 20 and less, especially children due to their activity and play in places where may they contact with infested host; results of this study may be due to the nature of the studied samples, which was based on the patient who attended the teaching hospital. According to microscopy examination about the location of lesion (Habat Bagdhad), it was evident that the most affected area was the arms with 40% (44 patients with lesion on the arm), leg and foot comes second with 20,90%, and then the face with 5,45% which is the least infected area in patient with leishmaniasis. This coincides with (7) and (8). This indicates that the parasite attacks the exposed areas of the body for the purpose of sucking a blood meal, and most of the areas infected are the most vulnerable to these stings, which are the legs and arms.

Results also indicated that rate of multiple lesions (78.18%) was higher than single (21.81%). This study is consistent with (9) and (10), where it was explained that the multiple lesions were the most common among the infected in Salahuddin province. Researchers attributed this to the nature of the agricultural area in which these people lived (an environment similar to the Diyala's environment), being agricultural areas in which the host insect is abundant and thus the chances of exposure to more than one bite are greater, and this may be due to insect's activity and spread.

Results of this study indicated that those infected with dry leishmaniasis were 56.36% that's more than those with wet leishmaniasis 43.65% with no significant differences, P-Value=0.182.This coincides with the study (8) which found that dry leishmaniasis cases are more than wet leishmaniasis ones. In this study a high infection rate of wet leishmaniasis disease is also noted, that may indicate the presence of the disease hosts like dogs and rodents, and this is confirmed by the current study results in terms of the presence of rodents in the living quarters of the infected, especially in rural areas as well as in the cities. The presence of rodents was 62.72% in the residential areas of the current study. Some of them were infected with wet leishmaniasis, others with the dry type. The insect was present in the areas of residence of all patients in this study. This is confirmed by previous studies that the prevalence of infection is associated with the presence of host animals and the transmitting insect in the areas studied and as shown in previous studies conducted by both (11) and (8) And (7) there was no significant difference for the residential areas of the infected despite the high rate of infection among the population of the city (55.5% ) compared to the countryside (44.5%). This agree with study number (6) which indicates that people living in the city are at more risk of infection from those living in rural areas, and it added that these areas might be semi-rural because it was mentioned in (6) that Diyala is a semi-rural area for having many agricultural areas.

## Histological Changes

This study indicated that there is a group of histological biopsies taken from the skin of patients with cutaneous leishmaniasis (CL), and these group were subdivided into two groups according to the time when the biopsy was taken (pre-treatment and thought treatment), and these histological changes were summarized.

Among these histological changes, in patients' tissues in the current study, were necrosis and hyperkeratosis in the epidermis, the rate of appearance of the latter symptoms in infected patients was 60% and 85%, respectively, as shown in Fig. (4). Cell necrosis and hyperkeratosis appear in the epidermis. The treatment revealed its healing effects on tissue layers, which decreased to 42.85% and 52.38%, respectively, see Fig. (4). Present results indicated significant differences between these two histological changes, which included necrosis and hyperkeratosis, where (P-value=0.023) for necrosis, whereas for hyperkeratosis it was 0.001 at a probability level of 0.05 and this coincides with (12) which indicted significant differences of dermal necrosis and skin hyperkeratosis pre- and through treatment, these changes occur in severe infection where the stratum corneum begins to separate from the epidermis layer and begins decaying after a long period of infection. This study does not coincide with (13) which revealed no significant differences in hyperkeratosis pre to and through treatment. This may be due to the nature of the treatment used in the study, which differs from the type of treatment there in, whereas Glucantime, Leishvacin and Bacillus Calmette-Guerin was used in (13) Pentostam was used in this study. Results revealed papilloma in the dermis layer, it increased from 30% pre-treatment to 28,85% post-treatment, (P-Value=0,951) and that indicates significant differences and coincides with (14) as demonstrated in Fig. (2) and (4), but this doesn't coincide with study (13) which stated that there are significant differences in papilloma pre-treatment and post-treatment and it further stated that the cause of theses tumors might be due to overlap of the dermis with the epidermis.

This study also indicated that among the histological changes occurring in the affected tissue is edema in the skin layer by 60% pre-treatment Fig. (2), decreased to 52.38% through treatment, also edema in the dermis decreased from 75% to 66.66 As shown in Fig. (3), this result is consistent with (15) as the histological sections infiltration of the phagocyte cells containing elliptical-shape Fig. (3).A decrease in the percentage in hyper-epidermis from 90% pre-treatment to 80.95% through treatment, as shown in Fig. (2) (3), respectively, and this is consistent with the study conducted by (16).

Results of this study revealed granuloma consisting of the pool of inflammatory cells in the dermis, its existence rate was 50% pre-treatment, see Fig. (4) and decrease through treatment to 38.09% and P-Value was 0.117 with no significant differences at the level of probability 0.05, as in Fig. (5), this coincides with (17) which indicated that the exacerbation of the infection, which leads to the infiltration of a large number and many types of inflammatory cells,

and that ultimately leads to the formation of granular tumors.Fig. (4) shows certain expansions from the epidermis to the dermis, which is called, which Rete ridges decreases from 65% (pre-treatment) to 42.85% (through treatment) as in Fig. (5). This coincides with (18), which demonstrated in the samples from patients with leishmaniasis, studied alongside with samples from patients with scabies, the manifestation of net edges in the skin, which is a descriptive term for hyperplasia in the epidermis, which takes palace when cells increase in number the stratum basale, due to increased cells' division rate, leading to a great increase in the cells numbers, and to accommodate this large increase in numbers, the epidermis starts expanding downwards into the dermis in the shape of regular elongations from the net edges, which leads to manifestation of camel hump like shapes. (19)

Fig. (4) and Fig. (5) other pathological effects are demonstrated, including increase in fibrosis, which increased from 60% pre-treatment to 75% through treatment. P-Value was 0.034 with significant differences at the probability level of 0.05. This is consistent with previous studies revealing that the increase in collagen fibers is evidence of the initiation of the healing process (13).

Fig. (5) shows the infiltration of lymphocytes, neutrophil cells, plasma cells, and the emergence of giant cells. This occurs in the dermis layer. This result is consistent with what is revealed in (20). They have shown that the presence of these cells in the lesion sites indicates a strong immune response as a result of infiltration of these cells causing the initial immune response to the inflammation changes, they also revealed that tissue changes are positively correlated with increased numbers of these cells. Coronation and necrosis increases with as necrosis area increases. The cause may be due to the role of T cells in the pathogenesis, its presence is associated with increased pass of interferon and necrosis, which has a role in the increasing necrosis and inducing cells to move the site of infection, and this increases inflammatory reactions

## REFERENCES

1. Daham, Amal Kamel and Al-Alusi, Tawfiq Ibrahim (2011). A temporal survey of leishmaniasis in the province of Salah al Din. Diyala Journal of Agricultural Sciences, 3 (2): 601-610.
2. Al-Samarai, A. M. and Al-Obaidi, H. A. H, Al-Jumaili, Z. K.; Jasim, M. M. and Qatal, S. (2016) cutaneous Leishmaniasis in iraq: a continuing endemic disease. Journal of Drug and Diseases Researches, 31(1): 1024-1031.
3. Ul-Bari, A. and Rahman, S. (2006) Correlation of clinical histopathological microbiological findings in 60 cases of cutaneous leishmaniasis. Indian Journal of Dermatology, Venereology and Leprology, 72(1):28-32.
4. Viana, A.G.; Mayink,W.; Frage, C.A.C., silva, L.M.; Domiagos, P.L.B.; Bonan, P.R.F.; Paual, A.M.B. and Botelho, A.C.C. (2013). Histopathological and Immunohistochemical aspects of American cutaneous leishmaniasis before and after different treatments. Anias Brasileinos de Dermatologia, 88(1) : 32-40.
5. Manamperi, N.H.; Oghumu, S.; Pothirana, N.; de Silva, M.V.; Abeyewichieme, W.; Satoskar, A.R. and Karunaweera, N.D. (2017). In situ immunopathological changes in cutaneous leishmaniasis due to *Leishmania donovani.* Parasites Immunology, 39(3), doi:10.1111/pim.12413.
6. Danas, M.L.; Oliveira, J.M.; Carvalho, L.; Passos, S.T.; Queiroz, A.; Guimmães, L. H.; Machado, P.; Carbalho, E. and Arrunda, S. (2014). Comparative analysis of the tissue inflammatory responses in human cutaneous and disseminated leishmaniasis. Memorios Institute Oswaldo Cruz, Rio de Janerio, 109:202-209.
7. Shirian, S.; Oryan, A.; Hatam, G. R. and Daneshbod, Y. (2012). Mixedmucosal leishmaniasis infection caused by *L. tropica* and *L. major*. Journal of Clinical Microbiology, 50(11): 3805-3808.
8. Shamsi- Meymandi, S.; Javadi, A.; Dabiri, Sh.; Shamsi-Meymandi, M. and Nadji, M. (2011). Comparative histological and immunohistochemical changes of dry type cutaneous leishmaniasis after administration of meghumine antimoniate, Imiquimod or compination therapy. Archives of Iranian Medicine, 14(4): 238-243.
9. Al-Musawi, N.D.; Al-Bayati, N.Y. and Al- Kadhemi, M.H. (2018). Histological changes resulting from parasitic infection (scabies). Diyala Journal of Pure Sciences., 14(2): 248-259.

10. Madke, B.; Doshi, B.; Khopkar, U. and Dongra, A. (2013). Appearance in dermapathology, the diagnostic and the deceptive. Indian Journal of Dermatology, Venereology, Leprology, 79:338-348.
11. Gonzălez, K.; Diaz, R.; Ferreira, A.; Garcia, V.; Paz, H.; Calzada, J.E.; Ruiz, M.; Laurenti, M. and Saldaňa, A. (2018). Histopathological characteristics of cutaneous leishmaniasis caused by Leishmania Viannia panamensis in Panama. Revista do Institute de Medicina Tropical de Săo Paulo, 60: e8-e16.

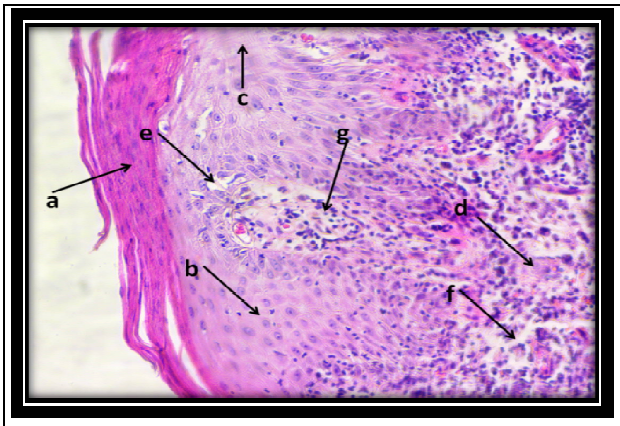


**Figure1. A longitudinal section in the skin of a patient with cutaneous leishmaniasis demonstrates a-keratosis. b-hyperepidermis. c- Skin necrosis in epidermis. d- Necrosis in the dermis. e- Edema in epidermis. f- Edema in dermis. g- Papilloma g (H & E 20 x)**

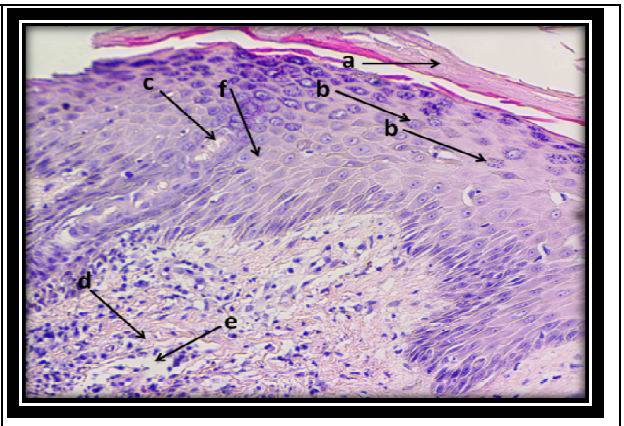


**Figure 2. Vertical section of the skin of a patient with CL through treatment stage, it shows separation of the keratosis layer from the epidermis a- Phagocytes containing the parasite in its parasitic phase. B- odema in the Skin. c- Cell necrosis in the corium. d- edema in the corium. f- Hyperepidermis (H & E 20x)**

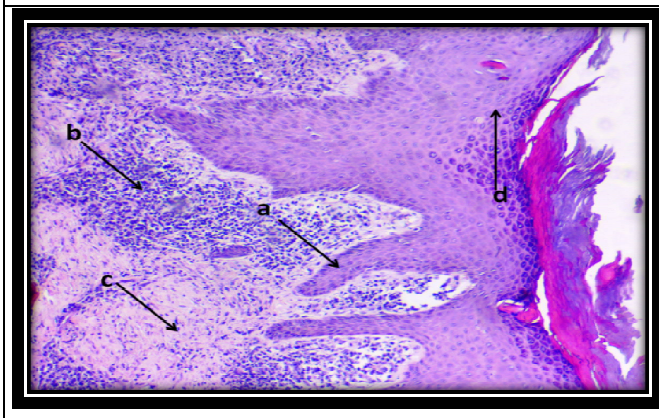


**Figure 3. Histological section of a pre-treated patient with leishmaniasis a- Rete ridges. b- Pelvic tumor. c- Collagen fibers. d- Acanthosis (H & E 20x).**

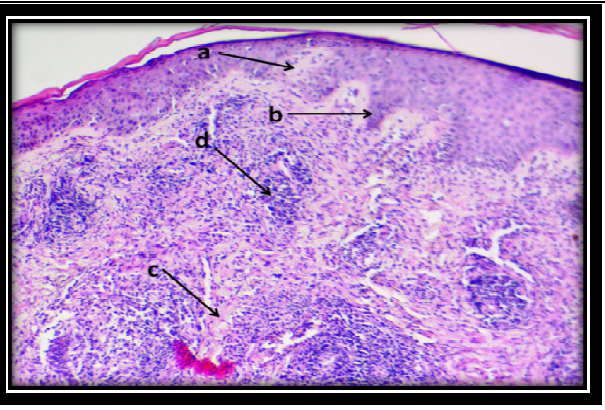


**Figure 4. Histological section in the skin of the leishmania during papilloma treatment a- Rete ridges. b- Collagen fibers. c- Pelvic tumor. d- (H & E20x).**

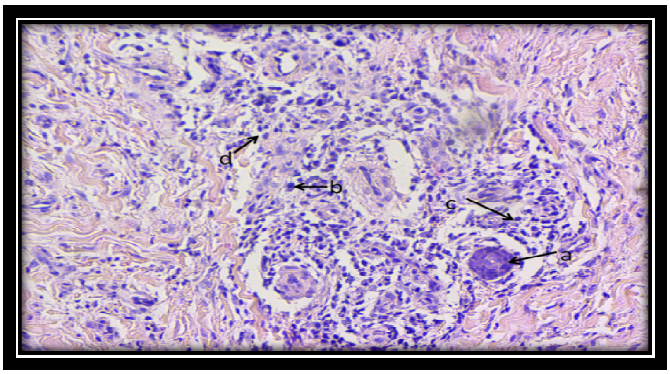


**Figure 5. A- vertical section of skin with leishmaniasis showing a-Giant cell. c- Plasma cell. d- Lymphocyte cell. f- Neutrophil cell (H & E 40x).**

*Indian Journal of Natural Sciences* www.tnsroindia.org.in ©IJONS

*Vol. 9 / Issue 50 /October 2018* *International Bimonthly* *ISSN: 0976 – 0997*

RESEARCH ARTICLE

# The use of Microstructures in Determination of Tectonic Phases Influence Evolution of Al- Tib Anticline, Southeastern Iraq

Atheer Edan Khalil Al- Hachem* and Mustafa Rasheed Al-Obaidi

Department of Geology, College of Science, University of Baghdad, Baghdad, Iraq.

Received: 14 July 2018 Revised: 18 Aug 2018 Accepted: 26 Sep 2018

***Address for Correspondence**
**Atheer Edan Khalil Al- Hachem**
Department of Geology,
College of Science,
University of Baghdad, Baghdad, Iraq.
Email : akhalil35155@gmail.com



## ABSTRACT

This paper represents microstructures analysis of Al-Tib Anticline in the Low Folded Zone, Northeastern Missan area, Southeastern part of Iraq. Where Late Miocene to recent rock units are cropping out.Al-TibAnticline runs along the NW- SE trending, the southwestern limb is steeper and shorter than the the northeastern limb make it asymmetrical fold.Different and many types of the fractures were measured in the study area, such as Veins, Joints, Faults and Striations, andthe structural analysis was carried out on it. The fractures were studied and geometrically classified with reference to the tectonic axes (a, b and c) into sets and systems in (ab, bc, ac, hkl, hol and okl). The majority of fractures are geometrically related to layering and fold axes. The dominant fracture sets at study area striking (NW-SE, NE-SW, E-W and N-S). It has been suggested that the reason for the slightly different orientations in some sets or systems in different rock units is related to the different behavior of the rocks at the time of fracturing producing a stress pattern which is inhomogeneous.

**Key words:** Microstructures, Joints, Low Folded Zone, Missan, fractures.

## INTRODUCTION

Iraq is one of the countries that are exposed to the tectonic activity due to its location. Zagros-Taurus Belt is located in the collision area between Arabian and Iranian Plates. The study area is one of relatively complex geological structure located in the Middle part of Zagros Belt southeastern Iraq.Several previous works e.g. [1] [2] [3] [4] [5] [6] [7] [8]have studied fractures in the northeastern Iraq. Some of these studies have put geometrical classification of the fractures. This study concentrates on the structural and tectonic analysis of Al- Tib Anticline in Northeastern Missan. Al-Tib Anticline lies southeastern part of Iraq, and it's located between latitudes (32° 15' - 32° 30' North) and longitudes (46°

55' - 47° 25' East), covering about (1121) Km². The boundary of the study area represents the Iraqi-Iranian border as shown in Figure (1).

### Aim of the Study

This paper aims to the geometrical fractures analysis to be classified and analyzed to find the geometrical and genetic relationship with the principal tectonic axes at Injana and Muqdadiya Formations of Al- TibAnticline that acts on the study area for paleostress analysis.

## MATERIALS AND METHODS

### Geological Setting

Tectonically, the study area belongs to the un stable shelf represented by two Zones, Foothills Zones, along the Iraqi-Iranian international boundaries and the Mesopotamian Zone, more precisely, the former is represented by Hemrin Sub zone ,whereas the latter by Tikrit-Amara Sub Zone as shown in Figure (2), [9]. The exposed rocks in the study area belong to the late Miocene and Late Pliocene ages. These rocks include Injana Formation (Late Miocene) ofthe southwestern limb at attitude (240°/40°)**.**Itcomprises of fine grained, molass sediments deposited initially in the coastal environment and later in fluvio- lacustrine environment. The basal unit comprises thin bedded sandstone, siltstone, marls and reddish brown and brownish grey mudstone.Muqdadiya Formation (Early Pliocene). It comprises pebbly sandstone; grey and brownish grey sandstone, red mudstone and marls. Sandstone rocks are often strongly characterized by cross- bedding and Bai-Hassan Formation (Late Pliocene).

It is characterized by interbedding of gray conglomerate, brown claystoneand lenses of gray sandstone. Bai-Hassan Formation was deposited in fluvio- lacustrine environment. The Upper boundary of Bai-Hassan Formation is eroded. The formation is overlain by terrace gravels and/or alluvial deposits and is covered by fine grain sediments of Quaternary age[10] [11] [12].

### Fractures Analysis in the study area

More than (370) reading of fracture planes were collected of Al-Tib Anticlinethrough the distributed on the (12) stations of the study area as shown in Figure 1. Strike and dipwere measured for the fracture planes as well as the attitude of the beddingplane which contain the fractures.Stereographic Projections and Rose Diagram Plots were used for projection different fractures. Fractures planes data of Al-Tib Anticline were collected from Injana and Muqdadiya Formations through twelve stations distributed in the study area as shown in Figure13. The fractures are described and classified geometrically in proportion to the orthogonal tectonic axes, into sets and systems as shown in Figure (3) as follows:

### ab fractures set

The planes of these fractures are perpendicular to c axis and parallel to both aandb axes. This set comprises all the planes parallel to bedding planeas shown in Figure(4)and Plate (1). The set ab fracturescommonly appear in surfaces parallel to bedding plane and usually intersected by other sets. Possibly they could be release fractures resulted from recent unloading or due to weathering process [13][14][15].The percentage of this set is (3.2 %) from the study stations.

**ac: fracture set**

The planes of this set of fractures are parallel to tectonic axes a andc, whereas a tectonic axis b is perpendicular to them. In other word (ac) sets are perpendicular to the axis of Al-Tib anticline as shown in Figure (5) and Plate(2).The general trend of this set is NE-SW within different geological formations of the study area, such as Injana and Muqdadiya Formations. The percentage of this set is (35.4%) from the study stations. Fractures of this set comprise joints and veins. The joints form the majority of fractures of this set and these joints are either closed or opened. Blocky and fibrous crystals of secondary gypsum are developed on the wall of these opened joints to form veins. These veins developed to reach (3) centimeters thick.

**bc fractures set**

The planes of this set of fractures are parallel to tectonic axes b and c and perpendicular on the aaxis as shown in Figure (6) and Plate (3). They are formed as a result of extensional stress perpendicular on the bedding planes. The general trend of this set is NW-SE within different geological formations of the study area, such as Injana and Muqdadiya Formations. The percentage of this set is (40%) from the study stations.

**hko system**

Planes of this system are parallel or sub parallel to the c tectonic axis and intersect both (a andb) tectonic axes. The planes of this system makes approximately orthogonal angle with the bedding planes. This system subdivided into the following sets of conjugate systems.

**hko acute about a system**

This system consists of intersecting two sets; the tectonic axis a bisects the acute angle between these two sets. Whereas, the tectonic axis bbisects the obtuse angle as shown in Figure(7)and plate(4). These fractures occur and observed through the exposed geological formations of the Al-Tib anticline in Injana and Muqdadiya Formations as conjugate sets. The percentage of this system is (2.5%) from the study stations, that form approximately (65°) with tectonic axis a.

**hko acute about b system**

The intersected two sets of this subsystem are bisected by the tectonic axes (b and a). The axes a andb bisect the obtuse and acute angle respectively as shown in Figure(8) and plate (5). The sets of this system were observed within Injana and Muqdadiya Formations in the studied area. The fractures of this system are joints and veins. The percentage of this system is (3.2 %) from the study stations, that form approximately (40°) with tectonic axisa.

**hol System**

The orientation of the planes for this system is parallel to tectonic axisb and intersects both (a andc) tectonic axes. These planes form an acute angle with bedding plane. This system subdivided into the follows sets of conjugate systems.

**hol acute about a system**

The intersected two sets of this system are bisected by the tectonic axes**(**a andc) and make an acute and obtuse angle around each of them respectively as shown in Figure(9) and plate (6). This system of fractures recorded in Muqdadiya Formation in the study area. The percentage of this system is (5.7 %) from the study stations.

**b-hol acute about c system**

This system is also consisting of two conjugate shears trending parallel to the b axis. The tectonic axis c bisects the acute angle between the two sets of this system, whereas the tectonic axis a bisects the obtuse angle as shown in Figure(10)and Plate (6). The fractures of this system were documented in Muqdadiya Formation in the study area. The percentage of this system is (5.4%) from the study stations.

**okl fracture system**

The planes of this fracture system are parallel to the tectonic axis a and intersect the tectonic axes (b and c). This system consists of two conjugate systems:

**a-okl acute about b system**

The tectonic axis b bisects the acute angle between the two set of this system. They are showing as conjugate sets or individual set as shown in Figure(11) and Plate (7). These fractures observed in Muqdadiy Formation in the study area. The percentage of this set is (2.7 %) from the study stations.

**b-okl acute about c system**

The two planes of this system intersect forming an acute and obtuseangle. Tectonic axis cbisects the acute angle between the two sets and the tectonic axis b bisects the obtuse angle as shown in Figure(12) and Plate (7).These fractures exists in the form of conjugate sets or individual set and their planes make angles range between (50° to 70°) with bedding plane. The fractures of system distributed mainly in the southwestern limb of Al- Tib anticline in Muqdadiya Formation. The percentage of this set is (1.9 %) from the study stations.

## RESULTS

Results include the tectonic interpretationof thefractures in the study area, as follows:

**Geometry and Kinematic Interpretation**

On the basis of geometry and kinematics, fractures were divided into tension sets (ab, ac, bc) and shear systems (hko acute about a, hko acute about b, ho1 acute about a, holacute about c, okl acute about b and okl acute about c). Generally the fracturing of rocks is related to folding and could haveoccurred during three stages, before, during and after folding.

**Dynamic interpretation**

The dynamic interpretation for each of these sets and systems is outlined with reference to their relative ages. Shear fractures hol are the oldest shear fractures and okl are the youngest shear fractures in Al- Tib Anticline of the study

area according to its arrangements depending on its percentage as shown in Table (1) and Figure(14). Generally, the fractures can be interrelatedin the study area into:

**Fractures of hko acute about a system and ac set**

Shear fractures in hko acute about a could have developed under a stress regime when the maximum principal stress axis (σ1) was approximately parallel to the a direction, the intermediate principal stress axis (σ2) parallel to c and the minimum principal stress axis (σ3) parallel to the fold axis. Since ac joints and veins intersect the dihedral angle between shears in hko acute about a and are perpendicular to the minimum stress axis, these surfaces could have developed contemporaneously as extension fractures.

**Fractures of hko acute about b system and bc set**

Shear fractures in hko acute about b could have formed when the maximum principal stress axis (σ1) was parallel to the fold axis, the intermediate principal stress axis (σ2) parallel to caxis and the minimum principal stress axis (σ3) parallel to a axis. Fractures in bc intersect the dihedral angle between shears in hko acute about b and are perpendicular to the minimum stress axis. They could have developed contemporaneously with hko shear acute about b as extension surfaces.

**Fractures of hol acute about a system and ab set**

shear fractures in hol acute about a indicates that they developed when the maximum principal stress axis (σ1) was parallel to a direction, the intermediate principal stress axis (σ2) parallel to b and the minimum principal stress axis (σ3) parallel to c. Joints in ab are not parallel to ho1 acute about a and the small angle between shears in ho1 acute about a and are perpendicular to the minimum principal stress axis.These joints could have formed contemporaneously with shear fractures in hol acute about a as extension surfaces.

**d: Fractures of hol acute about c system and bc set**

Shear fractures in hol acute about c could have formed when the maximum principal stress axis (σ1) was perpendicular to the layering, the intermediate principal stress axis parallel to the fold axis and the minimum principal stress axis parallel to a direction.

**Fractures of okl acute about c system and ac set**

Shear fractures in okl enclosing an acute about c, could have developed under a stress regime when the maximum principal stress axis was parallel to c direction, the intermediate principal stress axis parallel to a direction and the minimum principal stress axis parallel to b direction Some of the joints and veins in ac could have formed contemporaneously with this system.

## DISCUSSION

There are two systems of the fractures present in the Rose diagram (approximately corresponding between all types of fracture sets and systems based on their orientation), the first system is composing of two sets assuming the following orientations NE-SW and NW-SE, and the secondary system is composing two sets assuming the following orientations N-S and E-W.The dominant fractures trend is N45°E, which corresponds to the orientation of the maximum horizontal principal stress (σ1) (NE - SW). The minimum principal stresses (σ3) were oriented in NW-SE direction, while the intermediate principal stress (σ2) was oriented perpendicular to the plane containing (σ1) and

(σ3). Such possible orientation of (σ1) has formed ac fracture parallel to its direction, whereas, the (N –S) trend is represented tension fractures which are parallel to the main force (N- S), as well as (E - W) trend is considered also as tension fractures formed by releasing the stress during folding process.

## CONCLUSIONS

Shear Fractures system (hol) and tension fractures (bc) of Al-Tib Anticline might have been formed prior at early stages of folding, as the main extension stress which are in the trend of NW – SE. Fractures analysis revealed the geometrical and genetic relationship with the principal tectonic axes of Al- Tib Anticline as the main compression stress was representative in the form of shear fractures system (hko) and tension fractures (ac) which are in the trend of NE – SW, it might have been formed prior at last stages of folding.

## REFERENCES

[1]Al-Obaidi MR. A Study of Geological Structures of JabelSinjar: Un published M.Sc.Thesis, University of Baghdad, Iraq 1978.

[2]Alki HD. Structure Study of Hemrin South Mountain- Suddor area. Un published M.Sc. Thesis, College of Science, University of Baghdad. Iraq 1992.

[3] Barno JM.Structure Analysis of Kosrat Anticline and its Tectonic Implications, Northeastern Iraq. Unpublished Ph.D. Thesis, University of Baghdad,Iraq 2014.

[4]Shahab AT. Structural Analysis using Remote Sensing and GIS Techniques inthe High Folded Zone between Harir and Bardost Anticlines, Northeast Iraq. Unpublished M. Sc. Thesis, University of Baghdad, Iraq 2015.

[5]Al-Kubaisi MS, BarnoJM. Fold geometry and Kinematics of inversion tectonic for Kosrat anticline, northeastern Iraq. Arabian J Geosciences2015;8:9455-9469.

[6]Al-Mamaar AF.Newtectonic Analysis Using Remote Sensing and GIS Techniques in the High Folded Zone between Perat (Bekhme) and Bardost Anticlines, Northeast Iraq.UnpublishedM.Sc. Thesis, University of Baghdad, Iraq 2015.

[7]Al-Muathen AA.Structure Analysis of Selected areas in High Folded Zone of Duhok Governorate North of Iraq.Unpublished Ph.D. Thesis, University of Baghdad, Iraq 2016.

[8] Ward AH. Geometry and Structural History of Kkalakan Anticline North Eastern Iraq. Unpublished Ph.D. Thesis, University of Baghdad, Iraq 2018.

[9] Al-Khadimi JA, Sissakian VK, Fattah AS, Deikaran DB. Tectonic map of Iraq.State Company of Geological Survey and Mining, Baghdad, Iraq 1996.

[10]Barwary AM, Said FS. The Geology of Khanaqin Quadrangle, Sheet (NI 38-15), Report No. 2256.State establishment of Geology Survey and Mining (GEOSURV), Baghdad, Iraq 1992.

[11]Barwary AM. The Geology of Ali- Al Garbi Quadrangle.Report No. 2226, NI- b38-16(GM 28). State establishmentof Geology Survey and Mining (GEOSURV), Baghdad, Iraq 1993.

[12]Jassim SZ,Goff JC.Geology of Iraq. Published by Dolin, Moravian, Museum, Brno, Czech Republic 2006.

[13]Hancock PL. Brittle Microtectonic, Principles and practice.J StructuralGeology 1985;7:437-457.

[14]Van der Pluijm BA, Marshak S. Earth Structure: AnIntroduction to Structural Geologyand Tectonics. WCB/McGraw-Hill, USA; 2004.

[15] Fossen H. Structural Geology: United States of America, Cambridge University Press;2012.

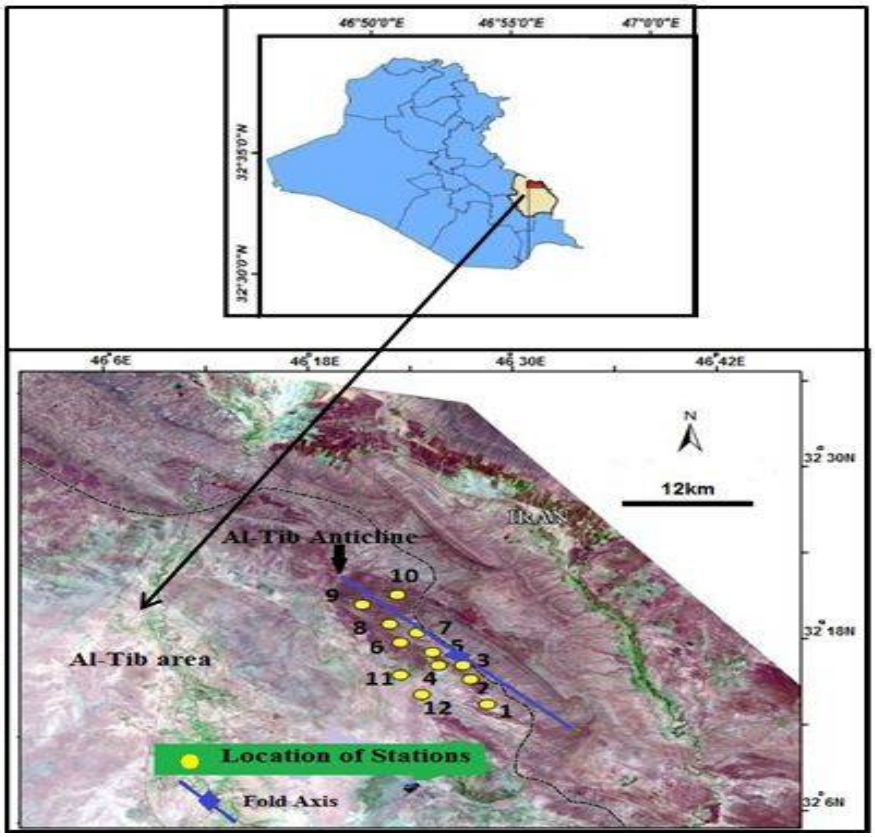


**Figure 1.Satellite image shows the oriented sample measurements in the study area.**

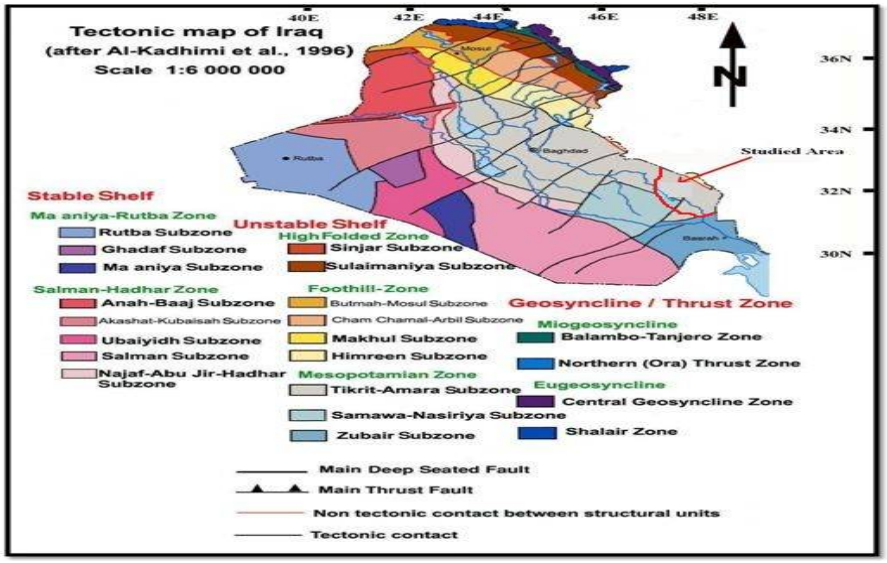


**Figure 2. Tectonic Map of Iraq [9].**

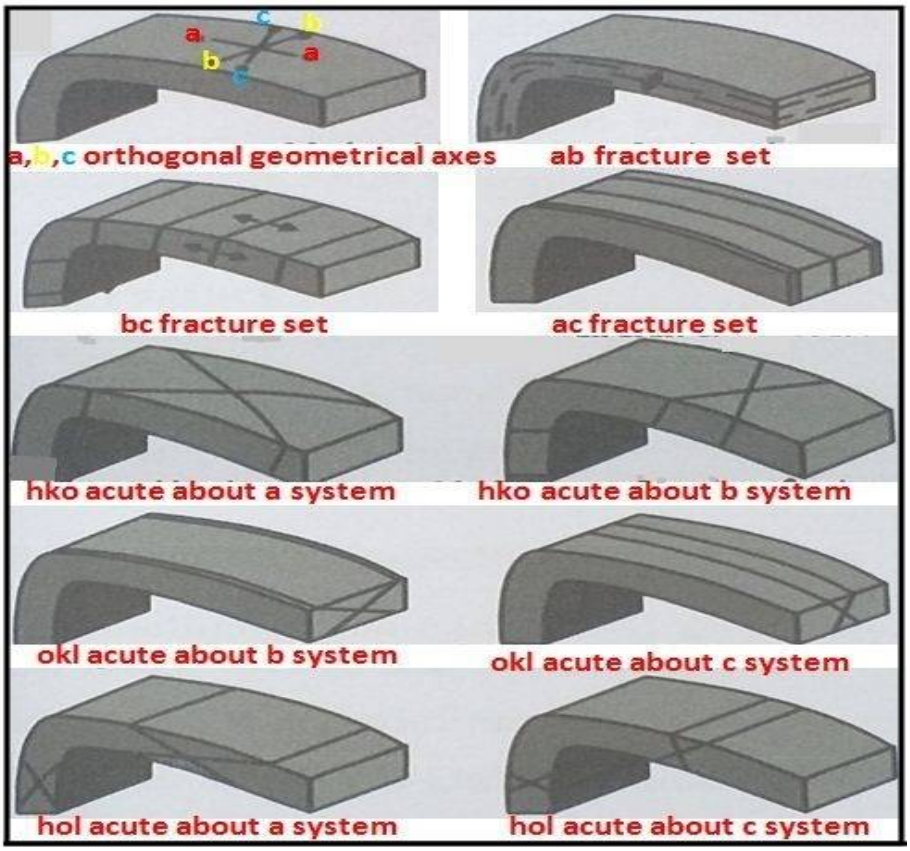


**Figure 3.Geometrical classification of fractures with respect to three orthogonal geometrical axes [13].**

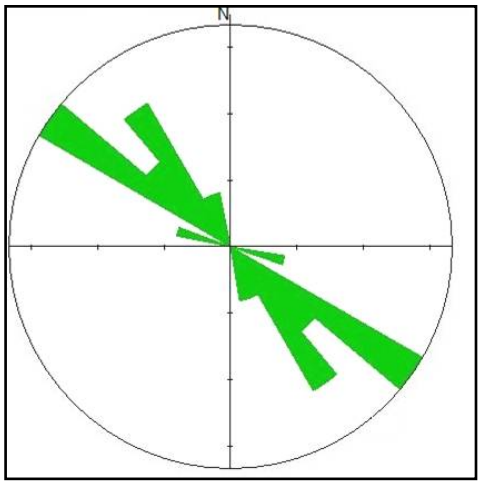


**Figure 4. Rose diagram of ab fractures set direction of the study area which is parallel to Al-Tib fold axis**

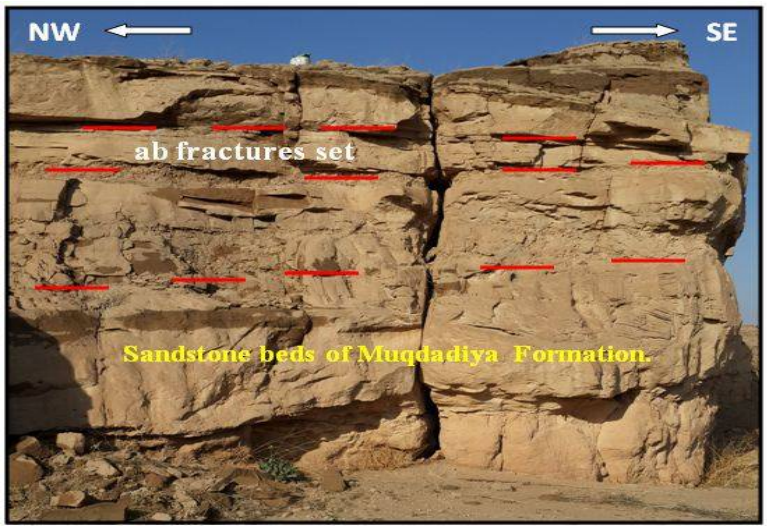


**Plate 1.Shows ab fractures set in Al-Tib Anticline.**

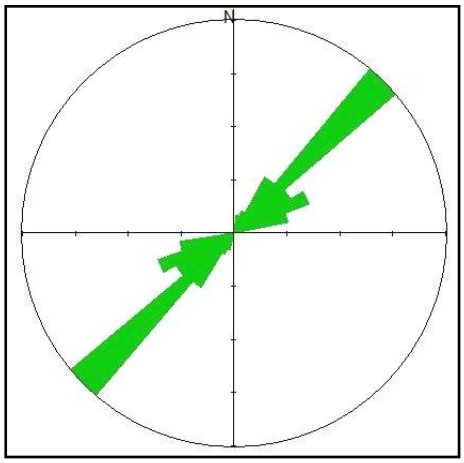


**Figure 5.Rose diagram of ac fractures set direction of the study area which is perpendicular to Al-Tib fold axis.**

a:b:


**Plate 2. Shows ac fractures set a:ac Joint b:ac vein in Al- Tib Anticline.**

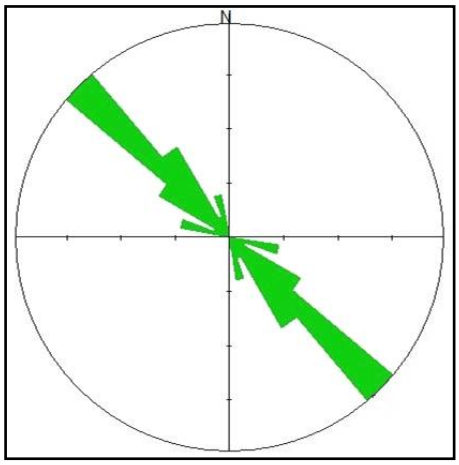


**Figure 6.Rose diagram of bc fractures set direction of the study area which is parallel to Al-Tib fold axis.**

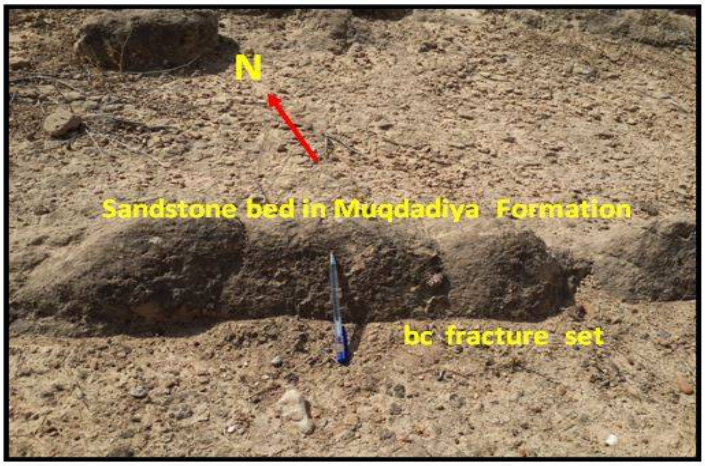


**Plate 3. Shows bc fractures set in Al-Tib Anticline.**

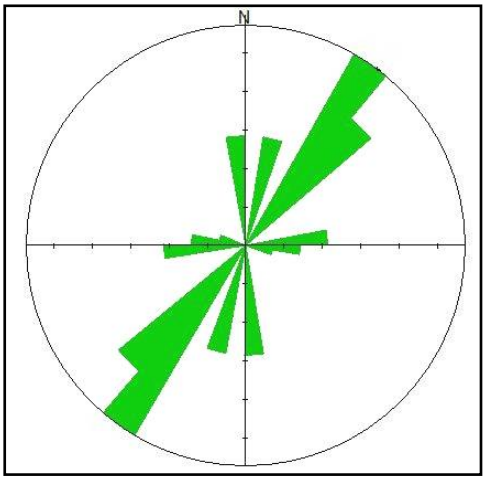


**Figure 7.Rose diagram of (hko acute about a) fractures system direction of the study area which is perpendicular to Al-Tib fold axis.**

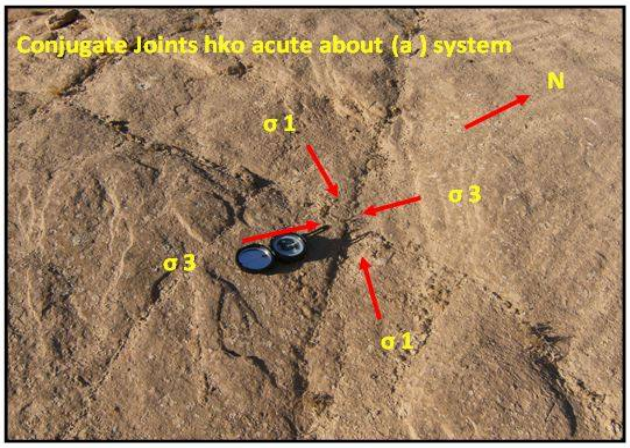


**Plate 4.Shows hko acute about a fractures in Al- Tib Anticline.**

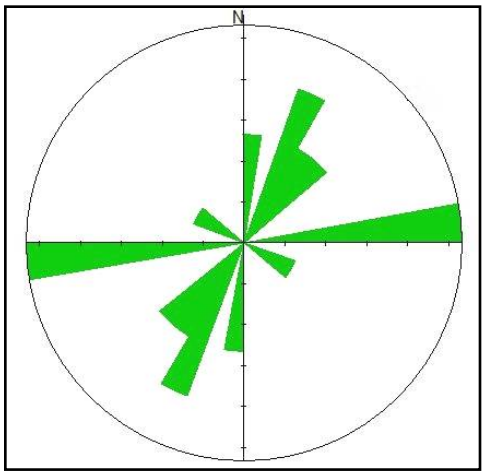


**Figure 8. Rose diagram of (hko acute about b) fractures system direction of the study area which is perpendicular to Al-Tib fold axis.**

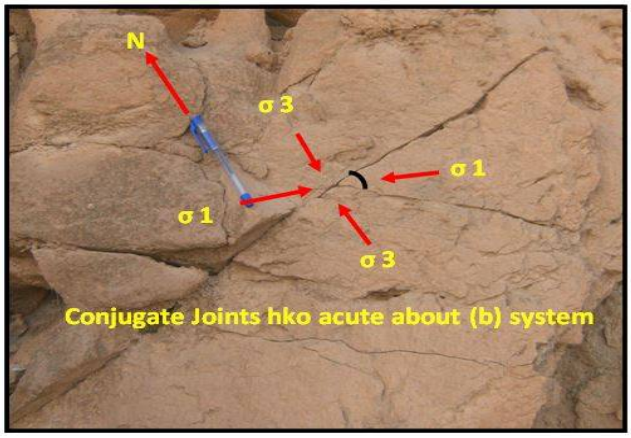


**Plate 5. Shows hko acute about b fractures in Al- Tib Anticline.**

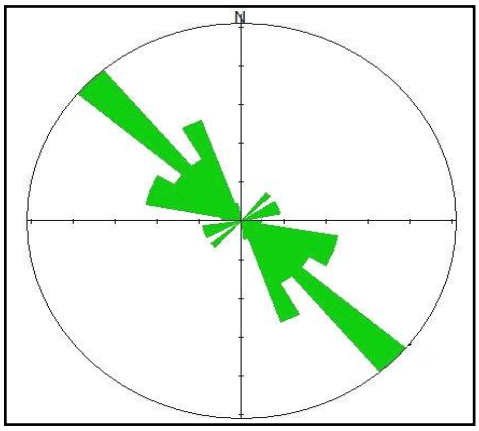


**Figure 9.Rose diagram of (hol acute about a) fractures system direction of the study area which is parallel to Al-Tib fold axis.**

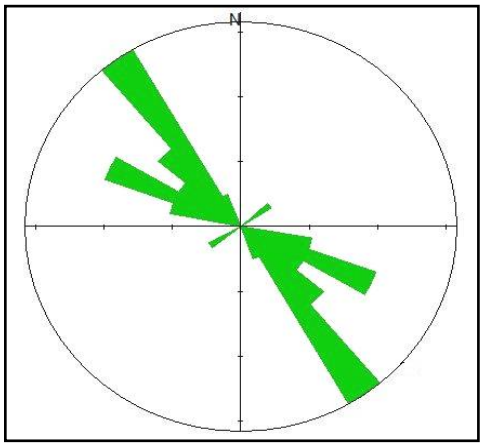


**Figure 10.Rose diagram of (hol acute about c) fractures system direction of the study area which is parallel to Al-Tib fold axis.**

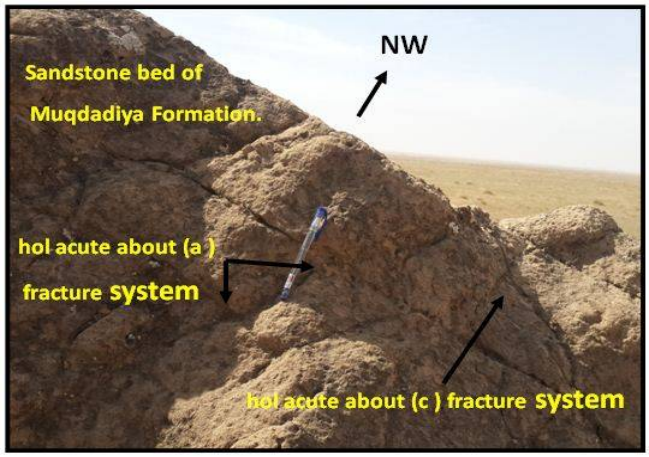


**Plate 6.Shows hol acute about (a andc) fractures system in Al-Tib Anticline.**

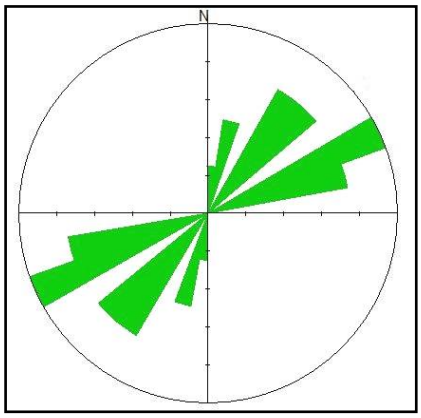


**Figure 11.Rose diagram of (okl acute about b) fractures system direction of the study area which is perpendicular to Al-Tib fold axis.**

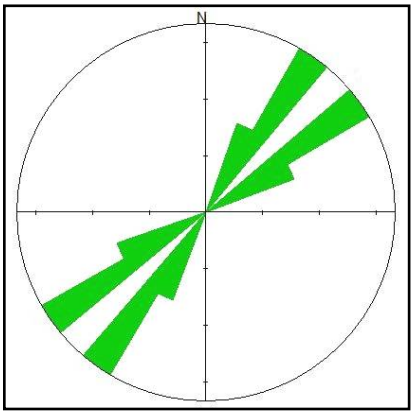


**Figure 12.Rose diagram of (okl acute about c) fractures system direction of the study areawhich is perpendicular to Al-Tib fold axis.**

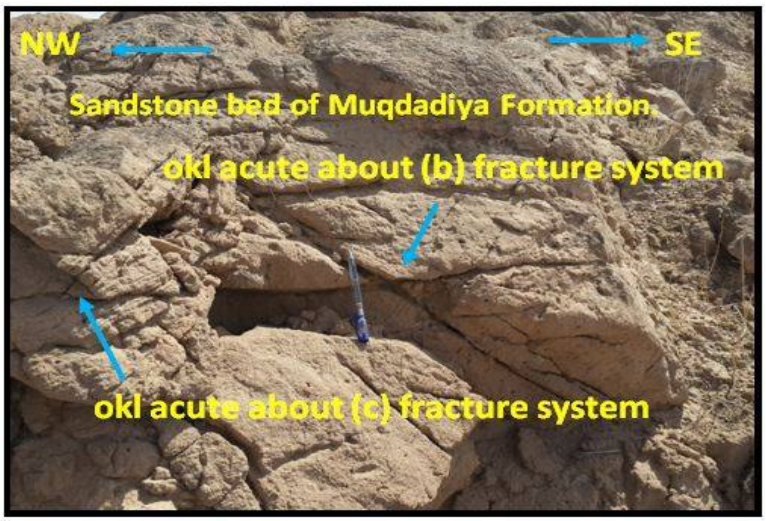


**Plate 7.Shows okl acute about (b and c) fractures system in Al- Tib Anticline.**

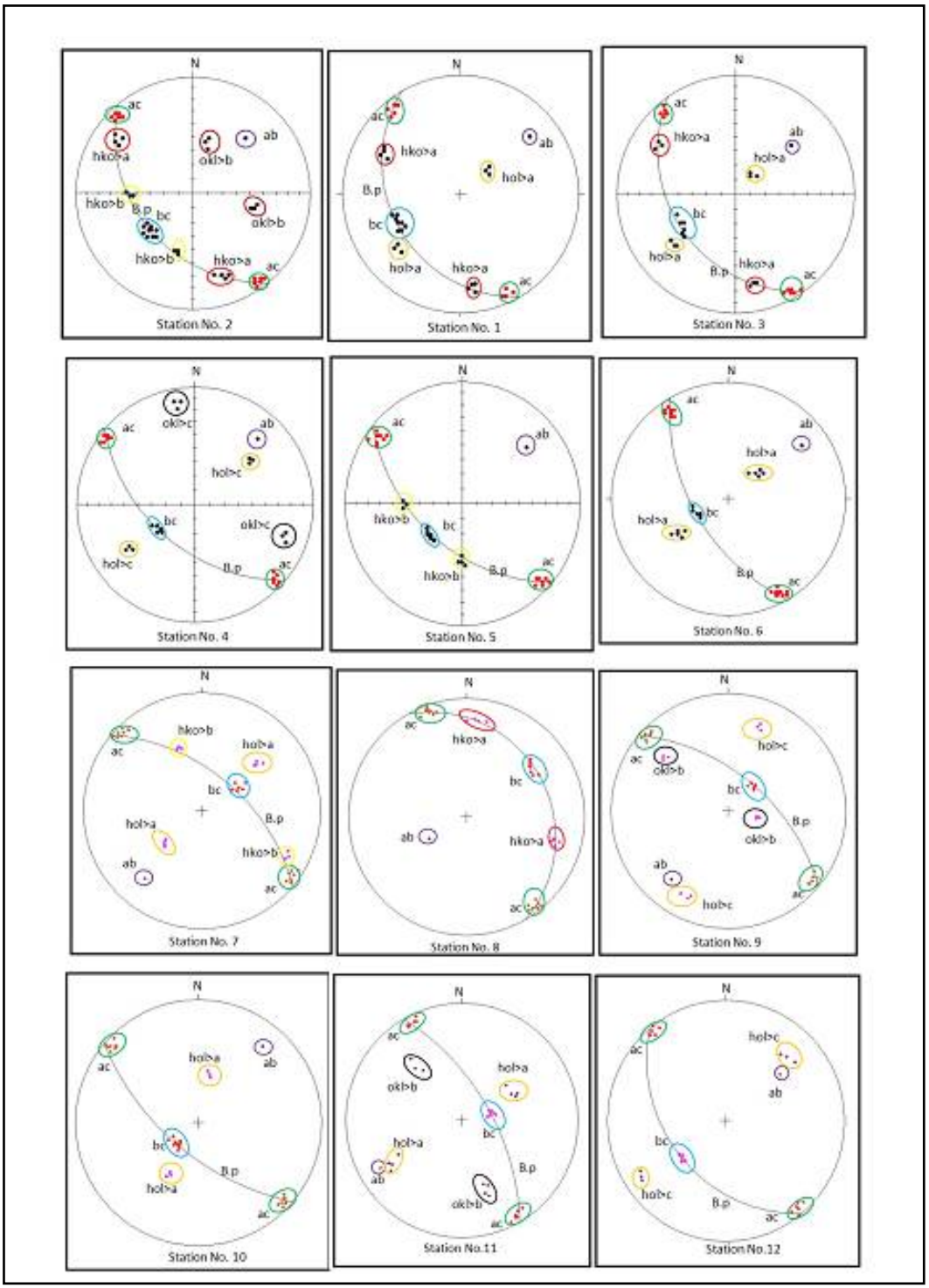


**Figure 13. Stereographic projections for different sets and systems of Al-Tib Anticline in (12) stations**

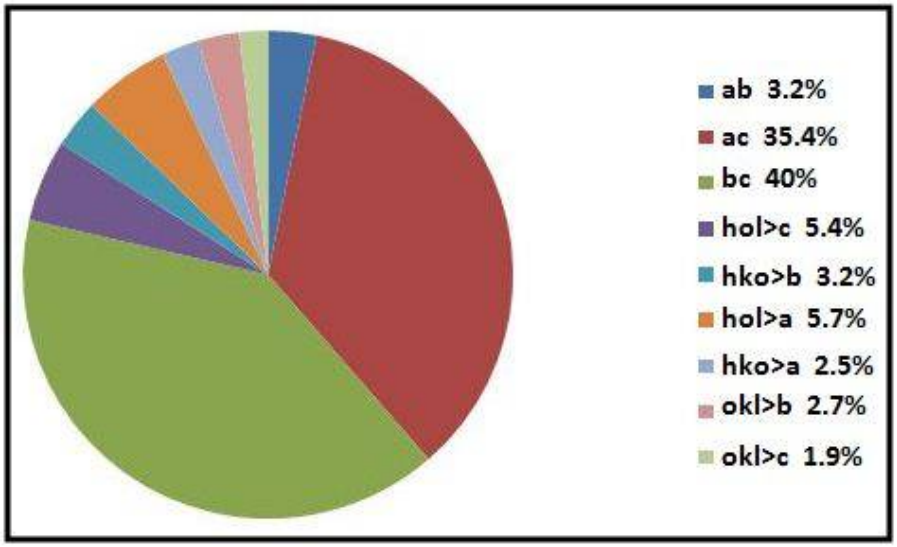


**Figure 14.Shows Shear and Tension Fractures Ratio of Al- Tib Anticline in the study area.**

**Table 1.Shows arrangement of the fractures according to it percentage of Al- Tib Anticline in the study**

| Shear Fracture Type | Percentage % | Forming |
|---|---|---|
| hol acute about a | 5.7 | Early stage of folding, the oldest |
| hol acute about c | 5.4 | Early stage of folding, the oldest |
| hko acute about b | 3.2 | Early stage of folding, the oldest |
| okl acute about b | 2.7 | Early stage of folding, the oldest |
| hko acute about a | 2.5 | Last stage of folding, the youngest |
| okl acute about c | 1.9 | Last stage of folding, the youngest |

*Indian Journal of Natural Sciences* www.tnsroindia.org.in ©IJONS

*Vol. 9 / Issue 50 /October 2018* *International Bimonthly* *ISSN: 0976 – 0997*

RESEARCH ARTICLE

# Video Data Image Compression using Block Truncation Method with Adaptive Motion Estimation Technique

Ebtisam F.Khanger* and Lina Awad and Ban Sabah

Department of Astronomy and Space, College of Science, University of Baghdad, Iraq.

Received: 20 July 2018 Revised: 23 Aug 2018 Accepted: 26 Sep 2018

***Address for Correspondence**
**Ebtisam F.Khanger**
Department of Astronomy and Space,
College of Science, University of Baghdad, Iraq.
Email : dr.efk33@yahoo.com



**ABSTRACT**

Digital image sequence processing has been an attractive research area because an image sequence, as a collection of images, may provide much compression than a single image frame. In this research, Block Truncation compression technique. This is technique depend on adopting the good points of other techniques. As well as algorithm of efficient block's position has been adopted to achieve this research. Also in this paper was introduce A modify of the orthogonal search algorithm (OSA) for searching scheme has been introduced which is contributed in decreasing the motion searching time of the successive inter frames.

**Key words:** Block Truncation, BTC, Orthogonal Search algorithm ,Video compression ,Motion estimation.

## INTRODUCTION

Effective image and video compression techniques have been active research areas for the last several years. Because of the vast data size of raw digital image and video signals and limited transmission bandwidth and storage space, image and video compression techniques are paramount in the development of digital image and video systems. It is essential to develop compression methods which can both produce high compression ratios and preserve reconstructed quality in order for the creation of highquality, affordable image and video products. Figure (1) represent video compression flow.The degree of data reduction achieved by a compression process or algorithm is called compression ratio, given by:

$$Compressio\,n \quad ratio = \frac{Uncompress\,ed \quad File \quad Size}{Compressed \quad File \quad Size} \qquad ..... \quad (1)$$

Therefore, measuring compression ratio as a function of the reproduced image quality defines the efficiency characteristics of the adopted lossy compression technique, rather than a signal compression ratio in the decompressed pictures.

The equivalent definition to the mean square $(SNR)_{ms}$ is the Peak Signal-to-Noise Ratio (PSNR) defined as [2,3]

$$\text{PSNR} = \frac{[\text{Peak to Peak of f(x, y)}]^2}{\text{MSE}} \quad \text{..... (2)}$$

The PSNR can be represented in decidable (dB) unit as:

$$\text{PSNR} = 10 \log_{10} \left[ \frac{gray \quad scale \quad of \quad image}{MSE} \right]^2 \quad \text{..... (3)}$$

Interframe predictive coding is often used to eliminate the large amount of temporal and spatial redundancy that exists in video sequences. It is also helps in achieving compression purposes. In conventional predictive coding the difference between the current frame and the predicted frame, which is based on the previous frame , is coded and transmitted. The better the prediction, the smaller the error and hence the lowest transmission bit rate. However, when there is motion in a sequence, then a pel on the same part of the moving object is a better prediction for the current pel. the use of the knowledge of the displacement of an object in successive frames is called Motion Compensation [4]. This called Block Matching Algorithm, this algorithm estimates the amount of motion as blocks basis, i.e., for each block in the current frame, a block from the previous frame is found, that is said to match this block, based on a certain criterion .Two of them are :
The Mean Absolute Difference (MAD), defined as :

$$MAD\ (dx, dy) = \frac{1}{mn} \sum_{i=-n/2}^{n/2} \sum_{j=-m/2}^{m/2} F(i, j) - G(i + dx, j + dy) \quad \text{.... (4)}$$

Where *F(i,j)* represents an *(m×n)* macro block within the current frame, *G(i,j)* represent the corresponding macro block within reference frame (past or future), *(dx,dy)* a vector representing the search location .
The Mean-Squared Difference (MSD) cost function is defined as :

$$MSD(dx, dy) = \frac{1}{mn} \sum_{i=-n/2}^{n/2} \sum_{j=-m/2}^{m/2} [F(i, j) - G(i + dx, j + dy)]^2 \quad \text{.... (5)}$$

**Image compression using Block Truncation method**

Most image data compression techniques achieve high data compression ratio. The trade off between data compression remains one of the difficult problems. Maintaining high compression ratios with good image quality is possible at a more or less high computational cost. One of the main goals for image data compression is to reduce redundancy in the image block a much as possible. That is, it is very important torepresent an image with as few bits as possible while maintaining good image quality.

Both compression and decompression algorithms should be simple and efficient.

(BTC) is one of the simple and easy to implement image compression algorithms.[block1] The BTC algorithm involves the following steps:

- Step1: The given image is divided into non overlappingrectangular regions. For the sake of simplicity the blocks were let to be square regions of size m x m.
- Step 2: For a two level (1 bit) quantizer, the idea is to select two luminance values to represent each pixel in theblock. These values are the mean x and standard deviation σ.

$$\bar{x} = \frac{1}{n}\sum_{i=1}^{n} x_i \quad \text{.....(6)}$$

$$\sigma = \sqrt{\frac{1}{n}\sum_{i=1}^{n}(x_i - x)^2} \quad \text{.....(7)}$$

Where xi represents the ith pixel value of the image block and n is the total number of pixels in that block.

- Step3: The two values x and σ are termed as quantizers of BTC. Taking x as the threshold value a two-level bit plane is obtained by comparing each pixel value xi with the threshold. A binary block, denoted by B, is also used to represent the pixels. We can use "1" to represent a pixel whose gray level is grater than or equal to x and "0" to represent a pixel whose gray level is less than

$$B = \begin{cases} 1 & x_i \geq \bar{x} \\ 0 & x_i < x \end{cases} \text{..... (8)}$$

By this process each block is reduced to a bit plane. For example, a block of 4 x 4 pixels will give a 32 bit compressed data, amounting to 2 bit per pixel (bpp).

- Step 4: In the decoder an image block is reconstructed by replacing '1's in the bit plane with H and the '0's with L, which are given by:

$$H = \bar{X} + \sigma\sqrt{\frac{p}{q}} \text{.....(9)}$$

$$L = \bar{X} - \sigma\sqrt{\frac{p}{q}} \text{.....(10)}$$

Where p and q are the number of 0's and 1's in the compressed bit plane respectively.

**Motion Estimation**

The goal of video compression is to remove the redundancy in the video signal.In still image coding, the main task is to improve the transform and entropy coding efficiency. However, the optimal performance of an individual video frame in

video coding is upper bounded by the entropy of its residual frame. Motion estimation plays an important role in video coding by taking advantage of the temporalRedundancy across the sequence. The general goals of motion estimation methods are to improve the prediction accuracy, or to reduce the implementation complexity.

## ORTHOGONAL SEARCH ALGORITHM

The orthogonal search algorithm (OSA) is proposed by A. Puri et. al. in 1987 [3]. It consists of pairs of horizontal and vertical steps with a logarithmic decrease in step size. Two search paths of OSA are shown in Figure 3. Starting from the horizontal searching step, three checking points in the horizontal direction are searched. The minimum checking point then becomes the center of the vertical search step that also consists of three checking points. Then step size is decreased to half and same search strategy is used. The algorithm ends with step size equal to one. For d=7, the SA algorithm requires a total of (3+2+2+2+2+2)=13 checking points. For general case, the OSA algorithm requires [1+4{log2(d+1)}] checking points.

### Interpolation (IBBP)

Interpolation is a simple yet efficient and important method in image and video compression . In image compression, we may only transmit, say, every row. We then try to interpolate these missing rows from the other half of the transmitted rows in the receiver . In this way, compress the data to half . since the interpolation is carried out within a frame, it is referred to as spatial interpolation . In video compression, for instance. In the receiver we may try to interpolate the dropped frames from the transmitted frames . This strategy immediately drops the transmitted data to one third. I or basic concepts of zero – order interpolation, bilinear interpolation, and polynomial interpolation ,readers are referred to signal processing texts . In temporal interpolation, the zero – order interpolation means creation of a frame by copying its nearest frame along the time dimension. The conversion of a 24 – frame –per – second motion picture to a 60 –frame –per – second . [11] .

The IBBP frame model is anew feature of video coding which consists of three pictures ( one p-picture and two BB-pictures ). The P-pictures are predicted from previous decoded (I) .The BB-pictures are bidirectional predicted both from the previous decoded ( I ) and P-picture . This model has been used in this work.

$$f(x,y,t)=\frac{I_2}{I_1+I_2}f(x,y,t_1)+\frac{I_1}{I_1+I_2}f(x,y,t_2) \quad \ldots\ldots(1)$$

## RESULTS

Producing a compression unit for digital security video cameras poses a unique challenge; ideally the encoder should be small and inexpensive, yet powerful enough to compress and transmit live video. In this paper, we will present a BTC based video compression algorithm that solves this problem. The algorithm is of low computational complexity.

The new efficient video image compression using block truncation with different block size is applied to grayEarth the image size (128x128) and reference block size is (4x4)( 8x8) and (16x16) pixel. Also was applied adaptive search for motion Estimation technique and reference block size is( 8x8) pixel .We will show the usefulness of the motion estimation in interframe compression. The compression and motion estemayion are performed using the visual basic. In performance tests of the proposed algorithm apply block truncation and **(OSA)** . The figure (3) represent the origin (Earth) images. Figure (4) represent the reconstruction (I), (p) frame when we apply block truncation block size (4x4). Figure (5) represent reconstruction images (I) and (P) and block different when we apply **(OSA)** used (MAD) criteria with thr.4, in figure shown the block different between (I),(P) frames . Figure (6) represent

reconstruction images (I) and (P) when we apply **(OSA)** used (MSD) criteria with thr.4, in figure shown the block different between (I),(P) frames . Figure (7) represented the frames (I), (B1),(B2) and (P) respectively Where BB-pictures are bidirectional predicted both from the previous decoded ( I ) and P-picture . Table (1) numerical result when we apply block truncation block size (4x4)**.** Table (2) numerical result when we apply block truncation block size (8x8). Table (3) numerical result when we apply block truncation block size (12x12)**,**

## CONCLUSION

From the result we were found the best image reconstruction at block size (4x4)) with good value of compression rati**o** but lowest C.R than block size (8x8)and (16x16). We have presented motion estimation technique, New Three Step Search( OSA), The experimental results show that this new method can significantly reduce the computational complexity and low search time while achieving comparable performance for many video sequences . Also we have found the criteria (MAD) was gave higher number of block different than criteria(MSD) then low C.R when we used(MAD) than (MSD).Threshold (4) was gave highest number of block different than other thresholds.

## REFERENCES

1. S.Immanuel, Dr.G. Josemin, and Becky Alma "Astudy on block matching algorithms for motion estimation" ISSN: 0975-3397 vol. 3 No. 1 Jan 2011.
2. Conzales, R.C. and Woods R.E. "Digital image processing" Addison Wesley,1992.
3. Chalidab H.J.C. "Fast motion vector estimation using multi- resolution-spatiol-temporal correlation" IEEE. Trans. On circuits and systems for video technology, Vol. 7, p. 477-488, June 1997.
4. Dehaan, Blezen, P.W.A.C., and Huijgen H. "True motion estimation with 3- D Reanrsive search block matching" IEEE. Trans. On circuits and systems for video technology, Vol.3, P. 368- 379, Oct. 1993.
5. Doaa Mohammed, Fatma Abou-Chadi (senior member IEEE.)"Image compression using Block truncation coding" February Edition, 2011.
6. A.Gyaourova, C. Kamath, and S.-C. Cheung "Block Matching for object Tracking" October 14, 2003.

**Table 1.Numerical result when we apply block truncation block size (4x4) Comp. ratio (I)= 5.2 PSNR= 30.3**

| Threshold | Tim of search(sec) | No. of block change | Over all comp. ratio | PSNR (B1) | PSNR (B2) | PSNR (P) |
|---|---|---|---|---|---|---|
| 4 (MAD) | 0.411 | 117 | 19.5 | 26.7 | 26.4 | 27.5 |
| 8 (MAD) | 0.232 | 85 | 22.5 | 26.7 | 26.4 | 27.5 |
| 12 (MAD) | 0.161 | 62 | 29.2 | 26.7 | 26.4 | 27.5 |
| 4 (MSD) | 0.411 | 75 | 21.9 | 26.1 | 25.3 | 26.7 |
| 8 (MSD) | 0.232 | 54 | 34.8 | 26.1 | 25.3 | 26.7 |
| 12 (MSD) | 0.161 | 42 | 38.7 | 26.1 | 25.3 | 26.7 |

**Table 2. Numerical result when we apply block truncation block size (8x8) Comp. ratio (I)=7.6 PSNR=28.2**

| Threshold | Tim of search(sec) | No. of block change | Over all comp. ratio | PSNR (B1) | PSNR (B2) | PSNR (P) |
|---|---|---|---|---|---|---|
| 4 (MAD) | 0.415 | 115 | 24.3 | 24.1 | 24.36 | 25 |
| 8 (MAD) | 0.223 | 83 | 27.4 | 24.1 | 24.36 | 25 |
| 12 (MAD) | 0.172 | 59 | 38.2 | 24.1 | 24.36 | 25 |
| 4 (MSD) | 0.411 | 73 | 26.4 | 23.6 | 24.5 | 24.7 |
| 8 (MSD) | 0.232 | 51 | 41.8 | 23.6 | 22.8 | 24.7 |
| 12 (MSD) | 0.172 | 39 | 48.7 | 23.6 | 22.8 | 24.7 |

**Table 3. Numerical result when we apply block truncation block size (16x16) Comp. ratio (I)=9.6 PSNR=27.1**

| Threshold | Tim of search(sec) | No. of block change | Over all comp. ratio | PSNR (B1) | PSNR (B2) | PSNR (P) |
|---|---|---|---|---|---|---|
| 4 (MAD) | 0.43 | 111 | 31.6 | 23.2 | 22.6 | 23.8 |
| 8 (MAD) | 0.24 | 80 | 39.9 | 23.2 | 22.6 | 23.8 |
| 12 (MAD) | 0.175 | 60 | 51.5 | 23.2 | 22.6 | 23.8 |
| 4 (MSD) | 0.43 | 75 | 39.7 | 22.9 | 21.9 | 24.2 |
| 8 (MSD) | 0.24 | 57 | 43.6 | 22.9 | 21.9 | 24.2 |
| 12 (MSD) | 0.172 | 48 | 57.2 | 22.9 | 21.9 | 24.2 |

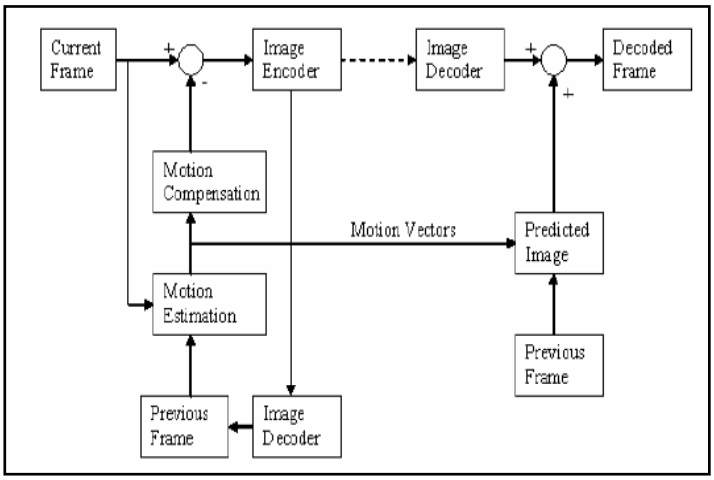


**Fig.1.MPEG /H.26x video compression process flow**

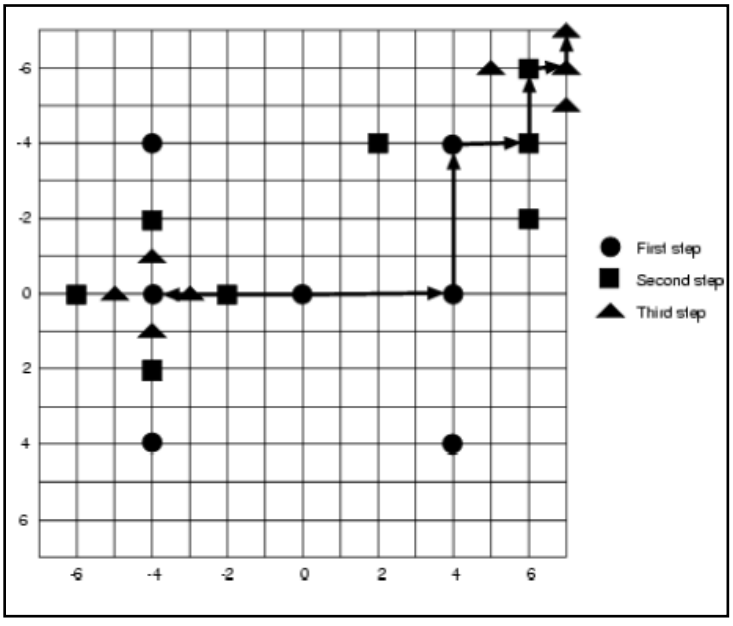


**Fig.2 Two Search paths of orthogonal search algorithm**

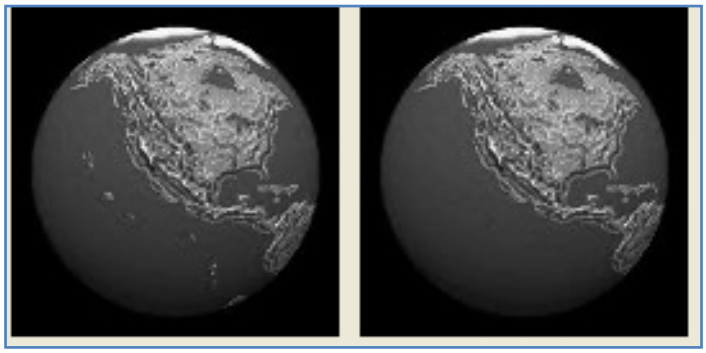

**(I)** **(P)**

**Fig.3. Represent the original images of Earth (I), (P) frame**

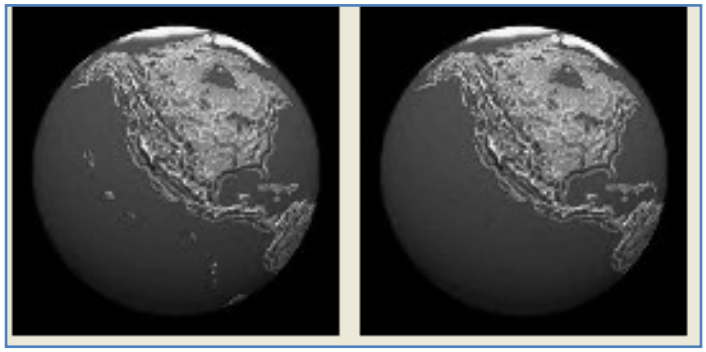

**(I)** **(P)**

**Fig.4. Represent the reconstruction images (I), (P) frames when apply block truncation method, block size (4z4).**

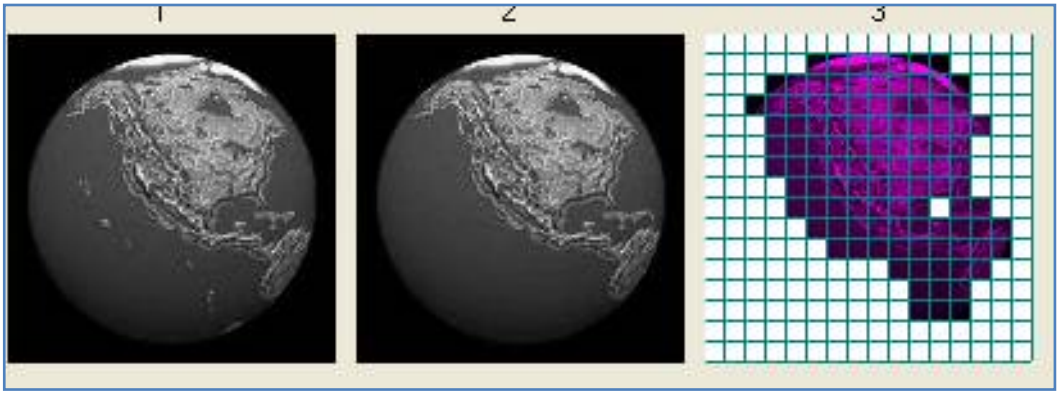

**(I)** **(P)** **Block different**

**Fig.5.Represent the (I), (P) frame and block different when we apply (OSA) used (MAD) ,with thr.4**

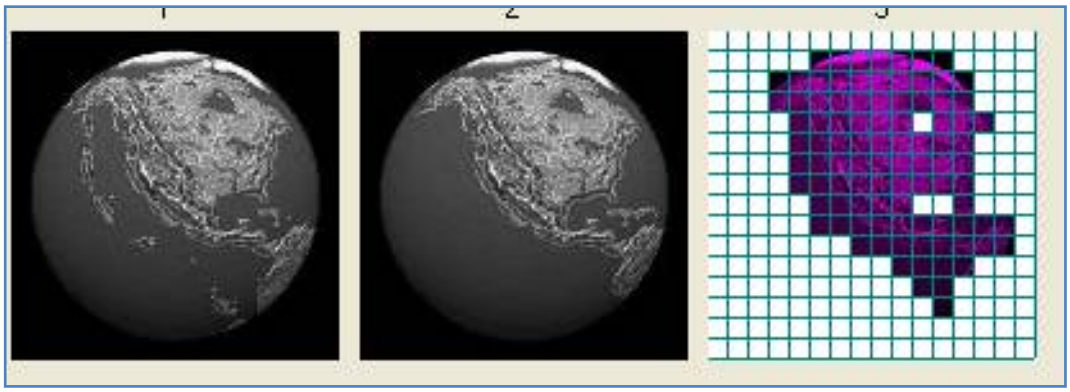

**(I)** **(P)** **Block different**

**Fig.6.Represent the (I), (P) frame with block different when we apply (OSA) used (MSD), with thr.4**

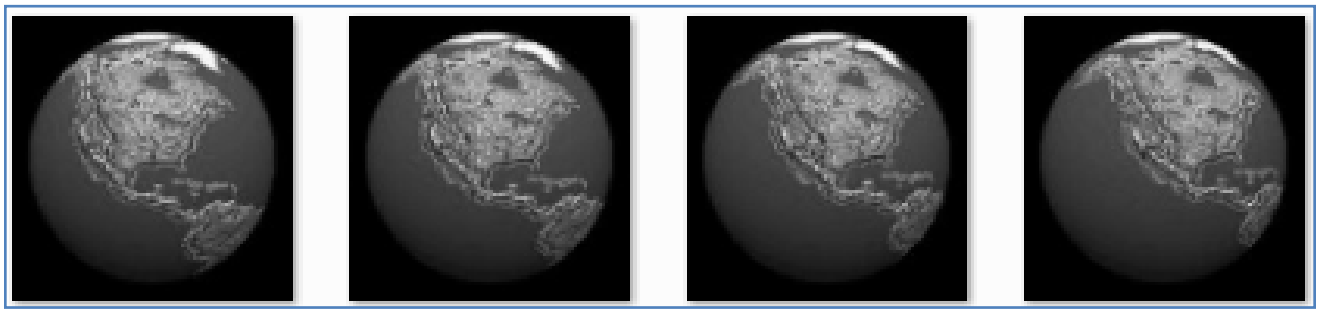

**Fig.7.Represent the (I), (B1),(B2) and (P) frame when we apply (OSA) used (MAD), with thr.4**

*Indian Journal of Natural Sciences* www.tnsroindia.org.in ©IJONS

*Vol. 9 / Issue 50 /October 2018* *International Bimonthly* *ISSN: 0976 – 0997*

**REVIEW ARTICLE**

# An Over Review on Chicken Genome and Its Significance

Chethan Raj R[1]*,Jeevan C[2], Kanaka K K[1], Bhanuprakash A G[1], Naresh V K[1], Balraj S[1], Sneha Smitha Panda[1], Mitek Tarang[1] and Dhanpal[1]

[1]Indian Veterinary Research Institute, Izatnagar, Utter Pradesh, India.
[2]National Dairy Research Institute, Karnal, Haryana, India.

Received: 16 July 2018 Revised: 20 Aug 2018 Accepted: 24 Sep 2018

*Address for Correspondence
**Chethan Raj R**
Department of Geology,
Indian Veterinary Research Institute,
Izatnagar, Utter Pradesh, India.
Email : chethanrajvet@gmail.com



**ABSTRACT**

Chicken research has had a significant impact on fundamental biology. Studies of developmental biology, physiology, immunology, oncology, and virology have traditionally capitalized on the amenable nature of the chicken to genetic studies, and these investigations will now be greatly enhanced by the availability of the chicken genome sequence. The chicken genome diverged from the human genome 310 million years ago.The first build of the chicken genome sequence appeared in March, 2004.Size of chicken genome is 1.2 billion base pairs and approximately 4,000 cM in length.In total, there may be 20,000–23,000 genes; suggesting we still have more to learn about gene prediction. Chicken genomics is likely to have major applications and benefitsin comparative genomics, evolutionary biology and systematics, models of development and human disease, and agriculture.

**Key words:** Chicken, Gene, Genome, Sequence**.**

## INTRODUCTION

Research in birds has contributed to fundamental biology and the chicken has been a popular model organism for at least 100 years, for example, with the discovery of B cells and tumour viruses (1). Ready access to the chicken embryo using incubated eggs and the ease of manipulation make this system ideal for studies of vertebrate development (2). The chicken has been used in many of the classical studies on the molecular basis of patterning in the vertebrate embryo, in particular, the limb bud. In recent times, other model organisms, such as the mouse and zebra fish, have been in greater demand because of increased genetic resources and theability to manipulate their genomes. The chicken EST and genome programs have removed many of these limitations in the chicken. In addition, new tools

such as the electroporation of chicken embryos and the use of RNAi to knock down gene expression are likely to make the chicken embryo a powerful model for the molecular study of development in vertebrates [2].

In meat-type chickens, there has been an increase in the incidence of congenital disorders, such as ascites and lameness, reduced fertility, and reduced resistance to infectious disease. In egg-type chickens, there has been an increase in the incidence of osteoporosis associated with increased egg production. Given the possibility that genetic progress in egg and meat production will reach its limit within the next twenty years [3], priorities in the poultry industry will be to reduce these costs and develop new products. The consumer wants high-quality products (e.g., increased egg shell strength), which requires greater uniformity and predictability in production. With an increased requirement for food safety, there will be a need to reduce the use of chemicals and antibiotics and increase genetic resistance to pathogens. These new traits are difficult and costly to measure by conventional genetic selection, and the developments in poultry genomics in the last few years promises new solutions to these problems.

The chicken is again re-emerging in importance as a model organism [2]. Studies of developmental biology, physiology, immunology, oncology, and virology have traditionally capitalized on the amenable nature of the chicken to genetic studies, and these investigations will now be greatly enhanced by the availability of the chicken genome sequence (International Chicken Genome Sequencing Consortium, 2004).

## Importance of chicken genome sequence

The chicken genome sequence is important for several reasons. The chicken shared a common ancestor with mammals ~310 million years ago (Mya) at a phylogenetic distance not previously covered by other genome sequences. It therefore fills a gap in our knowledge and understanding of the evolution and conservation of genes, regulatory sequences, genomes, and karyotypes. The chicken is also a major source of protein in the world, with billions of birds used in meat and egg production each year. It is the first livestock species to be sequenced and so leads the way for others. The sequence and the 2.8 million genetic polymorphisms defined in a parallel project are expected to benefit agriculture and cast new light on animal domestication. It is a model for the 9600 avian species thought to exist today. Many of the features of the chicken genome and its biology make it an ideal organism for studies in development and evolution, along with applications in agriculture and medicine

## Genome Organization

The chicken genome diverged from the human genome 310 million years ago. It is a modern descendant of the dinosaurs and the first non-mammalian amniote to have its genome sequenced. Diploid chromosome no 78 In addition to a pair of sex chromosomes, chickens have 38 pairs of autosomes: 5 macro-chromosomes, 5 intermediate and 28 microchromosomes. Since each chromosome arm must have at least one obligate crossover, it follows that the micro chromosomes will have the highest rate of recombination. Comparison of genetic maps and genome sequences confirms this expectation, with crossover rates of 2.8 cM/Mb for macro chromosomes and 6.4 cM/Mb for microchromosomes. This is in contrast to 1–2 cM/Mb for most human chromosomes, making the chicken ideal for genetic linkage studies.

The density of genes is highest on the microchromosomes, confirming earlier conclusions based on mapping genes [4] and CpG islands [5]. The estimated number of CpG islands based on bioinformatics approaches depends on the definition in use. In this case [6], ~70,000 CpG islands were predicted in the chicken, with 38% of these located in regions of conserved synteny with mammalian genomes. Since 48% are associated with a gene, CpG island density mimics gene density and is highest on microchromosomes. Conversely, sizes of introns and intergenic regions and density of repetitive elements correlate negatively with gene density and are reduced on microchromosomes. If we assume that genomes balance selective constraints favouring DNA loss over those that favour expansion and that selection will be most efficient in regions of high recombination where linkage of alleles are more readily broken [7],

then the correlation of the densities of genes, CpG islands, repeats, etc. With chromosome size (and therefore recombination rate) is to be expected.

## Genome sequence

The first build of the chicken genome sequence appeared in March, 2004, the first genome sequence of any animal agriculture species. That sequence was done primarily by whole genome shotgun Sanger sequencing, along with the use of an extensive BAC contig-based physical map to assemble the sequence contigs and scaffolds and align them to the known chicken chromosomes and linkage groups. Subsequent sequencing and mapping efforts have improved upon that first build, and efforts continue in search of missing and/or unassembled sequence, primarily on the smaller microchromosomes.

Size of chicken genome is1.2 billion basepairs and approximately 4,000 cM in length [8], Therefore, 1 cM is approximately equivalent to 300 kb of DNA in the chicken. In contrast, 1 cM in humans is about 1,000 kb of DNA, and thus, the chicken genome is about one-third the size of the human genome. It was the low repetitive DNA content, only 11% compared with 40%–50% found in mammals that was a key contributing factor to the quality of the finalassembly. This sequence employed DNA from a single inbred female Jungle Fowl [9] and represented a 6.6-fold coverage of thegenome.

Together with genetic and BAC maps, almost 100,000 contigs were assembled into a scaffold of 907 Mb,or 86% of a 1050-Mb genome. In birds, it is the female that is the heterogametic sex, with single copies of the Z and W chromosomes. Therefore, these chromosomes were poorly represented in the final assembly. In addition, unlike the rest of the genome, the W chromosome has a high repeat content and so very little sequence was assembled. Targeted sequencing of the sex chromosomes will be necessary to complete their assemblies. For autosomes, sequence coverage was 98% based on overlaps with an independent set of BAC clones sequenced to high quality. Overlaps with cDNA clones suggested 5%–10% of genes were missing from the final assembly; gene duplications and GC-rich sequences were a particular problem. The MHC region on chromosome 16, a rich source of duplicated genes, was very poorly represented. Further work to complete the chicken genome sequence to a high quality for comparative genomics and gene discovery is required.

There are 1,965 genetic markers mapped to 50 linkage groups and covering almost the entire 4,000 cM[8]expressed sequence tags (EST), the identification of genetic polymorphisms such as SNP ,about 2.8 million SNP (~1 every400 base pairs) in chicken genes has become a reality. Our laboratory has undertaken an in silico analysis of the chicken EST at the University of Delaware by using a Phred/Phrap/Polyphred/Consed pipeline to identify candidate chicken SNP. Initial scanning of 23,427 chickens EST identified a total of 1,209 candidate SNP, with at least 182 non-synonymous SNP that result in an amino acid change observedValidation of these candidate chicken SNP is on-going[11, 12].Placement of the SNP on the chicken genetic map will enhance marker density, thus allowing for mapping of complex traits through linkage analysis and linkage disequilibrium. Application of SNP to identify disease resistance genes in chickens is of special interest to our laboratory, especially in regards toMarek's disease and coccidiosis. Comparisons of the chicken genome to the human and mouse genomes indicate that there are highly conserved syntenic groups, particularly between the chicken and human [8, 10].

## Genes & proteins

In total, there may be 20,000–23,000 genes; suggesting we still have moreto learn about gene prediction [13]. When used toidentify novel genes missed in the current human gene set (Ensemble22,287 genes), only an additional 37 were predicted, which suggests we have identified most ofthe "conserved" genes found inbirds and mammals. Only 75 processed (or retrotransposed) pseudo geneswere found in the chicken genome[6], comparedwith 15,000 in mammals.The reason for this low numbermay be the sequence specificity ofreverse transcription by avian LINES

(long interspersed elements).Mammalian LINES are more promiscuous and able to retrotransposemost mRNAs.It was hoped that the lack of pseudogenes in the\ chicken would help to identify functional noncoding RNA genes in mammalian genomes via conservation of chromosomal gene location.(Because of their noncoding character, it is difficult to distinguish functional RNA genes from thelarge excess of RNA pseudogenes in mammals by ab initio methods.)

In chicken, 571 RNA genes in 20 distinct families were predicted and only the miRNA and snoRNA families (that usually lie within introns of coding genes) show conserved synteny to the extent that protein coding genes do. That the other noncoding RNA families did not suggests that they may transposethroughout the genome in ways that differ from coding genes571 ncRNA genes, about 2.8 million SNP (~1 every400 base pairs) &Estimated 20,000 to 23,000 protein-coding genes(International Chicken Genome Sequencing Consortium, *Nature* 2004). Comparisons between mammals and birds can also start toaddress questions about gene gains/losses [6]. Comparisons between human, chicken, and *Fugu* suggest a core set of almost one third of all genes (7606) is conserved in all vertebrates. These comparisons also suggest that the rates of gene loss were higher in the avian lineage and fewer gene duplications were found in birds. Careful comparisons detected some genes lost from the chicken lineage, including vomeronasal receptors, caseins, and some genes of the immune system. Similarly, birds have more keratins specific to feathers and mammals have lost the avidin egg proteins. The discovery that all enzymes inthe urea cycle were present but apparently not used for this function in birds was perplexing.

## New tools for genome analysis

Important by-products of any genome project are the resources (cDNA and BAC clones, genetic markers, etc.) and information itprovides for future research [14]. Together with chromosome paints, BAC clones (BPRC) have been used to define cytogenetically all chicken chromosomes [15]. Because of the nearly identical sizes of the microchromosomes in mitotic chromosome spreads, this was not previously feasible. A BAC map with 20-fold redundancy or 91% coverage of the chicken genome has been assembled into 260 contigs [16]. BAC contig maps are under construction for other birds; including turkey, California condor, and zebra finch [17]. These clones can be used to target specific genomic regions and to create whole genome BAC arrays for comparative surveys of avian genomes. These arrays may be able to classify many avian species into unique clades, a notoriously difficult task [17].

From the very start, ESTs and cDNA clones have been important [18], in particular for the prediction of chicken genes. ESTs have been used to create cDNA microarrays [19] and design DNA chips (Affymetrix) for high-throughput gene expression assays. A total of 4532 full-length cDNA clones [20], representing ~25% of known gene predictions in chicken, can now be used in evolutionary and functional studies (available from ARK-Genomics). RNAi and transgenic technologies are now available in the chicken, which when combined with the accessible chicken embryo, makes this a powerful system for functional studies in vivo [21, 22]. There are a number of databases distributed throughout the world, including genome browsers (Ensemble, NCBI, and UCSC), genetic maps (ARKdb and ChickACE), geneexpression (GEISHA), and others, but there is a need to integrate these views into a single Model Organism Database (GMOD).

## Applications of the chicken genome sequence

Taken together with the ready access to chicken embryos and as a major food source, chicken genomics is likely to have major applications and benefits in comparative genomics, evolutionary biology and systematics, models of development and human disease, and agriculture.

### Comparative genomics

A major reason for sequencing the chicken genome was to increase our understanding of the human genome through comparative genomics, for example, to define regions under selection such as coding and regulatory elements [6]. Comparisons with known functional sequences suggested that 75% of coding regions and 30%–40% of regulatory elements are conserved. Comparative genomics has identified ~400 ultra-conserved regions (UCR) greater than 200 bp sharing at least 95% sequenceidentity between human and chicken [22]. Surprisingly, highly conserved, noncoding regions like the UCR often exist far from any predicted gene within so-called "gene deserts" that are apparently free of any known protein-coding genes and are often clustered [23]. Genes with a role in transcriptional regulation and development flank many of these UCR and gene deserts. These regions are often far from genes and may represent distant regulatory signals. Parent-specific gene expression by genomic imprinting is only found in mammals and not birds or lower vertebrates.

Therefore, comparison of imprinted genes in mammals with orthologs in the chicken may uncover features about the origins of imprinting. Comparative mapping suggests these genes cluster on macrochromosomes in regions that preferentially undergo asynchronous DNA replication [25]. Analysis of the chicken region orthologous to the imprinted mammalian *ASCL2–H19* region [26] revealed extensive conservation of gene organization, except *H19*, a critical noncoding imprinted gene. This gene and its regulatory elements were absent from the chicken genome. These studies suggest that imprinted genes were clustered before the evolution of imprinting, an event that occurred after the divergence of birds and mammals ~310 Mya. Subsequently, imprinting control elements, such as the *H19* gene region, must have evolved by duplication and/or transposition into these gene clusters.

A long-standing question in genome evolution has been the question of genome size. The chicken genome is 35% the size of the human and 45% of mouse.In part, this can be explained in terms of the low frequency of repeats, pseudo genes, segmental duplication, and gene duplications [6]. However, these factors only account for 20%–25% of the variation in genomesize, so other factors are at work, possibly a dearth of ancient repeats (that are no longer detectably repetitive) or reduction in cell size and energy conservation [26].

### Developmental biology

Applications in developmental biology are likely to be another major beneficiary of the genome sequence. The chicken has always been a favourite among developmentalbiologists [2]because of easyaccess to the chick embryo and ease of manipulation. These features,when combined with the new tools of genomics, are idealfor testing gene function and predicted regulatory sequences invivo. For example, studies on the conservation of the avian *SOX2*genes have identified neural specific enhancers, confirmed invivo by electroporation of chick embryo neural tubes [27].

### Genetic variation and complex trait analysis

In parallel with the chicken genome sequencing project, a consortium [28,29]gener 2.8 million SNPs from a comparison of the Red Jungle Fowl reference sequence and partial genome scans of Silkie, Broiler, and Layer lines. Resequencing confirmed 94% of the total and 83% of the nonsynonymousSNPs. An initial surprise was that ~70% of SNPs were common to all breeds, suggesting an origin prior to domestication 5,000–10,000 years ago.Another possibility is that their ancestry has been lost because of extensive cross breeding between Asian and western poultry populations. The next steps are toverify a larger sample of SNPs and create high-resolution genetic and linkage disequilibrium maps of chicken populations. These assays will be used to map and identify genes controlling traits of economic and biological interest at quantitative trait loci (QTL). Currently, more than 600 QTL have been mapped using

microsatellites [30]. The availability of a standard set of 10,000 or more SNPs combined with the ease of building structured large resource populations hold much promise towards the identification of genes controlling these traits.

## Animal health and the avian immune system

One area that has benefited most from genomic approaches has been the characterization of the genes and proteins in the avian immune system. The MHC was the first major chicken genome sequence to be assembled [31] and was a surprise, being relatively compact and simpler than those of mammals. Since then, there has been slow progress in the isolation ofavian cytokines and other signaling molecules. The main problem has been their high rate of evolution, limiting their detection using homology to mammalian sequences [32]. Sequencesincluded interleukins, transcription factors, chemokines, differentiationantigens, receptors, genes involved in the Toll pathway, and MHC-associated genes. The discovery of *IL4* and othercytokines involved in the Th2 response was asurprise, since it had previously been speculated that the chickendoes not elicit a typical Th2 response [32]. Thereceptors for *IL10* and *IL13* were also identified, indicating thatthe chicken probably also contained these genes, which are typicalTr1 and Th2 cytokines. This was confirmed by sequencingspecific BAC clones identified assuming conservation of syntenybetween chicken and mammalian genomes.

A comprehensive analysis of the chicken genome sequence has identified many cytokines, chemokines, and their receptors [6]. Even genes once thought to be mammalian-specific, including *IL3, IL7, IL9, IL26, CSMF, LIF,* and Cathelicidin, were found [6]. These are proteins that evolve rapidly and require more effort to detect. A number of orthologs to human chemokines are absent from the chicken genome, including *CCL2, 7, 8, 11, 15, 18, 23, 24,* and *26; CXCL1–7, 9, 10,* and *11,* possibly products of independent gene duplications in mammals. Similarly, missing chemokine receptors included *CCR1,CCR3, CCR10, CXCR3,* and *CXCR6.* The lack of functional eosinophils correlates with the absence of the eotaxin genes (*CCL22, CCL24, CCL26*) and their receptor (*CCR3*). Chickens lack lymph nodes and also the genes for the lymphotoxins and their receptors. *TNF* is also absent, but its receptor, *TNFRSF1A* (*ENSGALG00000014890*) is present, suggesting thatfurther sequencing will reveal this gene in the chicken. Similar analyses have been performed on the leukocyte receptor complex that regulates the activity of Tand B-lymphocytes and NK cells. A model of evolution by repeated birth and death of these Ig-like receptors genes was proposed.

## Selection for Specific Disease Resistance

Selection for specific disease resistance particularly against MD, *E.coli* infectionhas been tried with variable results. However, at present this study is in progressboth at phenotypic and molecular level.At present there is increasing interest in breeding for increased disease resistance. With the availability of the draft chicken genome sequence,the genes that underlie the resistance loci can be identified and utilized

## Control of Emerging Diseases

Some of the emerging diseases like avian influenza are creating havoc lossesin the poultry industry. We may get rid of this problem through geneticmanipulation as well as effective health management practices

## Future opportunities

- Marker assisted selection
- Selection for Specific Disease Resistance
- Control of Emerging Diseases
- Proteomics
- Transcriptomics

- DNA microarray technology
- Gene silencing
- Embryonic stem cell lines.
- Transgenic vehicle and cloning.
- Pharmacogenomics
- Nutrigenomics

## CONCLUSION

Chicken being the most popular model for modern research in fundamental science, studying its genome organisation will further helpful in many aspects of science.Size of chicken genome is 1.2 billion base pairs and approximately 4,000 cM in length and estimated about 20000-23000 genes in its genome. In genetics still opportunities are their starting from gene to genome to proteomics and transfer of information from generation to generation which involves various genetic process could be studied well in chicken as its generation interval is small and large number of offspring can be obtained per parent.

## REFERENCES

1. Brown, G.D. and Gordon, S., 2003. Fungal β-glucans and mammalian immunity. Immunity, 19(3), pp.311-315.
2. Stern, C.D. 2004. The chick embryo—Past, present and future as a model system in developmental biology. Mech. Dev. 121: 1011–1013. 2005. The chick: A great model system becomes even greater. Developmental Cell 8: 9–17.
3. Burt, D.W., Bruley, C.K., Dunn, I., Jones, C.T., Ramage, A., Law, A.S.Morrice, D.R., Paton, I.R., Smith, J., Windsor, D., et al. 1999. Dynamics of chromosome evolution: Clues from comparative gene mapping in birds and mammals. Nature 402: 411–413.
4. Smith, J., Bruley, C.K., Paton, I.R., Dunn, I., Jone, C.T., Windsor, D., Morrice, D.R., Law, A.S., Masabanda, J., Sazanov, A., et al. 2000. Differences in gene density on the Chicken macrochromosomes and microchromosomes: A tool for gene discovery in vertebrate genomes. Animal Genetics. 31: 96–103.
5. McQueen, H.A., Siriaco, G. and Bird, A.P., 1998. Chicken microchromosomes are hyperacetylated, early replicating, and gene rich. Genome research, 8(6), pp.621-630.
6. Hillier, L.W., Miller, W., Birney, E., Warren, W., Hardison, R.C., Ponting, C.P., Bork, P., Burt, D.W., Groenen, M.A., Delany, M.E., et al. 2004. Sequence and comparative analysis of the chicken genome provide unique perspectives on vertebrate evolution. Nature432: 695–716.
7. Hill, W.G. and Robertson, A., 1966. The effect of linkage on limits to artificial selection. Genetics Research, 8(3), pp.269-294.
8. Groenen, M.A., Cheng, H.H., Bumstead, N., Benkel, B.F., Briles, W.E., Burke, T., Burt, D.W., Crittenden, L.B., Dodgson, J., Hillel, J. and Lamont, S., 2000. A consensus linkage map of the chicken genome. Genome Research, 10(1), pp.137-147.
9. FuMIHITO, A.K.I.S.H.I.N.O.N.O.M.I.Y.A., Miyake, T., Sumi, S.I., Takada, M., Ohno, S. and Kondo, N., 1994. One subspecies of the red junglefowl (Gallus gallus gallus) suffices as the matriarchic ancestor of all domestic breeds. Proceedings of the National Academy of Sciences, 91(26), pp.12505-12509.
10. Crooijmans, R.P., Dijkhof, R.J., Veenendaal, T., van der Poel, J.J., Nicholls, R.D., Bovenhuis, H. and Groenen, M.A., 2001. The gene orders on human chromosome 15 and chicken chromosome 10 reveal multiple inter-and intrachromosomal rearrangements. Molecular biology and evolution, 18(11), pp.2102-2109.
11. Suchyta, S.P., Cheng, H.H., Burnside, J. and Dodgson, J.B., 2001. Comparative mapping of chicken anchor loci orthologous to genes on human chromosomes 1, 4 and 9. Animal genetics, 32(1), pp.12-18.
12. Jennen, D.G., Crooijmans, R.P., Kamps, B., Açar, R., van der Poel, J.J. and Groenen, M.A., 2003. Comparative map between chicken chromosome 15 and human chromosomal region 12q24 and 22q11-q12. Mammalian genome, 14(9), pp.629-639.

13. Eyras, E., Reymond, A., Castelo, R., Bye, J.M., Camara, F., Flicek, P., Huckle, E.J., Parra, G., Shteynberg, D.D., Wyss, C. and Rogers, J., 2005. Gene finding in the chicken genome. BMC bioinformatics, 6(1), p.131.
14. Antin, P.B. and Konieczka, J.H., 2005. Genomic resources for chicken. Developmental dynamics: an official publication of the American Association of Anatomists, 232(4), pp.877-882.
15. Masabanda, J.S., Burt, D.W., O'Brien, P.C., Vignal, A., Fillon, V., Walsh, P.S., Cox, H., Tempest, H.G., Smith, J., Habermann, F. and Schmid, M., 2004. Molecular cytogenetic definition of the chicken genome: the first complete avian karyotype. Genetics, 166(3), pp.1367-1373.
16. Wallis, J.W., Aerts, J., Groenen, M.A., Crooijmans, R.P. Layman, D.Graves, T.A., Scheer, D.E., Kremitzki, C., Fedele, M.J., Mudd, N.K., etal. 2004. A physical map of the chicken genome. Nature432: 761–764.
17. Edwards, A.O., Ritter, R., Abel, K.J., Manning, A., Panhuysen, C. and Farrer, L.A., 2005. Complement factor H polymorphism and age-related macular degeneration. Science, 308(5720), pp.421-424.
18. Boardman, P.E., Sanz-Ezquerro, J., Overton, I.M., Burt, D.W., Bosch, E., Fong, W.T., Tickle, C., Brown, W.R., Wilson, S.A. and Hubbard, S.J., 2002. A comprehensive collection of chicken cDNAs. Current biology, 12(22), pp.1965-1969.
19. Burnside, J., Neiman, P., Tang, J., Basom, R., Talbot, R., Aronszajn, M., Burt, D. and Delrow, J., 2005. Development of a cDNA array for chicken gene expression analysis. BMC genomics, 6(1), p.13.
20. Hubbard, T., Andrews, D., Cáccamo, M., Cameron, G., Chen, Y., Clamp, M., Clarke, L., Coates, G., Cox, T., Cunningham, F. and Curwen, V., 2005. Ensembl 2005. Nucleic acids research, 33(suppl_1), pp.D447-D453.
21. Sang, H. 2004. Prospects for transgenesis in the chick. Mechanisms of Development. 121: 1179–1186.
22. Sandelin, A., Bailey, P., Bruce, S., Engström, P.G., Klos, J.M., Wasserman, W.W., Ericson, J. and Lenhard, B., 2004. Arrays of ultraconserved non-coding regions span the loci of key developmental genes in vertebrate genomes. BMC genomics, 5(1), p.99.
23. Ovcharenko, I., Loots, G.G., Nobrega, M.A., Hardison, R.C., Miller, W. and Stubbs, L., 2005. Evolution and functional classification of vertebrate gene deserts. Genome research, 15(1), pp.137-145.
24. Dünzinger, U., Nanda, I., Schmid, M., Haaf, T. and Zechner, U., 2005. Chicken orthologues of mammalian imprinted genes are clustered on macrochromosomes and replicate asynchronously. Trends in genetics, 21(9), pp.488-492.
25. Yokomine, T., Shirohzu, H., Purbowasito, W., Toyoda, A., Iwama, H., Ikeo, K., Hori, T., Mizuno, S., Tsudzuki, M., Matsuda, Y.I. and Hattori, M., 2005. Structural and functional analysis of a 0.5-Mb chicken region orthologous to the imprinted mammalian Ascl2/Mash2–Igf2–H19 region. Genome research, 15(1), pp.154-165.
26. Hughes, A.L. and Piontkivska, H., 2005. DNA repeat arrays in chicken and human genomes and the adaptive evolution of avian genome size. BMC evolutionary biology, 5(1), p.12.
27. Uchikawa, M., Takemoto, T., Kamachi, Y. and Kondoh, H., 2004. Efficient identification of regulatory sequences in the chicken genome by a powerful combination of embryo electroporation and genome comparison. Mechanisms of development, 121(9), pp.1145-1158.
28. Wong, G.K., Liu, B., Wang, J., Zhang, Y., Yang, X., Zhang, Z., Meng, Q., Zhou, J., Li, D., Zhang, J., et al. 2004. A genetic variation map for chicken with 2.8 million single-nucleotide polymorphisms. Nature432: 717–722.
29. Wang, J., He, X., Dai, M., Ruan, J., Chen, J., Zhang, Y., Hu, Y., Ye, C., Li, S., Cong, L., et al. 2005b. ChickVD: A sequence variation database in the chicken genome. Nucleic Acids Research. 33: D438–D441.
30. Andersson, L. and Georges, M., 2004. Domestic-animal genomics: deciphering the genetics of complex traits. Nature Reviews Genetics, 5(3), p.202.
31. Kaufman, J., Milne, S., Gobel, T.W., Walker, B.A., Jacob, J.P., Auffray, C., Zoorob, R., and Beck, S. 1999. The chicken B locus is a minimal essential major histocompatibility complex. Nature 401: 923–925.
32. Staeheli, P., Puehler, F., Schneider, K., Göbel, T.W., and Kaspers, B. 2001. Cytokines of birds: Conserved functions a largely different look. J. Interferon Cytokine Res. 21: 993–1010.

*Indian Journal of Natural Sciences* www.tnsroindia.org.in ©IJONS

*Vol. 9 / Issue 50 /October 2018* *International Bimonthly* *ISSN: 0976 – 0997*

RESEARCH ARTICLE

# Determination of the Paleostress Magnitudes of the Eastern Part of the Low Folded Zone, E- Iraq

Ali Kh. Al-Shwaily* and Mustafa R. Al-Obaidi

Department of Geology, College of Science, University of Baghdad,Iraq.

Received: 13 July 2018 Revised: 18 Aug 2018 Accepted: 25 Sep 2018

***Address for Correspondence**
**Ali Kh. Al-Shwaily**
Department of Geology,
College of Science,
University of Baghdad,Iraq.
E-mail: ali.kh.geosurv@gmail.com



## ABSTRACT

Fault slip data were collected from six fault data stations distributed across an area of 600 km$^2$, located within the eastern part of Low Folded Zone, the Western Zagros Thrust-Fold Belt, within Iraqi territory. Based on Mohr theory, Bott equation and vertical thickness, the magnitudes of the stress at the time of tectonic activities were estimated. Firstly, by using the TENSOR WIN software, the orientations of the principal stresses ($\sigma 1$, $\sigma 2$ and $\sigma 3$). Secondly using the rupture- friction laws, taking into account the depth of the overburden, the vertical stress ($\sigma v$) was calculated. Finally, the three dimensions Mohr representation is used to calculate the magnitudes of the paleostresses. In addition to the magnitudes of the paleostresses, this study shows, the existence of two types of faults, the reactivated faults, which lie on or above the cohesionless friction (sliding) line and Mohr envelope and the stable faults that lie on the great circles of Mohr diagram.

**Key words:** Paleostress, Magnitudes, Mohr circles, Low Folded Zone, Iraq.

## INTRODUCTION

Zagros Thrust-Fold Belt is the deformational product of Cretaceous- present day convergence of the Arabian-Iranian Plates. It extends more than 800 km from southern Turkey through north and north east Iraq to the Strait of Hormuz southwestern Iran. It has a thick folded and thrusted sedimentary pile, accumulated on the northeastern margin of the Arabian Plate (Alavi,2004; and Sherkati et al., 2005).Characterizing the distribution of stress orientationsand magnitudes in the crust is a major challenge in Earth Sciences. Motivation arises from applied purposes such asevaluation and mitigation of geological hazard, engineering activities and resource exploration, but also from academic purposes, such as understanding the mechanicalbehavior of geological materials and deciphering tectonic mechanisms at various scales (Lacombe,2012). The state of stress in rocks is generally anisotropic and is defined by

stress ellipsoid axes, which characterizes the magnitudes of the principal stresses (Kaymakci,2006). The reduced stress tensor concept and stress ratio have been proposed by Angelier (1975), which describe the shape of the stress ellipsoid from whichratios of principal paleostress magnitudes can be calculated. The qualitative and quantitaive analyses of brittle structures, that obtained from paleostress studies provide a reiable key to understand the distribution and evolution of paleostress fields through a succesive tectonic events (Angelier,1989). Despite of the reconstructed reduced stress tensor is linear fuction, it provides a vaulable information about the order and orientation of the three principal stresses are the same as for the actual stress tensor, which can used later in determining the magnitudes of palaeostresses.The study of the relationship between stress magnitudes and development of geological structures is inherently difficult. Determination of stress magnitudes associated with the tectonic history of rock masses relies upon establishing a close relationship between the state of stress and the development of a conspicuous element in the rock itself (Lacombe,2001)

The reactivated fault model has been applied by several authors to determine the magnitudes of the paleostresses (Sassi and Carey, 1987; Angelier, 1989; Salih,1990; Al-Handula, 1997; Al-Diabat,1999 ;and Al-Ubaidi and Al-Kotbah, 2003). The Mohr circle representation of the stress states in the three dimensions can be tested to represent the reactivation of faults. Most paleostress studies, which are executed in Iraq, deal with the orientations of the pricipal stress axes and there is a lack of studies involving quantitative measurementsof their magnitudes. However, only two studies concerned the magnitudes of the paleostresses, the first is carried out by Salih (1994), who studied the paleostress magnitudes within Sinjar anticline and the second, Al-Handula (1997), who studied the magnitudes of the paleostresses of the Low Folded Zone. Most studies concerning fault slip data aim to determine the principal stress orientations. However, the collected and the available data in this study allow to determine the magnitude and the orientation of the paleostresses from their ratios and directions. Furthermore, to estimate the burial depth at time of deformation.

## MATERIALS AND METHODS

### Location

The study area is located within the eastern part of the Low Folded Zone, within Wasit Governorate, along the Iraqi-Iranian international borders, it occupies, approximately, an area of 700 km$^2$ ( Fig. 1). Badrah, Zurbatiyah and Jassan represent the main cities that exist within the study area. It is limited by the following coordinates :

| | | |
|---|---|---|
| Longitudes | 45° 52` 45`` E | 46° 07° 45`` E |
| Latitudes | 33° 07° 35`` N | 33° 22` 37`` N |

### Geological setting

Tectonically,different plate boundaries exist along the Arabian Plate, collisional belt along the NE boundary (Zagros-Tauras thrust belt), rifting and sea floor spreading around the W and SW boundary, along Red Sea and Gulf of Aden, transform Plate boundary along the NW margin, along the Dead Sea and along Owen- Sheba fracture zones in SE boundary and active subduction margin along Makran belt (Emami,2008). Zagros Thrust-Fold belt is a part of the Alpine-Himalayan belt (Beydoun et. al., 1992). The Iraqi territory of the Zagros fold- thrust belt has been divided into several NW-SE trending longitudinal tectonic zones (Buday and Jassim (1987); Al-Kadhimi et al., (1996); Jassim and Goff (2006); and Fouad (2012). The Low Folded Zone represents a part of these longitudinal zones, it is a part of the Outer Platform of the Arabian plate (Fouad,2012), where the study area lies. The main structures within the study are: Hemrin anticline; is the major structure within the study area, it is NNW-SSE trending anticline, 33 km in length and its width ranges from 0.7 km up to 7 km. the NE limb of Hemrin anticline is thrust over its SW limb. KaniSakht anticline; is a narrow Asymmetrical fold, located along the eastern side of Hemrin Structure, with length of about 30 Km and variable width up to 1.5 km. It has NWN – SES trend. The dip of the southwestern limb is about (40 – 65)

degrees, whereas the dip of the northeast limb is about (47 – 52) degree. The study area is characterized by the development of three large scale thrust faults of NW – SE trend, Kachaa Fault extends for 25 km, Cea Koran Fault extends for 25 km in length, Koolic Fault, It runs parallel to the Iraqi – Iranian international borders, extends for 12 km in length.

From topographic point of view, the study area is characterized by its mountainous and hilly terrains, it descends in relief from its NE part, Geomorphologically, the study area is characterized by the hilly terrains, whereas the extreme western part represents the mountainous region (Yacoub, et, al., 2012). The structural elements such as faults and folds beside the lithological variations play an important role in the formation of the geomorphological landforms within the study area (Mahmoud et al., 2018).Stratigraphically, the study area is built up of sedimentary rocks, range in age from Oligocene to Pleistocene, brief description of the stratigraphy is hereinafter:Ibrahim Formation (Oligocene): It is exposed within the eastern part of the study area , this formation represents the oldest rock unit within the hanging wall of Koolic thrust fault, which is thrusted on Dhiban and Jeribe formations (foot wall), it consists of 130m of alternation of marl and marly limestone,The upper part of the formation is dominate of marl with thin beds of limestone while the middle part composed of thickly bed of marlylimestone and alternation of marlylimestone and marl in the lower part (Mahmoud et, al,.,2018).

Serikagni Formation (Early Miocene):It is exposed in the eastern parts of the study area, it consists of 22 m of marl, marly limestone and limestone.Dhiban Formation (Early Miocene):it exists within in the eastern parts of the study area, consists of 30 m of white, nodular textured and massive gypsum. Jeribi Formation (Middle Miocene):It comprises of 70 m of massive dolomitic limestone. Fat'ha Formation (Middle Miocene):The formation consists of cyclic alternation of calcareous claystone, limestone and gypsum. It is divided into two members (Al-Mubarak and Youkhanna,1979; and Ma`ala et, al., 1987), both Upper and Lower members of this formation are exposed in the study area, its maximum exposed thickness is 330 m, Fat'ha Formationis thrustedover Injana Formation along the major thrust fault. Injana Formation (Late Miocene):The formation is exposed only within south western limb of Hemrin anticline, Injana formation consists of alternation of claystone and sandstone**,** The uppermost part is characterized by very thick (up to 30 m) claystone and thin sandstone beds. the total thickness is 350 m. Mukdadiyah Formation (Late Miocene-Pliocene): It consists of 110 m of rhythmic clastic cycles of sandstone and claystone are lenticular as a mode of deposition, with many lateral changes to each other. Bai Hassan Formation (Pliocene – Pleistocene):The formation consists of thick and coarse conglomerates contain lenses of sandstones. its total exposed thickness is 25 m (Mahmoud et. al.,2018).

## Methodology

Under the assumption that a fault slips parallel to the direction of maximum resolved shear stress (Wallace-Bott hypothesis), fault kinematic data can be inverted to calculate palaeo-stress fields and fault-related deformation can be forward modeled in terms of orientations and magnitudes (Angelier, 1979; Aydin,1980; Etchecopar,*et.al.*,1981; Angelier, *et . al .*,1982;Angelier,1984; Michael, 1984; Aleksandrowski,1985;Angelier,1985; Frizzell and Zoback,1987; Hancock, *et . al .*,1987; Julien and Cornet, 1987; Lisle,1987; Pfiffner and Burkhard,1987; Reches,1987; Sassi and Carey-Gailhardis,1987; Caputo and Caputo, 1988; Célérier, 1988; Larroque and Laurent, 1988; Lisle,1988; Angelier,1989; Hardcastle,1989; Hatzor and Reches,1989; Manning and deBoer,1989; Wallbrecher and Fritz, 1989; and Burg**,** 2013)**.**

Three criteria are used to determine the paleostress magnitudes: rupture, fiction line and the vertical stress (Angelier,1989). Anderson (1951) assumed (Anderson classification of faults) the rock was initially intact and unfractured, which means each neoformed fault is related to an independent tectonic event and stress field (Hatcher, 1995). The existence ofneoformed conjugate faults can be easily detected withinthe fault slip data set according to their geometricalproperties (Anderson 1951).The magnitudes of normaland shear stress for conjugate faults correspondto a point on the largest Mohr circle, the largest Mohr circle should be tangent to the failure envelope at the corresponding point (Angelier,1989). However, the value of the vertical stress ($\sigma v$) can be estimated through

determining the lithostatic load and one of the principal stress axes is generally vertical during a tectonic event (rotations may occur later) (Fig.2) (Angelier,1989). at the time of the tectonic event, the depth can be determined as well as the average density of overlying rocks, additional information can be obtained (the value of one principal stress), using the following equation:

$$\sigma v = \varrho g z \quad \ldots\ldots\ldots\ldots (1)$$ (Price,1966; Sibson,1974 and Suppe, 1985)

Where:
ϱ: average density of the rock column
g: the acceleration of gravity
z: the paleodepth

### Calculating the stress ratio (R)

It is possible to calculate the stress ratio when the orientation of the principal stress axes are known, for each fault individually, by using Bott equation (eq. 2)(Al-Ubaidi and Al-Kotbah, 2003). In addition to the Mohr circles, Lisle stress diagram is used to represent the state of stress (Fig.3).

$$R = \tan\Theta Im - In^2 / n - n^3 \ldots\ldots\ldots\ldots (2)$$

Where:
R: the ratio of the principal stress difference
Θ:the pitch of the shear stress direction in the fault plane
I, m, n: are the direction cosines of the normal to the fault surface

TENSOR WIN software is used to compute and analyze the field data, by using the improved right dihedral and PTB methods (Delvaux 1993; Delvaux et al. 1997; Delvaux and Sperner 2003 ) and the orientations of the principal stress axes ($\sigma 1, \sigma 2$, and $\sigma 3$) were calculated.MohrPlotter software is used to produce Mohr diagram and GIS software is used for map layout.

## RESULTS

Within the field work and according to the practical sliding test, the friction angles of the fault surfaces, for different lithologies and smoothness were measured. It was estimated, for the smooth surfces (limestone), about 25°. Whereas, it is 35° for the rough surface (sandstones). The maximum thickness of the overburden, above the fault plane, for each station was also estimated (Table 1). It is worthy to mention that the present study uses 25° friction line angle in all stations. Seventy six fault slip data were collected, within six fault slip data stations, distributed across the study area (Fig.1). From these measurements, the orientations of the principal stress axes ($\sigma 1, \sigma 2$, and $\sigma 3$) and the ratio of the principal stress difference (R) were calculated. The average bulk density for the sedimentary rocks is estimated as 2300 gm/$c^3$ (Salih,1990), the vertical stress is calculated ($\sigma v = \varrho g z$) (Tables 2&3) and Finally, the rock cohesion values of both 0 and 100 bars were used as published of cohesion commonly lie in this range (Sassi and Carey, 1987).

Due to the reverse modes of the measured faults, the measured vertical stress, within each station is equal to the minimum principal stress ($\sigma 3$). For Mohr diagram representation, with fixed $\sigma v$ ($\sigma 3$) and fixed R, the horizontal stresses can be varied until the points representing fault planes are positioned on or nearly close to the two lines of limit sliding (Al-Diabat et, al., 2003). Furthermore, minimum, maximum sliding angles, minimum and maximum horizontal stresses are tested within each station (Table 4 and Figs. 4,5,6,7,8 and 9).

## DISCUSSION

The rocks of Neogene age ( Ibrahim Fn.- Injana Fn.) have been studied to determine the magnitudes of the principal paleostresses based on field analysis, Mohr theory, Bott equation and Lisle diagram. Furthermore, the reactivation of faults have been tested on 3D Mohr diagram, where the slip on discontinuities is controlled by the friction law, so that the points should lie between the sliding line and the failure envelope. The vertical thickness is constant for different typed of faults. Mohr diagrams reflects the relationship between the effective normal and shear stresses on fault surfaces and there is a proportional relationship between the reactivation on faults and the shear stress. The resulted diagrams from the analyzed stations show that some faults were associated with relatively low values of shear stress and high values of normal stresses. According to Mohr diagrams, some of the faults are located within the area that surrounded by the sliding line and the Mohr envelop, whereas, others are found to be along the Mohr circles.

The obtained results show that the estimated paleodepth during faulting ranges from (460m), in station one, up to (1060m) in station six. The calculated vertical stress ($\sigma$ v) is 104 bar in station one up to 239 bar in station six and all the stress magnitudes are calculated at 25° sliding line.

## CONCLUSIONS

Due to compressional stress regime, the collected faults within all stations, which are distributed across the study area, are of a reverse sense, which is in accordance with the oblique collision of the Arabian and Eurasian plates along their curved margins, and to the anticlockwise rotation of the Arabian plate relative to Eurasian plate. Within dry conditions, where the effect of the pore- fluid pressure has not taken into account, it is found that there is a proportional relationship between the paleodepth and the vertical stress ($\sigma$ v). Some poles of fault planes are found to be of low shear stress and high normal stress, which means there is no slip exists under these conditions. This calculation is clearly at odds with reality because movement occurred on these planes and the slip took place, this contraction could be explained as the following:

1.Tthese faults could be formed before the folding, and they changed their orientation after deformation.
2. These faults were formed at the first stage of folding (at the end of ductile stage) and changed their orientations at a later stage of folding.
3. These measurements could be mixed i.e. come from more than one population and represent the product of different stress states, because these are taken from large are.
4. It could be the effect of pore fluid pressure (pore fluid pressure reduces the magnitudes of principal effective stresses) has not been taken into account or it could be some errors in the overburden thickness estimates.
The first two explanations involve a shift of the fault points within the stress circles on the Mohr diagram. Whereas, the last reason would shift the Mohr circle bodily.

The poles of other group of faults mostly indicate high shear stress and low normal stress.. the diagrams also show the presence of two types of faults, the first group is the reactivated faults, which lie between the sliding line and the failure envelop and the second group, represents the faults that distributed along the boundaries of Mohr circles. These Mohr diagrams show that the stress magnitudes were enough to induce reactivation of faults in the area. The overburden pressure estimated by Salih (1994) and Handula (1997) for the Low Folded Zone in close agreement with stress determined by this study. According to these conclusions the two methods (PTB and the right dihedral methods) are applicable to these faults and using frictional sliding consideration allow the estimation the magnitudes of the two principal stresses when the third one is known. A comparison between the magnitudes of the principal stresses of this study and other studies shows the compatibility of the results.

## REFERENCES

1. Al- Diabat, A. A. and Salih, M. R. and Attalah, M., 2003, Magnitudes of the paleostresses at the eastern rim of the dead sea transition fault. Dirasat, pure sciences. Vol. 30,no. 1.
2. Aleksandrowski, P. 1985. Graphical determination of principal stress directions for slickenside lineation populations : An attempt to modify Arthaud's method. Journal of Structural Geology. **7**:73-8 2.
3. Al-Handula, R. E. J., 1997.Structural and stress analyses in the folded area north and northeast Iraq. Unpub. M. Sc. Thesis. Baghdad University, Iraq.
4. Al- Kadhimi, J. M. A., Sissakian, V. K., Fattah, A. S. and Deikran, D. B., 1996. Tectonic Map of Iraq, scale 1:1000000, 2nd edit.GEOSURV,Bagdad.
5. Al- Kotbah, A. M. and Al- Ubaidi, M. R., 2001. Principal stress orientation of Yemen faults in the Mesozoic age, Sana`a unv. Faculty of science Bull. Vol. 14, p. 85-103.
6. Al- Mubarak, M. A. and Youkhanna, R. Y., 1976. Report on the regional geological mapping of Al-Fatah – Mosul Area GEOSURV, int. rep. no. 753.
7. Al- Ubaidi, M. R. and Al- Kotbah, A. M., 2003. The Magnitudes of the paleostresses of the Yemen faults in the sedimentary cover. Sana`a unv. Faculty of science Bull. Vol. 16, p. 95-109.
8. Anderson, E. M., 1951, The dynamics of faulting and dyke formation with applications to Brittain: Edinburgh, Oliver & Boyd, 206 pp.
9. Angelier, J., 1979, Determination of the mean principal directions of stresses for a given fault population: Tectonophysics, v. 56, p. T17-T26.
10. Angelier, J., 1984, Tectonic analysis of fault slip data sets: Journal of Geophysical Research, v. 89, p. 5835- 5848.
11. Angelier, J., 1985, Extension and rifting: the Zeit region, Gulf of Suez: Journal of Structural Geology, v. 7, p. 605-611.
12. Angelier, J., 1989, From orientation to magnitudes in paleostress determinations using fault slip data: Journal of Structural Geology, v. 11, p. 37-50.
13. Angelier, J., Colletta, B., and Anderson, R. E., 1985, Neogene paleostress changes in the Basin and Range: A case study at Hoover Dam, Nevada-Arizona: Geological Society of America Bulletin,v. 96, p. 347-361.
14. Angelier, J., and Mechler, P., 1977, Sur unemethodegraphique de recherche des contraintesprincipalesegalmentutilisable en tectonique et en seismologie: La methode des diedresdroits: Bulletin de SocietieGeologique de France, v. 19, p. 1309-1318.
15. Angelier, J., Tarantola, A., Valette, B., and Manoussis, S., 1982, Inversion of field data in fault tectonics to obtain the regional stress. I, Single phase fault populations: A new method of computing the stress tensor: Geophys. J. R. Astron. Soc., v. 69, p. 607-621.
16. Angelier, J. 1994. Fault slip analysis and paleostress reconstruction. Continental Deformation, 53–100. Oxford: Pergamon Press.
17. Aydin, A.1980. Determination of the orientation of the principal stresses from three or more sets of contemporaneous faults (abstract ) . EOS: Transactions of the American Geophysical Union. V. 61: 1117.
18. Bot t, M . H . P . 1959. The mechanics of oblique -slip faulting. Geological Magazine. 96:109-117.
19. Buday, T. and Jassim, S., Z. 1987. The Regional Geology of Iraq, Vol. 2, Tectonism, Magmatism and Metamorphism. GEOSURV, Baghdad, 352pp.
20. Caputo , M. and Caputo, R. 1988. Structural analysis : New analytic a l approach and applications. AnnalesTectonicæ. V.2: p.84-8 9.
21. Célérier, B. 1988. How much does slip on a reactivated fault plane constrain the stress tensor? Tectonics. V. 7, p. 1257-1278.
22. Delvaux, D. 1993. The TENSOR program for paleostress reconstruction: examples from the east African and the Baikal rift zones. Terra Nova 5(1): 216.

23. Delvaux, D, R Moeys, G Stapel, C Petit, K Levi, A Miroshnichenko, and V San'kov. 1997. Paleostress reconstructions and geodynamics of the Baikal region, Central Asia, Part 2. Cenozoic rifting. Tectonophysics 282(1–4): 1–38.
24. Delvaux, D, and B Sperner. 2003. New aspects of tectonic stress inversion with reference to the TENSOR program. Geological Society, London, Special Publications 212(1): 75–100.
25. Emami, H., 2008. Foreland propagation of folding and structure of the mountain front flexure in pusht-e kuh arc (Zagros, Iran, PhD thesis, university De Barcelona, Spain.
26. Etchecopar, A. , Vasseur, G., and Daignieres, M. 1981. An inverse problem in microtectonics for the determination of stress tensors from fault striation analysis . Journal of Structural Geology. V.3, p.51-65.
27. Fouad, S. F.A., 2012. Western Zagros Fold- Thrust Belt, Part I, The Low Folded Zone. Iraqi Bull. Geol. Min., Special Issue, No. 5, p. 39-62.
28. Frizzell, V. A. and Zoback, M. L. 1987. Stress orientation determined from fault slip data in HampelWasharea, Nevada, and its relation to contemporary regional stress field . Tectonics. V.6, p.89-98.
29. Guiraud, M, O Laborde, and H Philip. 1989. Characterization of various types of deformation and their corresponding deviatoric stress tensors using microfault analysis. Tectonophysics v. 170, p. 289–316.
30. Hancock, P. L., Al -Kahdi, A., B a rk a , A. A., and Bevan, T. G. 1987. Aspects of analyzing Brittle structures . AnnalesTectonicæ. v.1, p.5 - 19.
31. Hancock, PL. 1985. Brittle microtectonics: principles and practice. Journal of Structural Geology. v. 7, p. 437–457.
32. Hardcastle, K. C. 1989. Possible paleostress tensor configurations derived from fault – slip data in eastern Vermont and western New Hampshire. Tectonics. v.8, p.265-284.
33. Hatcher, R. D., 1995. Structural geology: principals, concepts and problems. 2edit., Prentice-Hall, New Jersey.
34. Hatzor, Y. and Reches, Z. 1990. Structure and paleostresses in the Gilboaregion , western margins of the Dead Sea transform . Tectonophysics. v.180, p.87-100.
35. Jaeger, J. C . 1969. Elasticity , Fracture and Flow. 2nd edit. Methuen: London . 268 p p.
36. Jassim, S. Z. and Goff, J. C., 2006. Geology of Iraq. Prague and Moravian Museum,Brno,341pp.
37. Julien, P. and Cornet, F.1987. Stress determination from aftershocks of the Campania - Lucania earthquake of November 23, 1980. AnnalesGeophysicæ. v. 5B, p. 289-300.
38. Kaymakci, N. 2006. Kinematic development and paleostress analysis of the Denizli Basin (Western Turkey): implications of spatial variation of relative paleostress magnitudes and orientations.Journal of Asian Earth Sciences, Vol. 27, p. 207–222.
39. Lacombe, O. 2012. Do fault slip data inversions actually yield ''paleostresses'' that can be compared with contemporary stresses? A critical discussion. R.C. Geoscience. Vol.344, p159- 173.
40. Lacombe, O. 2001. Paleostress magnitudes associated with development of mountain belts: Insights from tectonic analyses of calcite twins in the Taiwan Foothills, Tectonics. Vol. 20(6), p.834–849.
41. Larroque, J. M. and Laurent, P. 1988. Evolution of the stress field pattern in the south of the Rhine Graben from the Eocene to the present . Tectonophysics. v.148, p.41-58.
42. Lisle, R. J., 1979. The representation and calculation the deviatoric component of the geological stress tensor. Journal of structural geology. vol. 1, p. 317-321.
43. Lisle, R. J. 1987. Principal stress orientations from fault s : An additional constraint . AnnalesTectonicæ. v.1, p.155-158.
44. Lisle, R. J. 1988. ROMSA: A BASIC program for paleostress analysis using fault – striation data . Computers & Geosciences. v.14, p.255-259.
45. Ma`ala, Kh. A., Fouad, S. A., Lawa, F. A., Philip, W. and Al-Hassny, N., 1987. Report on the geological investigation for northern sector of the Fatha- Mosul Sulfur District. GEOSURV. Int. rep. no. 1935.
46. Mahmoud, A. A., Ali, M. A., Mohammed, A. J., Al-Mikhtar, L. E., Al-kubaysi, K. N., Hussien, M. S., Al- Obaidy, R. A., Mohammed Ali, S. M., Tawfeeq, G., Jassim, M. K., Shnaen, S. R. and Kareem, A. Y. 2018. Detailed geological mapping of Iraq, Zurbatiyah region, east Iraq, scale 1:250000. GEOSURV. Int. rep. no. 3650.
47. Manning , A. H. and de Boer, J. Z. 1989. Deformation of Mesozoic dikes in New England. Geology. v.17, p.1016-1019.

48. Marzouk, I. M. and Sattar, M. A. 1994. Wrench tectonic in Abu Dhabi, UAE, the Middle east geosciences exhibition and conference, Bahrain, April25-27.
49. Michael, A. J. 1984. Determination of stress from slip data : Fault sand folds . Journal of Geophysical Research. v.89, p.1 1 ,517-1 1 ,526.
50. Pfiffner, O. A. and Burkhard, M. 1987. Determination of paleo-stress axes orientations from fault , twin and earthquake data. AnnalesTectonicæ. v. 1, p. 48-57.
51. Price, N. J., 1966. Fault and joint development in brittle and semi- brittle rocks. Pergamon Press. Oxford, 176pp.
52. Ramsay, J. G. and Lisle, R., J. 2000. Applications of Continuum Mechanics in Structural Geology. London: Acad. Press.
53. Salih, M. R., 1994. Stress field determination (orientation and magnitudes) and their relation to structural trends and overburden thickness for Sinjar and Bashiqa structures, N Iraq. J.Sc. Iraq. Vol. 35, p. 365-380.
54. Salih, M, R. 1990. The structural analysis of the Trimsaran, NW part of the South Wales coalfield. PhD Thesis, University of Wales.
55. Sassi, W. and Carey - Gailhardis, E. 1987. Interprétationméchanique de glissementsur les failles: Introduction duncritère de frottement. AnnalesTectonicæ. v.1, p.139-154.
56. Sibson, R. H., 1974. Frictional constrains on thrust wrench and normal faults. Nature, London. Vol. 249, p. 542-544.
57. Suppe, J., 1985. Principle of structural geology. Prentice-Hall, Inc. Englewood Cliffs, New Jersey.
58. Reches, Z. 1987. Determination of the tectonic stress tensor from slip a long faults that obey the Coulomb yield condition. Tectonics. v. 6, p. 849-861.
59. Wallace, R. E. 1951. Geometry of shearing stress and relation to faulting. Journal of Geology. v.59, p.118-130.
60. Wallbrecher, E. and Fritz, H. 1989. Quantitative evaluation of the shape factor and the orientation of a paleo - stress ellipsoid from the distribution of slickenside striations. AnnalesTectonicæ. v.3, p.110-122.
61. Yacoub, S. Y., Othman, A. A. and Kadim, T. H. , 2012. Geomorphology of the Low Folded Zone. Iraqi Bull. Geol. Min., Special Issue, No. 5, p. 7-37.

**Table 1.stratigraphic succession of the study area**

| No. | Formation | Thickness | Lithology |
|---|---|---|---|
| 1 | Bai Hassan | 1000 m | Alternation of conglomerate and claystone |
| 2 | Mukdadiyah | 900 m | Alternation of pebbly sandstone, sandstone and claystone |
| 3 | Injana | 900 m | Alternation of sandstone and claystone |
| 4 | Fat'ha | 300 m | Alternation of gypsum, marl and limestone |

**Table 2: The calculated principal stress orientations, stress ratio, paleodepth and the vertical stress of the study area, based on the improved right dihedral method**

| Station no. | σ 1 | σ 2 | σ 3 | R | Paleodepth(m) | σ v(bar) |
|---|---|---|---|---|---|---|
| St.1 | 04/265 | 14/174 | 76/011 | 5.3 | 460 | 104 |
| St.2 | 07/225 | 21/1322 | 68/332 | 0.45 | 790 | 178 |
| St.3 | 15/026 | 11/119 | 71/245 | 1.9 | 790 | 178 |
| St.4 | 17/195 | 28/096 | 57/313 | 2.67 | 860 | 194 |
| St.5 | 05/041 | 29/308 | 60/139 | 2.5 | 1060 | 239 |
| St.6 | 02/025 | 21/294 | 69/119 | 4.6 | 1060 | 239 |

**Table 3. The calculated principal stress orientations, stress ratio, paleodepth and the vertical stress of the study area, based on the PTB method**

| Station no. | σ 1 | σ 2 | σ 3 | R | Paleodepth(m) | σ v (bar) |
|---|---|---|---|---|---|---|
| St.1 | 03/056 | 04/326 | 86/183 | 9.2 | 460 | 104 |
| St.2 | 05/225 | 17/134 | 73/331 | 0.33 | 790 | 178 |
| St.3 | 18/038 | 08/131 | 70/243 | 1.28 | 790 | 178 |
| St.4 | 15/198 | 04/107 | 74/004 | 2.75 | 860 | 194 |
| St.5 | 15/198 | 04/107 | 74/004 | 2.6 | 1060 | 239 |
| St.6 | 04/028 | 15/297 | 74/133 | 4.25 | 1060 | 239 |

**Table 4. The maximum and minimum values of principal paleostress**

| | | PTB method | | | | Right dihedral method | | | |
|---|---|---|---|---|---|---|---|---|---|
| Station no | σ 3 (σ v) | σ 1 max. | σ 2 max. | σ 1 min. | σ 2 min. | σ 1 max. | σ 2 max. | σ 1 min. | σ 2 min. |
| 1 | 104 bar | 1030 | 890 | 920 | 797 | 1030 | 800 | 890 | 695 |
| 2 | 178 bar | 1440 | 520 | 1240 | 465 | 1440 | 620 | 1220 | 542 |
| 3 | 178 bar | 1440 | 900 | 1240 | 785 | 1500 | 1100 | 1105 | 825 |
| 4 | 194 bar | 1680 | 1400 | 890 | 760 | 1600 | 1080 | 890 | 760 |
| 5 | 239 bar | 1920 | 1400 | 1600 | 1180 | 1920 | 1150 | 1425 | 881 |
| 6 | 239 bar | 1900 | 1300 | 1500 | 1044 | 1920 | 1640 | 1600 | 1373 |

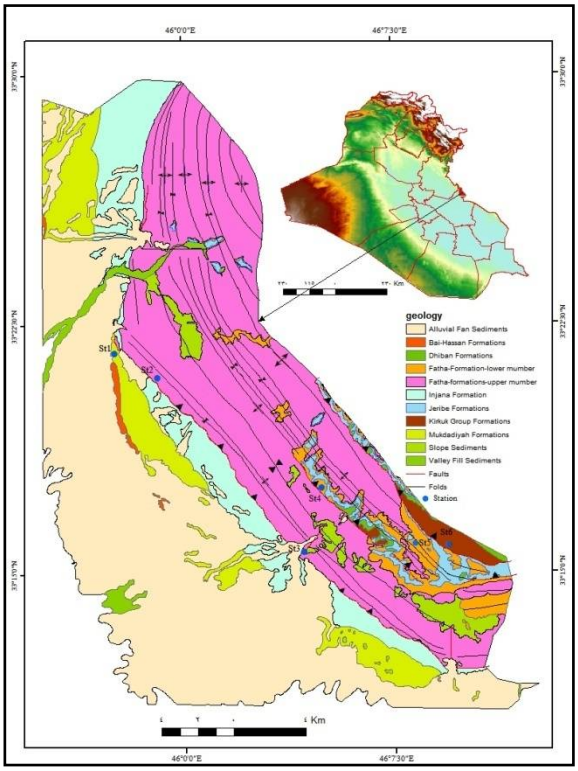


**Fig.1: Location and geological map of the study area (Mahmoud et, al,., 2018)**

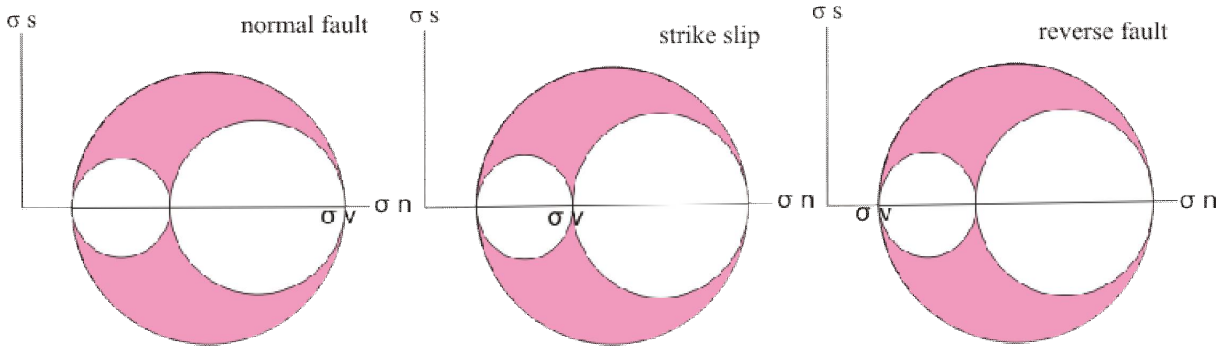


**Fig. 2: the magnitude of vertical principal paleostress (σv) depending on fault type (Angelier, 1989)**

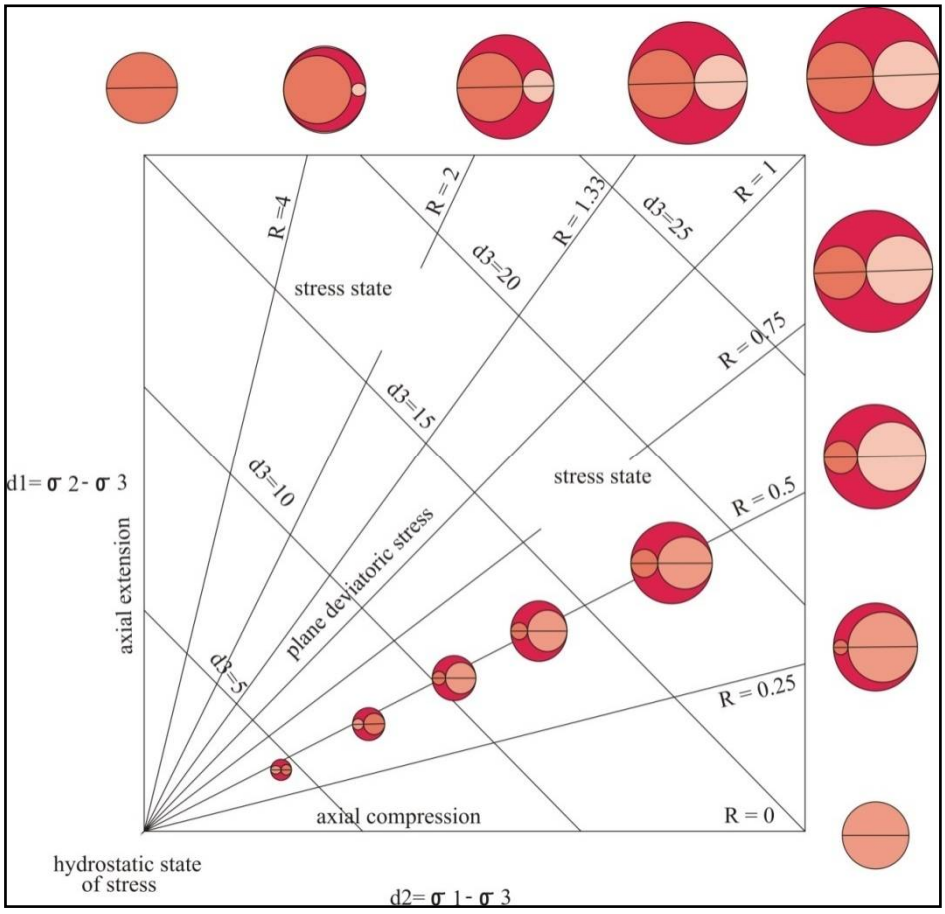


**Fig. 3: Lisle stress diagram (Lisle, 1979)**

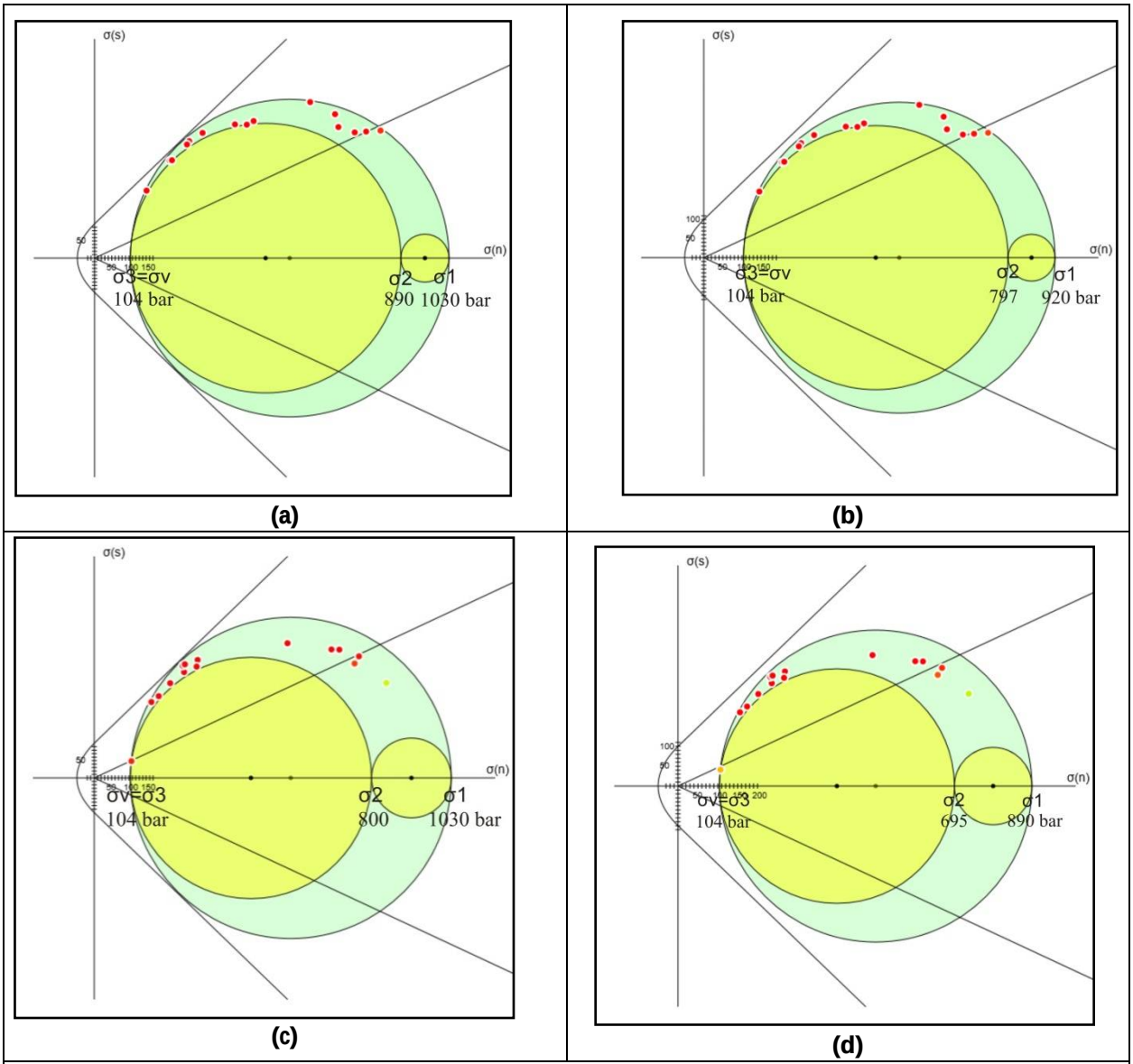


**Fig. 4: Determination of principal stress magnitudes using Mohr circles in station 1: (a) and (b) ;determination the maximum and minimum valuesat 25° sliding line, respectively, based on PTB method. (c) and (d): calculation the maximum and minimum values at 25° sliding line, based on right dihedral method.**

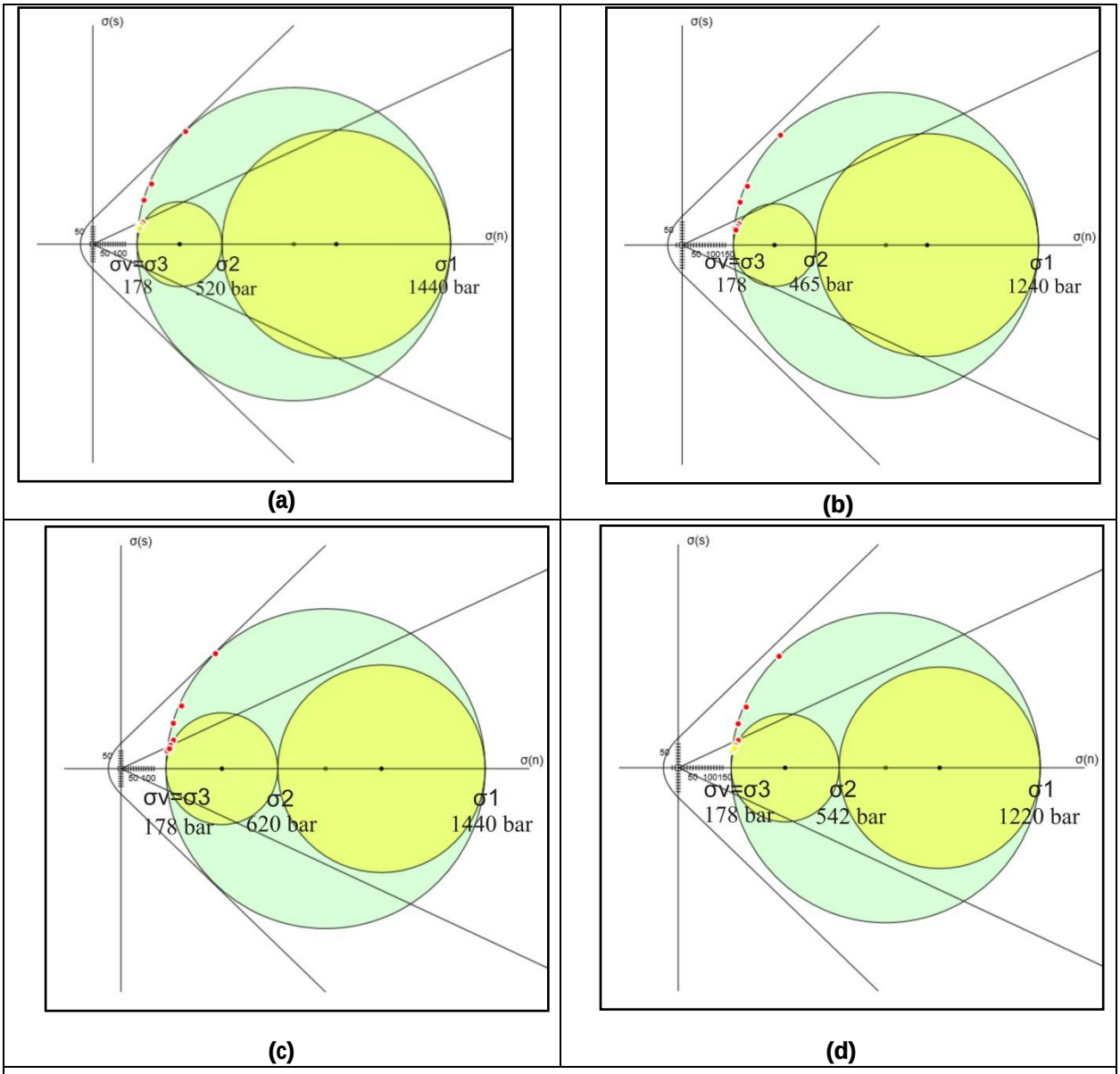


**Fig. 5: Determination of the principal stress magnitudes using Mohr circles in station 2: (a) and (b) ;determination the maximum and minimum values at 25° sliding line, based on PTB method.(c), and (d) calculation the maximum and minimum values at 25° sliding line, based on right dihedral method.**

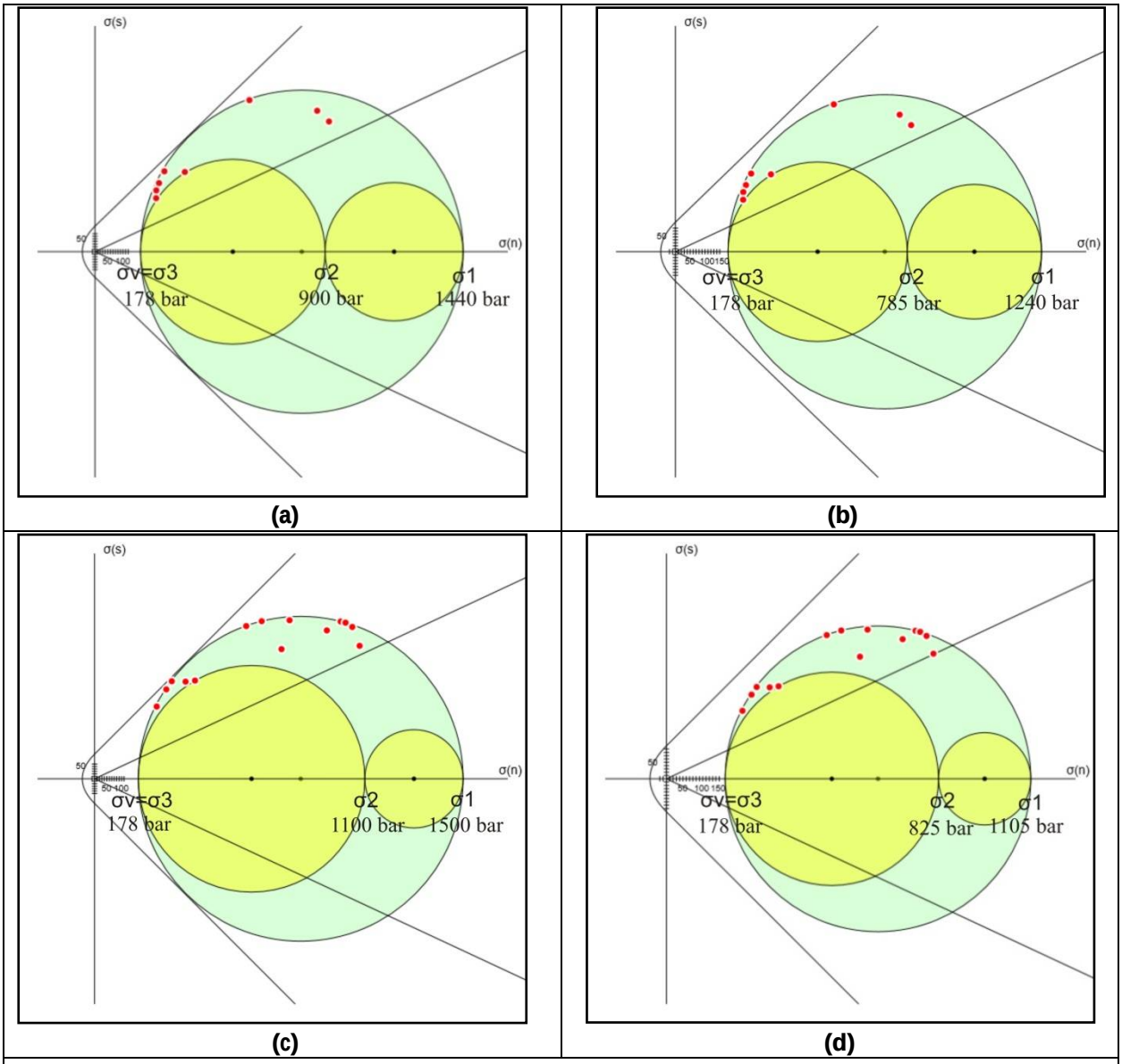


**Fig. 6: Determination of the principal stress magnitudes using Mohr circles in station 3: (a) and (b) ;determination the maximum and the minimum values at 25° sliding line, based on PTB method..(c) and (d) and are determination the maximum and minimum values at 25° sliding line, based on right dihedral method.**

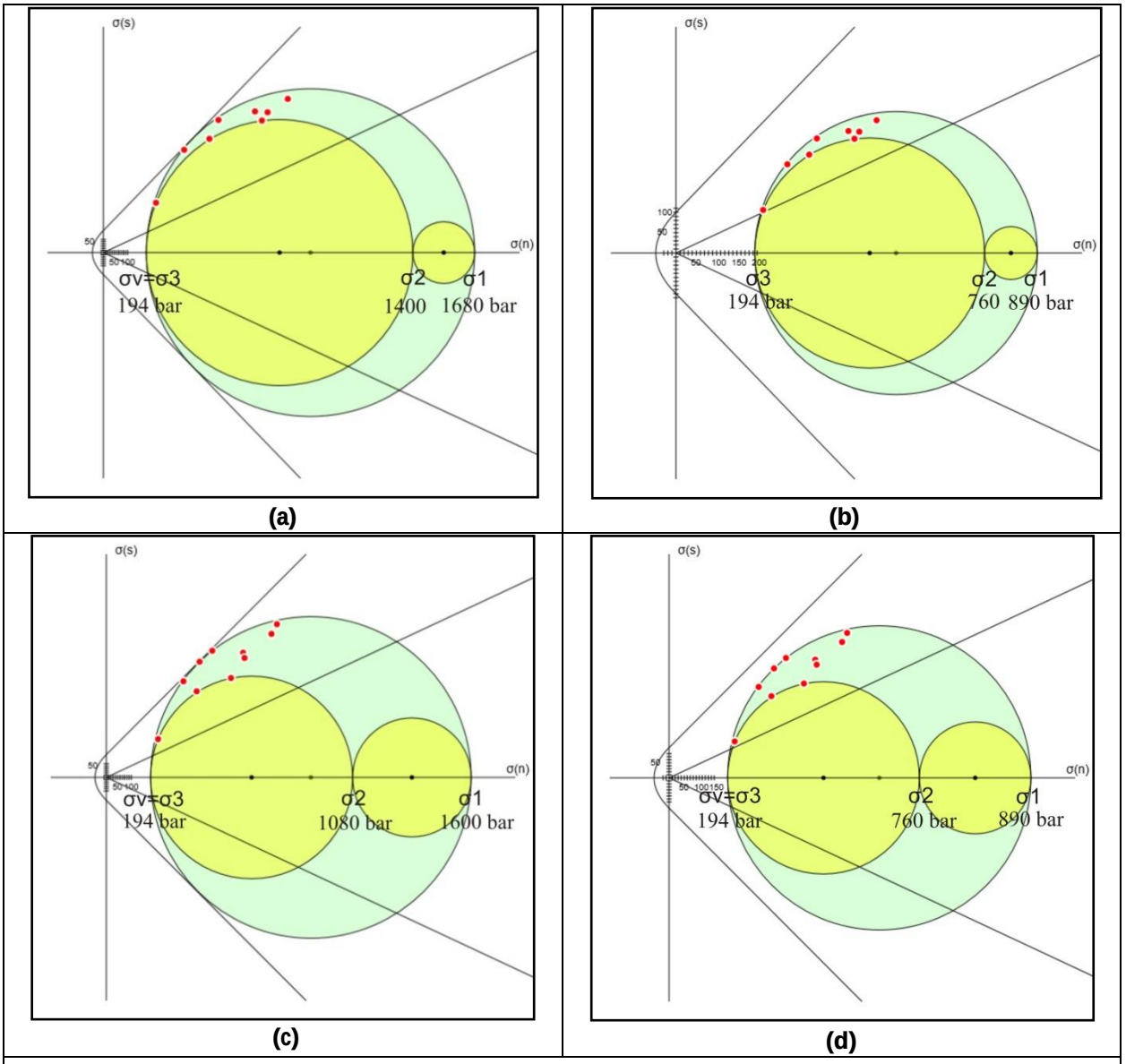


**Fig. 7: Determination of the principal stress magnitudes using Mohr circles in station 4: (a) and (b) ;determination the maximum and minimum values at 25° sliding line, based on PTB method. (c) and (d) are determination the maximum and the minimum values at 25° sliding line, based on right dihedral method.**

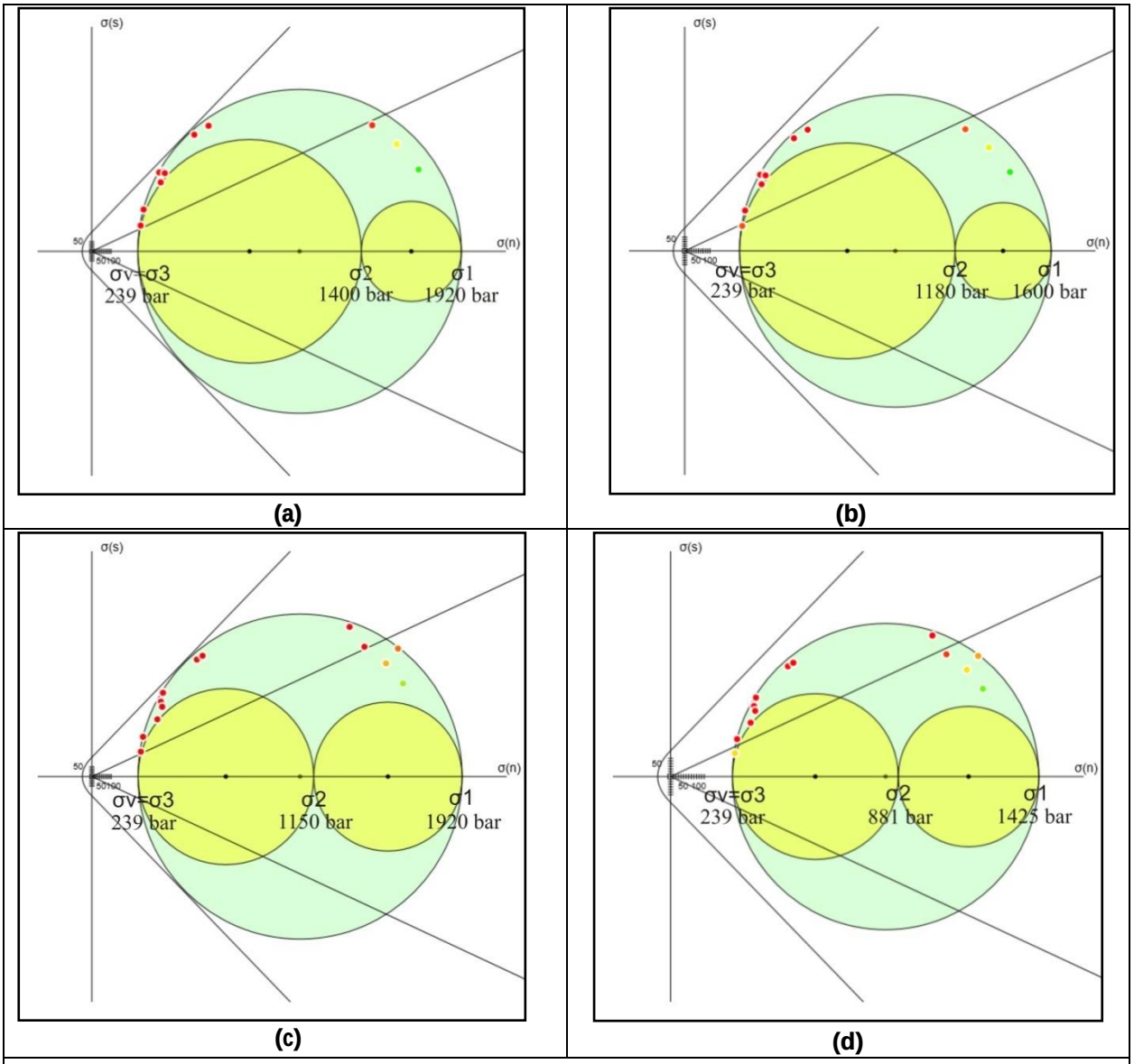


**Fig. 8: Determination of the principal stress magnitudes using Mohr circles in station 5: (a) and (b) ;determination the maximum and the minimum values at 25° sliding line, based on PTB method.(c) and (d) ; determination the maximum and minimum values at 25° sliding line, based on right dihedral method**

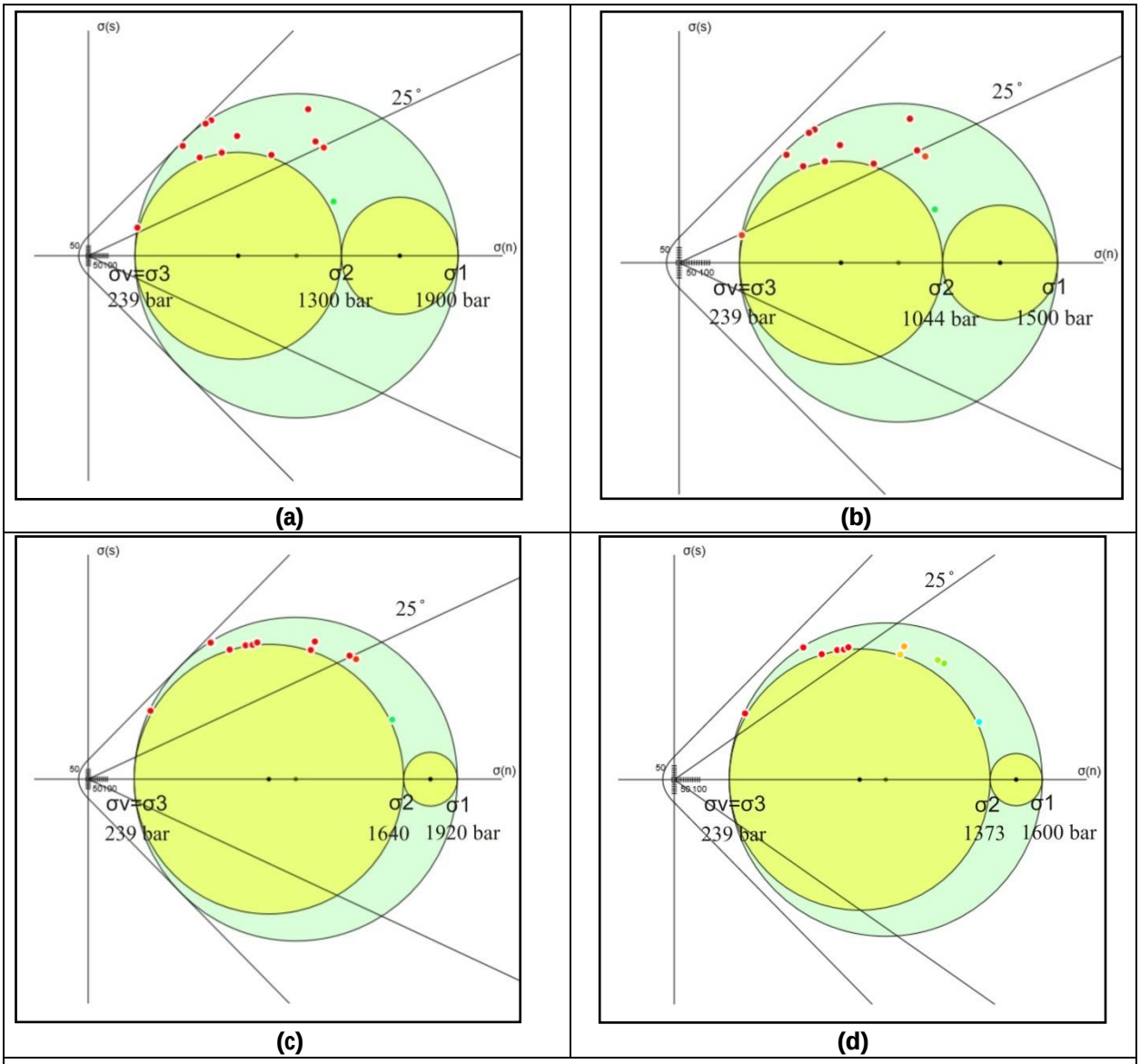


**Fig. 9: Determination of the principal stress magnitudes using Mohr circles in station 6: (a) and (b) ;determination the maximum and the minimum values at 25° sliding line, based on PTB method.(c) and (d) ; determination the maximum and minimum values at 25° sliding line, based on right dihedral method.**

*Indian Journal of Natural Sciences* www.tnsroindia.org.in ©IJONS

*Vol. 9 / Issue 50 /October 2018* *International Bimonthly* *ISSN: 0976 – 0997*

RESEARCH ARTICLE

# Evaluation of *In-vitro* Anthelminthic Activity of *Curcuma longa* Rhizome and *Diploclisia glaucescens* Leaves

Majida Farzana P[1], Ranjith. D[2]*, Sahla Kannatti[1], Surjith KP[3], Muhsina Rahman[4] and Juliet S[5]

[1]College of Veterinary and Animal Sciences (CVAS), Pookode, Wayanad, Kerala, India.
[2]Assistant Professor, Department of Veterinary Pharmacology and Toxicology, CVAS, Pookode, Kerala, India.
[3]Assistant Professor, Department of Veterinary Anatomy, CVAS, Pookode, Kerala, India.
[4] Research Assistant, Department of Veterinary Pharmacology and Toxicology, CVAS, Pookode, Kerala, I India.
[5]Assistant Professor and Head, Department of Veterinary Pharmacology and Toxicology, CVAS, Pookode, Kerala, India.

Received: 10 July 2018 Revised: 15 Aug 2018 Accepted: 12 Sep 2018

*Address for Correspondence
**Dr. Ranjith.D**
Assistant Professor,
Department of Veterinary Pharmacology and Toxicology
College of Veterinary and Animal Sciences
Pookode, Wayanad, Kerala, India.
Email ID: ranjithd@kvasu.ac.in



## ABSTRACT

The objective of the present investigation was to determine the anthelminthic activity of methanolic extract of herbal formulation containing *Curcuma longa* rhizomes and leaves of *Diploclisia glaucescens* in combination at equal proportion respectively. The phytochemical analysis of the formulation revealed methanolic extract showed maximum phytoconstituents and thus selected to study in vitro anthelminthic activity in Indian earth worm (*Pheretima posthuma*). The results of the study revealed a dose dependent anthelminthic activity. However further comprehensive chemical and pharmacological investigation shouldbe carried out to isolate the active compounds and appropriate elucidation of its mechanism of action and ithelps in the development of new pharmaceuticals to treat Helminthiasis.

**Key words:** *Curcuma longa*, *Diploclisia glaucescens,* phytochemical, activity, pharmaceuticals.

## INTRODUCTION

Livestock sector plays a momentous role for the upliftment of Indian economy, among which cattle and buffalo has major role (1). Though multifarious reasons has been elucidated for the production loss in animals, Helminthiasis stands at top infestation with Ascaris spp, Necatator, Trichuris and Ancylostoma species respectively.The major route of infection with worms includes contamination of pastures with eggs or larvae, hands and utensils contamination and also through skin penetration (2). World Health Organization (WHO) estimates an approximately 1.5 billion of the population in the world are infested with worms and ubiquitous in sub-tropical and tropical regions of America, Africa, China and Southeast Asia (3). The conventional and synthetic anthelminthic drugs becomes ineffective against various helminthic pathogens and they may also possess unwanted side effects and interactions causing afflictions in host. In these circumstances, developing a safe and effective drugs is a challenging tasks for scientific community to deal with this threat (4).

Since time immemorial, our system of traditional medicine and folklore claims that the medicinal plant as a whole or their parts being used for all types of ailments with multifarious activities like anticancerous, anti-inflammatory, analgesic, anthelminthic and antibacterial etc. Herbal medicines, because of their higher margin of safety and lower cost, were of good demand in both developed and also developing countries for primary health care with broader biological and medicinal activity (5). Multiple number of herbs has been screened for anthelminthic activity including seeds and latex of *Carica papaya*, leaf extract of *Coleus blumei,* fruit juice of *Ananas comosus,* twig extract of *Codiaceum variegatum,* Seed infusion of *Leucana leucocephala*, chloroform extract and hexane extract of *Morinda citrifolia* etc (6). The present investigation was carried out to disclose the anthelminthic activity of herbal formulation containing rhizomes of *Curcuma longa* and leaves of *Diploclisia glaucescens* respectively.

*Curcuma longa* Linn (Zingiberaceae) is a perennial herb with short stem and long oblong leaves. It contains oblong or pyriform, cylindrical or ovate rhizomes, usually branched and yellowish brown in colour with characteristic odour and pungent bitter in taste (7). The pharmacological use of turmeric includes analgesic, antibacterial, antioxidant, expectorant and flavouring agent. The rhizome powder is commonly used for the treatment of various inflammation as household remedy on empirical basis (8). *Diploclisia glaucescens* (Blume) Diels is a climbing deciduous shrub of family *Menispermaceae*, frequently found in moist and evergreen forests up to 1500 m and spread over India, Southern China, Sri Lanka and Southeast Asia (9). The leaf extract of *Diploclisia glaucescens* commonly given to Tanchangyas tribes for cure of diarrhoea in Rangamati, Bangladesh. Leaf powder with milk is given in gonorrhea, syphilis and biliousness and the stem part is used in diabetes, asthma and kidney stone in India (10). The seeds, stem and roots of *D.glaucescens* reported the isolation of 20-Hydroxyecdysone along with proaporphine alkaloid like stepharine, triterpenoids serjanic acid, phytolaccagenic acid and their glycosides (11). The leaves of *D.glaucescens* along with gingelly oil and coconut oil applied externally for sprain treatment.

The present study is an attempt in this regard to study the anthelminthic activity of herbal formulation containing an equal mixture of *Curcuma longa* rhizome and leaves of *Diploclisia glaucescens* against *Pheretima posthuma*, an Indian earth worm.

## MATERIALS AND METHODS

### Plant materials and their extraction

The rhizomes of *Curcuma longa* and leaves of *Diploclisia glaucescens* were collected in the month of June-August 2017 locally from the Meppadi regions of Wayanad district of Kerala and were authenticated by MS Swaminathan Research Foundation, Wayanad. The collected materials were shade dried and subjected to pulverization and sieved to get powder of uniform size. The powdered plant materials was extracted with different solvents in their increasing

order of polarity which includes petroleum ether, chloroform, ethyl acetate, methanol,ethanol and water by using Soxhlet apparatus continuously for 70 hrs respectively. Each time the plant material was dried and later extracted with next higher polar solvents (following the strategy of extraction in series of increasing the solvent polarity). All extracts were concentrated in Buchi rotary evaporator, followed by removal of traces of solvent by using desiccator and kept under refrigeration condition till further use. Each solvent extract and standard drug Albendazole were dissolved in 20% of Tween 80 in distilled water (v/v).

### Phytochemical screening

The dried extracts were reconstituted with suitable solvents and are subjected to multifarious screening protocols for identification of secondary metabolites from the herbal formulation such as alkaloids, flavonoids, glycosides, saponins, tannins, terpenoids / steroids (12)

### Experimental worms

All the experiments were carried out in Indian adult earthworms (*Pheretima posthuma*) of equal length and size, due to its anatomical significance with intestinal roundworm parasites of human beings (13). They were collected from moist soil and washed with normal saline to remove all unwanted organic matters including fecal matters.

### Administration of Albendazole

Albendazole (25 mg/ml) was prepared by using 20% v/v of tween 80 as suspending agent and used for experimental purpose

### Administration of Extract

The suspension of methanolic extract of *Curcuma longa* rhizome and *Diploclisia glaucescens* leaves of different concentration (25 mg/ml, 50 mg/ml, 75 mg/ml and 100 mg/ml) were prepared using 20% of tween 80 as suspending agent and final volume was made up to 40 ml per petridish for respective concentration. All the groups contains approximately equal length and size of earthworms consisting of six earthwormsindividually in each group were released in to in each 40 ml of desired concentration of drug and extract in the Petridishes.

### Experimental design

The anthelminthic activity was performed according to the method (14) with slight modification. Anthelminthic activity was evaluated on adult *Pheretima posthuma*, an Indian earth worm, as it has anatomical and physiological resemblance with the intestinal round worm parasites of human beings. Earthworms were divided in to six groups (6 each). Each Petridishes were placed with three worms each of two sets of petridishes for each groups. The first group (I) serviced the control group with 20% tween 80 in distilled water, Group II serviced the standard drug Albendazole at a dose level of 25 mg/ml. Group III, IV, V and VI received different doses of methanolic extracts says 25 mg/ml, 50 mg/ml, 75 mg/ml and 100 mg/ml respectively. Observations were made for the time taken for paralysis and death of individual worms respectively. Paralysis was confirmed when no movement of any sort could be observed, except when the worm is shaken vigorously. Death was concluded when the worm neither moved when shaken vigorously nor when dipped in warm water ($50^0$C) followed by fading away of their body colour. The test results were compared with reference standard, Albendazole (25 mg/ml) treated samples (13).

### Statistical analysis

All experiments were performed in triplicates (n=3) and the data are presented as the mean ± standard error mean. Differences between the means of the individual groups were analyzed using the analysis of variance procedure of SPSS software 20 Version (IBM). The significance of differences was defined at the $p < 0.05$.

## RESULTS AND DISCUSSION

Helminthiasis is a significant parasitic disease seen in both humans and animals that reflects both social and economic difficulties throughout the world. Generally, helminths are classified as eukaryotic endoparasites as they live inside the body. Most of the helminthes infections are chronic in nature as they probably cause higher morbidity and distinguished economic loss with more social deprivation in both animas and human beings respectively. World health organization estimates about 2 million people throughout the world affected with parasitic worm infection and the main reason is associated with poor management and inadequate control measures (16). Whilst, numerous efforts has been made to understand the transmission mode and therapeutic probabilities against Helminthiasis in last few decades, still no prominent product has been established to control specific helminthic infestations (15, 16 & 17). In India, occurrence of these infection is very high in wet seasons (as high as 100%), the drugs available in market is of high cost and limited effective control over parasitic infections (18, 19). Plant products are frequently considered to be less toxic and significantly free from side effects than synthetic ones (20). The present investigation was carried out to understand effectiveness of herbal formulation containing *Curcuma longa* rhizome and leaves of *Diploclisia glaucescens* in combination against Indian earth worm, *Pheretima posthuma* respectively. Initially the formulation was extracted with multifarious solvents in the increasing order of polarity range viz. chloroform, ethyl acetate, ethanol, methanol and water. Upon phytochemical analysis shown methanolic extract with maximum phytoconstituents so these extract was selected to study the anthelminthic activity against Indian earthworm. The phytochemical screening of methanolic extract showed the presence of all major phytoconstituents like alkaloids, flavonoids, glycosides, steroids, terpenoids and phenolic compounds. The herbal formulation also tested for the extractive yield, the result of the experiment showed, hydro alcoholic extract with maximum yield of 27.32 % followed by water, methanol and acetic acid yield of 25.68%, 19.79% and 18.63% respectively.

The anthelminthic activity of the methanolic extract of herbal formulation containing *Curcuma longa* rhizomes and leaves of *Diploclisia glaucescens* was tested against Albendazole as standard. From the results, it is observed that the herbal formulation showed potent anthelminthic activity, the activity result revealed dose dependent paralysis ranging from loss of motility to loss of response to external stimuli, which eventually progressed to death from starting dose of 25 mg/ml to 100 mg/ml respectively. The methanolic extract of herbal formulation exhibited dose dependent anthelminthic activity that caused paralysis at 144.52±2.81, 120.33±4.24, 90.17±2.67 and 49.33±2.12 at 25, 50, 75 and 100 mg/ml and death at 180.83±2.43, 168.33±2.49, 117.83±3.91 and 76.67±3.14 at 25, 50, 75 and 100 mg/ml respectively. The standard drug (Albendazole) shows paralysis within 11.67±1.23 min and time of death 76.67±3.14 min. All the test groups showed a statistically significant ($p<0.05$) anthelminthic activity as compared with control and standard group respectively. The observation of the result showed the methanolic extract of herbal formulation as more potent anthelminthic agent and sensitivity of earthworms increased by increasing dosage of the formulation.

The presence of phytochemical compounds such as polyphenols, tannins, saponins, and glycosides may contribute to anthelmintic activity of plant extracts (21-23). Potential anthelmintic activity of plant extracts may due to the presence of tannins in high concentration (24). Tannins are able to disturb the metabolism of Ascaris species through oxidative phosphorylation reaction (25). In addition, tannins can also bind to free protein nutrition which leads to larval starvation (26). Flavonoids can interact with the free proteins of gastrointestinal host or glycoproteins on the worm's cuticula and blocking tubulin polymerization leading to death of worm (27). Saponins causes vacuolization and disintegration of the tegmental worm through changing their cell membrane permeability (28). Glycosides and

steroids are antioxidant agents that decrease nitrate production; it leads to the inhibition of worm development (29). The mechanism of action of natural anthelmintic agents also involves inhibition of glucose uptake system that causing the loss of energy of worm (30). Breaking of mucopolysaccharide membrane structure of helminths will restrict their movement which may cause paralysis and finally the worm's death (31). According to Kundu *et al*. (2015) and Swargiary and Roy (2012), phytochemicals are also involved in blocking of attachment of the parasitic worm to host by damaging of worm's tegumental surface (32). The effects also involve the change of phosphatase enzymes in the tegument of parasites (33).

## CONCLUSION

The present study was conducted to unravel the *in vitro* anthelminthic activity of herbal formulation containing rhizomes of *Curcuma longa* and leaves of *Diplocl*isia *glaucescens* mixture in equal quantity. The examined methanolic extract of herbal formulation exhibited higher anthelminthic activity for both estimated parameters of paralysis and death. With these baseline information, a novel formulation can be prepared as new pharmaceutical drug for the treatment and curing of Helminthiasis. This justifies us the use of present combination used by the tribals of Wayanad regions of Kerala for various ailments including as potent anthelminthic agents. Still and all, further panoramic pharmacological and chemical investigations should be carried out to isolate the active constituents and elucidate appropriate mechanism of action for development of new herbal product.

## ACKNOWLEDGEMENTS

Authors are thankful to Sivan VV, Scientist, MS Swaminathan Research Foundation, Meppadi, Wayanad, Kerala, India for providing necessary raw materials for this research work.

### Conflict of Interest

None Declared

## REFERENCES

1. M. Das, D.K. Deka, A.K. Sarmah, P.C. Sarmah and S. Islam. 2017. Gastrointestinal parasitic infections in cattle and swamp buffalo of Guwahati, Assam, India. *Indian J. Anim. Res*., B 3427. 1-7.
2. WHO, Epidemiology of Soil-Transmitted Helminthiasis, Geneva: WHO, 2011, [Online] Available from: http://www.who.int/intestinal_worms/epidemiology. / en/ [Accessed on 9th September, 2018].
3. WHO, Media Centre: Soil-Transmitted Helminth Infections [Internet], Geneva: WHO, 2014, [Online] Available from: http://www.who.int/mediacentre/factsheets/ fs366/en/ [Accessed on 9th September, 2018].
4. Santhosh Anasuri, Uma Shankar Damu, ShankaraiahPulipaka and MadhuriTekurala. 2017. Phytochemical investigation and antimicrobial anthelmintic activities of the leaves of *Rubus moluccanus* Linn. J. of Pharmacog. and Phytochem. 6(6): 1392-1396.
5. SapanaKhandelwal and Parul Sharma, TribhuwanSingh ,RekhaVijayvergia. 2012. Anthelmintic and antimicrobial activity of *Hamelia patens*Jacq. (Rubiaceae). Int. J. of Nat. Products Res.. 1(3): 54-56
6. Satrija, F., Retnani, E.B., Ridwan, Y. and Tiuria, R., 2001. Potential use of herbal anthelmintics as alternative antiparasitic drugs for small holder farms in developing countries. Development of traditional herbal anthelminthics as an alternative for commercial anthelminthics in small holder farms in Indone. http://www.aitvm.kvl.dk/E_periurban/E6Satrija.htm (3 of 10)12/07/2005 12:12:00. Pp 1-10.
7. Rohinisingh A. Mehta, P. Mehta, K. Shukla. 2011. Anthelmintic activity of rhizome extracts of *curcuma longa* and Zingiber officinale (zingiberaceae). Int. J. of Pharmacy and Pharmaceut. Sci.. 3(2), 236237.

8. Mujumdar AM, Naik DG, Dandge CN and Puntambekar HM. 2000. Anti- inflammatory activity of *Curcuma amada*roxb. in albino rats. Ind. J. Pharmacol. 32:375-377.
9. Jayasinghe ULB, Wannigama GP, Balasubramaniam S, Habib Nasir and Atta Ur Rahman. 1992. Benzyl isoQuinoline alkaloids from AnamirtaCocculus and *Diploclisia glaucescens*. J of Natn Sci. Count. Srilanka. 20(2), 187-190.
10. Jayasinghe ULB, Fujimoto Y. 2005. Search for biologically active compounds from Sri Lankan Plants. Frontiers in Natural Products Chemistry. 1. 193-199.
11. Immanuel Sagayaraj M, S. John Britto, M. ThamacinArulappan, J. Krishnakumar, Sinjumol Thomas and Mariat George. 2014. Antimicrobial studies and phytochemical screening of the leaves in Tiliacoraacuminata (lam.) hook. &thomson and *Diploclisia glaucescens* (blume) diels. (Menispermaceae). Asian J. Pharm. Res. 4(2), 82-86.
12. Ranjith D and Maria L. 2017. A Review on Phytochemicals Based Extraction and their Qualitative Screening Protocols. *Indian Journal of Natural Sciences.* 8(44). 12794-12804.
13. SanghPartap, Saurabh Kumar, Amit Kumar, Neeraj K. Sharma, K. K. Jha. 2012. *In-Vitro* Anthelmintic Activity of *Luffa cylindrica* Leaves in Indian Adult Earthworm. Journal of Pharmacognosy and Phytochemistry. 1(2). 27-30.
14. Das SS, MonalishaDey, AK Ghosh. Determination of the anthelmintic activity of the leaf and bark extracts of the Tamarindus indica Linn; Indian journal of Pharmaceutical Sciences. 2011; 71(1):104-107
15. Gaikwad SA, Kale AA, Jadhav BG, Deshpande NR, Salvekar JP. Anthelmintic activity of Cassia auriculata L. extracts - in vitro study. J Nat Prod Plant Resour 2011; 1(2): 62-66.
16. Dama GY, Tare HL, Gore MS, Deore SR, Bidkar JS. Comparative helmintholytic potential of extracts obtained from Cymbopogoncitratus and Wrightia tinctoria leaves. Int J Pharm Bio Sci 2011; 2(1): 321-327.
17. SourovKuri, Md. MustahsanBillah, S. M. MasudRana, ZannatulNaim, Md. Mahmodul Islam, Md. Hasanuzzaman, Md. Ramjan Ali, RanaBanik. 2014. Phytochemical and *in vitro* biological investigations of methanolic extracts of *Enhydrafluctuans*Lour. Asian Pacific J. of Trop. Biomed. 4(4): 299-305.
18. Asolkar LV, Kakkar KK, Chakre OJ. Second supplement to Glossary of Indian Medicinal Plants with Active Principles. CSIR Publication. New Delhi.1992, 61.
19. Kritikar KR, Basu LM. Indian Medicinal plants.2000;841-3.
20. Dhandapani S, Vijayakumar R, Senthilkumar R, Nalini N. Hypolipidemic effect of Cuminum cyminum on alloxan-induced diabetic rats. Pharmacol Res. 2002;46(3):251-5. https://doi.org/10.1016/S1043-6618(02)00131-7.
21. Olusegun-Joseph TS, Ofodile LN, Oguntoke T. *In vitro* evaluation of anthelmintic activity of crude extract of the leaves of *Dalbergiellawelwitschii*. Int J Pharm Pharm Sci 2013;5Suppl 1:32-3.
22. Paria S, Maity S, Mookerjee M. Phytochemial investigation and evaluation of anthelmintic activities of *V. Negundo*leaf extract. Int J Res Pharm Biomed Sci 2012;3:1143-6.
23. Joshi N, Bhatt S, Dhyani S, Nain J. Phytochemical screening of secondary metabolites of *Argemonemexicana*linn flowers. Int. J Curr Pharm Res 2013;5:144-7.
24. Azaizeh H, Halahleh F, Abbas N, Markovics A, Muklada H, Ungar ED, *et al.* Polyphenols from *Pistacialentiscus*and *Phillyrealatifolia*impair the exsheathment of gastro-intestinal nematode larvae. Vet Parasitol 2013;191(1-2):44-50.
25. Kumar BS, Lakshman K, Jayaveera KN, Velmurugan C, Manoj B, Sridhar SM. 2010. Anthelmintic activity of methanol extract of *Amaranthus caudatus*Linn. Internet J Food Saf. 12:127-9.
26. Jain P, Singh S, Singh SK, Verma SK, Kharya MD, Solanki S. 2013. Anthelmintic potential of herbal drugs. Int J Res Dev Pharm L Sci.2(3):412-27.
27. Hussain A, Sonkar AK, Ahmad MP, Wahab S. 2012. *In vitro* anthelmintic activity of *Coleus aromaticus*root in Indian adulth earthworm. Asian Pac J Trop Dis. 2 Suppl 1:425-7.
28. Wang GX, Han J, Zhao LW, Jiang DX, Liu YT, Liu XL. 2010. Anthelmintic activity of steroidal saponins from *Paris polyphylla*. Phytomed. 17(14):1102-5.
29. Borba HR, Freire RB, Albuquerque AC, Cardoso ME, Braga IG, Almeida ST, *et al.* 2010. Anthelmintic comparative study of *Solanum lycocarpum*St. Hill extracts in mice naturally infected with *Aspiculuristetraptera*. Nat Sci. 8(4):94-100.

30. Gaikwad SS, Kale AA, Jadhav BG, Deshpande NR, Salvekar JP.2011. Anthelmintic activity of *Cassia auriculata* L. Extracts-*In vitro* study. J Nat Prod Plant Resour. 1(2):62-6.
31. Chandrashekhar CH, Latha KP, Vagdevi HM, Vaidya VP. 2008. Anthelmintic activity of the crudeextracts of *Ficus racemosa*. Int J Green Pharm. 2(2):100-3.
32. Kundu S, Roy S, Nandi S, Ukil B, Lyndem LM. 2015. *In vitro* anthelmintic effects of *Senna occidentalis*(L.) Link (Leguminosae) on rat tapeworm *Hymenolepisdiminuta*. Int J Pharm Pharm Sci. 7(6):268-72.
33. Swargiary A, Roy B.2015. *In vitro* anthelmintic afficacy of *Alpinianigra*and its bioactive compound, astragalin against *Fasciolopsisbuski*. Int J Pharm Pharm Sci. 7(10):30-5.

**Table No.1: Results of Preliminary phytochemical analysis of Methanolic extract of Herbal formulation containing *Diploclisia glaucescens* leaves and *Curcuma longa* rhizomes**

| Sl No. | Phytoconstituents | Pet. Ether | Chloroform extract | Ethyl acetate extract | Ethanol extract | Methanol extract | Water extract |
|---|---|---|---|---|---|---|---|
| 1 | Alkaloids | A | A | P | P | P | P |
| 2 | Flavonoids | A | P | A | P | P | P |
| 3 | Glycosides | A | A | A | A | P | A |
| 4 | Steroids | P | A | A | A | P | P |
| 5 | Tannins | P | P | P | A | P | A |
| 6 | Phenolic compounds | P | P | A | A | P | A |
| 7 | Terpenoids | A | P | P | P | P | A |
| 8 | Saponins | A | A | A | A | P | A |
| 9 | Gums and mucilages | A | A | A | A | A | A |
| 10 | Carbohydrates | A | A | A | A | A | P |
| 11 | Oils and Fats | A | A | A | A | A | A |
| 12 | Proteins and amino acids | A | A | A | A | P | A |

A – Absent, P – Present

**Table No. 02. Results of the Extractive values of Herbal formulation**

| Solvents | Extractive Yield (%) | Solvents | Extractive Yield(%) | Solvents | Extractive Yield(%) |
|---|---|---|---|---|---|
| Water | 25.68 | Aniline | 17.65 | Toluene | 1.92 |
| Hydro alcoholic | 27.32 | Ethyl acetate | 1.89 | Xylene | 1.85 |
| Acetic acid | 18.63 | Acetone | 8.65 | Cyclohexane | 2.65 |
| Methanol | 19.79 | CCL4 | 8.65 | Petroleum ether | 3.52 |
| Ethanol | 17.25 | Dichloromethane | 9.78 | Hexane | 1.96 |
| Isopropanol | 3.85 | Chloroform | 9.10 | Diethylether | 3.96 |
| Acetonitrile | 2.58 | Benzene | 1.25 | | |

**Table No. 03. Anthelminthic activity of Methanolic extract of Herbal Formulation against *Pheretima posthuma***

| Groups | Conc. (mg/ml) | Time taken for Paralysis (min) | Time taken for death of worm (min) |
|---|---|---|---|
| **10% Tween 80 in Distilled water** | ---- | --- | ----- |
| **Albendazole** | 25 | $11.67\pm1.23^{A}$ | $20.33\pm1.20^{A}$ |
| **Herbal Formulation (HF)** | 25 | $144.52\pm2.81^{B}$ | $180.83\pm2.43^{B}$ |
| | 50 | $120.33\pm4.24^{C}$ | $168.33\pm2.49^{C}$ |
| | 75 | $90.17\pm2.67^{D}$ | $117.83\pm3.91^{D}$ |
| | 100 | $49.33\pm2.12^{E}$ | $76.67\pm3.14^{E}$ |

Values are expressed in Mean ± SEM, n=6 in each group, HF- Herbal Formulation
Means with different superscripts (A, B, C) are statistically ($p<0.05$) highly significant between the groups in the single reaction time (in minutes) parameter.

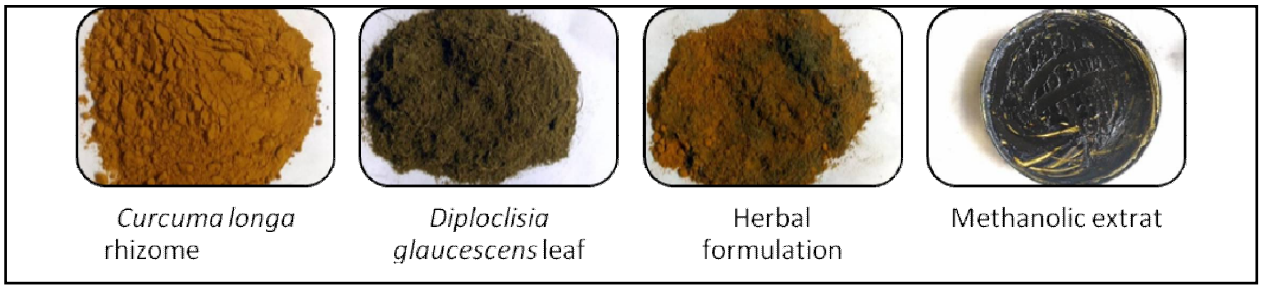


**Fig. 01. Preparation of Herbal formulation for Anthelminthic activity**


**Fig.02. Experimental worms in different groups for Anthelminthic activity of Herbal formulation**